
N7721074

**PRELIMINARY DESIGN OF A REDUNDANT STRAPPED
DOWN INERTIAL NAVIGATION UNIT USING
TWO-DEGREE-OF-FREEDOM TUNED-GIMBAL
GYROSCOPES**

LITTON SYSTEMS, INC., WOODLAND HILLS,
CALIF

OCT 1976

PRELIMINARY DESIGN OF A REDUNDANT
STRAPPED DOWN INERTIAL NAVIGATION UNIT
USING TWO-DEGREE-OF-FREEDOM
TUNED-GIMBAL GYROSCOPES

(NASA-CR-145305) PRELIMINARY DESIGN OF A
REDUNDANT STRAPPED DOWN INERTIAL NAVIGATION
UNIT USING TWO-DEGREE-OF-FREEDOM
TUNED-GIMBAL GYROSCOPES (Litton Systems,
Inc.) 582 p HC A25/MF A01

77-21074

Unclass
25708

CSCL 17G G3/04

For



Litton

GUIDANCE & CONTROL SYSTEMS

5500 Canoga Avenue, Woodland Hills, California 91364



Document No. 403314
NASA CR-145305
October 1976

PRELIMINARY DESIGN OF A REDUNDANT
STRAPPED DOWN INERTIAL NAVIGATION UNIT
USING TWO-DEGREE-OF-FREEDOM
TUNED-GIMBAL GYROSCOPES

Prepared Under Contract No. NAS1-13847

For



Publication of this report does not constitute NASA approval of the findings or conclusions indicated in the report. It is published for the exchange of information and stimulation of ideas.



GUIDANCE & CONTROL SYSTEMS
5500 Canoga Avenue, Woodland Hills, California 91364

TABLE OF CONTENTS

<u>Paragraph</u>	<u>Title</u>	<u>Page</u>
	I. INTRODUCTION	1
	II. SUMMARY.	3
2.1	General Program Description	3
2.2	System Description.	6
	III. SPECIFICATION OF SYSTEM REQUIREMENTS. . .	35
3.1	Cost Factors.	35
3.2	Reliability	37
3.3	Accuracy.	39
3.4	System Input/Output	39
3.5	Reaction Time	41
3.6	Modes of Operation.	41
3.7	Environment	42
	3.7.1 Flight Profile Operating Conditions . .	42
	3.7.2 Ambient Temperature	43
	3.7.3 Cooling Air	43
	3.7.4 Vibration	44
	3.7.5 Shock	46
3.8	Power	46
3.9	Memory Non-Volatility	47
3.10	Packaging Philosophy.	47
3.11	Form-Factor/Weight.	48
3.12	Installation Provisions	48
3.13	Maintenance Philosophy.	49
3.14	Maintainability Design.	49
3.15	Test/Calibration.	50
3.16	Operational Service Life.	50
3.17	Electromagnetic Interference.	51
3.18	Humidity.	51
3.19	Explosive Atmosphere.	51
3.20	Atmospheric Pressure.	51

TABLE OF CONTENTS (cont)

<u>Paragraph</u>	<u>Title</u>	<u>Page</u>
	IV. SYSTEM SYNTHESIS AND DESIGN.	53
4.1	General Design Requirements.	53
	4.1.1 General Construction	54
	4.1.2 Module Designs	54
	4.1.3 Software Generation.	55
	4.1.4 Test and Calibration	55
4.2	Element Block Diagrams	55
	4.2.1 Non-Redundant System Block Diagram	55
	4.2.2 Gyro Mechanization	56
	4.2.3 Accelerometer Mechanization.	63
	4.2.4 IMU/Computer Interface	63
	4.2.5 Digital Computer Design.	65
	4.2.6 Computer Input/Output.	68
	4.2.7 Power Supply and Support Electronics	69
	4.2.8 Software	69
4.3	System Redundancy Tradeoffs.	73
4.4	Instrument Redundancy Trade-Offs	84
	4.4.1 General Concepts	84
	4.4.2 Two-Degree-Of-Freedom Gyro (TDF) Considerations	85
	4.4.3 3-Gyro FDI Singularities	86
	4.4.4 Gyro Geometries.	96
	4.4.5 Accelerometer Geometries	99
	4.4.6 Parity Equations	100
	4.4.7 Error Detection and Isolation Methods.	108
	4.4.8 Switching Methods.	112
	4.4.9 Failure Coverage	115
4.5	Software Trade-offs.	121
	4.5.1 Redundancy Management Software Design.	121
	4.5.2 Radio Aid Updates.	126
	4.5.3 Instrument Compensation.	127
4.6	Hardware Packaging Options	128
4.7	Redundant Strapdown INS Trade-Off Summary.	137

TABLE OF CONTENTS (cont)

<u>Paragraph</u>	<u>Title</u>	<u>Page</u>
	V. SYSTEM ANALYSES	141
5.1	Dynamic Error Analysis	143
5.1.1	Computation Errors	145
5.2	Error Simulation of Radio-Strapdown Navigator.	178
5.2.1	Introduction	178
5.2.2	Strapdown Inertial Error Model	178
5.2.3	Radio Error Model and Budget	184
5.2.4	Inertial Error Budgets	185
5.2.5	Updating Concept	185
5.2.6	Simulated Trajectory	188
5.2.7	Simulation Program	193
5.2.8	Performance of Inertial Budget #5.	196
5.2.9	Performance of Inertial Budget #4.	207
5.3	System Reliability	220
5.3.1	Analytical Approach.	220
5.3.2	Probability of Flight Control System Output Failure.	224
5.3.3	Probability of Navigation Output Failure	230
5.3.4	Summary of Study Results in Advanced Techniques for Failure Detection and Isolation.	232
	VI. PRELIMINARY SYSTEM DESIGN	239
6.1	System Block Diagram	239
6.2	Hardware Design.	239
6.2.1	G-6 Gyro and Loop Dynamics	239
6.2.2	Gyro Rebalance Loop Electronics.	259
6.2.3	A-1000 Accelerometer and Loop Dynamics.	269
6.2.4	Accelerometer Rebalance Electronics.	272
6.2.5	IMM/Computer Interface	272
6.2.6	Computer Description	278
6.2.7	Input/Output System Description.	285
6.2.8	Power Supply and Support Electronics.	286
6.2.9	Self-Test.	288

TABLE OF CONTENTS (cont)

<u>Paragraph</u>	<u>Title</u>	<u>Page</u>
	6.2.10 Packaging Design.	289
6.3	Software Design	296
	6.3.1 Computational Considerations.	296
	6.3.2 Equation Summary.	298
	6.3.3 Computer Resource Estimates	320
	6.3.4 Future Software Refinements	328
	VII. FACTORY TEST EQUIPMENT	331
7.1	Module Testing.	331
	7.1.1 Manufacturing Flow.	331
	7.1.2 Test Programs	331
	7.1.3 Test Equipment.	334
7.2	G-6 Gyro Test	342
	7.2.1 G-6 Process Flow.	342
	7.2.2 G-6 Final Test Station.	342
7.3	A-1000 Accelerometer Test	346
	VIII. COST ANALYSIS.	347
8.1	Baseline Cost Estimate.	347
8.2	Basis of Estimate	348
APPENDIX A	REDUNDANT STRAPDOWN INERTIAL NAVIGATION SYSTEM SPECIFICATION.	A-1
APPENDIX B	PARITY EQUATIONS.	B-1
APPENDIX C	LOGISTICS ANALYSIS.	C-1
APPENDIX D	STRAPDOWN GYRO TRANSFER FUNCTION.	D-1
APPENDIX E	PENDULOUS ACCELEROMETER ANALYSIS.	E-1
APPENDIX F	DERIVATION OF DESIGN EQUATIONS FOR TETRAHEDRAL ARRAY OF 4 TDF GYROS.	F-1
APPENDIX G	RELIABILITY DATA.	G-1
APPENDIX H	COMPUTER FLOW CHARTS.	H-1
APPENDIX I	ADVANCED FAILURE DETECTION AND ISOLATION ALGORITHM	I-1
APPENDIX J	PROBABILITY OF EFFECTIVELY SIMULTANEOUS FAILURE OF TWO GYROS AND IMPACT ON FAILURE ISOLATION AND SYSTEM FAILURE.	J-1

LIST OF ILLUSTRATIONS

<u>Figure</u>	<u>Title</u>	<u>Page</u>
2-1	Four Channel Installation Configuration	4
2-2	Split-Sensor Installation Arrangement	5
2-3	Redundant Strapdown INS	7
2-4	Inertial Navigation Module	9
2-5	G-6 Gyroscope and A-1000 Accelerometer	10
2-6	Four-Channel Software Mechanization	17
2-7	Gyro Parity Equations, Semi Octahedral Gyro Spin Axis Orientation	18
2-8	Simulation Results of 50 Percentile Velocity and Position Error With Radio Update	23
2-9	Simulation Results of 1 σ and 50% Position and Velocity Errors, Free Inertial	24
2-10	One Channel of the Redundant Strapdown INS	27
2-11	Instrument Block	28
2-12	Redundant Strapdown INS Installation	29
2-13	Redundant Strapdown INS Mount Details	30
2-14	INS Reliability Growth Curve	32
2-15	Calculated System Failure Probabilities	34
4-1	Non-Redundant INS Simplified Block Diagram	57
4-2	G-6 Gyro Interface	58
4-3	Digital Gyro Rebalance Loop Mechanization	60
4-4	IMU/Computer Interface Block Diagram	64
4-5	Power Supply and Support Electronics	70
4-6	Simplified Block Diagram of Strapdown System Software	71
4-7	Channel vs Modular Redundancy Options	74
4-8	Approximate System Reliability vs Coverage	75
4-9	Modular Redundant Configuration	78
4-10	Selected Channel Redundancy System Configuration	79
4-11	Intercomputer I/O Options	82

LIST OF ILLUSTRATIONS

<u>Figure</u>	<u>Title</u>	<u>Page</u>
4-12	Gyro Assemblies and Gyro Associated Electronics	87
4-13	Three Orthogonal TDF Gyro Configuration	89
4-14	Failure Error Vector	91
4-15	Error Angle Versus Time	92
4-16	Non Dimensional Isolation Error For $0 \leq \theta \leq 45^\circ$.	94
4-17	Failure Isolation Error vs Direction of Gyro Error (3 Orthogonal TDF Gyro Spin Axes)	95
4-18	Octahedral Spin Axis Orientation	98
4-19	Gyro Parity Equations. Semi-Octahedral Gyro Spin Axis Orientation	101
4-20	Physical Interpretation of Parity Equations (Tetrahedron Example)	102
4-21	Illustration of 3-Gyro Isolation Singularity . .	104
4-22	Failure Isolation Error vs Direction of Gyro Error (3 of 4 Tetrahedral TDF Gyro Spin Axes) . .	106
4-23	Flattened Semi-Octahedron	107
4-24	Polar Plots of Isolation Error vs Gyro Drift Direction 3 and 4 TDF Gyros	110
4-25	Tetrahedron Illustration of 3-Gyro Ambiguity . .	114
4-26	Hypothetical Polar Plot of Soft-Failure Probability Density ($P/\Delta\psi$) vs Error Direction (ψ)	118
4-27	Polar Plots of Isolation Error vs Gyro Drift Direction	120
4-28	4-Channel Software Mechanization	123
4-29	Packaging Options	129
4-30	Illustration of Tetrahedron Via Cube	133
4-31	Successive 180° Rotation of the Cube	134
4-32	Symmetrical Chassis Implementation	135
4-33	Achieving Tetrahedron With 90° Rotations About Single Axis	136
4-34	Conceptual Packaging Design With 90° Rotations .	138

LIST OF ILLUSTRATIONS

<u>Figure</u>	<u>Title</u>	<u>Page</u>
5-1	System Analysis Methodology	142
5-2	Normalized Random Vibration Spectrum	151
5-3	RMS Acceleration Input vs Bandwidth of Wide Band Random Linear Vibration	152
5-4	RMS Rate Input vs Bandwidth of Wide Band Random Angular Vibration	153
5-5	Gyro Loop Rectification Error Coefficient	154
5-6	Gyro Loop Rectification Error Coefficient	155
5-7	Gyro Anisoinertia Error Coefficient	156
5-8	Gyro Scale Factor Asymmetry Error For Random Input Rates	157
5-9	Accelerometer Loop Rectification Error Coefficient	158
5-10	Accelerometer Scale Factor Asymmetry Error For Random Input Accelerations	159
5-11	Coning Drift Coefficient	160
5-12	Uncompensated Pseudo Coning Error Coefficient	161
5-13	Pseudo Coning Error Coefficient due to Mismatched Gyro Loops	162
5-14	Pseudo Sculling Error Coefficient Due to Sensor Loop Mismatch	163
5-15	Gyro Loop Rectification Error vs Vibration Bandwidth - Direct Axis	164
5-16	Gyro Loop Rectification Error vs Vibration Bandwidth - Cross Axis.	165
5-17	Anisonertia Error vs Vibration Bandwidth	166
5-18	Gyro Anisoelastic Error vs Vibration Bandwidth	167
5-19	Accelerometer Loop Rectification Error vs Vibration Bandwidth	168
5-20	Accelerometer g^2 Error vs Vibration Bandwidth	169
5-21	Coning Error vs Vibration Bandwidth	170
5-22	Uncompensated Pseudo Coning Error vs Vibration Bandwidth, No Computer Attenuation	171

LIST OF ILLUSTRATIONS

<u>Figure</u>	<u>Title</u>	<u>Page</u>
5-23	Pseudo Coning Error vs Vibration Bandwidth, Computer Frequency Response Included	172
5-24	Pseudo Coning Error Due To Mismatched Gyro Loops vs Vibration Bandwidth	173
5-25	Sculling Error vs Vibration Bandwidth	174
5-26	System Dynamic Error Description	175
5-27	Computer Frequency Response	176
5-28	Computer Roundoff Error	177
5-29	Coordinate Frames	179
5-30	Simulated Updating Concept	187
5-31	Strapdown Trajectory TRAJ002 (Complete)	189
5-32	First Station Detail	190
5-33	Second Station Detail	191
5-34	Third Station Detail	192
5-35	Simplified Structure of the MOD6DF Program	194
5-36	Free Inertial Position Errors (Budget #5)	197
5-37	Free Inertial Velocity Errors (Budget #5)	197
5-38	Heading Error (Budget #5)	198
5-39	Pitch Error (Budget #5)	199
5-40	Roll Error (Budget #5)	200
5-41	Radio-Inertial East Position Error Residual (Budget #5)	201
5-42	Radio-Inertial North Position Error Residual (Budget #5)	202
5-43	Radio-Inertial CEP Residual (Budget #5)	203
5-44	Radio-Inertial East Velocity Error Residual (Budget #5)	204
5-45	Radio-Inertial North Velocity Error Residual (Budget #5)	205
5-46	Radio-Inertial CEV Residual (Budget #5)	206
5-47	Free Inertial Errors (Budget #4)	208

LIST OF ILLUSTRATIONS

<u>Figure</u>	<u>Title</u>	<u>Page</u>
5-48	Free Inertial Velocity Errors (Budget #4)	209
5-49	Heading Error (Budget #4)	210
5-50	Pitch Error (Budget #4)	211
5-51	Roll Error (Budget #4)	212
5-52	Radio-Inertial East Position Error Residual (Budget #4)	213
5-53	Radio-Inertial North Position Error Residual (Budget #4)	214
5-54	Radio-Inertial CEP Residual (Budget #4)	215
5-55	Radio-Inertial East Velocity Error Residual (Budget #4)	216
5-56	Radio-Inertial North Velocity Error Residual (Budget #4)	217
5-57	Radio-Inertial CEV Residual (Budget #4)	218
5-58	Assumptions Used in System Reliability Analysis .	222
5-59	Single-Channel Reliability Diagram	224
5-60	Calculated Channel Failure Rate and MTBF	225
6-1	Redundant Strapdown INS	240
6-2	Inertial Navigation Module	241
6-3	Photograph of Litton G-6 Strapdown INS Gyroscope	242
6-4	Strapdown Gyro Block Diagram	252
6-5	Electronics for Strapdown Compensation	255
6-6	Frequency Response for Dual-Axis Compensation (Integral Gain Not Shown)	256
6-7	Closed-Loop Pickoff Excursion vs Frequency . . .	257
6-8	Frequency Response of Strapdown Gyro	258
6-9	Compensation Response for Single-Axis Control . .	260
6-10	Strapdown Gyro Loop Pickoff Response (Direct) . .	261
6-11	Strapdown Gyro Loop Pickoff Response (Cross Axis)	262
6-12	Strapdown Gyro Loop Frequency Response (Direct) .	263

LIST OF ILLUSTRATIONS

<u>Figure</u>	<u>Title</u>	<u>Page</u>
6-13	Strapdown Gyro Loop Frequency Response (Cross Measurement).	264
6-14	Typical Pulse-Rebalance Loop	265
6-15	Rebalance Electronics Bridge Arrangement	266
6-16	Rebalance Loop Waveforms	268
6-17	A-1000 Accelerometer	270
6-18	Strapdown Accelerometer Block Diagram	271
6-19	Accelerometer Loop Pickoff Response	273
6-20	Accelerometer Loop Frequency Response	274
6-21	Functional Block Diagram IMM/Computer Interface	277
6-22	Functional Block Diagram of CPU Using AMD Chips	280
6-23	4-Bit Bipolar Microprocessor Slice	281
6-24	Power Supply and Support Electronics Block Diagram	287
6-25	One Channel of the Redundant Strapdown INS	290
6-26	Redundant Strapdown INS Installation	292
6-27	Redundant Strapdown INS Mount Details	293
6-28	Instrument Block	294
6-29	INM Software	297
6-30	INM Compensation	300
6-31	Gyro Failure Detection and Isolation Block Diagram	307
6-32	Coordinate Conversion	312
6-33	Baro-Inertial Loop	319
6-34	Semi-Octahedral Coordinate Frames	321
6-35	Navigation Frame Relationship	322
7-1	Module Manufacturing Flow	332
7-2	LN-31 INU Multiplex Station	335
7-3	Load Station	337
7-4	Rate Calibration Station	339

LIST OF ILLUSTRATIONS

<u>Figure</u>	<u>Title</u>	<u>Page</u>
7-5	Three Axis Automatic Test Stand	340
7-6	G6 Factory T/E Process Flow	343

LIST OF TABLES

<u>Number</u>	<u>Title</u>	<u>Page</u>
2-1	FAILURE DETECTION, ISOLATION, SWITCHING CONCLUSIONS	20
2-2	COMPUTER RESOURCE ESTIMATES	21
4-1	TRUTH TABLE FOR ISOLATION OF A FAILED GYRO FOR 3 ORTHOGONAL TDF GYRO CONFIGURATION WITH ORTHOGONAL SENSING AXES	88
4-2	HYPOTHETICAL SYSTEM FAILURE DISTRIBUTION.	116
4-3	GYRO PAIR SELECTION VS FAILURE INDICATION	124
5-1	DYNAMIC ERROR SUMMARY (SINGLE AXIS-1 σ).	146
5-2	DYNAMIC ERROR SUMMARY-SINUSOIDAL VIBRATION (3 σ)	147
5-3	DYNAMIC ERROR SUMMARY-RANDOM VIBRATION (3 σ)	149
5-4	PERFORMANCE ENVIRONMENT SUMMARY	150
5-5	LANGLEY ERROR BUDGETS	186
5-6	UPDATE LOSS PERIODS	196
5-7	FREE INERTIAL SUMMARY PERFORMANCE (BUDGET #5)	207
5-8	FLIGHT CONTROL OUTPUT FAILURE PROBABILITY VERSUS ARCHITECTURE, FLIGHT TIME, AND CHANNEL MTBF	229
5-9	NAVIGATION OUTPUT FAILURE PROBABILITY VERSUS FLIGHT TIME AND CHANNEL MTBF, INFLEXIBLE ARCHITECTURE.	231
6-1	GYRO NOMENCLATURE	248
6-2	ACCELEROMETER NOMENCLATURE.	275
6-3	SENSOR LOOP OPERATIONAL PARAMETERS.	276
6-4	4516 GENERAL CHARACTERISTICS.	283
6-5	TYPICAL INSTRUCTION TIMES	284
6-6	INSTRUCTION MIX FOR REDUNDANT STRAPDOWN INS	298
6-7	DUTY CYCLE ESTIMATE FOR A STATE OF THE ART 16-BIT COMPUTER	299
6-8	SEMI-OCTAHEDRON UNIT VECTORS.	305
6-9	INSTRUMENT PAIR SELECTION VS FAILURE INDICATION	310

Preceding page blank

LIST OF TABLES (cont)

<u>Number</u>	<u>Title</u>	<u>Page</u>
6-10	LEAST SQUARES WEIGHTING FACTORS.	311
6-11	COORDINATE FRAMES.	323
6-12	GLOSSARY	324
6-13	COMPUTER RESOURCE ESTIMATES.	327
8-1	REDUNDANT STRAPDOWN INS PREDICTED AVERAGE COST, 200 SYSTEMS.	347

I. INTRODUCTION

This report documents results of the redundant strapped-down (strapdown) Inertial Navigation System (INS) preliminary design study conducted by Litton Industries Guidance and Control Systems division under contract number NAS1-13847 for the NASA Langley Research Center (LaRC). This study is part of the LaRC VTOL Automatic Landing Technology (VALT) program. The purpose of the VALT program is to foster the development of the various technologies needed by the VTOL aircraft in an intra-urban setting. Low-cost, highly reliable avionics are essential for the economic viability of this mode of transportation.

One means of achieving lower costs for both VTOL and conventional aircraft is improved integration of avionics functions. Currently, there is considerable interest in replacing the multiple flight control sensors of a typical, modern commercial aircraft with a skewed array of strapdown inertial navigation sensors, and using redundant computers to perform multiple functions such as flight control, air data, and strapdown navigation. Net cost has been shown to be less than current, non-integrated systems. Inertial navigation capability is thus available without additional cost. This integrated avionics approach depends upon redundancy to achieve the reliability needed in flight control loops. VTOL and other modern aircraft will be designed to depend upon the flight control avionics for their flight stability in order to achieve various performance and economic improvements. Thus, flight control system reliability and flight safety depend upon integrated avionics reliability. Thorough analysis of skewed sensor system reliability, then, is essential.

This redundant strapdown INS preliminary design study demonstrates the practicality of a skewed sensor system configuration by means of:

- Devising a practical system mechanization utilizing proven strapdown instruments.
- Thoroughly analysing the skewed sensor redundancy management concept to determine optimum geometry, data processing requirements, and realistic reliability estimates.
- Implementing the redundant computers into a low-cost, maintainable configuration.
- Providing a practical, maintainable packaging concept suitable for airline use.
- Estimating system size, weight, power and cost for a production system configuration.

The redundant strapdown INS design is founded upon proven strapdown gyros and accelerometers used in Litton's LN-50 developmental strapdown system. This system, undergoing flight test at the time this report was written, is proving the practicality of strapdown navigation using two-degree-of-freedom (TDF), tuned-gimbal gyroscopes. These gyroscopes are an extension of the type of instrument used on a wide variety of production, gimballed inertial systems manufactured by Litton, and other companies. They employ conventional, non-exotic techniques very close to a production configuration.

The TDF capability of these tuned-gimbal gyroscopes is particularly suited to a redundant system configuration. A fail-operational/fail-operational (fail-op/fail-op) system can be achieved using only four gyros versus six single-degree-of-freedom instruments. Tuned-gimbal gyro costs are quite low compared to present forms of exotic instruments, resulting in a particularly low cost for the high-reliability, redundant system.

The compact size of the tuned-gimbal gyro lends itself to a redundant system, resulting in a small net configuration. This is useful in solving aircraft installation problems, improving maintainability, and in assuring the required gyro-to-gyro mechanical alignment stability needed for accurate strapdown navigation.

The preliminary electronics estimates of the remaining system constituents are based on current technology. Extensive technology extrapolations are not employed. The size and cost estimates presented in this study are thus very realistic for application of such a system into airline use in the early 1980's.

II. SUMMARY

2.1 General Program Description

This report documents the preliminary design of a redundant strapdown navigator using four, two-degree-of-freedom, tuned-gimbal gyroscopes. NASA/Langley Research Center requirements defined in Contract NAS1-13847 are for fail-operational/fail-operational reliability with a failure probability per 0.5 hour flight of less than 10^{-6} . Accuracy is required to be 1.03 m/sec (2 knots) with radio aid updates having drop-outs up to 60 seconds in duration. Exceptionally low system cost is a firm requirement.

The fail-op/fail-op navigator designed to meet these requirements in this study has been configured to consist of four, interchangeable plug-in units for lowest cost. Each unit contains one channel of hardware consisting of a TDF tuned gimbal gyro, two linear accelerometers, a computer, and a power supply.

The gyro/accelerometer axes are skewed within each chassis so that when the four channels are installed as shown in figure 2-1, the four gyro, eight accelerometer axes are distributed in space. This distribution assures that normal operation continues regardless of which two sensors fail. A precision alignment block would be located within the central core of the array. Thus, accurate angular registration between instruments of the four channels can be obtained easily.

Some applications may require a physical separation between channels to reduce overall system susceptibility to a common disaster. Other solutions to this susceptibility are preferred, however, such as proper location of the units in the aircraft and/or structural and thermal isolation. If these methods are not adequate, the four channels can be split into pairs as shown in figure 2-2. Stiffness of the aircraft must be assured or the reliability and performance of the second fail-op level are significantly degraded. Added software is also needed if precision boresighting between location is to be avoided. This report concentrates on the preliminary system design for the installation method of figure 2-1.

The system characteristics for the full fail-op/fail-op redundant strapdown INS are as follows:

Power:	540 watts
Weight:	27.7 Kg (61 pounds)
Dimensions:	0.33m x 0.33m x 0.36m (13" x 13" x 14")

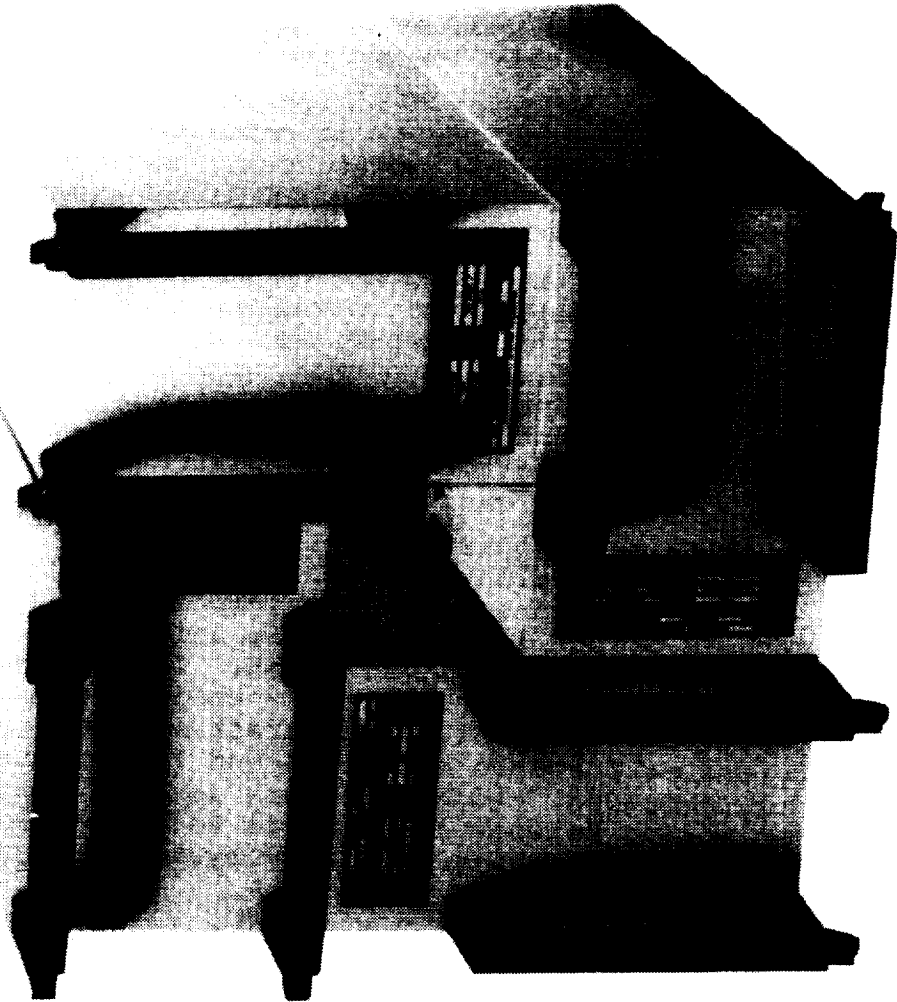


Figure 2-1. Four Channel Installation Configuration



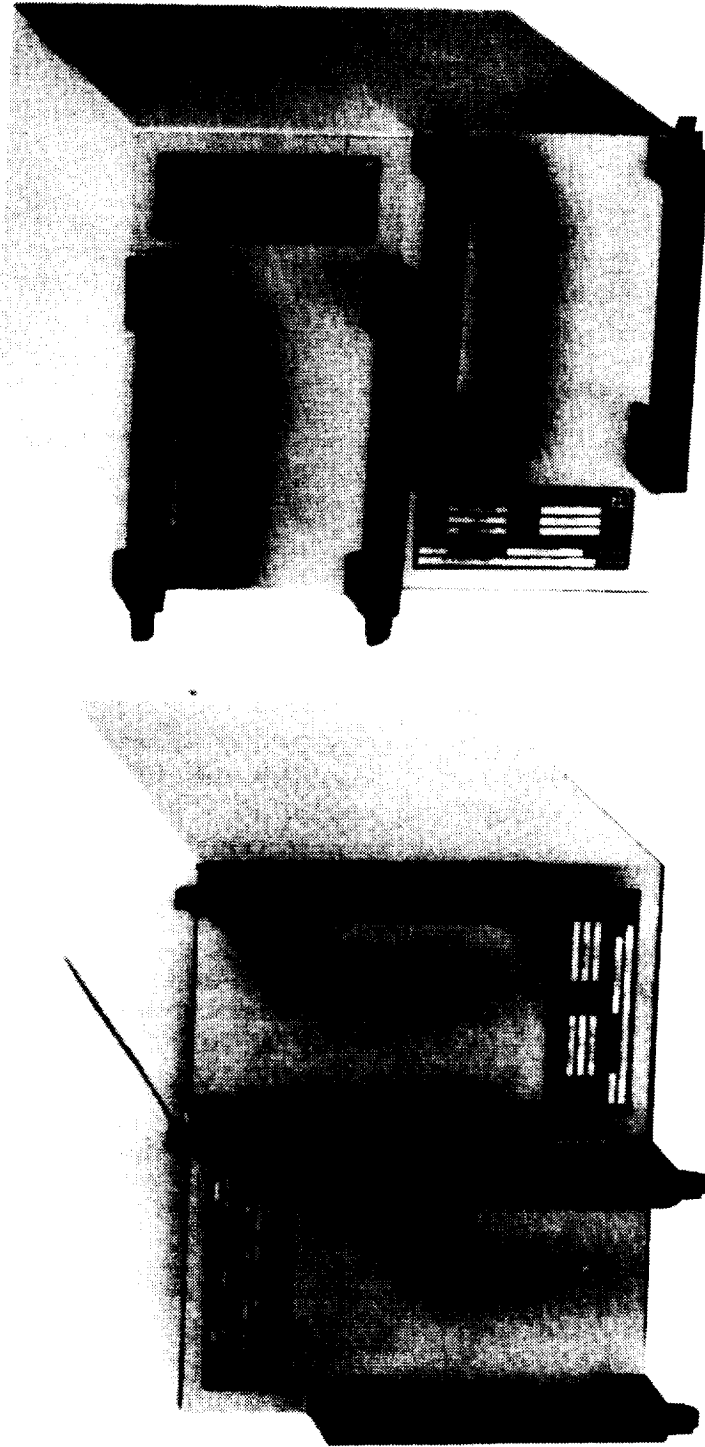


Figure 2-2. Split-Sensor Installation Arrangement



Accuracy*:	1.03 m/sec (2 knots)(95%)
Reliability, 1 hour flight	
Flight control outputs:	0.4×10^{-10}
Navigation outputs:	0.5×10^{-9}
Cost (production):	\$98,000

A baseline system specification is included as Appendix A of this report. The preliminary design of the redundant strapdown INS indicates that production equipment meeting these specifications could be available in the early 1980's.

2.2 System Description

A simplified system block diagram for the redundant strapdown INS is shown in figure 2-3. The complete system is composed of four identical channels. Each channel of the INS consists of the following elements:

- a. An Inertial Measurement Module (IMM) containing the basic inertial sensing devices, one TDF tuned gimbal gyro and two axes of acceleration measurement, with the associated electronics.
- b. A computer which performs redundancy management, instrument compensations, coordinate transformations, and the inertial navigation computations.
- c. External I/O which interfaces the computer with other aircraft equipment. Note that there is no self-contained voting in the system between the computers and these outputs. The external equipment must perform some voting between channels (in addition to using validity information provided by each channel) in determining the final navigation variable to be used.
- d. Inter-computer I/O which is used to transfer gyro and accelerometer measurement data from one channel to all others for use in redundancy management, and for derivation of the full 3-dimensional rate and acceleration inputs.
- e. A power supply used to drive all elements in a channel. Note that there is no cross-feeding of power between

*With position updates from DME, differential Omega, Loran C, or GPS.

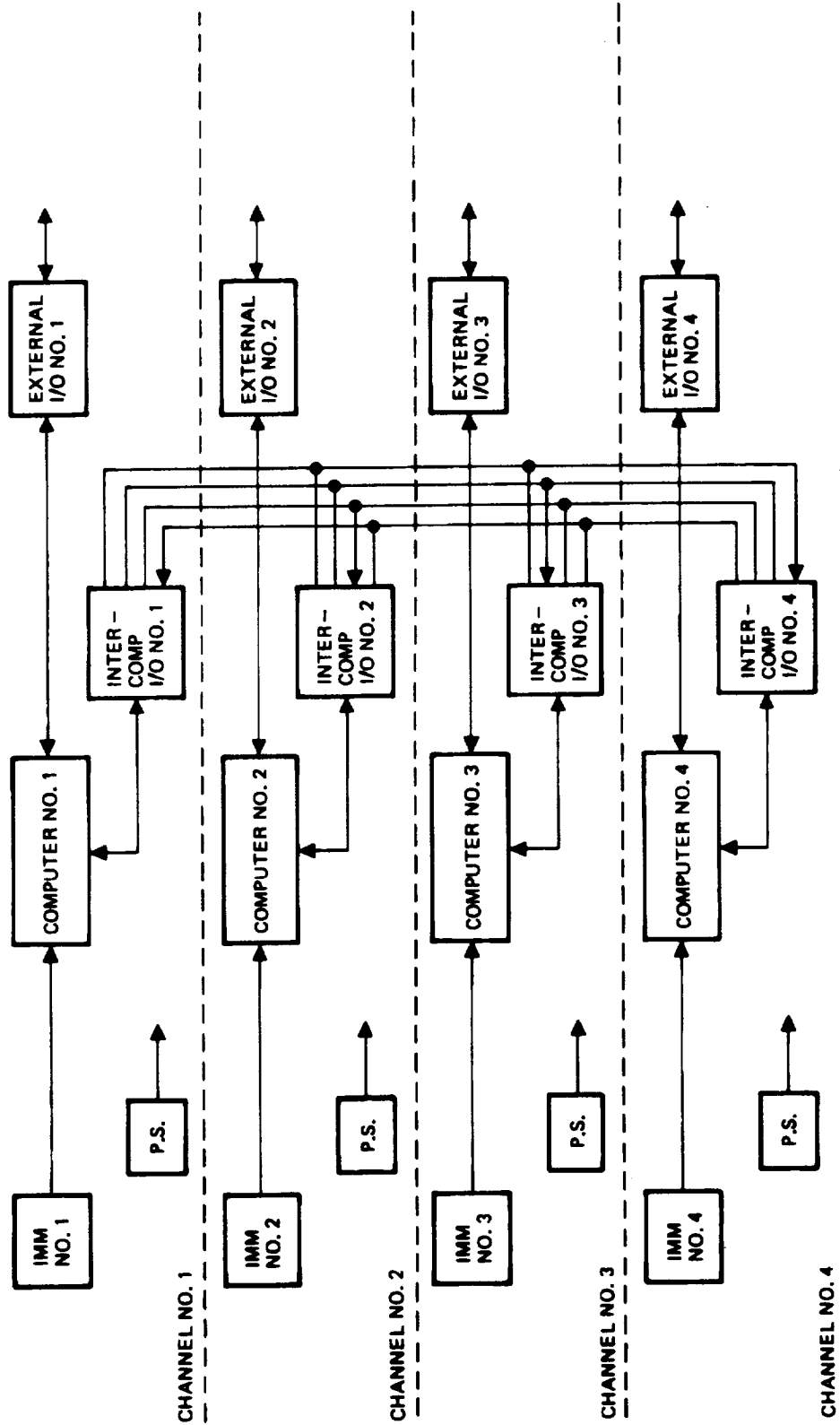


Figure 2-3. Redundant Strapdown INS

channels. This results in a simple, low-cost power supply design with a negligible decrease in system reliability over a modularly redundant power supply configuration

A more detailed block diagram for one of the four Inertial Navigation Modules (INM) is shown in figure 2-4. The equipment shown is packaged in its own chassis and four of these chassis installed into a common mount comprise the complete redundant strapdown INS.

G-6 Gyroscope (Figure 2-5)

The baseline gyroscope for the production program is designated the G-6. It is used in the LN-50 program and has proven performance. The design is based on the production Litton G-1200 gyro used in the LN-30 family of gimballed inertial navigation systems and the LTN-72 commercial system. It has a considerably increased torquing rate capability (up to 240°/sec) to be suited to strapdown INS usage. A smaller, lower-performance, lower-cost version of this instrument (designated the G-7) is currently under development. Its applicability to LaRC requirements has been considered due to the stringent cost goals of the study program.

Both the G-6 and G-7 are TDF, tuned gimbal, nonfloated gyroscopes. The gyroscopic element is attached to the rotor of a synchronous motor by means of two pairs of flexible hinges separated by an intermediate gimbal. The kinetic forces on the gimbal when rotating at operating speed are designed to cancel the hinge torques occurring at normal gyroscope displacement angles. Thus the gyroscope is capable of accurately measuring the extremely small angular rates required for inertial navigation.

Electromagnetic pick-offs are provided to sense displacements between the gyro case and the gyroscope rotating wheel. These pick-off outputs are then used in electronic circuitry to precess the gyro wheel to null the displacement in a high-speed, closed loop.

Gyro precession is produced by a pair of electromagnetic torquers attached to the gyro case, acting against a permanent magnet on the rotating wheel. The amount of current in the torquers required to keep the pick-offs nulled is the measure of vehicle angular rate about the two torquing axes. Special design features are provided in the torquing mechanization so that the torquing current accurately represents precession rate over the wide dynamic range appearing in a strapdown INS.

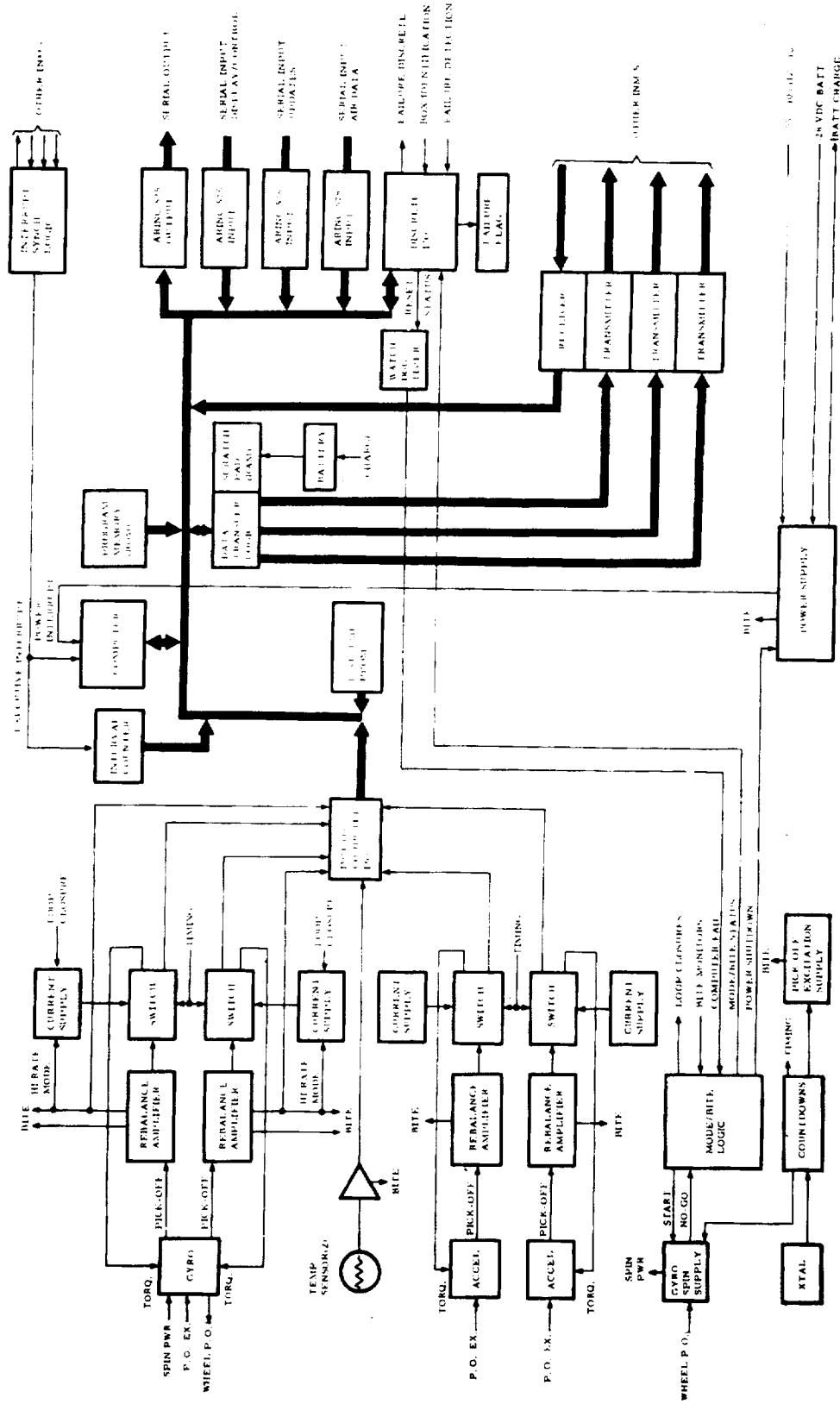


Figure 2-4. Inertial Navigation Module

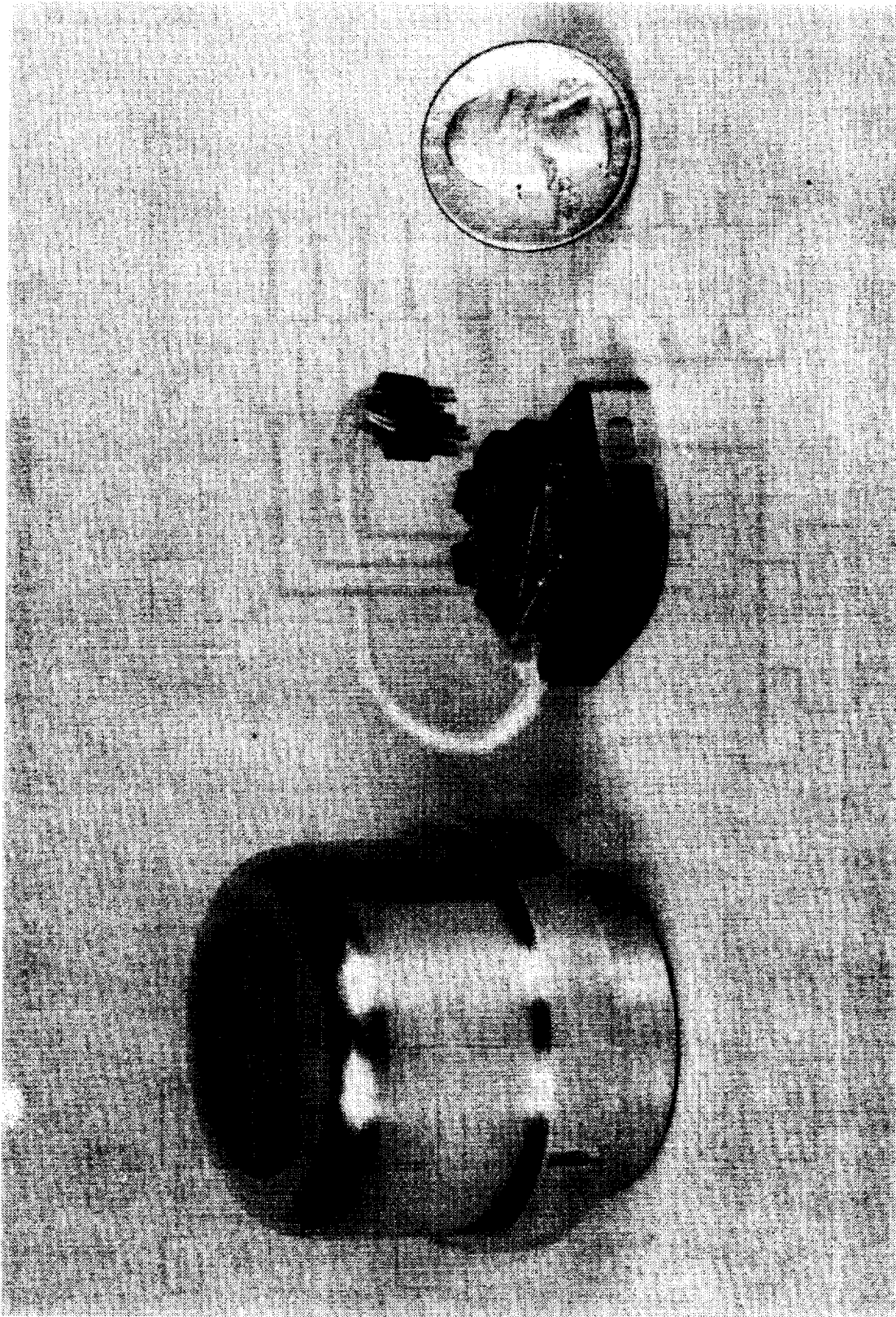


Figure 2-5. G-6 Gyroscope and A-1000 Accelerometer

Reproduced from
best available copy.



A-1000 Accelerometer (Figure 2-5)

The baseline accelerometer selected for the production program is designated the A-1000. It is a single-degree-of-freedom instrument used in the production LN-30 gimballed inertial navigation systems, the LTN-72 commercial gimballed systems, and the LN-50 strapdown navigation program. Minor modifications are made to the external instrument circuitry when used in the strapdown program to provide for digital rebalance instead of the normal analog rebalance.

The A-1000 accelerometer is a flexible hinge (dry), torque-to-balance instrument. It has a capacitive pick-off to detect rotations of the rotary, pendulous sensitive element. Pick-off deflections are then used in external electronics to produce current in an electromagnetic permanent magnet torquer in the accelerometer to drive the pick-off to null. The torquer current is then a measure of vehicle acceleration normal to the pendulous and rotary axes.

Gyro/Accelerometer Rebalance Electronics

Each of the gyro and accelerometer rebalance electronics takes essentially the same form, as shown in figure 2-4. The gyro loops have more difficult requirements so the following loop description and design criteria will be directed towards their concepts. Accelerometer loops are somewhat simpler but with wider bandwidth.

The gyro pick-offs are amplified, demodulated from their 54 KHz carrier, and the resultant is further amplified with frequency compensation. This compensation provides appropriate characteristics when the loop is closed through the gyro torquer. When the output of the compensation amplifier crosses a threshold, the duty cycle of a switched, constant-current supply is modified proportionately to change the gyro torquing level. This closed loop system is designed to be of a wide bandwidth within the capability of the gyroscope (approximately 80 Hz), and thus provides an accurate representation of vehicle angular rates during normal vehicle vibration. Dynamic errors which might occur during such vibration may then be compensated in the computer.

Designed in this manner (fixed-frequency square wave, duty-cycle modulated), the loop design is linear and well-behaved. An excellent incremental angle resolution of 0.5 arc seconds is achieved. Furthermore, loop compensation design is much simpler than for nonlinear systems. High noise methods such as lead

networks and cross-coupled loops can be avoided in the stabilization of gyro nutation and for the elimination of spin-frequency pick-off noise.

The switch which injects a constant current of alternating polarity into the gyro torquer is carefully designed to achieve exactly equal current in each direction. Imbalance of current leads to an equivalent gyro drift which is proportional to the maximum current supplied. To further decrease the electronics contribution to gyro drift, a mode change is incorporated which increases the current by a factor of 8 at high vehicle angular rates. Thus, during normal flight, the dynamic range of gyro torquing (the ratio of maximum vehicle rate to maximum allowable sensor rate error) is reduced for improved performance.

Temperature Sensitivity Correction

The gyro and rebalance electronics parameters are designed to have low sensitivity to operating temperature. There are limits to how insensitive these devices can be made, however. The residual coefficients are sufficiently stable with time so that the net system error budget can be achieved either with

- monitoring of component operating temperature, with computer corrections applied using factory-calibrated coefficients, or
- rapid component warmup and temperature control.

The advantages of the calibration method are:

- system power consumption is reduced
- component operating temperature is lower, resulting in improved reliability.

Additional benefits derived from avoiding a large thermal transient at turn-on are: 1) Electronics failures are often induced by the stresses associated with large thermal gradients, so net reliability is further improved over straight parts-count considerations; 2) A thermal, and thus instrument performance transient during ground alignment is eliminated. Such a transient can seriously contaminate gyrocompassing if not controlled. The instrument/electronic thermal design becomes very critical in temperature-controlled systems so that transients are completed soon enough to achieve alignment in the required 10 minutes.

Increased calibration costs result with this method, however, since instrument/electronic constants must be derived at a number

of temperatures instead of at a single point. Test equipment complexity, test time, and the number of testers needed for significant production rates are all increased.

The final tradeoff of whether or not to temperature-control instruments is left until the final production equipment design. System design is described for a compensated implementation.

Inertial Instrument/Computer Interface

The interface between the inertial instruments, the gyros and accelerometers, and the digital computer is shown in the block diagram of figure 2-4. Four of the inputs are the duty-cycle modulated squarewaves from the gyro and accelerometer digital rebalance loops. An indication of high rate mode is also required to change pulse weighting.

The conversion of duty-cycle modulated square-waves to a parallel digital word for entry into the computer is performed by up-down counters. While gyro or accelerometer torquer current is positive, the count in a register increments at some fixed clock rate. When torquer current switches negative, the register count decrements. The net counter value over one digital torquing interval (approximately 500 microseconds for gyros, 250 microseconds for accelerometers) is representative of the angular change of the vehicle about that axis during the interval for gyros, and velocity change for accelerometers. No unusual design techniques are needed for this function since clock rates of approximately 400 kHz can be employed. The main constraint is that the digital rebalance duty-cycle transition occurs only at one of the counter clock pulses so that no information is lost.

Temperature sensors are installed at the instruments for computed compensations. These sensors are platinum resistance elements put into a bridge circuit, the outputs of which are dc voltages proportional to temperature. Thus a 10-bit analog-to-digital converter is needed to develop the digital words for application to the computer data bus.

Since the digital rebalance circuits have their own sensitivity to temperature, gradients between the gyro temperature sensor and the thermally sensitive electronic components with, for example, different cooling air flows must also be considered. Adding a temperature sensor to the electronics implies that instruments and electronics are calibrated at the factory separately. This not only increases cost, but also may be impractical due to the accuracy requirements. Therefore, sensitive portions of rebalance electronics will be closely packaged with their corresponding instruments to assure a common thermal environment, and then will be calibrated together.

Digital Computer Design

A specific digital computer was not selected for the production redundant strapdown INS. There are two reasons for this decision.

- Digital computer technology is evolving so rapidly that lowest system cost can be achieved by making such a choice when production system detailed design is started. Cost and reliability estimates for the preliminary design are made based on use of components recently announced in the literature with price extrapolation.
- The primary use of a redundant strapdown INS is in a highly integrated avionics suit. Therefore, computer duty cycle and memory margin are needed for other functions such as flight control and display. A firm computer choice cannot be made until these other functions are delineated.

The redundant strapdown computation requires approximately 8000 words of memory. Throughput requirement is approximately 198 000 instructions per second. Modern digital computers employing features such as microprogrammability, general registers, vectored hardware interrupts, floating point, DMA, etc. are available with more than adequate speed. 32-bit arithmetic, including multiplication, is highly desirable.

A combination ROM/RAM semiconductor memory was chosen for lowest cost. This choice is based on the assumption that few software changes will be needed once the program is de-bugged. This assumption is valid for the LaRC problem as defined since the redundant strapdown INS is basically a sensor. If functions such as steering, flight control, or display are added, these would generally change from aircraft to aircraft. Therefore, higher-cost approaches such as all-RAM, EAROM, EPROM, or core would need to be considered.

The RAM chosen is of the CMOS type. The lower power dissipation of CMOS allows the addition of a small battery which prevents loss of memory (self-test data, modified calibration values, initial position) during power shutdown. A high speed construction technique such as Silicon-on-Sapphire (SOS) is needed to maintain throughput.

A PROM is also included which stores factory-derived instrument coefficients such as bias, scale-factor, g-sensitivity, etc. It is read out by the computer at the start of every flight. It is programmed only at the factory or repair depot following system calibration.

Computer I/O

Input/output format between each redundant strapdown INS computer and external avionics has been assumed to be in a serial format commonly used by commercial aircraft, ARINC-575. This format is clearly subject to change in future avionics. The low bit-rate (approximately 10 kHz) is quite marginal for modern-day, digital avionics. I/O cost, however, was felt to be representative. A failure output discrete is also planned, in addition to the serial data, to inform external equipment and failure annunciators of channel failure condition.

The internal I/O consists primarily of computer-to-computer data transfer. During normal operation the data to be transferred between computers is relatively light, consisting basically of corrected instrument measurement, 6 words at a rate of 128 times per second. Initialization modes are provided to correct one potentially erroneous computer with a known good one following a pre-flight channel replacement and following some instrument failures. A transfer of about 75 words of the variable-data memory would then be required.

Data transfer is shown in figure 2-4 as a read-only function from the RAM. This assures that failure of one of the three other INM computers cannot cause destruction of RAM data. Since instruction storage is in unmodifiable ROM, the possibility of multiple-channel instruction-sequencing failure modes is precluded.

Serial data transfer between channels is preferred due to the reduced connector/wiring requirements. Data transfer rates must be high enough to achieve the above initialization timing. Bit rates of 1 to 2 MHz are practical with present technology.

Interrupt Synchronization

The software in each computer is driven by an external interrupt occurring once for each fast cycle (128 per second). Since gyro and accelerometer data are transferred between computers and time-coherence of samples is required, each computer must start its fast cycle at the same time. Circuitry is needed to lock the four interrupt pulse generators together. In addition, the circuit design must be protected so that failure of circuitry in one interrupt generator does not cause failure in any other unit's interrupt and deactivate its computer.

Power Supply

The INM power supply design is conventional, based primarily on use of a converter-regulator and switching regulators for high power-utilization efficiency. Primary power is assumed to be 115v, 400 Hz from one of the aircraft generator busses.

One relatively high-voltage supply (80 volts) is needed to generate the high temporary currents needed when gyro rebalance loops switch into the high rate mode.

Software

The software organization for the four-computer system is shown in figure 2-6. Gyro and accelerometer data are requested via the I/O. Static and dynamic compensation are then applied as follows:

Accelerometer Compensation

- a. Scale Factor
- b. Axis alignment
- c. Bias

Gyro Compensation

- a. Scale factor (normal/high rate)
- b. Torquer axis transformation
- c. Inertial compensation
- d. Spin axis alignment
- e. G-Sensitive drift
- f. Bias

Following compensation and transformation from skewed instrument coordinates to aircraft body coordinates, the corrected gyro and accelerometer data are available for use by other channel computers. Note that each computer compensates only one gyro. Thus, the selected redundant configuration has a lower computer throughput requirement than a nonredundant (2-gyro) strapdown system. The inertia compensation must be performed at high rates to be effective so is very significant in duty cycle calculations.

The FDI equations accept data from the four (or three during failure modes) gyros and up to 8 accelerometer axes for failure detection, isolation, and system reconfiguration. The selected instrument axis orientation is shown in figure 2-7. Spin axes S_i are configured normal to faces of one-half of an octahedron, represented by the pyramid constructed from equilateral triangles. Gyro torquer axes and accelerometer input axes, x_i , y_i , are also shown.

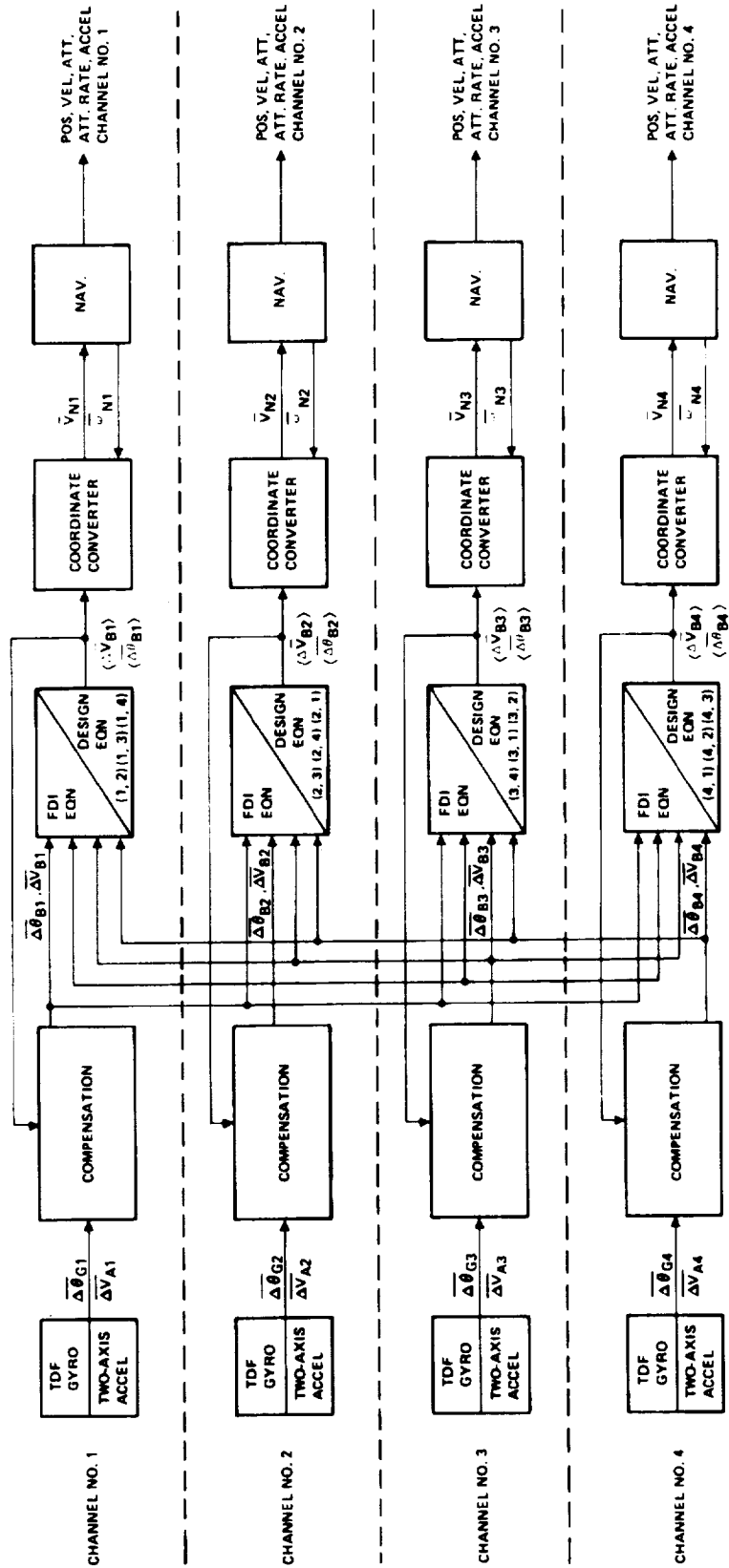
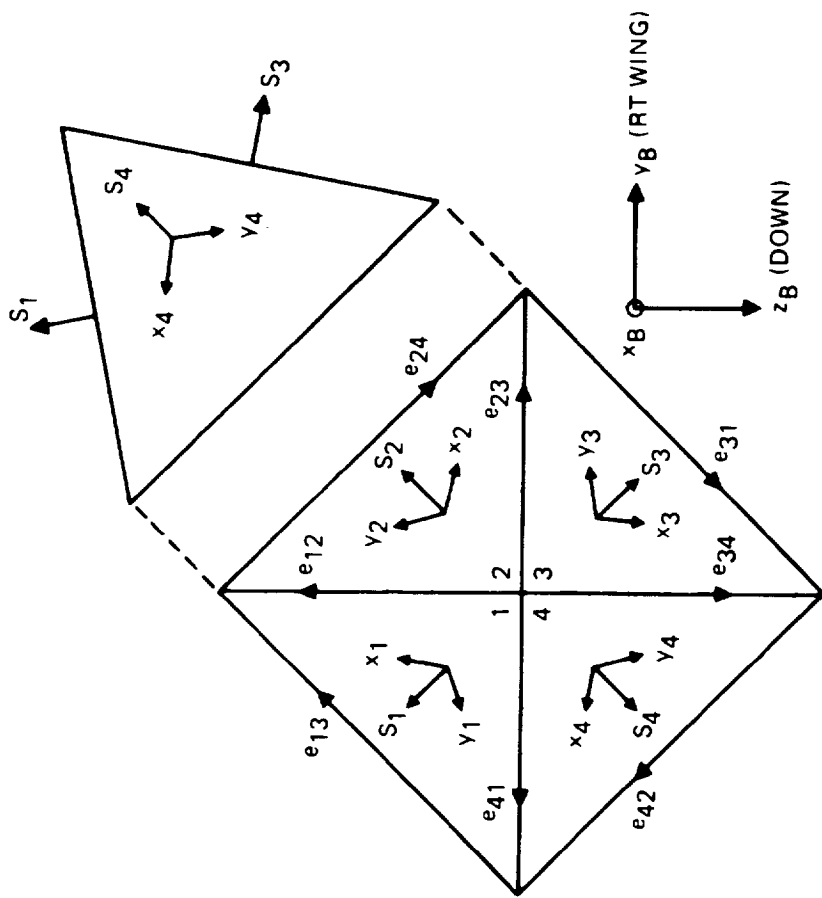


Figure 2-6. Four-Channel Software Mechanization



EDGE TESTS

$$T_{ij} = \text{FILTERED} (\bar{\omega}_i - \bar{\omega}_j) \cdot \hat{e}_{ij}$$

$$i, j = \{1, 2, 3, 4; i < j\}$$

FAILURE TESTS

$$F_{ij} = \{ |T_{ij}| > \delta\theta \}$$

GYRO FAILURE LOGIC

(4 - GYRO CASE)

- G₁ = F₁₂ F₁₃ + F₁₂ F₁₄ + F₁₃ F₁₄
- G₂ = F₁₂ F₂₃ + F₁₂ F₂₄ + F₂₃ F₂₄
- G₃ = F₁₃ F₂₃ + F₁₃ F₃₄ + F₂₃ F₃₄
- G₄ = F₁₄ F₂₄ + F₁₄ F₃₄ + F₂₄ F₃₄

(3 GYRO - CASE)

G ₁ FAILED	G ₂ FAILED	G ₃ FAILED	G ₄ FAILED
G ₂ = F ₂₃ F ₂₄	G ₁ = F ₁₃ F ₁₄	G ₁ = F ₁₂ F ₁₄	G ₁ = F ₁₂ F ₁₃
G ₃ = F ₂₃ F ₃₄	G ₃ = F ₁₃ F ₃₄	G ₂ = F ₁₂ F ₂₄	G ₂ = F ₁₂ F ₂₃
G ₄ = F ₂₄ F ₃₄	G ₄ = F ₁₄ F ₃₄	G ₄ = F ₁₄ F ₂₄	G ₃ = F ₁₃ F ₂₃

SEMI-OCTAHEDRAL GYRO AXIS ORIENTATION

Figure 2-7. Gyro Parity Equations, Semi Octahedral Gyro Spin Axis Orientation

Parity equations are derived by comparing one gyro's rate measurement with another's along a direction e_{ij} parallel to the intersection of the two gyro measurement planes. Since the gyro measurement planes are on the faces of the octahedron, the edges of the octahedron are these intersections. Thus, two gyro measurements of the same component of vehicle angular rate can be directly compared to detect errors.

Six unique parity equations T_{ij} are available as shown in figure 2-7. If two or more equations involving a specific gyro indicate an error condition, that gyro is classified as failed. After one gyro failure, only three equations remain. The "two-or-more" criterion still applies, however. A more sophisticated detection/isolation method is presently under consideration and will be described in Paragraph 5.3.

Processing of a parity equation involves an imperfect integration. For very small nonfailure gyro drift errors, the output remains below the error detection threshold. The threshold may thus be kept constant as a function of time. For large drift errors, the output is essentially an angle. Thus, angular transients to the flight control system during failure modes can be kept below a desired level.

Design equations form a least-squares solution of the angular rates from two gyros (format is similar for accelerometers) to derive three orthogonal axes of data from four measurement axes. The logic for selection of instruments to be used in the design equations is shown in figure 2-6. When all four channels are operating normally, channel 1 design equations use instrument data from channels 1 and 2. If channel 2 is determined to be in error by parity equations, instrument data from channels 1 and 3 are used, etc.

The resultant rates and acceleration data are then processed by the coordinate converter to determine aircraft body angles relative to the inertial navigation coordinate system and to convert body accelerations into that system. A partial 5th order quaternion integration algorithm is employed.

The basic inertial navigation equations are of a relatively conventional form, and include provisions for rapid ground alignment with optimally-derived, time-varying coefficients. Inertial angular rates are derived based on alignment equations on the ground, or vehicle position and velocity during flight to correct the body-to-computer axis quaternions.

The computation rates for the various software modules will be as follows:

Gyro compensation	128/sec
Accelerometer compensation	128/sec
Parity equations	128/sec
Design equations	64/sec
Quaternion integration	64/sec
Coordinate transformation	64/sec
Outputs	32/sec
Navigation	8/sec
Alignment	8/sec

Table 2-1 lists the major software FDI features recommended as a result of the study. Table 2-2 gives a conservative estimate of word-count and duty cycle requirements for the baseline computer. Various means of reducing computation time will be investigated during system final design. They include reduction of compensation and quaternion integration iteration rates by a factor of two, and use of special microprogrammed instructions.

TABLE 2-1. FAILURE DETECTION, ISOLATION, SWITCHING CONCLUSIONS

- PROCESS EACH PARITY EQUATION WITH SIMPLE LOW-PASS FILTER
- USE TABLE LOOK-UP OR LOGIC EQUATIONS FOR FAULT ISOLATION
- CONSIDER ADDITION OF PROCESSED PARITY EQUATIONS FOR TIGHTER DETECTION LEVELS
- EQUATIONS AND/OR SWITCHING LEVELS SHOULD BE MODIFIED BETWEEN GROUND ALIGNMENT, NORMAL AND MANEUVERING FLIGHT SINCE ERROR MODEL CHANGES
- CONTINUE MONITORING SOFT-FAILED GYRO.
- CONSIDER USE OF SOFT-FAILED GYRO FOR THIRD FAIL-SAFE OR TO RESOLVE 3-GYRO ISOLATION AMBIGUITY
- TREAT ACCELEROMETER AND GYROS AS BEING INDEPENDENT

TABLE 2-1. FAILURE DETECTION, ISOLATION, SWITCHING CONCLUSIONS (Cont)

- IF ONE AXIS OF A CHANNEL FAILS, SWITCH OUT BOTH AXES
- CONSIDER REINITIALIZATION FOLLOWING ANY SWITCHING
- CONSIDER COMPARISON BETWEEN OUTPUT TABLES IF SOFTWARE, AND REINITIALIZATION IF SIGNIFICANT ERROR IS DETECTED. ACCOUNTS FOR COMPUTER TRANSIENT ERRORS BETWEEN INSTRUMENT COMPARISONS AND OUTPUT FORMULATION
- USE RADIO AID UPDATES TO DETECT SMALL ERRORS OR TO RESOLVE 3-GYRO ISOLATION AMBIGUITY

TABLE 2-2. COMPUTER RESOURCE ESTIMATES

TASK	DUTY CYCLE (%)	MEMORY	RATE (Hz)
COMPENSATION - FAST	15.2	500	128
COMPENSATION - SLOW	0.3	200	2
FDI - DESIGN EQN	16.6	700	128
COORDINATE CONVERTER	15.9	750	64
NAVIGATION - FAST	2.1	650	8
NAVIGATION - SLOW	2.1	300	2
ALIGNMENT GAIN SELECT	0.1	100	1
MODE CONTROLLER	0.7	600	1
BARO-ALTITUDE	0.1	150	2
EXECUTIVE-SCHEDULER	4.8	250	128
OUTPUT FORMATTER	2.1	200	32
DATA BASE - SUBROUTINES		2000	
TOTALS	60.0	6400	

Accuracy/Input-Output

The redundant strapdown INS will have the following output accuracy:

Attitude rate	0.05°/sec, rms, per axis
Attitude	0.1°, rms, per axis
Heading, True	0.2°, rms, 0.5 hr. flight
Position Rate	1.03 m/sec (2 knots)(95%) radial with external updates every 5 sec., update noise of 122m rms, zero correlation time, 61m, rms, 20 sec correlation time per axis, 30 minutes flight duration
Acceleration	0.003m/sec ²

This accuracy applies with either 0, 1, or 2 hardware failures, and through the required operational environment. It is assumed that aircraft installation errors are not included, aircraft parking coordinates have been entered perfectly and a full gyro-compassing alignment has been completed in 10 minutes after turn-on, at a latitude of 45° prior to first aircraft motion.

The system error expected per channel is illustrated in figures 2-8 and 2-9. The simulations are based on a realistic error budget and show 50 percent probability errors with and without radio aid updating. Aided performance is essentially 1 m/sec (95%) as required.

Outputs provided by the redundant strapdown INS are as follows:

Category	Quantity	Resolution	Range	Bits	Cycle Time
Attitude	Pitch (Elevation)	$2\pi/2^{15}$	$\pm\pi/2^*$	14	0.031 sec
	Roll	$2\pi/2^{15}$	$\pm\pi$	15	0.031 sec
	Heading, true	$2\pi/2^{15}$	$\pm\pi$	15	0.031 sec
Attitude Rate	Pitch rate	0.05°/sec	± 4 rad/sec	14	0.031 sec
	Roll rate	0.05°/sec	± 4 rad/sec	14	0.031 sec
	Yaw rate	0.05°/sec	± 4 rad/sec	14	0.031 sec

STRAPDOWN, RADIO UPDATED: TRAJECTORY = TRAJ002 (HOME LAT = 45 DEG)
LANGLEY 005, RADIO 001, UPDATE 004, 20 MONTE CARLOS

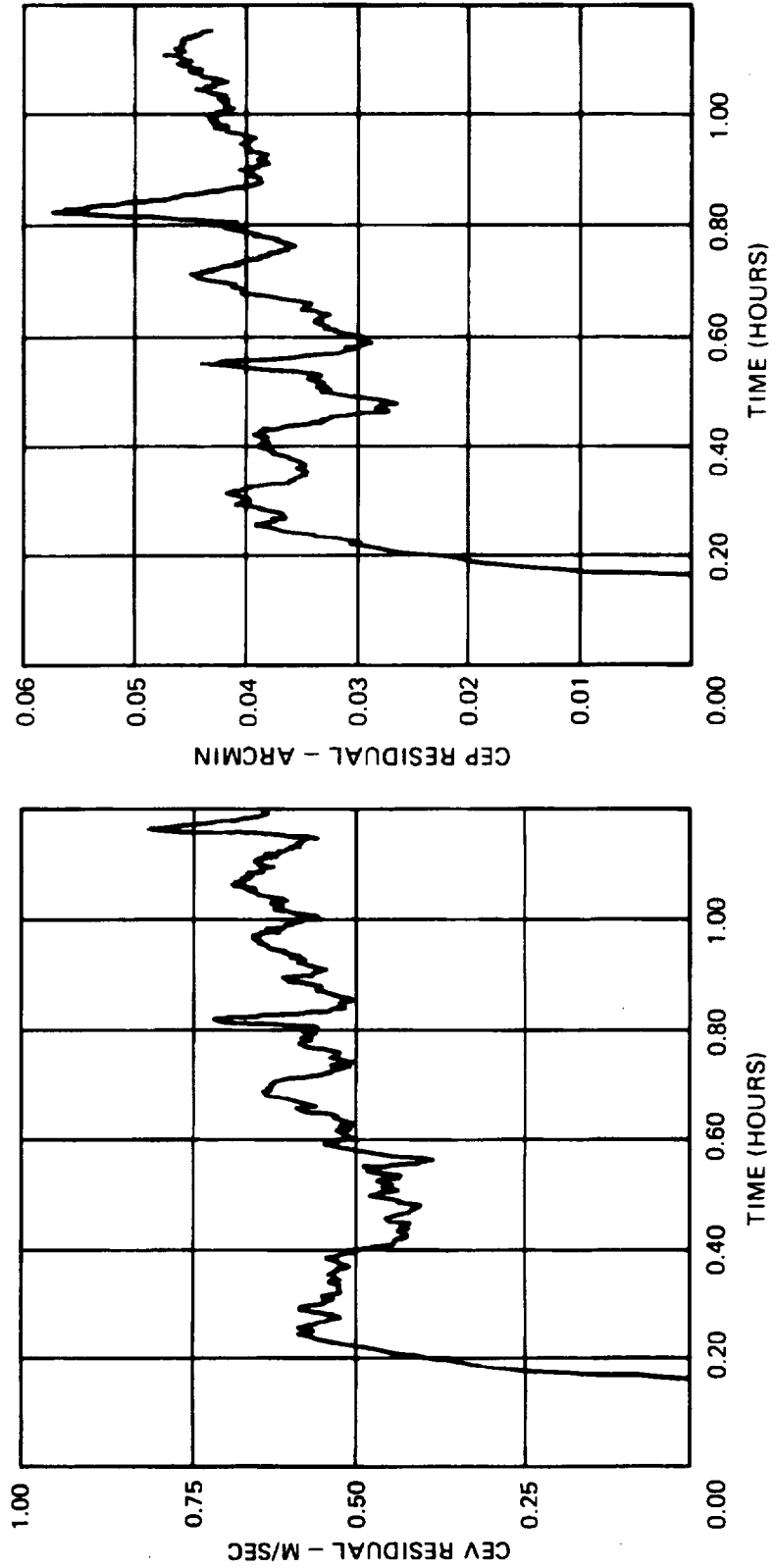


Figure 2-8. Simulation Results of 50 Percentile Velocity and Position Error with Radio Updates

STRAPDOWN FREE INERTIAL: TRAJECTORY = TRAJ002 (HOME LAT = 45 DEG)
LANGLEY ERROR BUDGET 005
20 MONTE CARLOS

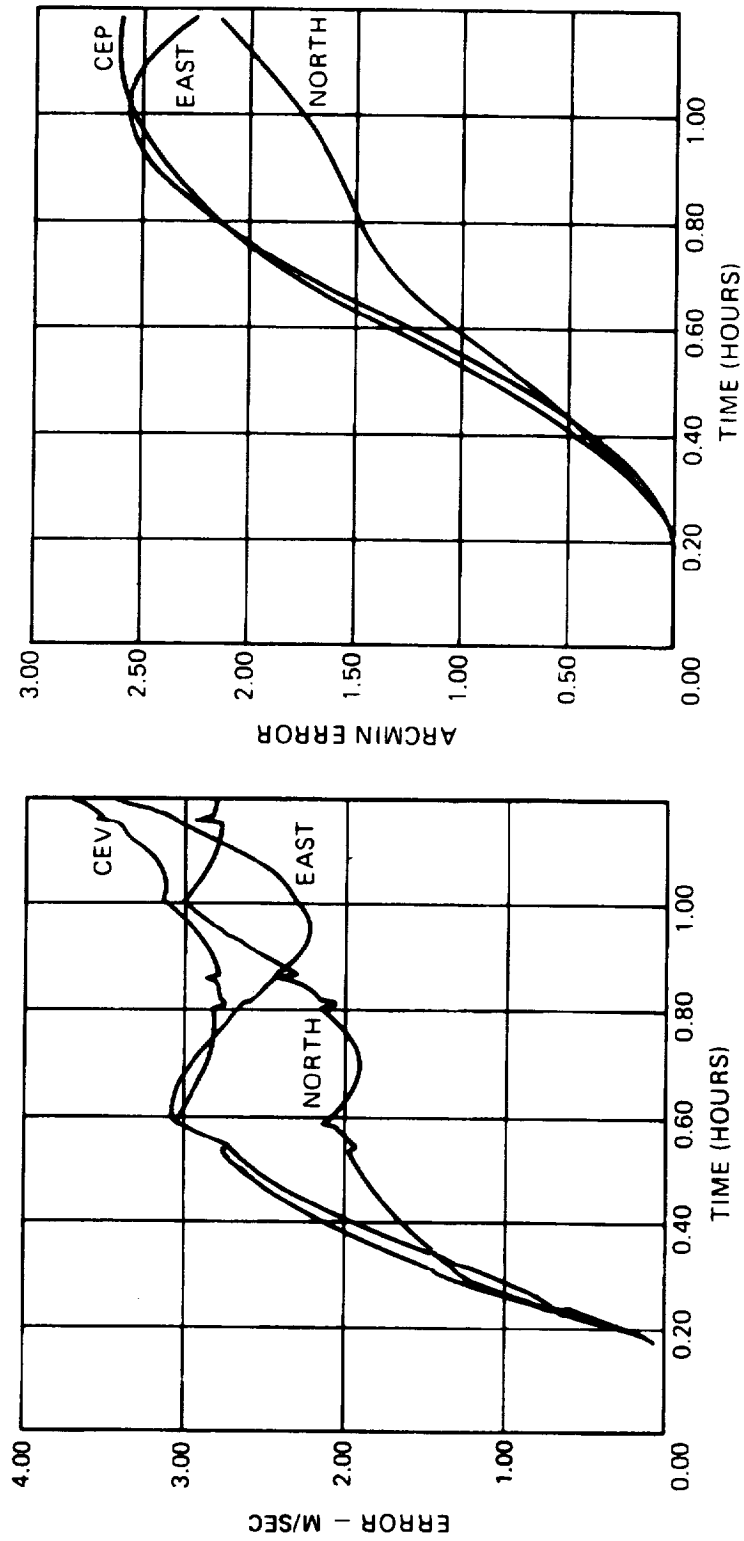


Figure 2-9. Simulation Results of 1 σ and 50% Velocity and Position Errors, Free Inertial

Category	Quantity	Resolution	Range	Bits	Cycle Time
Body** Accel.	Longitudinal Accel.	0.003 m/ sec ²	±10 g	11	0.031 sec
	Lateral Accel.	0.003 m/ sec ²	±10 g	11	0.031 sec
	Vertical Accel. (Body)	0.003 m/ sec ²	±10 g	11	0.031 sec
Nav Outputs	North Velocity	0.03 m/ sec	±1686 m/sec	16	0.125 sec
	East Velocity	0.03 m/ sec	±1686 m/sec	16	0.125 sec
	Vertical Velocity (Earth)	0.03 m/ sec	±1686 m/sec	16	0.125 sec
	Latitude	$2\pi/2^{19}$	± $\pi/2^*$	18	0.125 sec
	Longitude	$2\pi/2^{19}$	± π	19	0.125 sec
	Altitude	0.3 m	-305m to 18.3 km	16	0.125 sec
<p>*These outputs are generally scaled at ±π.</p> <p>**Installation is assumed to be at the aircraft center of gravity, so lever-arm accelerations are not included.</p>					

An output line indicating failure of one or more system components/subsystems will be provided from each redundant computer.

Input requirements consist of altitude from an air-data system and update data, for example, Kalman filter updates based on VOR/DME or OMEGA data. Baseline update quantities are 2 velocities and 2 position, (4 total) at a rate of one full update at least every 30 seconds. Additional inputs, TBD, will be received from a display.

Packaging Description

The complete redundant strapdown INS consists of 4 identical inertial navigation modules plugged into a common mount. One of

the inertial navigation modules is illustrated in figures 2-10. It consists of the chassis, power supply, electronics cards, and an instrument block, and has a weight of approximately 5.9 Kg. Cooling is assumed to be direct impingement of cabin air on the components, so no heat exchanger is required.

The instrument block is attached to the chassis by means of a lever mechanism. When the chassis is plugged into the common mount, a plunger pushes on the engagement lever causing the block to move so the alignment feet can engage a central alignment block in the mount. This mechanism provides for angular alignment accuracy of 10-20 arc seconds between the four instrument blocks of the entire system. Each instrument block consists of one G-6 Gyro, two A-1000 Accelerometers, and an electronics card, as shown in figure 2-11.

The mount chassis shown in figure 2-10 forms a common shell for the four inertial navigation modules. The mount chassis weight is approximately 4 Kg for a total installed weight of under 27.7 Kg. Module orientations are rotated by 90 degrees within the mount chassis. This allows all four plug-in inertial navigation modules to be identical yet achieve the desired gyro and accelerometer axis orientations. After an inertial navigation module is inserted into a slot, a lever on the actuator assembly is pushed forward, causing the instrument block to be pressed onto a common alignment block in the rear of the mount.

The unit cam-lock handles are of a type used on commercial avionics. The bottom of the handle engages a hook on the mount (figure 2-12), and when the lever in the handle is pushed in, the chassis mates with the connector and the unit is locked in place.

Figure 2-13 shows some details of the actuator assembly and the alignment block.

Environmental/Aircraft Characteristics

General environmental and aircraft specifications are derived from the present commercial inertial specifications, ARINC 561, and the LaRC SOW. To make the redundant strapdown INS more broadly applicable, civil or general aviation performance limits are assumed to apply. The required and desired aircraft operational performance limits are:

	VTOL	Civil or General Aviation
Angular Rates	4 rad/sec	4 rad/sec
Angular Acceleration	50 rad/sec ²	50 rad/sec ²
Linear Accel (maneuver)	±3 g	±3 g

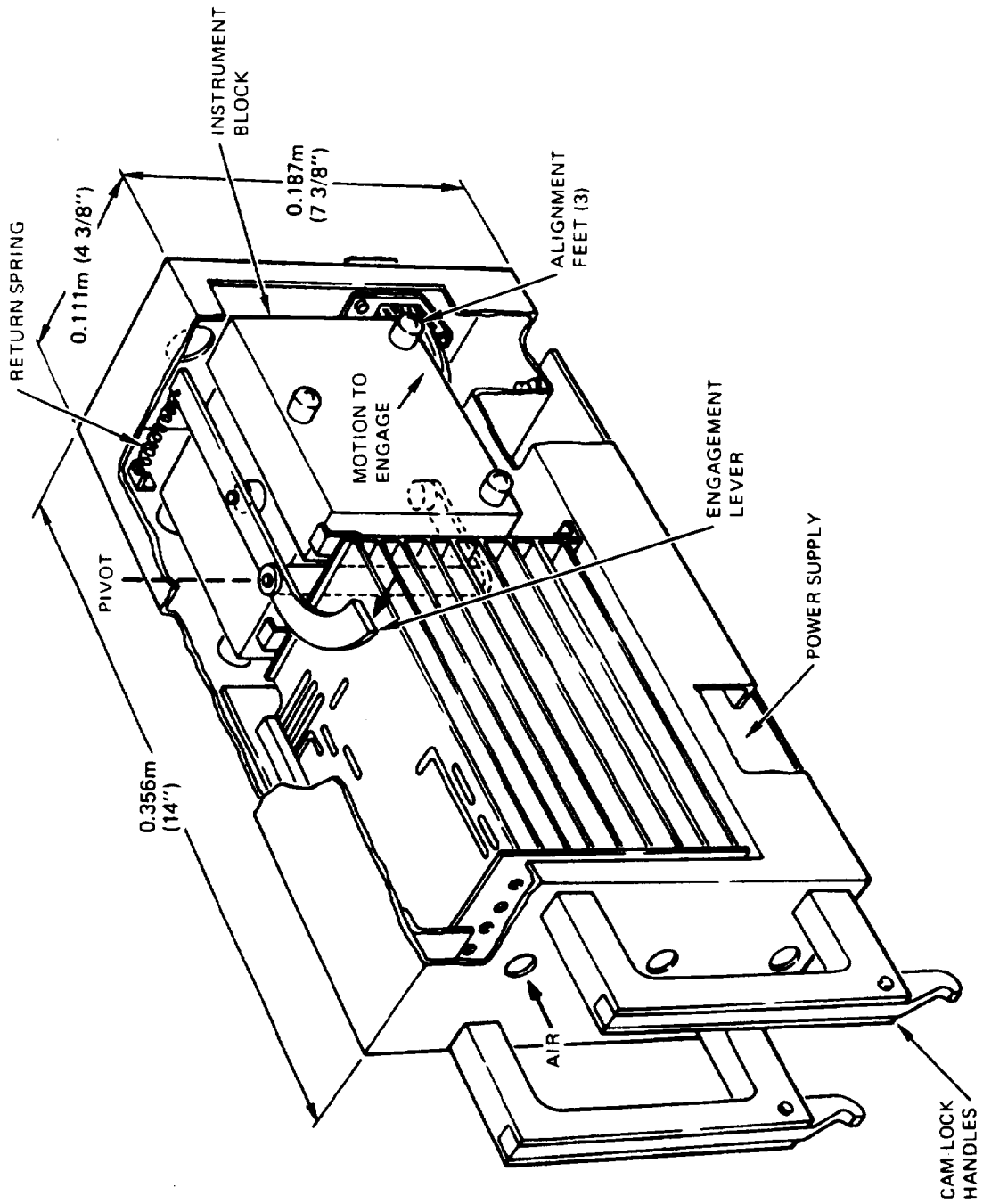


Figure 2-10. One Channel of the Redundant Strapdown INS

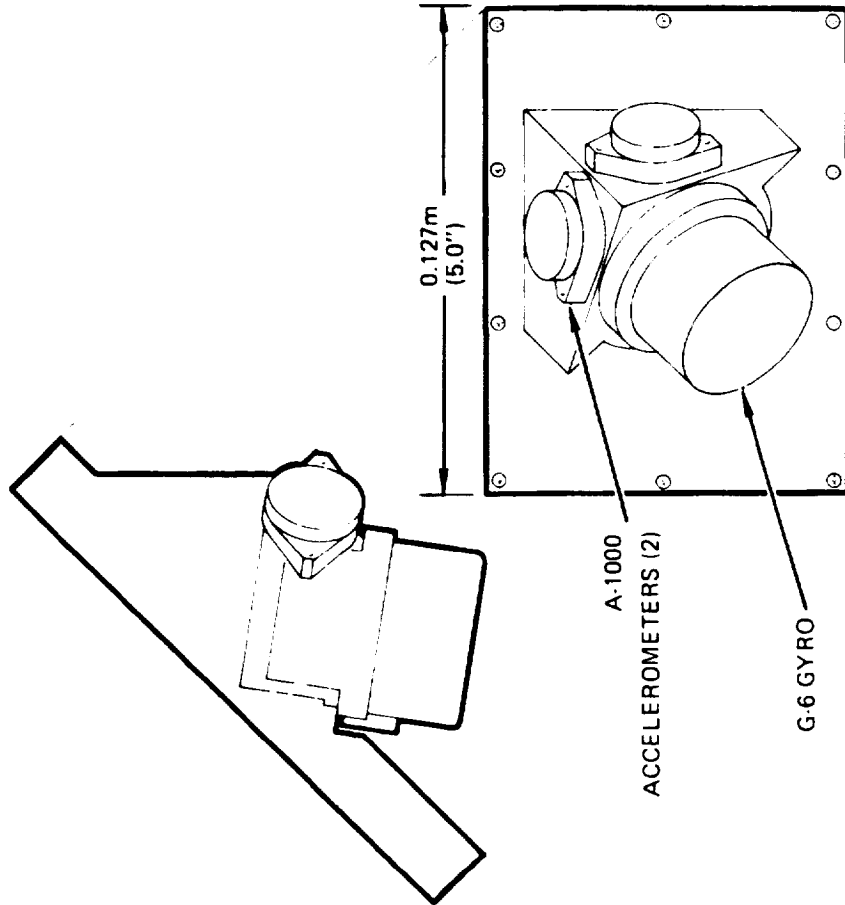
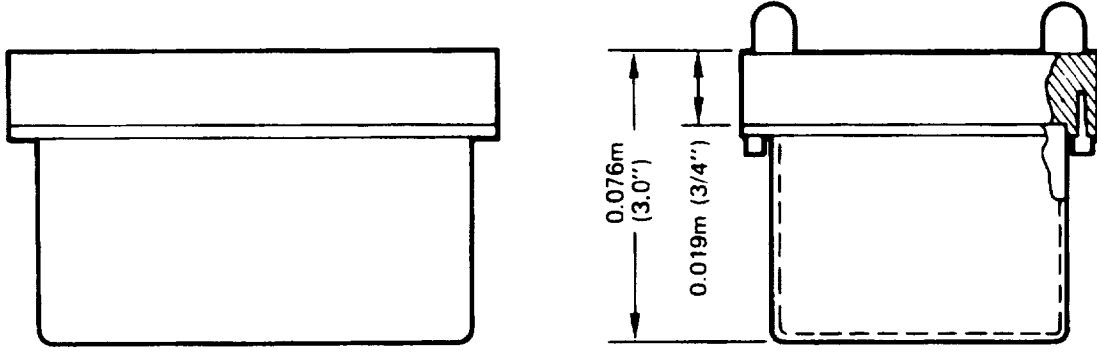


Figure 2-11. Instrument Block

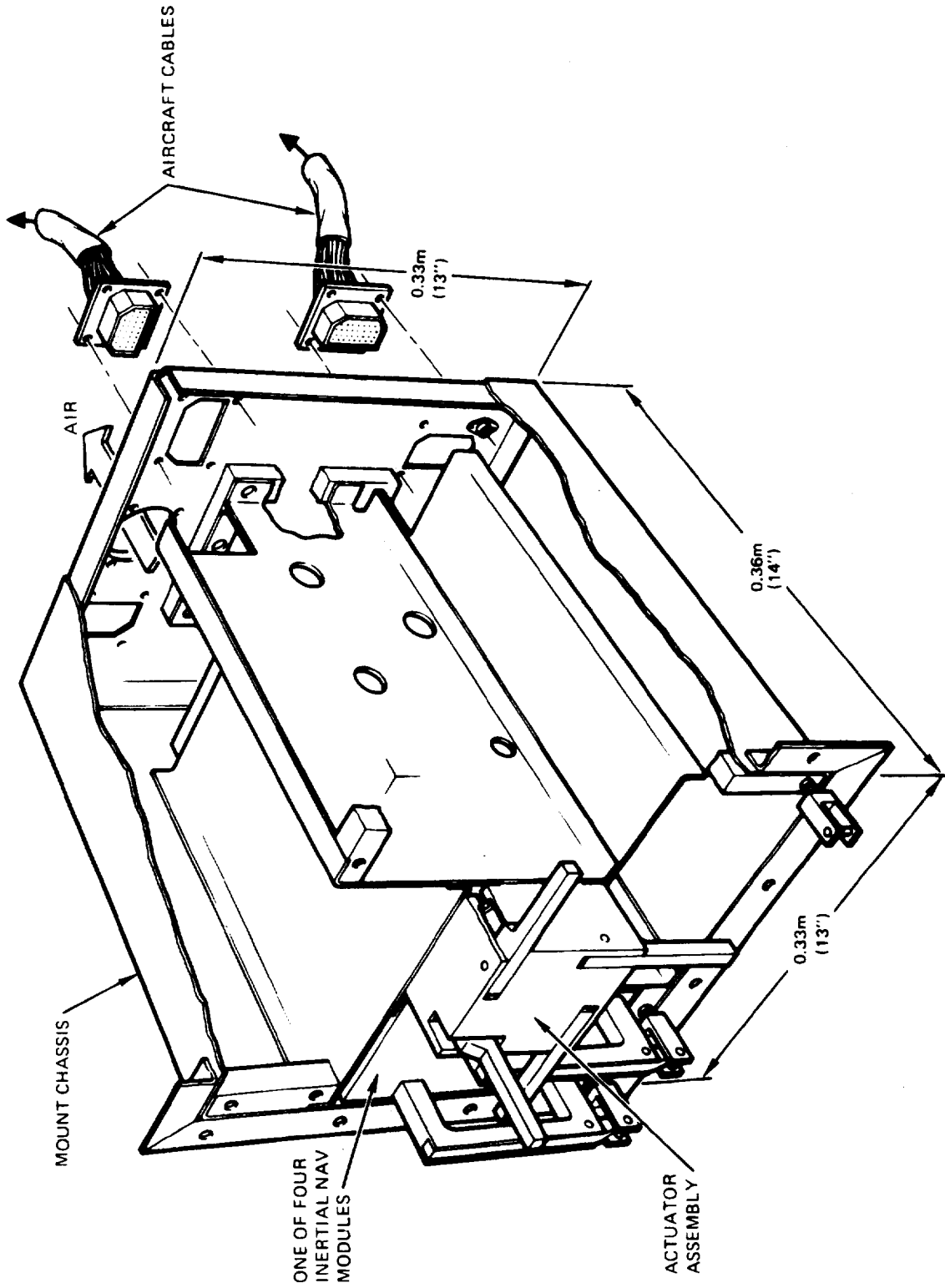


Figure 2-12. Redundant Strapdown INS Installation

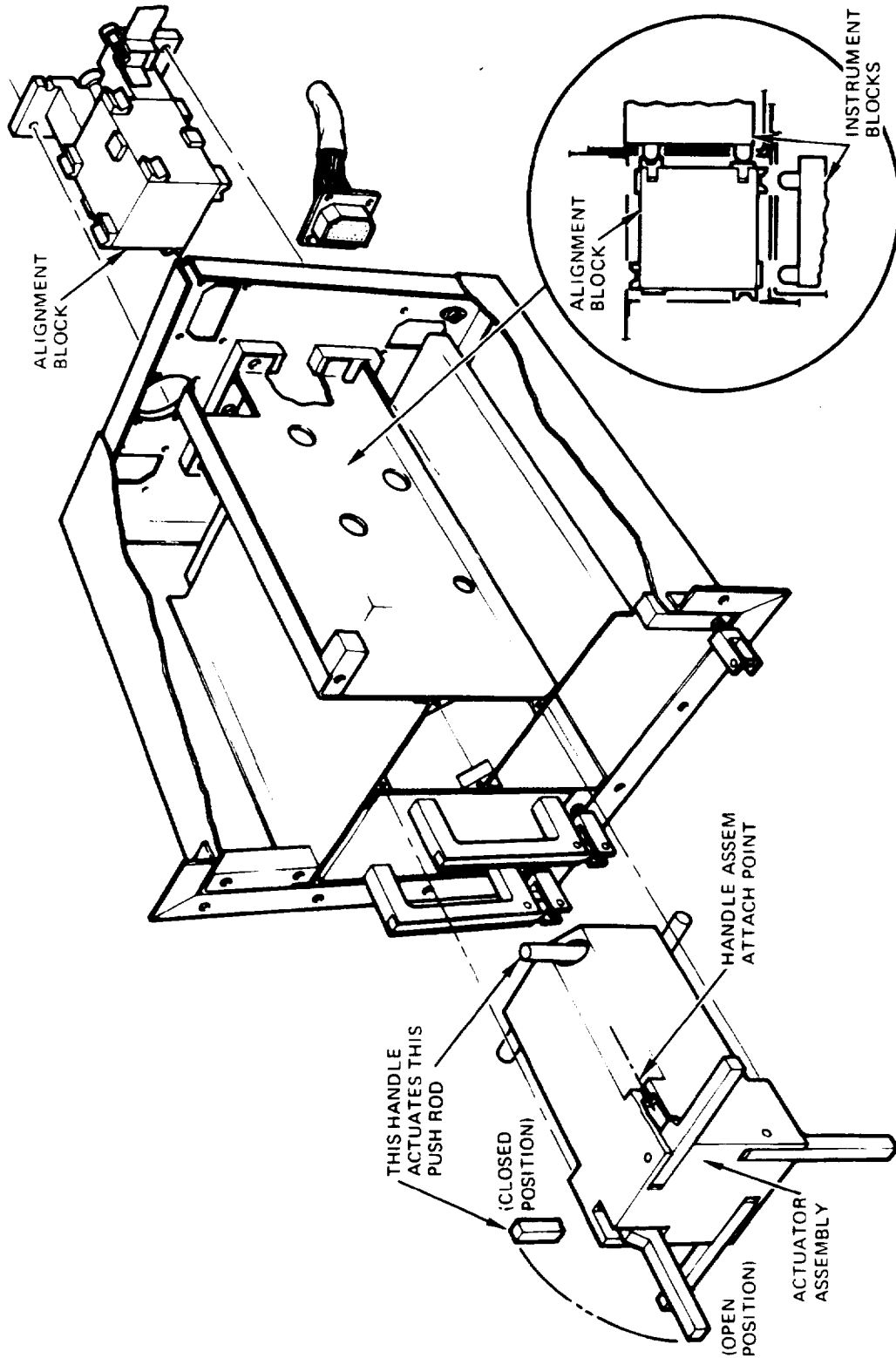


Figure 2-13. Redundant Strapdown INS Mount Details

	VTOL	Civil or General Aviation
Velocity (max)	154 m/sec	1029 m/sec (ARINC 561)
Altitude	3,048 m	18,288 m (ARINC 561)
Aircraft tilt (parked)	±5°	±5°
Range of operation (Lat)	±70°	Worldwide
Normal ambient temperature:		30°C (ARINC 561)
Maximum continuous operation:		50°C
Short-term (30 min) overtemp:		71°C
Low operating temp:		-15°C
Vibration (flight)		0.762 mm 10-55 Hz 5 g 55-500 Hz

It is assumed that ARINC 404 cooling air will be available with a flow of 13.6 kg/hour/100 watts of dissipation, but that the ARINC 404 form factor and cooling air attachment methods are not applicable. ARINC 600 will require review when available.

Reliability

The reliability of a single channel of the redundant strapdown INS has been calculated to be 4100 hours MTBF. This calculation is based on MIL-HDBK-217B failure rates, an "Airborne Inhabited" application with part ambient temperatures stabilized at a maximum of 70°C. The detailed failure rate breakdown is given in Appendix G.

This reliability may be expected for a production system in commercial airline use at some time after introduction into service. Reliability is expected to grow with time from some initial value as marginal components and circuits are weeded out of the system. An example of this reliability growth is shown in figure 2-14 for a first generation gimballed commercial inertial system. Approximately three years is needed to achieve mature reliability. One channel of the redundant strapdown involves considerably less equipment than a present ARINC system (no gimbals, one less gyro, one less accelerometer, smaller power supplies, more modern computer, considerably less I/O) so 4000 hours MTBF appears a reasonable prediction for mature channel reliability.

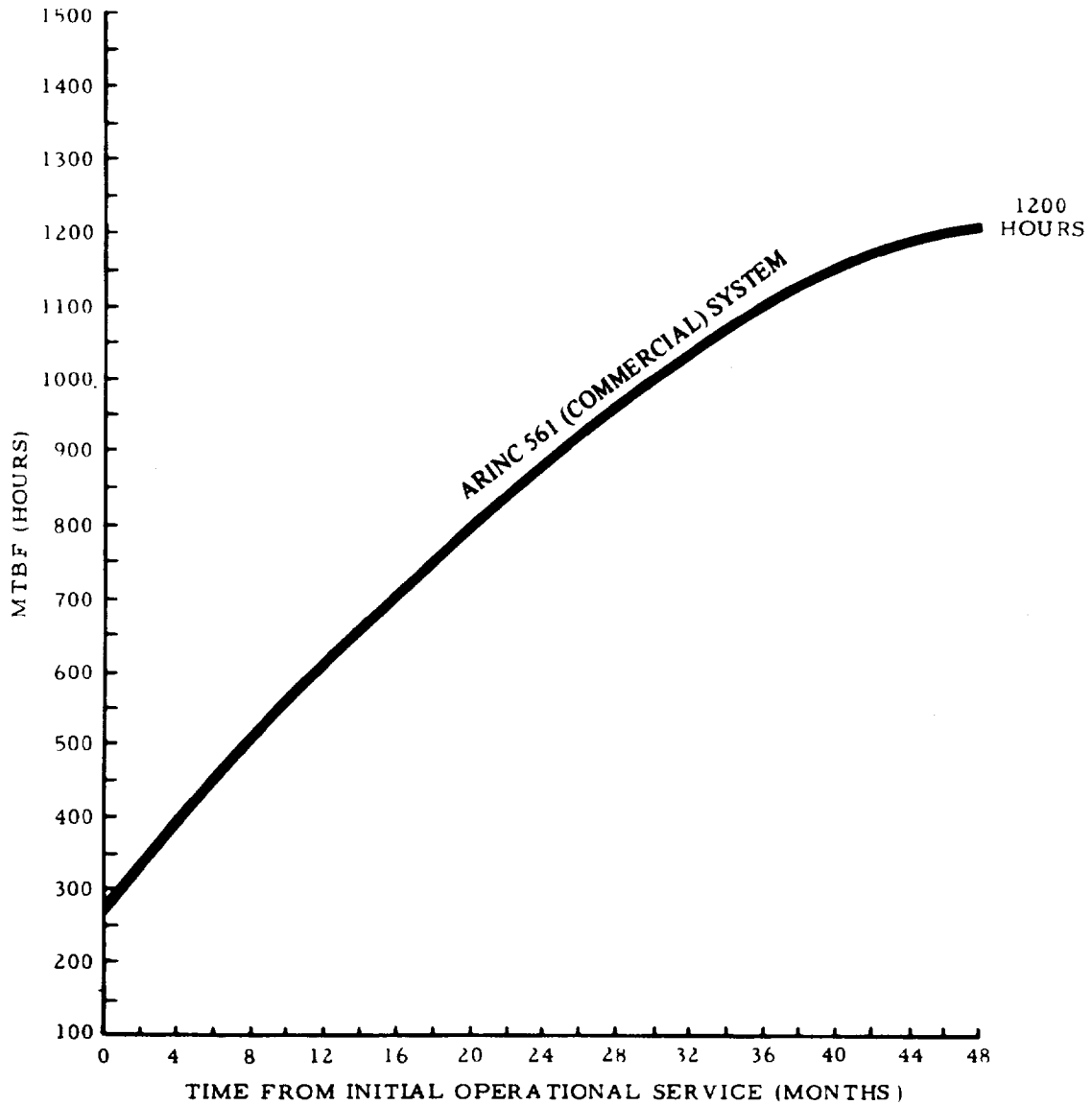


Figure 2-14. INS Reliability Growth Curve

The system failure probabilities are given in figure 2-15 for a channel MTBF of 2000 or 4000 hours, flight durations of 0.5, 1 and 8 hours. In addition, reliability is also a function of the allowable errors, improving significantly for outputs to the flight control system where it is needed for flight safety. Instrument noise, probability of two simultaneous failures, and information limitations of the 4 and 3 TDF gyro array were considered in these calculations.

Note that for flight durations of 8 hours, reliability is significantly degraded. Reliability can be improved for these long missions, particularly for flight control outputs, with a more flexible I/O structure between instruments and computers so any computer can read any instrument without other computers working. Probability of flight control reference failure is reduced by a factor of 40. For the short flight-time VTOL application, the lower-flexibility, lower-cost configuration is adequate.

Maintainability

Particular attention was focused on airline maintainability considerations during the preliminary system design. For example, the total cost of spares needed by the airlines to support the equipment during operational use is considerably reduced by having the system consist of four identical modules.

Since the redundant strapdown INS is designed to provide signals to the flight control system, it must be considered a dispatch critical item. This means that if any of the four channels indicates a failure, the aircraft will not take off. Thus, removal and replacement time must be minimized in order to limit dispatch delays - a costly action for airlines, particularly in short-haul applications.

The packaging design of the redundant strapdown INS was especially directed toward rapid removal and replacement of a module in the aircraft. Very simple latching mechanisms are used to engage the connector, lock the unit in place, and lock the inertial instruments into precise alignment with each other. Furthermore, this maintenance action can be performed without removing power to the remaining 3 channels so therefore the ground gyrocompassing mode need not be reinitiated, further shortening dispatch delay. Once redundancy management equations are satisfied, the complete fail-op/fail-op system is ready for takeoff.

	CHANNEL MTBF (HR)	FLIGHT			TIME		
		0.5 HR	1.0 HR	8.0 HR	0.5 HR	1.0 HR	8.0 HR
FULL SYSTEM ACCURACY	2000	4.6×10^{-10}	1.8×10^{-9}	1.2×10^{-7}	4.6×10^{-10}	1.8×10^{-9}	1.2×10^{-7}
	4000	1.3×10^{-10}	5.2×10^{-10}	3.3×10^{-8}	1.3×10^{-10}	5.2×10^{-10}	3.3×10^{-8}
OUTPUTS TO FLIGHT CONTRL SYSTEM*	2000	4.7×10^{-11}	3.8×10^{-10}	1.9×10^{-7}	4.7×10^{-11}	3.8×10^{-10}	1.9×10^{-7}
	4000	4.5×10^{-12}	3.6×10^{-11}	1.9×10^{-8}	4.5×10^{-12}	3.6×10^{-11}	1.9×10^{-8}

*ATTITUDE RATES AND ACCELERATIONS IN BODY COORDINATES.

Figure 2-15. Calculated System Failure Probabilities

III. SPECIFICATION OF SYSTEM REQUIREMENTS

The detailed INU design requirements are based first upon the LaRC Statement of Work [1]. Expansions upon these requirements are also provided in the Litton proposal to LaRC [2] and the preliminary study for NASA, CR-132419 [3]. The means utilized to fill in the remainder of design requirements is to use the commercial INS specifications, ARINC 561 and 571 [4] and [5] as guides. Additional material is utilized where appropriate with the source identified.

ARINC 561 formed the basis for introduction of inertial systems into commercial airlines. It was prepared by a committee composed of both INS manufacturers and airlines and thus represents environmental, installation, and design standards accepted by the majority of the commercial avionics community. It also references the other applicable general specifications accepted by the airlines such as for packaging and environmental testing. Some ARINC 561 requirements are not applicable to redundant strapdown INS, and these will be analyzed as required. The input/output and display requirements of the strapdown INS will not be included in this report except in a very general manner.

3.1 Cost Factors

The system cost goal of the redundant strapdown navigator shall be under \$50,000 for initial production quantities of approximately 200 units. The cost data are to be presented in the form of CR-132419 [3], tables 4 and 5, per the LaRC SOW. Amortized design, development and test equipment costs shall be included so that unit cost to an airline is developed. Cost of warranty and training shall not be included at this time.

This system cost goal is a considerable challenge judging from present generation, non-redundant INS costs of \$80K - \$100K per unit, and the conclusion from CR-132419 (page 278) that a best-case 10^{-6} reliability system would cost about \$78K (excluding development and test equipment). The CR-132419 report concluded that only an "advanced strapdown configuration" requiring significant technology advances could meet the goal. Further, fail-op/fail-op capability adds considerably to the amount of redundant hardware needed. In fact, the system reliability requirement is effectively increased from a 10^{-6} failure probability to almost a 10^{-9} failure probability for a 30-minute flight. Best-case INS cost for this reliability is projected to be about \$90K in the CR-132419 report, excluding development, test equipment and tooling.

The redundant strapdown INS is considered to consist of the following elements, as a minimum:

- Four two-degree-of-freedom tuned gimbal gyroscopes.
- Eight single axis accelerometers.
- Capture electronics for each of the above.
- Temperature sensor/control electronics for the above, as needed to meet system accuracy requirements.
- Redundant computers to process data from the instruments to produce required system outputs. For the purpose of preliminary design, four computers will be assumed.
- Redundant instrument-to-computer input/output provisions.
- Redundant computer-to-computer interface provisions.
- Representative system digital input/output channels to tie the redundant strapdown INS to displays and other aircraft avionics.
- Redundant power supplies, clocks, etc. required for system operation.

The design of the redundant computers with associated I/O will be based on representative hardware expected to be available for production go-ahead in the late 1970's. Digital subsystem designs will only be detailed to the extent needed for costing and reliability estimating and will not necessarily reflect the optimum redundancy management approach.

To achieve a clearer understanding of cost vs. system design parameters, trade-off analyses are required in the following categories:

- a. Derive cost as a function of packaging philosophy. The optimum packaging to be employed for all the various elements of the redundant strapdown INS is a function of not only unit cost, but also airline maintenance methods and aircraft dispatch constraints. A broad analysis, including airborne-incurred cost factors such as spares costs and dispatch-delay costs is required.
- b. Determine optimum power supply (including clocks, reference voltages, etc.) configuration (three with switching as described in the Litton proposal [2] vs four unswitched).
- c. Determine the lowest-cost redundancy mechanization which will meet the fail-op/fail-op and system reliability requirements.

A common means of reducing the cost of an item is to increase the production base through sales to a variety of customers. The ARINC 561 INS is a good example. A standardized design allowed application of the system to a variety of customers, commercial and private. This increased the production base and maintained a relatively low price for an item of rather sophisticated avionics. Therefore, the redundant strapdown INS should not be tailored precisely to expected VTOL needs unless the cost benefits are clear.

Present generation INS have a material/labor split of approximately 60%/40%, respectively. Labor costs normally follow a learning curve such as the Northrop 87 curve, and would reduce by approximately 13% if the system quantity is doubled (200 to 400 systems). Material costs savings only benefit if large single buys can be made. Assuming labor cost savings only, a system costing \$50K at quantity 200 will cost \$47K for 400. Therefore, some cost penalties may be allowed in the interest of standardization for an increased production base. One example of this concept is to include a small amount of extra computer memory for wider aircraft altitude, speed, and latitude capability rather than limiting performance to the VTOL envelope.

3.2 Reliability

The redundant strapdown INS shall be a fail-op/fail-op design, such that any two failures of any component or subsystem can be detected, isolated and disconnected without compromising system performance as specified in Paragraph 3.3 of this report.

The probability that more than two failures occur or are detected and disconnected (even if they did not occur), shall be less than 10^{-6} for a 30-minute flight. It is assumed that take-off will not proceed if one or more failures have been detected prior to flight.

Failures are classified as either hard or soft failures. A hard failure is defined as a condition where a subsystem (gyro, accelerometer, computer, power supply) becomes totally incapable of performing its intended function due to a component failure or out-of-tolerance failure mode. A soft failure is defined as a condition where a subsystem loses a portion of its intended function due to a component failure or out-of-tolerance failure mode, resulting in degradation of system output accuracy.

A "failure" of the redundant strapdown INS is defined as the condition where the outputs required in Paragraph 3.4 are not available due to a number of hard failures, or where the accuracy of one or more of the system outputs has degraded to greater than (TBD) times the required rms accuracy.

Completely separate computer I/O channels to other aircraft avionics will be assumed for each computer, with the selection of the proper channel performed by the external equipment, based on redundant strapdown INS self-test indications and external voting logic. All other redundancy management and switching will be self-contained. Any switching circuitry included for redundancy management is also subject to the fail-op/fail-op requirement.

Present generation commercial (e.g., Litton LTN-72) INS are currently achieving an in-service MTBF of about 2000 hours. Therefore meeting considerably better than 10^{-6} probability of complete system failure for the redundant strapdown INS is assured once the fail-op/fail-op design is implemented. Achieving high total part-count MTBF is also highly desirable, however, in order to reduce maintenance costs and minimize dispatch delays. A sound system thermal design is essential to meet this goal. As stated in ARINC 561, "...the rule of thumb on electrical component failures indicates a four-fold increase in failure rates when the normal operating component temperature is increased 30 to 50°C." While calculations performed at Litton using RADC Reliability Notebook failure rates indicate degradation of only about 20-30% for a typical modern inertial system under these thermal conditions, adequate cooling provisions are still essential to good system design.

Aircraft and personnel safety are of primary concern in the design of the failure detection and disconnection mechanizations.

Redundancy management switching due to soft failures shall not cause transients or steps in the output signals. Reconfigured outputs shall transition from the previous to the new value with a time constant long enough to not cause passenger discomfort. System elements removed from output calculations shall still be monitored for both hard and soft failure criteria. In the event of more than two component failures, the soft-failure component may be restored to operation if still available, if aircraft safety is thereby improved. Once a component is rejected for a hard failure it shall not be used for the remainder of the flight.

The concept of redundancy also includes the external effects on proper INS operation. Thus, separate aircraft power circuits must be available for the redundant INS power supplies. This concept could be carried further to the cooling system. However, since the INS can probably be designed to operate for 30 minutes without cooling air, redundant cooling is not required. Triple redundant INS are presently installed side-by-side in the Boeing 747, cooled by the same down-draft blower. While it is also desirable that redundant elements be located in different parts of the aircraft so they are not subject to the same

catastrophic event (e.g., lightning strike, explosion, etc.) it appears impractical to do so with strapdown system components. Substantial accuracy degradation occurs with aircraft flexure. Aircraft designers must locate the strapdown redundant INS away from rotating machinery such as engines or APU's which could shed debris during failure modes and thus simultaneously cause complete redundant strapdown INS failure.

Chain type failures must also be avoided within the INS, partly to reduce maintenance costs but primarily to avoid excessive heat or tripping of breakers which could lead to loss of other redundant functions. The need for partial power supply shut-down, short-circuit and overvoltage protection should be considered for this purpose.

3.3 Accuracy

The redundant strapdown INS shall have the following output accuracy:

Attitude rate	0.05°/sec, rms, per axis
Attitude	0.1°, rms, per axis
Heading	0.2°, rms
Position rate	1.03 m/sec (95) radial with external updates every 5 seconds, update noise of 122m rms, zero correlation time, 61m rms, 20 second correlation time, per axis
Acceleration	0.003 m/sec ²

This accuracy shall apply with either 0, 1 or 2 hardware failures, through the operational environment described in paragraph 3.7 of this report and with an external update outage of 60 seconds. It is assumed that aircraft installation errors are not included, aircraft parking coordinates have been entered perfectly and a full gyrocompassing alignment (paragraph 3.5) has been completed at a latitude of 45° prior to first aircraft motion.

3.4 System Input/Output

Output requirements are as listed in the following table.

CATEGORY	QUANTITY	RESOLUTION	RANGE	BITS	CYCLE TIME
Attitude	Pitch (Elevation)	$2\pi/2^{15}$	$\pm\pi/2^*$	14	0.03125
	Roll	$2\pi/2^{15}$	$\pm\pi$	15	0.03125
	Heading, true	$2\pi/2^{15}$	$\pm\pi$	15	0.03125
Attitude Rate	Pitch Rate	$0.05^\circ/\text{sec}$	± 4 rad/sec	14	0.03125
	Roll Rate	$0.05^\circ/\text{sec}$	± 4 rad/sec	14	0.03125
	Yaw Rate	$0.05^\circ/\text{sec}$	± 4 rad/sec	14	0.03125
Body** Acceleration	Longitudinal Accel.	0.003 m/sec ²	± 10 g	11	0.03125
	Lateral Accel.	0.003 m/sec ²	± 10 g	11	0.03125
	Vertical Accel (body)	0.003 m/sec ²	± 10 g	11	0.03125
Navigation Outputs	North Velocity	0.03 m/sec	1686 m/sec	16	0.125
	East Velocity	0.03 m/sec	1686 m/sec	16	0.125
	Vertical Vel. (earth)	0.03 m/sec	1686 m/sec	16	0.125
	Latitude	$2\pi/2^{19}$	$\pm\pi/2^*$	18	0.5
	Longitude	$2\pi/2^{19}$	$\pm\pi$	19	0.5
	Altitude	0.3 m	-305 m to 18.3 Km	16	0.5

*These outputs are generally scaled at $\pm\pi$.

**Installation is assumed to be at the aircraft center of gravity, so lever-arm accelerations are not included.

This list contains the minimum of items typically provided by an aircraft INS. It does not include special functions such as way-point steering which are assumed to be performed by a central computer complex and display. For the purposes of size, weight, reliability and cost estimates, one ARINC 575 serial output channel shall be provided for each of the redundant INS computers. The capacity of this type of I/O is 439 24-bit words/sec vs 300 words/sec for the above list, not including the display. The parts count for implementation is considered representative of moderate performance, serial digital I/O techniques.

A separate output line indicating failure of one or more system components/subsystems shall be provided from each redundant computer.

Input requirements consist of altitude from an air-data system and filter updates based on VOR/DME or OMEGA data. Baseline update quantities are 2 velocities and 2 position, (4 total), at a maximum rate of one full update every 5 seconds. Additional inputs, TBD, will be received from a display. The present ARINC 575 digital I/O format cannot drive a receiver from more than one transmitter. For the purposes of size, weight, reliability and cost estimates, therefore, three ARINC 575 serial digital input channels shall be provided for each of the redundant INS computers. Additional channels may be needed for inter-computer data transfer (not necessarily to ARINC format).

3.5 Reaction Time

The redundant strapdown INS shall complete its self-contained alignment in less than 10 minutes from system turn-on. No external inputs shall be required, with the exception of aircraft latitude and longitude entered within two minutes after system turn-on. Aircraft motion during alignment shall consist of the model described in Paragraph 3.7.4.1 of this report. The alignment time required applies for a starting ambient temperature greater than 0°C (ARINC 561) and less than 50°C and for a latitude less than 70°.

3.6 Modes of Operation

OFF	All power is removed from the system.
ALIGN	Automatic sequencing through the various steps needed for alignment shall be provided. The align mode is initiated only on the ground. Automatic transfer to the navigate mode shall occur if aircraft motion is detected via the INS accelerometers.

- NAV All outputs shall be provided to full accuracy in this mode.
- UPDATE External inputs to the INS shall be accepted while in the NAV mode to correct INS position and velocity.
- ATTITUDE Consideration shall be given to use of a pendulous attitude mode in flight during certain failure conditions if the end reliability of attitude and attitude rate outputs can be improved.

3.7 Environment

The redundant strapdown INS shall be designed in accordance with ARINC 414 [6] except as modified herein, and be capable of being tested in accordance with RTCA Paper 120-61/DO-108, [7], with conditions modified to be consistent with this specification.

3.7.1 Flight Profile Operating Conditions

A typical flight profile for the VTOL application consists of:

- a. System turn-on at 20°C, start alignment, passenger loading/refueling in progress, aircraft subject to wind gusts, ground power applied to the aircraft.
- b. Engine turn-on after 5 minutes.
- c. System advanced to Navigate Mode after 10 minutes, remove ground power.
- d. Engage rotors, perform vertical take-off.
- e. Climb to 300 m altitude, turn left 90° at a turn rate of 3°/sec.
- f. Accelerate to 103 m/sec and cruise for 6 minutes.
- g. Turn left 90° then spiral down at turn rates of 3°/sec. (typical peak turn rate of 30°/sec is indicated in the data of the reference [10] CH-46 flight testing).
- h. Decelerate and perform vertical descent to touchdown.
- i. Disengage rotors, unload/reload passengers for 3.5 minutes.
- j. Repeat d. thru h. two additional times, then turn off system power.

The non-VTOL applications are assumed to have the flight profile as follows:

- a. through c. - Same as above
- d. Take-off, climb to 9,000 m altitude, accelerate to 257 m/sec,
- e. Turn left 90° at a turn rate of 3°/sec.,
- f. Cruise for 2 hours with two 10° course changes at turn rates of 1°/sec.

The required and desired aircraft operational performance limits are:

	<u>VTOL</u>	<u>CIVIL OR GENERAL AVIATION</u>
Angular Rates	4 rad/sec	4 rad/sec
Angular Acceleration	50 rad/sec ²	50 rad/sec ²
Linear Accel.(maneuver)	±3 g	±3 g
Velocity (max.)	154 m/sec	1029 m/sec (ARINC 561)
Altitude	3,048 m	18,288 m (ARINC 561)
Aircraft tilt (parked)	±5°	±5°
Range of operation (latitude)	±70°	Worldwide

3.7.2 Ambient Temperature (Per ARINC 561)

Normal ambient temperature:	30°C
Maximum continuous operation:	50°C
Short term (30 min.) overtemp:	71°C
Low operating temp:	-15°C

Note: The ARINC Airlines Electronics Engineering Committee is currently reviewing all avionics installation methods for next-generation aircraft. Revised packaging and cooling methods contained in ARINC 600, not released at this time, require further review.

3.7.3 Cooling Air

It is highly desirable that the redundant strapdown INS operate without requiring the use of cooling air since ARINC 404 cooling (impingement) produces internal contamination. This could be accomplished if the aircraft installation design limits the maximum continuous ambient temperature to 30°C. In order to provide installation flexibility, however, ARINC 404 [8] cooling

provisions should also be included, with a cooling air flow of 13.6 Kg/hour/100 watts of dissipation. The use of heat exchangers having small openings shall be avoided due to the high likelihood of closure with dust. If the installation requires extended operation at 50°C ambient conditions, the cooling air will be utilized to achieve highest reliability.

3.7.4 Vibration

3.7.4.1 Ground

Movement of the aircraft while parked may occur due to wind gusts impinging on the fuselage, loading and unloading of passengers, refueling activities, and engine vibrations. The statistical properties of wind are described in NACA Report 1272. When this power spectrum is applied to a typical parked aircraft transfer function, the resulting horizontal motion may be modeled as a first order Markov process with a standard deviation of 4mm and a correlation time of 20 seconds. This model will need to be reviewed once the VTOL weight, form factor and INS location in the aircraft are established. The above model is felt to be conservative.

Data are available [9] on aircraft motion while parked for a number of aircraft, including the British Canberra, Comet, and the Boeing 707. These data were not reduced into a statistical model, but horizontal motion of the Canberra (which is approximately 21m in length and weighs 13,600 Kg vs 13m and 9,000 Kg for the CH-46) was under 3mm peak-to-peak during wind gusts of up to 12 m/sec and from varying directions.

Another effect described in [9] is excitation of the aircraft undercarriage resonance, approximately 1 cps for these aircraft, by wind, refueling and passenger movement. Motions of 2.5 arc minutes, peak-to-peak in roll and 3.8 arc minutes in yaw were recorded.

Data on motion of a CH-46 were taken [10] to determine errors of a strapdown navigator in the helicopter vibration environment. Unfortunately, the main data reduction of the report was limited to flight data (discussed in the next section of this report). A review of partially reduced ground data from [10] indicates an apparent CR-46 undercarriage resonance at approximately 4.5 cps, and angular motion of roughly 0.4 arc minutes peak-to-peak. For the purposes of this report, pure coning motions of 4 arc minutes (cone whole-angle) at 1 cps and one arc minute at 4.5 cps shall be assumed.

Passenger loading also causes variable compression of the aircraft undercarriage. Vertical motions of up to 0.1 m have been recorded [9]. This could result in pitch or roll rotations of

up to 0.5° , depending on the dimensions of the aircraft and the location of oleo struts. Also, this motion is sudden as the static friction of the oleo struts is overcome. Sudden changes of yaw up to 2.5 arc minutes were also observed.

In the flight profile of Paragraph 3.7.1 of this report, it was assumed that the INS would be transferred to the navigate mode before rotors are engaged. While this may generally be the case, it is possible that the reverse will occur. Comparison of the partially reduced CH-46 ground data from [10] (rotors on) with flight data shows PSD vibration peaks to be factors of 4 to 100 less than those occurring during flight. Therefore, it will be assumed that 1/4 of the in-flight coning and sculling vibration power levels are also occurring on the ground during alignment.

3.7.4.2 Flight

The redundant strapdown INS shall operate with specified accuracy during vibration as specified by RTCA Paper 120-61/DO-108, Category A. This vibration level consists of a constant total excursion of 0.762 mm from 10 to 55 cps with a maximum of 5 g, and of 5 g from 55 to 500 cps.

3.7.4.3 Coning and Sculling Motions

The power spectral density and Co and Quad spectral density plots for the CH-46C, as derived from flight test [10], can be represented by the approximate environment shown below:

	SINUSOIDAL	RANDOM
Linear	$0.3 g_{RMS} @ 28 \text{ HZ}$	$0.00045 (g_{RMS})^2/\text{HZ}$ $0-200 \text{ HZ } (0.3g_{RMS})$
Angular	$1.0 \text{ DEG/SEC}_{RMS} @ 15 \text{ HZ}$	$0.033 (\text{DEG/SEC}_{RMS})^2/\text{HZ}$ $0-30 \text{ HZ } (1.0 \text{ DEG/SEC}_{RMS})$
Linear/Angular	$0.1 g_{RMS} - \text{DEG/SEC}_{RMS} @ 15 \text{ HZ}$	$0.0033 (g_{RMS} \text{ DEG/SEC}_{RMS})/\text{HZ}$ $0-30 \text{ HZ } (0.1 g_{RMS} \text{ DEG/SEC}_{RMS})$

Further analysis of these data is presented in [11]. These data may be used to determine redundant strapdown INS errors due to aircraft coning and sculling. (Coning is an angular motion of a body described by sinusoidal velocities about one body fixed axis and one space-fixed axis which will cause a third axis to prescribe a pure cone in inertial space. The two oscillatory rates are in quadrature to produce the conical motion of the third.)

(Sculling motion is made up of a combination of a linear vibration along one axis and an angular oscillation around a perpendicular axis - both at the same frequency.)

These data are taken from a vibration measurement system flown in a CH-46C helicopter at Langley Research Center in August 1969. The motions of the vehicle were recorded for various conditions, both on the ground and in flight. A one-minute portion of the recorded motions during level flight with the start of a deceleration was used to generate power and cross spectral densities. Analog spectral analysis equipment was used to generate the in-phase and quadrature portions of the spectra. The resulting spectra indicate that most of the environment is near dc, due to the normal maneuvering of the vehicle and near 15 Hz and 27 Hz which is coming from the rotors. There is some energy near 400 Hz which would come from the helicopter turbine engines.

3.7.5 Shock

Operational: 6 g with a time duration of at least 10 milliseconds, in accordance with the procedure of RTCA Paper 120-61/DO-108.

Crash Safety: 15 g with a time duration of at least 10 milliseconds, in each direction.

3.8 Power

The aircraft power supply characteristics, utilization and general guidance, are given in ARINC 413. The redundant strapdown INS shall be designed to use 115V AC single phase power, per MIL-STD-704, Category B. A separate input shall be utilized for each redundant power supply.

Capability of operation from an external battery, equivalent to Sonotone P/N CA-51N, shall be provided with each redundant power supply. In addition, each supply shall contain a battery charger, as required by ARINC 561. Due to the dependence of the INS upon the battery during power interruptions such as transfer from ground to aircraft power, the INS suppliers have traditionally insisted upon retaining the responsibility for maintaining the battery in a charged state. The redundant strapdown INS shall

also have the capability of operating from redundant standby computer DC buses for backup power, as defined in ARINC 571, paragraph 2.4.5.1, in lieu of the battery.

3.9 Memory Non-Volatility

The computer program memory shall not be altered by short or long primary power interruptions. In addition, permanent gyro/accelerometer constants such as scale factors and non-orthogonalities, shall be stored in a non-volatile memory. Also, the last computed values of following variables shall be retained after system power shut-down for use during the next alignment:

- a. Gyro compensation constants
- b. Accelerometer compensation constants
- c. Other modifiable calibration constants
- d. Latitude and longitude
- e. Maintenance related data, e.g., self-test results

3.10 Packaging Philosophy

While redundant navigation/autopilot equipment currently in use by airlines consists of separate, non-redundant boxes, no FAA directive has been found giving this approach as a firm requirement. The overriding concern of systems using redundant elements is that a failure in one element not cause a failure of another. Separate packaging of each element is helpful in achieving this requirement. Electrical interactions are more common problems, however, and avoidance of these is more a function of good design practice rather than the physical arrangement.

Low system cost in service is a major design constraint. Packaging all components into a single unit reduces the number of connectors, chassis cost, wire harness cost and special components to drive/receive signals through cables. A more modular concept, on the other hand, reduces the total number of spares required (each VTOL-port needs spares since takeoff cannot occur with failures in any redundant element), and conceivably could reduce dispatch time if the total system can be left running during replacement of the failed element. The selection of the packaging concept will be made after a cost tradeoff, as discussed in paragraph 3.1 of this report. To assure non-interactive failures, the following design constraints shall apply:

- a. Redundant elements shall not be packaged into the same card or plug-in module.

- b. Separate ground buses shall be used to prevent high failure currents from interfering with other elements.
- c. Redundant signals may share the same external connector but pins must be sufficiently separated that a bent pin will not interfere with another element.
- d. A high current drain due to a failure shall not cause a power supply failure if that supply is used by another element.
- e. Consideration should be given to electromagnetic isolation and/or power shutdown where high RFI conditions may result from a failure.
- f. The module designs shall be such that they may be packaged into a non-redundant strapdown INS unit if desired for other applications.

3.11 Form-Factor/Weight

The Airlines Electronic Engineering Committee (AEEC) of ARINC is currently reviewing packaging and installation requirements for future avionics. Revised packaging, form-factor, cooling, etc., requirements may result from this review. In the meantime, however, as a goal ARINC 404 [8] packaging methods are assumed to apply. Deviations to this requirement shall be supported by cost trade-off data. For ease of handling, the weight of any unit replaceable on the aircraft shall be less than 20.4 kg (this is the approximate weight of present-generation ARINC 571 [5] ISS).

3.12 Installation Provisions

The redundant strapdown INS shall use the mounting provisions and handles similar to current commercial INS, per ARINC 561, if practical. Units shall be capable of installation into the aircraft by personnel with minimum training and in a maximum time duration of 1 minute.

The redundant strapdown INS shall have the capability of installation with the unit long dimension either along-ship or cross-ship. It is assumed that computer software (or firmware) modifications are needed to change installation orientation.

The redundant strapdown INS unit will be installed in the aircraft with an installation tolerance of ± 6 arc minutes in pitch and roll and ± 12 arc minutes in azimuth (per ARINC 561 for SST aircraft) as a goal, with ± 12 arc minutes in all axes as a firm requirement. The system accuracy requirement of paragraph 3.3 of this report does not include the effects of this misalignment.

The INS base (mount), if needed, is considered part of the redundant strapdown INS.

3.13 Maintenance Philosophy

The maintenance philosophy generally desired by commercial airlines is to do all of their own repairs, down to the piece-part level. This is partly to protect themselves against vendor problems such as strikes, bankruptcy, etc.. In the case of INS, however this policy is modified since test equipment and training costs are high. Large airlines or airline pools do most of their own repairs, with the exception of gyros and accelerometers. Some airlines only do module replacement, smaller users send the entire unit back to the manufacturer under a maintenance contract (a fixed cost/unit/operating hour).

The maintenance levels have been characterized by Litton as follows:

- Level 1. Unit replacement, in aircraft
- Level 2. Module replacement, in the shop
- Level 3. Module repair (excluding gyros and accelerometers)
- Level 4. Gyro/accelerometer repair

Maintenance levels 3 and 4 will not be considered further in this report.

Level 1 maintenance is performed at all airports serviced by the airline for units designated dispatch items. Take-off is not allowed with a failure in a piece of avionics so designated since flight safety is involved. The redundant strapdown INS falls into this category since it is required by the flight control/stability augmentation system. The speed at which such a unit replacement may be made is very important to airlines since flight delays result in significant cost penalties. Ability to replace a portion of a redundant system without turning off system power or requiring a realignment would be a very desirable feature.

3.14 Maintainability Design

Plug-in assembly construction shall be used to the greatest extent practical. All modules bearing the same part number shall be interchangeable. As a goal, electronic modules shall not require adjustment or recalibration after replacement. Care should be exercised in locating and mounting of modules and components for ease of accessibility.

Each aircraft-replaceable unit shall have a failure indicator, visible from the front panel which indicates that one or more of the internal modules has failed. This indication shall be present with or without power applied to the system and shall only be reset upon successful completion of self-test.

Highly reliable self-test shall be included, consistent with redundancy management requirements. All self-test provisions shall be continuous and automatic, with no pilot-initiated tests.

Sufficient unit test points shall be included to allow fault isolation to the module level using the test equipment defined in paragraph 3.15 of this report. Module test points shall be provided to allow fault isolation to the failed component without probing.

3.15 Test/Calibration

A. Level 1 Maintenance - in aircraft.

No test equipment shall be required for operation/calibration of the redundant strapdown INS while it is installed in the aircraft. An automatic partial-calibration of gyro drifts shall be performed during ground alignment. The redundant sensor data (during conditions of no failures) may be used for self-calibration to the extent practical.

B. Level 2 Maintenance - in shop.

Special purpose test equipment requirements shall be identified for use during routine maintenance. It shall be capable of performing strapdown sensor calibrations as required for accurate system operation and of entering these constants into the non-volatile airborne system memory. The design of this test equipment shall allow its use for Level 2 maintenance by airline personnel.

C. Level 3 Maintenance - not considered at this time.

D. Level 4 Maintenance - not considered at this time.

3.16 Operational Service Life

The redundant strapdown INS shall be capable of operation for at least 3,000 hours, preferably 5,000 hours, without additional lubrication, adjustment or replacement of components (per ARINC 414). Scheduled calibrations required to be performed during Level 2 maintenance, shall be minimized.

3.17 Electromagnetic Interference

The redundant strapdown INS shall meet the conducted and radiated susceptibility and emission requirements of ARINC 413, and the test requirements of RTCA Paper 120-61/DO-108, for Category A equipment. Grounding and shielding practices shall be used in accordance with ARINC 413. (NOTE: Category A is for aircraft greater than 5670 kg, Category B is for light aircraft and is less stringent).

3.18 Humidity

The redundant strapdown INS shall be capable of normal operation during conditions of a relative humidity varying from 10% to 100%, combined with temperature and altitude cycling encountered in normal aircraft operation, as defined by ARINC 414, for Category A (standard) environment.

3.19 Explosive Atmosphere

Explosive atmosphere is not normally encountered by electronics equipment in airline type aircraft. Specific installations where explosive vapor presents an operating hazard are normally defined by the airframe manufacturer.

3.20 Atmospheric Pressure

Normal atmospheric pressure range is from -305 m to 13,700 m. Decompression from a pressure altitude of 2,133 m to 13,700 m in 15 seconds or less shall not degrade system performance, per ARINC 414.

IV. SYSTEM SYNTHESIS AND DESIGN

The approach used to reach the preliminary design concept in this report is to first present general design constraints (paragraph 4.1), followed with a description of hardware and software needed to implement a non-redundant, strapdown INS (paragraph 4.2). Redundancy is then introduced to the overall system, to the instruments, and to the complete system software mechanization. The advantages and disadvantages of various alternative configurations are presented, along with the rationale for selection of the final design.

System redundancy requirements are analyzed in paragraph 4.3. Methods of achieving the system reliability requirement with a fail-op/fail-op configuration are described. The effects of imperfect failure detection and isolation are considered in achieving the recommended system configuration.

The information content of three and four TDF gyro systems is analyzed in depth in paragraph 4.4. Means of estimating failure detection and isolation probability for a three gyro array is presented. Discussion of instrument geometry, parity equations used for failure detection and isolation, processing of parity equations in the presence of system noise and methods of switching information following the isolation process are also covered in this section.

Software mechanization options are discussed in paragraph 4.5. The selected mechanization considers maintaining visibility of subtle errors throughout the processing to allow external improvements in failure detection and isolation processing. Capability of complete recovery from failures without retaining errors needed to perform failure detection and isolation is also provided. Software requirements for INS updating from radio aids, and a trade-off of software compensation of strapdown instrument errors are presented.

System packaging options are presented in paragraph 4.6. A cost-of-ownership trade-off illustrates the large impact that the packaging arrangement can have in airline cost. A baseline packaging arrangement is developed.

System design decisions are summarized in paragraph 4.7.

4.1 General Design Requirements

Section III of this report gives the requirements imposed on the redundant strapdown INS by the application. These requirements stem from various customer or potential customer needs, including those imposed by the total operational environment. Internal to redundant strapdown INS, additional design constraints, guidelines or assumptions may be imposed prior to system synthesis,

either to achieve more realistic cost/reliability estimates or based on current manufacturing trends.

4.1.1 General Construction

The general construction of units has a strong impact on cost, both unit cost and in-service cost. The following guidelines will be applied to the preliminary design of the redundant strapdown INS:

- Simplicity of construction is more important than minimum size.
- Internal inter-module wiring should use low-cost production techniques such as flex-print, multilayer laminates, or automatic wiring machines, as applicable, with that order of preference.
- Electronic modules should be designed to use modern production assembly methods such as automatic component insertion and wave soldering, as applicable. Hand-soldering should be minimized.
- The total number of electronic modules (printed circuit boards) should be limited, consistent with vibration integrity and modularity needs, to reduce the number of connectors, total printed circuit board cost, and test cost. A multitude of small assemblies should be avoided.

4.1.2 Module Designs

The gyro design will be assumed to be the Litton G-6, tuned-gimbal gyro. The accelerometer will be the production Litton A-1000 (single axis).

The electronics designs should use low-power techniques where practical. Having a low power requirement not only reduces power supply costs, but also simplifies electronics packaging. Heat exchangers may be eliminated or simplified and the overall structure may be reduced. Reliability also benefits from lower component operating temperature. In addition, aircraft battery requirements to cover power interruptions are simplified.

Power supply cost may be further reduced by standardizing power supply voltages. A fewer number of voltages to be generated tends to cut down on the number of regulators needed.

The expanded use of digital components in the electronic design (with a corresponding reduction of analog components, such as operational amplifiers, capacitors, and even resistors) is highly desirable. Digital component technology is evolving very rapidly through the use of MSI and LSI (medium and large-scale integration) techniques. Component costs are reducing

dramatically, with lowered power dissipation and use of a single power supply voltage (normally) as added benefits.

The digital computer which will be assumed for the purposes of the study is a modern hi-performance strawman machine utilizing state-of-the-art components while meeting the strapdown speed requirements. Computers in this class are state-of-the-art and available in quantity at competitive prices. The computer memory will be a semiconductor version. A core memory may be used for flight test of early models of the redundant strapdown INS for software validation. Production models, however, would benefit from the lower cost of semiconductor memory.

4.1.3 Software Generation

It will be assumed that the software will be generated in assembly language rather than in some higher order language such as FORTRAN or JOVIAL. Inefficiencies incurred with compilers as well as difficulties in real-time application result in 20%-50% memory word-count and time penalties. The lowest unit cost, therefore, will result from the most efficient computer programming. This trade-off should be reviewed when the computer is selected for the implementation phase of the redundant strapdown program. Computer memory costs are becoming so low that some memory hardware could be wasted if the costs of programming can be significantly reduced.

4.1.4 Test and Calibration

Computer-controlled module/unit test and calibration will be assumed for minimum cost. This will have a significant impact on unit price since electronic labor costs are already small through the use of automated assembly methods.

The design of the redundant strapdown INS units and modules should include capability of automatic test. This determines the number and type of test points (this may require additional or larger connectors) and some additional components for isolation of sensitive circuits.

4.2 Element Block Diagrams

The system design will now be synthesized from the basic, non-redundant constituents. Various alternative mechanizations are shown, and trade-off discussions presented where applicable.

4.2.1 Non-Redundant System Block Diagram

A simplified block diagram of a non-redundant strapdown INS is shown as figure 4-1. The G-6 tuned-gimbal gyro has two degrees-of-freedom and thus there is a redundant (R) channel. In addition, it is essentially a displacement gyro, as opposed to a

rate gyro. Therefore, an amplifier is needed to derive angular rate by precessing (torquing) whenever an angular displacement (pick-off) occurs. Similarly, accelerometers are of the torque-to-balance type where an amplifier produces an electrical current into the electromagnetic torquer of the accelerometer. This torque balances out the torque produced by the vehicle acceleration acting through a pendulous mass in the instrument.

Gyro and accelerometer torquer signals must be converted into a form which the computer can use and this conversion is designated IMU/computer I/O. After solution of alignment, attitude and navigation equations, the computer forms the required outputs for the aircraft avionics. Inputs are also accepted by the strapdown INS for update purposes. Special circuitry, assumed to be all-digital, is required for this system I/O since the computer signal format is not usually adaptable for use with aircraft wiring.

An alternative gyro and/or accelerometer torquing method is shown on figure 4-1 with dashed lines. In this method, the computer closes the loop around gyros and/or accelerometers, thus simplifying the analog amplifiers. Since a single computer cannot solve both the loop closures and the strapdown equations due to the speed limitations of modern computers, additional computational capacity must be added. This will not be discussed further in this report since it is more of a detailed circuit-design rather than system-design option.

4.2.2 Gyro Mechanization

The G-6 gyro input and output requirements are shown in figure 4-2. System mechanization factors which need consideration are:

- Gyro rebalance loop design.
- Temperature sensitivity correction.
- Spin motor power.
- Pickoff excitation supply.
- Angular axis alignment methods.

Gyro Rebalance Loop Design

The G-6 tuned gimbal gyro input/output characteristics are shown in figure 4-2. Since it is basically a limited range displacement gyro rather than a rate gyro, electronics is needed to sense displacements and drive them to a null. The driving signals into the two torquer coils are a measure of the vehicle angular rate about two axes.

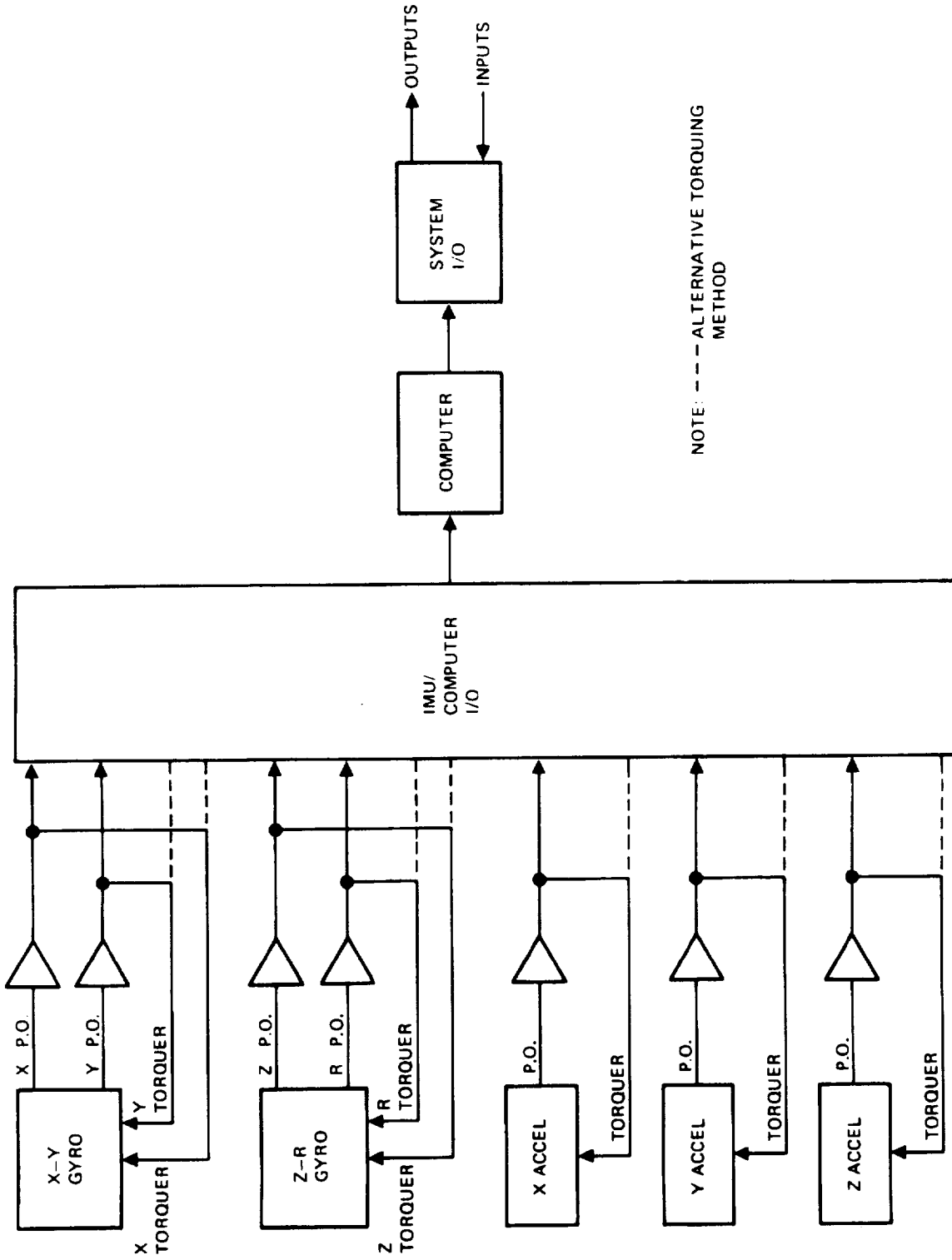


Figure 4-1. Non-Redundant INS Simplified Block Diagram

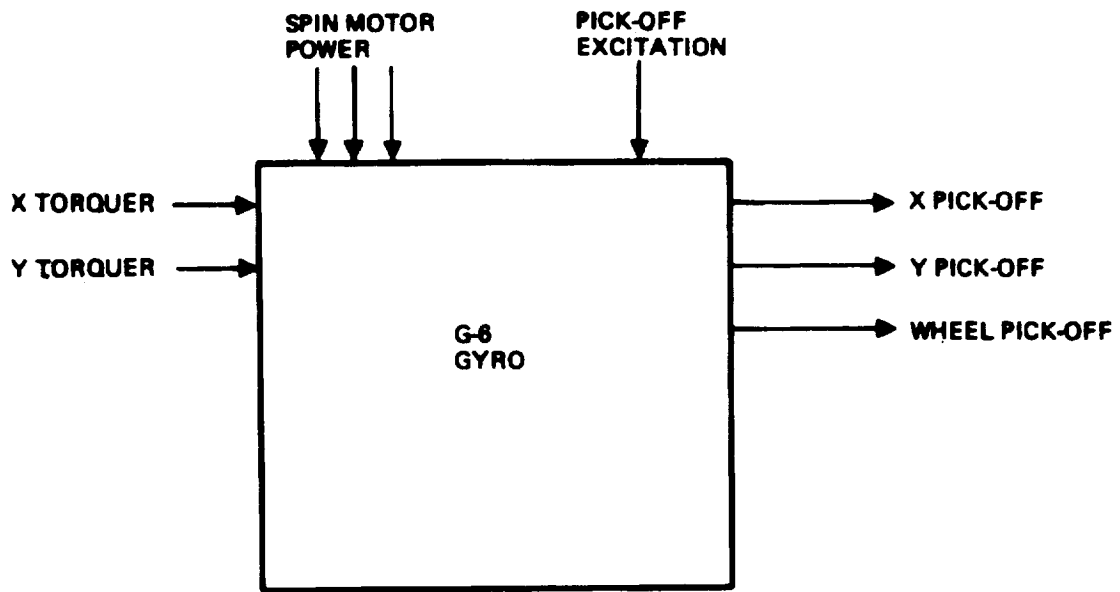


Figure 4-2. G-6 Gyro Interface

Loop closure can be performed either in an analog fashion or digitally. Analog rebalance requires an analog-to-digital converter for input of rate measurements into the digital computer. An analog mechanization is sometimes considered to have a tighter loop gain with less noise than a digital technique. The A/D conversion accuracy requirement on the other hand, is very difficult to achieve. Practical circuits have been implemented, however.

A digital mechanization produces loop closure by means of pulses into the torquer coil rather than a direct current. It is not the purpose of this study to determine the most cost-effective means of gyro rebalance loop implementation, but Litton prefers the digital method over analog plus A/D conversion on the basis of minimum circuitry.

Reference [13] describes a number of pulse torque loop mechanizations. Litton uses a method very similar to what is termed "forced binary loop" in reference [13]. With this method, a fixed frequency square wave is derived where the duty cycle is modulated as a function of the gyro pick-off signal.

Figure 4-3 illustrates this mechanization. Each marker clock pulse (approximately 2 KHz) switches a positive current into the gyro torquer coil. When the amplified, shaped pick-off signal crosses a threshold, the next data clock pulse (approximately 400 KHz) causes the current to switch negative. The net number of data pulses between marker pulses, counting positive during positive torquing, negative during negative torquing, is proportional to average gyro precession rate during the interval. External counting logic determines net pulse changes between computer sampling intervals for input of $\Delta\theta$ to the computer. The need and desirability of cross-coupling between the two gyro rebalance loops is discussed in the detailed loop design description given in paragraph 6.2.1.

The wheel pick-off signal may be used to detect synchronization between wheel motion and motor power supply frequencies and is thus useful for self-test purposes.

The advantages of the forced binary loop implementation are:

- a. For high marker pulse rate, the loop is essentially analog, and thus linear, resulting in high closed-loop gain and band-width. Selection of high marker pulse rate reduces digital noise to acceptable levels.
- b. Good $\Delta\theta$ resolution can easily be achieved (0.5 arc second).
- c. Power into the torquer coil is constant, resulting in constant gyro thermal characteristics and improved performance.

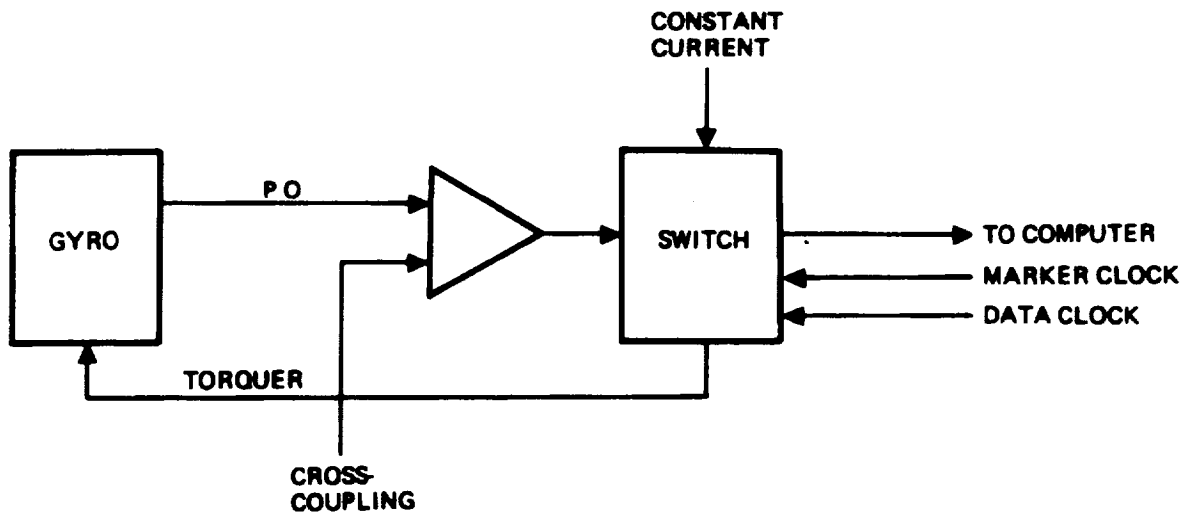


Figure 4-3. Digital Gyro Rebalance Loop Mechanization

- d. Parts count is reduced over the analog-A/D method.
- e. Excellent positive-to-negative torquing symmetry can be achieved.

The "sampling error" described in [13] for this mechanization is easily eliminated by synchronization of computer interrupts with marker pulses, or by buffer registers.

A critical aspect of any rebalance loop implementation is retaining stable symmetry between positive and negative torquing scale factors. Any asymmetry drift from a calibrated condition causes errors when the vehicle is in a dynamic environment through a rectification of positive/negative motion. Achieving 0.01% scale factor stability (100 ppm) is a lesser challenge.

Null stability errors are a function of the balance between positive and negative torquing, including pulse rise-time and fall-time contributions. These are difficult parameters to control and require careful circuit design. Since this bias error is proportional to the maximum torquing rate, and very high vehicle rates (up to 4 radians per second) are present for very short time durations, a rate switch is included. One current level representing 30°/sec is used during normal operation. A second current level, 240°/sec, is applied during extreme vehicle maneuvers.

If the aircraft autopilot is rate-limited in all three axes for passenger comfort or other reasons, this extra rate switching circuitry is generally not used. Safety considerations, however, require that the sensor measurement range be higher than the basic airframe capability.

Temperature Sensitivity Correction

The gyro and rebalance electronics parameters are designed to have low sensitivity to operating temperature. There are limits to how insensitive these devices can be made, however. The residual coefficients are sufficiently stable with time so that the net system error budget can be achieved either with

- rapid component warmup and temperature control, or
- monitoring of component operating temperature with computer corrections applied using factory-calibrated coefficients.

The advantages of the calibration method are:

- system power consumption is reduced
- component operating temperature is lower, resulting in improved reliability.

Additional benefits derived from avoiding a large thermal transient at turn-on are: 1) Electronics failures are often induced by the stresses associated with large thermal gradients, so net reliability is further improved over straight parts-count considerations; 2) A thermal, and thus instrument performance transient during ground alignment is eliminated. Such a transient can seriously contaminate gyrocompassing if not controlled. The instrument/electronic thermal design becomes very critical in temperature-controlled systems so that transients are completed soon enough to achieve alignment in the required 10 minutes.

Increased calibration costs result with this method, however, since instrument/electronic constants must be derived at a number of temperatures instead of at a single point. Test equipment complexity, test time, and the number of testers needed for significant production rates are all increased.

The final tradeoff of whether or not to temperature-control instruments is left until the final production equipment design. System design is described for a compensated implementation.

Spin Motor Power

The G-6 gyro spin motor has been designed to operate with a square-wave, three-phase supply voltage. This allows use of a high-efficiency switching-type power source.

Tuned gimbal gyros are susceptible to vibrations at the spin speed and especially at twice spin speed. Therefore, if each gyro is run at a slightly different spin speed, coupling between gyros through self-induced vibration effects, such as bearing noise is avoided. If this coupling is significant, separate spin motor power supplies are needed for each gyro.

A signal is available from the G-6 gyro, the wheel pickoff, providing a voltage pulse for each rotation of the gyro wheel. This signal is useful for self-test purposes to detect gyro motor or major bearing failures. The pulse frequency is equal to 1/4 the motor power supply frequency when the motor is operating synchronously. This pulse train could also be used to determine motor hunting, and thus compensate for some dynamic gyro errors. This type of compensation is not expected to be needed in a CH-46 type of environment, as described in paragraph 4.5.3.

Pickoff Excitation Supply

The supply for gyro pickoff excitation is of straightforward design. It must be sinusoidal, however, with low harmonic content.

Angular Axis Alignment Methods

Gyro axis misalignments of the spin axis and the torquer axes, relative to the mounting structure, are needed to be known to an accuracy of approximately 10 arc seconds. The cost of machining to this tolerance would be quite high, so the approach assumed is to machine to relatively loose tolerances and then calibrate the misalignment angles during test. Thus, gyro axis misalignments will be derived during the calibrations described for temperature compensation, though these will probably not vary with operating temperatures. This adds four constants per gyro to be stored in a non-volatile memory for read-in by the computer at the start of each flight.

4.2.3 Accelerometer Mechanization

The characteristics of the A-1000 accelerometer are very similar to that of the gyro, except, of course, there is no spin motor. The accelerometer rebalance loop may be mechanized in a manner very similar to the gyro loop. Again, a digital loop is favored for reduced parts count.

Accuracy requirements for the accelerometer rebalance loop torquing are slightly less stringent than for the gyro, especially during flight. Approximately 10 ppm repeatability (100 micro-g out of 10g maximum) is typically acceptable. During ground alignment, however, accelerometer bias drifts are indistinguishable from gyro bias. Equivalent bias drift must be under 3 micro-g per minute ($0.01^\circ/\text{hr}$) to achieve reasonable ground alignment accuracy. Pulse torquing circuitry can be of a common design between the gyro and accelerometer, except that there is no mode equivalent to the high rate condition in the accelerometer loop. Also, avoiding temperature control with its attendant transient will aid in achieving the low bias drift needed during ground alignment.

4.2.4 IMU/Computer Interface

The interface between the Inertial Measurement Unit components, the gyros and accelerometers, and the digital computer is shown in the block diagram of figure 4-4. The diagram is structured for a complete inertial navigator including two gyros (with one redundant axis) and three accelerometer axes. G_x through G_R are the duty-cycle modulated square-waves from the gyro digital rebalance loops and A_x through A_z are the equivalent signals from accelerometer loops.

The conversion of duty-cycle modulated square-waves to a parallel digital word for entry into the computer is performed by the up-down counters. While gyro or accelerometer torquer current

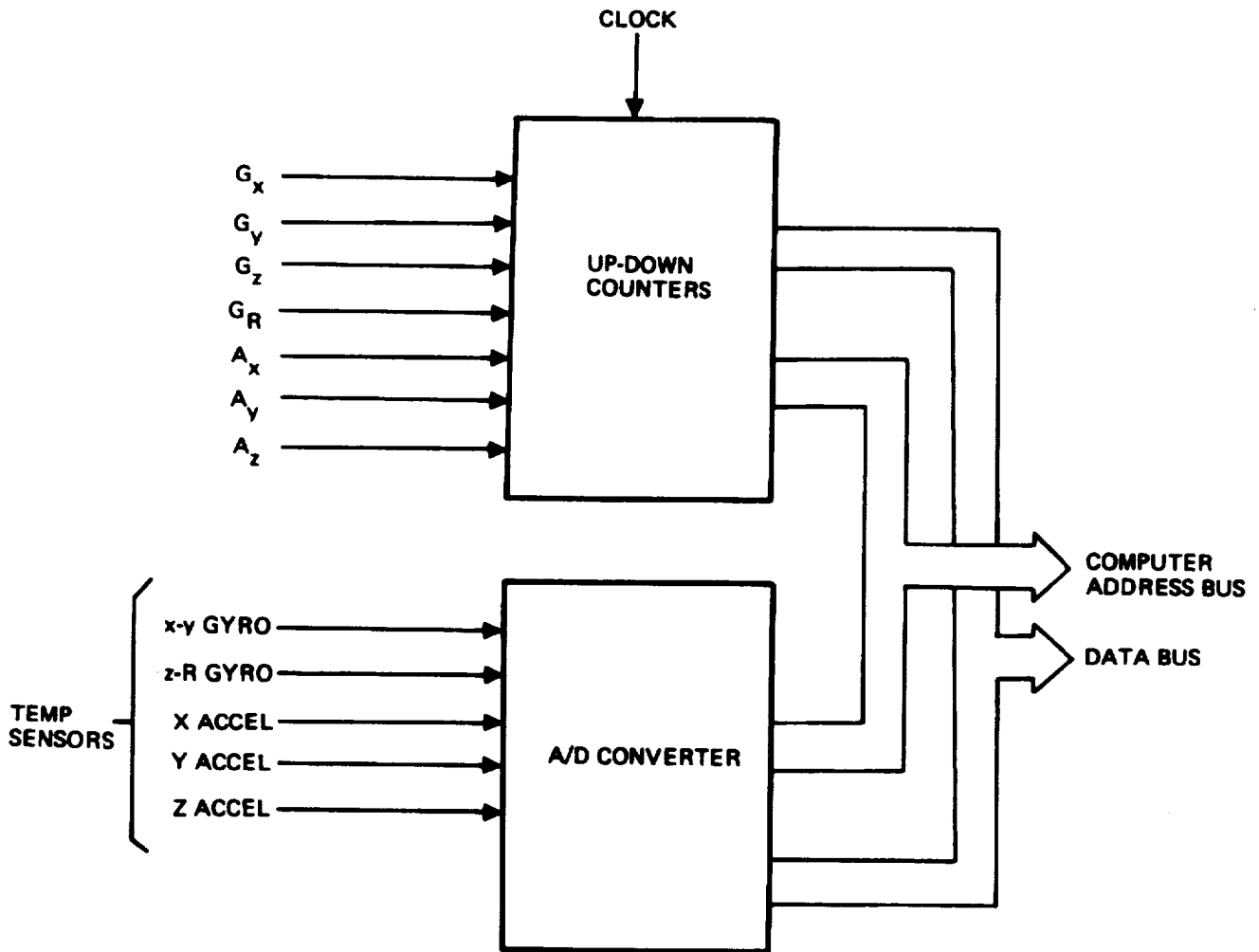


Figure 4-4. IMU/Computer Interface Block Diagram

is positive the count in a register increments at some fixed clock rate. When torquer current switches negative, the register count decrements. The net counter value over one digital torquing interval (approximately 500 microseconds for gyros, 250 microseconds for accelerometers) is representative of the angular change of the vehicle about that axis during the interval for gyros, and velocity change for accelerometers. No unusual design techniques are needed for this function since clock rates of approximately 400kHz can be employed.

The main constraint is that the digital rebalance duty-cycle transition occurs only at one of the counter clock pulses so that no information is lost.

Temperature sensors are required at the instruments for computer compensation. These sensors are typically a variable resistance element, such as platinum, which are put into a bridge circuit, the output of which may be a dc voltage proportional to temperature. Thus, a 10-bit analog-to-digital converter is needed to develop the digital words for application to the computer data bus. The number of sensors needed depends upon the thermal design of the instrument block and the thermal gradients expected under a variety of environments and power conditions.

Since the digital rebalance circuits have their own sensitivity to temperature, gradients between the gyro temperature sensor and the thermally sensitive electronic components with, for example, different cooling air flows must also be considered. Adding a temperature sensor to the electronics implies that instruments and electronics are calibrated at the factory separately. This not only increases cost but also may be impractical due to the accuracy requirements. Therefore, rebalance electronics will be closely packaged with their corresponding instruments to assure a common thermal environment, and then will be calibrated together.

4.2.5 Digital Computer Design

The basic computer performance and memory requirements for strapdown navigation are defined elsewhere in this report. Other aspects of the computer design such as architecture, I/O provisions, etc., are functions of detail design trade-offs rather than preliminary design. This type of trade-off considers design features which may add to unit CPU cost but reduce memory cost and/or one-time programming costs. Only general design trends likely to be applicable to a strapdown INS will be covered in this preliminary design report.

16-bit computer architecture is used extensively in the mini-computer field for data words, with single or multiple words used as instructions. 24-bit computers are sometimes used in avionics for simplified addressing and reduced double-precision

requirements. The strapdown problem requires a significant amount of higher-precision arithmetic so some 32-bit arithmetic capability is very desirable. This function is included in the typical instruction mix used in the throughput definition described in paragraph 6.3, so is contained in the throughput specification. In other words, the problem may be solved by a fast 16-bit computer using software 32-bit subroutines, or by a slower computer having hardware 32-bit arithmetic. The lower-cost unit meeting the throughput requirement is the natural selection. The added memory for the 32-bit subroutines should also be considered, but the downward cost trends of semiconductor memory make this a relatively small factor. 16-bit architecture with good 32-bit arithmetic capability is assumed for the baseline redundant strapdown computer.

Floating-point arithmetic is also a highly desirable feature, primarily to simplify the variable-scaling aspects of programming. While the wider dynamic range is a help in some cases, it is not as essential as in a problem such as Kalman filtering where covariances can assume such a wide range of values. To be of use, the floating point capability would need to be reasonably fast and use a mantissa of 24-bits or greater. Fixed point capability would still need to be retained in the computer for high-speed portions of the problem. Low cost implementations of floating point arithmetic are generally significantly slower than fixed-point.

The use of index registers as pointers to memory areas has been found very valuable in simplifying programming and reducing memory. The general trend is to have some of the index registers also capable of operation as an accumulator (general register), with register-to-register arithmetic capability. These type of non-memory-reference operations are usually very fast and add to net throughput performance.

Many modern computers have microprogrammable instruction sets so they can more easily be tailored to a specific application and/or available software. Thus a computer can be configured to emulate a previous design, with potentially significant savings in software generation costs, or a particular instruction may be included for a more efficient solution of the problem. For the strapdown problem, for example, there may be an instruction format which could solve the quaternion integration with lower word-count/duty-cycle impact. Speed may be improved if the instruction takes the place of several normal instructions, since only a single instruction-fetch is required. Execution time of normal, long instructions, however, such as multiply and divide, is degraded, if these are microprogrammed instead of implemented in hardware. Thus, net performance gains, if any, need to be clearly established.

Most modern computers can be configured to perform input/output operations either under software control or under hardware control through direct memory access (DMA) by the external device during times the CPU is not accessing memory. DMA capability is very useful in many applications in conserving duty cycle.

The software of a real-time problem is often controlled by means of an interrupt pulse. These pulses, occurring at some fixed rate control the software executive. Counting of these pulses is then used to schedule the various software tasks. An additional interrupt, usually the primary interrupt, is used to start a sequence of software operations in the event of loss of primary power. An example of such an operation is the rapid storage of self-test results in non-volatile memory to aid in post-flight evaluation of failures. A fairly simple computer interrupt mechanization can be suitable to vector the software to the correct memory location containing the interrupt subroutine. Extensive multi-level, vectored interrupt schemes are not required. Special design features needed for redundancy are discussed in a later section.

The total computer memory requirement may be divided into four categories:

- a. Program memory
- b. Scratchpad memory
- c. Electrically alterable, non-volatile memory
- d. Factory-derived, instrument constant memory

The program memory contains the sequence of instructions to be performed by the CPU. Many types of computer applications require that the instruction memory be electrically alterable (but non-volatile when power is off) so that program changes can be easily incorporated. Core memories, CMOS semiconductor RAM with a battery for non-volatility, and silicon nitride MOS devices fall into this category. Ultra-violet-erasable PROM also provides program modification flexibility.

Since the redundant strapdown INS as presently conceived is basically a sensor, it is assumed that the software will have very few changes once the system is debugged and proven. Therefore, low-cost ROM (read-only semiconductor memory) will be assumed. This memory will also contain various constants needed for program execution. A variety of devices of this type are currently available at low cost with more than adequate speed for this application.

Scratchpad memory provides temporary storage for system variables, flags, etc., during processing and I/O operations. It may

be volatile since battery protection against short power interruptions will be provided for the entire system, and the variables are all reinitialized when the system is energized at the start of a flight.

Some variables are required to be retained following system deactivation, however. For example, position coordinates of the aircraft at shutdown may be used during the next start-up sequence if accumulated system errors are not too great. Some system calibrations such as partial gyro biases need to be retained so that further biasing during the next flight can improve on past estimates.

In addition, it is very useful to retain a record of system variables and redundancy management or self-test results after a failure is indicated. Since many failure modes cause a rapid power shut-down (100 usec is typical) to avoid chain-type failures, the write time of the non-volatile, read/write memory holding these variables must be faster than the power supply shutdown time constant. Silicon nitride memories now becoming available, cannot be used for this function since write-times are too long.

The total read/write memory function is assumed to be implemented with a CMOS memory supported by a small battery. Several months of non-volatility can be obtained with such a small battery. SOS (silicon on sapphire) versions of CMOS are now becoming available with adequate speed for this application.

The instrument constant memory (a read-only memory which is programmed only once using a special item of test equipment) is required to store some instrument constants which are not normally subject to change. This includes instrument non-orthogonalities which are determined during manufacture. A silicon nitride memory is not recommended since certain types of computer failures might cause alteration of the constants, thus necessitating instrument recalibration, a time-consuming maintenance action. The instrument constant memory would be implemented in a programmable ROM (PROM).

4.2.6 Computer Input/Output

The input/output between the digital computer and other aircraft avionics has been designated to be all-digital, serial and in the format defined in ARINC 575. For the non-redundant configuration, there are no unique design problems associated with this circuitry.

4.2.7 Power Supply and Support Electronics

The remainder of electronics needed to complete a non-redundant strapdown INS is shown in block diagram form in figure 4-5. Primary aircraft power is converted to DC which is used to derive the various voltages needed by the electronic components. It is also used to charge the battery which provides the backup power in the event of aircraft power interruptions.

Self-test circuits monitor critical gyro, accelerometer, and power supply signals. When a failure is detected, the computer is sent an interrupt so it can perform its shutdown subroutine, and a failure indication is provided to other aircraft avionics.

A variety of frequency references are provided by the crystal oscillator and countdown circuitry for such things as instrument pickoff excitation, gyro spin power, digital rebalance loop control, I/O circuit counting and timing, computer clock, the software executive interrupt, and a computer-read time word used in the solution of the equations to compensate for computational time delays. A watch-dog timer is also incorporated, reset periodically by software. If a problem develops and software cannot reset the timer, self-test circuits are activated to indicate a computer failure.

Mode sequencing circuits are used to initiate gyro spin power once power supply voltages are stabilized and close gyro and accelerometer digital rebalance loops once gyro motors are up to speed.

4.2.8 Software

The general software mechanization of a strapdown inertial navigation system implemented with TDF tuned-gimbal gyroscopes is shown in figure 4-6. Following read-in of counts representing the incremental change in angle and velocity occurring over the previous sampling interval, in instrument coordinates, software compensation is applied. Compensation converts the data into the body coordinate system and applies correction to calibrated or predictable error functions.

Accelerometer compensation consists of a scale-factor correction, rotation of data through calibrated misalignment angles, and bias correction. Gyro compensation consists of similar corrections plus compensation for gravity-dependent bias and dynamic error mechanisms.

The type of dynamic error compensation employed depends upon the vibration environment of the vehicle, gyro parameters, gyro rebalance loop characteristics, and the desired net system accuracy. There is a significant penalty in use of computer duty cycle so software tends to be tailored to the application.

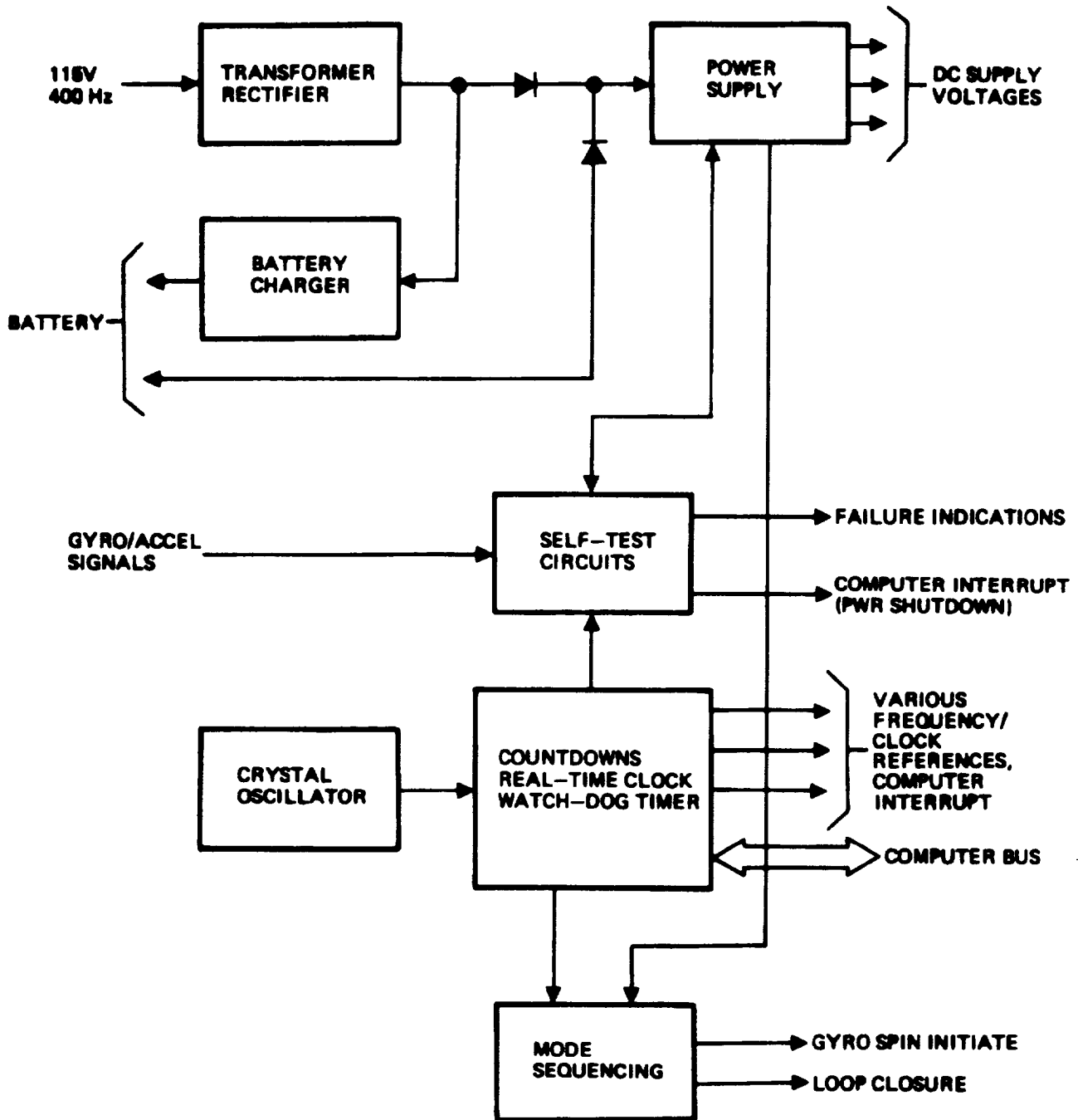


Figure 4-5. Power Supply and Support Electronics

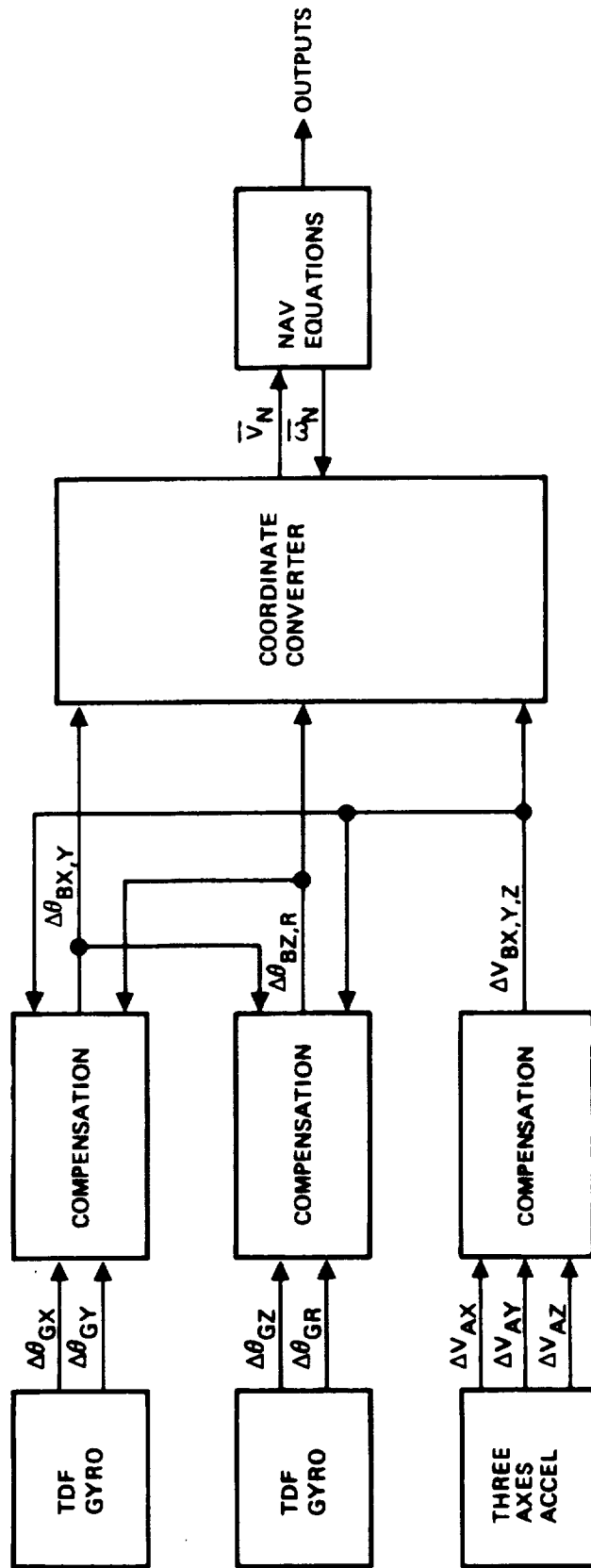


Figure 4-6. Simplified Block Diagram of Strapdown System Software

The most significant dynamic compensation used in strapdown applications corrects for gyro inertia effects. When a gyro is torqued, it not only processes 90° from the torquing and spin axes, but also deflects about the torquing axis. This is a very predictable effect but must be compensated at a high speed in software to minimize errors due to angular vibration of the vehicle.

Another compensation often employed uses gyro pick-off displacements to offset rectification which could occur in a vibration environment due to finite rebalance loop compliance. This compensation is smaller and may be considered for elimination in error budget trade-offs.

Compensated gyro outputs are then integrated in a quaternion integration algorithm to determine the angle between the aircraft body coordinate system and the coordinate system used in the inertial navigation equations. In general, higher order integration algorithms such as second or fourth are used with reasonable computer solution rates to prevent errors due to circulatory vehicle vibration (coning).

Velocity increments are transformed from body coordinates to navigation coordinates using these quaternions. From this point on, equations to be solved are identical to the inertial navigation equations of gimballed systems. The inertial rate of the navigation coordinate system is also derived and returned to the quaternion integration algorithm in a manner directly analogous to gyro torquing.

Leveling and gyrocompassing are performed on the ground prior to flight in the same manner as gimballed inertial systems. Time-varying gains are normally employed, with high initial gains to remove large initial conditions, gradually reducing to a low value to provide filtering of either internal noise effects or unpredictable motion of the aircraft due to wind gusts, passenger loading, refueling, etc. The optimum time-schedule of the gain is often determined using an off-line Kalman filtering technique.

The design of compensation and quaternion integration must be performed carefully to avoid undue airborne computer time consumption. In a current strapdown program at Litton, approximately 40% of the total utilized duty cycle was consumed by instrument compensation, 40% for quaternion integration and 20% for the remainder of tasks. Compensation and quaternion time consumption can be reduced for systems with reduced accuracy requirements or reduced vibration environment, or can be reduced by use of advanced techniques such as higher-order algorithms, time-staggered $\Delta\theta$, ΔV read-in, and special microprogrammed computer instructions.

4.3 System Redundancy Tradeoffs

System Design

The synthesis of the remainder of the redundant strapdown INS is based on comparison of a channelized approach vs lower level modular redundancy. This tradeoff is illustrated by figure 4-7. In the channelized approach, failure of any element of the channel (IMM, computer, I/O, power supply) causes failure of the entire channel. The IMM redundancy management requires communication between channels which then also provides the instrument measurements to all computers.

The modular redundancy approach provides fault detection and isolation at each module so that a failure of a power supply or computer, for example, does not deactivate any other module. The reliability of this method is higher than the channelized approach, at some extra cost for monitoring and switching hardware. This is a well-documented redundancy tradeoff [14].

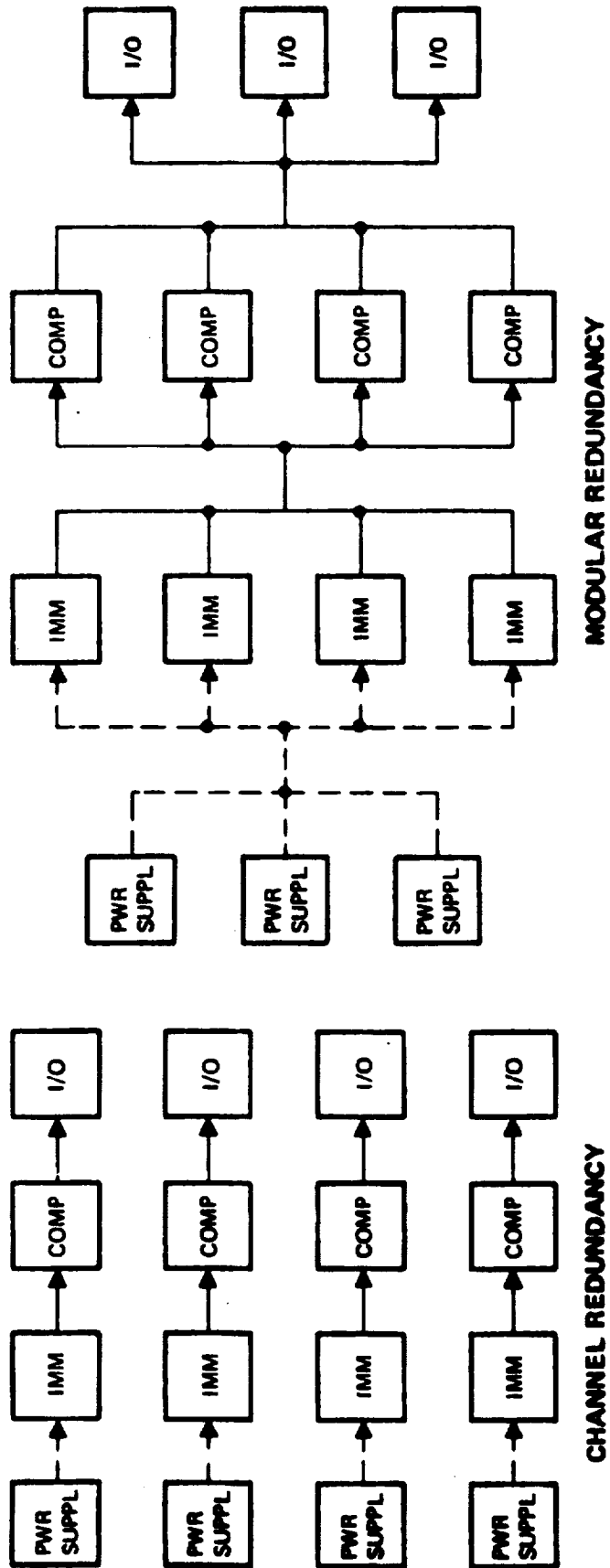
An approximate calculation of redundant strapdown INS reliability with the channelized approach will serve to scope the problem. If reliability is marginal with this method, some modular redundancy would need to be introduced.

One channel of the four redundant channels is expected to have an MTBF of at least 3000 hours. This is consistent with reliability actually experienced on ARINC 561/571 INS of 1500-2000 hours. These INS contain 2 gyros, 3 accelerometers, gimbals, sliprings, servo amplifiers, considerable input/output circuitry, and older, less-integrated component technology vs 1 gyro, 2 accelerometer axes, minimum I/O, and medium and large scale integrated (LSI) circuitry in one redundant strapdown INS channel.

A calculation of system reliability must take into account the failure coverage* at each fail-operational level. The sensitivity of system reliability to this variable, at each level, is illustrated in figures 4-8a and 4-8b taken from reference [16].

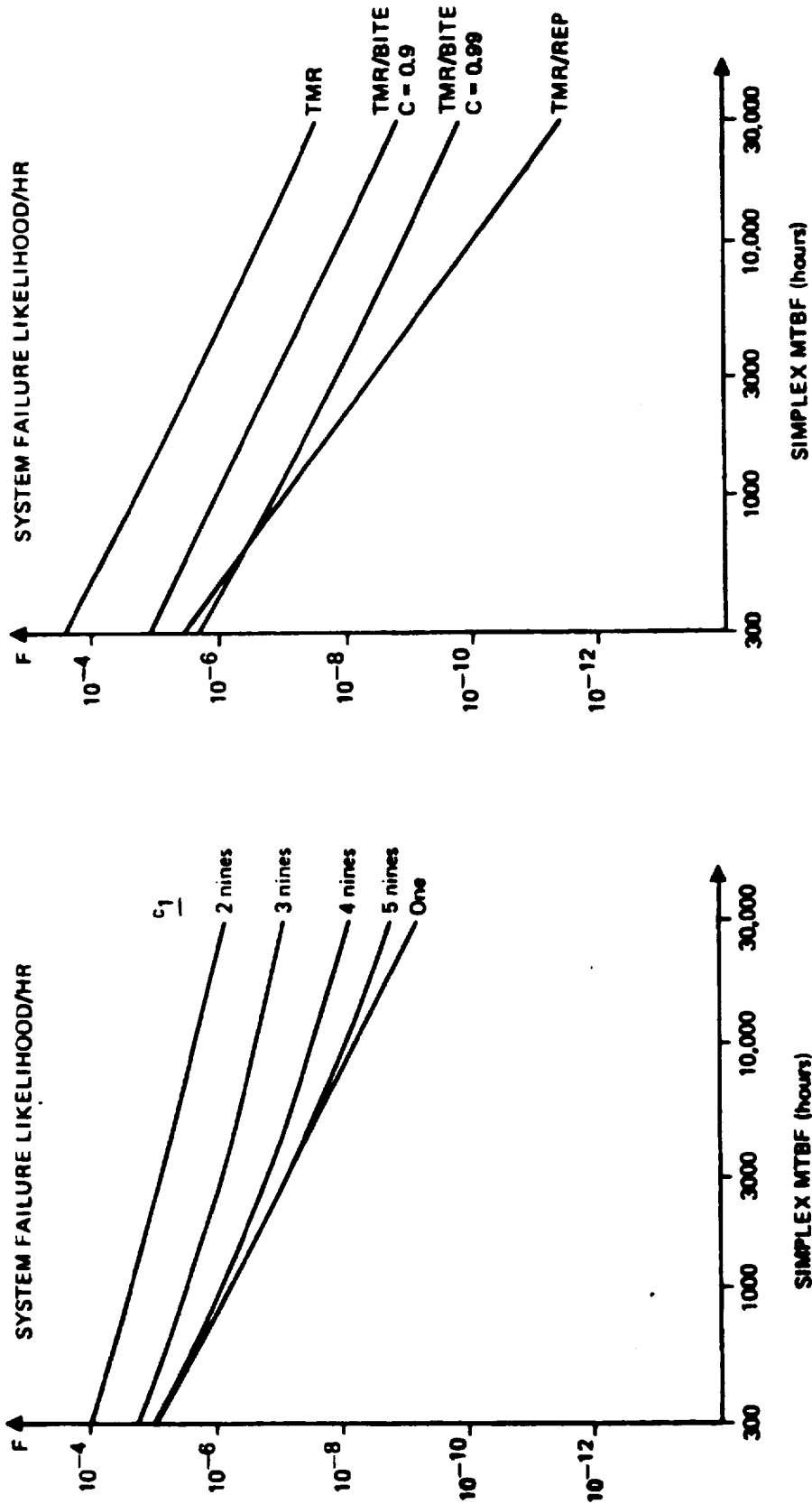
Figure 4-8a (figure 3 of [16]) shows the effect of non-unity coverage for the first failure, with a coverage of 0.9 for the second. The system configuration for these curves is three channels, the first failure detected by voting and the second by BITE. While this condition is not identical to the redundant strapdown INS, reliability trends are applicable. It is clear

*The term "coverage" has been defined in the literature [15][16] as the likelihood of detection and recovery given that a failure has occurred. Thus coverage measures the confidence associated with a fail-operational capability.



"IMM" is an inertial measurement module consisting of 1 gyro, 2 accelerometer axes and associated rebalance electronics

Figure 4-7. Channel vs Modular Redundancy Options



- a) Failure likelihood for 3 channel system, c_1 variable, $c_2 = .9$
- b) Failure likelihood for 3 channel voted system with BITE and 4 channel voted system TMR/REP

"Coverage" is the likelihood of detection and recovery given that a failure has occurred.

Figure 4-8. Approximate System Reliability vs Coverage

that nearly perfect coverage for the first failure (C_1) is needed to make full use of the inherent equipment reliability, preferably better than 0.99999. One source of imperfect coverage is the detection level used in the parity equations to detect soft gyro or accelerometer errors. This detection level must be set high enough that false failure isolation due to normal measurement noise has a very low probability.

Figure 4-8b), a combination of figures 6 and 7 of [16], illustrates the effect of non-unity coverage of the second failure. The top curve represents a 3-channel system with voting logic (coverage of unity for one failure) and no BITE. This is analogous to zero capability to fault-isolate the second gyro failure. The second two curves show addition of BITE with increasing probabilities of correct fault detection and isolation. The fourth curve is a 4-channel voted system (triple modular redundancy with a standby replacement channel) with perfect coverage for two failures. From these curves it is clear that coverage for the second failure should be greater than 0.9, preferably greater than 0.99 to make full use of the inherent equipment reliability. The analysis of the next section of this report shows the practicality of achieving greater than this degree of coverage for the second instrument failure.

From these curves, it appears that a reliability of approximately 1×10^{-8} (for 0.5 hr) can be achieved with the channelized approach, assuming a 3,000 hr MTBF/channel and considering realistic failure coverage conditions.

The previous discussion is general and approximate. A more rigorous presentation of reliability performance for the selected system configuration is given in paragraph 5.3 of this report. For purposes of system configuration trade-offs, however, the following conclusions may be reached:

- a. Low-level redundancy is not needed to meet the 10^{-6} failure probability requirement once the system is configured to be fail-op/fail-op, except where necessary to meet coverage requirements. The design should be driven primarily by cost factors.
- b. Coverage for the first failure should be greater than 0.9999, preferably 0.99999.
- c. Coverage for the second failure should be greater than 0.99, preferably 0.999. A small amount of BITE circuitry should be employed to achieve this goal.
- d. BITE circuitry to provide fault isolation for a third failure is not needed. The primary function of BITE

will be to prevent further damage following a failure such as power supply burn-out, gyro hinge damage, or other secondary failures.

As an illustration of the first point, two system configurations may be considered. Figure 4-9 shows complete redundancy of computers* and system input/output. The computer subsystem may thus be designed to be fault-tolerant and the techniques described in the literature, [17] and [18] for example, may be applied in some form. This often includes redundancy at the computer module level, CPU or memory, for further reliability improvement. There is additional hardware needed for this redundancy, however. Each computer needs to be able to accept data from all four IMM's, and the redundant I/O needs to have considerable monitoring and switching circuitry.

Based on the need for a low cost design, the concept of figure 4-10 is recommended. An IMM interfaces with only 1 computer, simplifying that hardware. Data is made available to other computers for IMM redundancy management through the basic inter-computer I/O. External I/O is dedicated to a computer with final voting performed by the equipment tying into the redundant strapdown INS.

This recommended approach essentially provides redundancy on a channel level. Failure of any element of the channel causes failure of the entire channel but not the failure of another channel. This is consistent with the earlier conclusion that low level redundancy is not needed.

The assumption that external subsystems can accept four inputs and perform their own voting and fault masking appears reasonable in light of redundant systems presently in service and since future interfacing systems will probably contain a computer of their own.

Gyro and Accelerometer Electronics

Gyro and accelerometer rebalance loops must be operating continuously to provide accurate redundancy management. Therefore, there is no circuitry reduction which may be achieved over including separate circuits for each instrument. Since each gyro

*The use of 4 computers was a basic assumption of this study program to limit the required amount of trade-off analysis. While 3 computers are considered to have fail-op/fail-op capability when used in conjunction with BITE, added BITE circuitry and I/O tends to offset the cost reductions offered by one less computer. This is particularly true considering the cost trends of computers vs special-design I/O.

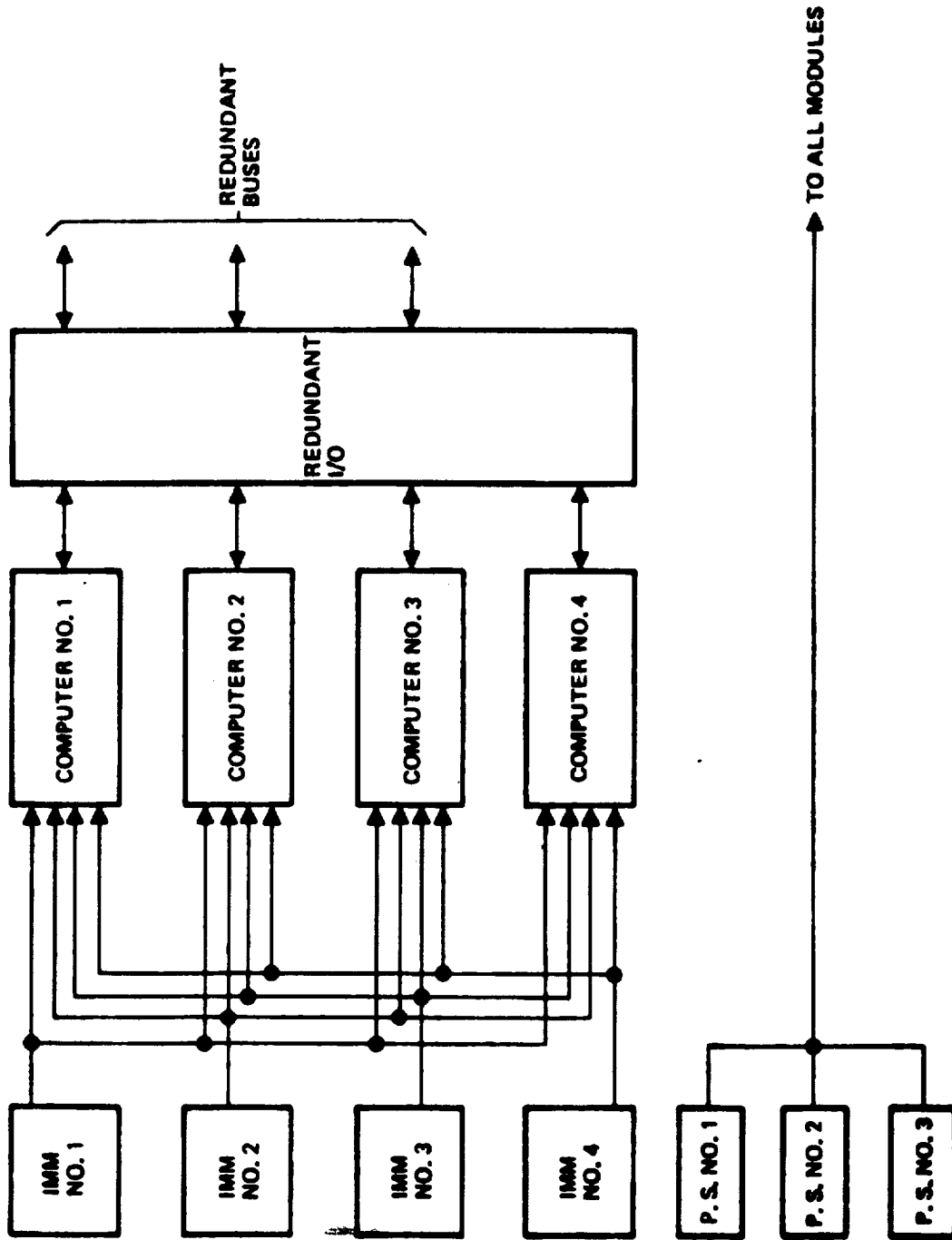


Figure 4-9. Modular Redundant Configuration

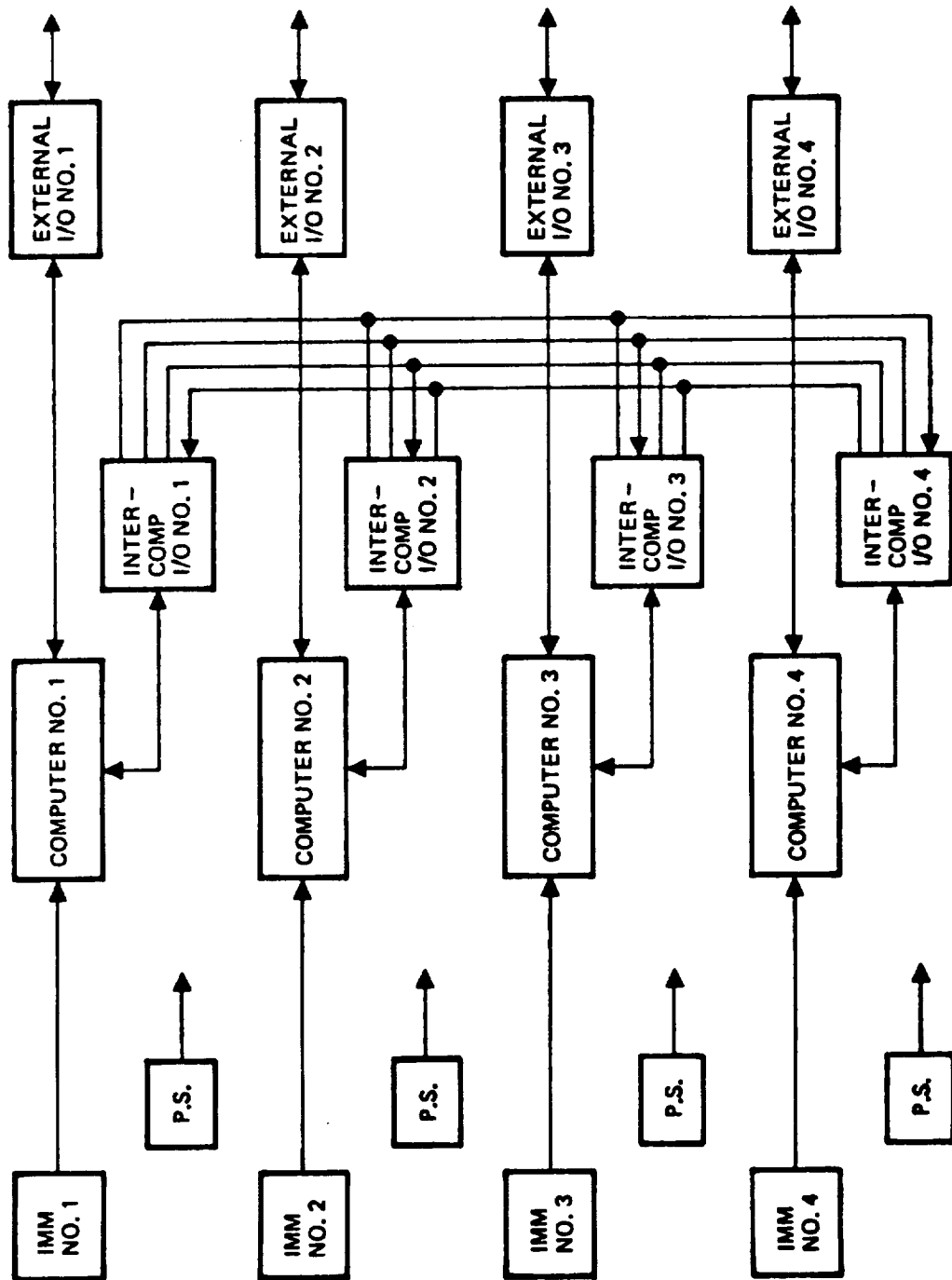


Figure 4-10. Selected Channel Redundancy System Configuration

operates at a slightly different spin speed to eliminate the possibility of errors due to vibrational crosscoupling, four gyro spin supplies are also desirable.

IMM/Computer Interface

The interface between the instruments and the computer is actually simpler for the redundant IMM configuration than for a non-redundant Inertial Measurement Unit (IMU). This is due to use of the channelized approach previously described where a computer is dedicated to a single IMM (1 gyro, 2 axes of acceleration). This dedication not only reduces the number of inputs but also simplifies timing requirements so that each IMM/Computer channel may run essentially asynchronously from the others.

Digital Computer

The recommended system approach eliminates the need for hardware voting. Any comparison of data between channels is performed in software. This then eliminates the need for additional levels of interrupt to reconfigure the system, recover from transients, etc. Thus unique design features are not needed for redundancy, controlling cost.

The use of an ROM program memory is considered a Reliability Enhancement Technique since it cannot be altered during excessive noise conditions. It would be desirable to have the capability of reinitializing the RAM since the integration type of processing in an INS does not recover from transient failures. This is a rare condition so only minor cost penalty should be incurred to provide it.

Computer I/O

The recommended system approach where a computer is dedicated to a single IMM (1 gyro, 2 axes of acceleration) requires intercommunication between all computers in the system in addition to communication to the external world. It is assumed for purposes of this discussion that communications to the external world will be provided via standard ARINC 575 Serial I/O Buses.

The inter-computer communication scheme, however, requires careful consideration since it can greatly affect reliability analysis and redundancy considerations. A key consideration in the system design should be a method to ensure that a faulty processor cannot destroy data in another processor.

Approximately 75 variables need to be transferred from every computer to every other computer. Transfer of variables from the other three computers (225) should be initiated by software and be available in a computer before the next executive interrupt (128 per second). The gyro and accelerometer data (6 words per

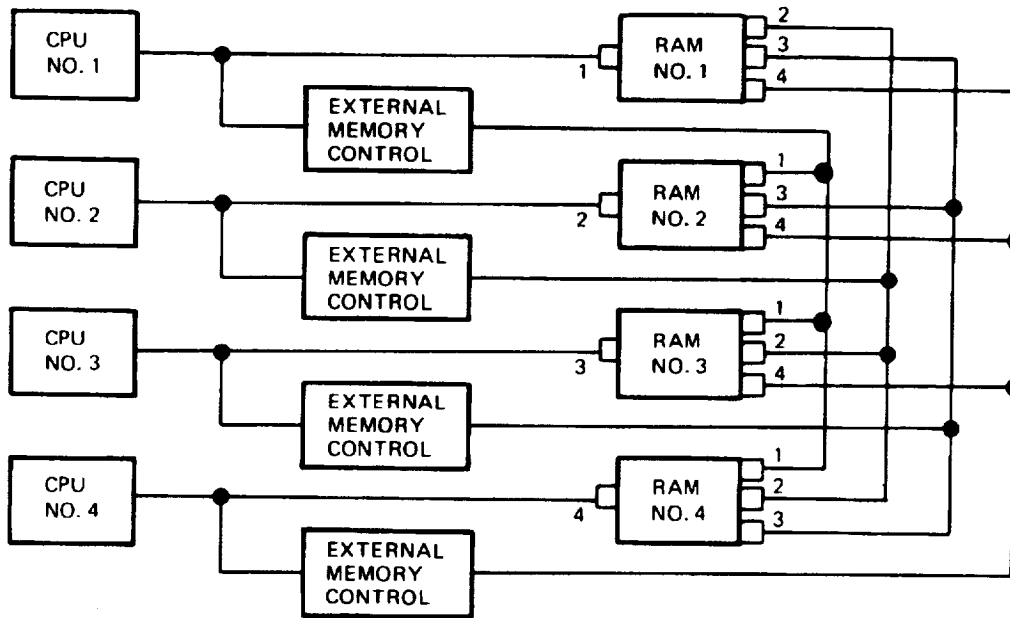
computer) should be transferred first since the software must wait before performing other functions until these measurements are available from the other three computers. Thus the wait-time between data transfer initiation and receipt of instrument data consumes computer duty cycle and should be minimized. The use of DMA for data transfer is highly desirable due to its speed and low impact on duty cycle.

One method of implementing this I/O is to provide every memory unit with four ports, one local port with both read and write capability and three external ports with read only capability. Each computer therefore has the capability of reading all the state variables and data of every other computer. Software voting algorithms will be employed to effect fault detection and recovery processes.

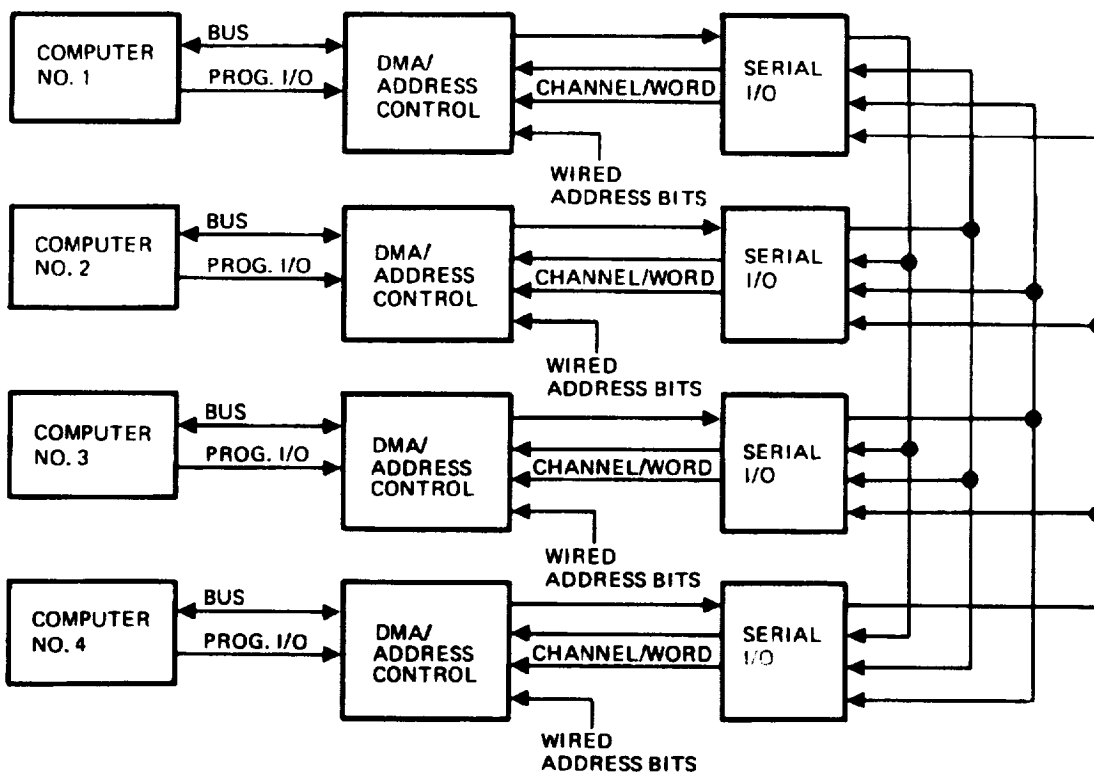
Two port-methods of transferring the data between the four computers have been considered. The first approach is to use a 16-bit parallel bus that time shares data and address lines. Assuming approximately four control lines (Address Strobe, Data Strobe, Memory Request, Memory Enable) for completely asynchronous operation, this approach requires at least 80 signals lines of interconnect between the four systems for computer-to-computer communication. It has the inherent advantage of being simple to implement with very fast response time to error detection. In addition, in the event of a channel failure just prior to take-off, substitution of a channel and IMU reinitialization could be effected rapidly since all system variables are available and may be transferred from the three active systems to the replaced system within a few milliseconds.

In this approach the RAM memory (approximately 1024 16-bit words for each channel) of the entire system is contiguous within the memory address structure. A discrete bit provided in the electronic harness will identify to the software the channel number (1, 2, 3 or 4) of the local processor. If a program is operating out of processor 2, therefore, it will be able to read addresses within the entire spectrum but write only between addresses 2K thru 3K. It is assumed that with parallel busses interconnecting the four computers, data can be read directly from another channel without any delay or extra buffering.

A second port method is to use a serial transmission scheme between the computers. This approach can reduce the signal line interconnect count to approximately twelve lines. A serial-to-parallel converter is required at each receiving memory port and a parallel-to-serial converter is required at each External Memory Controller (see figure 4-11a). The disadvantage of this approach is the relative slowness of the data transfer and the extra complexity of the I/O Controller.



a) DATA TRANSFER VIA READ - ONLY MEMORY PORTS



b) DATA TRANSFER VIA CONVENTIONAL SERIAL I/O

Figure 4-11. Intercomputer I/O Options

In a serial scheme the delay encountered in receiving a given variable may adversely effect the fast iteration loops. Therefore a block transfer of variables is assumed and a contiguous addressing structure for the four computers is not needed.

The serial External Memory Controller of figure 4-11a) can accept the following type command:

Read n variables from location $i \rightarrow i + n$ from system s
and store in local locations $l \rightarrow l + n$.

The command is sent to the controller and the CPU then continues with another program task. The port structure of the memory will contain logic to ensure that no single requestor can hang up a RAM. At completion of the data transfer, the External Memory controller could then signal the requesting processor via an interrupt.

A third method of data transfer is illustrated in figure 4-11b). When data is ready in a particular computer, a programmed I/O function initiates serial data transfer from that computer to all other computers. When the serial I/O is receiving data from a particular channel, the channel number, word count and wired bits are used to form the memory address for DMA logic. Use of this method requires that there be no component failure mode which could cause multi-channel failure.

Selection of the specific inter-computer I/O mechanization has been deferred to the detailed design phase. No matter which method is selected, careful failure analysis must be performed to retain a fail-op/fail-op capability at all levels.

Power Supply and Support Electronics

The power supply could also be configured to be modularly redundant, i.e., a single power supply failure would not cause failure of any other system element. Since monitoring (BITE) circuits for power supplies are relatively straightforward, only 3 supplies would be needed for fail-op/fail-op capability. Coverage could be made adequate for both failures.

After two power supply failures, however, one supply is driving all 4 channels. Each of the supplies would need this power drive capability, resulting in an inherent power drive capability of 4 X 3 or 12 channels, only 4 of which are applied at any one time. For a channelized approach, a power supply is preassigned to a single IMM/Computer. Thus a net drive capability of only 4 channels is required for the total redundant strapdown system. Since power supply cost is strongly dependent upon power drive capability, there is a significant system cost penalty for the small amount of increased reliability provided by modular redundancy (not even considering monitoring and switching components

needed to switch-out the failed unit). Therefore, a channelized approach for the power supply is selected, where a power supply failure will cause loss of one IMM and one computer function.

Self-test circuits are applied for detection of hard instrument and power supply failures to assist the redundancy management function and to prevent further damage to instruments or other components during this condition. Power shutdown of an entire channel would be activated during such failures. Therefore, these self-test circuits are best designed completely on a channel basis, having minimum or no interaction with other channels.

The various frequency references needed for system implementation could also be implemented to be independently redundant. There is a relatively minor amount of circuitry involved so the final decision is influenced by other factors such as packaging and maintainability. Again, it appears that having separate channels is preferred to eliminate elaborate detection and switching circuits. There needs to be some interaction between channels, however, to approximately synchronize computations so that data comparisons are made following calculations within the same computer iteration. This is attained by producing the software executive interrupt simultaneously in all 4 channels. Local clock stability would then produce adequate synchronization for the remainder of the iteration. Monitoring and switching circuitry is needed to prevent a single failure from deactivating more than one channel.

Mode sequencing circuits for system start-up require a minor amount of circuitry to produce outputs for activation of a specific channel, such as computer reset, gyro spin-up, and loop closures, based on power supply mode status. Thus, the design clearly requires a channel approach vs modular redundancy, with no interaction between channels.

4.4 Instrument Redundancy Trade-Offs

4.4.1 General Concepts

The preceding channel redundancy approach does not apply to the inertial instruments. Each so-called channel contains only two axes of information and thus is not a complete navigator. Instruments, therefore, are treated in a modular fashion, with Failure Detection, Isolation (FDI) and subsequent system reconfiguration included so that a single instrument failure will not cause the deactivation of any other instrument. This FDI and reconfiguration has been chosen to be performed in computer software for lowest system cost.

Definitions of the following terms are taken from reference [19]. Detection is the decision that a degradation or failure has

occurred at a threshold level established by mission phase requirements. Isolation is the subsequent decision of which particular instrument output is responsible for the system degradation or failure.

A missed alarm is defined as an actual failure that remains undetected and/or unisolated after the desired threshold limit on system attitude or velocity error (or any other such detection criterion) is exceeded.

False alarms occur when the inertial system truly has no failures but transients or noise trigger the FDI system to falsely indicate failure of a good instrument. False and missed alarm probabilities together should form a valid criterion for measuring the effectiveness (i.e., reliability) of a particular FDI method. A more comprehensive judgment of the worth of FDI in a particular system is derived by judging the overall reliability of the composite system by combining the mean time before failure (MTBF) estimates of the system components with the FDI false and missed alarm probabilities over the critical mission flight time.

Coverage is the probability of a successful system recovery after any failure has occurred. Coverage then, is by this definition, the probability of a correct alarm when a failure occurs. It is not a complete overall concept because it does not take into account the probability of the FDI method having a false alarm.

4.4.2 Two-Degree-Of-Freedom Gyro (TDF) Considerations

Much of the published work on strapdown gyro redundancy management has been directed toward application of single-degree-of-freedom gyros. References [20], [21], [22] and [23] present some of the dodecahedron work of the Charles Stark Draper Laboratory, [24], [25] and [26] the work of TRW and [27] that of Honeywell.

A major problem in the use of single-degree-of-freedom (SDF) gyros is the large number of gyros (6) needed for fail-op/fail-op capability. This leads to high system cost. SDF gyros have not differed significantly in cost from TDF gyros in the past, and this fact has led to the dominance of TDF gyros in the highly competitive aircraft inertial system marketplace. The projections to strapdown instruments, such as the laser gyro (\$4,000 ea., per reference [28]) indicate the same trend. Noting that a 4-TDF gyro system is fail-op/fail-op while a 4-SDF gyro system is only fail-safe highlights this comparison. Considerable producibility efforts are needed on laser gyros to offset the inherent TDF advantage of the tuned-gimbal gyro.

The present published work on TDF gyro redundancy management, references [3], Teledyne, and [29], Kearfott make very restrictive assumptions as to how a TDF gyro will fail. Considering the number of possible failure modes and the extent of interaction between the two axes of a TDF tuned-gimbal gyro, these assumptions do not appear warranted.

Figure 4-12 illustrates the tuned-gimbal gyro components and their supporting electronics. Some failure modes result in drift errors on a single input axis. The circuitry which transfers the digital data from each axis to the computer for example, may have single-axis failure modes. This depends upon the actual mechanization, however, since multiplexing is a common digital design technique. The portion of the loop electronics or gyro torquer which produces precision torquing from the digital signal has a number of soft failure modes which result in a difference between the rate indicated to the computer and the actual gyro precession rate and thus a system error. Since the rebalance loop may still be operating satisfactorily, there could be little or no cross-coupling to the other axis.

Failures of components which are used in common between axes, such as the gyro rotor and suspension system, magnet, bearings and motor, result in degradation of performance of both axes. In addition, errors are dependent on aircraft maneuvers. The error due to a scale factor shift depends upon the axis about which the aircraft is rotating. An error due to a high g-sensitivity depends upon the instantaneous magnitude and direction of the g-vector.

Thus, the error of a TDF gyro should be considered a vector quantity in the measurement plane of the gyro. There also exists some probability density distribution vs. the direction of the angle with higher probability densities in the vicinity of the measurement (torquer) axes.

4.4.3 3-Gyro FDI Singularities

When all four TDF gyros are operating, there is a considerable amount of redundant information. FDI algorithms leading to 100% coverage of the first failure are relatively straightforward, regardless of the gyro failure direction. Detection levels must be set high enough above normal gyro drift transient effects to avoid false alarms and missed alarms, but still be within the level set by system accuracy requirements.

After one gyro failure, however, the ability to isolate a second gyro failure is somewhat limited, depending on the magnitude and direction of the failure. The majority of gyro failures are catastrophic--they fail to spin, the rebalance loop opens, etc.,

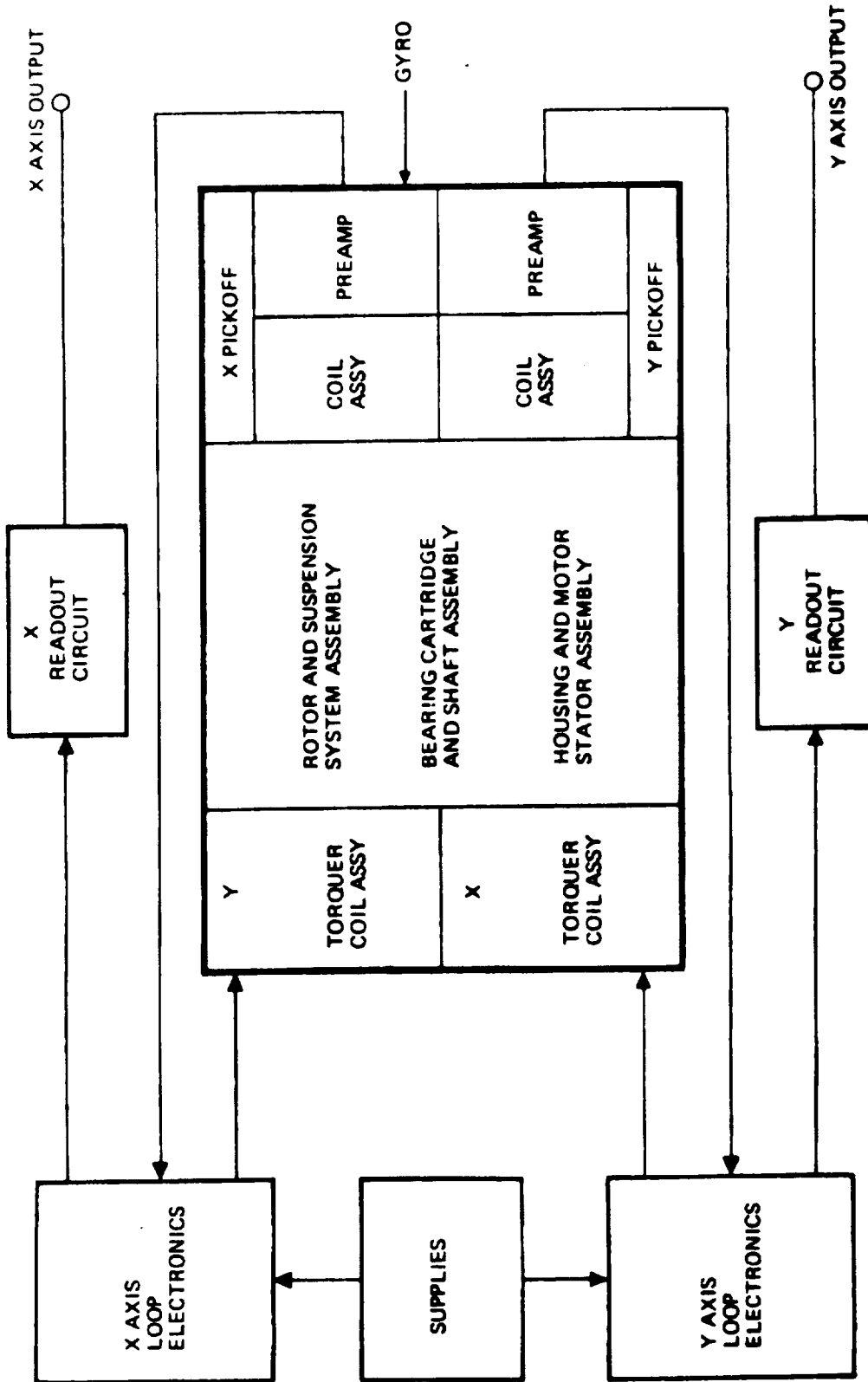


Figure 4-12. Gyro Assemblies and Gyro Associated Electronics

and are detectable by hardware means. The computer FDI is only concerned with soft failures.

The FDI limitations for the 3 TDF gyro conditions may be conveniently analyzed considering three gyros with spin axes orthogonal and, initially, with torquer axes along the three principal axes.

The orientation of the three gyros relative to the reference coordinate set is shown in figure 4-13. Gyro numbers 1, 2 and 3 have their spin axes aligned along X, Y, and Z axes of the reference coordinate set. The gyro outputs are denoted by ω 's with subscripts and superscripts. The subscripts denote the reference axis about which the measurement is made and the superscripts denote the number of the gyro which performed the measurement.

Failure isolation equations (parity equations) can be written by inspection of figure 4-13, as follows.

$$K_1 = \omega_Z^1 - \omega_Z^2 \quad (1)$$

$$K_2 = \omega_Y^1 - \omega_Y^3 \quad (2)$$

$$K_3 = \omega_X^2 - \omega_X^3 \quad (3)$$

Using equations (1), (2), and (3) we may construct a truth table.

TABLE 4-1. TRUTH TABLE FOR ISOLATION OF A FAILED GYRO FOR 3 ORTHOGONAL TDF GYRO CONFIGURATION WITH ORTHOGONAL SENSING AXES

Gyro # Failed	K_1	K_2	K_3
None	0	0	0
1	1	1	0
2	1	0	1
3	0	1	1

In the Truth Table 4-1, the symbol of unity denotes that a failure has occurred and the isolation threshold level has been exceeded. The symbol zero denotes no failure.

Since gyro outputs are incremental angles subject to noise, rate measurements may be partially integrated for smoothing. Therefore, isolation thresholds are often expressed in angle and thus the symbol of unity represents a state in which the set angular threshold has been reached or exceeded. Isolation error is defined as the total angular error made in the time period

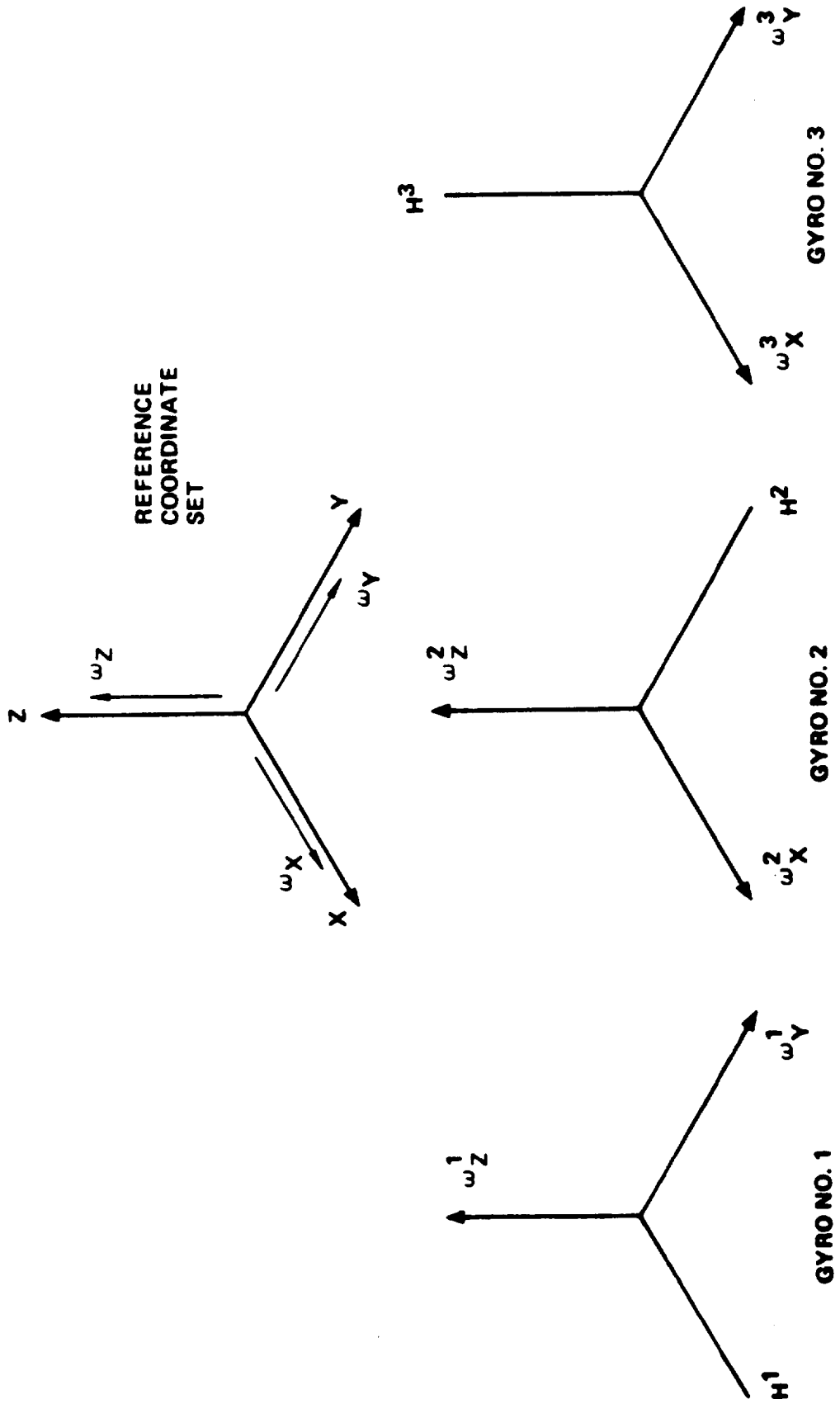


Figure 4-13. Three Orthogonal TDF Gyro Configuration

bounded by the occurrence of a failure and determination of which gyro caused the failure.

During certain failure modes, only one of the parity equations has exceeded its threshold. Therefore, a determination of the failed gyro from the Truth Table cannot be made. To determine the cause and effect of this condition, let us assume that a soft failure has occurred in gyro No. 1 and that the magnitude and direction of this failure is represented by an error vector shown in Figure 4-14. This error vector $\dot{\phi}$ is measured relative to the gyro axes Y^1 and Z^1 . Although the angle θ may assume any value between 0° and 360° , it will be assumed for the purpose of the initial discussion that $0 \leq \theta \leq 45^\circ$.

It is noted that for $0 \leq \theta \leq 45^\circ$, the error rate along the Y^1 axis is larger or equal to the rate along the Z^1 axis. The error angle accumulated along the gyro No. 1 axes is shown in figure 4-15. At the time t_1 , the output of the Y^1 axis reaches the angular detection threshold level ϕ_0 . At this time the failure detection system is aware of the fact that a failure has occurred. The failure isolation mechanism is not actuated because it is not known whether the error is caused by gyro No. 1 or gyro No. 3. Referring to equation (2), it is noted that K_2 can assume a value of unity when either gyro No. 1 or No. 3 fails. At time t_2 , the output of Z^1 axis reaches the angular detection threshold level ϕ_0 . Thus at time t_2 the failure isolation mechanism is actuated and the failed gyro No. 1 is switched from the system. During time t_2 , isolation error has been accumulated. From figure 4-15, the magnitude of the isolation error as a function of the angle θ is as follows:

Error angle accumulated about the Z^1 axis is:

$$\phi_0 = (\dot{\phi} \sin \theta) t_2 \quad (4)$$

Error angle accumulated about the Y^1 axis is:

$$(\dot{\phi} \cos \theta) t_2 \quad (5)$$

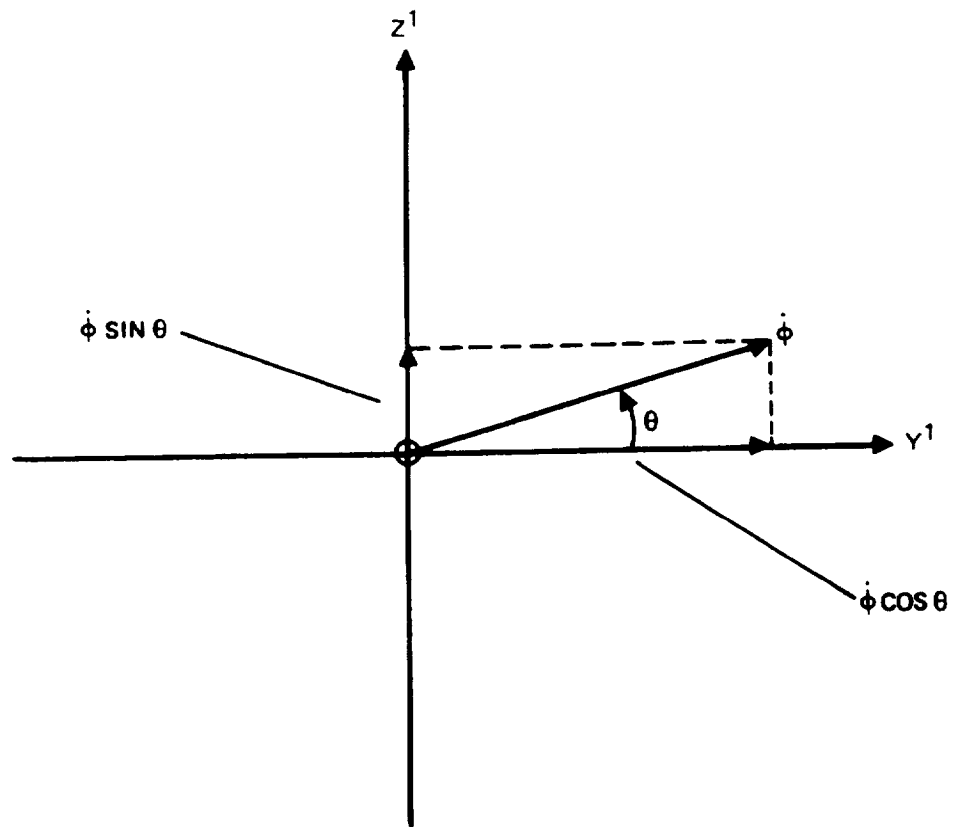


Figure 4-14. Failure Error Vector

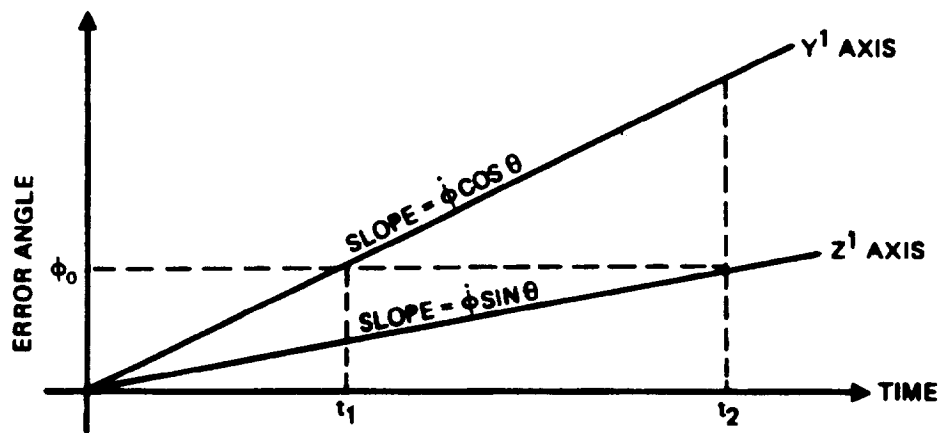


Figure 4-15. Error Angle Versus Time

Assuming the error angles are small so that they can be treated as vectors, then the resultant isolation error is

$$\phi_{\epsilon} = \sqrt{\phi_0^2 + [(\dot{\phi} \cos \theta)t_2]^2} \quad (6)$$

Substituting t_2 from equation (4) into equation (6),

$$\begin{aligned} \phi_{\epsilon} &= \sqrt{\phi_0^2 + \phi_0^2 \frac{1}{\tan^2 \theta}} \\ &= \phi_0 \sqrt{\phi_0 \frac{\sin^2 \theta + \cos^2 \theta}{\sin^2 \theta}} \\ &= \phi_0 \frac{1}{\sin \theta} \end{aligned} \quad (7)$$

The isolation error in nondimensional form is shown plotted in figure 4-16. Similar reasoning that led to equation (7) can be extended for values of $45 \leq \theta \leq 360$, thus obtaining nondimensional isolation error for $0 < \theta < 360$ as shown in figure 4-17.

As seen from figure 4-17, fault isolation singularities (isolation error approaching infinity) occur for gyro error directions of 0° , 90° , 180° and 270° . For gyro errors along these directions, parity equations can detect that an error has occurred (one of the parity equations exceeds the threshold ϕ_0) but a determination cannot be made as to which gyro has failed. In table 4-1, two parity equations must exceed their detection levels for fault isolation to occur. If only one equation exceeds the detection level, only one of the 3 gyros can be classified as good.

With gyro sensitive axes aligned along principal axes, that is coincident with the spin axis of another gyro, a single-axis gyro failure cannot be isolated. Since single-axis gyro failures are expected to have a slightly higher probability of occurrence than, for example, an exactly equal drift rate about both axes simultaneously, it is appropriate to physically rotate the sensitive axes away from the singular directions. A 45° rotation of the gyro about its spin axis was suggested by Teledyne in reference [3]. This reorientation does not remove the singularities but simply moves them relative to probable gyro failure modes.

A physical interpretation of the singularities may be obtained by referring to figure 4-13. In the direction along one of the

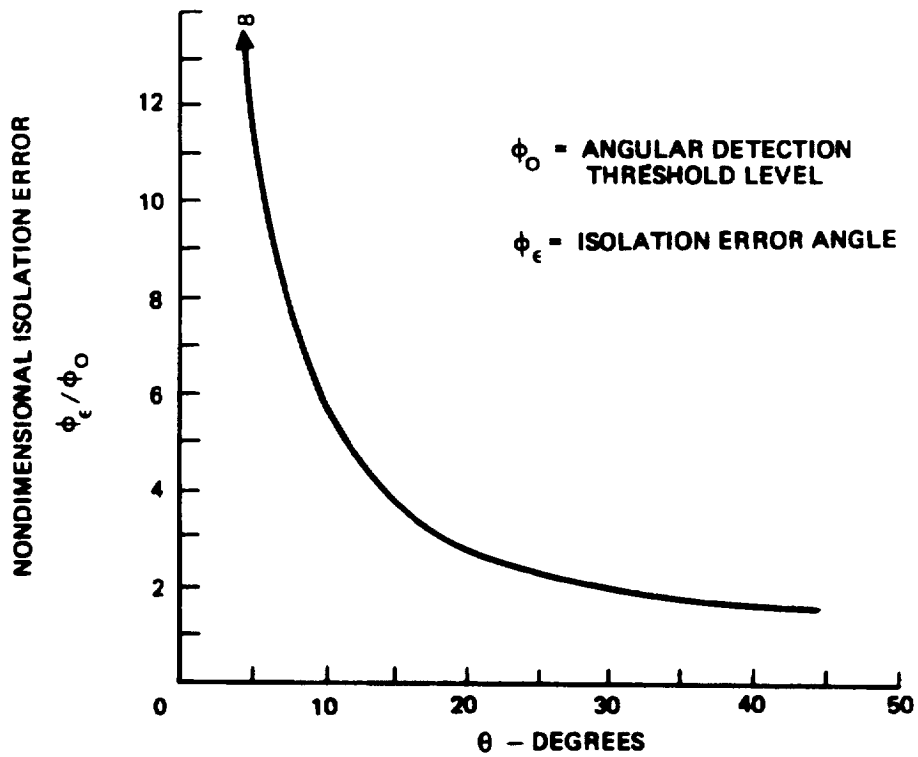


Figure 4-16. Non Dimensional Isolation Error
For $0 \leq \theta \leq 45^\circ$

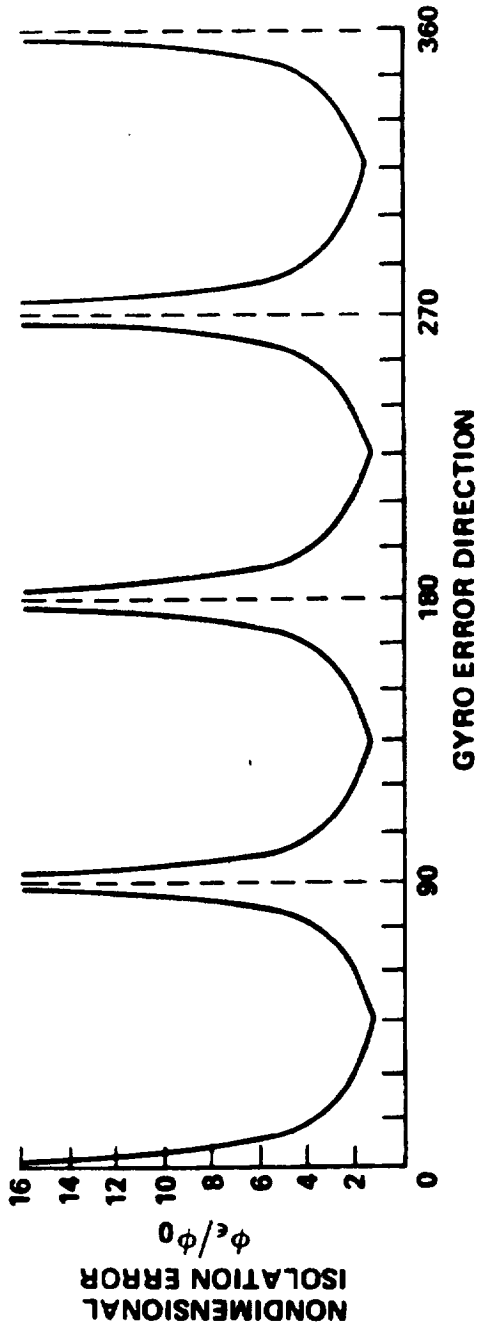


Figure 4-17. Failure Isolation Error vs Direction of Gyro Error
(3 Orthogonal TDF Gyro Spin Axes)

gyro spin axes, say H^3 , there are only two measurements of angular rate, ω_Z^1 and ω_Z^2 . If an error in gyro #1 occurs along this axis, it appears in only one parity equation, which is insufficient for the solution of two unknowns, the two gyro drift rates. Physical rotation of the torquers about the gyro spin axis does not introduce any more information since the same effect can be achieved by a computational rotation.

The fault isolation singularities occur with any geometrical arrangement of three TDF gyros, not only the orthogonal arrangement, except for the trivial case of three coincident gyros. The impact of this constraint on system design is that software must be configured to handle the rare cases of failures along the singular directions, gyro input axes should be oriented away from the singular directions, and total system reliability is slightly reduced due to non-unity coverage of the second failure. It will be shown that coverage is much closer to unity for large allowable isolation errors, as required for flight control use, than for navigation errors.

4.4.4 Gyro Geometries

The geometry selected by Teledyne in reference [3] was to orient three of the gyro spin axes orthogonal with sensitive axes rotated 45° from coincidence with another gyro's spin axis, and with the fourth gyro spin axis bisecting the orthogonal set. This results in a rather unsymmetric condition, where performance (FDI and navigation) and equations to be solved by the computer after the first failure depend upon which gyro failed first - the bisector or one of the three orthogonal gyros. A more symmetric arrangement is desirable computationally and from packaging considerations, provided that the computational burden is not increased significantly.

An obvious symmetrical choice is a tetrahedron where spin axes are directed toward the four vertexes and each gyro measurement plane is one of the faces. Spin axes are thus distributed uniformly in space. Another form of the tetrahedron is half of an octahedron. With this configuration, spin axes are distributed uniformly about a hemisphere. This latter orientation is directly analagous to the dodecahedron of Draper Labs, reference [20]. In that case, distributing sensitive axes on faces of a cube (hexahedron) results in pairs of coincident (one negative, one positive) sensitive axes. Since the computer can make a sign reversal, the desired angular distribution is not achieved. Use of a dodecahedron achieves the desired distribution without parallel axes. The octahedron has a property similar to the dodecahedron in that pairs of the eight faces are parallel.

Therefore, gyros on four non-parallel faces of the octahedron are evenly distributed in space.

Figure 4-18 illustrates the octahedron, formed from equilateral triangles, and two possible selections of gyro spin vectors. The octahedron may be viewed as being composed of two pyramids with the square bases tied together. In figure 4-18(a) the four gyros are attached to only one pyramid. In figure 4-18(b) two of the gyros are moved to the parallel opposite octahedral faces. It can be shown that this latter configuration is equivalent to the tetrahedron where the angles between any two spin vectors are the familiar 109.46° .

In terms of information content, these two geometries are identical. Certain error terms, however, behave differently in the two configurations. In the tetrahedron, the net angular velocity of the 4-gyro array is zero and some error terms, notably the inertia term, cancel. Since the system must work with one or two failed gyros, this feature cannot be fully exploited. The semi-octahedron arrangement has certain packaging advantages so that it is preferred over the tetrahedron.

The tetrahedron could be achieved by reversing the spin motors of two of the semi-octahedrally mounted gyros. Many of the instrument calibration coefficients such as bias, scale factor and g-sensitivity, would not precisely reverse polarity with reversed spin, so there would be additional calibration costs. Again, the semi-octahedron is preferred for lowest system cost.

The symmetry of the semi-octahedron could still be retained with some angle other than 109.46° between alternate spin vectors. Considering spin vectors to be on a cone, this would be equivalent to varying the cone angle to potentially improve some system parameter. Some accuracy degradation would be expected since the amount of measurement along the cone axis relative to the measurement made in the base of the pyramid would change. Since reliability is one of the most important of the system parameters, some accuracy degradation might be acceptable if improved coverage of the second failure could be achieved.

Reducing the cone angle to zero makes all four gyro spin axes coincident. This orientation is very good for reliability (perfect coverage for the 3-gyro condition) but disastrous for navigation since there are only two axes of information. As soon as the cone angle deviates from 0° sufficiently to obtain a measurement about the third axis, the 3-gyro singularities appear. A minor improvement in coverage could be achieved by reducing the cone angle to a very small angle, say 30° . For this condition, large pitch or roll rate errors, i.e., $10^\circ/\text{sec}$, can be detected and isolated. Due to the improbability of such a failure mode,

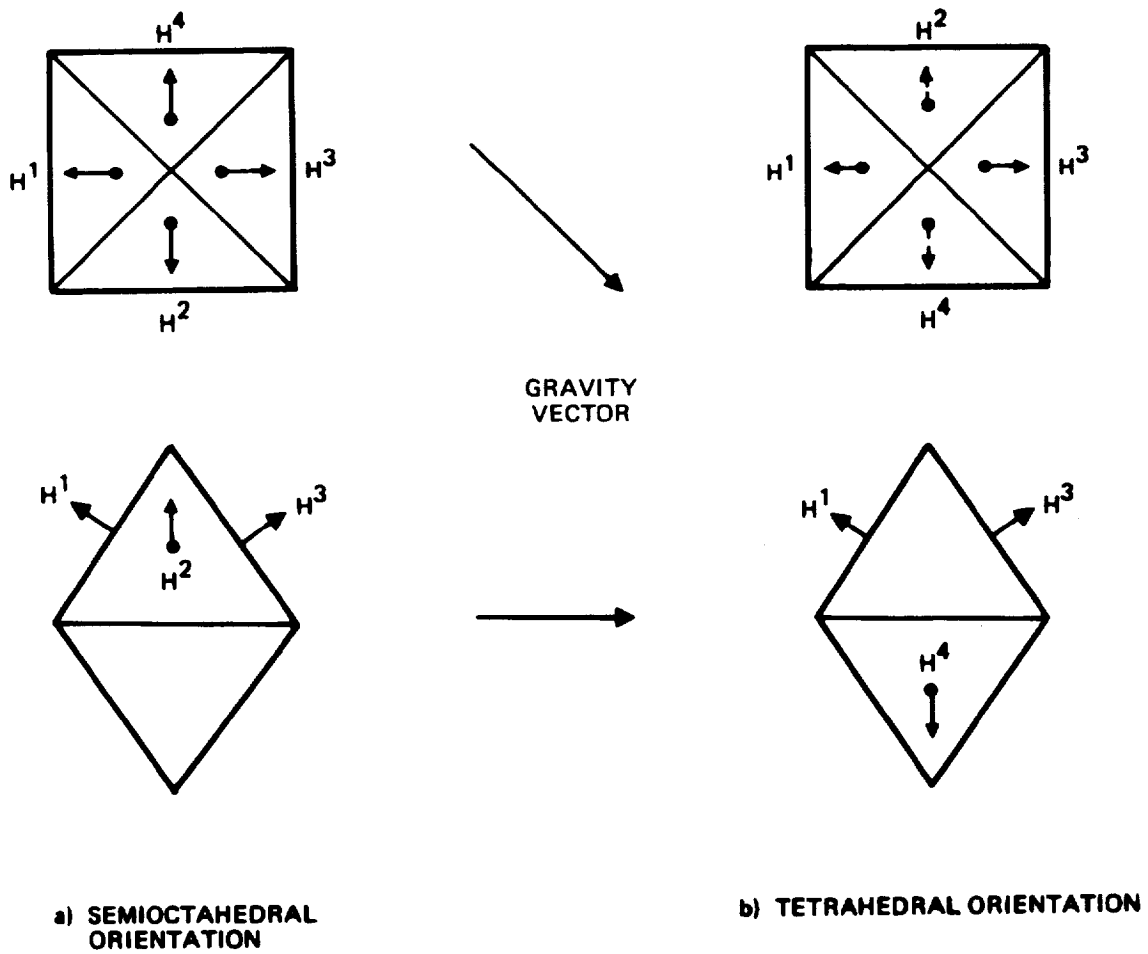


Figure 4-18. Octahedral Spin Axis Orientation

coupled with packaging and computational disadvantages, this non-regular tetrahedral orientation will not be considered further.

Another trade-off which may be made is analagous to the single-degree-of-freedom analysis performed by Pejsa in reference [27]. A gyro's performance is improved when its spin axis is near vertical due to elimination of errors which are a function of acceleration or gravity normal to the spin vector. Since navigation performance is less influenced by error in measurement of angular rate about the local vertical, optimum performance should occur with cone angles smaller than the ideal octahedral 109.46° (assuming the cone axis is vertical). This is particularly true for flight durations of about an hour and thus is potentially applicable to some of the short-haul VTOL missions.

The application under consideration, however, includes nearly continuous position updating from radio aids. The important inertial system parameter is thus rate-of-change of velocity error since this establishes how well velocity may be calibrated from position updates and how well it will hold this calibration during position aid outages. Velocity error is caused by a large number of error sources and small improvements of only one of these, for example g-sensitive bias, will not have a strong impact on net performance. Therefore, the instrument skew angle will be retained in the nominal octahedral orientation. A secondary benefit of this skew angle is that large g-sensitive drifts, one of the normal tuned gimbal gyro failure modes, can be detected and isolated before flight or while flying straight and level rather than just during maneuvers.

Once spin axis skew angles have been selected, sensitive axis definition is largely governed by avoidance of 3-gyro singularities. Since tuned gimbal gyros are sensitive to the g-vector in both axes simultaneously, there is no optimum orientation relative to gravity. The final orientation will thus be selected for ease of computation and packaging.

Figure 4-18 shows the selected relationship between the earth's gravity vector and the gyro spin axes. For this orientation, all gyros are subject to the same portion of earth's gravity.

4.4.5 Accelerometer Geometries

If a SDF accelerometer is to be employed, only 6 accelerometers would be required for fail-op/fail-op capability. They could be oriented in a dodecahedron orientation with redundancy management similar to that performed, for example, on the Draper Labs SIRU. The channel redundancy approach and the subsequent low-cost-of-ownership packaging method described in a subsequent section of this report are lost, however.

Since the proposed packaging arrangement more than compensates for the added accelerometer costs and general computational efficiency is improved, 8 accelerometer axes will be assumed, coincident with their associated gyro sensitive axis.

4.4.6 Parity Equations

Parity equations will now be presented for the semioctahedral spin axis orientation. Equations are based on gyro measurements but are applicable in form to both gyro and accelerometer outputs.

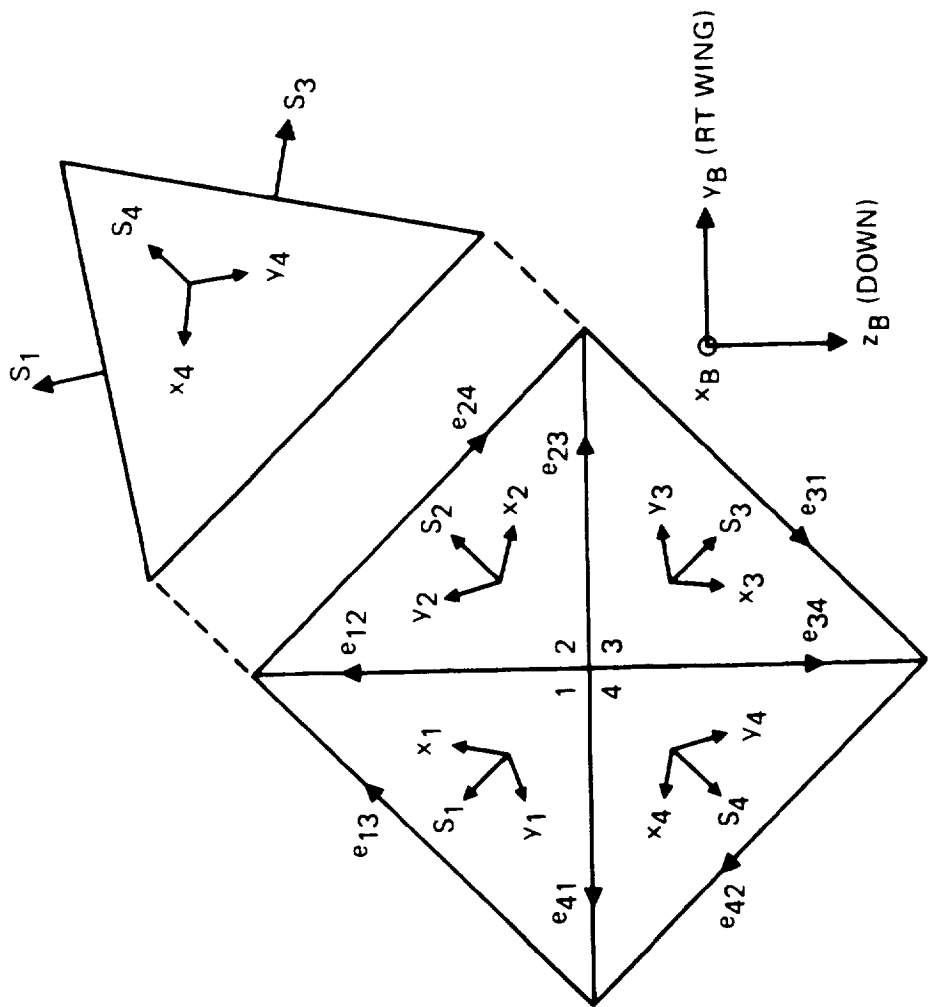
Gyro parity equations and axis definitions are given in figure 4-19. These equations are derived in Appendix B of this report. Gyro number is designated by subscript i or j . The gyro spin vector is identified by the letter S_i and subscripts x_i and y_i define the gyro sensitive axes.

A parity equation, T_{ij} , represents a direct comparison between the angular rate measured by the i and j gyros about some common test direction e_{ij} . The test direction is along the intersection of the measurement planes of the two gyros. These components may be directly compared to remove vehicle rate and thus expose any gyro error rates.

Another form of the parity equations was investigated, namely comparison of a gyro rate to the least-squares solution of the other gyro measurements projected onto the plane of that gyro. The benefits obtained were not found to be sufficiently great compared to simple intersection comparisons to warrant the added computational complexity.

A simple method of isolating a fault to the failed gyro is to integrate (approximately) each parity equation and compare the output against some detection threshold, $\delta\theta$, as shown in figure 4-19. Logic is then employed in the computer such that if two or more equations involving a gyro exceed the threshold, that gyro is classified as failed and switched out of the output computation. Other detection, isolation and switching options are discussed in the next subsections of this report.

A physical interpretation of the parity equations for a tetrahedron may be achieved by means of figure 4-20. The faces of the tetrahedron, #1, #2, #3, and #4, represent the four TDF gyro measurement planes. A parity equation is formed at each edge of the tetrahedron, the intersection of two gyro measurement planes. For example, ω_{1A} is the rate measured by gyro #1 in the A direction and ω_{3A} is the rate measured by gyro #3 in the A direction. Since the two measurements are of the same quantity,



EDGE TESTS

$$T_{ij} = \text{FILTERED} (\bar{\omega}_i - \bar{\omega}_j) \cdot \hat{e}_{ij}$$

$$i, j = \{1, 2, 3, 4; i < j\}$$

FAILURE TESTS

$$F_{ij} = \{ |T_{ij}| > \delta\theta \}$$

GYRO FAILURE LOGIC

(4 - GYRO CASE)

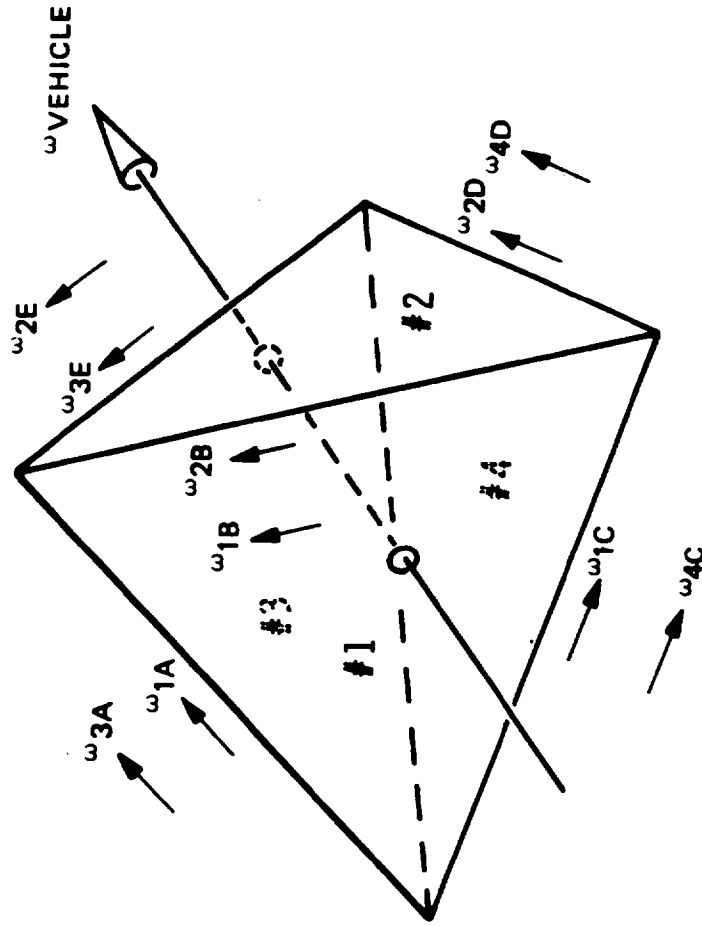
- G₁ = F₁₂ F₁₃ + F₁₂ F₁₄ + F₁₃ F₁₄
- G₂ = F₁₂ F₂₃ + F₁₂ F₂₄ + F₂₃ F₂₄
- G₃ = F₁₃ F₂₃ + F₁₃ F₃₄ + F₂₃ F₃₄
- G₄ = F₁₄ F₂₄ + F₁₄ F₃₄ + F₂₄ F₃₄

(3 GYRO - CASE)

- | | | | |
|--|--|--|--|
| G ₁ FAILED | G ₂ FAILED | G ₃ FAILED | G ₄ FAILED |
| G ₂ = F ₂₃ F ₂₄ | G ₁ = F ₁₃ F ₁₄ | G ₁ = F ₁₂ F ₁₄ | G ₁ = F ₁₂ F ₁₃ |
| G ₃ = F ₂₃ F ₃₄ | G ₃ = F ₁₃ F ₃₄ | G ₂ = F ₁₂ F ₂₄ | G ₂ = F ₁₂ F ₂₃ |
| G ₄ = F ₂₄ F ₃₄ | G ₄ = F ₁₄ F ₃₄ | G ₄ = F ₁₄ F ₂₄ | G ₃ = F ₁₃ F ₂₃ |

SEMI-OCTAHEDRAL GYRO
AXIS ORIENTATION

Figure 4-19. Gyro Parity Equations. Semi-Octahedral Gyro Spin Axis Orientation



PLANES OF TETRAHEDRON REPRESENT TDF GYRO MEASUREMENT PLANES

Figure 4-20. Physical Interpretation of Parity Equations (Tetrahedron Example)

namely the component of the total vehicle angular rate, ω_{VEHICLE} , in the A direction, the two measurements may be differenced to determine measurement error.

Consider a vector measurement error made by gyro #1 in a direction perpendicular to edge B. The ω_{1B} component of rate measured by gyro #1 will therefore not contain any error - it would be a perfect measurement of the component of ω_{VEHICLE} in the B direction. Assuming no errors in gyro #2, the B edge parity equation will thus be zero. The A and C edge parity equations will expose the error, however, and thus fault isolation can be achieved.

If gyro #4 had previously failed, the C, D and F edge parity equations are lost. For the gyro #1 error rate perpendicular to edge B, only the A edge parity equation exceeds its threshold. This condition could also be caused by a gyro #3 error rate perpendicular to edge E. Therefore, this vector direction of gyro error is a fault isolation singularity of the same type described for three orthogonal gyros. Note that no reference was made to the particular tetrahedron angles. This condition applies to any non-collinear orientation of three gyros.

The preceding is not a general proof of the existence of the isolation singularities occurring with 3 TDF gyros, however, since parity equations may take forms other than the tetrahedron edge comparisons. A general proof is obtained with the aid of figure 4-21.

Consider three gyros, the sensitive axes of each represented by a plane surface. The orientation of the two gyro input axes in this plane is immaterial since measurements made in one orientation can be changed to another with a simple coordinate transformation about the spin axis.

Consider next a vehicle angular rate $\bar{\omega}$ along the spin axis of gyro #1 of figure 4-21. The rates sensed by each gyro are the projections of $\bar{\omega}$ onto each measurement plan, where $\bar{\omega}_1 = 0$.

Given the gyro measurements $\bar{\omega}_2$ and $\bar{\omega}_3$, one can reconstruct an estimate of $\bar{\omega}$ along the intersection of two planes - one plane is normal to gyro measurement plane #2 and along $\bar{\omega}_2$, the other plane is normal to gyro measurement plane #3 and along $\bar{\omega}_3$. This reconstructed $\bar{\omega}$ is also consistent with $\bar{\omega}_1 = 0$.

If gyro #3 has an error $\Delta\bar{\omega}_3$ along the direction of $\bar{\omega}_3$, the error in the reconstructed $\bar{\omega}$, $\Delta\bar{\omega}$, is along the direction of $\bar{\omega}$. The same error could have been caused by an error in gyro #2 along

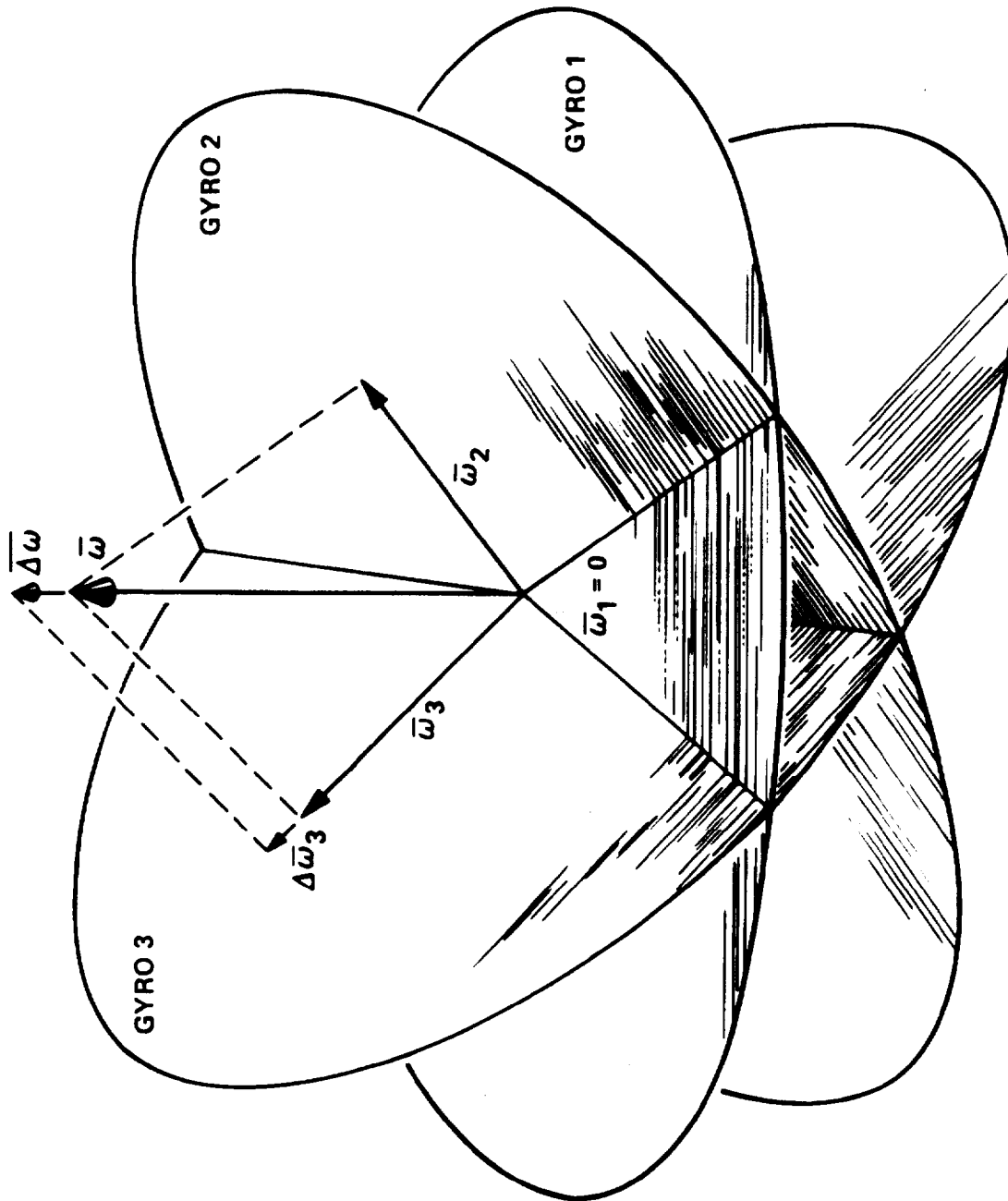


Figure 4-21. Illustration of 3-Gyro Isolation Singularity

the direction of $\bar{\omega}_2$. Gyro #1 cannot contribute information in determining whether $\bar{\Delta\omega}$ was caused by gyro #1 or gyro #2 since $\bar{\Delta\omega}$ is normal to its measurement plane. Therefore, isolation singularities occur in each gyro measurement plane for gyro drift errors along the projections of the other gyro spin axes onto that plane.

Isolation error may again be plotted vs. gyro error direction, figure 4-22, where the origin of the abscissa is the perpendicular to edge B of the tetrahedron. This plot is directly comparable to figure 4-17, for orthogonal gyros. The location of singularities has changed to account for tetrahedral geometry.

If the detection level ϕ_0 is set at the noise level of the gyro, the curve of figure 4-22 indicates that there is an amplification of this basic noise level as a function of gyro drift direction due to geometry, analogous to the geometrical amplification of errors in a LORAN C net. If the allowable isolation error is very large (for example, flight control requirements may tolerate $1^\circ/\text{sec}$. error compared to $0.5^\circ/\text{hr}$ or less for navigation needs) gyro failure modes having drift directions very close to the singular direction can still be isolated since the noise level of inertial-grade gyros is so low. Therefore, the effective angular width of the singularities decreases compared with 360° , and thus the probability of non-isolation decreases. Flight control reliability, then, will be much higher than navigation reliability. This relationship will be expanded upon in later sections of this report.

Parity equations for the semioctahedron form of the tetrahedron, figure 4-19, are essentially the same as for a regular tetrahedron. The parity equations are again formed at the edges of the polyhedron. Note that the intersection between gyros i and k is parallel to the upper and lower horizontal edges. Each face of the octahedron is still composed of an equilateral triangle, so the behavior of parity equations is identical to the standard tetrahedron. The selection of gyro sensitive axes has been made to avoid coincidence with any possible singularity.

It is interesting to review the reduced cone-angle trade-off of paragraph 4.4.4 in light of the above interpretation. Figure 4-23 illustrates a flattened semioctahedron. Faces of the octahedron now deviate from equilateral triangles, approaching right isosceles triangles. Clearly navigation errors will deteriorate due to geometrical dilution of measurements along an axis out of the peak of the pyramid. If this axis is made the aircraft yaw axis, net navigation performance might be acceptable.

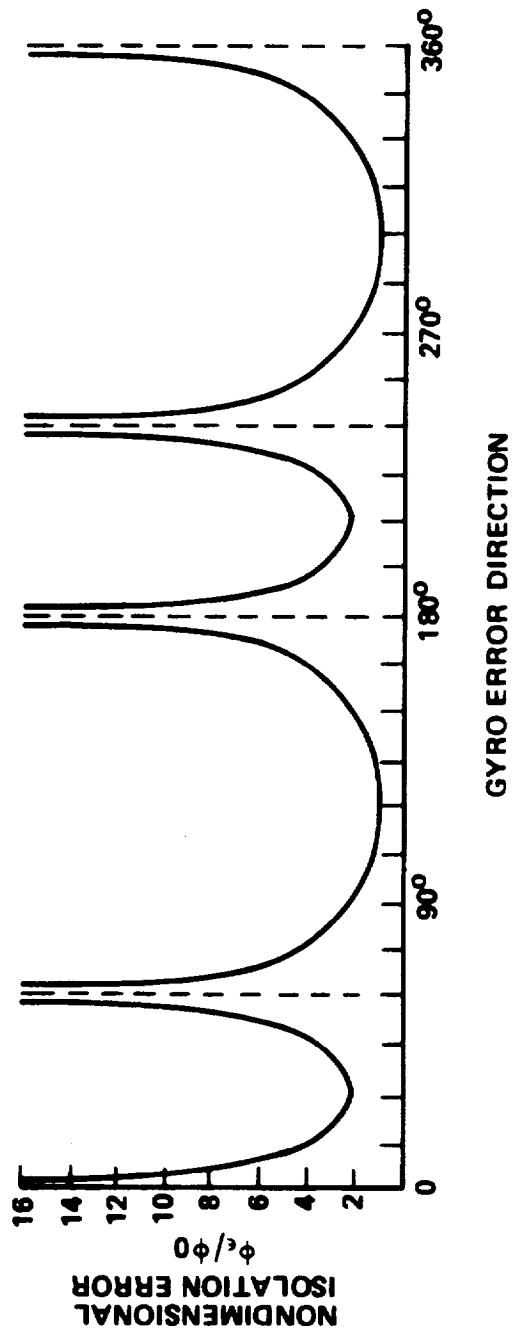


Figure 4-22. Failure Isolation Error vs Direction of Gyro Error
(3 of 4 Tetrahedral TDF Gyro Spin Axes)

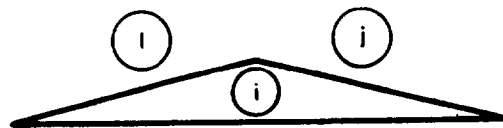
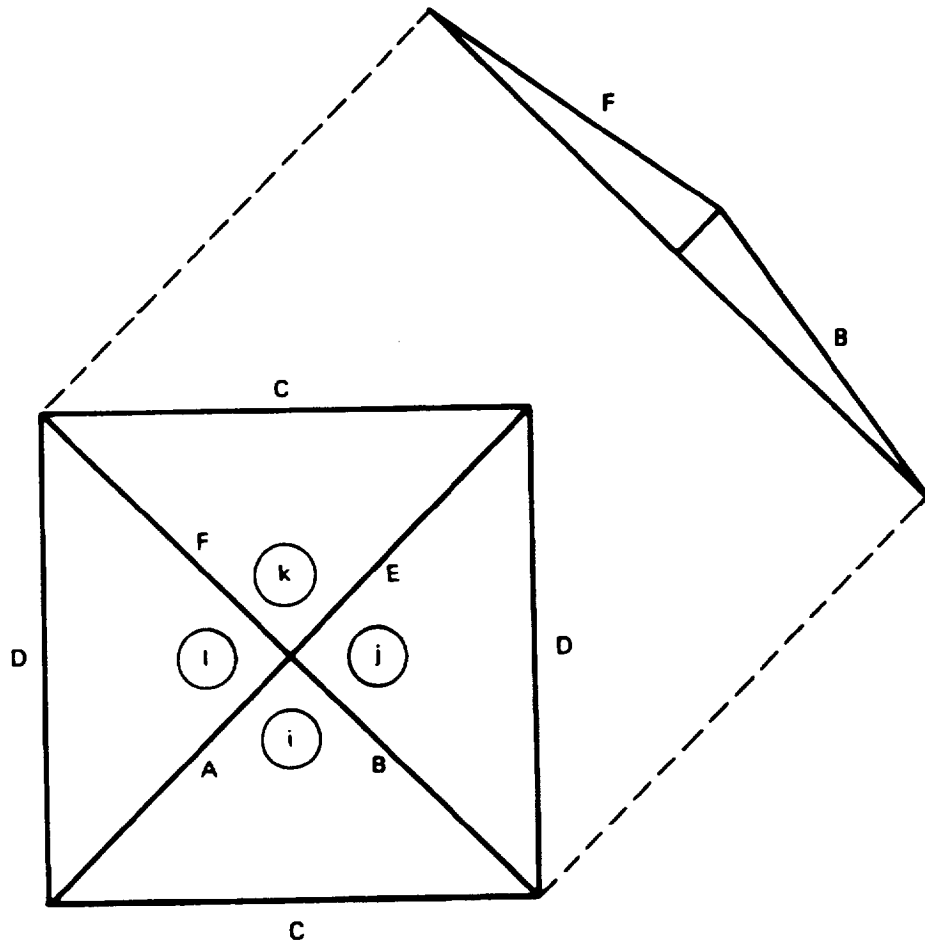


Figure 4-23. Flattened Semi-Octahedron

Parity equations for this geometry would be very similar to those described for the regular octahedron. 3-gyro singularities appear as before except at different angles. Considering gyro i in figure 4-23, singularities are perpendicular to edges A and B if gyro k has failed, and perpendicular to edges A and C if gyro j has failed.

The only apparent benefit from this geometry is that an improved reasonableness test could be performed during the remote possibility of a large gyro failure along a singular direction during 3-gyro operation. Consider a prior k-gyro failure and an i-gyro error in a direction parallel to B. The error shows up in the B edge test with gyro j, but not in the A edge test with gyro l. Therefore, the error is detected but not isolated to either the i or j gyro. However, because the B and F edges are nearly colinear, a crude comparison can be made between the i and l gyros, limited by how much aircraft yaw rate can be coupled through the angle between the B and F edges. If the measurement difference is greater than the maximum possible coupled yaw rate, fault isolation between i and j gyros can be made.

As described in paragraph 4.4.4, the disadvantages in computational efficiency and packaging incurred for a reduced cone angle outweigh the minor fault isolation improvement achieved for a remote failure mode. Therefore the regular octahedron skew angle will be retained.

4.4.7 Error Detection and Isolation Methods

Since the outputs from the gyros and accelerometers are incremental in nature, angle and velocity increments, respectively, determination of angular rate and linear acceleration would require differentiation of these sensed values in the computer. This processing method is impractical due to amplification of noise and data quantization which would lead to a high false alarm rate in the redundancy management.

Integration of parity equations produces the desired smoothing. Error detection would then be on the basis of angle and velocity. However, accelerometers and gyros contain a variety of normal-mode errors, including bias. Integration of these normal bias errors over a long period of time tends to obscure failure-error buildups. A simple lag filter washes out the bias errors while acting as an integrator over short periods of time. Use of a simple, low-pass digital filter was used on SIRU, [20], [23], as part of the TSE (total squared error) FDI (failure detection and isolation) and is also selected for this study.

A simple means of processing the "integrated" parity equations is to compare each individually against a predetermined threshold.

When thresholds are exceeded, a logic truth table such as that shown in paragraph 4.4.3 is then used to determine the failed gyro.

Other methods involving a combination of parity equations have been described in the literature for SDF gyros, such as the TSE [23], Minimax [22], Maximum Likelihood [25], Kalman-Bucy and others [26]. These cannot be directly employed for TDF gyros except conceptually.

In order to view drawbacks of the simple table look-up method, consider again figure 4-22. This curve may be considered as a boundary or threshold for error detection for a 3-gyro condition, using uncombined parity equations. If ϕ_0 is taken to be the noise level of the gyro, the error detection limit must be set well enough above the noise to avoid false alarms and missed alarms. (NOTE: The curve of figure 4-22 assumes that only one gyro has an error and is thus incomplete. It is used for illustration only.) Figure 4-24a is a polar plot of figure 4-22. A $1/\sin$ function is simply a straight line on a polar plot.

Direct use of parity equations in the 4-gyro case, with fault detection and isolation based on two equations exceeding detection limits, is equivalent to processing gyro data using three gyros at a time. Thus the detection threshold versus gyro error direction for the full four-gyro set may be derived by superposition of three curves of the form of figure 4-24a, each rotated by 60° from the rest. This superposition process is illustrated in figure 4-24b.

The inner portion of each of the plots of figure 4-24b represents the parity equation pair which produces the smallest isolation error for a given gyro drift and is thus the pair with which the error is first detected. A composite of the isolation error which considers this isolation logic is shown in figure 4-24c.

For both the four and three gyro conditions, it is clear that the isolation threshold is not constant as a function of the angle of the gyro drift. If the threshold is set at the largest value allowed by system requirements and this is very close to the point of the star for four gyros, system errors smaller than this value produce a failure indication a significant portion of time. These failure indications might still be arbitrarily classified as "failure" conditions even though real errors are smaller than the system error limit, so would not contribute to false alarm rate.

Real false alarm rate could be reduced, however, by processing parity equations to achieve a more constant detection level vs failure angle and make full use of the information contained in these equations. Note that at the points of the star of figure 4-24c, all three parity equations exceed the threshold but in

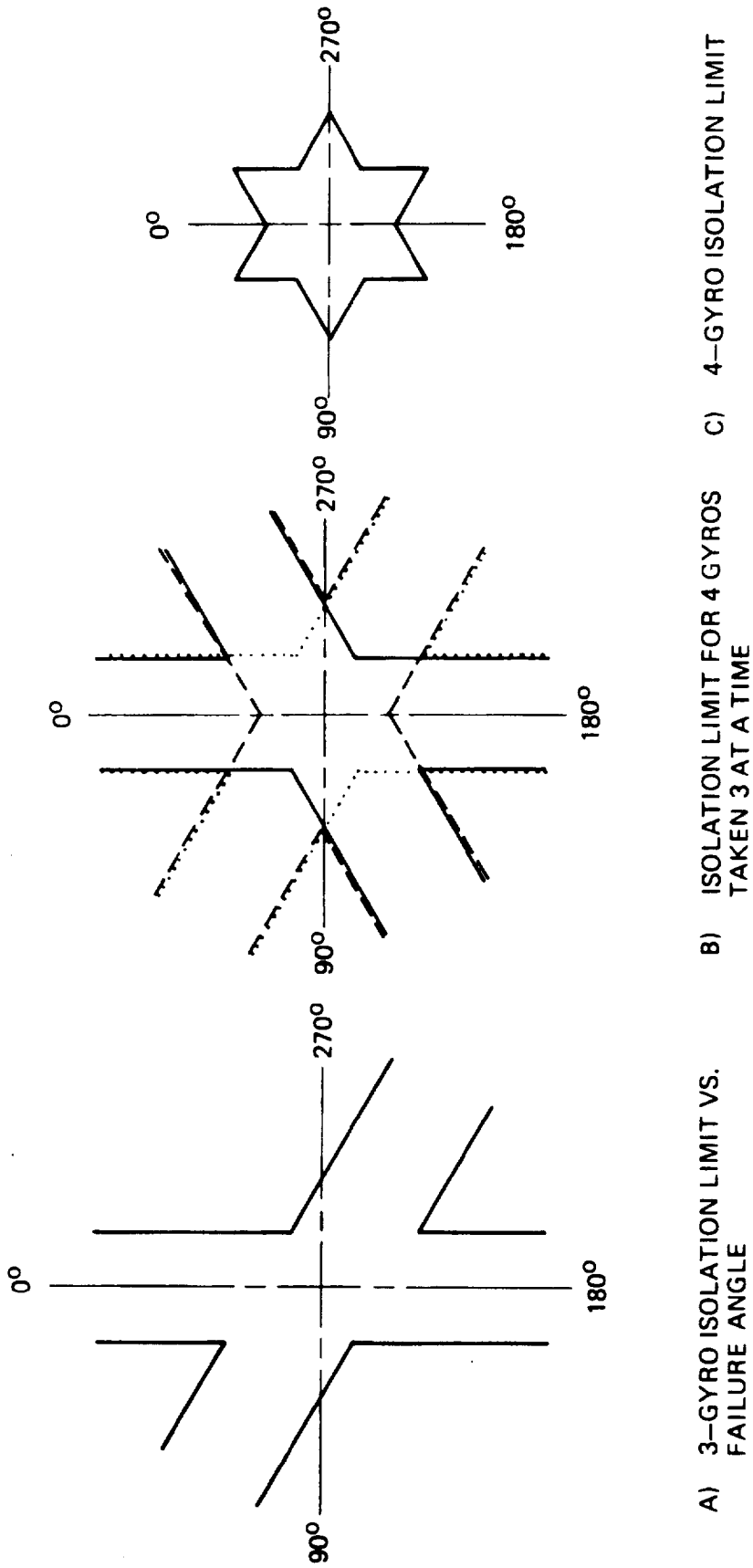


Figure 4-24. Polar Plots of Isolation Error vs Gyro Drift Direction 3 and 4 TDF Gyros

reality only two are being used. Better processing could achieve either tighter detection limits or reduced false alarm/missed alarm rates.

When large gyro errors occur, speed of detection is important to avoid transients in the aircraft flight control system. Due to the simplicity of the table look-up method which operates on uncombined parity equations, a high computer iteration rate can be used for this test. Since a combination of parity equations is primarily applicable to detection and isolation of small errors which takes a long time anyway, such processing can be performed at a low rate with little impact on computer duty cycle. Thus, inclusion of both methods is desirable. The derivation of parity equation combinations is given in paragraph 5.3 of this report.

Methods have been proposed in the literature [21] for classifying a gyro drift as either a step or ramp function and then applying a compensation to the faulty instrument to bring it back to a useful state. This approach may have application to space systems where vehicle maneuvers are limited. In an aircraft system, however, normal turns produce time-varying gyro errors since scale-factor, g-sensitivity, and axis alignment error coefficients are exercised. Therefore, this approach is felt to be inapplicable to the aircraft redundant strapdown system.

Significant errors occur during a turn due to deviation of each gyro scale factor from its nominal value. For a $3^\circ/\text{sec}$ turn and 100 ppm scale factor error, there is a gyro drift error of $1^\circ/\text{hr}$ for the duration of the turn. A 180° turn lasts 60 seconds and results in an error buildup of 1 arc minute if the turn rate is about the gyro sensitive axis. Considering that 100 ppm is a typical 1-sigma value and near-continuous turning may need to be provided for, scale factor effects need to be either accommodated or compensated.

The study program covered by this report includes only a brief examination of scale factor compensation in paragraph 5.3. Insufficient time was available for a thorough analysis. This appears to be worth further study, however, to allow a reduction of gyro drift detection levels. The effects of other maneuver-dependent errors must also be considered in determining the effectiveness of scale-factor compensation, but due to the magnitude of the scale factor effect, compensation appears a promising technique for improving error detection and isolation sensitivity.

There is a finite probability that two gyro failures can occur simultaneously. This is particularly true for small failures since several minutes of time may be needed to detect and isolate a given drift. Provisions should be included in FDI algorithms

for multiple failure modes where practical. Excessive computation should be avoided due to the low probability of occurrence. There exists a dual failure mode condition where the parity equations remain satisfied (a failure is not detected). For this situation to occur the two simultaneous failures need to be equal in amplitude and each be in a specific vector direction. The joint probability that these events all occur simultaneously is considerably less than the total system failure probability and is estimated in paragraph 5.3.

4.4.8 Switching Methods

Once an error has been detected and isolated, further action is required to prevent the erroneous information from affecting system outputs. The most obvious method is to simply switch out the gyro from all computations. Consideration should be given to minimizing switching transients in flight control functions, however. Weighting schemes such as described in [30] may need to be considered if transients are troublesome.

Vehicle angular rate and linear acceleration, in body coordinates, are required as outputs. Computer switching from instrument to instrument could cause very small transients in these outputs. Error detection levels, however, are set orders of magnitude smaller than the normal accuracy required of these outputs. Therefore, switching transients are insignificant.

Attitude, heading, velocity, and position outputs are one or more integrations away from the instruments. Switching of instruments thus does not cause transients in these outputs. The only way in which transients could occur is if switching is performed directly on these functions or during reinitialization modes during error recovery. This is discussed in paragraph 4.5.1 relative to the software mechanization. Weighted combinations of instrument outputs to eliminate transients therefore is not needed.

A secondary purpose of combining instrument outputs in a weighted manner is to reduce system error. Monitoring of parity equations during normal operation yields some information regarding relative performance of instruments. Since parity equations are strongly influenced by noise during these conditions, weighting factors must be determined from error probabilities. This technique is of value during very soft failures, near the instrument noise characteristics, and during soft failure modes during 3-gyro operation. Simplified methods should be used in order to limit the computer penalties since system performance benefits derived from this mechanization are subtle.

Once a gyro has been classified as failed, it should continue being monitored, but not be involved in output computations. It could then be reinstated into the computation if required. Thus false alarms due to noise are less important since use of the gyro is not lost for the full duration of the flight. Also, a soft-failed gyro may still be good enough to resolve the 3-gyro isolation ambiguity in the rare event that it occurs. Furthermore, use of a marginal gyro for monitoring and backup following a second failure is better than having none at all.

If a gyro failure having a constant direction is detected, should the entire gyro be switched out of the computation, or should the data normal to the failure direction be retained? A special case of this question is whether or not it is necessary to isolate failures to a specific instrument or is it sufficient to merely eliminate the bad data. This is of particular interest when a failure is along one of the 3-gyro isolation singularities.

Figure 4-25 may be used to illustrate this procedure. Consider gyro #4 to have previously failed, thus leaving the three edge parity equations A, B, and C. Assume that the A edge parity equation is indicating a failure but that B and C are zero. The failure must be either gyro #1 or gyro #2 for this condition to be true. Therefore gyro #3 is good. The two possible error vectors which could cause this condition are perpendicular to edge B for gyro #1 or perpendicular to edge C for gyro #2, as shown. The gyro measurements perpendicular to these possible error vectors in the measurement planes are parallel to gyro #3. Thus an unambiguous measurement normal to the known good gyro is unavailable.

There are some gyro failure modes where one axis exhibits poor performance but the other axis is still good. An electronics scale factor shift is an example. This is a sufficiently rare condition that special software provisions for partial gyro data retention do not appear warranted. Therefore, when a gyro exhibits a failure drift, it will be completely switched out of the output computations.

Since the two accelerometer axes are implemented with two independent instruments, failure modes are also independent except when it involves some common function such as the power supply. A very minor increase in system reliability could be obtained by switching out one accelerometer when a failure is indicated. On a preliminary basis, however, both axes are switched for software simplicity.

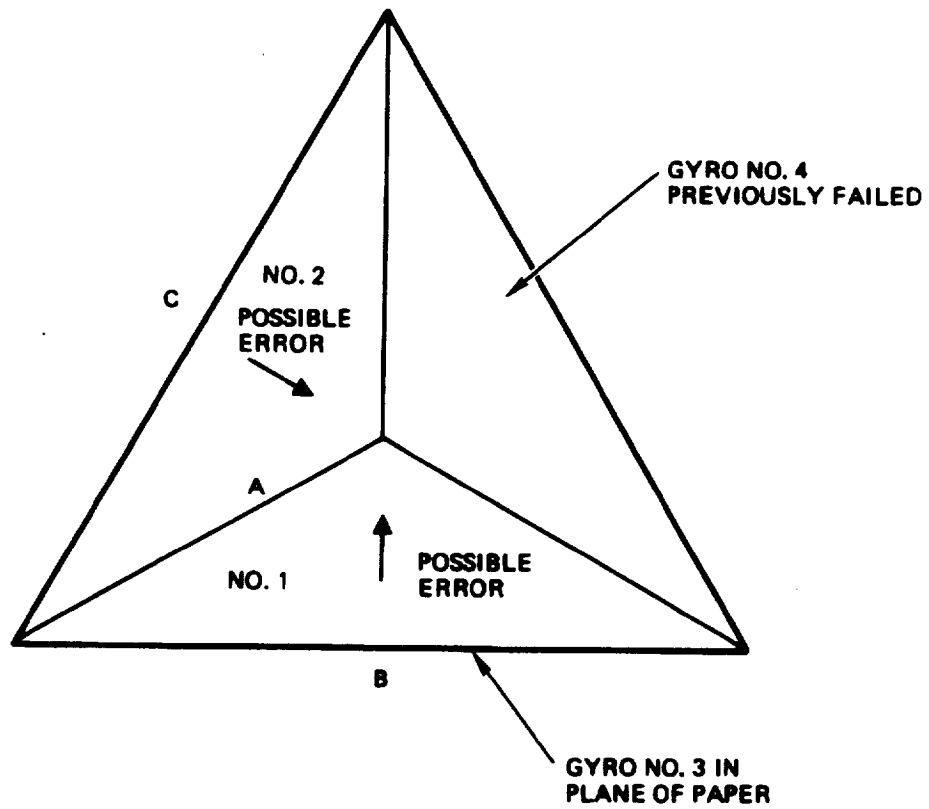


Figure 4-25. Tetrahedron Illustration of 3-Gyro Ambiguity.

4.4.9 Failure Coverage

Determination of failure coverage depends strongly upon definition of a failure. In other words, what output errors (1 sigma, 3 sigma, 6 sigma) result in a failure condition which jeopardizes flight safety or proper completion of the flight, and how long may the errors be present (is time-rmsing applicable)? The instrument errors which can cause this condition must then be derived.

Derivation of the definition of an instrument failure is complicated by the fact that system performance requirements include updates from an external radio aid using some form of combinational filter. Gyro drift requirements are very much a function of the accuracy of the radio aid and the sophistication of the filter.

In a redundant system, component error budgeting is influenced by error detection and isolation requirements relative to the allowable system errors just prior to switching-out a "failed" component. Instrument tolerances may need to be tighter for a redundant system than for a single-string system since failure detection limits must be set much higher than normal component tolerances (e.g., 5 sigma) to limit false alarms. This statement is somewhat contrary to the normally accepted fact that system accuracy is improved slightly over a non-redundant system by averaging the redundant data. This accuracy improvement only applies to the zero-failure condition, however. Since system accuracy must be undegraded after two failures, improved zero-failure performance is of minor overall benefit.

Use of probabilistic weighting coefficients derived from parity equations, parity equation combination processing, and scale factor compensation described in paragraphs 4.4.7 and 4.4.8 can all tend to offset the degradation of system performance just prior to switching-out a failed component. Thus these techniques are very useful in reducing the impact of redundancy management on the instrument error budget while retaining low false alarm rate and high failure coverage.

A full analysis considering the interaction between system performance, redundancy management algorithms and component error budgets, is beyond the scope of this preliminary design report. The error budget is determined essentially from single-string requirements (with a simple filter and some assumed radio noise model). Error detection and isolation thresholds are set to be large enough to avoid high false and missed alarm rates, with little consideration of pre-alarm performance transients. Means of recovery from these small transients to reduce their time duration, however, will be included in the computer mechanization.

The coverage of the first failure will be essentially unity since it will be designed to be so. All coordinates have sufficient measurement information for completely unambiguous "failure" detection and isolation. The coverage of the second failure must consider the effects of the 3-gyro isolation singularity coupled with the full spectrum of gyro failure modes.

If a large number of redundant strapdown systems were operated for a long period of time, there would be some distribution of the aggregate failures between hard failures, detectable by simple self-test, and soft failures, those needing redundancy management. The soft failures would also be distributed among a variety of failure modes, and only a portion of these would be subject to the 3-gyro isolation singularity. Table 4-2 shows a hypothetical distribution of system failures. While not based on real data, it is useful in approximating coverage of the second failure.

TABLE 4-2. HYPOTHETICAL SYSTEM FAILURE DISTRIBUTION

	Nav. Accuracy (%)	Flight Control Accuracy (%)
Hard Failures	90	95
Soft Failures	10	5
Electronics	2	
Accelerometer	2	1
Gyro	6	4
Variable Direction	4	2
Constant Direction	2	2
Non-Singular	1.5	1.98
Singular	0.5	0.02

Self-test is commonly felt to be effective for 90-95% of failure modes. There are many more failure modes producing small accuracy degradation of navigation variables than flight control variables where a few degrees per second may be acceptable. Thus it is assumed that the split between hard and soft failures is 90/10 for navigation performance and 95/5 for flight control. The slightly better MTBF for flight control channel reliability will be ignored.

Soft failures are distributed between gyros, accelerometers, and the remaining electronics. The gyros are assigned a major share since they are generally of more complex design. The gyro failures are then distributed between those whose vector direction is constant and those whose vector direction varies with time. Since a failure mode generally produces an uncontrolled condition and since many failures are flight-path dependent, it is assumed that most failures fall into this latter category. If the gyro failure vector direction varies, the failure is not subject to the 3-gyro isolation singularity.

Of the remaining constant-direction failures, only a portion of them fall into the isolation singularity bands. First, there is some probability density distribution for gyros as a function of failure angle. Figure 4-26 shows the general form such a distribution might take, in polar coordinates. Again, real world data is unavailable for an accurate plot.

Peaks are expected to occur in the failure probability distribution in the vicinity of the gyro input axes since there are a number of components in the electronics and gyro specifically related to axes. The integral of probability density over 360° , excluding the vicinity of input axes, may be called the probability of a dual axis failure. In general, the probability of a dual axis failure is expected to be higher than the probability of an input axis failure since there is a strong interaction between axes of a TDF gyro.

The probability of a failure along some arbitrary direction, ψ_A , within a narrow angular band, $\Delta\psi$, however, is expected to be lower than the probability of failure along an input axis, since dual-axis failure modes are distributed among a wide number of possible directions. This rationale leads to the conclusion that gyro input axes should not be coincident with any possible 3-gyro isolation singular direction. The exact form of the probability density distribution is unknown. It is assumed uniform between input axes for simplicity.

The effective angular width of the 3-gyro isolation singularity is smaller for large allowable errors (flight control) than for

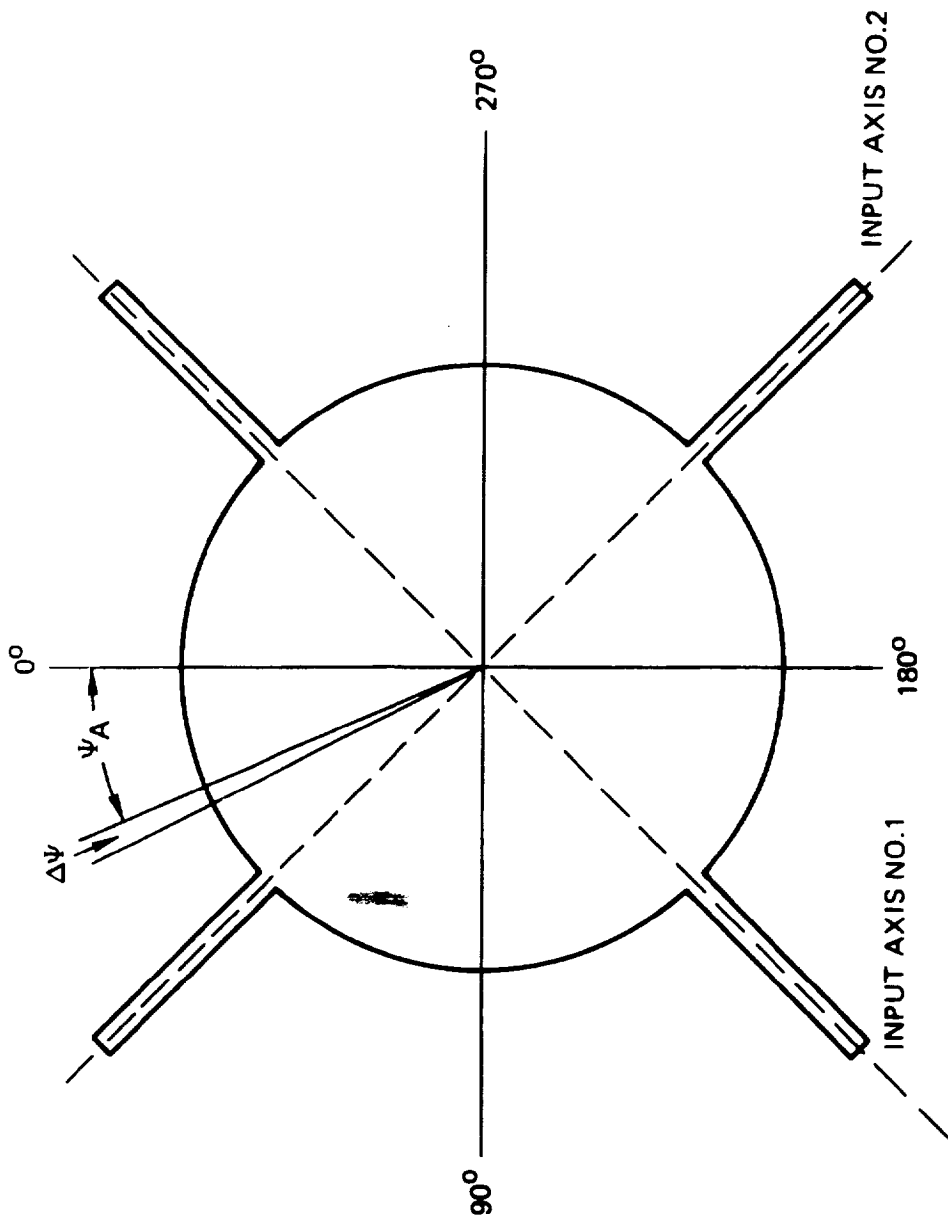


Figure 4-26. Hypothetical Polar Plot of Soft-Failure Probability Density ($P/\Delta\psi$) vs. Error Direction (ψ)

small allowable errors. This may be seen with the aid of figure 4-27, a repeat of the noise boundary curve of figure 4-24a.

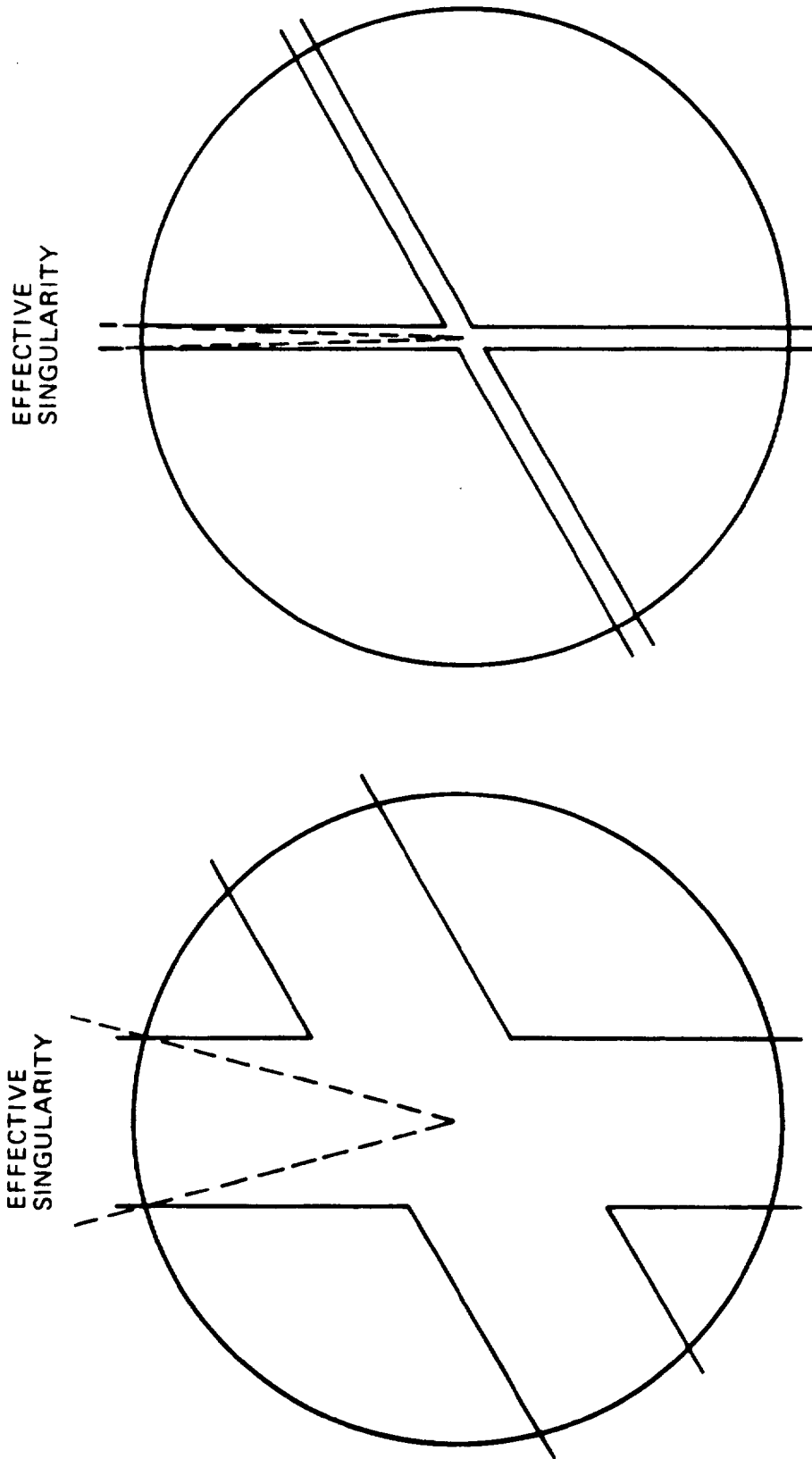
When error detection limits are set very close to the system noise level, as would be required to bound navigation errors (position/velocity), the effective isolation singularity is fairly broad, as shown in figure 4-27a. For large allowable errors, orders of magnitude larger than the normal instrument noise level, the effective singularity becomes quite narrow, as shown in figure 4-27b.

When this view of effective singularity width is coupled with the gyro failure probability density distribution previously described, one can see that the percentage of failures occurring within the isolation singularities reduces considerably for large allowable errors, thus increasing coverage. Hypothetical distributions are shown in table 4-2. No attempt is made to rigorously quantify these functions since net probability is well within LaRC requirements.

It may be noted that some additional external data would be useful in resolving the rare occurrence of the isolation ambiguity. Since radio aids are planned in the LaRC scenario, they could be applied toward further improvement in system reliability. The computer mechanization will be directed toward allowing this to be done, however its application will not be used in the reliability calculation.

There is some variation of coverage with time since many of the terms of the instrument error models are a function of flight dynamics. This consideration is of particular concern during ground alignment. System errors due to gyro scale factor and vibration-dependent errors are much smaller at this time than when the aircraft is stationary. On the other hand, failure tolerances on the parity equations can be tightened up during this condition for better detectability of static errors. Since inertial instruments are of such high quality compared to flight-control requirements, errors which would directly affect flight safety can be adequately detected on the ground. The remaining, navigation degradation errors would generally be detected during lift-off.

It is highly desirable to detect errors of this type as early as possible before takeoff to allow maintenance action. Provision for accentuating these errors by hardware means shortly after power is applied to the system should be investigated during the system design phase.



a) NAVIGATION DETECTION LEVEL

b) FLIGHT CONTROL DETECTION LEVEL

Figure 4-27. Polar Plots of Isolation Error vs Gyro Drift Direction

4.5 Software Trade-offs

4.5.1 Redundancy Management Software Design

Consideration has been given to a classical approach where all instrument data are combined in each computer prior to output processing. The computer mechanization which has been selected, however, uses instruments in pairs in order to achieve better overall redundancy management, including radio aid contributions, and to allow recovery from system error build-ups during the isolation process. This includes recovery from isolation errors which may be amplified by the 3-gyro isolation singularities.

The method generally proposed for processing of redundant instrument data following redundancy management, is to combine the redundant measurements in a least-squares fashion prior to use. Net accuracy is thus better than a single-string configuration. Equations for combining gyro or accelerometer data when oriented in a tetrahedral or octahedral geometry have been derived for 4, 3, and 2 TDF units, and are presented in Appendix F.

With this approach, each of the four computers is solving the same problem. This is then consistent with fault-tolerant computer methods. Each processor solves the same problem in approximate synchronization, each output should thus be identical, and outputs can be compared bit-by-bit with simple hardware devices for computer fault detection and isolation. Computer problems can thus be easily isolated.

A major drawback of using combined instrument data in the output solutions, is that a degraded instrument which escapes detection or isolation in parity equation processing is combined with good instruments. The opportunity of resolving the occasional 3-gyro isolation singularity or detecting performance degradation less than INS thresholds with radio aid data is thus lost, or at least considerably complicated. INS degradation would be detected when compared against radio data, but determination of which unit is marginal to initiate maintenance action may be extremely difficult.

In the assumed system mechanization, each computer output is sent to other avionics elements individually. This implies that some other avionics system performs a comparison between INS outputs and radio aid data. Since this involves an arithmetic process, this further means that the voting between the four redundant strapdown outputs must utilize arithmetic rather than simple bit-by-bit comparisons.

In other avionics implementations, voted or weighted combinations of redundant data could be derived in a using device such as an actuator or display using modern microprocessor technology. Therefore, there is no firm requirement for compatibility with

simple bit-by-bit voters. Such compatibility could be achieved, however, with a final voting/combining subroutine in each redundant INS computer. Since each computer iteration is synchronized, all computer outputs can be made identical in software prior to transmission to external voters. For the purposes of this study, however, it is assumed that external systems contain arithmetic capability.

Figure 4-28 shows a preferred 4-computer implementation. Each computer accepts data from one TDF gyro and two accelerometers. Compensation of various instrument parameters is then performed, including transformation from the skewed instrument coordinate system into aircraft body axes. Each computer solves this compensation and transformation for the instruments of only one channel. Since these are high rate, time-consuming computations, net computer speed requirements are significantly reduced from an equal-computer approach.

At this point, each computer receives corrected gyro and accelerometer data from the other three computers, solves parity equations and performs associated FDI processing. There would be only minor savings in splitting parity equations and processing between the four computers since they are not complex. Design equations are then solved which determine a least squares solution of two TDF gyro rate measurements (4 SDF accelerometers) in body coordinates. From this point on, the solution is that of a conventional strapdown INS with quaternion conversion to the navigation coordinate system followed by conventional inertial navigation equations.

Four separate navigation solutions are thus being performed in the computer array, each based on a different pair of gyros. All six possible two-gyro combinations are not needed since radio data can isolate one marginal instrument with only four. The six solutions would be desirable for simple detection and isolation of a condition where two gyros degrade simultaneously but the increase in computer speed needed to perform the additional solutions does not appear warranted.

The logic selected for determination of which gyro pair is to be used in each of the four output computations is shown in figure 4-28 in the Design Equation block. The gyro/accelerometers of a given channel are always used in that channel's design equations. The second gyro/accelerometer-pair is that from the next sequential channel satisfying the parity equations. Thus, the first choice for channel 1 is gyros 1 and 2. If gyro 2 fails, gyro 3 is used, if gyro 3 fails 4 is used.

Table 4-3 illustrates the alternate selections for various failure modes. Note that following two gyro/accelerometer-pair failures, two computers are operating on the same gyro pair.

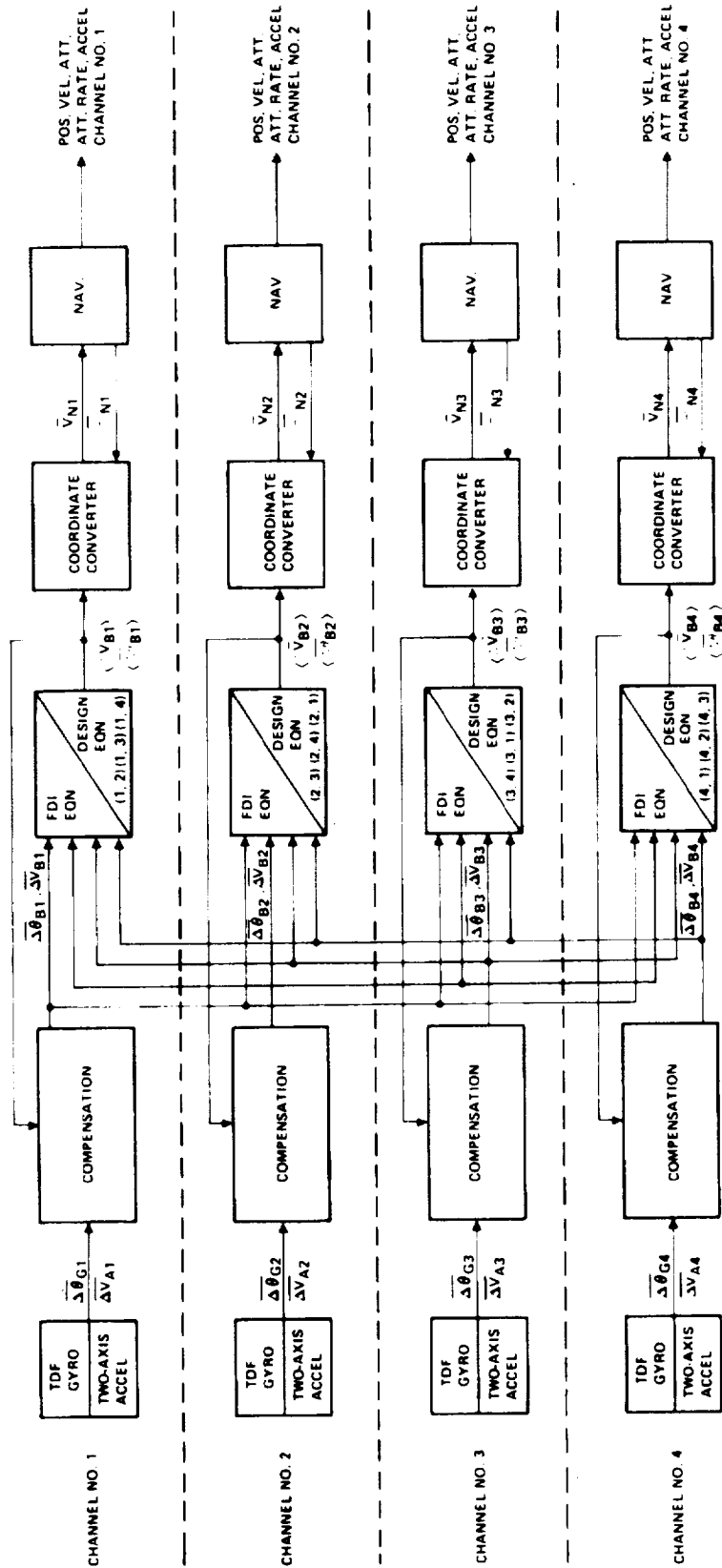


Figure 4-28. 4-Channel Software Mechanization

TABLE 4-3. GYRO PAIR SELECTION VS FAILURE INDICATION

CHAN	0	1	2	3	4	1/2	1/3	1/4	2/3	2/4	3/4
1	1,2	1,2	<u>1,3</u>	1,2	1,2	<u>1,3</u>	1,2	1,2	<u>1,4</u>	<u>1,3</u>	1,2
2	2,3	2,3	2,3	<u>2,4</u>	2,3	2,3	<u>2,4</u>	2,3	<u>2,4</u>	2,3	<u>2,1</u>
3	3,4	3,4	3,4	3,4	<u>3,1</u>	3,4	3,4	<u>3,2</u>	3,4	<u>3,1</u>	<u>3,1</u>
4	4,1	<u>4,2</u>	4,1	4,1	4,1	<u>4,3</u>	<u>4,2</u>	<u>4,2</u>	4,1	4,1	4,1

This gives a measure of fail-safe error detection capability with a limited third-fail-op-mode, depending upon self-test failure isolation efficiency.

Further pair-selection options could be employed. For example, if gyros 3 and 4 have failed, computers 3 and 4 could also perform the 1, 2 gyro solutions, presumably as backup to computers 1 and 2. However, since computers 1 and 2 are in series with gyros 1 and 2 for I/O and compensation, this backup capability is of no practical value. Gyro/accelerometer-to-computer I/O would need to be expanded for this modular type of redundancy and, as discussed in paragraph 4.3, is not needed to meet LaRC reliability requirements. Applications requiring considerably higher reliability may need the added I/O and software modes.

In the normal, 4-channel or 3-channel modes, degradation of an instrument affects two channels. The effect is not necessarily of equal magnitude in each channel since a gyro error may be averaged with its mate's output in one channel (if the error is in a direction parallel to the appropriate tetrahedron edge) but enter more strongly in the other channel since less averaging applies. The error is visible relative to radio data in each channel involved so the marginal gyro number can be easily deduced. It is assumed that the external computer will indicate the marginal instrument to the INS for use in its redundancy management and to alert maintenance personnel.

Behavior of position and velocity outputs for operation in the 3-gyro isolation singularities can be obtained by considering an orthogonal triad with a gyro error along one of the spin axes (one of the 3-gyro isolation singular directions). One can deduce that for the previous mechanization consisting of paired solutions, there will be three outputs of position and velocity. The correct solution, using two good gyros, is either the largest or the smallest position/velocity calculation depending

on the sign of the error. The computer using both ambiguous gyros is the exact middle solution. The computer using the known good gyro and the bad (but non-isolatable) gyro is either smallest or largest. Since the differences between the middle solution and either end are identical, no fault isolation can be made on a self-contained basis. Assuming two perfect gyros, the middle solution has exactly half the error of the worst solution since the error of the bad gyro is averaged with the good gyro. A similar result is expected with three non-orthogonal gyros. As the direction of the gyro error changes away from the singular direction the two "bad" solutions approach each other.

In all cases, radio aid data can be used to determine the bad gyro, assuming errors are large enough. Therefore, the size of position or velocity updates may be used to decide which channel should be used in the final display or steering calculation, viz., the channel requiring the smallest updates. Averaging of this decision is probably needed to avoid continuous switching between channels. During periods of radio aid loss, the last-selected channel should continue in use since it probably has the lowest rate-of-change of error. Monitoring of channel failure indications and errors between channels should continue in the external computer, however, so that switchover can be performed rapidly upon detection of a channel failure. The criteria for such a switchover are not defined at this time.

Rapid detection of errors within the redundant strapdown INS is needed to avoid large transients in outputs, particularly those used by the flight control system, and to limit the build-up of errors which might be retained within the INS and thus affect the remainder of the flight. From the computer mechanization diagram of figure 4-28, it can be seen that errors are monitored and switched prior to their use in the design equations. This assures that excessive errors are not propagated in the coordinate transformation and navigation solutions. Also parity equation monitoring is performed at the full strapdown integration rate of 64 iterations per second, providing error detection and isolation faster than the output rate of 32 per second.

Reinitialization of a computer can be performed following large error build-up, based on data from one of the other working computers. These data consist of quaternions, vehicle velocity and direction cosines. Other functions may be computed from these variables once they are available. The conditions for which initialization would be performed are:

- a. following replacement of a bad channel on the ground so that the flight need not be delayed for a complete gyrocompass alignment, or

- b. following a gyro or accelerometer performance recovery, to correct for the error build-ups which occurred during temporarily poor operation.

Another condition for which re-initialization might be considered is following elimination of any instrument from the inertial calculation due to errors. Since there is at least one channel in operation which does not contain errors due to the failure, the channel which has reconfigured could eliminate the quaternion or navigation errors which accumulated during the detection/isolation process.

There is some risk to this process, however, since a single computer failure could cause major errors in two channels if the failure occurred during the brief period of time between data sampling for parity equations and data sampling for reinitialization. Using parity and initialization data from the same iteration may eliminate the extremely low probability of a dual-channel failure mode. The decision of whether to employ this form of reinitialization is deferred until the final design phase since many hardware details must first be established.

4.5.2 Radio Aid Updates

Assumptions have been made regarding radio aid information, accuracy, and filter characteristics. These assumptions are:

- a. Radio aid produces geodetic position information with no geometric dilution, as with Loran C, and with no correlation to INS heading errors, as with airborne radar.
- b. Radio aid data does not include direct position rate information (GPS is not considered).
- c. Radio aid bias errors have been removed by some means, such as additional states in the filter.
- d. Radio aid position error consists of 122m rms white noise and 6lm, 20 second correlation time, correlated noise, per axis, no correlation between axes.
- e. The combinational filter generates updates of position and velocity only, with fixed gains.
- f. INS position and radio aid position coordinates are differenced in the external computer, the weighted differences are sent back to the INS for correction of indicated position and velocity.

Updates of this type are best applied to the INS in a manner which does not cause pumping of Schuler and 24-hour oscillations due to radio noise. Therefore, updates are accumulated in

separate integrators for combination with inertial measurements in an open loop fashion.

From simulation data presented in paragraph 5.2, it appears that update of inertially derived attitude and heading (in addition to position and velocity) is highly desirable. With large gyro drifts of a lower cost system, error build-up during turns and radio aid outages is excessive due to attitude and heading errors. Control of these functions via the radio aid information and a more sophisticated filter would probably make such a lower cost INS applicable to the VTOL mission. Use of time-variable gains of a Kalman approach is also beneficial if the update rate of the radio aid is variable due to atmospheric or terrain conditions.

4.5.3 Instrument Compensation

Instrument compensation can be classified into two major categories: (1) static and (2) dynamic.

Static compensation proposed for implementation in the INM include the following terms:

- a. Gyro scale factor.
- b. Gyro torquer axis misalignment.
- c. Gyro spin-axis misalignment.
- d. Gyro g-sensitive biases.
- e. Gyro biases.
- f. Gyro scale factor temperature sensitivity.
- g. Gyro g-sensitive bias temperature sensitivity.
- h. Gyro bias temperature sensitivity.
- i. Accelerometer scale factor.
- j. Accelerometer bias.
- k. Accelerometer input axis misalignment.
- l. Accelerometer scale factor temperature sensitivity.
- m. Accelerometer bias temperature sensitivity.

The only dynamic compensation required to meet accuracy in the assumed vibration environment consists of the inertia compensation. The dominant remaining error term then becomes that due to the gyro loop rectification. This term can be reduced by software compensation at the cost of additional hardware to enter gyro pick-offs into the computer. Furthermore, this error term is small for most applications since it is a multi-axis error phenomenon, requiring coherency for error rectification.

It was therefore concluded not to include this term until the environment can be better identified. Adequate computer duty cycle is available for this compensation if it is required.

4.6 Hardware Packaging Options.

The packaging approach selected for the redundant strapdown INS is to divide the total system into four, identical units. This configuration results in a low system cost to the airlines when compared with alternative methods due to reduced spares costs. The trade-off discussion leading to this conclusion is presented in this section.

The lowest unit acquisition cost for a redundant strapdown INS would probably result if all system components are packaged into a single unit. This approach results in minimum structure, connectors, etc. Other factors, however, also influence the packaging design. For example, spare units must be provided at all airports serviced by the VTOL, or if there are more airports than VTOL's, which might be the case in low traffic areas of the country, carrying spares on the VTOL would be more cost effective. With single unit packaging, therefore, this means that real avionics cost could be up to double the basic system acquisition cost.

Other packaging arrangements are illustrated in figure 4-29. It should be pointed out that the digital rebalance electronics must be located with the inertial instruments so they are in the same thermal environment and can thus be calibrated simultaneously, and to avoid noise pick-up from inter-unit wiring. For convenience, a module consisting of a gyro, 2 axes of accelerometer, and their associated digital rebalance electronics is called an Inertial Measurement Module or IMM.

OPTION A

A two-unit configuration (e.g., figure 4-29A) has the advantages that the total cost of units in the repair pipeline is reduced. For a single-unit configuration, when a component fails it (and all the remaining good parts) is sent to some repair depot. This process may take a significant length of time, during which the good components are not in use. The two-unit approach leaves at least a portion of the good components in the aircraft. As with any capital investment, including the aircraft itself, the highest utilization rate results in the lowest overall cost.

A slightly higher packaging cost results with the two-unit approach. There are added connectors, interfacing hardware, and total sheet-metal structure. Furthermore, both units need to be kept as spares either at the airport or on-board. Thus, cost of

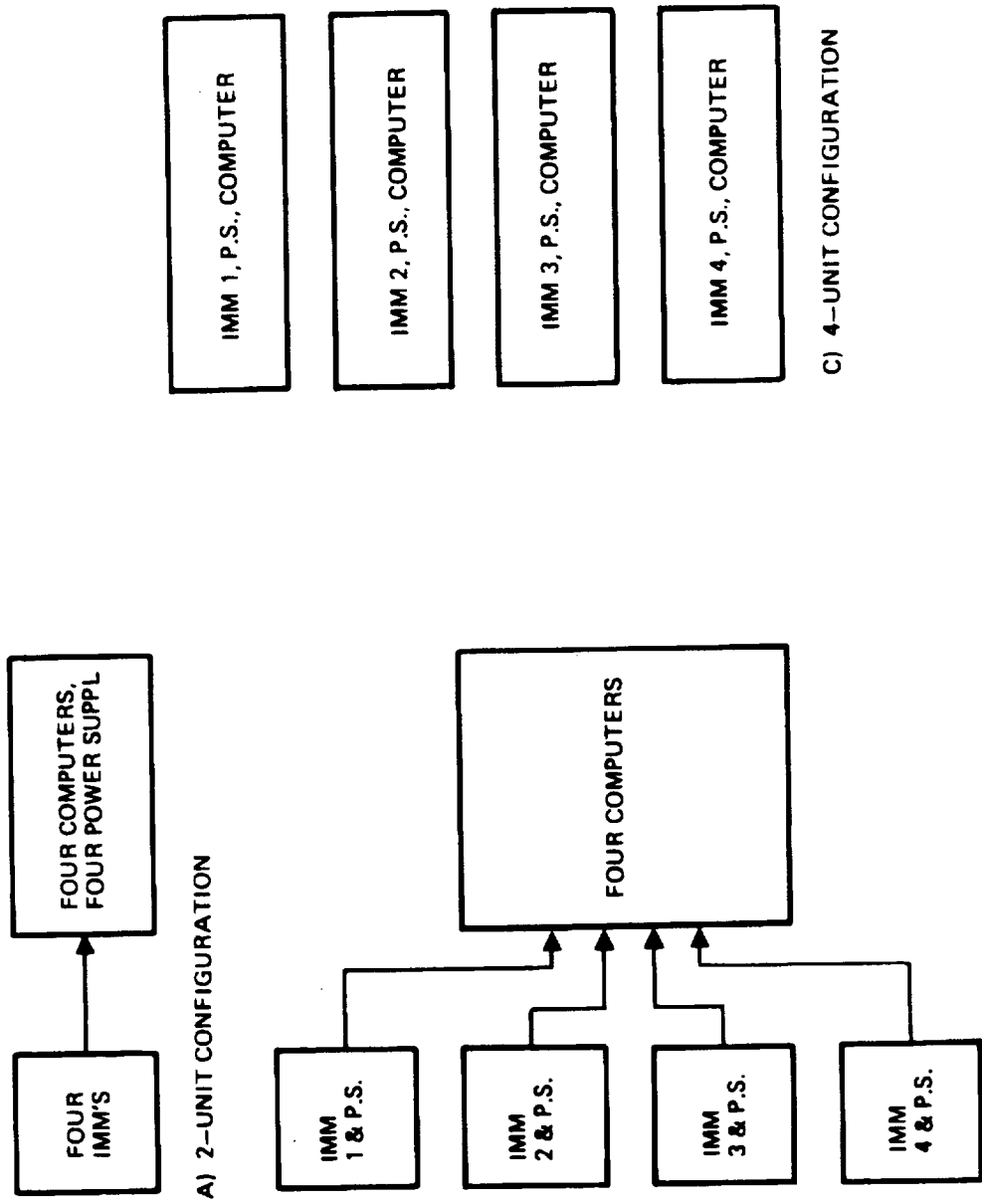


Figure 4-29. Packaging Options

spares outside of those in the repair pipeline is not reduced from the single-chassis approach. An additional disadvantage is in the area of fault isolation by means of self-test. An IMM failure could cause an apparent power supply or computer failure. Thus, there may be a significant number of cases where the wrong unit is replaced. Resolving this by having a power supply within each unit adds to net unit cost.

Some of the above disadvantages can be alleviated by having two identical units, each containing two IMM's, two computers and two power supplies. This approach is similar to Option C of figure 4-29, and will be discussed in connection with it.

OPTION B

The 5-unit approach of figure 4-29B further lowers the cost of the replaceable unit. In addition, if the 4 IMM's can be made identical and interchangeable, the production savings in this commonality will tend to offset the cost of an increased number of chasses. Also, perhaps most importantly, total cost of spares can be reduced and dispatch delays can be minimized by replacement of the faulty IMM with the other three still in operation.

The fault isolation problems of having a power supply (including the crystal oscillator, countdowns, etc.) in another unit also apply to this configuration. Again, separate power supplies in each unit increases net cost. In addition, particular care must be exercised in the transfer of data from the IMM to the computer. It may be desirable to have some of the IMM/computer interface circuitry in the IMM unit to avoid timing problems and loss of data. This could lead to further fault-isolation difficulties.

OPTION C

A further extension of the concept introduced by Option B is shown in figure 4-29C. An IMM, a computer, and a power supply are all contained within a single unit. Four units, preferably identical, are interconnected to form the redundant strapdown system. Some means must be devised to rotate the axes of the IMM's during installation to achieve the desired coordinate system.

The advantages of this packaging configuration are:

- If the four modules are identical and interchangeable, only one need be maintained as a spare in many airports. This is a function of the amount of traffic through the airport and unit failure rate. In the limiting case of on-board spares, only a single unit is required. Program cost is approximately 1.25/2.00 or 62.5% of the single-unit packaging cost.

- Net hardware in the spares pipeline is only 25% of that in the single-unit design.
- A nearly complete function is contained within a unit simplifying fault isolation. (The single-unit design has the advantage, however, in essentially eliminating the need for self-contained fault isolation capability to subsystems except for redundancy management.)
- Self-contained fault isolation separating computer failures from IMM failures is not needed.
- A unit may be replaced with the other three running, potentially reducing dispatch delays due to pre-flight failures.
- The added amount of hardware for four chasses tends to be offset by the cost savings of higher quantity purchases of identical chasses.
- Other users may only need fail-op or simplex. Simple deletion of one or two channels achieve the desired configuration.

A quantitative trade-off of the above considerations is presented in Appendix C. In summary, total cost of ownership is reduced by more than 12 million dollars over a 10-year period (200 aircraft), from a single-unit package, by applying the above 4-module packaging approach.

If the above concept is extended into 8-modules by separating each computer into a unit, the power supply and fault isolation aspects become difficult and more costly. Flightline or on-board spare requirements are not reduced, only repair pipeline unit costs are improved. This net minor improvement, however, is not felt worth the added complications.

Many of the above benefits can be achieved by having 2 IMM's, 2 computers, and 2 power supplies in one module, with a total system composed of 2 such modules. The full savings of spares cost cannot be achieved as effectively as with the 4-module method, however.

IMM AXIS ORIENTATION

The packaging arrangement of Option C promises significant program cost savings, provided that all four modules can be made identical and interchangeable. Also, since a physical rotation is involved and module-to-module alignments must be held to approximately 10 arc seconds, the practicality of the approach must be demonstrated. Such a simple practical implementation was found and is described in paragraph 6.2.10 of this report. The remainder of this section describes other implementations which were considered.

The geometry of a tetrahedron may be illustrated by means of a cube, as shown in figure 4-30A. Clearly, the sides of the tetrahedron connecting the four corners of the cube are equal since each of the diagonals of the cube faces are equal.

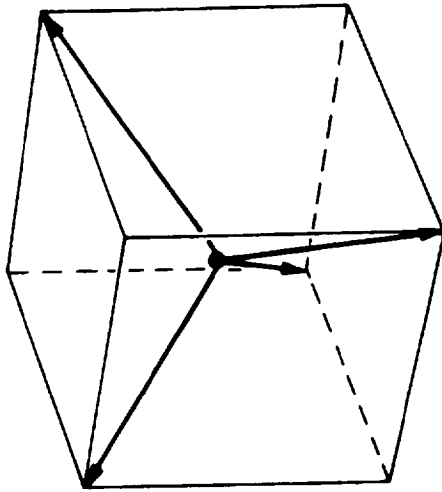
The gyro spin axes may now be placed in a tetrahedral configuration by placing a vector from the geometric center of the cube to each of the four corners of the tetrahedron, as shown in figure 4-30B. The orientation of each of the two gyro input axes will be discussed later.

Figure 4-31 shows how one gyro spin axis may be moved from one of the tetrahedral axes to another by means of 180° rotations about two axes 90° apart. This is convenient from a packaging point of view since electronics boxes are usually rectangular in shape. Rotation of the cube containing a single gyro spin axis 180° about the dashed horizontal line of figure 4-31 (1) results in an orientation of the spin axis along another of the tetrahedral axes (2). Rotation of the cube 180° about a vertical axis lines up the spin axis in the third tetrahedral axis (3). Rotation 180° again about the horizontal axis places the spin axis in the fourth orientation (4), completing the tetrahedron.

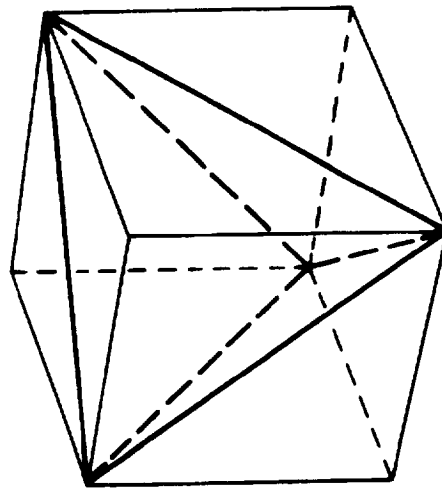
One manner of implementing an electronic chassis design is illustrated in figure 4-32. The chassis is made symmetrical about the vertical and horizontal axes to allow the above rotations. The inertial instruments are installed in the center. The connectors need not have symmetry about the horizontal axis since the aircraft or installation rack connectors can be 180° apart between positions. The four instrument packages would need to be compliant relative to the electronics portion of each chassis to provide some self-aligning as the four units are clamped together. This general method appears impractical, however, due to the tight requirements on alignment repeatability (10 arc seconds). Errors build up from one end of the stack to the other, and clamping over that great a distance, e.g. 10 inches, produces uneven pressures resulting in unpredictable alignment. An additional disadvantage is that a single unit cannot be replaced without disturbing the other three. Therefore, the ground alignment process must be discontinued during the maintenance activity.

A method of achieving the desired tetrahedral orientation is through four 90° rotations. A spin reversal of the gyro for two of the orientations can be used to exactly produce the tetrahedron. If the spin reversal is not done, the orientation is identical to the semioctahedral geometry described earlier.

The manner in which the tetrahedron can be produced with 90° rotations about a single axis is illustrated in figure 4.33. Positions (2) and (4) with spin direction reversals from the



GYRO SPIN AXES TO VERTEXES TETRAHEDRON



TETRAHEDRON ON FACE OF CUBE

Figure 4-30. Illustration of Tetrahedron Via Cube

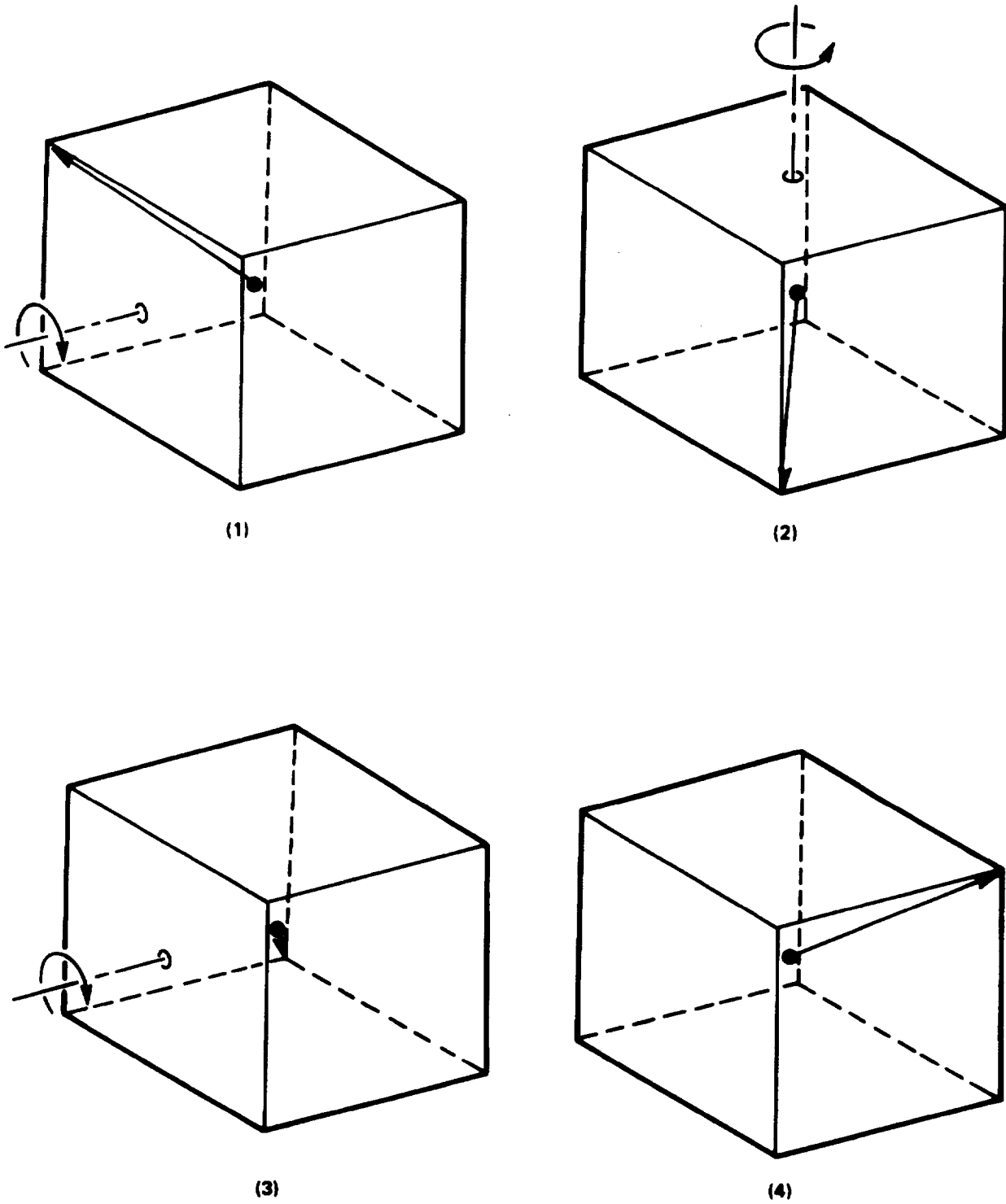


Figure 4-31. Successive 180° Rotation of the Cube

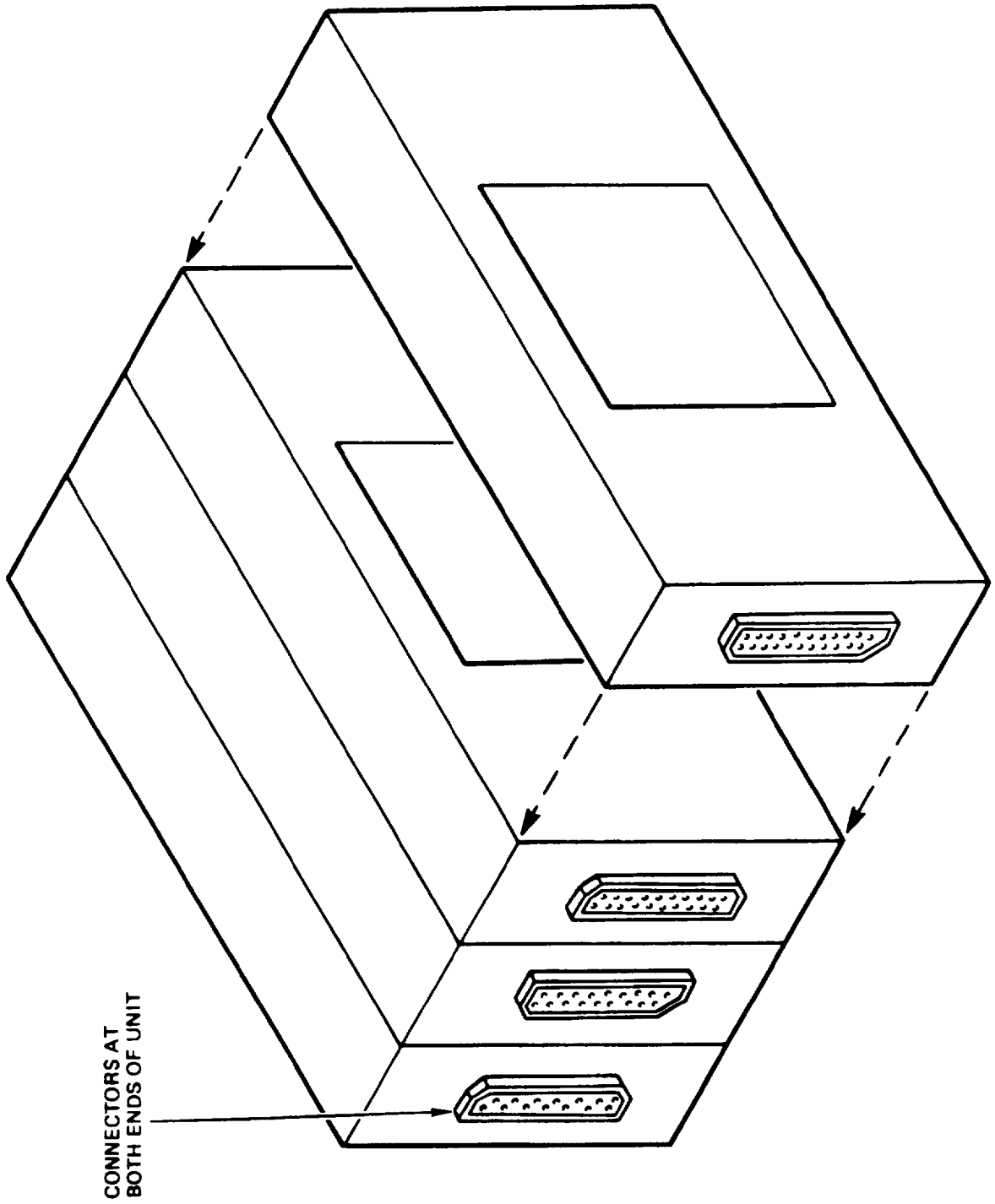


Figure 4-32. Symmetrical Chassis Implementation

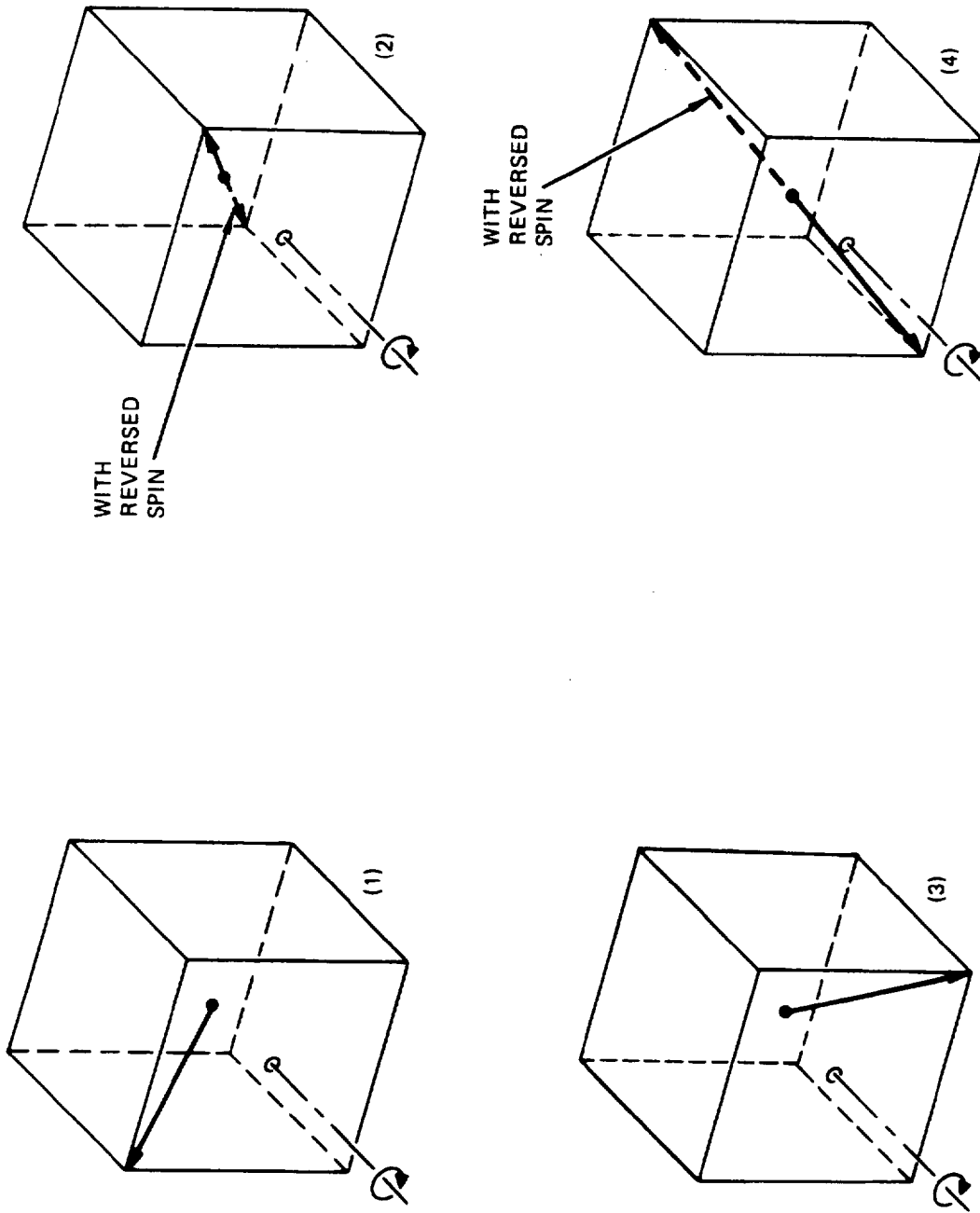


Figure 4-33. Achieving Tetrahedron With 90° Rotations About Single Axis

nominal condition are identical to positions (3) and (4) of figure 4-31. The packaging simplifications are clear from the conceptual drawing in figure 4-34. The four instrument blocks are not allowed to rotate relative to the electronics but contain sufficient compliance to allow being drawn or pushed against a common alignment block. This alignment block is of relatively small size and high rigidity and thus repeatable alignments will be achieved.

A preliminary packaging design which requires separate actions for connector and block engagements is given in paragraph 6.2.10 of this report. Further investigation is warranted to devise a single-action locking mechanism for improved maintainability. Factory calibration equipment restrictions also indicate that it is desirable to have block engagement on the end of the unit rather than on the side. Several similar units can then be installed side-by-side on the rate table used for factory calibration for more efficient utilization of this high cost item.

Gyro and accelerometer input axis orientations are easily maintained through the 90° rotations for the geometry selected in figure 4-19. Maximum avoidance of all potential 3-gyro isolation singularities is also provided.

The geometry recommended in the preliminary CR-132419 report was to orient three gyros orthogonally with the fourth bisecting the orthogonal triad. The inherent asymmetry of this approach does not allow the simplified packaging arrangement of the tetrahedron or semioctahedron. It thus produces clear cost-of-ownership disadvantages and is not recommended for use.

4.7 Redundant Strapdown INS Trade-Off Summary

The redundant strapdown INS design features resulting from the trade-off study described in this report are summarized below:

- The total redundant strapdown INS comprises four identical plug-in modules for low cost-of-ownership.
- Module-level redundancy (printed-circuit card, circuit element, CPU, etc.) is not employed except in the case of instruments, to achieve minimum system cost. Probability of complete system failure through both fail-op levels is significantly lower than LaRC requirements.
- Hardware failure detection and isolation (FDI) is not used (software only), except for a small amount in computer synchronization logic. The final vote is assumed to be in external hardware.
- The system consists of 4 TDF tuned-gimbal gyros and 8 SDF accelerometers oriented in a regular semioctahedral geometry, with 4 GP digital computers. This results in

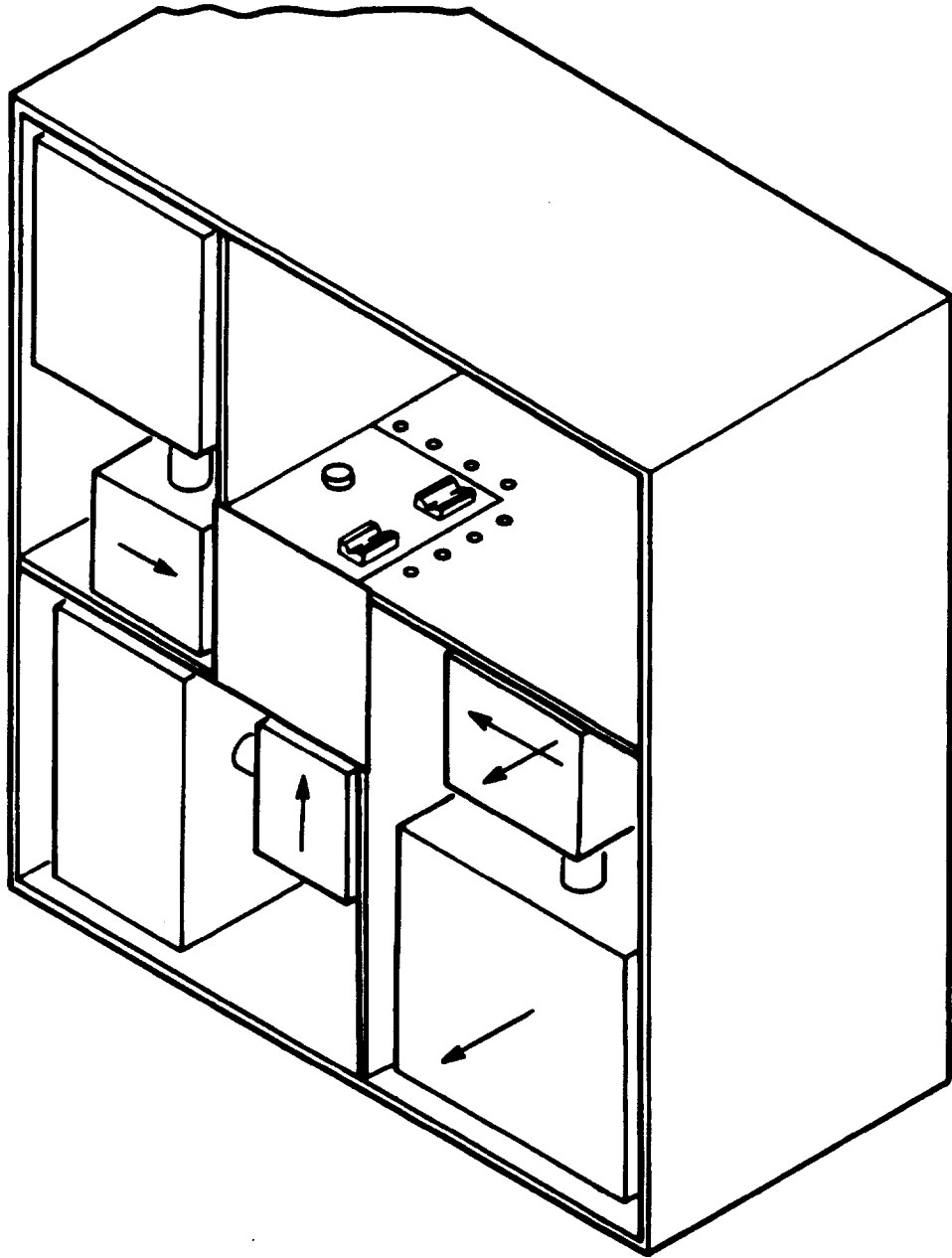


Figure 4-34. Conceptual Packaging Design With 90° Rotations

a low cost packaging approach and uniform redundancy management with very straightforward software processing.

- Gyro and accelerometer data of each module are input to only the computer of that module. Compensation for predictable errors is applied in only that computer for minimum I/O and computer duty cycle penalty.
- The probability of recovery from some second failures is less than unity due to information limits of 3 TDF gyros. These failures are always detectable, thus resulting in a fail-safe condition. Furthermore, recovery probability is sufficiently high to meet the system reliability specification, and approaches unity on outputs to the flight control system.
- Gyro input axes are oriented away from 3-gyro failure isolation singularities resulting from these information limits to improve recovery probability.
- The mechanization of the computer ensemble is structured to allow aid to self-contained FDI from external radio updates and to allow complete recovery from extended operation in 3-gyro isolation singularities when the failed gyro is finally isolated.
- Parity equations are formed by comparison of gyro measurements at the edges of a semioctahedron.
- Processing of parity equations consists of a low pass filter.
- Fault isolation consists of a computer table look-up process. Further processing of filtered gyro parity equations including compensation for normal scale factor deviations and computation of error probabilities is recommended to reduce system errors just prior to redundancy management switching. Incorporation of these refinements will be done at a later date following further analysis, simulation and/or testing.
- Instruments which are indicated as failed will simply be switched out of the computation. Weighted combinations for output transient suppression are not needed.
- Instruments switched out of computations due to soft failure detection continue to be monitored and if only marginally bad will be re-used for a third fail-op level or to resolve ambiguous second failures.

- All four computers will do the same FDI processing.
- A computer always uses its attached instruments in its output computations. The choice of the second instrument depends upon redundancy management decisions.
- Reinitialization of one computer to another is performed following replacement of a bad channel before flight. Consideration will be given in the future to reinitialization following any failure switching, or a computer error transient. The impact of a failure mode within or near a 3-gyro isolation singularity is thus considerably reduced.
- Tighter error detection limits will be used during ground operation to reduce the probability of take-off with failed or marginal instruments.

V. SYSTEM ANALYSES

The analytical results presented in this section indicate the following performance.

TWO CHANNEL PERFORMANCE PREDICTIONS

Predicted Performance**		Requirement
1. Position Error:	$56 + 41t^*$ meters CEP	
2. Velocity:	0.50 m/sec cev	0.49 m/sec cev
3. Attitude:		
a. Verticality (Pitch and Roll):	$0.3 + 1.4t \widehat{\min} (1\sigma)$	0.1° rms
b. Heading:	$5.8 + 7.5t \widehat{\min} (1\sigma)$	0.2° rms

*t is in hours

**with radio updates

As discussed in paragraph 4.5.3, 'Instrument Compensation', the errors encountered in strapdown inertial navigation systems may be categorized into two general classifications, (1) dynamic errors and (2) static errors.

Dynamic errors are those produced as a result of the vibration environment. Paragraph 5.1 contains the results of this analysis. The assumed environment encountered includes wide band noise plus a sinusoidal resonance. The results of the dynamic analysis are in terms of equivalent instrument biases. These biases are then introduced into the strapdown simulation program together with the static errors (instrument frequency independent errors). Figure 5-1 illustrates this methodology.

The final results were obtained from a Monte Carlo simulation of the strapdown inertial navigation system operating in a closed path trajectory over a 1.2 hour period, with open loop velocity and position updating. Paragraph 5.2 presents the results of this simulation and a description of the simulator.

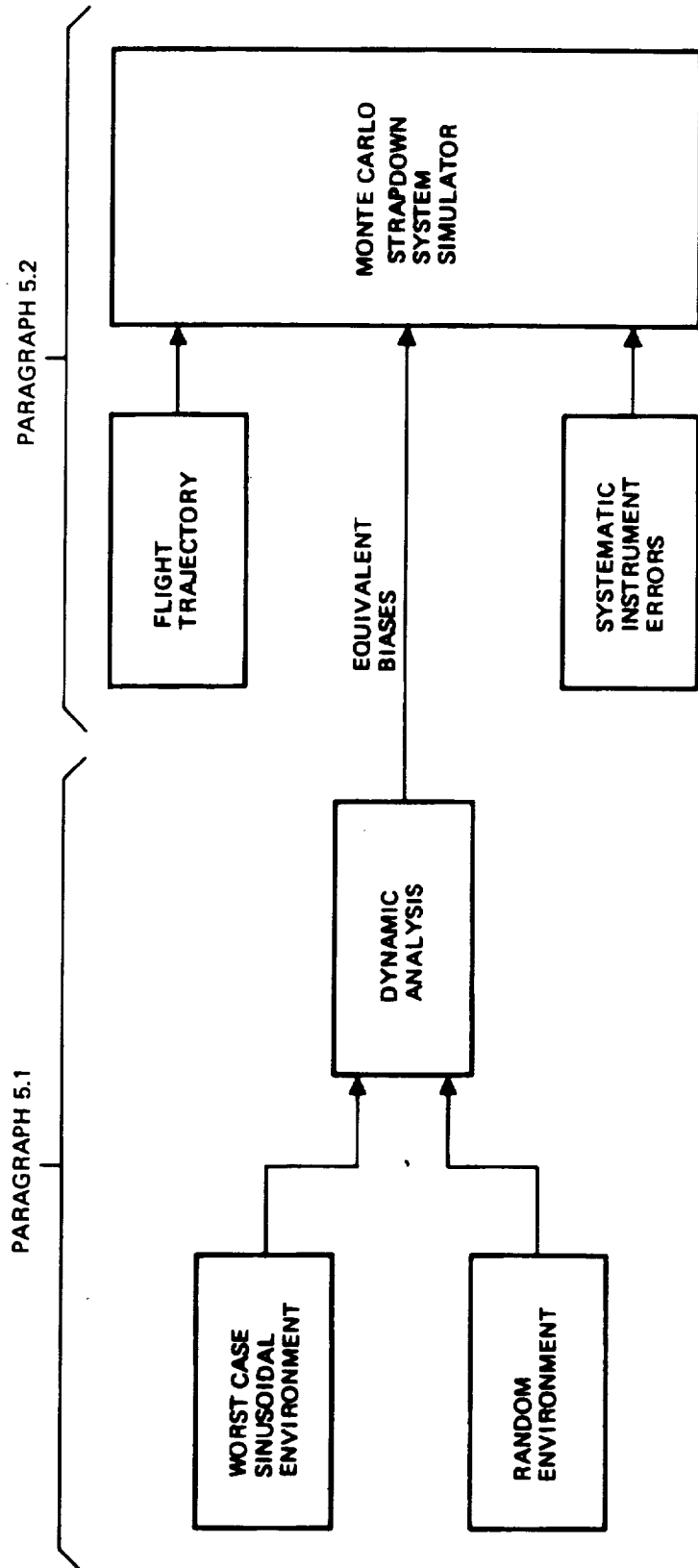


Figure 5-1. System Analysis Methodology

The system reliability calculation results in the following probability of system failure:

	Channel MTBF (Hr)	Flight	Time
		0.5 Hr	1.0 Hr
Full System Accuracy	2000	4.6×10^{-10}	1.8×10^{-9}
	4000	1.3×10^{-10}	5.2×10^{-10}
Outputs to Flight Control System*	2000	4.7×10^{-11}	3.8×10^{-10}
	4000	4.5×10^{-12}	3.6×10^{-11}

It is well within the 10^{-6} failure probability requirement for a 0.5 hour flight. Very conservative assumptions have been used in calculating system reliability. Furthermore, use of radio and update data can improve system reliability by resolving the 3-gyro isolation ambiguity, but this capability is not included in the failure probability determination.

5.1 Dynamic Error Analysis

The dynamic errors have been evaluated for a strapdown navigation system while operating in a helicopter-type of environment. The resulting errors on a per channel basis, are summarized in table 5-1. For a combined sinusoidal and random environment, the resulting dynamic biases are 1 ug and .02°/hr/channel.

The total bias/channel is made up of errors due to gyro loop, accelerometer loop, and system type dynamic errors. A separate analysis was performed for both an assumed sinusoidal and random vibration environment. The detailed breakdown of all the error sources considered, and their resulting contribution to the total error, are shown in tables 5-2 and 5-3, (sinusoidal and random environments respectively). Each table shows the individual error source, the coefficient used, the vibration motion and the resulting maximum error. For errors dependent upon multiaxis motion, the error was reduced by .3 to account for phase correlation probability.

The environments used in this analysis are summarized in table 5-4. These were based on review of available data, primarily reference [10]. The total environment is considered to be made of an overall random spectrum with some discrete frequencies of vibration.

The dynamic errors are computed for the dry-tuned instrument rebalance loops as described in paragraph 6.2.1.

*Attitude rates and accelerations in body coordinates.

The errors as shown in tables 5-2 and 5-3 are generated with the following assumptions:

- a. All error sources are excited simultaneously.
- b. The environments exist at the same levels at all times on all axes.
- c. The phasing of the vibrations are always such as to maximize the resulting error.
- d. The random and sinusoidal environments exist simultaneously.
- e. The environments used are worse case levels from test data.
- f. The total error is reduced by 50% for time weighting of their existence during flight.
- g. All errors are assumed to be independent and thus RSS'd for a total error.
- h. A computer utilizing a partial fifth order algorithm at a 64 Hz iteration rate.
- i. Only pseudo coning correction included in the software compensation.

The errors shown in table 5-2 for the sinusoidal environment of table 5-4 are computed as follows:

$$\text{Error} = (\text{Error Coefficient})_{f_i} \times (\text{Vibration})_{f_i} \\ \times (\text{Computer Attenuation})_{f_i}$$

The error coefficients are shown in figures 5-5 through 5-14 for those which are frequency dependent. The error coefficients shown on table 5-2 are obtained from these figures at the frequency (f_i) of the input vibration. A brief description of system dynamic errors is shown in figure 5-26. The computer attenuation for system errors based on a 64 Hz, fifth order algorithm is shown in figure 5-27.

The errors shown in table 5-3 for the random vibration environment of table 5-4 are computed as follows:

$$\text{Error} = \int (\text{Error Coefficient}) \times (\text{Power Spectral Density}) \\ \times (\text{Computer Attenuation}) df$$

The coefficients are shown in figures 5-5 through -14 for those which are frequency dependent. Before arriving at the final

error, an analysis was performed to estimate the dynamic errors as a function of vibration bandwidth for a normalized random environment. The normalized environments are shown in figure 5-2. The resulting RMS values as a function of bandwidth are shown in figures 5-3 and -4 for the linear and angular spectra respectively. The resulting integrated error coefficient vs vibration bandwidth are shown in figures 5-15 and -25. If new vibrations of different bandwidths or levels are used, the resulting errors can be quickly determined.

5.1.1 Computation Errors

The quaternion integration routine proposed is a partial fifth order algorithm. The truncation error for this order algorithm will introduce negligible quaternion drift for input angular rates above several hundred degrees per second.

Figure 5-28 illustrates the error related to the use of finite digital word lengths. A plot of word length versus equivalent quaternion drift in degrees per hour illustrates the proportionate relationship of equivalent drift to computer iteration rate. Note for a 32 Hz quaternion computation rate with a 32 bit word length introduces an equivalent drift rate of .0016 deg/hr in the worst case.

TABLE 5-1. DYNAMIC ERROR SUMMARY
(SINGLE AXIS-1σ)

ERROR	VIBRATION			RSS
	SINUSOIDAL	RANDOM		
LINEAR	2.0 μg	2.0 μg		2.8 μg
ANGULAR	0.035 DEG/HR	0.027 DEG/HR		0.044 DEG/HR

WITH 50% TIME WEIGHTING

ERROR	VIBRATION			RSS
	SINUSOIDAL	RANDOM		
LINEAR	1.0 μg	1 μg		1.4 μg
ANGULAR	0.017 DEG/HR	0.013 DEG/HR		0.022 DEG/HR

TABLE 5-2. DYNAMIC ERROR SUMMARY-SINUSOIDAL VIBRATION (30)

ERROR SOURCE	ERROR COEFFICIENT	VIBRATION (EACH AXIS)	MAX. ERROR	PHASE CORRELATION COEFFICIENT	RESULTING ERROR
<u>GYRO LOOP:</u>					
LOOP RECTIFICATION-DIRECT CO	$.14(^{\circ}/\text{HR})/(^{\circ}/\text{SEC}_{\text{PK}})^2 @ 15 \text{ Hz}$	$1.0^{\circ}/\text{SEC}_{\text{RMS}} @ 15 \text{ Hz}$	$.280^{\circ}/\text{HR}$.3	$.084^{\circ}/\text{HR}$
QUAD	$.06(^{\circ}/\text{HR})/(^{\circ}/\text{SEC}_{\text{PK}})^2 @ 15 \text{ Hz}$	$1.0^{\circ}/\text{SEC}_{\text{RMS}} @ 15 \text{ Hz}$	$.120^{\circ}/\text{HR}$.3	$.036^{\circ}/\text{HR}$
LOOP RECTIFICATION-CROSS CO	$.002(^{\circ}/\text{HR})/(^{\circ}/\text{SEC}_{\text{PK}})^2 @ 15 \text{ Hz}$	$1.0^{\circ}/\text{SEC}_{\text{RMS}} @ 15 \text{ Hz}$	$.004^{\circ}/\text{HR}$.3	$.001^{\circ}/\text{HR}$
QUAD	$.018(^{\circ}/\text{HR})/(^{\circ}/\text{SEC}_{\text{PK}})^2 @ 15 \text{ Hz}$	$1.0^{\circ}/\text{SEC}_{\text{RMS}} @ 15 \text{ Hz}$	$.036^{\circ}/\text{HR}$.3	$.011^{\circ}/\text{HR}$
ANISOINERTIA	$.04(^{\circ}/\text{HR})/(^{\circ}/\text{SEC}_{\text{PK}})^2 @ 15 \text{ Hz}$	$1.0^{\circ}/\text{SEC}_{\text{RMS}} @ 15 \text{ Hz}$	$.080^{\circ}/\text{HR}$.3	$.024^{\circ}/\text{HR}$
SCALE FACTOR ASYMMETRY	$.02(^{\circ}/\text{HR})/(^{\circ}/\text{SEC}_{\text{PK}}) @ 15 \text{ Hz}$	$1.0^{\circ}/\text{SEC}_{\text{RMS}} @ 15 \text{ Hz}$	$.028^{\circ}/\text{HR}$	1.0	$.028^{\circ}/\text{HR}$
ANISOELASTIC	$.01(^{\circ}/\text{HR})/(g_{\text{PK}})^2 @ 28 \text{ Hz}$	$.3g_{\text{RMS}} @ 28 \text{ Hz}$	$.006^{\circ}/\text{HR}$.3	$.002^{\circ}/\text{HR}$

TABLE 5-2. DYNAMIC ERROR SUMMARY SINUSOIDAL VIBRATION (3σ) (cont)

ERROR SOURCE	ERROR COEFFICIENT	VIBRATION (EACH AXIS)	MAX. ERROR	PHASE CORRELATION COEFFICIENT	RESULTING ERROR
<u>ACCELEROMETER LOOP:</u>					
LOOP RECTIFICATION - CO	$20(\text{UG})/(\text{G}_{\text{PK}})^2 @ 28 \text{ Hz}$.3G _{RMS} @ 28 Hz	4UG	.3	1UG
QUAD	$26(\text{UG})/(\text{G}_{\text{PK}})^2 @ 28 \text{ Hz}$.3G _{RMS} @ 28 Hz	5UG	.3	2UG
NON-LINEAR G ²	$15(\text{UG})/(\text{G}_{\text{PK}})^2 @ 28 \text{ Hz}$.3G _{RMS} @ 28 Hz	3UG	1.0	3UG
SCALE FACTOR ASYMMETRY	$7(\text{UG})/(\text{G}_{\text{PK}}) @ 28 \text{ Hz}$.3G _{RMS} @ 28 Hz	3UG	1.0	3UG
<u>SYSTEM</u>	0.0016				
TRUE CONING	$(^\circ/\text{HR})/(\text{SEC}_{\text{PK}})^2 @ 15 \text{ Hz}$	1.0 [°] /SEC _{RMS} @ 15 Hz	0.0032 [°] /HR	.3	0.001 [°] /HR
PSEUDO CONING (COMPENSATED)	$0.005 (\text{SEC}_{\text{PK}})^2 @ 15 \text{ Hz}$	1.0 [°] /SEC _{RMS} @ 15 Hz	0.01 [°] /HR	1.0	0.01 [°] /HR
LOOP MISMATCH (20%)	$0.056 (\text{SEC}_{\text{PK}})^2 @ 15 \text{ Hz}$	1.0 [°] /SEC _{RMS} @ 15 Hz	0.112 [°] /HR	.3	0.033 [°] /HR
SCROLLING - CO	$19(\text{UG})/(\text{G}_{\text{PK}})^2 @ 15 \text{ Hz}$.1G _{RMS} ^{-°} /SEC _{RMS} @ 15 Hz	4 UG	.3	1.2 UG
-QUAD	$37(\text{UG})/(\text{G}_{\text{PK}})^2 @ 15 \text{ Hz}$.1G _{RMS} ^{-°} /SEC _{RMS} @ 15 Hz	8 UG	.3	2.4 UG

TOTAL ERROR/CHANNEL (RSS)

ANGULAR: 0.105[°]/HR (3 SIGMA)
0.035[°]/HR (1 SIGMA)

LINEAR: 5UG (3 SIGMA)
2UG (1 SIGMA)

TABLE 5-3. DYNAMIC ERROR SUMMARY - RANDOM VIBRATION (3σ)

ERROR SOURCE	ERROR COEFFICIENT	INTEGRATED RESPONSE	RANDOM VIBRATION	MAXIMUM ERROR	PHASE CORRELATION COEFFICIENT	RESULTING ERROR
GYRO LOOP						
LOOP RECTIFICATION - DIRECT						
CO	FIGURE 5-5	FIGURE 5-15	A IN PHASE	0.240 DEG/HR	0.3	0.072 DEG/HR
QUAD	FIGURE 5-5	FIGURE 5-15	A QUADRATURE	0.026 DEG/HR	0.3	0.008 DEG/HR
LOOP RECTIFICATION - CROSS						
CO	FIGURE 5-6	FIGURE 5-16	A IN PHASE	0.026 DEG/HR	0.3	0.008 DEG/HR
QUAD	FIGURE 5-6	FIGURE 5-16	A QUADRATURE	0.033 DEG/HR	0.3	0.010 DEG/HR
ANISOTROPY	FIGURE 5-7	FIGURE 5-17	A IN PHASE	0.063 DEG/HR	0.3	0.019 DEG/HR
SCALE FACTOR ASYMMETRY	0.03 (DEG/HR)/(DEG/SEC ² RMS) FIGURE 5-8	---	A IN PHASE	0.030 DEG/HR	1.0	0.030 DEG/HR
ANISOELASTIC	0.02 (DEG/HR)/(gRMS) ² FIGURE 5-8	FIGURE 5-18	B IN PHASE	0.002 DEG/HR	0.3	0.001 DEG/HR
ACCELEROMETER LOOP						
LOOP RECTIFICATION						
CO	FIGURE 5-9	FIGURE 5-19	B IN PHASE	8.6 μg	0.3	2.6 μg
QUAD	FIGURE 5-9	FIGURE 5-19	B QUADRATURE	2.3 μg	0.3	0.7 μg
NON LINEAR g ²	30 (μg)/(gRMS) ²	FIGURE 5-20	B IN PHASE	2.7 μg	1.0	2.7 μg
SCALE FACTOR ASYMMETRY	8 (μg)/(gRMS) (FIGURE 5-10)	---	B IN PHASE	2.4 μg	1.0	2.4 μg
SYSTEM						
TRUE CONING	FIGURE 5-11	FIGURE 5-21	A IN PHASE	0.0225 DEG/HR	0.3	0.007 DEG/HR
PSEUDO CONING						
(UNCOMPENSATED)	FIGURE 5-12	FIGURE 5-22	A IN PHASE	0.081 DEG/HR	1.0	0.081 DEG/HR
COMPENSATED	---	FIGURE 5-23	A IN PHASE	0.01 DEG/HR	1.0	0.01 DEG/HR
LOOP MISMATCH (20%)	FIGURE 5-13	FIGURE 5-24	A IN PHASE	0.042 DEG/HR	0.3	0.012 DEG/HR
SCULLING						
CO	FIGURE 5-14	FIGURE 5-25	C IN PHASE	1.0 μg	0.3	0.3 μg
QUAD	FIGURE 5-14	FIGURE 5-25	C QUADRATURE	3.6 μg	0.3	2.0 μg

ENVIRONMENT:

A - 0.033 (DEG/SEC²RMS)²/HZ. 0.30 HZ TOTAL ERROR/CHANNEL (RSS) LINEAR 5 μg (3 SIGMA)

B - 0.00045 (gRMS)²/HZ. 0.200 HZ ANGLUAR 0.083 DEG/HR (3 SIGMA) 2 μg (1 SIGMA)

C - 0.003 (gRMS - DEG/SEC²RMS)/HZ. 0.30 HZ 0.027 DEG/HR (1 SIGMA)

TABLE 5-4. PERFORMANCE ENVIRONMENT SUMMARY

	<u>SINUSOIDAL</u>	<u>RANDOM</u>
LINEAR	0.3 g_{RMS} @ 28 Hz	.00045 (g_{RMS}) ² /Hz 0-200 Hz (.3 g_{RMS})
ANGULAR	1.0 deg/sec _{RMS} @ 15 Hz	.033 (deg/sec _{RMS}) ² /Hz 0-30 Hz (1.0 deg/sec _{RMS})
LINEAR/ANGULAR	.1 g_{RMS} - deg/sec _{RMS} @ 15 Hz	.0033 (g_{RMS} deg/sec _{RMS})/Hz 0-30 Hz (.1 g_{RMS} deg/sec _{RMS})

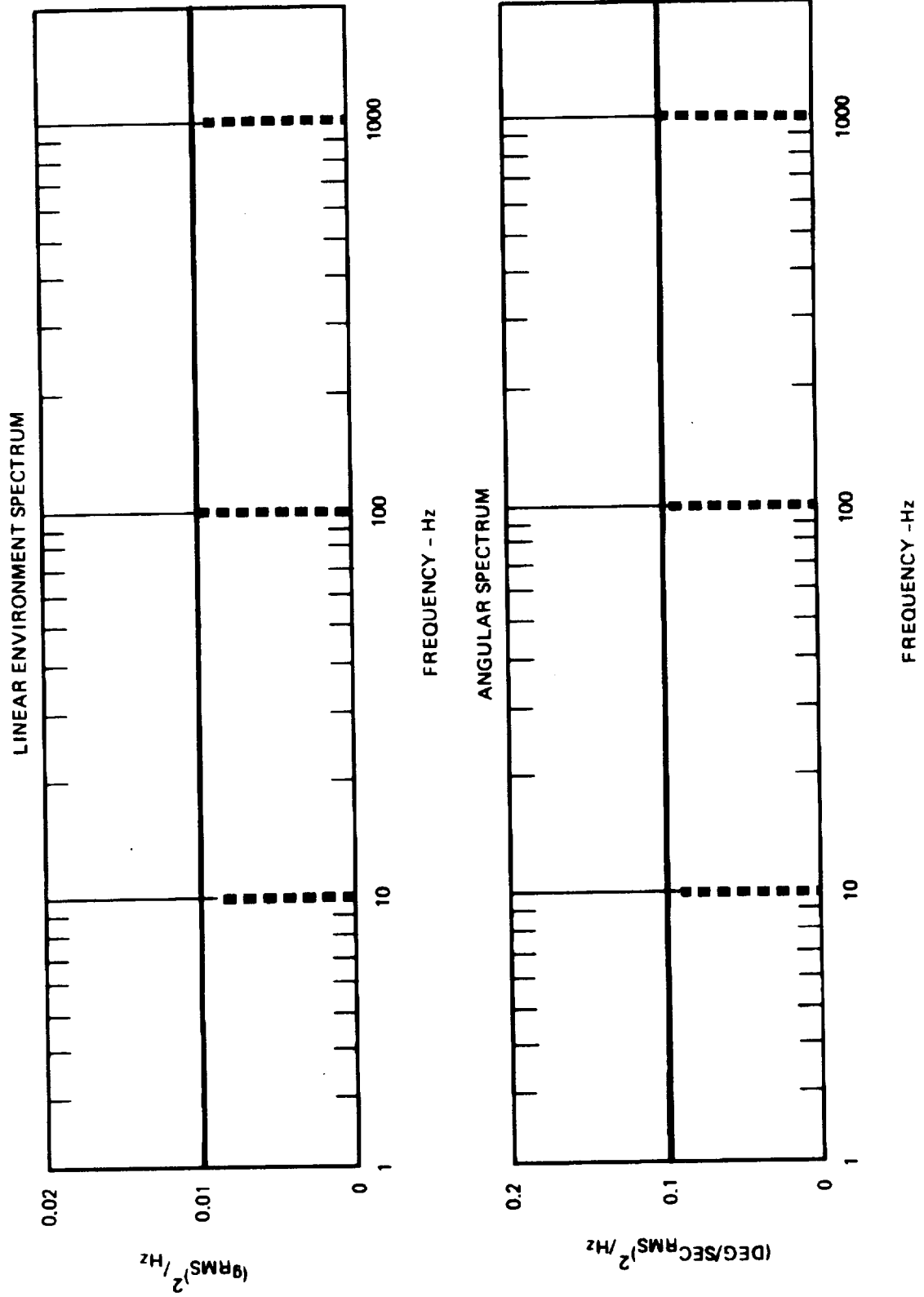


Figure 5-2. Normalized Random Vibration Spectrum

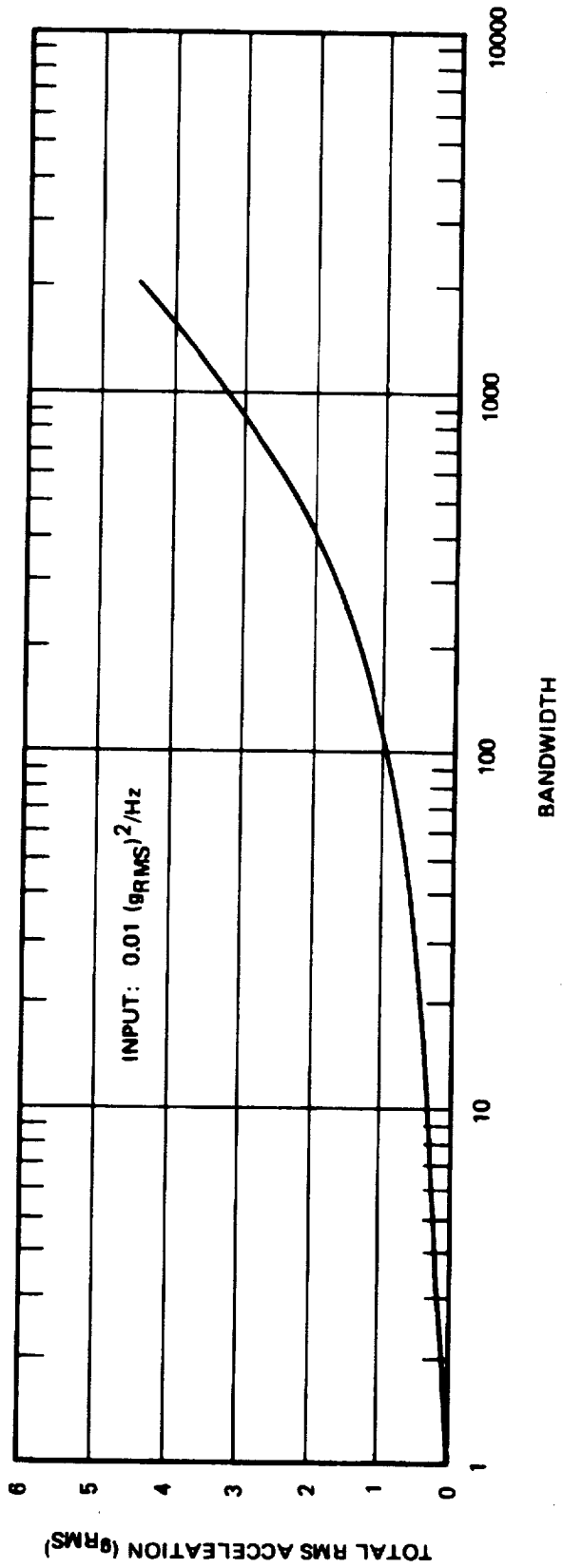


Figure 5-3. RMS Acceleration Input vs Bandwidth of Wide Band Random Linear Vibration

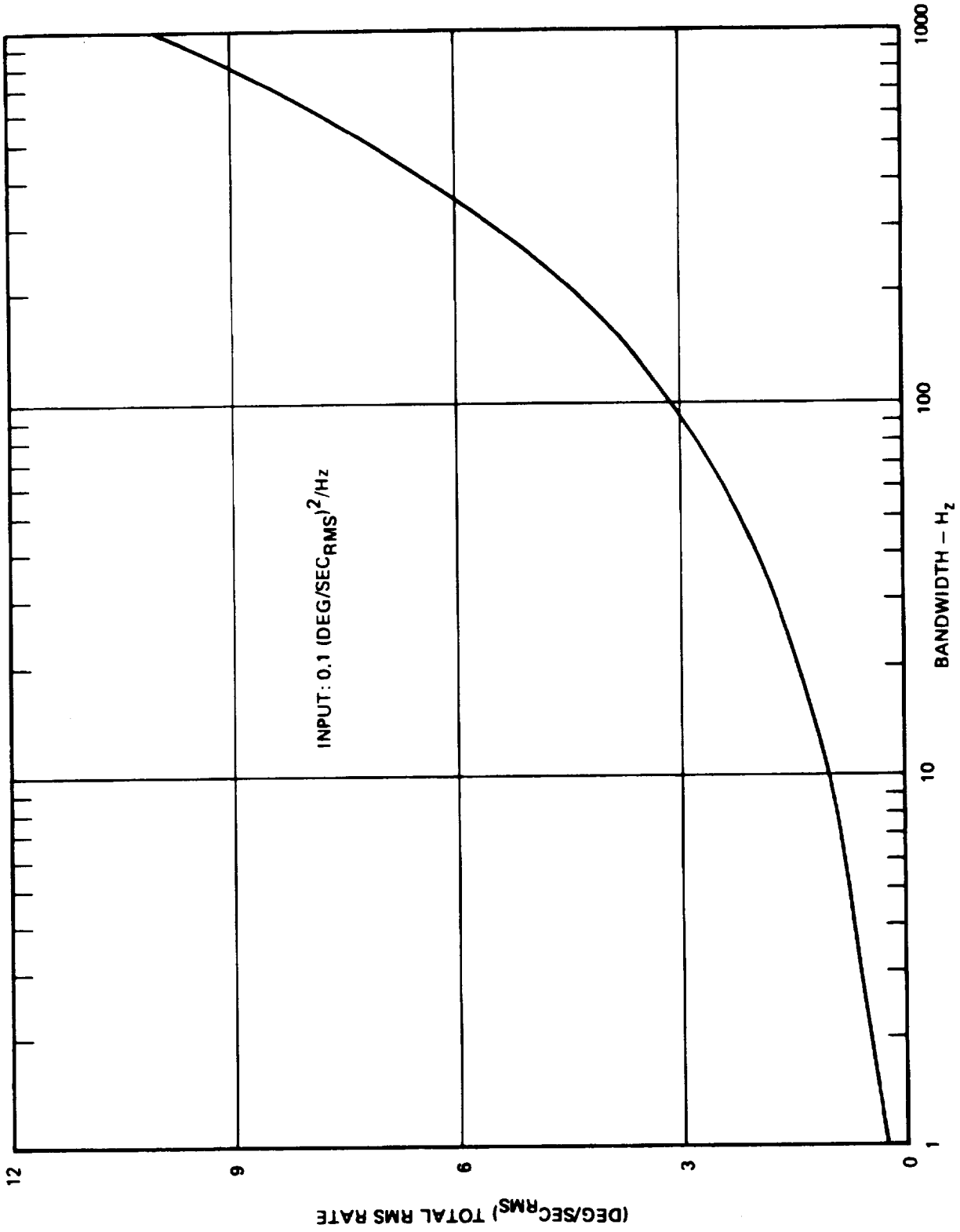


Figure 5-4. RMS Rate Input vs Bandwidth of Wide Band Random Angular Vibration

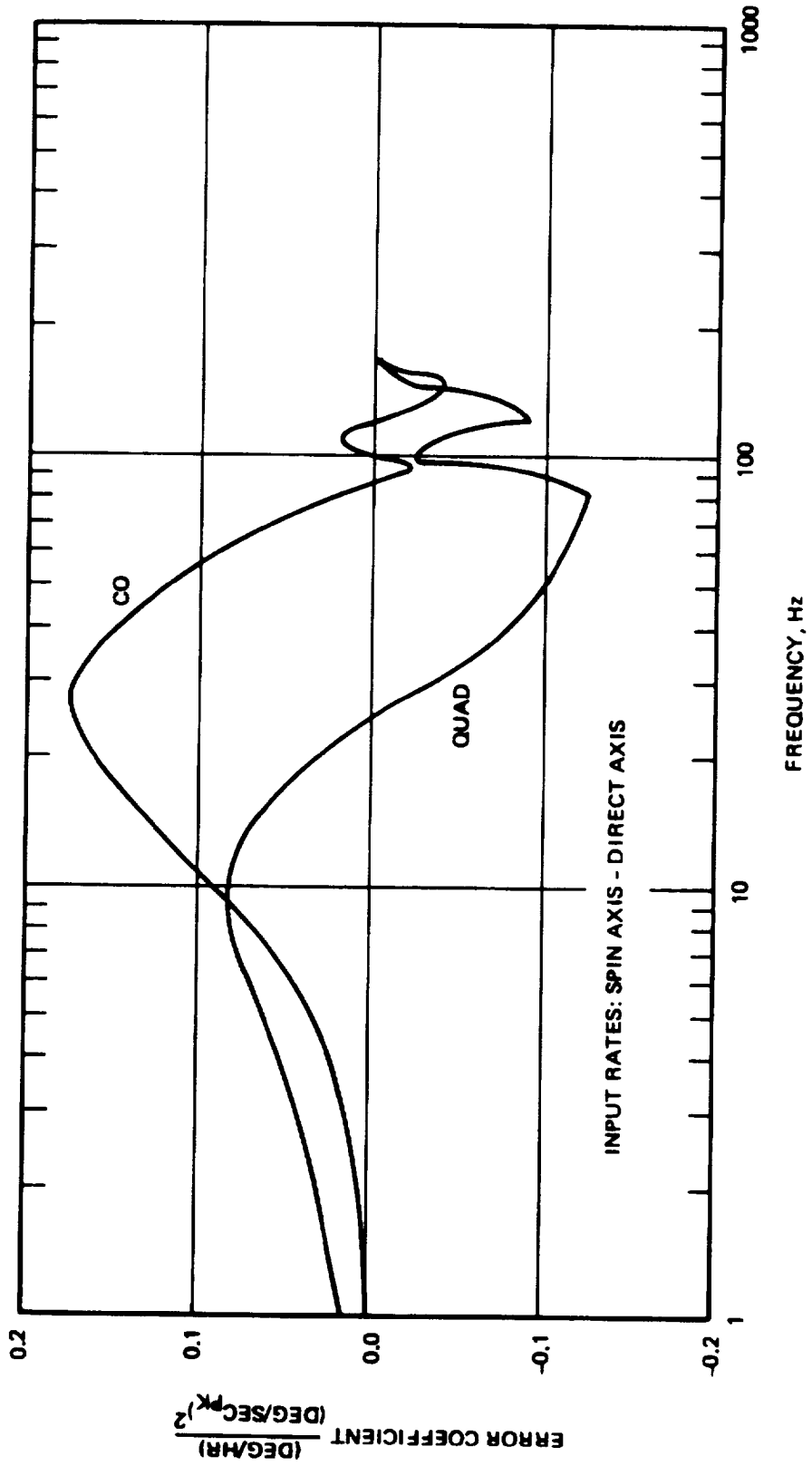


Figure 5-5. Gyro Loop Rectification Error Coefficient

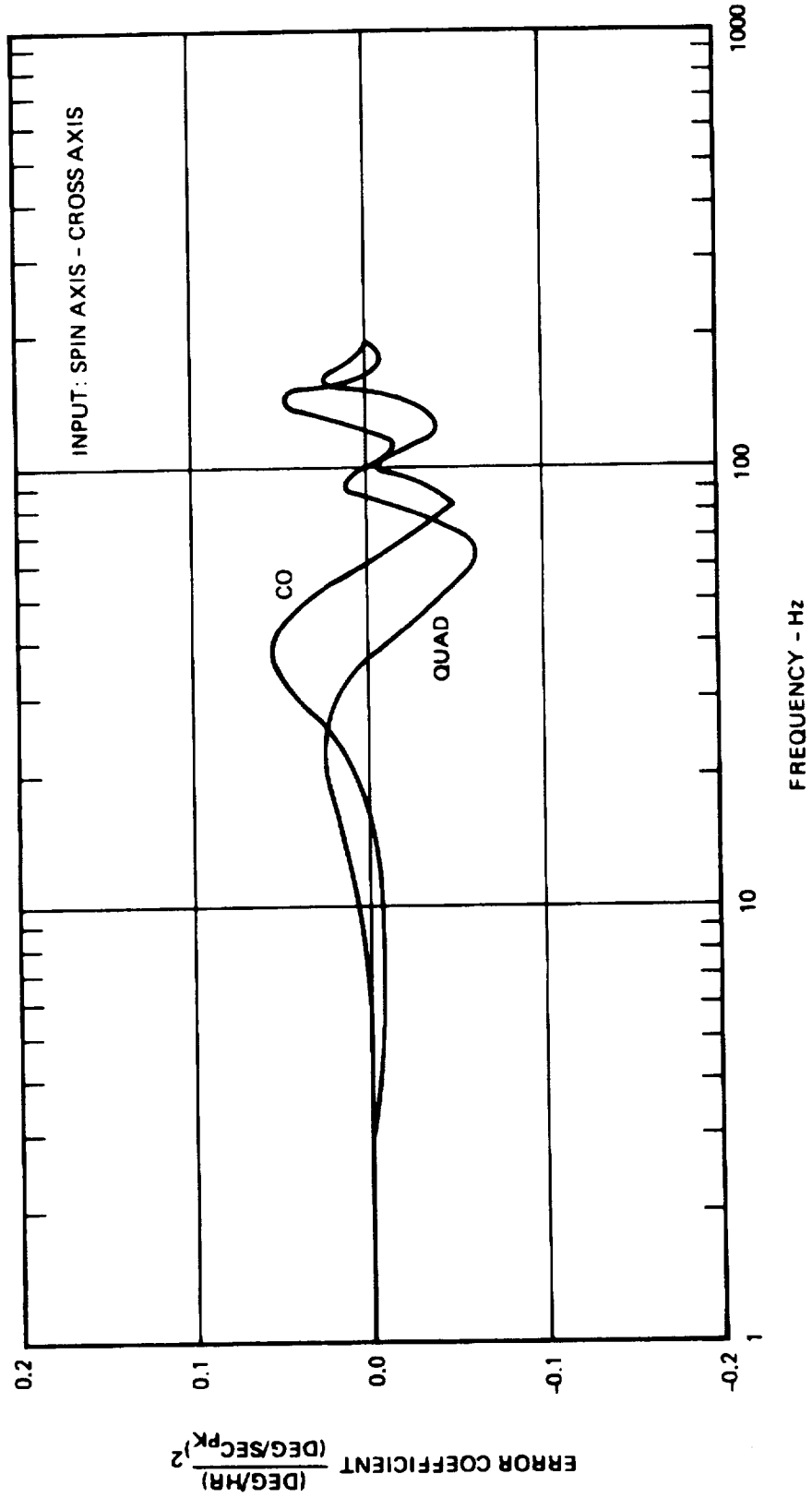


Figure 5-6. Gyro Loop Rectification Error Coefficient

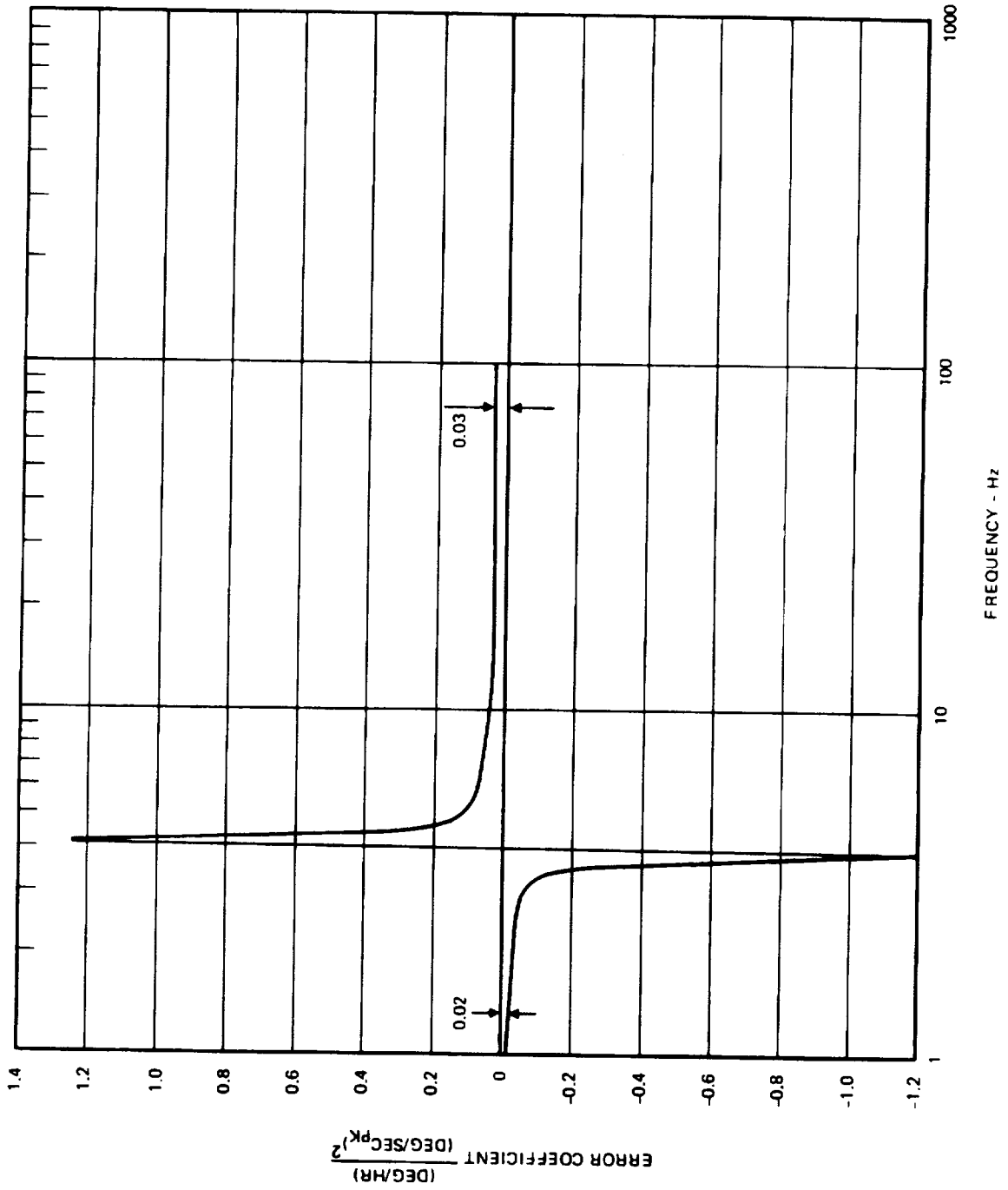


Figure 5-7. Gyro Anisoinertia Error Coefficient

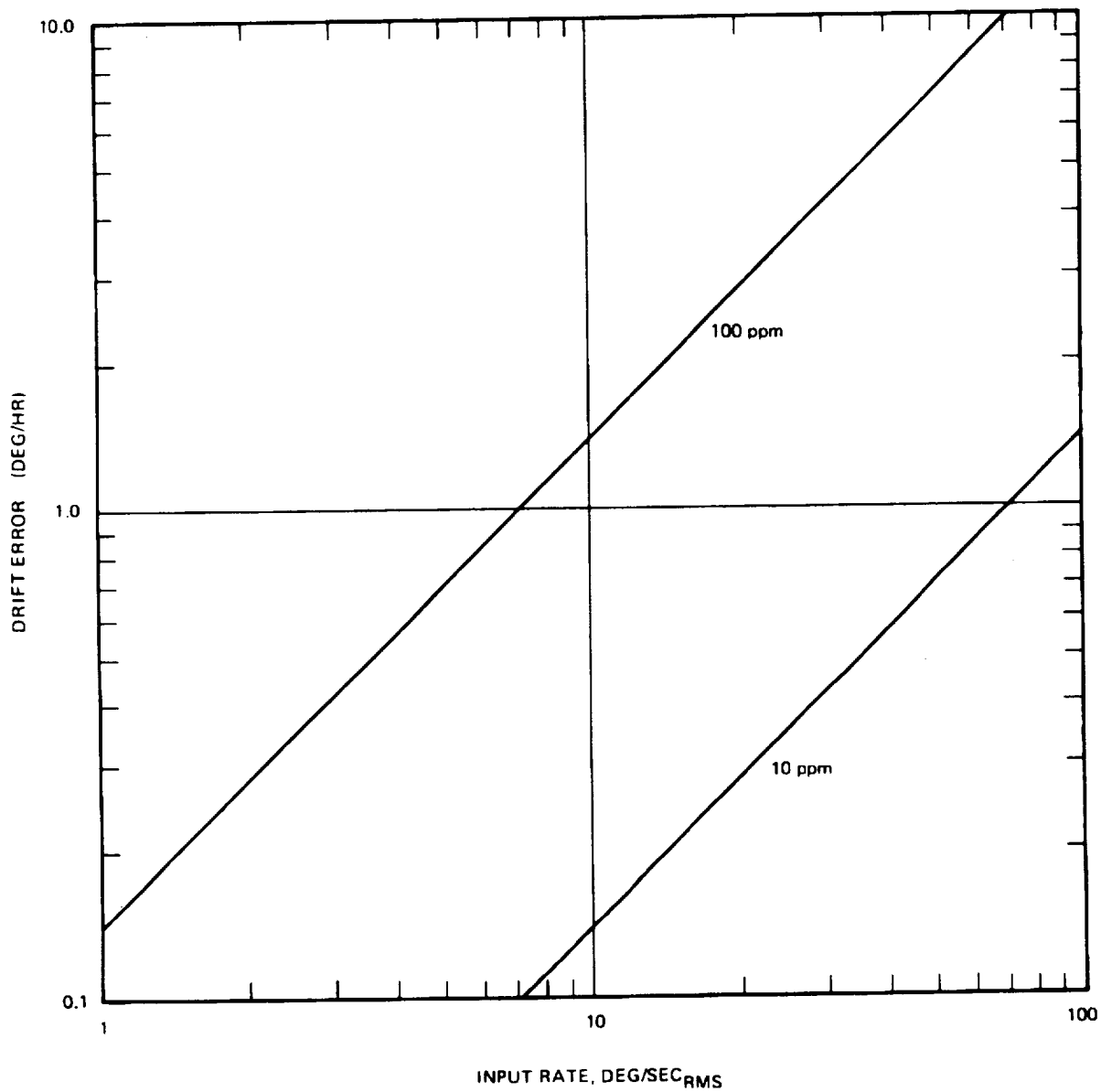


Figure 5-8. Gyro Scale Factor Asymmetry Error For Random Input Rates

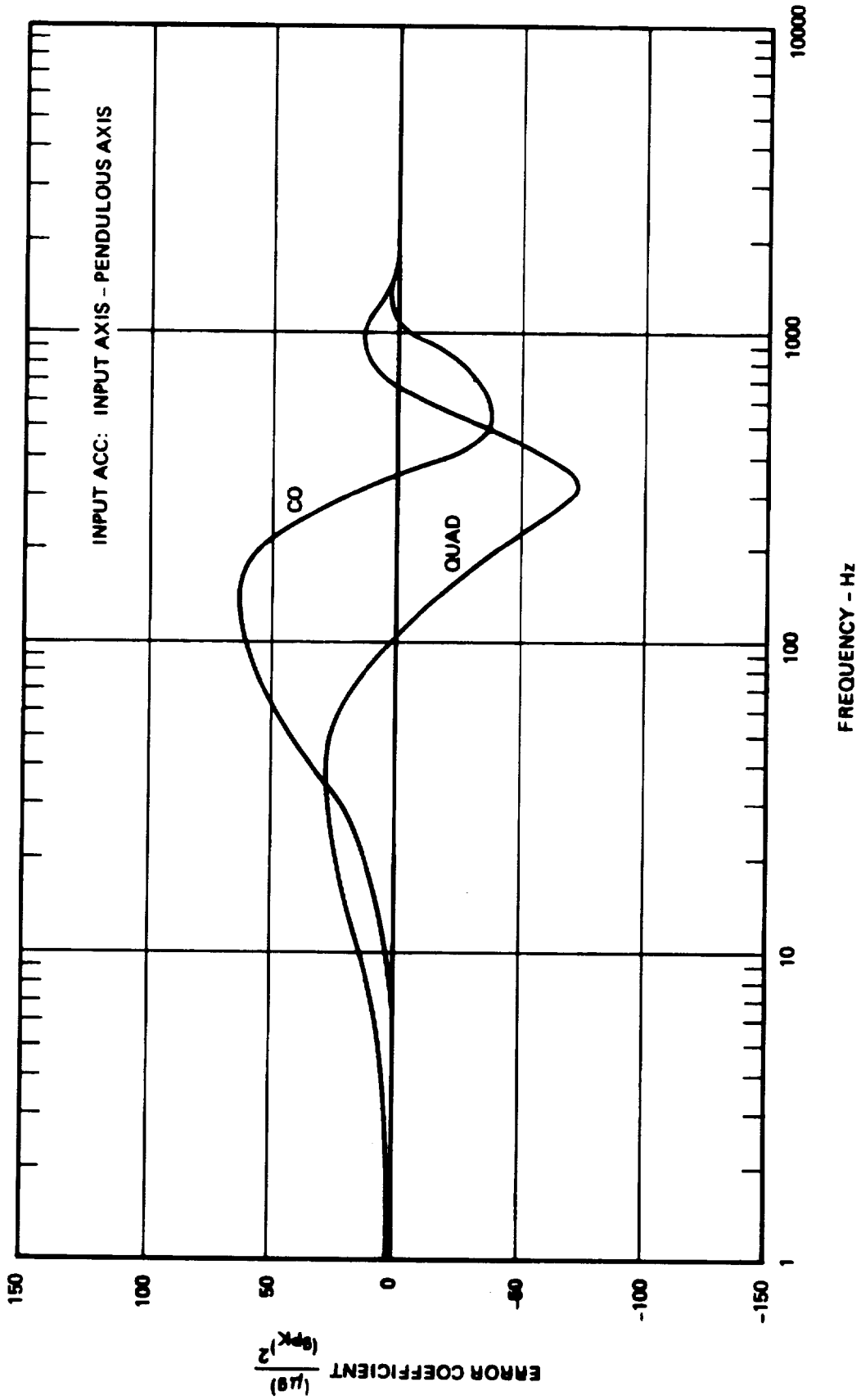


Figure 5-9. Accelerometer Loop Rectification Error Coefficient

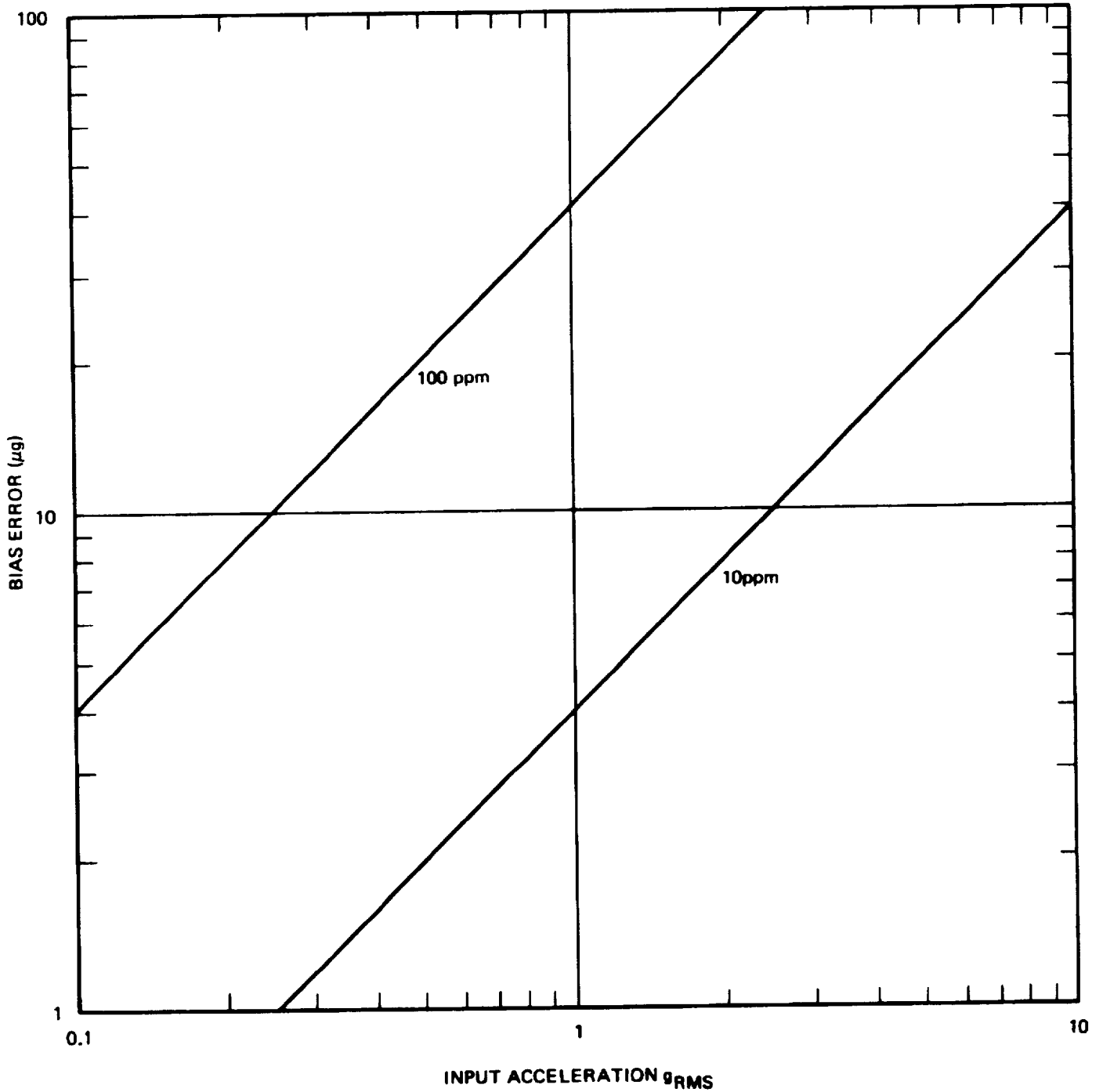


Figure 5-10. Accelerometer Scale Factor Asymmetry Error For Random Input Accelerations

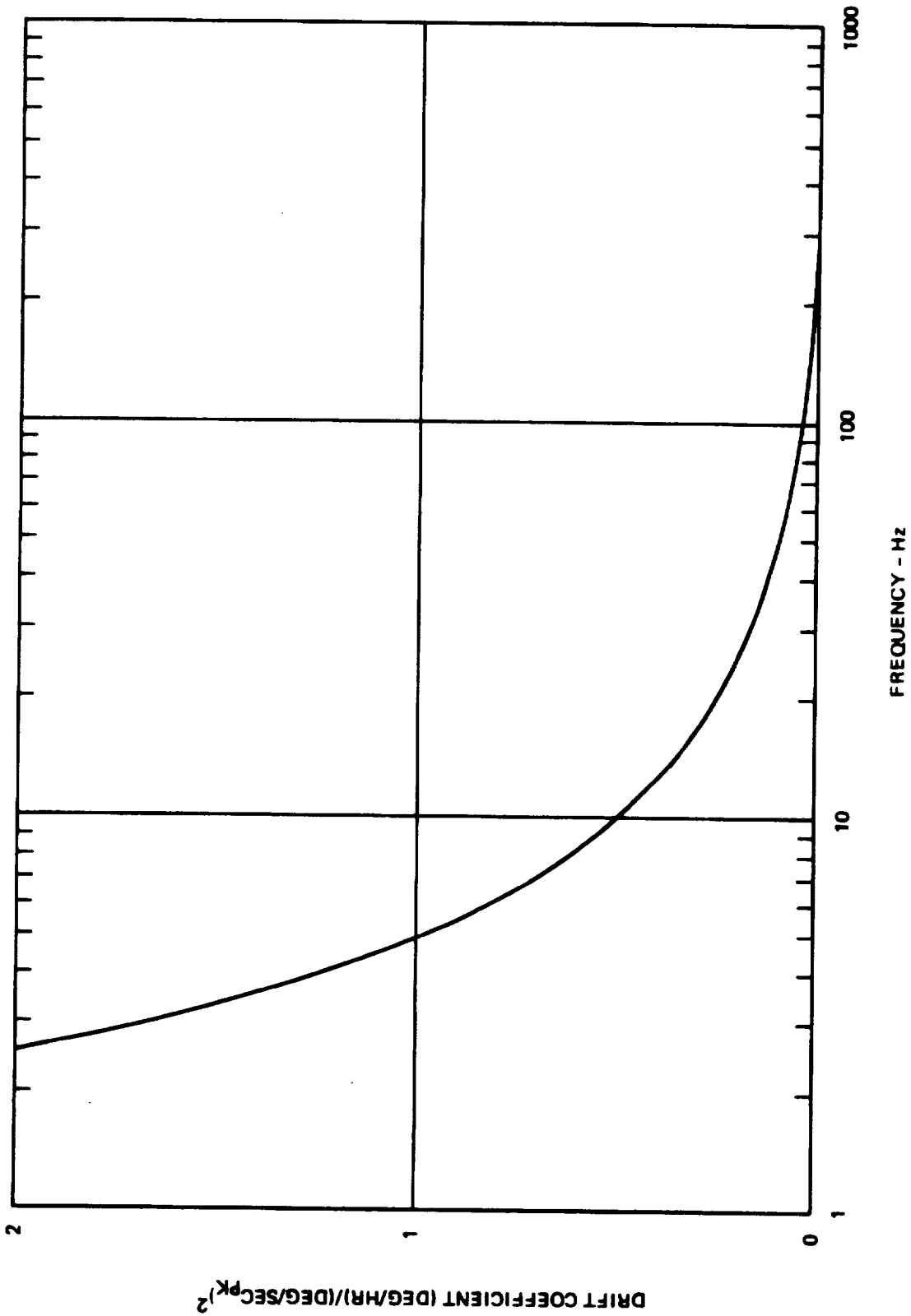


Figure 5-11. Coning Drift Coefficient

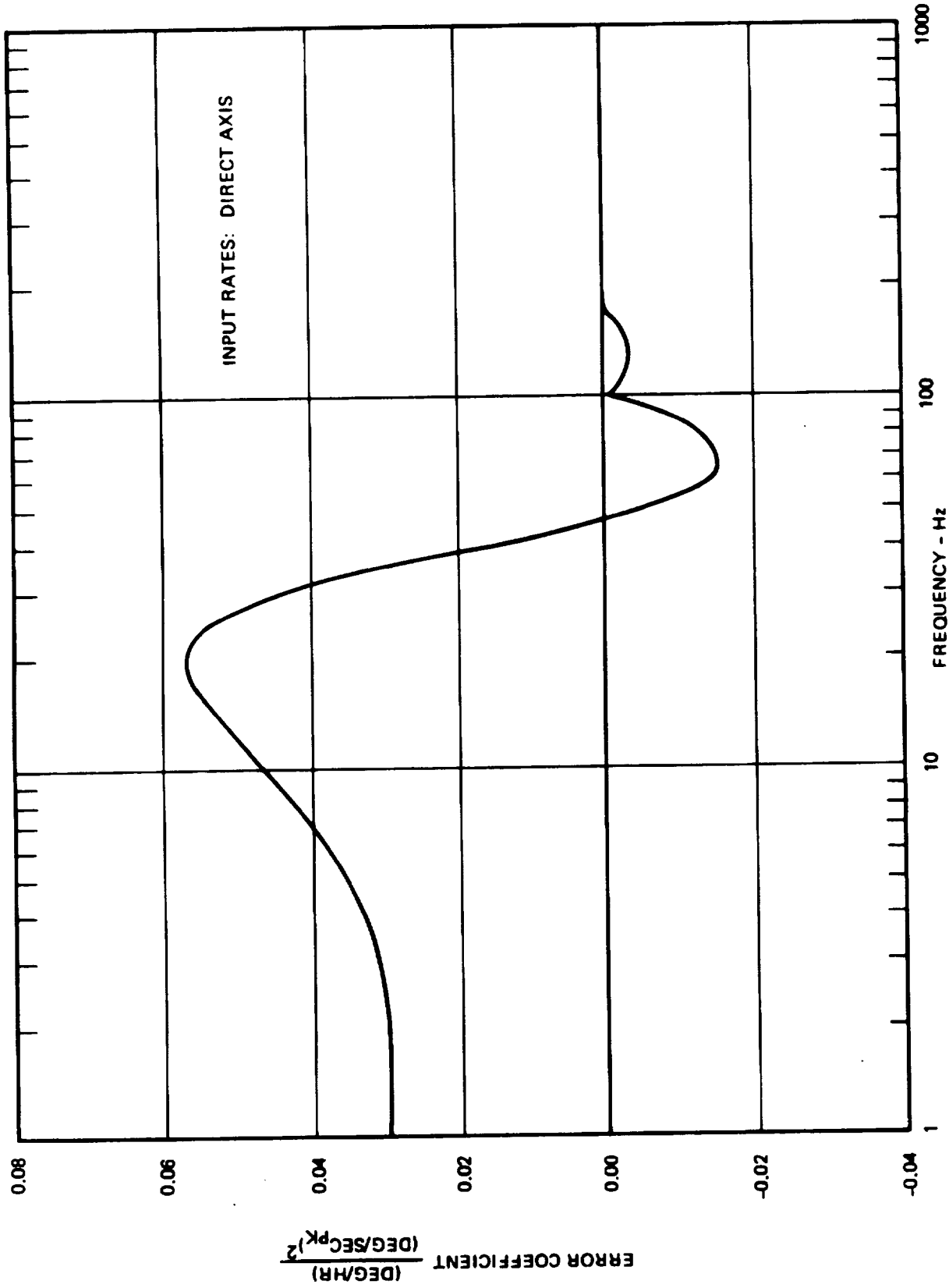


Figure 5-12. Uncompensated Pseudo Coning Error Coefficient

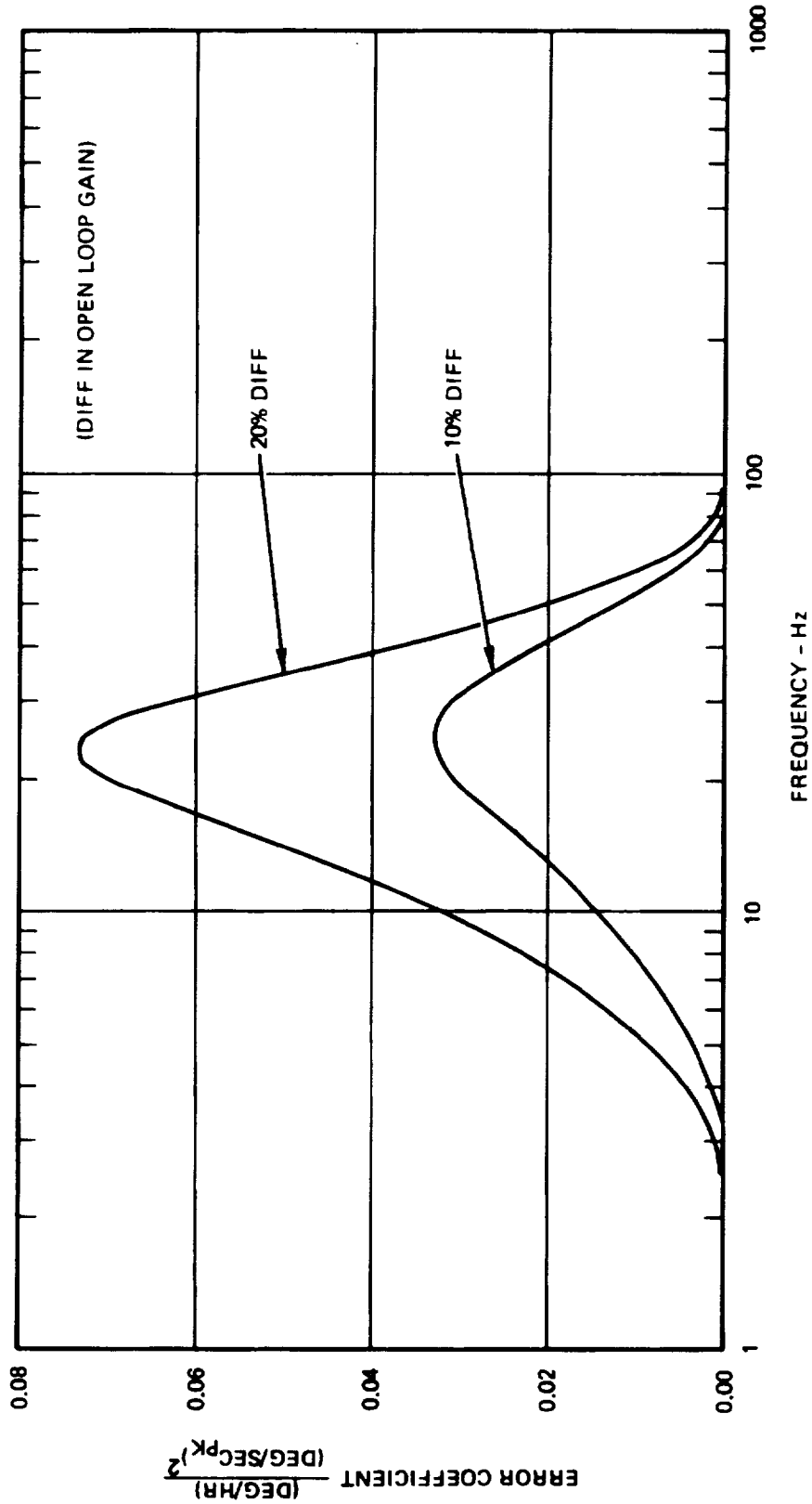


Figure 5-13. Pseudo Coning Error Coefficient due to Mismatched Gyro Loops

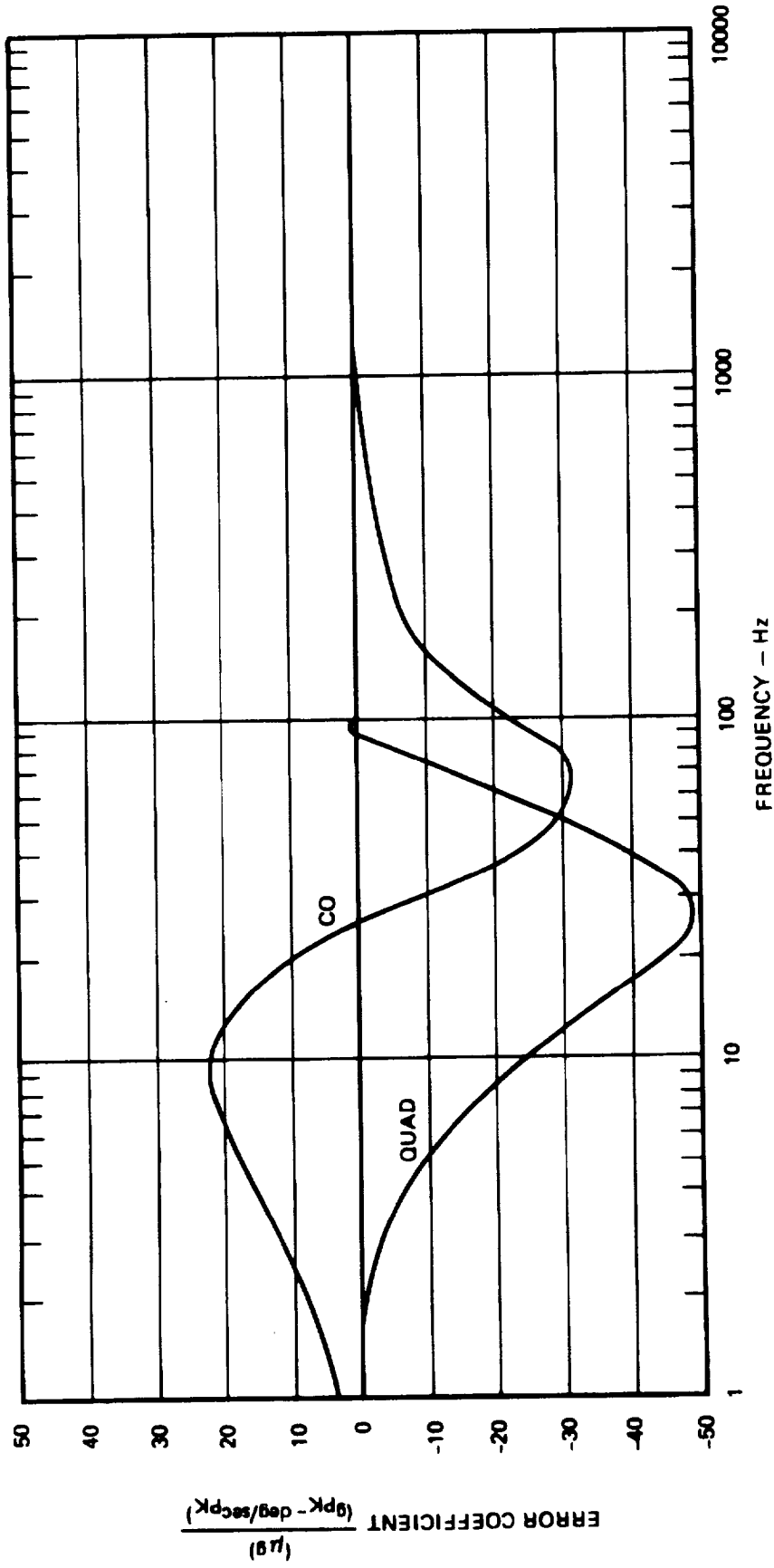


Figure 5-14. Pseudo Sculling Error Coefficient Due to Sensor Loop Mismatch

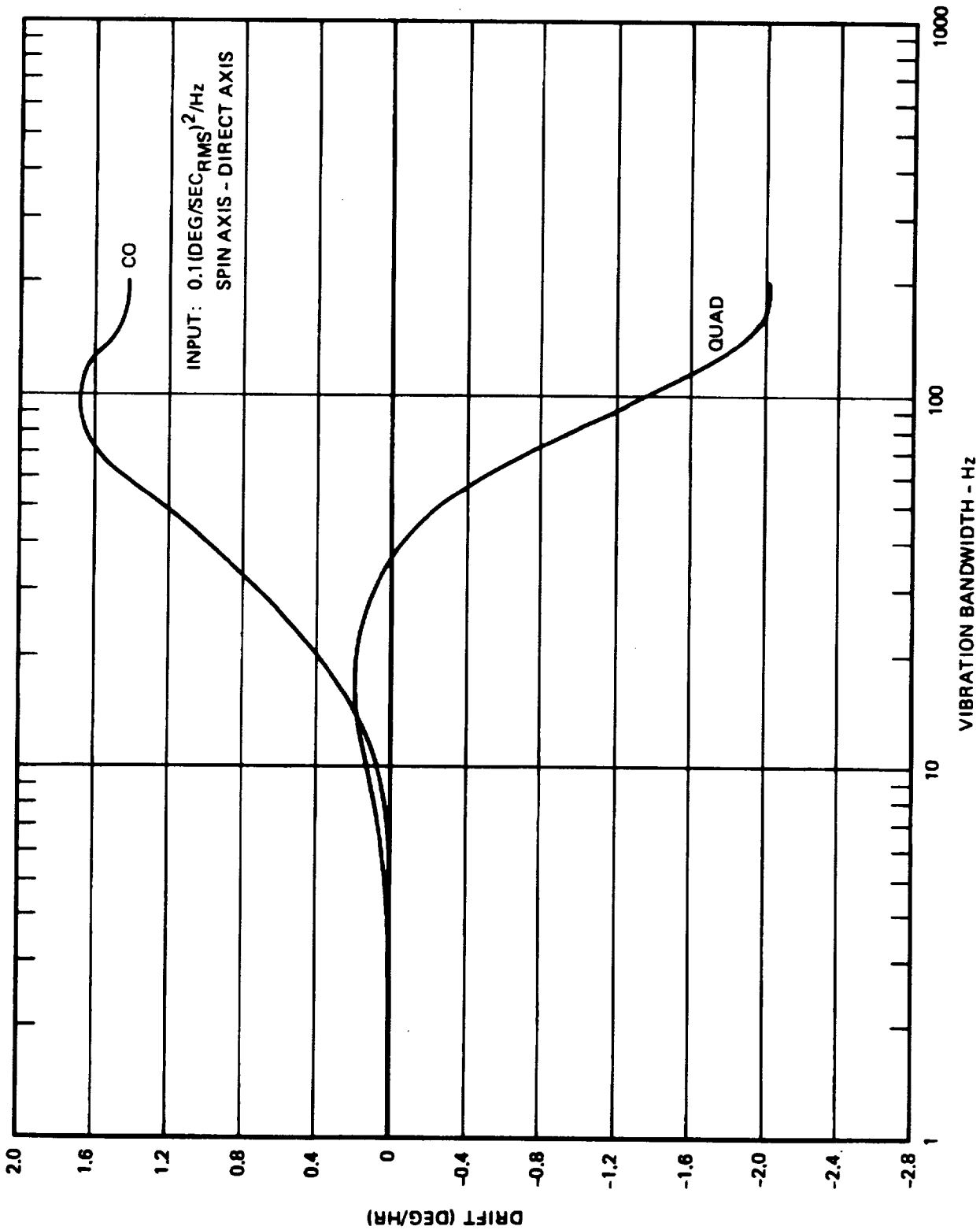


Figure 5-15. Gyro Loop Rectification Error Vs Vibration Bandwidth-Direct Axis

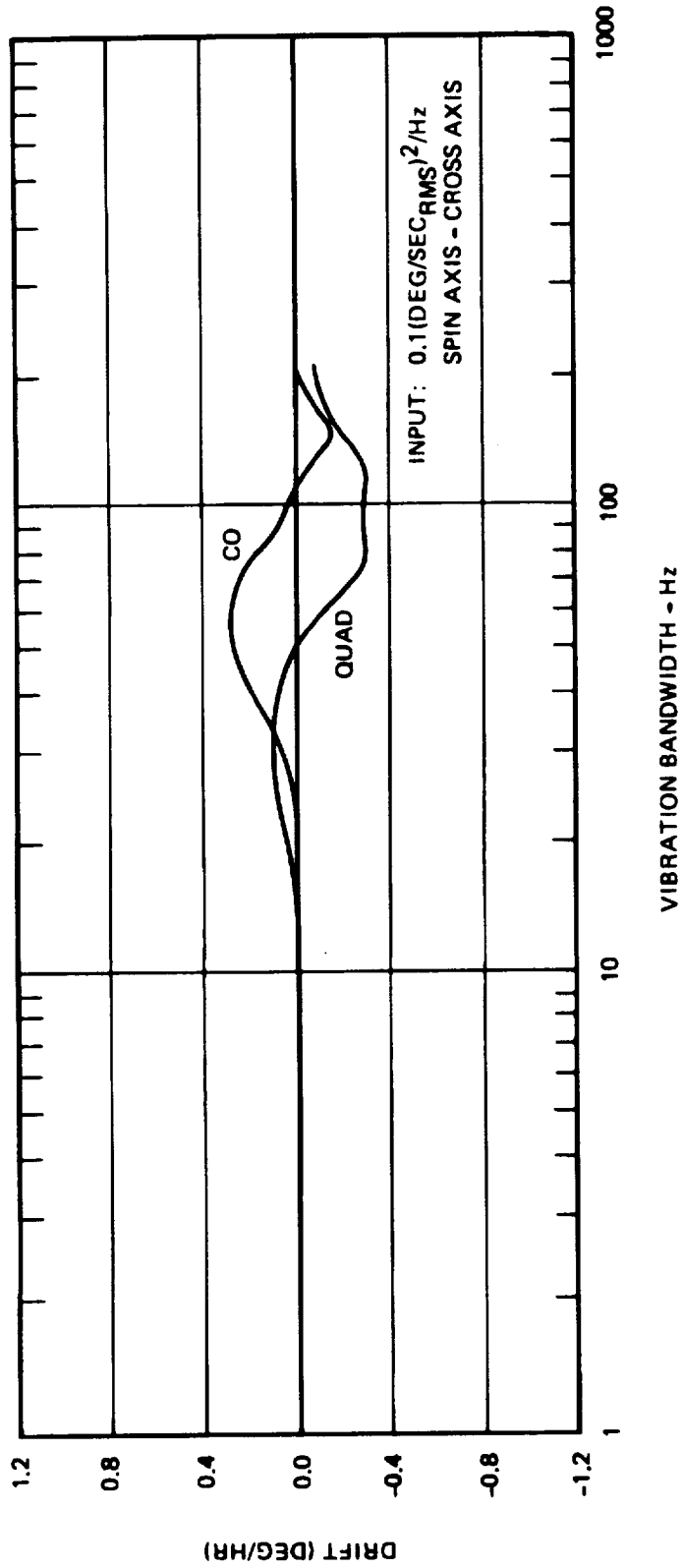


Figure 5-16. Gyro Loop Rectification Error Vs Vibration Bandwidth-Cross Axis

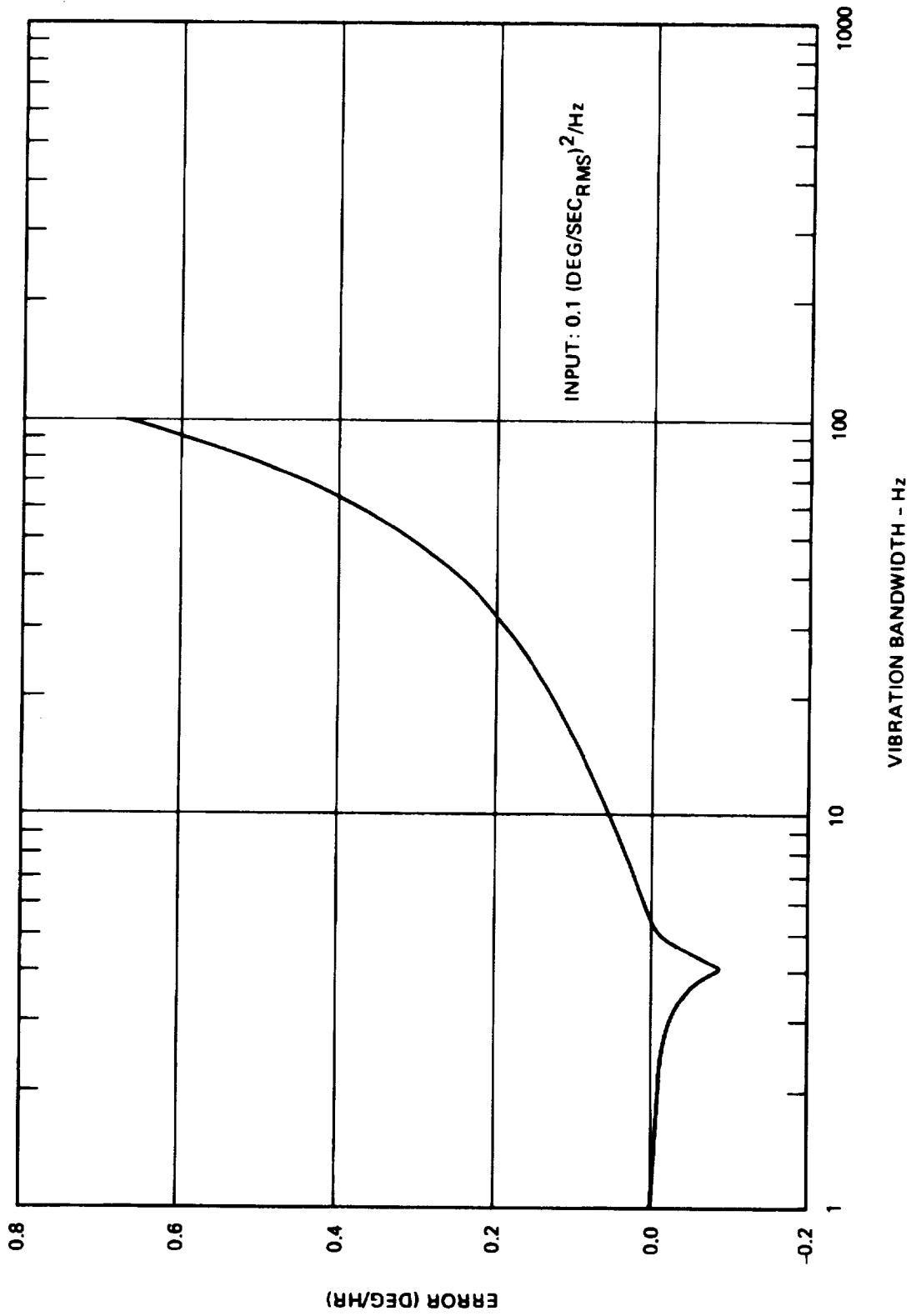


Figure 5-17. Anisoinertia Error Vs Vibration Bandwidth

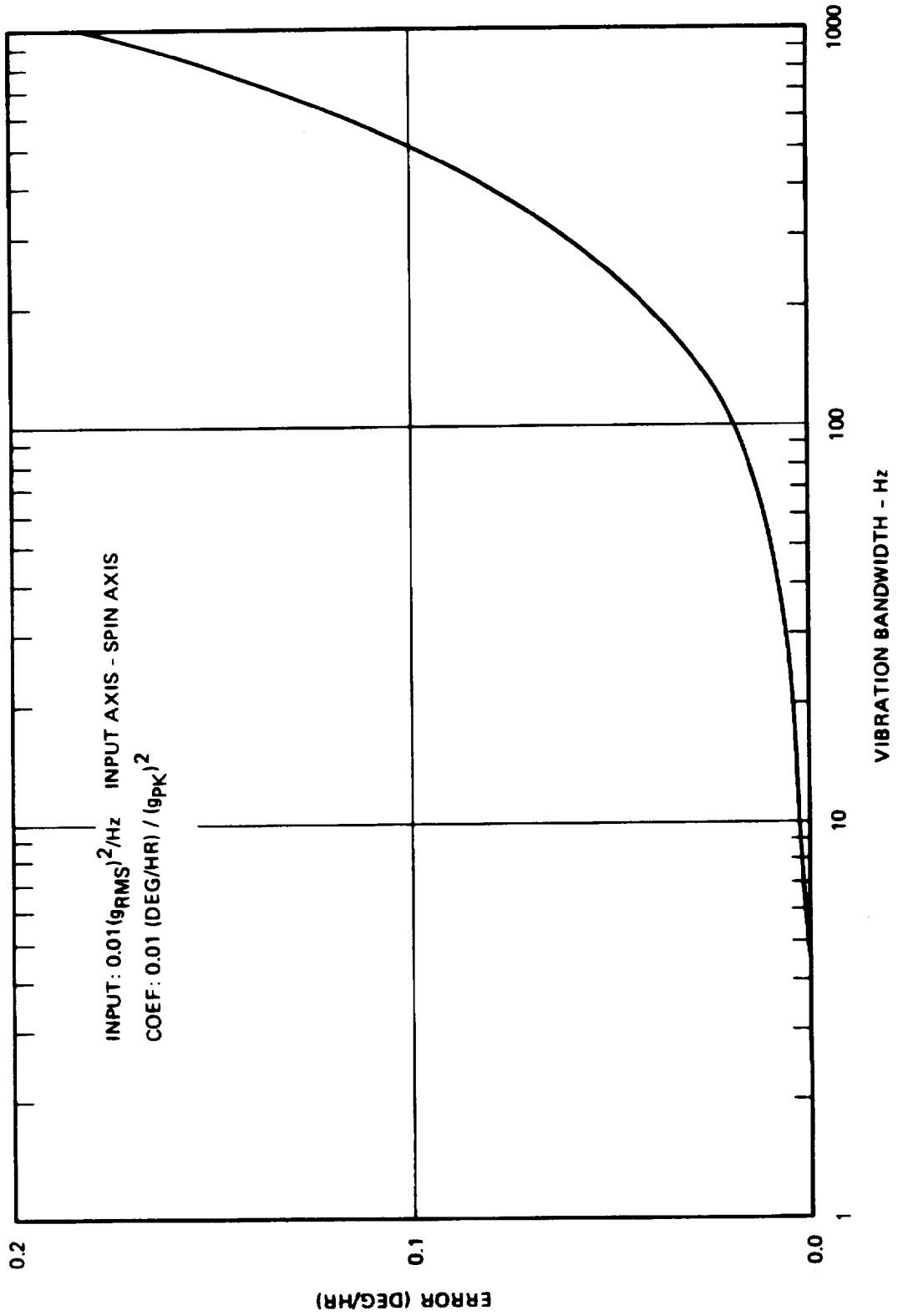


Figure 5-18. Gyro Anisoelastic Error Vs Vibration Bandwidth

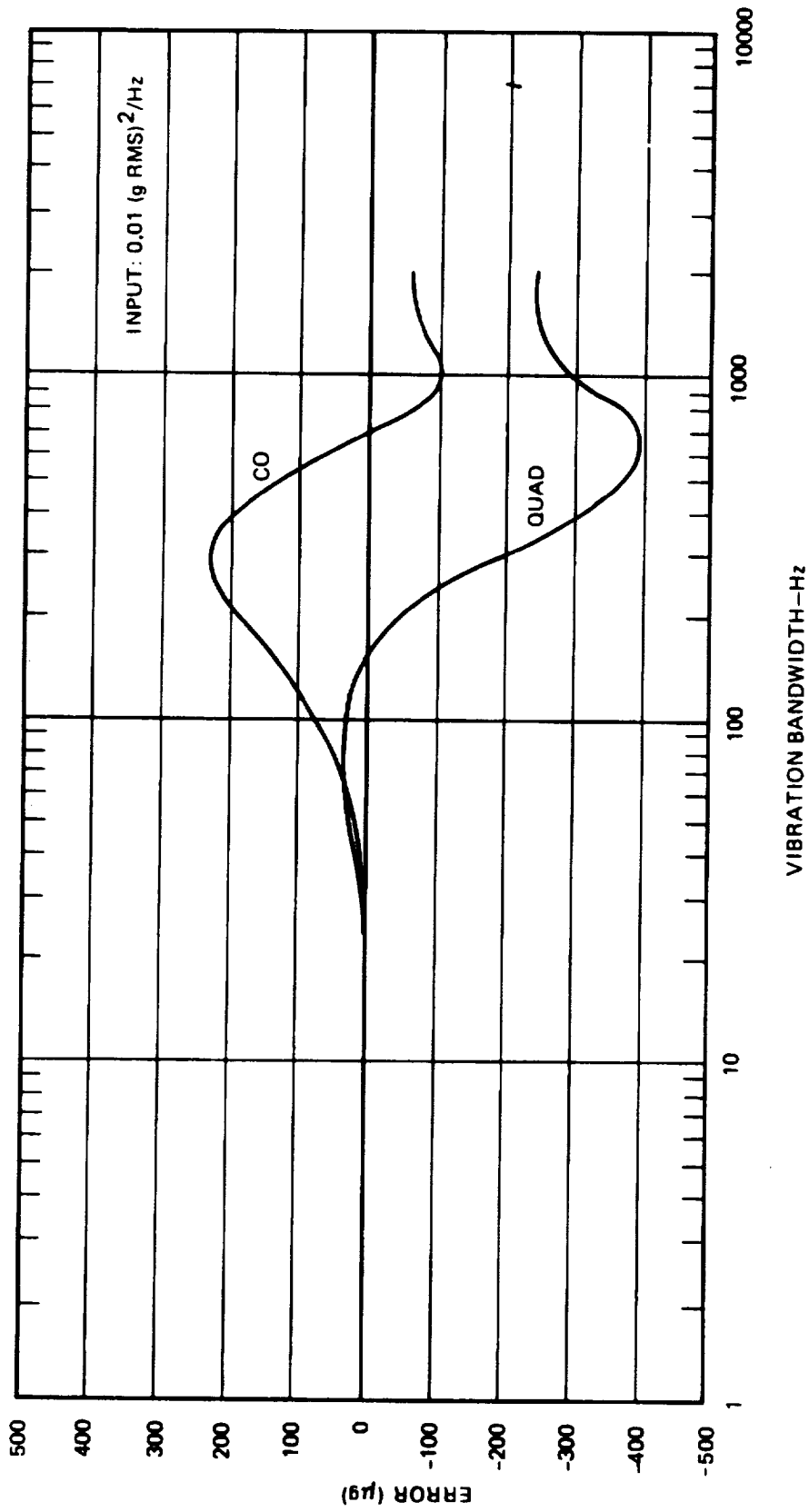


Figure 5-19. Accelerometer Loop Rectification Error Vs Vibration Bandwidth

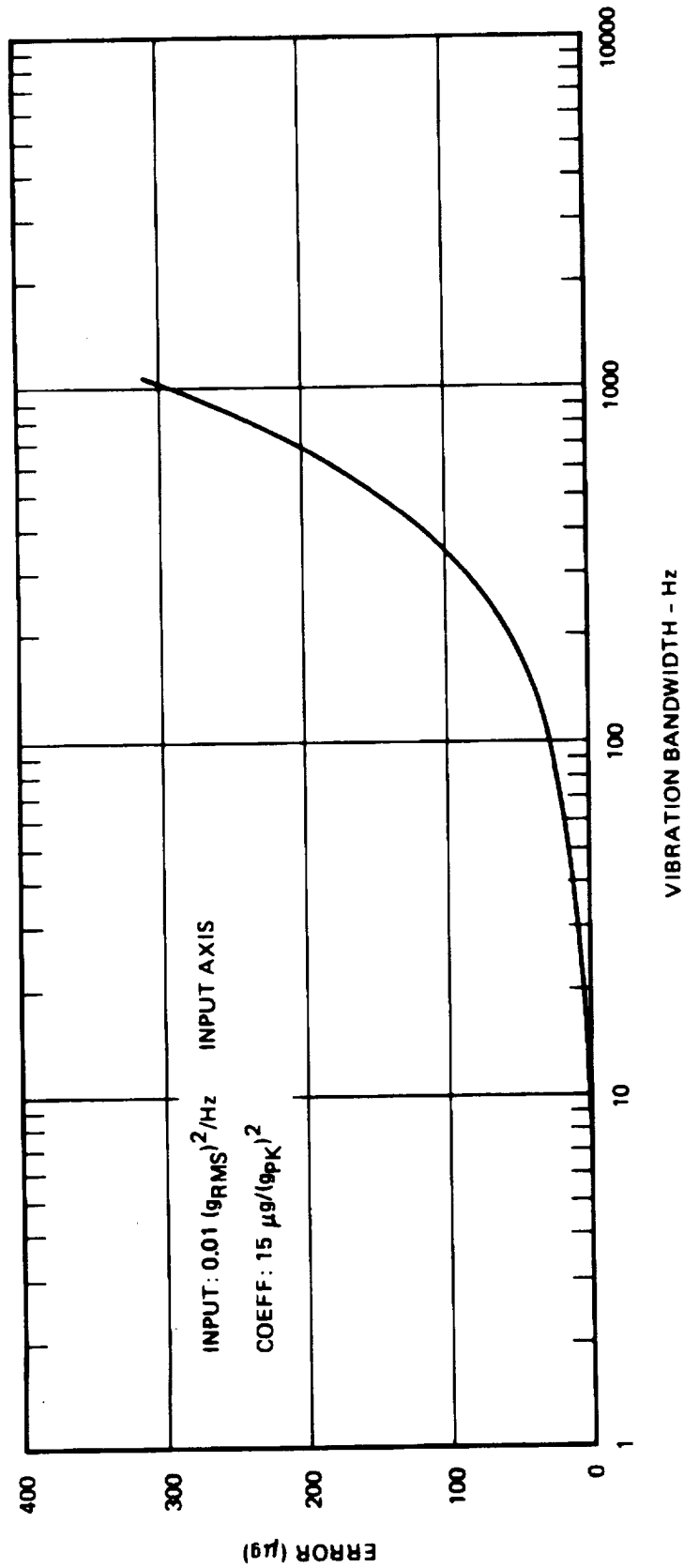


Figure 5-20. Accelerometer g² Error Vs Vibration Bandwidth

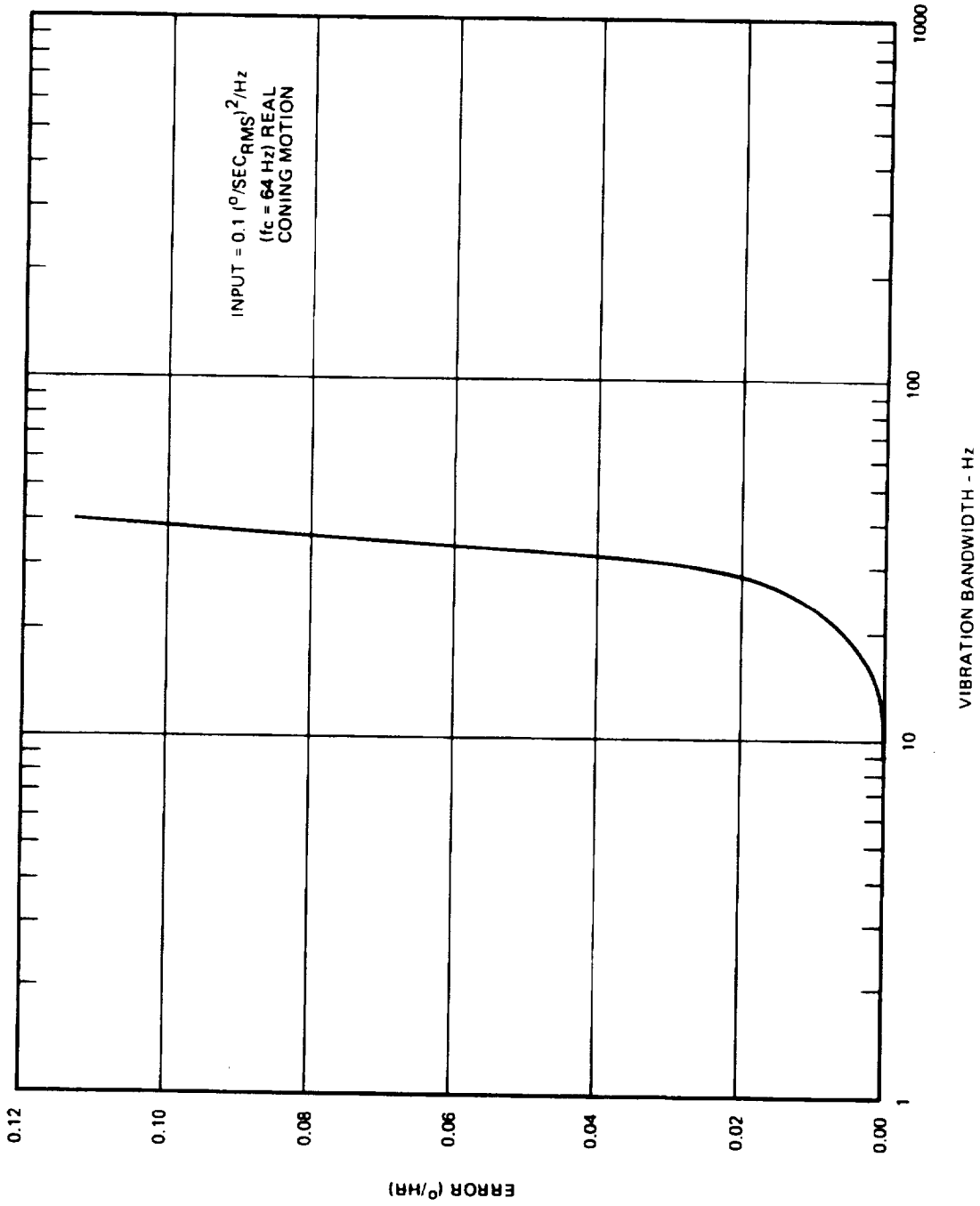


Figure 5-21. Coning Error Vs Vibration Bandwidth

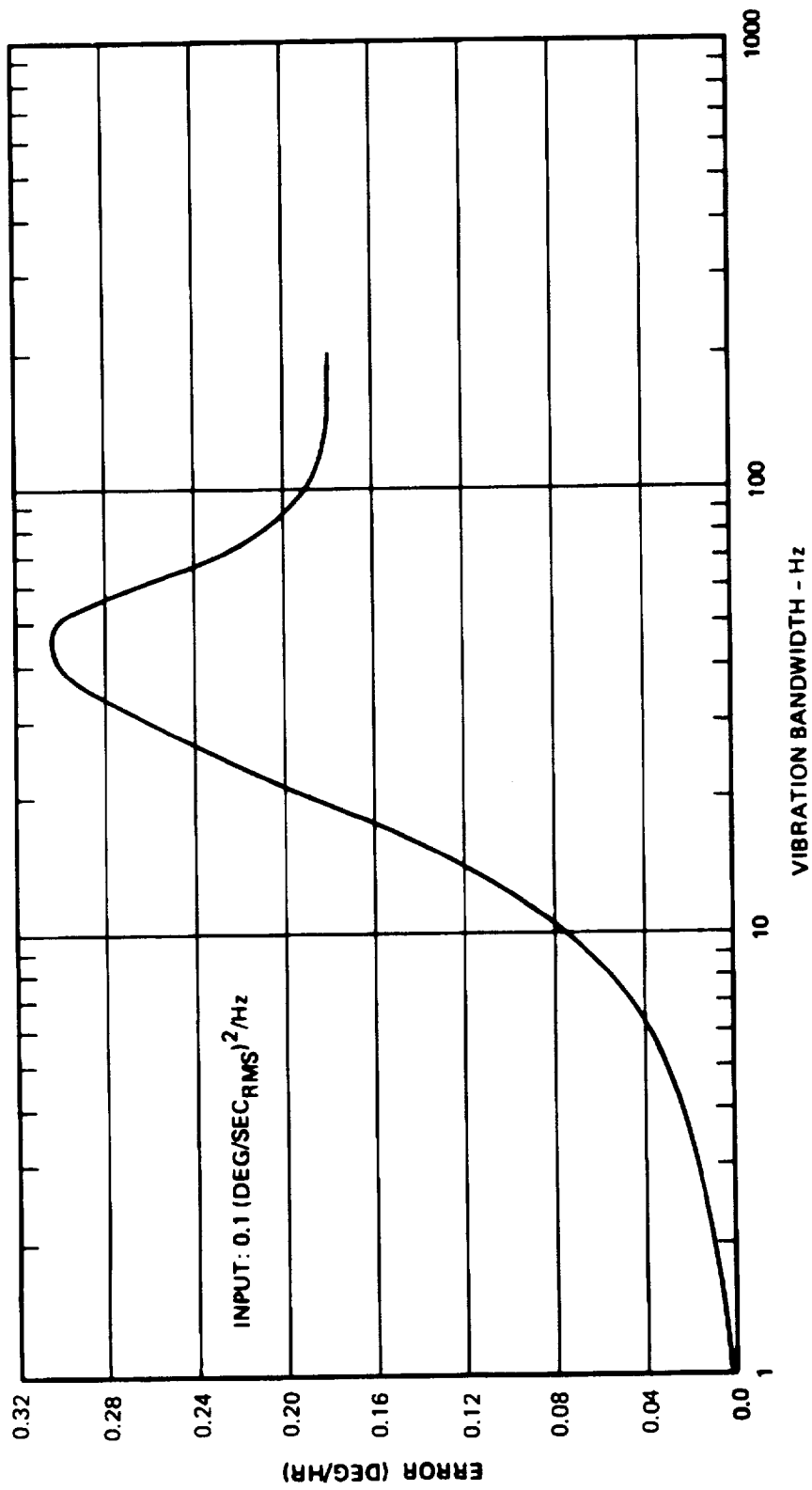


Figure 5-22. Uncompensated Pseudo Coning Error Vs Vibration Bandwidth,
No Computer Attenuation

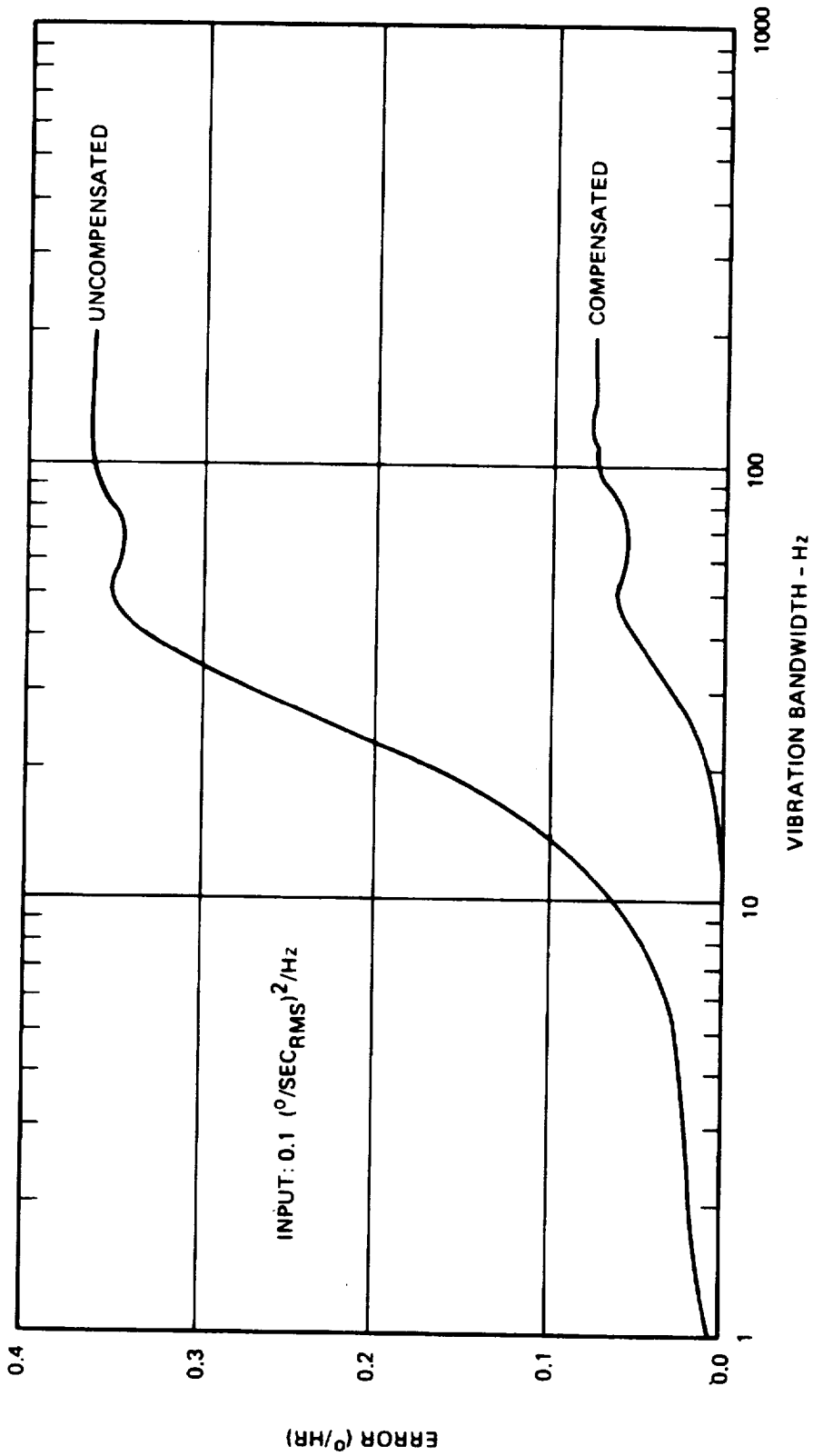


Figure 5-23. Pseudo Coning Error Vs Vibration Bandwidth, Computer Frequency Response Included

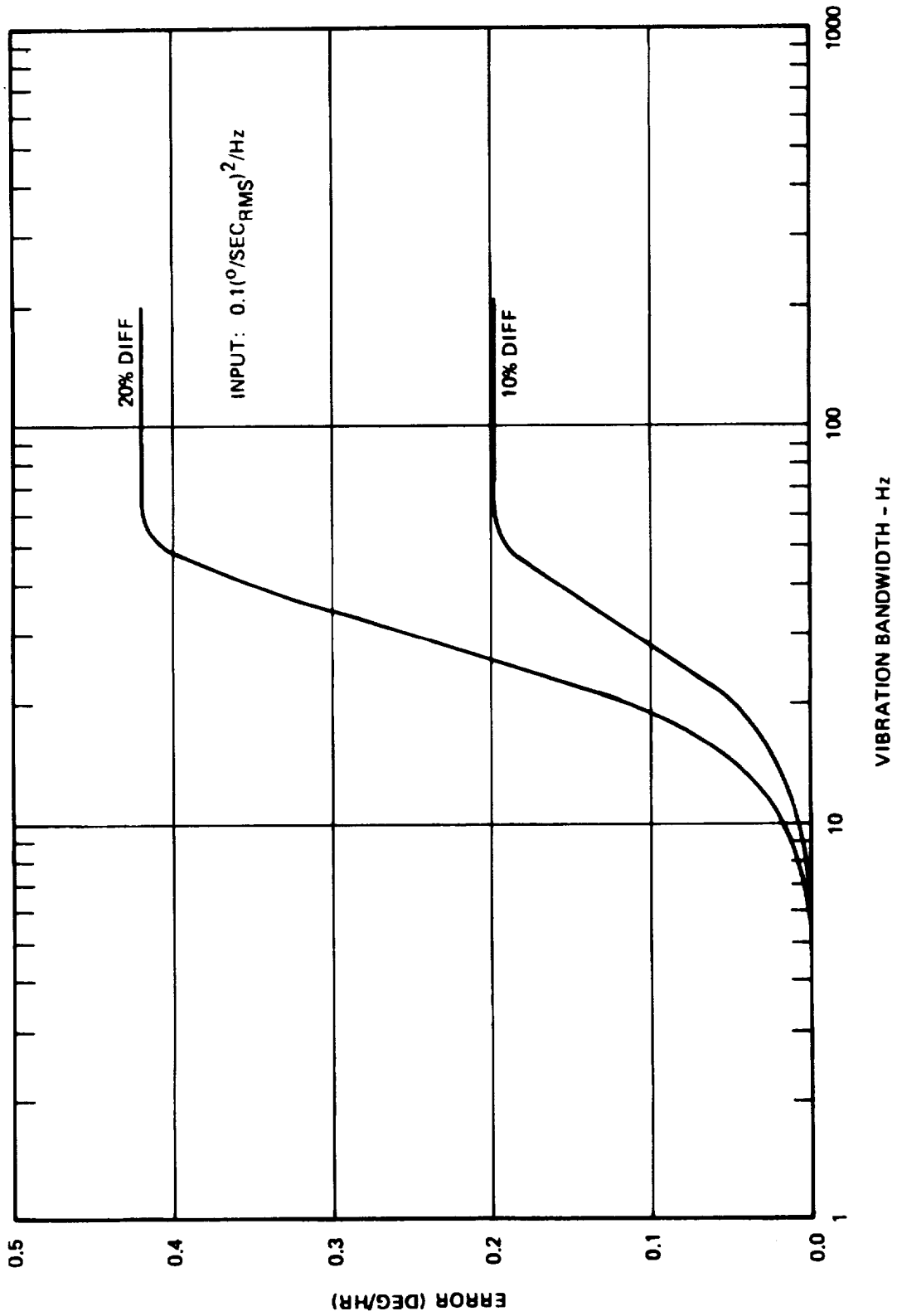


Figure 5-24. Pseudo Coning Error Due To Mismatched Gyro Loops Vs Vibration Bandwidth

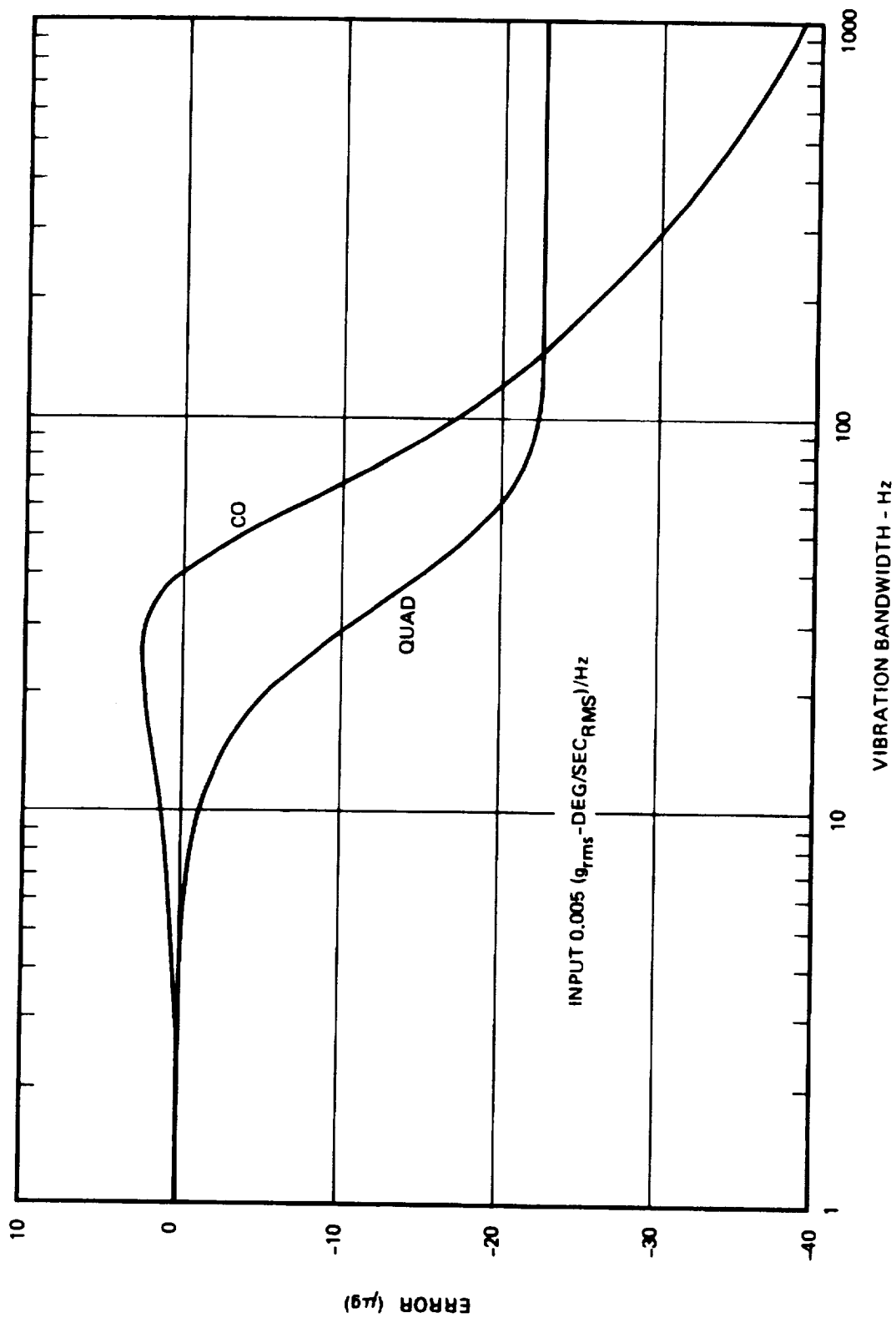


Figure 5-25. Sculling Error Vs Vibration Bandwidth

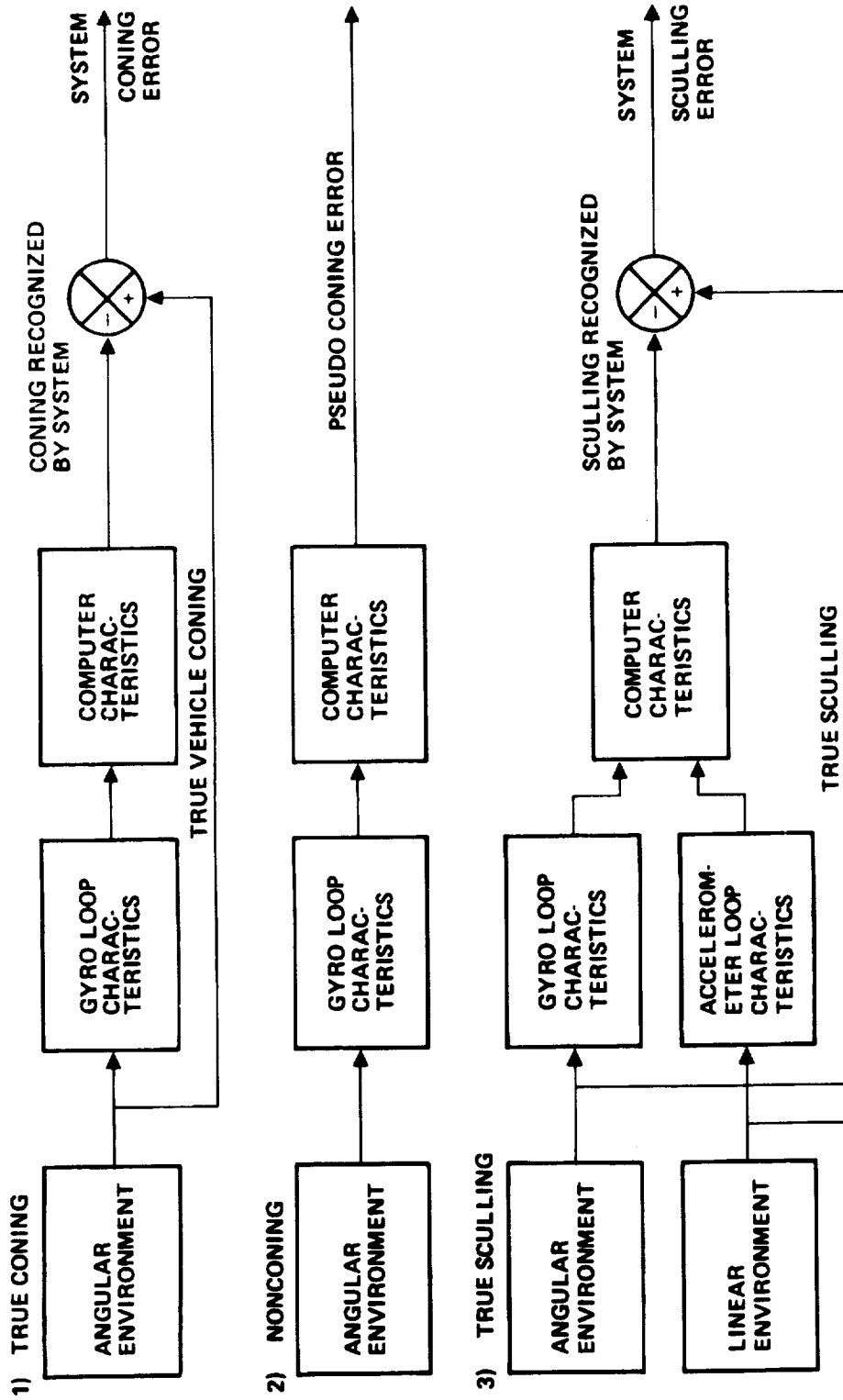


Figure 5-26. System Dynamic Error Description

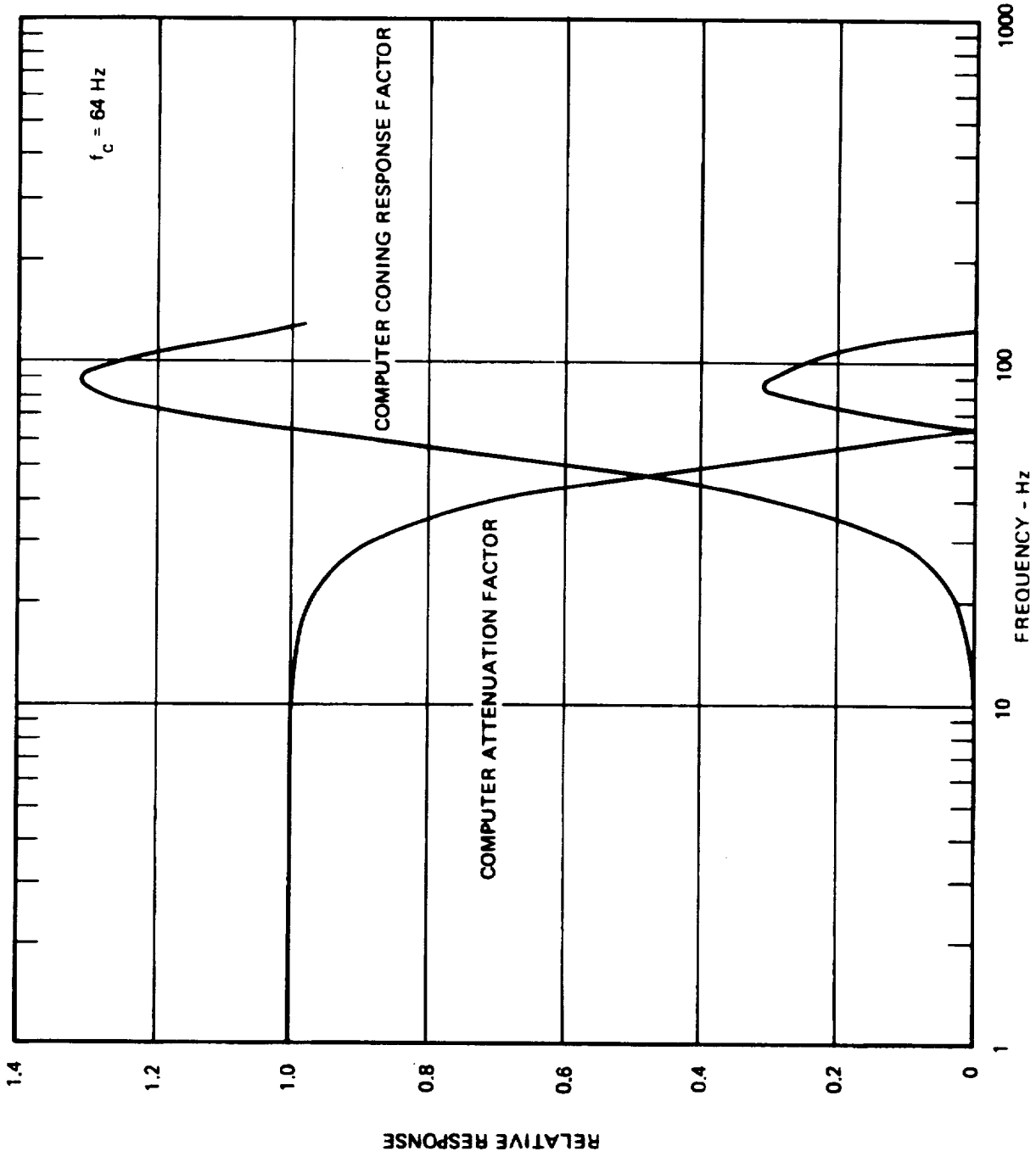


Figure 5-27. Computer Frequency Response

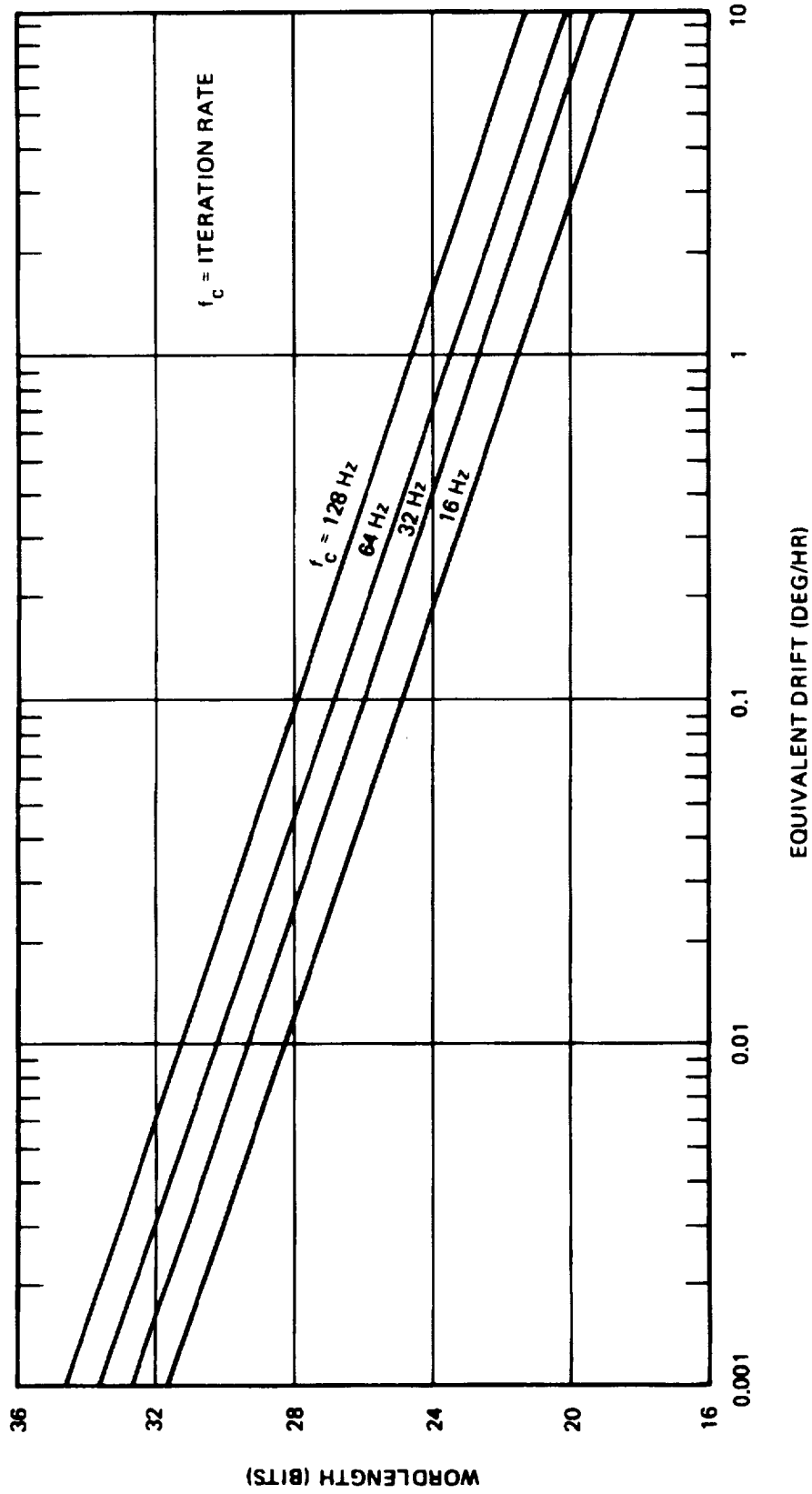


Figure 5-28. Computer Roundoff Error

5.2 Error Simulation of Radio-Strapdown Navigator

5.2.1 Introduction

An error simulation of a radio-inertial (strapdown) navigator traversing a 1.2 hour closed trajectory was performed using a digital computer program developed under Litton's IRAD program 76G-1D(B). The simulation does not as yet take into account the instrument redundancy concepts incorporated in the Langley study, but models instead a simple orthogonal triad configuration. Results are thus conservative, applying essentially to performance of one airborne computer output without averaging the four computer outputs.

The inertial error budgets (two are simulated for tradeoff purposes) are each composed of 45 error sources and the radio error budget of four error sources (two per axis). The radio and inertial position data is used to estimate the errors in both position and velocity via a simple open loop constant gain estimator. No error estimates of heading and attitude were made.

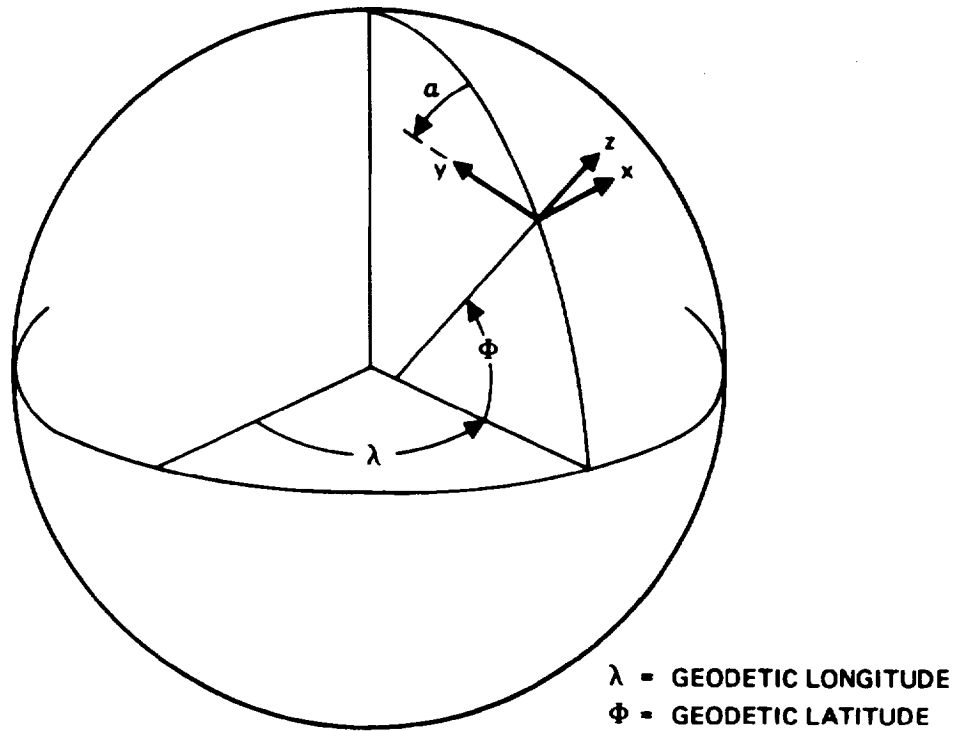
Paragraphs 5.2.2, 3 and 4 present the error models and budgets simulated. Paragraph 5.2.5 displays and discusses the simulated updating concept. Details of the trajectory are presented in paragraph 5.2.6. A brief discussion of the simulation program is contained in paragraph 5.2.7. Paragraphs 5.2.8 and 5.2.9 present and discuss both the free-inertial and the radio-inertial error profiles for the two inertial error budgets simulated. Finally paragraph 5.2.10 relates the results to the Langley specification.

5.2.2 Strapdown Inertial Error Model

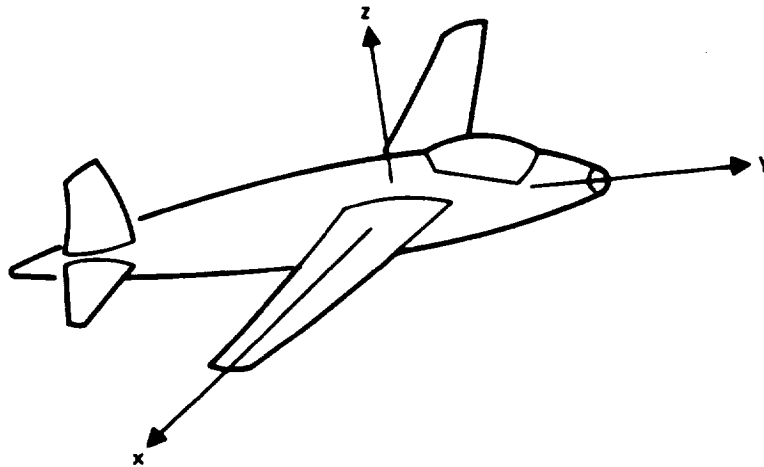
The inertial error model incorporated into the simulation program is based on a navigator consisting of an orthogonal instrument set (gyros and accelerometers) affixed to the aircraft, and computing in a local level frame. The local level computation frame is a wander azimuth frame whose wander angle α is given by

$$\dot{\alpha} = -\dot{\lambda} \sin \phi \quad (5.2-1)$$

See figure 5-29.



A) COMPUTATION FRAME



B) INSTRUMENT FRAME

Figure 5-29. Coordinate Frames

The error dynamics are summarized (not derived herein) in equations 5.2-2 to 5.2-20, where the symbols are defined as follows (all components are in the computation frame):

$\Omega_{x, y, z}$	Components of earth rate
$\rho_{x, y, z}$	Components of transport rate of computation frame
$\omega_{x, y, z}$	Components of inertial angular rate of computation frame
$\mu_{x, y, z}$	Components of transport rate plus earth rate
$V_{x, y, z}$	Components of vehicle velocity relative to earth
$R_{x, y}$	Radii of curvature
$A_{x, y, z}$	Components of specific force
$\delta\rho_{x, y, z}$	Transport rate error
$\delta\theta_{x, y, z}$	Computation frame attitude errors
$\phi_{x, y, z}$	Instrument frame attitude errors
$\delta V_{x, y, z}$	Velocity errors
δh	Altitude error
τ	Alignment, updating, etc controls
$\epsilon_{x, y, z}$	Components of composite gyro drift
$\nabla_{x, y, z}$	Components of composite accelerometer bias

$$\omega_x = \rho_x + \Omega_x \quad (5.2-2)$$

$$\omega_y = \rho_y + \Omega_y \quad (5.2-3)$$

$$\omega_z = \rho_z + \Omega_z \quad (5.2-4)$$

$$\mu_x = \rho_x + 2\Omega_x \quad (5.2-5)$$

$$\mu_y = \rho_y + 2\Omega_y \quad (5.2-6)$$

$$\mu_z = \rho_z + 2\Omega_z \quad (5.2-7)$$

$$\delta\rho_x = -\delta V_y/R_y + (V_y/R_y^2) \delta h \quad (5.2-8)$$

$$\delta\rho_y = \delta V_x/R_x - (V_x/R_x^2) \delta h \quad (5.2-9)$$

$$\delta\rho_z = 0 \quad (5.2-10)$$

$$\dot{\delta\theta}_x = \delta\rho_x - \rho_y \delta\theta_z + \rho_z \delta\theta_y + \tau_{cx} \quad (5.2-11)$$

$$\dot{\delta\theta}_y = \delta\rho_y - \rho_z \delta\theta_x + \rho_x \delta\theta_z + \tau_{cy} \quad (5.2-12)$$

$$\dot{\delta\theta}_z = \delta\rho_z - \rho_x \delta\theta_y + \rho_y \delta\theta_x + \tau_{cz} \quad (5.2-13)$$

$$\dot{\phi}_x = \delta\rho_x + \Omega_y \delta\theta_z - \Omega_z \delta\theta_y - \omega_y \phi_z + \omega_z \phi_y + \tau_{px} - \epsilon_x \quad (5.2-14)$$

$$\dot{\phi}_y = \delta\rho_y + \Omega_z \delta\theta_x - \Omega_x \delta\theta_z - \omega_z \phi_x + \omega_x \phi_z + \tau_{py} - \epsilon_y \quad (5.2-15)$$

$$\dot{\phi}_z = \delta\rho_z + \Omega_x \delta\theta_y - \Omega_y \delta\theta_x - \omega_x \phi_y + \omega_y \phi_x + \tau_{pz} - \epsilon_z \quad (5.2-16)$$

$$\begin{aligned} \delta \dot{V}_x = & A_y \phi_z - A_z \phi_y - \mu_y \delta V_z + \mu_z \delta V_y - V_z \delta \rho_y + V_y \delta \rho_z \\ & - 2(V_y \Omega_y + V_z \Omega_z) \delta \theta_x + 2\Omega_x V_y \delta \theta_y + 2\Omega_x V_z \delta \theta_z + \tau_{vx} + \nabla_x \end{aligned} \quad (5.2-17)$$

$$\delta \dot{V}_y = A_x \phi_z - A_z \phi_x - \mu_x \delta V_z + \mu_z \delta V_x - V_x \delta \rho_z + V_z \delta \rho_x$$

TABLE 5-5. LANGLEY ERROR BUDGETS

ERROR SOURCE	NO. 005	NO. 004
X GYRO BIAS DEG HR	1.4000E-02	1.0000E-01
Y GYRO BIAS DEG HR	1.4000E-02	1.0000E-01
Z GYRO BIAS DEG HR	1.4000E-02	1.0000E-01
X ACC BIAS MICRO G	6.5000E 01	6.5000E 01
Y ACC BIAS MICRO G	6.5000E 01	6.5000E 01
Z ACC BIAS MICRO G	6.5000E 01	6.5000E 01
X GYRO MISALIGNMENT (WY) - MICRO RADIANS	7.5000E 01	7.5000E 01
X GYRO MISALIGNMENT (WZ) - MICRO RADIANS	7.5000E 01	7.5000E 01
Y GYRO MISALIGNMENT (WZ) - MICRO RADIANS	7.5000E 01	7.5000E 01
Y GYRO MISALIGNMENT (WX) - MICRO RADIANS	7.5000E 01	7.5000E 01
Z GYRO MISALIGNMENT (WX) - MICRO RADIANS	7.5000E 01	7.5000E 01
Z GYRO MISALIGNMENT (WY) - MICRO RADIANS	7.5000E 01	7.5000E 01
X ACC MISALIGNMENT (AY) - MICRO RADIANS	7.5000E 01	7.5000E 01
X ACC MISALIGNMENT (AZ) - MICRO RADIANS	7.5000E 01	7.5000E 01
Y ACC MISALIGNMENT (AZ) - MICRO RADIANS	7.5000E 01	7.5000E 01
Y ACC MISALIGNMENT (AX) - MICRO RADIANS	7.5000E 01	7.5000E 01
Z ACC MISALIGNMENT (AX) - MICRO RADIANS	7.5000E 01	7.5000E 01
Z ACC MISALIGNMENT (AY) - MICRO RADIANS	7.5000E 01	7.5000E 01
X GYRO G DRIFT (-AX)-DEG/HR/G	1.0000E-02	1.0000E-02
X GYRO G DRIFT (-AY)-DEG/HR/G	1.0000E-02	1.0000E-02
Y GYRO G DRIFT (-AY)-DEG/HR/G	1.0000E-02	1.0000E-02

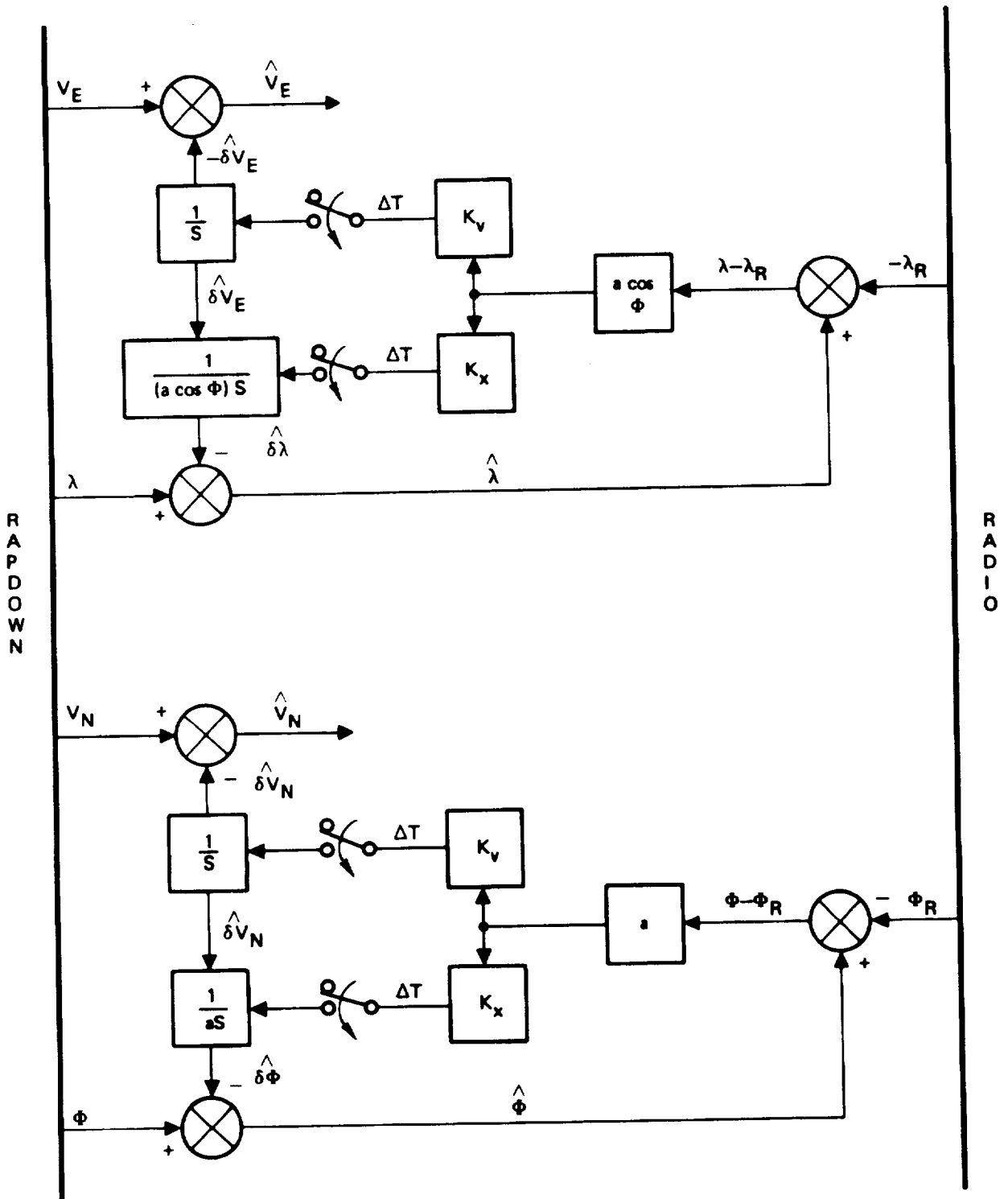


Figure 5-30. Simulated Updating Concept

The inertially derived latitude (ϕ) is first corrected with the present estimate of its error ($\delta\hat{\phi}$), yielding the best estimate of present latitude for display purposes. A similar procedure is used to obtain the best estimate of north velocity

($\hat{V}_N = V_N - \delta\hat{V}_N$) for display purposes.

At an update time (every ΔT), the best estimate of present latitude is compared with the radio indicated latitude, forming the observable difference ($= a(\hat{\phi} - \phi_R)$). The observable difference multiplied by the constant gains K_V and K_X form the incremental error estimates for velocity and position respectively. These incremental estimates are added to the existing error estimates thus forming new (updated) error estimates. Note that between updates the velocity error estimate remains constant, but the position error estimate is changed by the time integral of the velocity error estimate.

5.2.6 Simulated Trajectory

A plan view of the simulated trajectory is shown in figure 5-31. It consists of three take-offs and three landings around a closed loop, simulating an intracity airbus. The total time of the flight is 1.2 hours.

Each take-off consists of a turning climb during which the aircraft changes heading by 180° . The landing patterns at stations two and three are similar and consist of a descent followed by a turning descent during which the aircraft changes heading by 270° . The landing at station one differs from that at two and three in that the heading change is 225° .

Each of the maneuvers (climb, descent, turn) is performed by pitching and/or rolling the aircraft. Since the strapdown instruments are attached to the aircraft body, they will, of course, experience a change in geographic direction just as the aircraft body does. Thus, for example, when taking off after ground alignment, the accelerometer biases rotate 180° due to the change in aircraft heading.

Figures 5-32, -33 and -34 show detailed plan views of the first, second and third stations respectively. In each case the plot is made with the station at the origin.

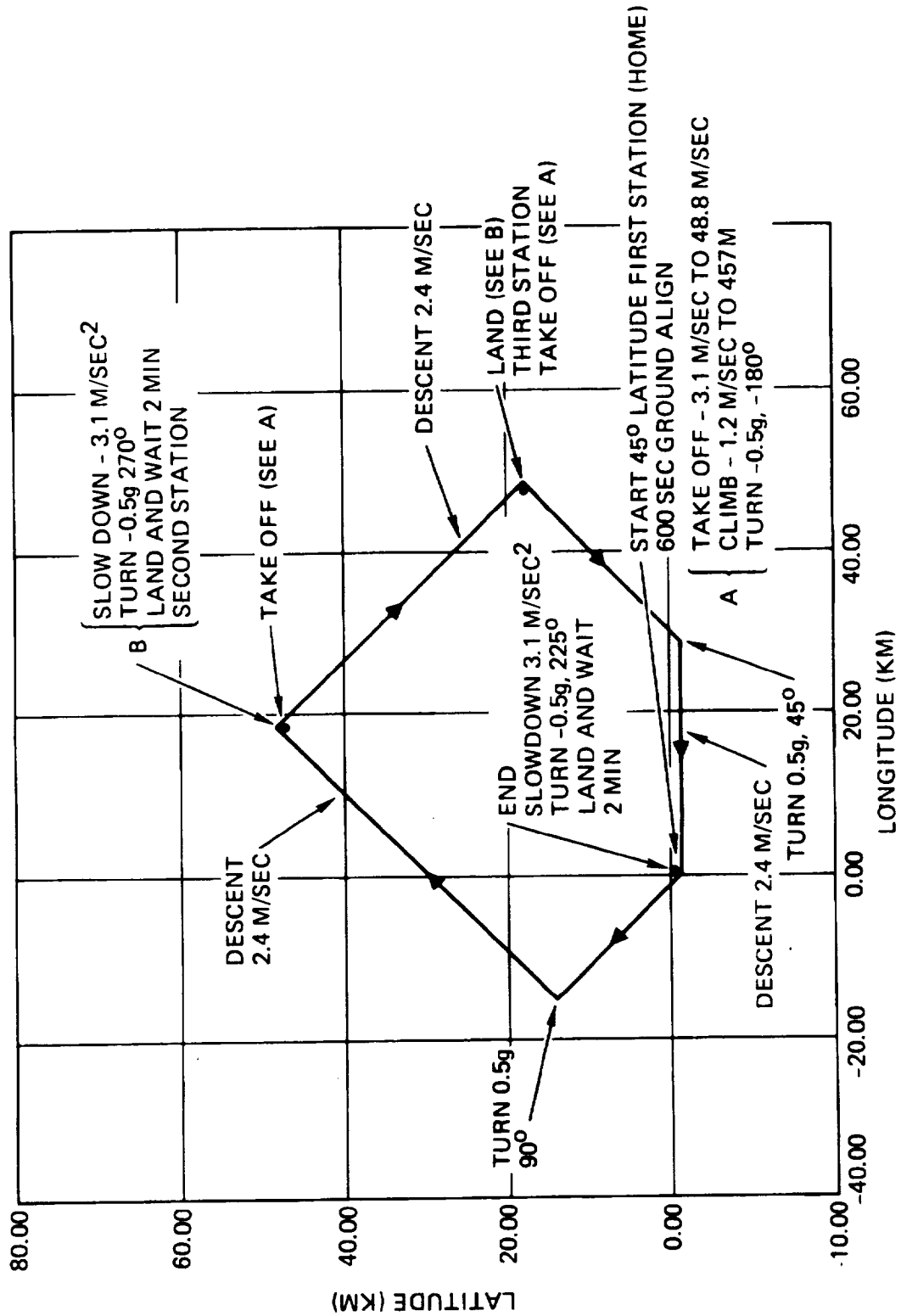
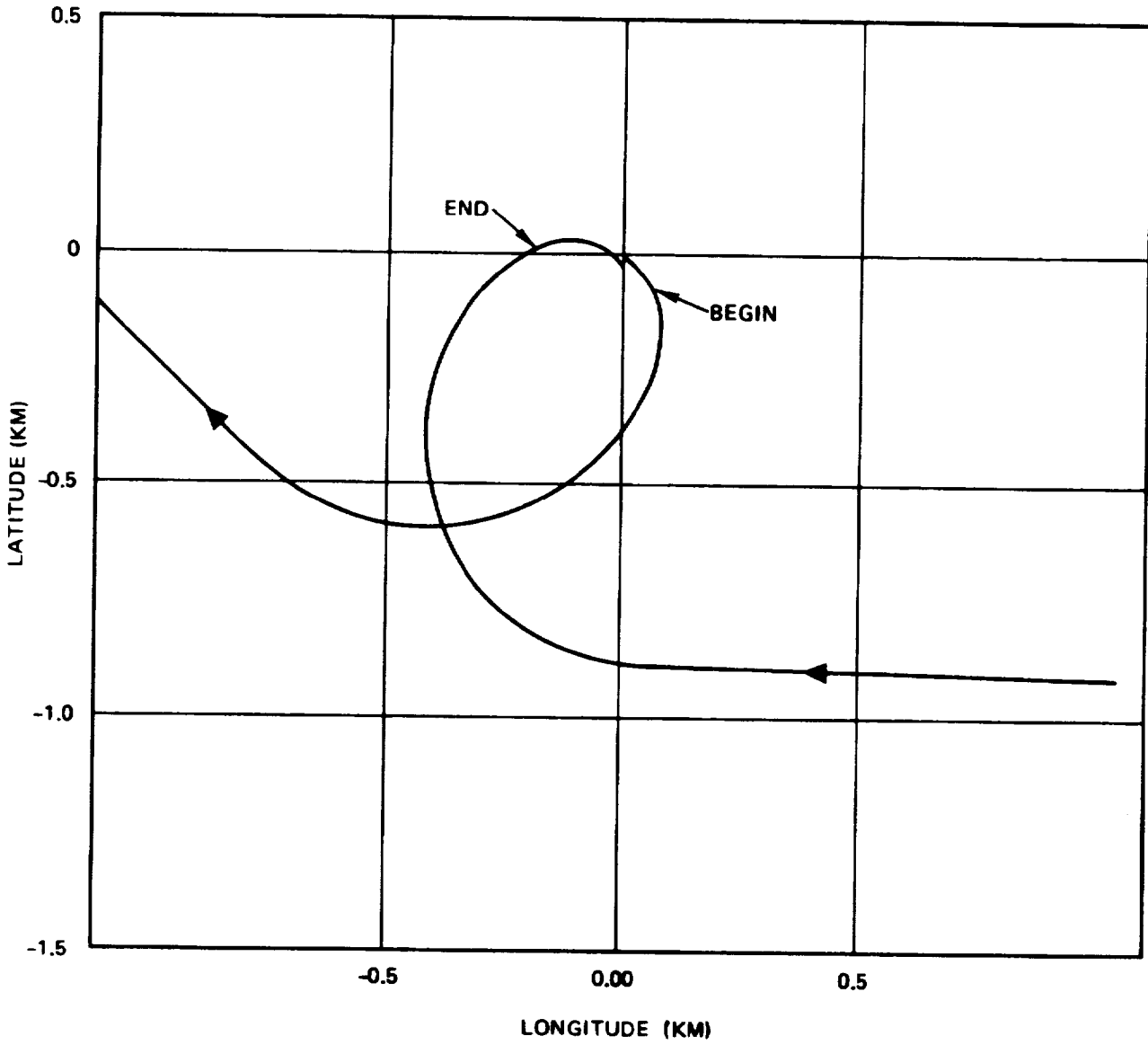
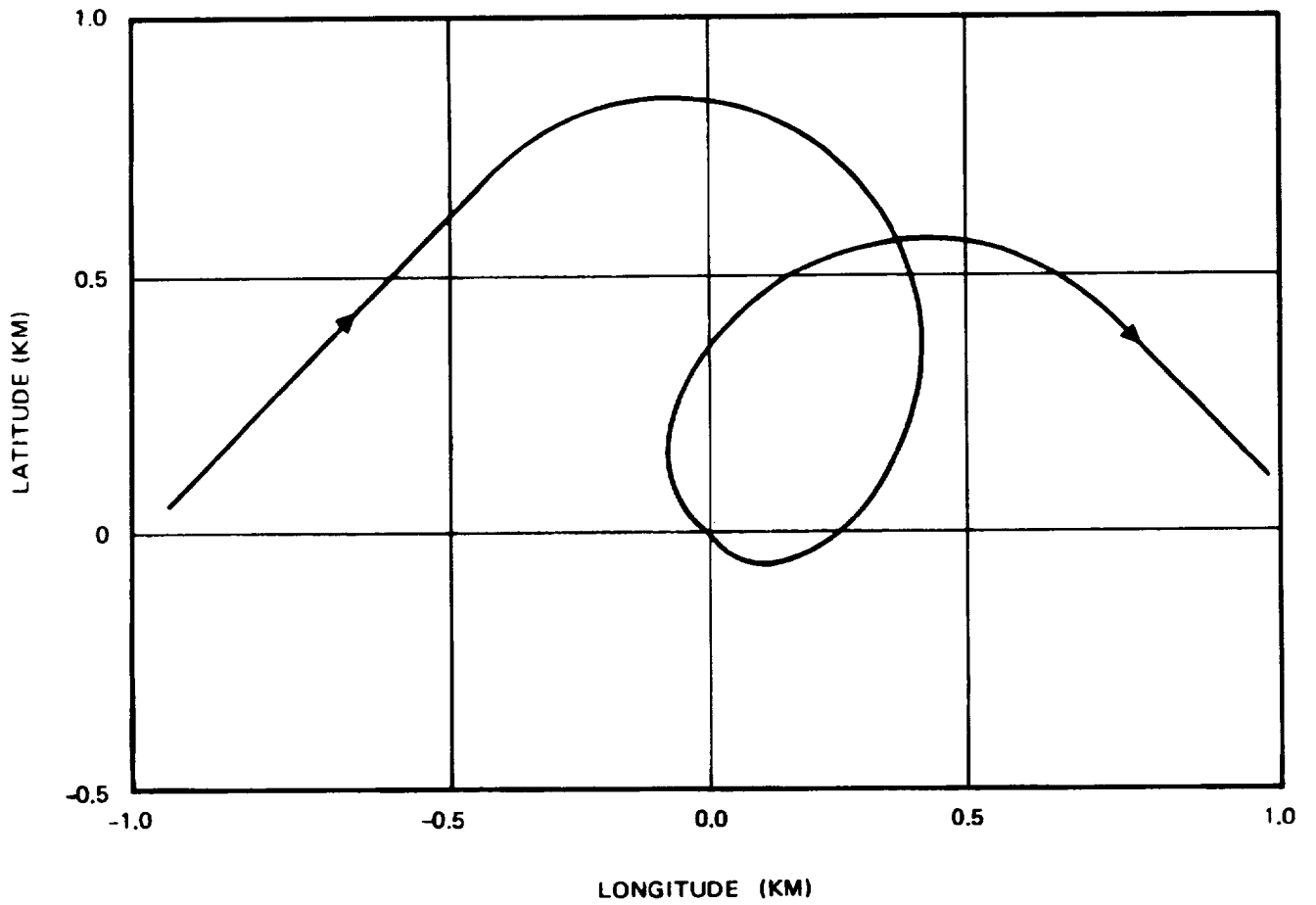


Figure 5-31. Strapdown Trajectory TRAJ002 (Complete)



STRAPDOWN TRAJECTORY TRAJ002 (FIRST STATION DETAIL)

Figure 5-32. First Station Detail



STRAPDOWN TRAJECTORY TRAJ002 (SECOND STATION DETAIL)

Figure 5-33. Second Station Detail

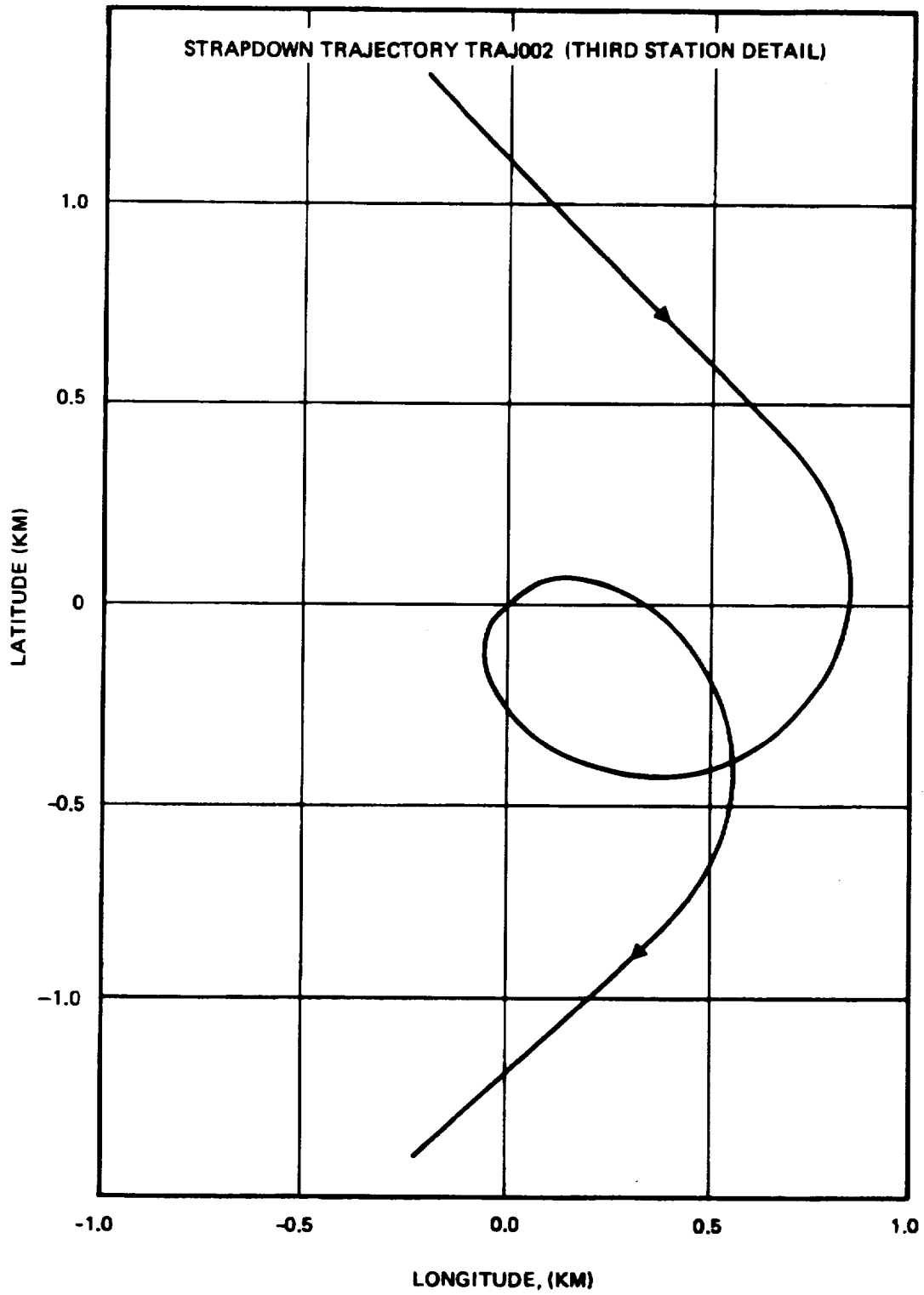


Figure 5-34. Third Station Detail

5.2.7 Simulation Program

The basic program used for the strapdown radio-inertial error simulations is Litton's MOD6DF. It is written entirely in FORTRAN and has been compiled on many computer systems including the IBM 7094, 7040, 360 and 370 series.

Since the inception of the program, Litton has expanded it (principally in size) to accommodate the ever increasing demand for more complex simulations. Because of its modular structure it is adaptable to numerous different types of simulations (aircraft, ship, missile and jeep dynamics, Kalman filters, navigation error dynamics, etc.).

The simplified structure of the computer program is illustrated in figure 5-35. As shown, the physical system being simulated consists of a group of modules or "black boxes". Typically, these represent computer functions, sensors, and the vehicle frame and its external environment. After the usual executive functions have been performed, including input of data, the actual mission trajectory simulation begins. Using a fourth-order Runge-Kutta integration algorithm, the trajectory progresses at each point in time by processing the differential equations in each module to advance the solution one step Δt in time.

The integration is automatic and unaffected by modifications in old modules or the inclusion of new module subroutines, even though these contain new variables to be integrated. Similarly, random noise sources can be called automatically at each step of the integration. If so desired, it is possible to replace the Runge-Kutta integration algorithm with a simpler integration algorithm. This in fact is done when simulating Kalman filter covariance matrix propagation.

At the end of the mission trajectory simulated, post-processing of data can occur (such as statistical processing), as well as computations required in automatically setting up the next run of a series of runs. Extensive RMSing, RSSing and plotting programs augment the MOD6DF program.

The various concepts and modules required for the strapdown inertial error simulation were developed under Litton's IRAD program 76G-1D(B). The specific application to the Langley study particularized the error values and the updating concept.

The procedure used to perform the simulations contained herein consisted of four principal computer job steps. Selection of four job steps economizes on the computer time required for the simulations. The four job steps are

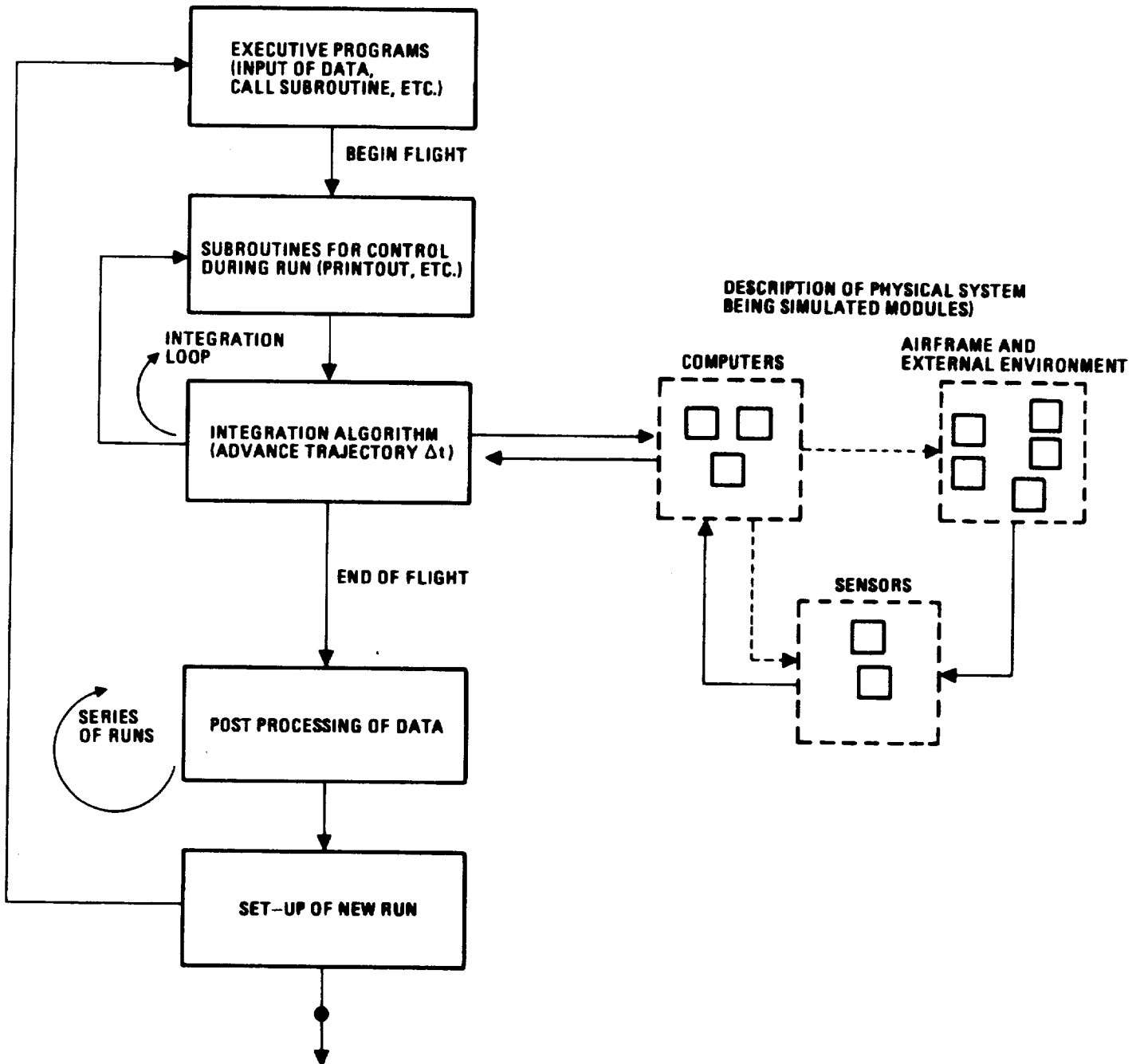


Figure 5-35. Simplified Structure of the MOD6DF Program

- a. Trajectory variables' generation and storage
- b. Strapdown free inertial error response generation and storage
- c. Radio and inertial updated error responses generation and storage
- d. RSSing and storage of radio and inertial updated error responses

Additional job steps are used to obtain the desired graphical outputs.

The first job step is concerned with only trajectory generation. The aircraft is commanded in pitch, roll and thrust to traverse the desired flight profile. During this portion of the simulation all the trajectory variables required for the strapdown free inertial error response generation job step are stored as a data set. These data include, for example, components of specific force and angular rate in both the body and navigation coordinate systems. In addition the transformation matrix relating the body and navigation coordinate systems is also stored. This seemingly redundant storage of data avoids the necessity of performing some transformations during the second job step, thus saving computer time.

During the second job step the computer program reads the stored trajectory data and propagates specified error sources through the strapdown free inertial error dynamics. Specifically, for the simulations performed herein, all 45 inertial error sources were propagated simultaneously through the dynamics, twenty times, being randomly selected for each run (twenty Monte Carlos). These results were RMS'd to give the final RMS response of the system (free inertial). In addition the longitude ($\delta\lambda \cos \phi$), latitude ($\delta\phi$), east velocity (δV_E) and north velocity (δV_N), error time histories for each Monte Carlo were stored. These data form the input for the third job step.

The third job step propagates the stored $\delta\lambda \cos \phi$, $\delta\phi$, δV_E and δV_N through the updating model (20 Monte Carlos) forming the RMS response and also generates the RMS updated response of 20 Monte Carlos of the radio error. These data are stored and finally RSS'd to give the radio-inertial RMS response for twenty Monte Carlos.

The generation of separate updated responses for the radio and inertial error provided comparative data for the rational selection of the gains used in the updating scheme.

5.2.8 Performance of Inertial Budget #5

The inertial error budget given in table 5-5 (005) was used to obtain the results presented in this section. Figures 5-36 to 5-40 summarize the free inertial error responses and figures 5-41 to 5-46 summarize the radio-inertial residual error responses. Since the error estimation and updating process is performed open loop and involves only position and velocity, the heading, pitch and roll error responses (figures 5-38, -39 and -40) are invariant to the updating.

The gains used for the updating were "tuned" for Error Budget #5 and are

$$K_x = 3.24 \times 10^{-2} \text{ m/m} \quad (5.2-30)$$

$$K_y = 3.65 \times 10^{-4} \text{ m/sec/m} \quad (5.2-31)$$

The updating occurred every 5 seconds starting at 605 seconds except for three periods where the loss of updating for sixty seconds was simulated. These periods are shown in table 5-6.

TABLE 5-6. UPDATE LOSS PERIODS

SEC	HOURS
1920 - 1980	0.533 - 0.550
2900 - 2960	0.806 - 0.822
4140 - 4200	1.150 - 1.167

These periods occur just prior to landing and are meant to simulate the possible loss of the radio signal by shadowing effects due to the low altitude of the vehicle.

The characteristics of the RMS free inertial responses are highly sensitive to the particular aircraft maneuvering. This is obvious in the velocity, heading, pitch and roll responses (figures 5-36, -38, -39 and -40). Each time the aircraft changes heading the velocity error is seen to abruptly change slope principally due to the geographic rotation of the gyro and accelerometer biases. Table 7 summarizes the free inertial performance for Budget #5.

STRAPDOWN FREE INERTIAL: TRAJECTORY = TRAJ002 (HOME LAT = 45 DEG)
 LANGLEY ERROR BUDGET 005
 20 MONTE CARLOS

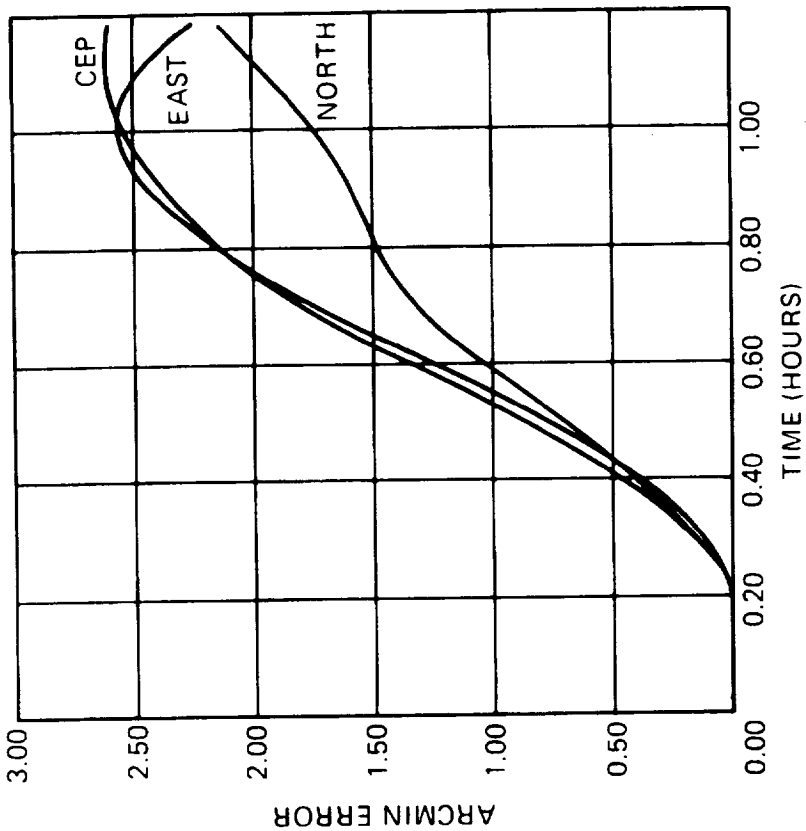


Figure 5-37. Free Inertial Position Errors (Budget #5)

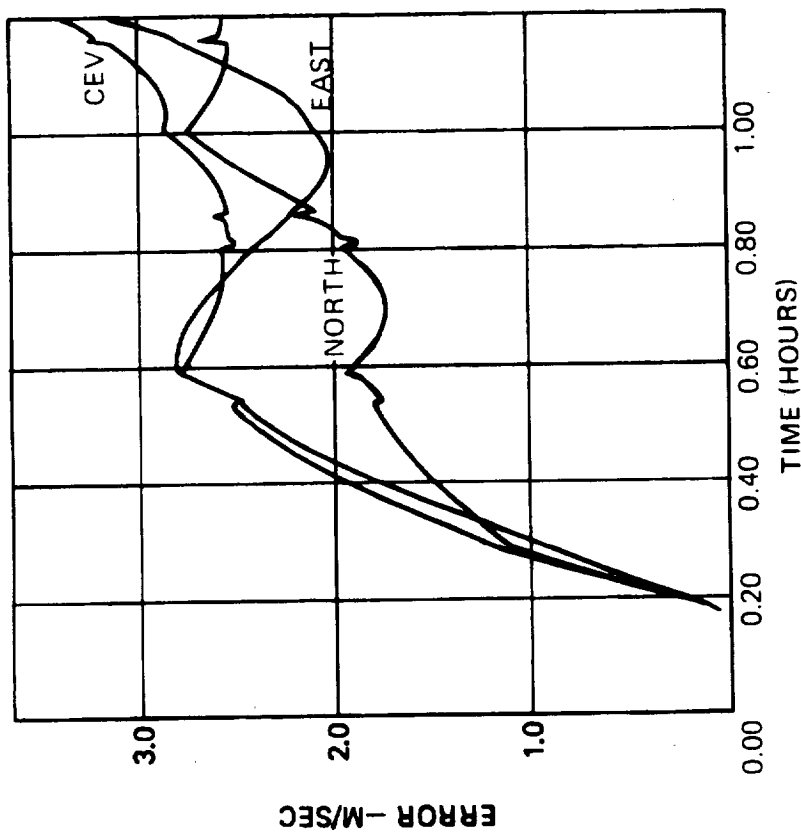
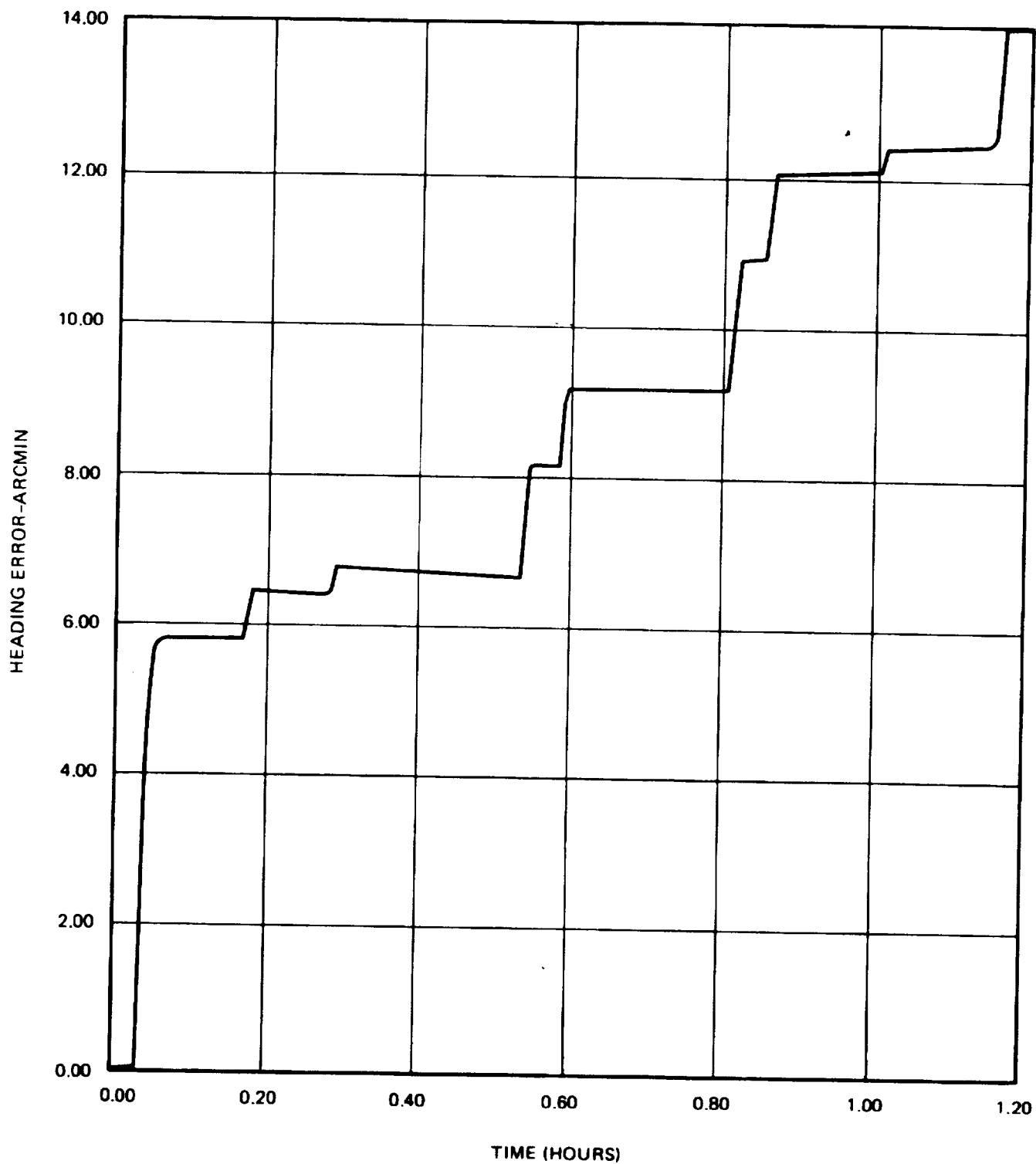
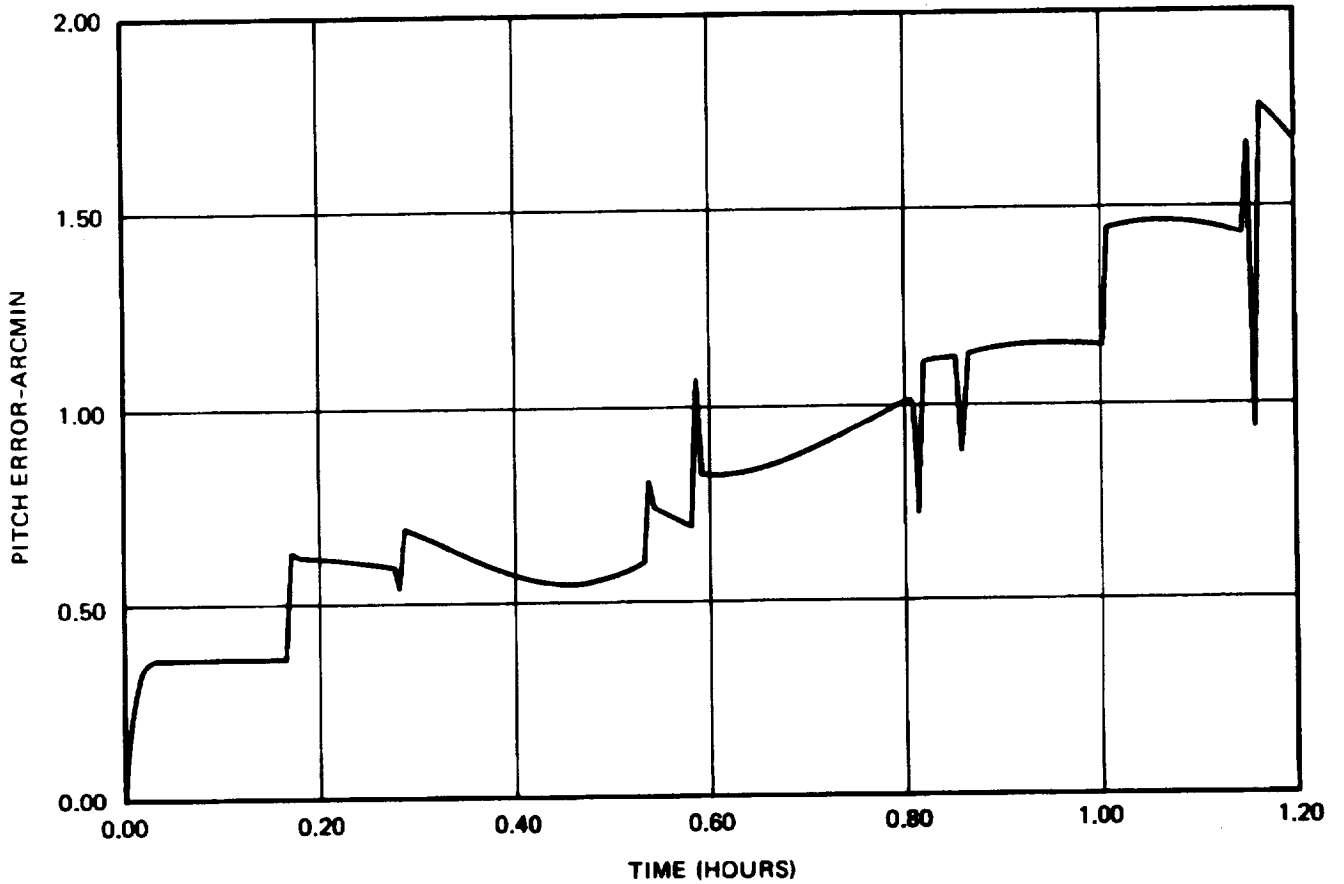


Figure 5-36. Free Inertial Velocity Errors (Budget #5)



STRAPDOWN FREE INERTIAL: TRAJECTORY = TRAJ002 (HOME LAT=45DEG)
LANGLEY ERROR BUDGET 005 20 MONTE CARLOS

Figure 5-38. Heading Error (Budget #5)



STRAPDOWN FREE INERTIAL: TRAJECTORY = TRAJ002 (HOME LAT=45DEG)
LANGLEY ERROR BUDGET 005 20 MONTE CARLOS

Figure 5-39. Pitch Error (Budget #5)

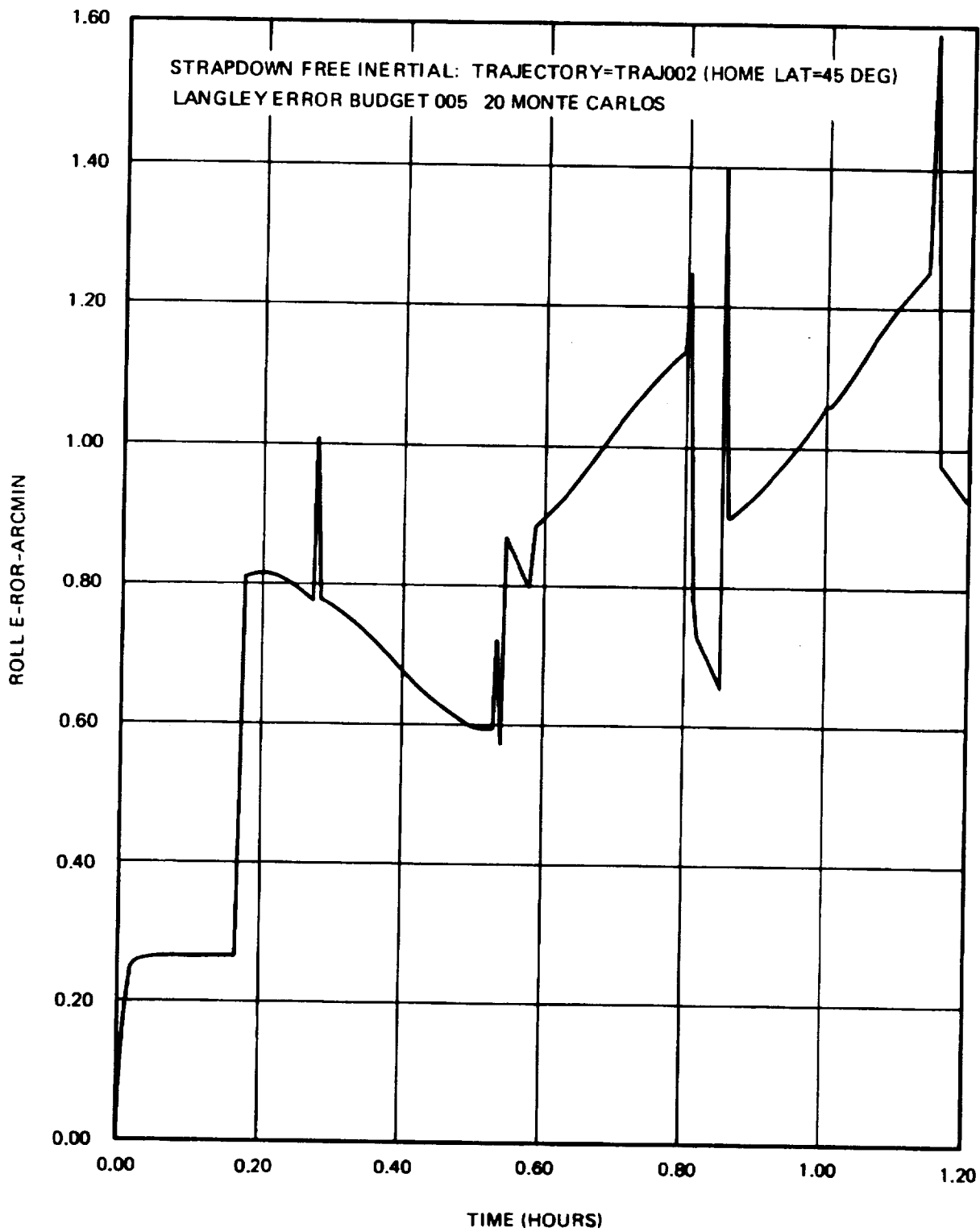
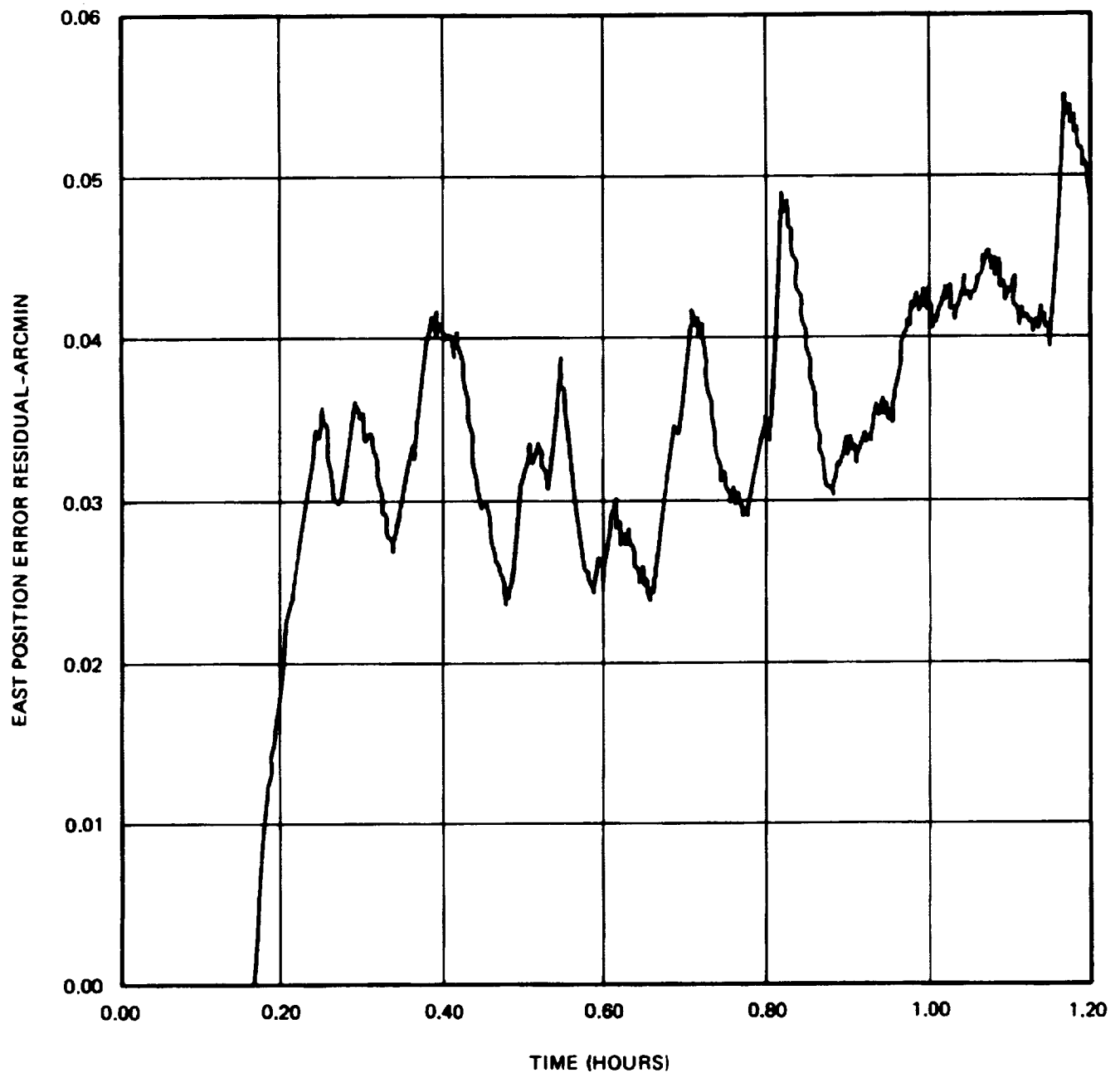
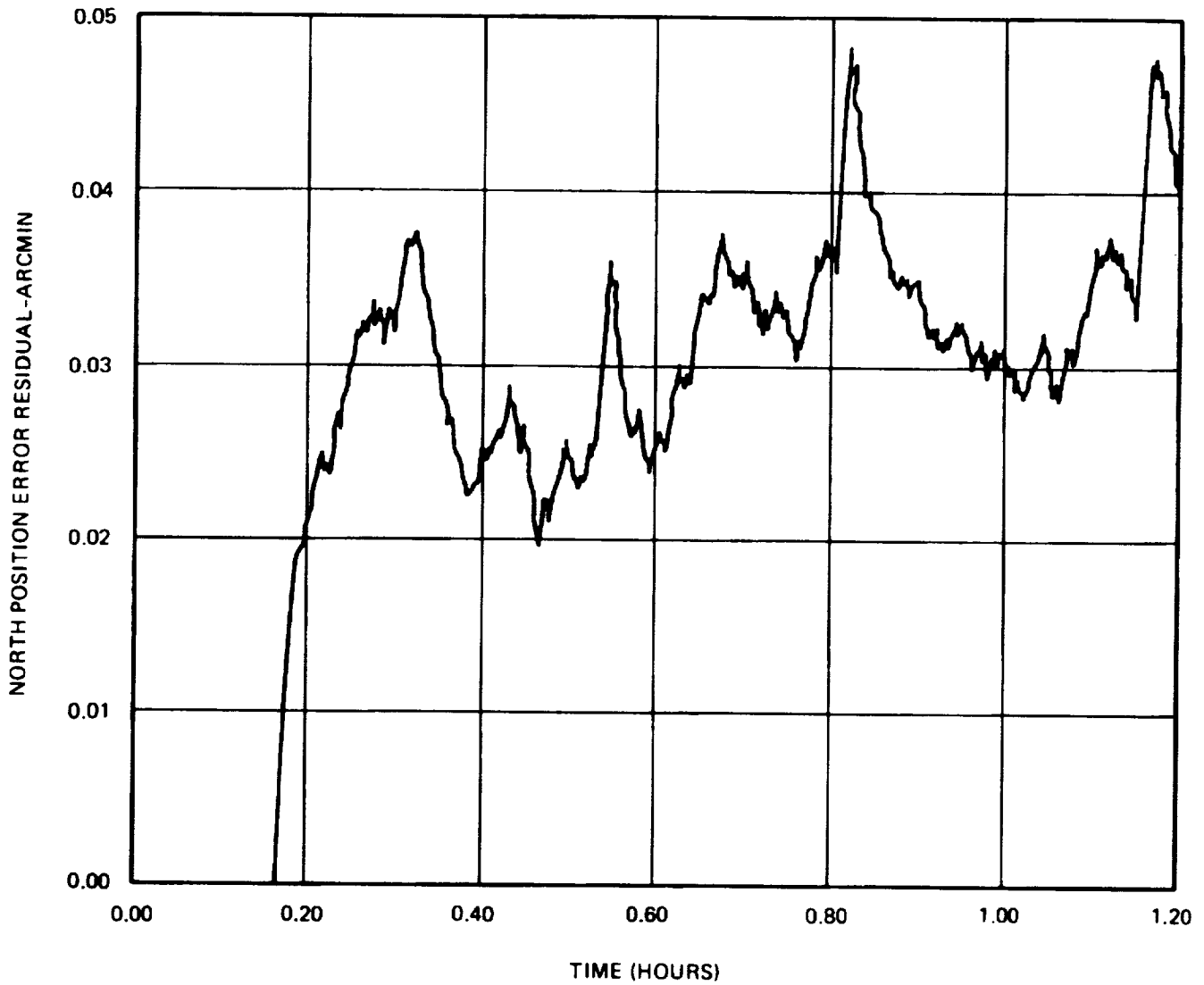


Figure 5-40. Roll Error (Budget #5)



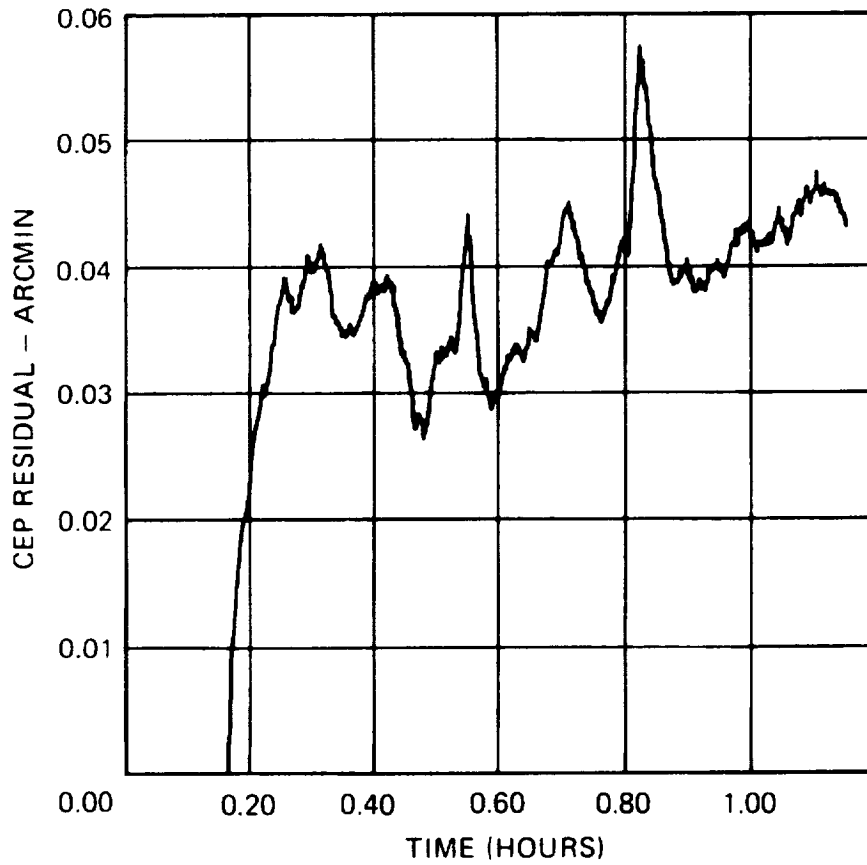
STRAPDOWN, RADIO UPDATED: TRAJECTORY=TRAJ002 (HOME LAT=45DEG)
LANGLEY 005, RADIO 001, UPDATE 004, 20 MONTE CARLOS

Figure 5-41. Radio-Inertial East Position Error Residual (Budget #5)



STRAPDOWN, RADIO UPDATED: TRAJECTORY=TRAJ002 (HOME LAT=45DEG)
LANGLEY 005, RADIO 001, UPDATE 004, 20 MONTE CARLOS

Figure 5-42. Radio-Inertial North Position Error Residual (Budget #5)



STRAPDOWN, RADIO UPDATED: TRAJECTORY = TRAJ002 (HOME LAT = 45 DEG)
LANGLEY 005, RADIO 001, UPDATE 004, 20 MONTE CARLOS

Figure 5-43. Radio-Inertial CEP Residual (Budget #5)

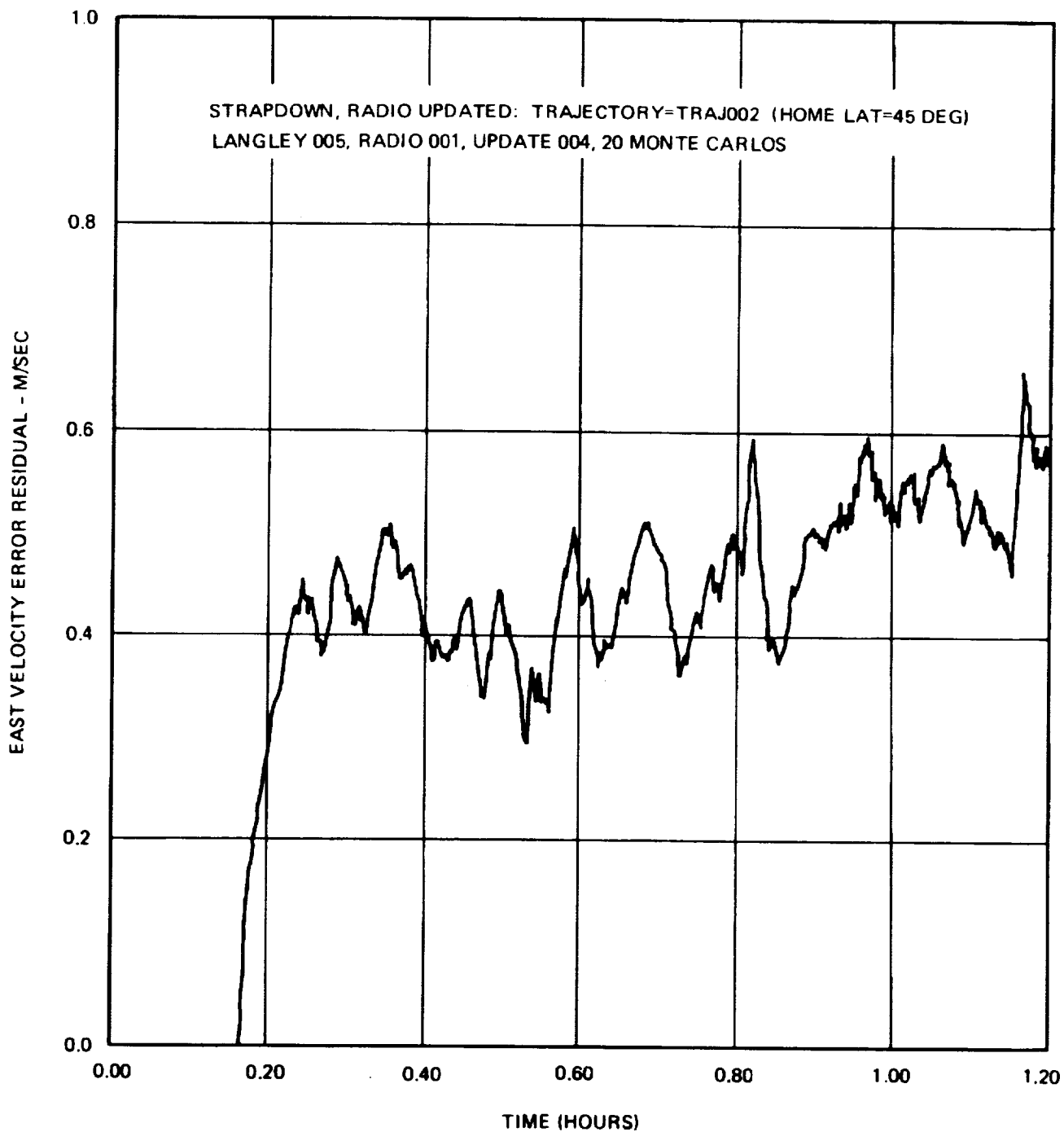
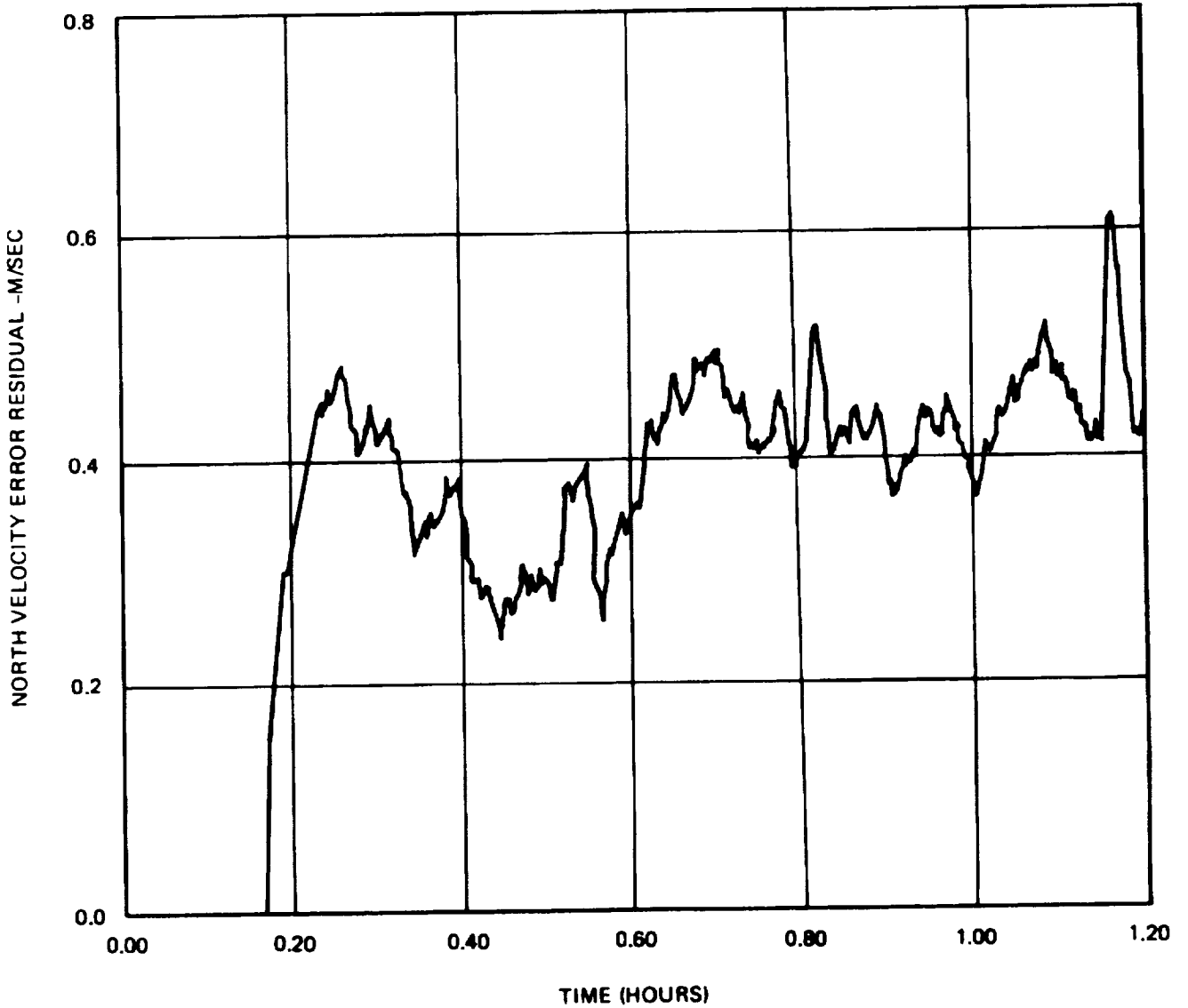


Figure 5-44. Radio-Inertial East Velocity Error Residual (Budget #5)



STRAPDOWN, RADIO UPDATED: TRAJECTORY=TRAJ002 (HOME LAT=45DEG)
LANGLEY 005, RADIO 001, UPDATE 004, 20 MONTE CARLOS

Figure 5-45. Radio-Inertial North Velocity
Error Residual (Budget #5)

STRAPDOWN, RADIO UPDATED: TRAJECTORY = TRAJ002 (HOME LAT = 45 DEG)
LANGLEY 005, RADIO 001, UPDATE 004, 20 MONTE CARLOS

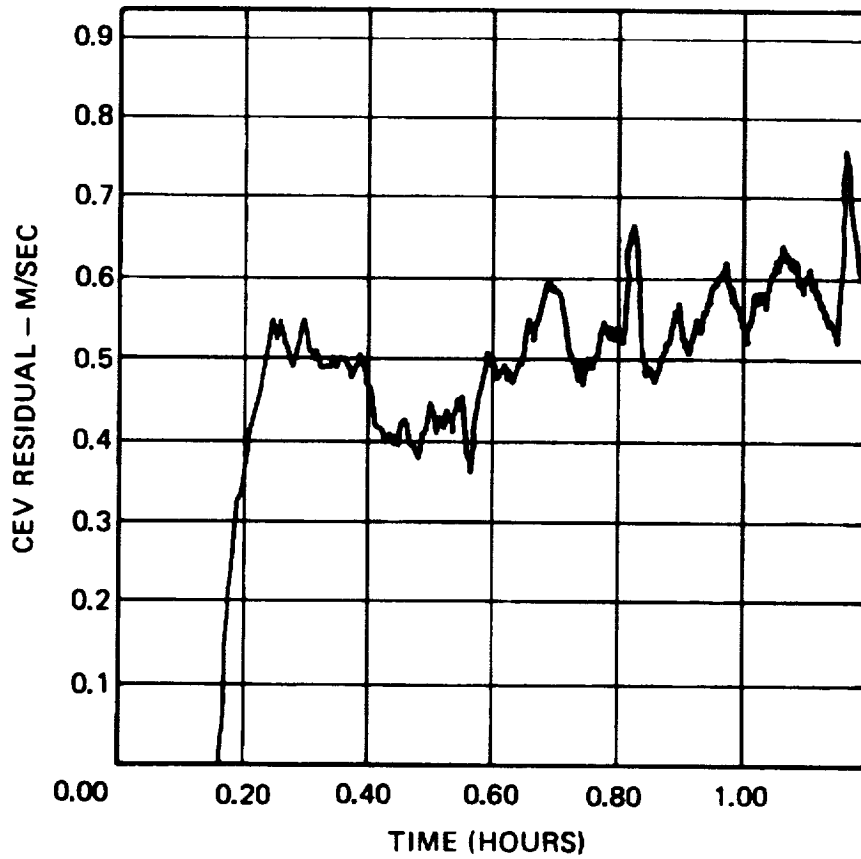


Figure 5-46. Radio-Inertial CEV Residual
(Budget #5)

TABLE 5-7. FREE INERTIAL SUMMARY
PERFORMANCE (BUDGET #5)

Position	5.6 Km/hr CEP
Velocity	2.7 m/sec CEV
Heading	6 min + 8 min/hr RMS
Pitch	0.4 min + 1 min/hr RMS
Roll	0.2 min + 1 min/hr RMS

Utilization of the radio information to estimate the position and velocity error considerably improves the error profiles.

The position error (figures 5-41, -42, and -43) indicates about a 73 m error CEP with a small (43 m/hr) increasing slope. The three update outage periods coincide with the 270° turns before landing and can be identified by 30 m (approximately) error spikes in the curves. If updating had continued these spikes would have been considerably reduced in size because of the tight coupling to the radio position.

The velocity error (figures 5-44, -45, -46) indicates a CEV of approximately 0.53 m/sec (somewhat lower at the beginning of the flight). Since the update outages coincide with the 270° turns before landing it is not clear from the data presented whether the spikes seen at these times are due primarily to the existing attitude and heading errors or the outage itself. Simulation analysis on Error Budget #4 indicates that little improvement in the velocity performance is obtained by eliminating the outages and therefore the spikes are primarily due to attitude and heading errors. It is concluded therefore that the same is true for Error Budget #5.

5.2.9 Performance of Inertial Budget #4

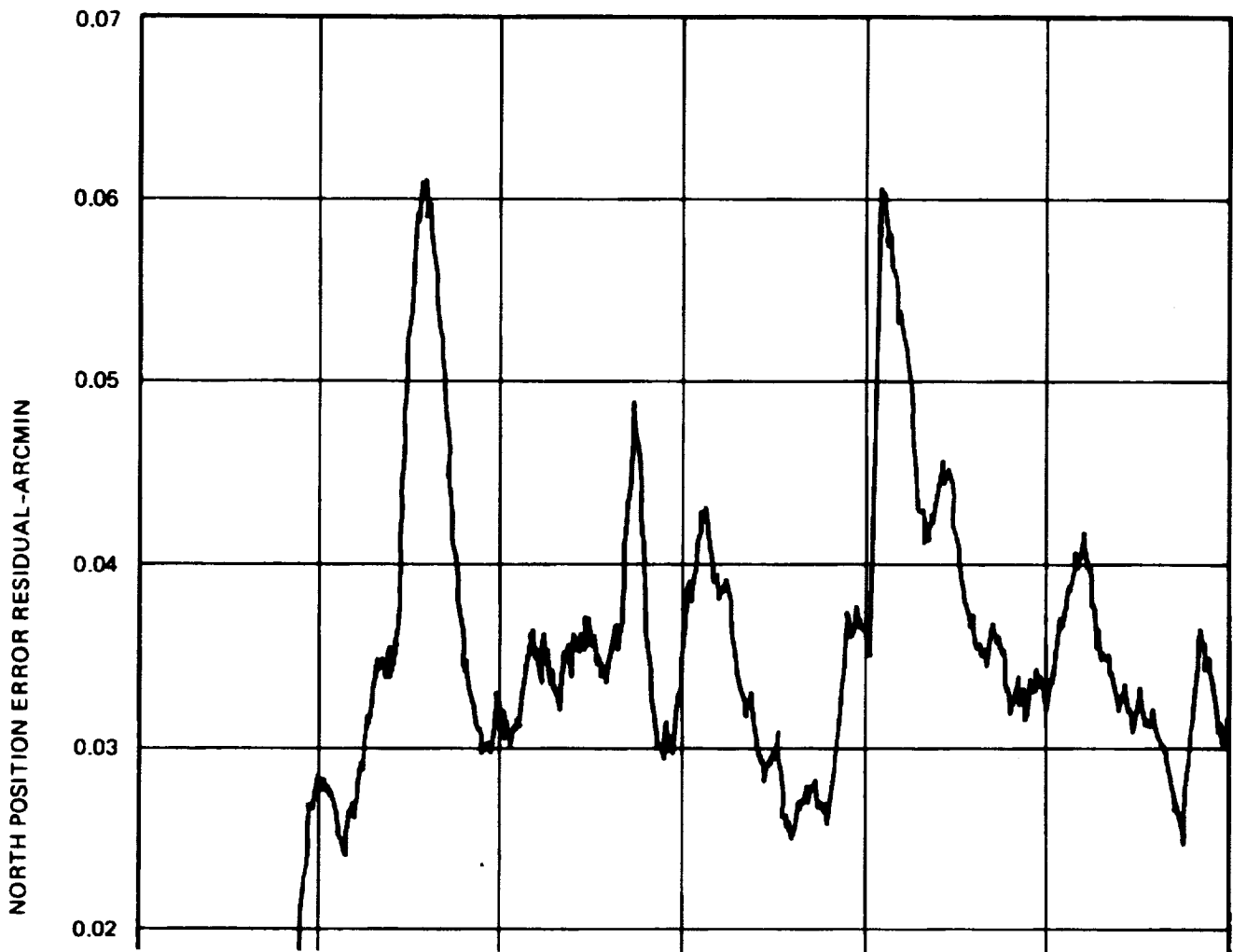
The inertial error budget given in table 5-4 (004) was used to obtain the results presented in this section. Figures 5-47 to 5-51 summarize the free inertial error responses and figures 5-52 to 5-57 summarize the radio-inertial residual error responses. As mentioned in paragraph 5.2.8, the heading, pitch and roll error responses (figures 5-49, -50, and -51) are invariant to the updating.

403314

403314

403314

403314



STRAPDOWN, RADIO UPDATED: TRAJECTORY - TRAJ002 (HOME LAT = 45 DEG)
LANGLEY 004, RADIO 001, UPDATE 005. 20 MONTE CARLOS

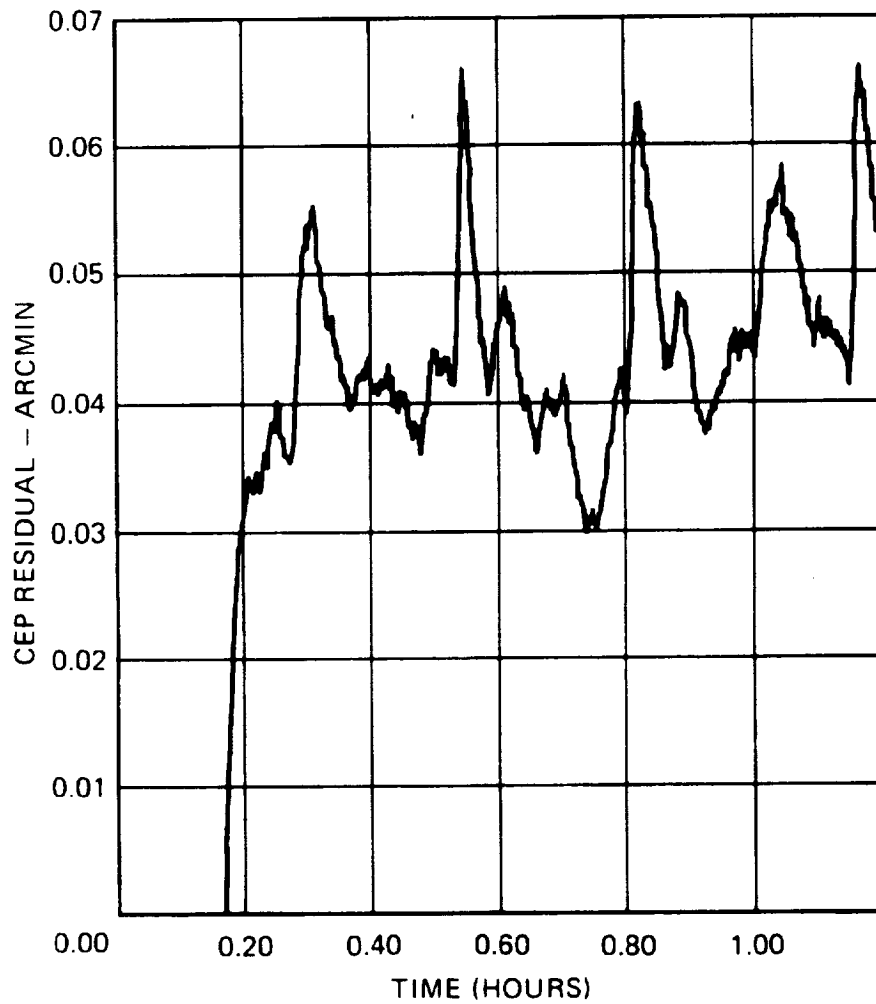
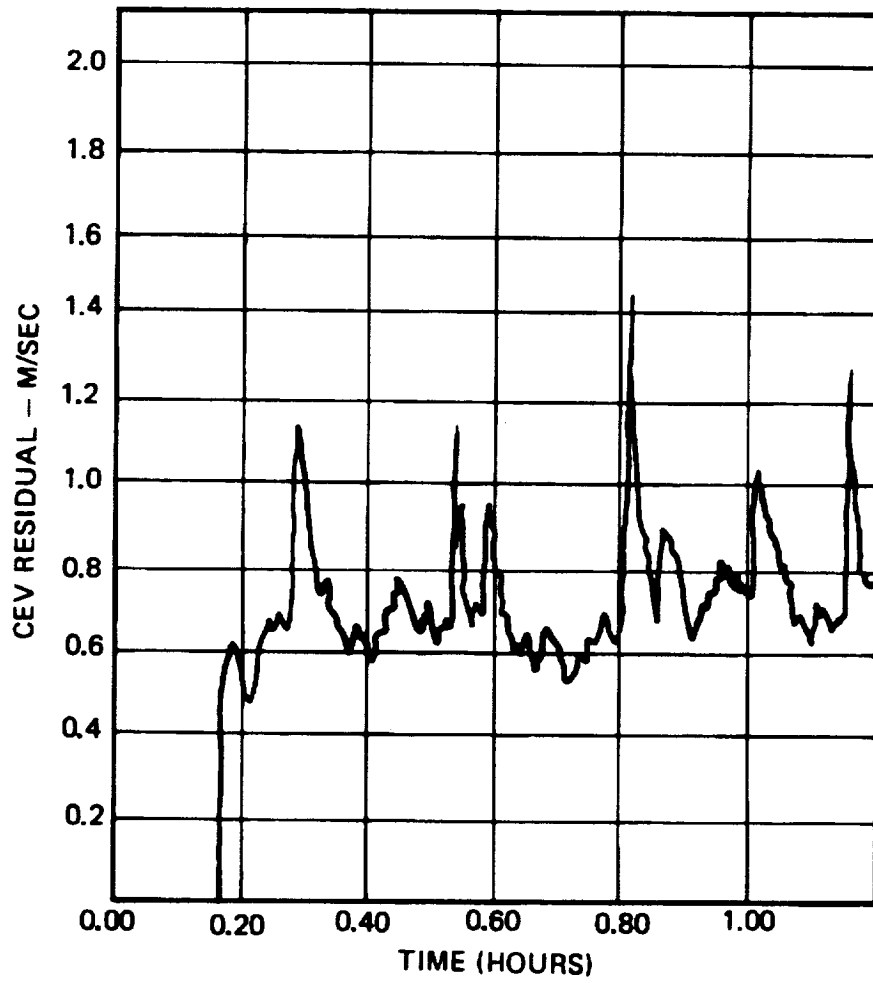


Figure 5-54. Radio-Inertial CEP Residual (Budget #4)

403314

403314



The gains used for the updating were "tuned" for Error Budget #4 and are

$$K_x = 4.25 \times 10^{-2} \text{ m/m} \quad (5.2-32)$$

$$K_v = 6.31 \times 10^{-4} \text{ m/sec/m} \quad (5.2-33)$$

The updating times for this simulation are exactly the same as those used for Error Budget #5, inclusive of the loss of updating (see paragraph 5.2.8, table 5-6).

Compared to Error Budget #5, the free inertial error responses for Error Budget #4 are considerably larger. The large variations of the velocity, pitch and roll error responses make it difficult to characterize the free inertial performance as was done for Error Budget #5 (see table 5-7). Because of the large gyro drifts the heading error incurred at alignment (due to equivalent east gyro drift rate) remains the heading error for the entire flight for all practical purposes. From the CEP plot (figure 5-47) the free inertial performance can be characterized as 14.8 km/hr CEP.

As for Error Budget #5 the radio updating improves the error profiles. The position errors (figures 5-52, -53, and -54) indicate about an 82 m CEP with a small (~43 m/hr) increasing slope. Compared to Error Budget #5 the responses are considerably less smooth. The various large spikes occurring can be correlated with the heading changes of the aircraft. An additional simulation made (but not included herein) shows that the spikes occurring when the aircraft turns and simultaneously experiences an update outage are considerably reduced if the updating had continued. This is because of the tight coupling to the radio position.

The velocity error (figures 5-55, -56, and -57) indicates a CEV of approximately 0.8 m/sec. As for position the various large spikes can be correlated with the heading changes of the aircraft. Eliminating the update outages changes the performance very little during these periods. Thus the velocity performance is practically independent of the outages simulated. The spikes can be related to the heading error at the time of the turn. For example, the 90° turn at 0.28 hours requires a velocity change of

$$\Delta V_E = 69 \text{ m/sec} \quad (5.2-34)$$

$$\Delta V_N = 0 \text{ m/sec} \quad (5.2-35)$$

therefore it would be expected that the east velocity error would not be affected and that the north velocity error would increase by the heading error (40 min) times the east velocity change, that is 0.7 m/sec. From figure 5-55 and -56 it is seen that this is what happened.

One important consideration relative to the observed velocity error spikes is the time required to recover from them especially at the time of landing. From the graphs it is estimated that the recovery time is one to two minutes.

5.2.10 Conclusions

The Langley velocity error specification is

1.03 m/sec radial 95%

or in terms of 50% radial (CEV)

0.49 m/sec CEV

Error Budget #5 is estimated to be slightly above the specification. However it is observed that the performance from initial takeoff to the first landing is within specification. Since the simulation did not take advantage of the time period on the ground to realign, it is anticipated that such a procedure would improve the overall performance to that seen in the first airborne period. As mentioned previously, the velocity performance is highly uncorrelated to the update outage. Therefore further improvement in performance requires a somewhat more sophisticated error estimator. In particular it is anticipated that including attitude and heading in the error estimator would bring the velocity well within the specification. Some form of simple Kalman filter would probably be required.

Error Budget #4 is not within specification. The comments for Budget #5 relative to performance improvement are equally applicable for Error Budget #4. In addition it might be necessary to incorporate some form of gyro biasing.

5.3 System Reliability

5.3.1 Analytical Approach

System reliability is expressed in terms of the probability of a complete system failure to produce required outputs, for a half-hour flight duration. The failure probability calculation is based upon the selected system mechanization, and predicted component failure rates. The predicted failure rate and hardware MTBF are derived in Appendix G and are based on a preliminary list of electronic components for the redundant strapdown INS.

The definition of a failure depends upon the manner in which system outputs are used. Two levels of system performance "failure" are defined, one relative to navigation data failures and the other relative to flight control system failures. The former requirement is generally less stringent since other navigation data such as radio aids, ground radar, or visual sighting are generally available. Reliability requirements for the latter, however, are very stringent since aircraft safety is affected.

To facilitate discussions of system reliability we define different levels of gyro drift (D) failure as follows:

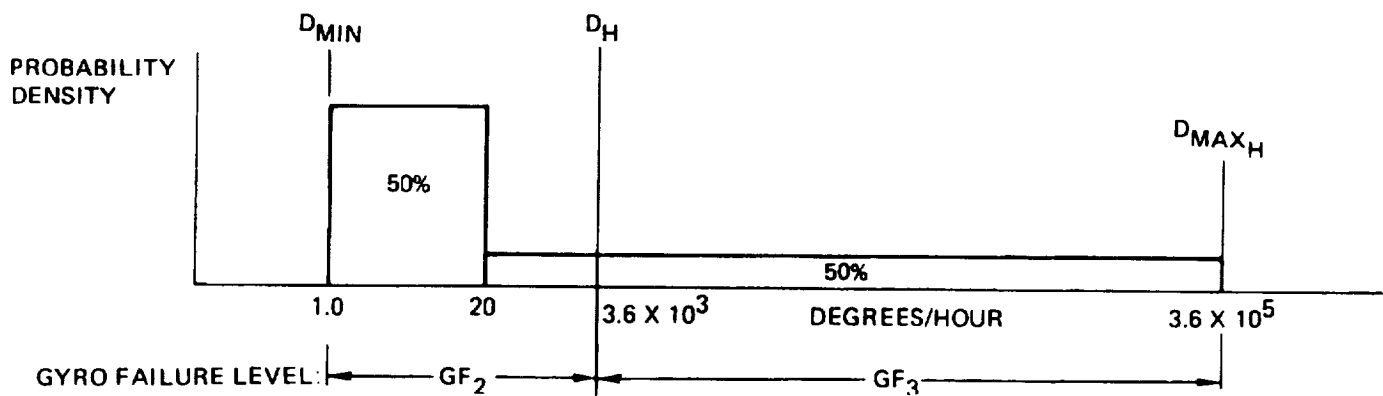
- Hard Failure - The channel of the gyro is non-functional. The failure may be detected and isolated to a channel by self-contained self test.
- GF₃ - The gyro has drift rate exceeding the requirement D_H for attitude rate reference.
- GF₂ - The gyro failure has drift rate less than GF₃ but exceeding the requirement D_{min} for navigation.
- GF₁ - Gyro drift rate less than D_{min} but more than three times the specified gyro drift rate.

Considering the total population of failures which might occur over a long period of time, there will be a distribution of failures into these various categories. Since precise data are lacking on this distribution, a set of assumptions has been made, as shown in figure 5-58.

The assumptions of $D_{min} = 1^\circ/\text{hr}$ and $D_H = 1^\circ/\text{sec}$ are preliminary, as described in paragraph 4.4.9. An angular threshold for large drift errors of 1 arc minute is also assumed. These detection levels cannot be used during aircraft maneuvering since normal scale factor and misalignment tolerances can produce errors of this magnitude for short periods of time. The means of accounting for these effects, such as maneuver-dependent limits or dynamic compensation, have not been defined at this time.

A higher probability has been assigned to the region of small drifts since there are many more mechanisms contributing to slight performance degradations.

It is further assumed that the vector angle of a failure drift is constant and that the angle of a failure has a uniform probability density over 360° . This is also a very conservative assumption since the angle will vary in many cases due to erratic performance or aircraft maneuvering. In either case, the 3-gyro isolation ambiguity will be avoided if the failure occurs as a second failure. To be conservative, the increase of probability density in the area of gyro input axes is ignored.



- 50% OF GYRO FAILURES ARE DETECTED BY SELF-TEST.
- DISTRIBUTION OF GYRO FAILURES WITH AMPLITUDES IS SHOWN ABOVE.
- DISTRIBUTION OF SOFT GYRO FAILURES WITH ANGLE IS UNIFORM AND INDEPENDENT OF AMPLITUDE
- EXTERNAL AVIONICS CAN DETECT, ISOLATE, AND RECONFIGURE FROM TWO INU_{RS} I/O FAILURES WITH UNITY COVERAGE
- HARDWARE FDI OF INU_{RS} SOFTWARE INTERRUPT HAS UNITY COVERAGE FOR TWO FAILURES
- THE INTER-COMPUTER I/O DOES NOT HAVE MULTI-CHANNEL FAILURE MODES

Figure 5-58. Assumptions Used in System Reliability Analysis

The ultimate use of redundant strapdown INU (INURS) data will require a final vote on the four channel outputs to be performed in order to derive a single activity, such as a display of navigation data, or to drive flight control actuators. The INURS reliability calculation assumes this final vote is performed with unity coverage for two failures.

The preliminary design described herein has not included hardware design such as for the inter-channel data transfer and synchronization of the four software executive interrupts. It is assumed that these hardware designs do not detract from coverage of two failures.

The reliability diagram for a single channel is illustrated in figure 5-59. The main failure rates, indicated in failures per million hours, reflect a channel MTBF of about 4000 hours. The failure rates in parentheses are for a 2000 hour MTBF, degraded due to exposure to a more severe environment. A summary of module failure rates, extracted from Appendix G, is shown in figure 5-60.

The system failure probability is calculated for each of the failure rates and for two failure detection levels, D_H and D_{min} , representing flight control and navigation degradation, respectively. The failure detection amplitude determines the probability that a given second soft gyro failure results in failure-isolation ambiguity and complete system failure. In practice, this condition can be remedied by reference to radio updates, or by pilot intervention, however, these possibilities are not assumed for the failure probability calculation.

Several system architectures have been assumed for trade-off purposes. They are:

- a. Flexible IMM-to-computer I/O (a computer can receive all sensor data with all other computers in a failed condition) with full accelerometer selection flexibility (the alternate I/O path shown in figure 5-59).
- b. Same as above but with both accelerometers of a channel rejected if one fails.
- c. IMM data input to only one computer (cross-channel comparison after computer processing of figure 5-59 only) and inflexible accelerometer processing.

Option c is the selected mechanization. Options a and b are included for trade-off purposes, and may be applicable to missions with longer flight duration.

Paragraph 5.3.2 describes the flight control failure probabilities (sensor-related), and 5.3.3 describes navigation failure probabilities for the various mechanizations, MTBF's, and flight duration.

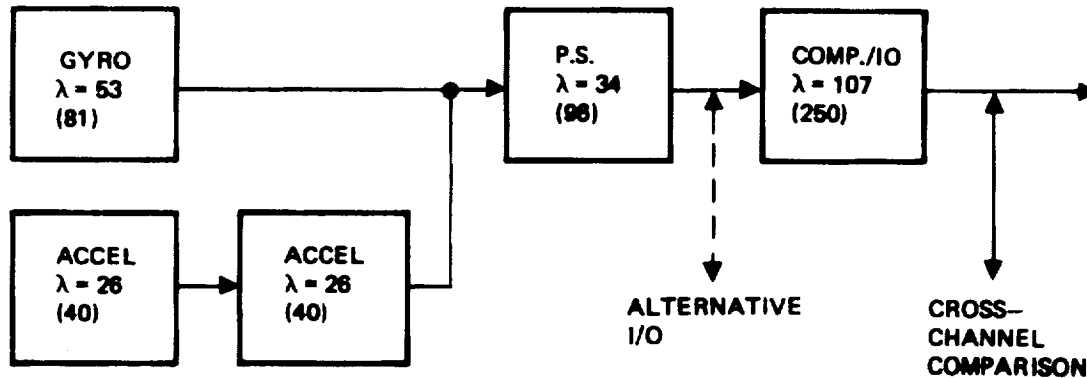


Figure 5-59. Single-Channel Reliability Diagram

An advanced method of FDI has been formulated using the parity equations derived in Appendix B. This algorithm would be used in conjunction with the simple table look-up approach for improved FDI sensitivity and for reduced INS error buildup just prior to redundancy management reconfiguration. Further work is required to consider effects of normal scale factor error, etc. Present work on the advanced FDI method is presented in Appendix I and is summarized in paragraph 5.3.4.

5.3.2 Probability of Flight Control System Output Failure

The attitude rate measurement functions of the redundant strap-down INS are regarded as failed if an attitude rate measurement has an error with a magnitude D_H , where $D_H = 1.^\circ/\text{sec}$. To minimize the probability of attitude rate failure the software should select gyro pair channels (in the event of three failures including GF_2 type, or two gyro failures including a GF_2 type with an ambiguity) so as to accept as valid any GF_2 failed gyros. Use of SDF accelerometers precludes accelerometer FDI ambiguity so it is assumed that coverage of these failures is unity.

QUANT (n)	PART TYPE/ASSEMBLY	70°C INHABITED RATES		90°C UNINHABITED RATES	
		INDIVIDUAL FAILURE RATE (λ)	TOTAL FAILURE RATE (nλ)	INDIVIDUAL FAILURE RATE (λ)	TOTAL FAILURE RATE (nλ)
1	INSTRUMENT BLOCK ASSEMBLY	90.143	90.143	125.655	125.655
1	INSTRUMENT REBALANCE CARD	13.544	13.544	33.556	33.556
1	IMM I/O CARD	12.729	12.729	25.977	25.977
1	GYRO SPIN/INTERRUPT CARD	7.322	7.322	18.635	18.635
1	CPU CARD NO. 1	15.552	15.552	37.418	37.418
1	CPU CARD NO. 2	31.562	31.562	81.602	81.602
1	RAM CARD	22.727	22.727	45.340	45.340
1	PART LOGIC CARD	4.484	4.484	11.831	11.831
1	I/O CARD NO. 1	6.809	6.809	17.072	17.072
1	I/O CARD NO. 2	6.947	6.947	15.541	15.541
1	I/O CARD NO. 3	5.722	5.722	15.182	15.182
1	MODE CARD	9.220	9.220	23.595	23.595
1	POWER SUPPLY ASSEMBLY	8.993	8.993	21.548	21.548
4	CONNECTOR, 90 PIN	2.034	8.136	7.840	31.360

504.3
1983

CHANNEL FAILURE RATE/10⁶ HRS 243.9
CHANNEL MTBF, HOURS 4100

Figure 5-60. Calculated Channel Failure Rate and MTBF

The probability* of system failure with full IMM-to-computer I/O flexibility is:

$$\begin{aligned}
 P_F = & f_p^4 + \binom{4}{3} f_p^3 (1 - f_p) + \binom{4}{2} f_p^2 (1 - f_p)^2 \left\{ f_c^2 + (1 - f_c^2) \left[f_{g_3}^2 + \binom{2}{1} f_{g_3} (1 - f_{g_3}) + (1 - f_{g_3})^2 G \right] \right\} \\
 & + \binom{4}{1} f_p (1 - f_p)^3 \left\{ f_c^3 + (1 - f_c^3) \left[f_{g_3}^3 + \binom{3}{2} f_{g_3}^2 (1 - f_{g_3}) + \binom{3}{1} f_{g_3} (1 - f_{g_3})^2 P_{A_3} y_3 \right] \right. \\
 & \left. + \left[(1 - f_{g_3})^3 + \binom{3}{1} f_{g_3} (1 - f_{g_3})^2 (1 - P_{A_3} y_3) \right] H \right\} + (1 - f_p)^4 \left\{ f_c^4 + (1 - f_c^4) \left[X_3 + (1 - X_3) J \right] \right\}
 \end{aligned}$$

where, for fully flexible accelerometer logic, (1)

$$G = \sum_{n=2}^4 \binom{4}{n} f_a^n (1 - f_a)^{4-n} \quad (2)$$

$$H = \sum_{n=4}^6 \binom{6}{n} f_a^n (1 - f_a)^{6-n} \quad (3)$$

$$J = \sum_{n=6}^8 \binom{8}{n} f_a^n (1 - f_a)^{8-n} \quad (4)$$

$$X_3 = f_{g_3}^4 + \binom{4}{3} f_{g_3}^3 (1 - f_{g_3}) + \binom{4}{2} f_{g_3}^2 (1 - f_{g_3})^2 P_{A_3} y_3 \quad (5)$$

f_p , f_c , and f_a are the power supply, computer (and I/O), and accelerometer failure probabilities based on their λ , from figure 5-59, times 10^6 , times flight duration; f_{g_3} is the probability of gyro failure drift greater than D_H including the failure versus

*Using binomial distribution $\binom{n}{k} p^k q^{n-k}$

amplitude distribution of figure 5-58, and approximately 0.5 times the gyro λ of figure 5-59, times 10^6 , times flight duration. y_3 is the portion of gyro failures with amplitude greater than D_H and not detected by self-test which are subject to failure isolation ambiguity. That is, from figure 5-58, $y_3 \approx 0.25$.

P_{A_3} is the probability that a given soft second gyro failure falls into a fault-isolation ambiguity. Assuming a uniform distribution of failure angles over 360° , and a D_{\max_H} of 3.6×10^5 °/hr,

$$P_{A_3} = \int_{D_H}^{D_{\max_H}} \frac{C}{D_F} \frac{dD_F}{(D_{\max_H} - D_H)} \quad C = \frac{4\sigma}{\pi} N$$

$$= \frac{1.26 \sigma N}{(D_{\max_H} - D_H)} \cdot \ln \left(D_{\max_H} / D_H \right) \quad (6)$$

where σN is the noise level. For $\sigma N = 0.1^\circ/\text{hr}$,

$$P_{A_3} = \frac{1.26 (0.1) 4.6}{0.36 \times 10^6} = 1.6 \times 10^{-6}$$

If two gyro failures occur simultaneously, and are of comparable amplitudes with certain failure directions, FDI ambiguity may occur. (Described in Appendix J.) The probability of simultaneous failures during a 0.5 hour mission is a function of the time to detect errors greater than D_H . If the detection level is set to 1 min, time to detect an error of $1^\circ/\text{second}$ is $1/60$ second. Probability of simultaneous failures in a half-hour flight is then 10^{-5} . The probability of two gyro failures not detectable by self-test being greater than D_H is $(0.5 \times f_{g_3})^2 = 2 \times 10^{-10}$. Of such cases, from Appendix J, only the small fraction

$$\frac{D_{\min}}{2\pi} \cdot \frac{\ln \left(D_{\max_H} / D_H \right)}{D_{\max_H}} \approx 10^{-6} \quad (7)$$

cause failure. The combination of these three probabilities is 10^{-21} which is negligible.

If accelerometers are rejected in pairs instead of a fully-flexible choice, the following terms apply:

$$G = 1 - (1 - f_a)^4 \quad (8)$$

$$H = \sum_{n=2}^3 \binom{3}{n} \left[1 - (1 - f_a)^2 \right]^n (1 - f_a)^{6-2n} \quad (9)$$

$$J = \sum_{n=3}^4 \binom{4}{n} \left[1 - (1 - f_a)^2 \right]^n (1 - f_a)^{8-2n} \quad (10)$$

If IMM-to-computer I/O is made inflexible, that is a computer can only read other channel data through their computer, and inflexible accelerometer selection is assumed system failure probability becomes:

$$\begin{aligned} P_F = & f_{pc}^4 + \binom{4}{3} f_{pc}^3 (1 - f_{pc}) + \binom{4}{2} f_{pc}^2 (1 - f_{pc})^2 \\ & \left\{ f_{g_3}^2 + \binom{2}{1} f_{g_3} (1 - f_{g_3}) + (1 - f_{g_3})^2 G \right\} \\ & + \binom{4}{1} f_{pc} (1 - f_{pc})^3 \left\{ f_{g_3}^3 + \binom{3}{2} f_{g_3}^2 (1 - f_{g_3}) \right. \\ & + \binom{3}{1} f_{g_3} (1 - f_{g_3})^2 P_{A_3} y_3 \\ & \left. + \left[(1 - f_{g_3})^3 + \binom{3}{1} f_{g_3} (1 - f_{g_3})^2 (1 - P_{A_3} y_3) \right] H \right\} \\ & + (1 - f_{pc})^4 \left[X_3 + (1 - X_3) J \right] \quad (11) \end{aligned}$$

where f_{g_3} , X_3 , and y_3 are as previously defined, G , H , and J are those definitions for inflexible accelerometer selection, equations (8), (9), and (10), and

$$f_{pc} = \left[1 - (1 - f_p) (1 - f_c) \right]$$

The terms of equations (1) and (11) represent the various system failure modes. Thus, the first term applies to four power supply failures during the flight. The second term indicates three power supply (or computer, for equation (11)) failures. The third term is for two power supply failures plus an additional failure such as a gyro.

Evaluation of equation (1) with and without flexible accelerometer selection and equation (11) without flexible accelerometer selection for the two system MTBF's and for different flight durations leads to system failure probabilities shown in table 5-8.

TABLE 5-8. FLIGHT CONTROL OUTPUT FAILURE
PROBABILITY VERSUS ARCHITECTURE,
FLIGHT TIME, AND CHANNEL MTBF

ARCHITECTURE	FLIGHT TIME (HR)	MTBF	
		4000 HR	2000 HR
FULL FLEXIBILITY	0.5	1.1×10^{-13}	1.3×10^{-12}
	1.0	8.7×10^{-13}	1.0×10^{-11}
	8.0	4.4×10^{-10}	5.1×10^{-9}
INFLEXIBLE ACCELS.	0.5	4.1×10^{-13}	3.5×10^{-12}
	1.0	3.3×10^{-12}	2.8×10^{-11}
	8.0	1.7×10^{-9}	1.5×10^{-8}
INFLEXIBLE I/O	0.5	4.5×10^{-12}	4.7×10^{-11}
	1.0	3.6×10^{-11}	3.8×10^{-10}
	8.0	1.9×10^{-8}	1.9×10^{-7}

The following conclusions may then be drawn:

- a. All architectures meet the required 10^{-6} failure probability for 0.5 hour flights.
- b. Full flexibility in computer instrument selection leads to about 1/40 of the failure probability of the most inflexible architecture.

- c. Rejecting accelerometers in pairs results in about 4 times the failure probability of the full flexibility method.
- d. If channel MTBF is halved, failure probability increases by about a factor of 10.
- e. Applications of long flight durations would probably require the more flexible architecture.

5.3.3 Probability of Navigation Output Failure

The probability of system failure for navigation outputs has the same form as equation (1) except that the full distribution of gyro failures with amplitude applies. The equation then becomes:

$$\begin{aligned}
 P_F = & f_p^4 + \binom{4}{3} f_p^3 (1 - f_p) + \binom{4}{2} f_p^2 (1 - f_p)^2 \left\{ f_c^2 + (1 - f_c^2) \left[f_g^2 + \binom{2}{1} f_g (1 - f_g) + (1 - f_g)^2 G \right] \right\} \\
 & + \binom{4}{1} f_p (1 - f_p)^3 \left\{ f_c^3 + (1 - f_c^3) \left[f_g^3 + \binom{3}{2} f_g^2 (1 - f_g) + \binom{3}{1} f_g (1 - f_g)^2 P_A y \right. \right. \\
 & \left. \left. + \left[(1 - f_g)^3 + \binom{3}{1} f_g (1 - f_g)^2 (1 - P_A y) \right] H \right\} + (1 - f_p)^4 \left\{ f_c^4 + (1 - f_c^4) \left[X + (1 - X) J \right] \right\}
 \end{aligned}
 \tag{12}$$

where f_p , f_c , and f_g are as previously defined and G , H , and J are defined in equations (2), (3), and (4), or (8), (9), and (10), depending on accelerometer rejection logic. y is essentially equal to y_3 (0.25), for the assumed distribution, and,

$$X = f_g^4 + \binom{4}{3} f_g^3 (1 - f_g) + \binom{4}{2} f_g^2 (1 - f_g)^2 P_A y \tag{13}$$

Evaluation of P_A primarily involves the failure distribution, from figure 5-58, from 1 to 20°/hr. Using these values in equation (6) for D_{\min} and D_{\max} , respectively, yields $P_A = 0.0195$.

The average time to detect errors under 20°/hr is 30 seconds (for a minimum drift of 1°/hr and a detection level of 1 arc minute). The probability of two simultaneous failures in a 0.5 hour flight is $30/1800 = 0.0167$. The probability of two GF₂ failures not detectable by self-test is $(0.25 \times f_g)^2 = 2 \times 10^{-10}$. Of such cases only the fraction, from equation (7), 0.025, apply. The net probability, $0.0167 \times 2 \times 0.025 \times 10^{-10} \approx 10^{-13}$, is insignificant.

The equation for probability of navigation output failure with the inflexible architecture, similar to equation (11), is:

$$\begin{aligned}
 P_F = & f_{pc}^4 + \binom{4}{3} f_{pc}^3 (1 - f_{pc}) + \binom{4}{2} f_{pc}^2 (1 - f_{pc})^2 \\
 & \left\{ f_g^2 + \binom{2}{1} f_g (1 - f_g) + (1 - f_g)^2 G \right\} \\
 & + \binom{4}{1} f_{pc} (1 - f_{pc})^3 \left\{ f_g^3 + \binom{3}{2} f_g^2 (1 - f_g) \right. \\
 & + \binom{3}{1} f_g (1 - f_g)^2 P_A Y \\
 & \left. + \left[(1 - f_g)^3 + \binom{3}{1} f_g (1 - f_g)^2 (1 - P_A Y) \right] H \right\} \\
 & + (1 - f_{pc})^4 \left[X + (1 - X) J \right] \tag{14}
 \end{aligned}$$

Using the previously defined values of G, H, and J (equations (8), (9), and (10)), and X (equation (13)), f_{pc} and computed values of y and P_A , equation (14) may be evaluated for the two values of MTBF, as shown in table 5-9.

TABLE 5-9. NAVIGATION OUTPUT FAILURE PROBABILITY
VERSUS FLIGHT TIME AND CHANNEL MTBF,
INFLEXIBLE ARCHITECTURE

FLIGHT TIME	MTBF	
	4000 HR	2000 HR
0.5	1.3×10^{-10}	4.6×10^{-10}
1.0	5.2×10^{-10}	1.8×10^{-9}
8.0	3.3×10^{-8}	1.2×10^{-7}

The improvement to be gained by using the more flexible I/O and accelerometer selection architecture is not as great for navigation output reliability. It can be shown to be less than a factor of 3. The reason this occurs is that the probability of isolation ambiguity is much more significant for the smaller gyro drifts needed for navigation than for flight control failure detection levels.

5.3.4 Summary of Study Results in Advanced Techniques for Failure Detection and Isolation

The navigation system will fail if errors in craft rate exceed $1^\circ/\text{hr}$ during flights where craft rates of $>10^\circ/\text{sec} = 3.6 \times 10^4^\circ/\text{hr}$ can occur. Failure detection and isolation techniques based on comparison of gyro torquer outputs should correspond to the same directions to within a fraction of $1^\circ/\text{hr}/3.6 \times 10^4^\circ/\text{hr} \approx 0.3 \times 10^{-4} \text{ rad} = 6. \text{ sec}$. For this reason, directions in which angular rate is sensed by more than one gyro are important for comparative testing. For the tetrahedral array the sensing planes of only two gyros intersect in the same direction. Each intersection is at an edge of the tetrahedron defining a test direction along the edge for a comparison of components of observed angular rate obtained by resolution of the two torquer outputs of each gyro. Each difference of angular rate components T_{rs} of gyro r and gyro s along the commonly sensed direction of a tetrahedron edge, is a member of the set of six edge test observations,

$$T_{12}, T_{13}, T_{14}, T_{23}, T_{24}, T_{34}$$

which comprise the primary information of angular rate outputs of the gyros. The computation and smoothing of T_{rs} quantities is described in Appendix B. The analysis of Appendix I evolves advanced techniques for failure detection and isolation. The study first seeks an answer to the question of what test functions F_g of contemporaneous T_{rs} ,

$$F_g (T_{12}, T_{13}, T_{14}, T_{23}, T_{24}, T_{34}) \quad g = 1, 2, 3, 4$$

give a measure of whether gyro g has failed? More general functions could involve past and present T_{rs} but here the dependence on past T_{rs} is limited to previous decisions regarding gyro failure based on past T_{rs} magnitudes. Say gyro \bar{g} was previously isolated as failed. Then the new question is, what functions $F_g(\bar{g})$ not involving the failed gyro \bar{g} , where for example $\bar{g} = 4$, and we have

$$\bar{F}_g (4) = F_g (T_{12}, T_{13}, T_{23}) \quad g = 1, 2, 3$$

give a measure of whether gyro g has failed?

To facilitate the generation of gyro failure isolation functions F_g for the four gyro case and $\bar{F}_g(\bar{g})$ for the three gyro case, we directly implement a definition of failure of a gyro according to total drift rate in the sensing plane, a failed gyro corresponding to

$$\vec{D}_g \cdot \vec{D}_g > \epsilon^2$$

where ϵ is a test drift rate level. Derived functions may be directly used or, as in the three gyro case, an equivalent form of the functions is shown to involve simplified testing.

A second criterion to facilitate the generation of test functions is the assumption that only one gyro has failed in the test period. In the three gyro case this criterion is not a limitation since two gyro failures means certain navigation system failure. In the four gyro case, once deriving the implied functions F_g , it is necessary to provide special secondary procedures for the infrequent situation of two gyros failing within the test smoothing time (see Appendix J). The frequency and provision for such cases are analyzed in another section.

In the four gyro case it is shown in Appendix I-1 that if a single gyro \bar{g} failed with drift rate $D_{F\bar{g}}$ then functions F_g [$g = 1...4$] given by (6a), (6b) take on the values, in the absence of noise,

$$F_g = D_{F\bar{g}}^2 \cdot \delta_g^{\bar{g}}$$

where

$$\delta_g^{\bar{g}} = \begin{cases} 1 & \text{if } g = \bar{g} \\ 0 & \text{otherwise} \end{cases}$$

Gyro failure detection and isolation is given by failure of the test $F_g < \epsilon^2$ [$g = 1...4$].

An equivalent form of F_g [$g = 1...4$] defined by (6a), (6b), Appendix I is

$$F_g = \frac{2}{3} \left\{ F_0 - \bar{F}(g) \right\}$$

where

$$\bar{F}(1) = T_{23}^2 + T_{24}^2 + T_{34}^2 + (T_{23} - T_{24} + T_{34})^2$$

$$\bar{F}(2) = T_{13}^2 + T_{14}^2 + T_{34}^2 + (T_{14} + T_{34} - T_{13})^2$$

$$\bar{F}(3) = T_{12}^2 + T_{14}^2 + T_{24}^2 + (T_{12} + T_{14} - T_{24})^2$$

$$\bar{F}(4) = T_{12}^2 + T_{13}^2 + T_{23}^2 + (T_{12} - T_{13} + T_{23})^2$$

$$F_0 = T_{12}^2 + T_{13}^2 + T_{14}^2 + T_{23}^2 + T_{24}^2 + T_{34}^2$$

In this algebraic form the calculation of test functions for four gyros make functions $\bar{F}(g)$ available for:

- a. Special procedures for detection and provision for two effectively simultaneous failures
- b. Failure detection and isolation in the three gyro case.

For four gyros the test $F_g < \epsilon^2$ can be made equivalently by tests

$$\bar{F}(g) > F_0 - \frac{3}{2} \epsilon^2 \quad g = 1 \dots 4$$

as indicated in the preliminary FORTRAN list of the advanced failure detection and isolation program listed in Appendix I-5. The statistical properties of the four gyro test procedure in the presence of gyro noise are analyzed in some detail in Appendix I. The fractional variation from gyro noise of F_g if gyro g failed is

$$\frac{F_g}{F_g \text{ average}} = \frac{2}{\sqrt{3}} r \sqrt{1 + r^2} \quad , \quad r = \frac{\sigma_N}{D_{Fg}}$$

so for noise $\sigma_N = 0.1^\circ/\text{hr}$ and $D_{Fg} = D_{F_{\min}} = 1.0^\circ/\text{hr}$ the 1σ variation of F_g from noise for the minimum failure rate is 11.6%. If none of the gyros failed, the effect of gyro noises in producing outputs of F_g is to produce 1σ output of $-.63\%$ to $+1.63\%$ of that of a minimally failed gyro at $1.0^\circ/\text{hr}$. An exact probability

distribution* for F_g from noise is derived from which the false alarm probability PFA for test level ϵ^2 is shown to be

$$PFA = \frac{5}{7} \cdot e^{-\frac{3}{5} \left(\frac{\epsilon}{\sigma_N} \right)^2} \quad \text{Four Gyro Case}$$

For noise level $\sigma_N = .1^\circ/\text{hr}$ and test level $\epsilon = .5^\circ/\text{hr}$

$$P_{FA} = 2 \times 10^{-7}$$

for which the fraction f_{FA} of false alarms to actual failures is

$$f_{FA} = \frac{P_{FA}}{\tau_s} \cdot (\text{MTBF}) = .5 \times 10^{-4} \quad \text{Four Gyro Case}$$

for mean time before failure $\text{MTBF} = 3000 \text{ hr}$, test smoothing time $\tau_s = 60.0 \text{ sec}$. The probability of non-detection is a more involved calculation and necessarily uses approximations good for the range of test levels considered. Assuming a relatively flat distribution of failure drift rates with minimum value D_{Fmin} , the probability of non-detection at the recommended failure test level ϵ^2 , with $\epsilon = (\delta_N + D_{Fmin}) / 2$ is

$\frac{D_{FL}}{\sigma_N}$	PND
11	10^{-24}
9	10^{-13}
8	10^{-6}
7	3×10^{-5}

* A modified Rayleigh distribution.

Techniques were evolved for evaluation of the probability distribution of relevant classes of test functions. Probability distribution is requisite to determine probability of rare events such as false alarm and non-detection.

The three-gyro case was analyzed to obtain test functions based on the same criteria of failure definition and single failure at a time, obtaining failure detection and isolation functions for gyro g where gyro \bar{g} has previously failed,

$$F_g < \epsilon^2$$

where

$$F_g = \frac{2}{3} [\bar{F}(\bar{g}) - 2k \cdot T_{rs}^2] \quad \begin{array}{l} \text{Three Gyro Case} \\ r \neq s \neq g \neq \bar{g} \end{array}$$

where $\bar{F}(\bar{g})$ is defined for the four gyro case above.

It is shown $k > 0$ should be as high as tolerable for the gyro noise level,

$$K = \frac{3}{8} \epsilon \cdot D_{F_{\min}}^2 / \sigma_N^2$$

for test decision purposes, despite the fact that other smaller K makes F_g a better estimate D_g^2 when the other gyros are drifting. The tests for $F_g < \epsilon^2$ to determine validity of each gyro g other than gyro \bar{g} are equivalent to failure tests,

$$\text{Test \#}g \quad T_{rs}^2 > (\bar{F}(\bar{g}) - \frac{3}{2} \epsilon^2) / 2K \quad \begin{array}{l} \text{Three Gyro Case} \\ r \neq s \neq g \neq \bar{g} \end{array}$$

such that if only Test # g fails then gyro g has failed. In the event two of the three tests fail we have the ambiguous case in which the direction of the failure drift is near normal to a test direction. The Test # g is incorporated in the preliminary FORTRAN list of the advanced failure detection and isolation program listed in Appendix I-5, in the test of $S(L) \equiv T_{rs}^2$ against $TL \equiv (\bar{F}(\bar{g}) - 3/2 \epsilon^2) / 2K$. In the ambiguous case where two of the three tests fail, it is known that one gyro g whose test passed

is good. To find which gyro failed, gyro r or gyro s, the statistic

$$\Delta = (T_{rg}^2 - T_{sg}^2)$$

is analyzed for probability distribution given gyro r failed or gyro s failed in the presence of gyro noise. From these probability distributions are derived the probability that gyro r failed, $P_{F_r}(\Delta)$. Then the reliability of the decision of which gyro failed is calculable in terms of edge test observations. Operational requirements determine the use of decision reliability, for example if below a prescribed level of certainty to signal to the pilot a system failure. In Appendix I-5 a particular utilization of the probability of correct decision, extracted from a stored table is considered, namely, the assignment of gyro validity

$$v_r = P_{F_r}(\Delta)$$

for weighting of navigation channel estimates or according to level for logical validity.

It is proposed that improved navigation accuracy with four valid gyros be obtained by weighting channels according to drift level estimates of the gyros of each channel. Soft failures GF_1 which markedly degrade navigation of a channel using such gyros would be downgraded in a weighting of channel estimates of a variable χ ,

$$\hat{\chi} = \frac{\sum_{i=1}^4 \omega_i \cdot \chi_i}{\sum_{i=1}^4 \omega_i}$$

where

$$\omega_i = [2F_0 - \bar{F}(r) - \bar{F}(s) + C]^{-1} \quad \text{Channel } i \text{ uses gyro } r, \text{ gyro } s$$

the functions F_0 , $\bar{F}(r)$ and $\bar{F}(s)$ being available from the gyro failure detection and isolation program. The case of three gyros and ambiguous two gyros are of interest for weighted navigation, for example, using

$$\omega_i = [T_{rs}^2 + C]^{-1} \quad \text{Channel } i \text{ uses gyro } r, \text{ gyro } s$$

VI. PRELIMINARY SYSTEM DESIGN

6.1 System Block Diagrams

A simplified system block diagram is shown in figure 6-1. The complete redundant strapdown INS is composed of four identical channels. Each channel of the INS consists of the following elements:

- a. An Inertial Measurement Module (IMM) containing the basic inertial sensing devices, one TDF tuned gimbal gyro and two axes of acceleration measurement, with their associated electronics.
- b. A computer which performs redundancy management, instrument compensations, coordinate transformations, and the inertial navigation computations.
- c. External I/O which interfaces the computer with other aircraft equipment. Note that there is no self-contained voting in the system between the computers and these outputs. The external equipment must perform some voting between channels (in addition to using validity information provided by each channel) in determining the final navigation variable to be used.
- d. Inter-computer I/O which is used to transfer gyro and accelerometer measurement data from one channel to all others for use in redundancy management, and for derivation of the full 3-dimensional rate and acceleration inputs.
- e. A power supply used to drive all elements in a channel. Note that there is no cross-feeding of power between channels. This results in a simple, low-cost power supply design with a negligible decrease in system reliability over a modularly redundant power supply configuration.

A more detailed block diagram for one of the four Inertial Navigation Modules (INM) is shown in figure 6-2. The equipment shown is packaged in its own chassis and four of these chassis installed into a common mount comprise the complete redundant strapdown INS. The entire system will have a weight of 28 kg and a power consumption of 540 watts.

6.2 Hardware Design

6.2.1 G-6 Gyro and Loop Dynamics

The G-6 gyro, figure 6-3, consists of only five major subassemblies, resulting in a simple, low-cost design. The subassemblies are: the gyro case, bearing assembly capsule, torquer coils,

· Preceding page blank

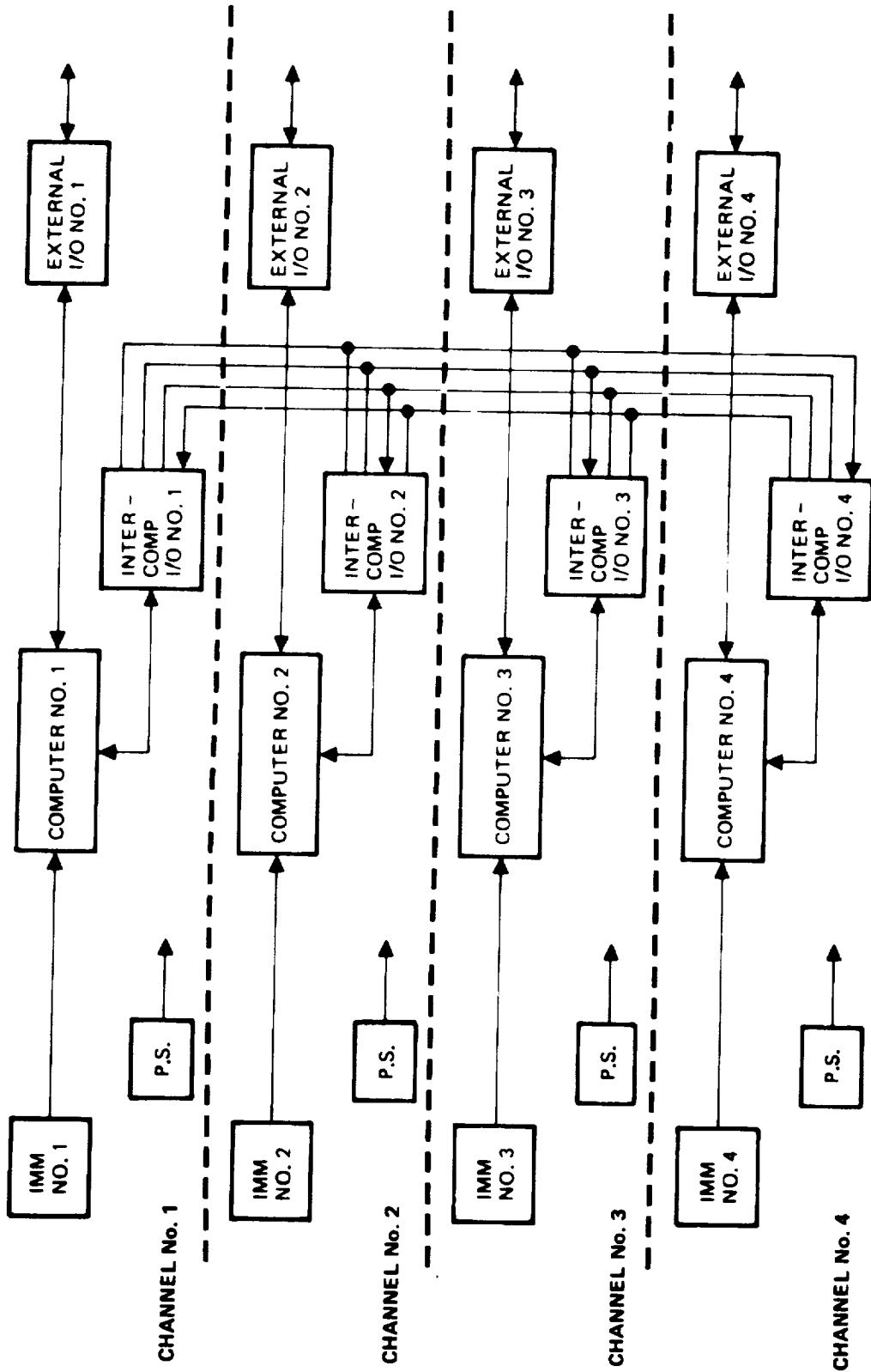


Figure 6-1. Redundant Strapdown INS

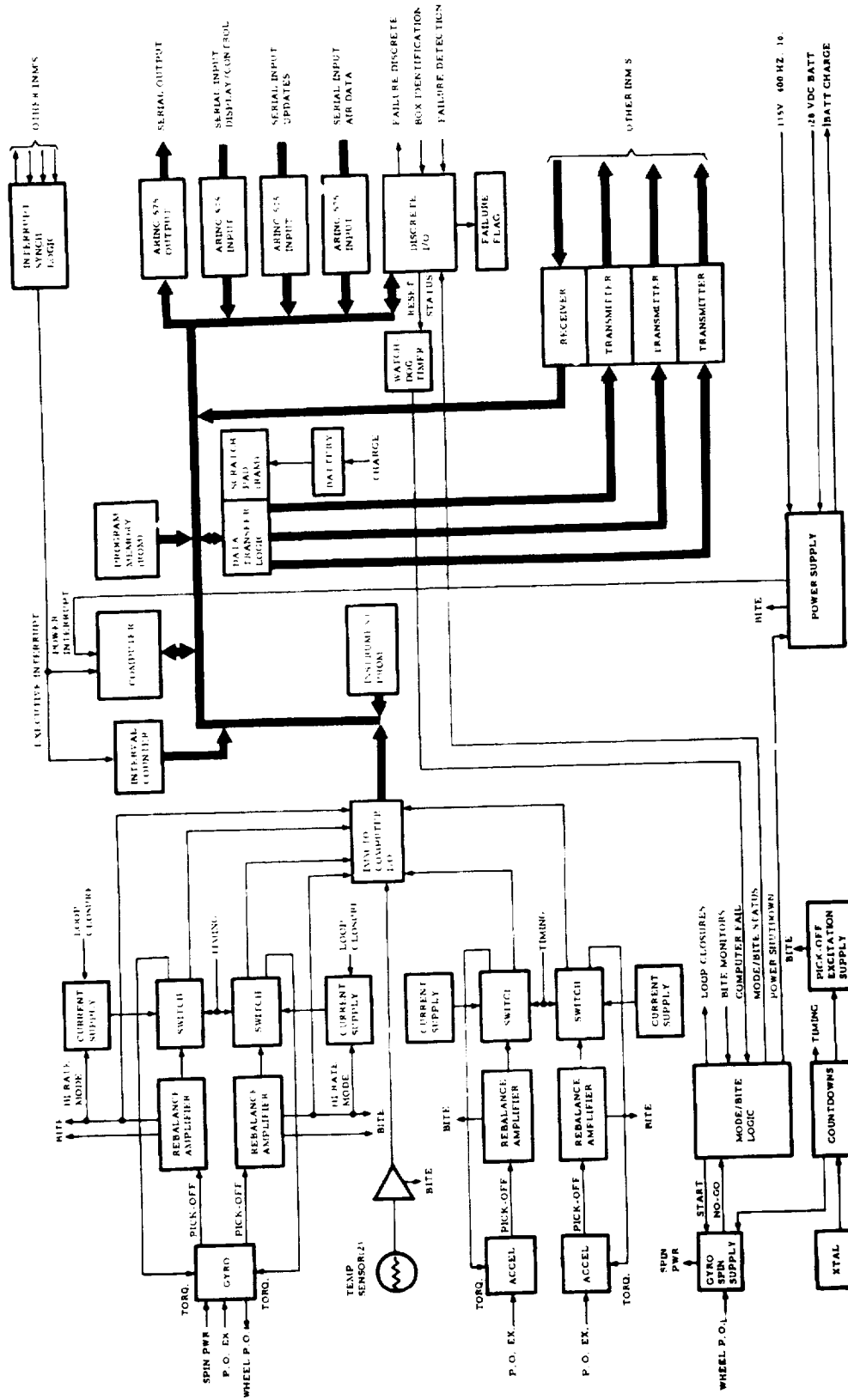


Figure 6-2. Inertial Navigation Module



REPRODUCIBILITY OF THE
ORIGINAL PAGE IS POOR

Figure 6-3. Photograph of Litton G-6 Strapdown INS Gyroscope

pickoffs, and the rotor with its tuned suspension. The torquer, pickoff, and bearing subassemblies are mounted in the case containing the spin motor stator. The replaceable bearing assembly contains the prealigned shaft and bearing assembly. The motor hysteresis ring is mounted on one end, and the rotor and suspension are mounted on the other. End covers, when soldered in place, provide an hermetic seal for the gyro. All five major subassemblies are interchangeable with other like subassemblies.

The Suspension System

The function of the suspension system is to provide translational support for the rotor in such a way that the effective torsional coupling between the rotor and the gyro case about any axis that is perpendicular to the rotor spin axis is zero. The suspension system in a tuned gyro is analogous to that of a universal joint and in its simplest form consists of an inertia element (the gimbal) and the torsional elements (the flexures). Typically, four cross-leaf flexures are used. Two of these flexures connect the gimbal to the shaft, forming one torsion axis of rotor and gimbal freedom relative to the shaft. The remaining two flexures, whose axis of torsion is orthogonal to that established by the first two flexures, connect the rotor to the gimbal and thus form the second axis of rotor freedom. When such a suspension system and the rotor are run at a speed corresponding to the tuned frequency, the dynamically induced spring rate due to the gimbal motion is equal to the physical spring rate of the flexures and the resultant spring rate coupling the rotor to the shaft is zero. This condition is attained by the adjustment of the moments of inertia of the gimbal such that the tuned frequency is equal to the frequency of the synchronous motor speed.

Through careful selection of the ratio of rotor to gimbal inertias and gyro operating spin speed, Litton has eliminated the need for complex tuning techniques and procedures often used in this class of instruments. This new approach not only significantly reduces gyro cost but also inherently enhances performance. Reduced long-term mass shifts (spin axis mass unbalance) and thermal instability of mass shifts are obtained. There are no adjustment weights on the rotor assembly. All balancing is done at the subassembly level by a static balance procedure in which unbalances are measured and appropriate material is removed. Gyro tuning is also adjusted at this subassembly level.

References [31], [32], and [33] provide a description of the operation and errors caused by the tuned suspension system.

Torquers and Pickoffs

The function of the pickoffs and torquers is to control the attitude of the rotor relative to the gyro case. When an input rate is applied to the gyro case, the case fixed pickoffs sense the change of rotor attitude relative to the case and cause the rebalance loop to provide current to the torquers in such a sense as to reduce this change to zero. In an ideal strapdown gyro the torquer maintains the spin axis of the rotor aligned with the shaft spin axis and thus the rotor has the same angular velocities as the case about the input axes. The torquers are designed such that the currents through their coils are directly proportional to the moment outputs and thus the torquer current is a direct measure of the input rate to the gyro.

The gyro torquer is a permanent magnet of the voice coil type and is capable of exerting moments on the rotor about two nominally orthogonal axes that are perpendicular to the rotor spin axis. The torquer consists of two elements; one element consists of permanent magnets attached to the rotor and thus spinning with the rotor, and the other is the torquer coil assembly fixed to the gyro case. The permanent magnets are radially magnetized and, when assembled on the rotor, establish a radially oriented magnetic field across the airgap containing the conductors of the torquer coils.

The high-permeability rotor provides the return path for the magnetic flux. There are two diametrically opposite torquer coils per axis connected in series in such a way that the moments produced by the individual coils are additive. The average torque produced by the coils is proportional to the product of the effective field density, the ampere turns, the effective circumferential length of the conductors and the radius of the airgap.

The pickoff used is a high frequency variable reluctance type. There are two diametrically opposite E cores per axis, each carrying a primary and a secondary winding. The reluctance path associated with each core consists mainly of the airgap that separates the E core from the flux return path mounted on the rotor. Thus, the field set up by the primary winding and linking the secondary winding is mainly a function of the airgap length. The voltages induced in the secondary windings of the two diametrically opposite cores are connected in series-opposition. The overall pickoff output is thus only sensitive to the angular motions of the rotor relative to the case about the pickoff axis.

Summary of Capture Loop Technique

Pulse rebalance torquing with binary duty cycle modulation has been selected by Litton for capturing the sensitive elements of the inertial instruments (accelerometer and gyro). Pulse-torquing

has significant advantages in terms of higher accuracy, less complexity, higher reliability, and lower cost than other methods considered. Other important advantages of pulse torquing are (1) elimination of torquer nonlinearity, (2) constant torquer power dissipation, and (3) elimination of linear power amplifiers.

Each axis of the G-6 gyro is captured using a simple single-axis loop, i.e., the X pickoff drives the Y torquer, and the Y pickoff drives the X torquer. A major disadvantage in using a dual-axis approach (i.e., what is recommended in reference [3] where each torquer is controlled by both pickoffs) is the rectification effect from high current directed into the torquers at harmonics of the spin speed. The dual-axis loop has relatively high gain at frequencies above the bandwidth of the gyro and readily couples the everpresent harmonic noise from a pickoff into the torquers. This effect is compounded by the fact that the noise from both pickoffs is directed into each torquer at high gain levels (with considerably more circuitry required).

The single-axis capture loop (using a pure lag network with a notch at spin speed) attains essentially the same bandwidth as the dual-axis but reduces the torquer noise by two or more orders of magnitude. In so doing, (1) the dynamic range is not degraded, (2) torquer rectification effects become negligible, (3) the gyro bias is insensitive to gain variations, and (4) much shorter periods of time are required to ascertain drift rate since the data channel is not dithered by noise. All this is gained simply, more reliably, and at lower cost.

The predicted performance of single-axis control using pulse torquing techniques has been verified by tests of the G-6 gyro.

Gyro Capture Loop Groundrules

In order to obtain superior performance from the strapdown system, any significant errors generated at the gyro outputs and in subsequent computer processing must be minimized or compensated. With this in mind, certain ground-rules have evolved from the tests and studies of various capture loops for dry two-degree-of-freedom gyros. These investigations have contributed to optimizing the significant parameters affecting the quality of the gyro output.

Listed below are some of the critical factors which have been considered in the design. These factors are especially relevant with regard to realizing the advantages of pulse-torquing.

- a. The noise level of the capture-loop signals which are directed into the pulse-torquing networks should be low. More specifically, both the noncoherent and spin-speed coherent "noise" levels of the signal which controls the pulse widths should be less than that required to switch

from one discrete pulse-width level to the next. This requirement of course, is a function of various factors including bandwidth, pulse repetition frequency, and the pulse modulation frequency.

- b. The closed-loop dynamic behavior (bandwidth, relative stability, etc.) must meet conditions which are compatible with the gyro characteristics as well as with the computer processing techniques. For instance, errors associated with pickoff excursions, even if compensated, should be minimized by insuring that the bandwidth is as high as possible without unduly exceeding the computer processing rate. Too high a bandwidth may torque the gyros unnecessarily at frequencies which will not be processed fast enough by the computer, and consequently the error compensation by the computer would become ineffective.
- c. The pulse-torquing resolution should be fine enough such that initial alignment can be accomplished within the desired period of time.
- d. Asynchronous pulse-torquing is essential to eliminate any shutdown unrepeatability which may occur as a function of the rotor synch position. If the pulsing is synchronous with the wheel speed, the torquing pulses act upon the same portions of the rotor for each rotor revolution. If the gyro is shut down and restarted, the rotor may synch in a new position relative to the pulse modulation frequency, and the torquing pulses would then act upon different portions of the rotor; to negate this effect, the pulsing is applied asynchronously relative to the rotor speed.

Gyro Capture-Loop Design

The basic equations for the G-6 strapdown gyro are presented in Appendix D. Using these equations the general technique for studying the capture-loops was developed and the above ground rules were then incorporated as constraints.

The equations in Appendix D do not assume the simplifications made for the gyro model in reference [3]. Those simplifying approximations which were made (1) show nutation occurring at twice the spin speed which is misleading, (2) will indicate that no open-loop resonance will occur for rate inputs at this assumed nutation frequency, which again is misleading, and (3) do not involve the physical parameters of the gyro to facilitate studying the effects of parameter variations.

The equations in Appendix D allow for the real values of moment of inertia and for the effective angular momentums H and H_C which result from the rigorous derivation of the equations of motion for dry tuned gyros as developed in reference [31]. The equations also reduce to the standard equations applicable to TDF floated gyros, in which case $H = H_C (F_m \rightarrow \infty), \tau \rightarrow \infty$, D equals the flotation fluid damping, and K_D equals the pigtail spring rate.

To capture the rotor, torques M_{ax} and M_{ay} are applied as a function of the pickoff signals θ_x and θ_y . Generally torque can be applied about either axis (or both) from each pickoff. Therefore torque about X and Y are functions of θ_x and θ_y . The matrix in equation (3) in Appendix D can be modified to include the torquing function. To examine the capture loop behavior, the off-tuning condition, damping and time-constant effect can be neglected, i.e., let $\tau \rightarrow \infty, D = 0$ and $\Delta N = 0$. Then from (3) in Appendix D,

$$\begin{bmatrix} AS^2 + F_D(S) & H_C S + F_C(S) \\ -[H_C S + F'_C(S)] & AS^2 + F'_D(S) \end{bmatrix} \begin{bmatrix} \theta_X(S) \\ \theta_Y(S) \end{bmatrix} = \begin{bmatrix} \text{input} \\ \text{driving} \\ \text{functions} \end{bmatrix} \quad (1)$$

where

$F_D(S)$ is the "direct-axis" gain and compensation and

$F_C(S)$ is the "cross-axis" gain and compensation

Definitions of other terms are given in table 6-1.

The characteristic equation determined from the determinant of the matrix on the left hand side of (1) is useful in assessing the stability and behavior of the closed-loop. There are a number of ways of analyzing this equation. Assuming that the gain and compensation are the same (symmetric) for both axes ($F'_D = F_D$ and $F'_C = F_C$), the characteristic equation is:

$$\left[AS^2 + F_D(S) \right]^2 + \left[H_C S + F_C(S) \right]^2 = 0$$

Note that this expression is in the form of:

$$P^2(S) + Q^2(S) = [P(S) - jQ(S)][P(S) + jQ(S)] = 0 \quad (2)$$

TABLE 6-1. GYRO NOMENCLATURE

A	Rotor transverse moment of inertia
C	Rotor polar moment of inertia
D	Rotor damping relative to case
F_C	"Cross-axis" capture loop compensation
F_D	"Direct-axis" capture loop compensation
$\overline{F_{DC}}$	Composite complex compensation, $\overline{F_{DC}} = F_D - jF_C$
F_m	Figure of merit
G_D, G_C	Amplitude of pickoff error response
H	Angular momentum associated with rotor and case rates relative to inertial space ($\theta_X = \theta_Y = 0$)
H_C	Angular momentum associated with rotor rates relative to the gyro case ($\phi_X = \phi_Y = 0$)
j	Complex notation for $\sqrt{-1}$
K	Capture-loop gain factor
K_D	Gyro in-phase spring rate
K_P	Pickoff scale factor
K_T	Torquer scale factor
M_{aX}, M_{aY}	Torques applied to rotor (from torquer)
M_{aXY}	Vector form of applied rotor torque, $M_{aXY} = M_{aX} + jM_{aY}$
M_{eX}, M_{eY}	Disturbance or error torques
N	Rotor spin speed
S	Laplace variable
θ_X, θ_Y	Angular displacements of the rotor relative to the case (pickoff angles)
θ_{XY}	Vector form of gyro pickoff signal, $\theta_{XY} = \theta_X + j\theta_Y$
ξ_D, ξ_C	Phase of pickoff error response
τ	Gyro dynamic time constant
τ_T	Torquer electrical time constant
ϕ_X, ϕ_Y	Angular displacements of the case relative to inertial space
ϕ_{XY}	Vector form of case input, $\phi_{XY} = \phi_X + j\phi_Y$
ω	Radian frequency

and the roots of such an equation can be found from either factor of equation (2). Any complex root in one factor will have its complex conjugate in the other factor. With $P(S) = AS^2 + F_D(S)$ and $Q(S) = H_C S + F_C(S)$, and by arbitrary choice of a factor in (2).

$$P(S) - jQ(S) = [AS^2 + F_D(S)] - j[H_C S + F_C(S)] \quad (3)$$

To find the roots of this factor as a function of the gains (by root-locus techniques, for example) the form is:

$$\frac{F_D(S) - jF_C(S)}{AS^2 - jH_C S} = -1 = 1 \angle 180^\circ \quad (4)$$

A new variable $\overline{F_{DC}}(S)$ can be defined which represents a complex gain element.

$$\overline{F_{DC}}(S) = F_D(S) - jF_C(S) \quad (5)$$

substituting (5) into (4)

$$\frac{\overline{F_{DC}}(S)}{AS(S - jH_C/A)} = 1 \angle 180^\circ \quad (6)$$

By trying various compensations, $\overline{F_{DC}}(S)$, a suitable closed loop response can be developed. $F_D(S)$ can then be determined from the real parts of $\overline{F_{DC}}(S)$, and $F_C(S)$ from the imaginary parts of $\overline{F_{DC}}(S)$.

Another powerful mathematical technique* for examining stability from the set of equations represented by (1) generates a transfer function in complex form (vector form) for which the real parts of the transfer function characterize the behavior of the rotor about the X-axis, and the imaginary portion characterizes the behavior about the Y-axis. By adding the first equation in (1) to j times the second equation gives

$$\begin{aligned} [AS^2 + F_D(S)] [\theta_X(S) + j\theta_Y(S)] + [H_C S + F_C(S)] [\theta_Y(S) - j\theta_X(S)] \\ = (\text{summation of driving terms}) \end{aligned} \quad (7)$$

*See Ref. [34]

By defining a new variable (in vector form) as follows:

$$\theta_{XY}(S) = [\theta_X(S) + j\theta_Y(S)]$$

and substituting into the left hand side of (7) yields:

$$\left[AS^2 + F_D(S) \right] \theta_{XY}(S) - j \left[H_C S + F_C(S) \right] \theta_{XY}(S)$$

or,

$$\left\{ \left[AS^2 + F_D(S) \right] - j \left[H_C S + F_C(S) \right] \right\} \theta_{XY}(S)$$

Note that the term in brackets is the same as in (3) and indeed represents the characteristic determinant. This can then be put in the same form as (5) and (6).

The importance of this analysis is that the input-output relationships can now be determined by solving for $\theta_{XY}(S)$ for any input condition desired and noting that $\theta_X(S)$ and $\theta_Y(S)$ can be obtained separately (resolved) into the real parts and the imaginary parts of $\theta_{XY}(S)$. The resolved outputs can also be determined from:

$$\theta_X = \frac{\theta_{XY} + \bar{\theta}_{XY}}{2} \quad \text{and} \quad \theta_Y = \frac{\theta_{XY} - \bar{\theta}_{XY}}{2j}$$

where $\bar{\theta}_{XY} = (\theta_X - j\theta_Y)$, the complex conjugate of θ_{XY} .

Input driving functions for (7) will also be in the form of $M_{eXY}(S)$ or $\phi_{XY}(S)$, where any symbol in the form of f_{XY} is defined as:

$$f_{XY} = f_X + jf_Y \quad \text{and} \quad \bar{f}_{XY} = f_X - jf_Y \quad (8)$$

Note also that the feedback torques M_{aX} and M_{aY} are (in vector form), dropping the Laplace operator S ,

$$\begin{aligned} M_{aXY} &= M_{aX} + jM_{aY} = -\bar{F}_{DC} \theta_{XY} \\ &= -(F_D - jF_C)(\theta_X + j\theta_Y) \end{aligned}$$

and that:

$$\begin{aligned} -M_{aX} &= F_D \theta_X + F_C \theta_Y \quad (\text{Real parts}) \\ -M_{aY} &= F_D \theta_Y - F_C \theta_X \quad (\text{Imaginary parts}) \end{aligned} \quad (9)$$

or in matrix form:

$$\begin{bmatrix} M_{aX} \\ M_{aY} \end{bmatrix} = - \begin{bmatrix} F_D & F_C \\ -F_C & F_D \end{bmatrix} \begin{bmatrix} \theta_X \\ \theta_Y \end{bmatrix}$$

The sign of the feedback was chosen with some forethought with regard to stability, and this resulted in the form $\overline{F_{DC}}(S)$ instead of $F_{DC}(S)$. The signs of the feedback, of course, could be arbitrary, but the stability of the closed loop would reflect the choice as a positive or negative feedback. The stability analysis would reveal the desired choice, however.

A block diagram of the captured gyro is shown in figure 6-4. This block diagram represents equations (1) and (2) from Appendix D, with equation (9) above substituted for M_{aX} and M_{aY} .

Using this block diagram the optimum compensation can be determined. Certain characteristics of the compensation are essential if the basic ground rules are to be met, for instance, it is desirable to include integral gain in the capture loop (type I servo) to insure a negligible hang-off error for constant input rates. A notch at the gyro spin speed is also desirable. The "noise" signal which may be generated at spin speed is characteristic to all tuned rotor gyros and is nominally minimized by mechanical adjustments on the gyro rotor. However, to allow for greater freedom in the mechanical adjustment a notch is provided to reject this signal.

With these factors in mind the characteristic equation for the dynamic behavior can be developed. From equation (6):

$$\frac{\overline{F_{DC}}(S)}{AS(S - jH_C/A)} = 1 \angle 180^\circ \quad (6)$$

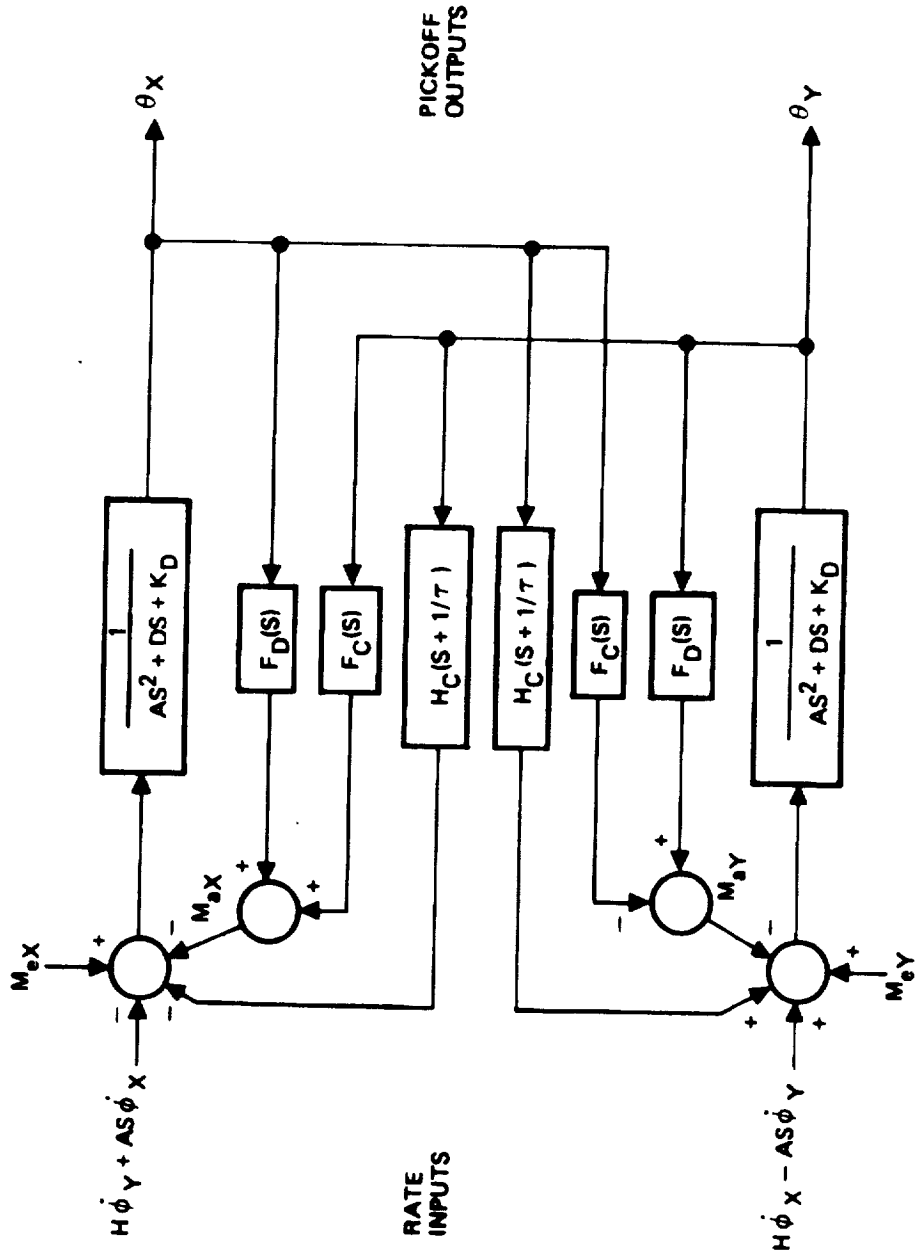


Figure 6-4. Strapdown Gyro Block Diagram

where:

$$\overline{F}_{DC}(S) = F_D(S) - jF_C(S)$$

H_C/A is the nutation frequency ω_n

$F_D(S)$ is the gain and compensation for direct-axis torquing, i.e., X pickoff driving the X-torquer, and Y-pickoff driving the Y-torquer

$F_C(S)$ is the gain and compensation for cross-axis torquing

From basic principles of gyrodynamics, torques which act on the rotor at low frequencies cause gyroscopic precession on an axis at right angles to the applied torque vector, but at the higher frequencies (near and beyond the nutation frequency) the gyro rotor acts more like a pure inertia and the rotor tends to displace about the same axis as the torque vector. This characteristic suggests using a pure gain for the cross-axis compensation $F_C(S)$ and a lead term for the direct-axis compensation $F_D(S)$. This approach is indeed optimum for capturing the gyro rotor to obtain high bandwidth, but generally uses more components to mechanize than the normal capture loops which Litton uses for rebalance. The standard capture loop is mechanized with only the "gyroscopic" cross-torquing function $F_C(S)$ and the loop essentially meets all the requirements desired. If extremely high bandwidth is found to be advantageous, then the direct-axis torquing function $F_D(S)$ can easily be included but caution is advised since the torquer noise will be high.

After examining the capture-loop compensation suggested in reference [3] which incorporated direct-axis capture, it has been concluded that the network was synthesized solely for its control characteristics without any concern for noise considerations.

A plot of the frequency response in reference [3] shows gains which are more than two orders of magnitude higher at the harmonics of spin speed than at the lower, controlled frequencies. The generation of relatively high output signals at these frequencies probably explains why the test data in reference [3] shows rotor excursions which are more than three times the theoretical value (12 mrad/rad/sec peak values instead of approximately 4 mrad/rad/sec) since the gain was probably limited to values much less than that desired.

This shows the importance of rolling-off lead networks at as low a frequency as possible after they have served their purpose, or noise will become a very serious problem.

Dual-axis Capture-Loop Compensation

The optimum dual-axis capture loop compensation is shown below. The gains are rolled-off as soon as possible after the required lead near the nutation frequency (for the direct-axis). The gain beyond the notch is only slightly higher at its peak than at midband (but orders of magnitude lower beyond the notch than the gain suggested in reference [3]). Let:

$$\overline{F}_{DC}(S) = \frac{K (S^2 + N^2) (S - jN)}{(S + 5N)^2 (S^2 + 2\xi NS + N^2)} \quad (10)$$

then

$$F_D(S) = \frac{KS (S^2 + N^2)}{(S + 5N)^2 (S^2 + 2\xi NS + N^2)}$$

and

$$F_C(S) = \frac{KN (S^2 + N^2)}{(S + 5N)^2 (S^2 + 2\xi NS + N^2)}$$

Note that the direct-compensation has no gain at DC and acts as a lead term at higher frequencies. The cross-compensation is effective at DC but rolls off at higher frequencies. The electronic circuitry for realizing this compensation is shown in figure 6-5. The frequency responses for these compensations are shown in figure 6-6 with $\xi = 0.3$.

Equation (10) is substituted into equation (6) and a root-locus plot is drawn. The optimum closed-loop gain is selected and the gain factor K is determined.

Closed Loop Frequency Response

Using the gain and compensation determined by the root-locus the closed-loop frequency responses can be evaluated for the pickoff error signals θ_x and θ_y and the rebalance torque M_{ax} and M_{ay} as a function of input angular rates $\dot{\phi}_x$ and $\dot{\phi}_y$. A computer program was developed which solves the block diagram shown in figure 6-4. The values of $F_D(S)$ and $F_C(S)$ above were used; in addition integral gain was included, with lead recovery at 60 rad/sec. Plots of these responses are shown in figures 6-7 and 6-8.

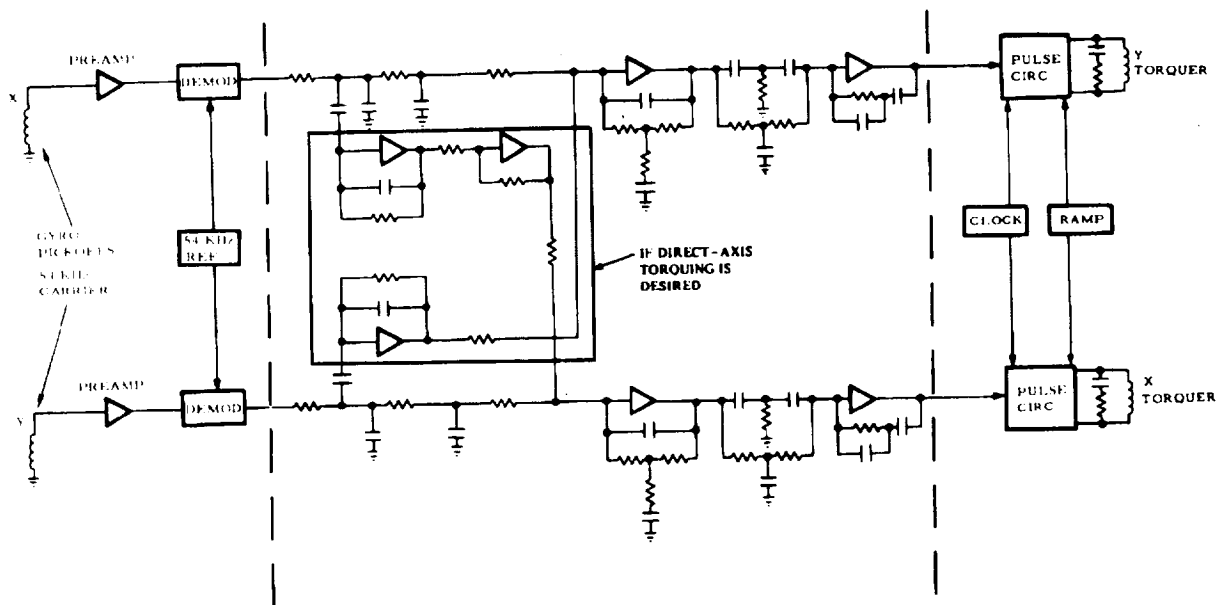


Figure 6-5. Electronics for Strapdown Compensation

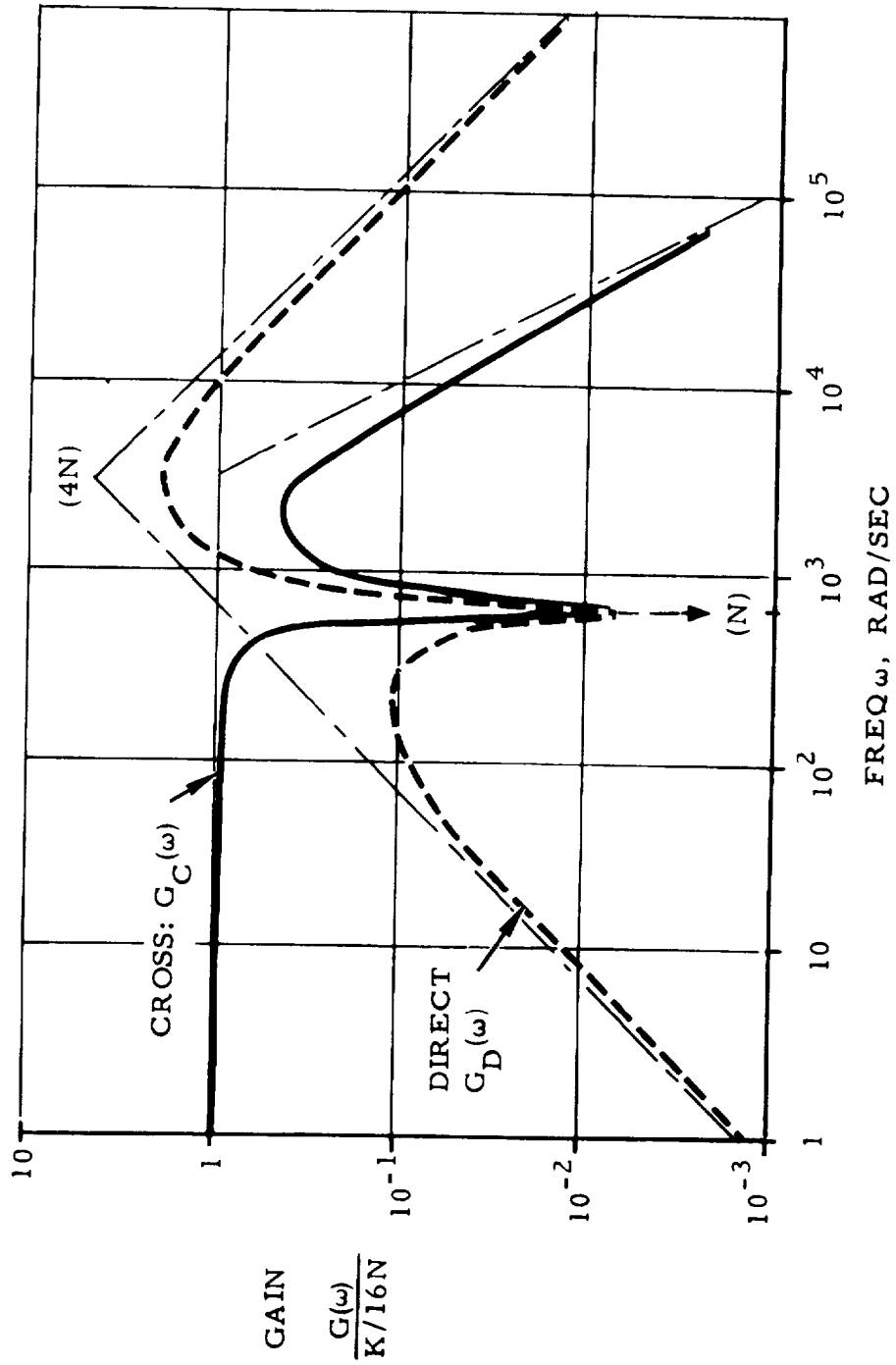


Figure 6-6. Frequency Response for Dual-Axis Compensation
(Integral Gain Not Shown)

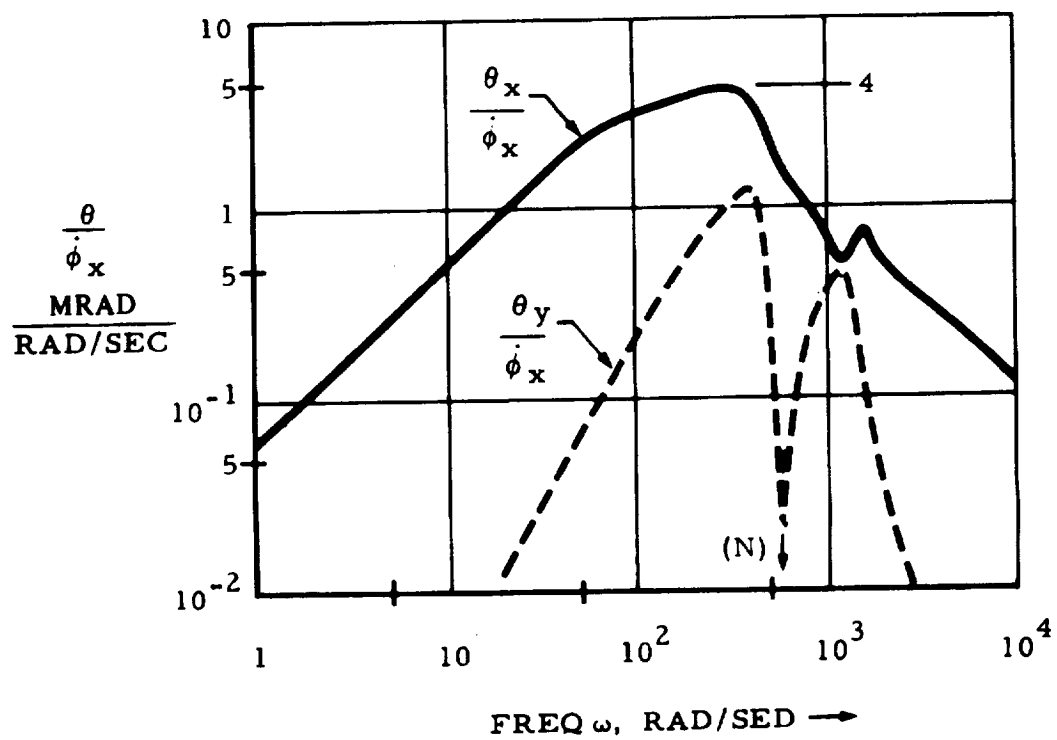


Figure 6-7. Closed-Loop Pickoff Excursion vs Frequency

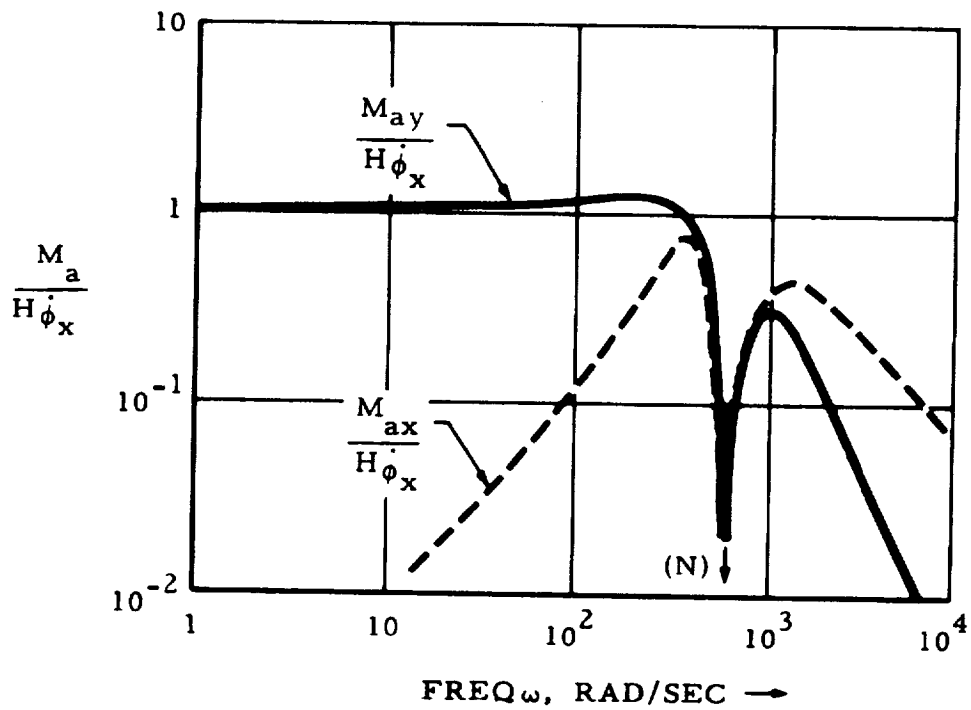


Figure 6-8. Frequency Response of Strapdown Gyro

Single-Axis Capture-Loop Compensation

The recommended method of capture is to implement only the cross-axis compensation $F_C(S)$. The reasons for this conclusion have been previously stated. Since a notch is used at the spin-speed, the bandwidth of the gyro is certainly limited to less than spin-speed using either capture loop approach. The bandwidth obtained in either case is also more than adequate for the system.

The following compensation is found to be optimum for single-axis capture:

$$F_C(S) = \frac{K [(S/N)^2 + 1] (S + 55)}{S [(S/2N) + 1]^3 [(S/N)^2 + (2\xi S/N) + 1]}, F_D(S) = 0$$

This compensation is characterized by a twin-T notch at spin speed N , three lags at twice the spin speed, a low-Q bandpass at spin speed ($\zeta = 0.03$), and integral gain with lead recovery at about 9 Hz. The frequency response for the compensation itself is shown in figure 6-9. It can be seen that there is a high rejection of signals beyond the bandwidth since this compensation consists primarily of lag networks. It is important that the phase of the torque at nutation be more than 90° lagging behind the pickoff to guarantee damping at this frequency. Tests using this circuit show extremely low noise for such a high bandwidth.

Frequency response plots for the pickoff error signal and rebalance torque are shown in figures 6-10 to 6-13.

6.2.2 Gyro Rebalance Loop Electronics

The basic design approach to rebalance the inertial strapdown sensors is through pulse duration modulation, a well known technique which provides direct digital output while still maintaining superior linearity and environmental capability. The basic block diagram of a loop is shown in figure 6-14. Functionally, vehicle angular motion produces a signal out of the gyro pickoff. This signal is amplified, demodulated, filtered and then compared with a sawtooth signal to produce a time modulated rebalance current through the gyro torquer to balance the input motion. This loop is basically a servo system which nulls the pickoff. The gyro torquer is electrically part of an "H" bridge arrangement. A constant current source, which is driven from a precision voltage reference, is switched by control signals from the voltage to pulse converter. Figure 6-15 shows a representation of the bridge arrangement. A higher voltage is switched into the bridge during large angular rates of the vehicle.

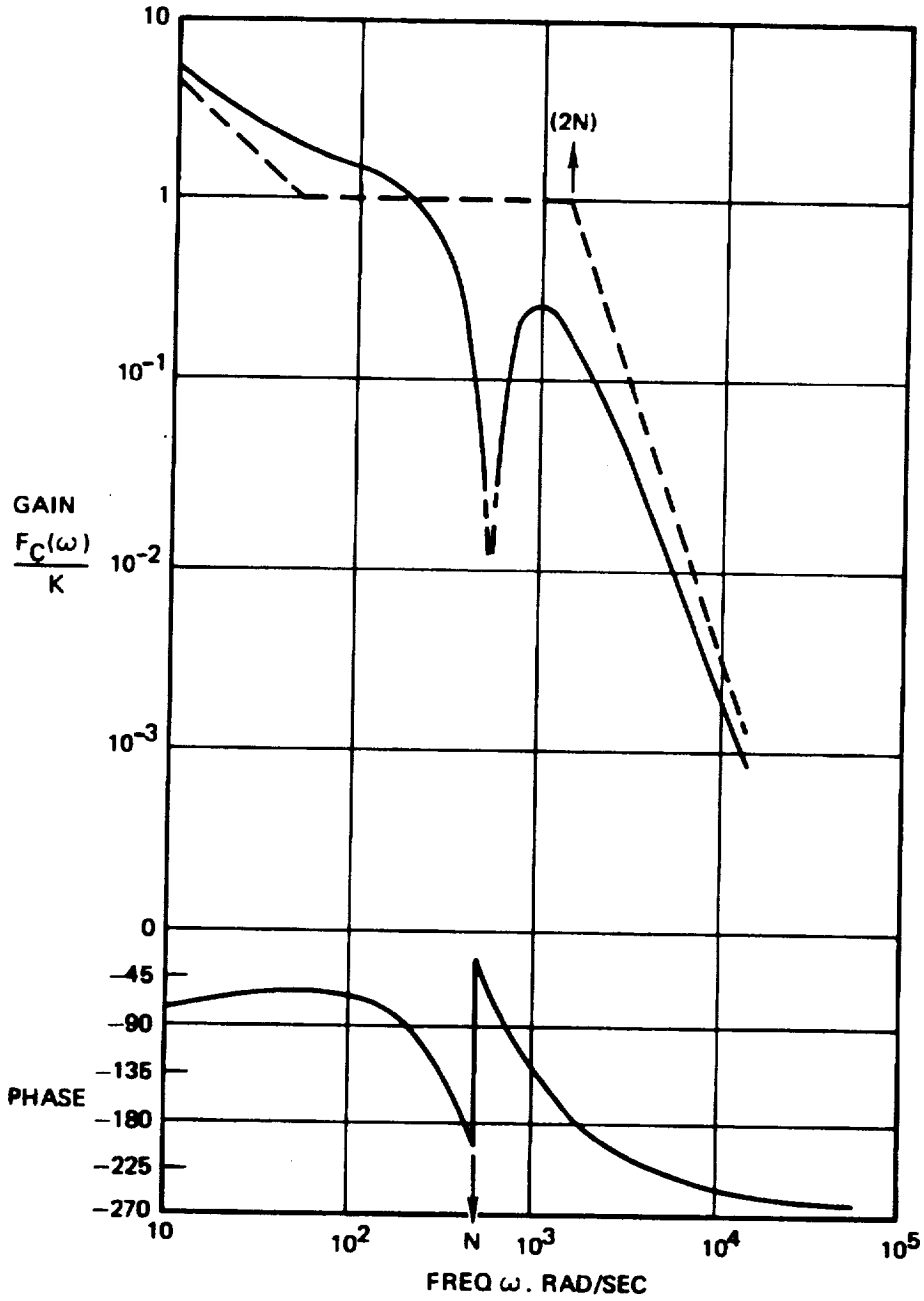


Figure 6-9. Compensation Response for Single-Axis Control

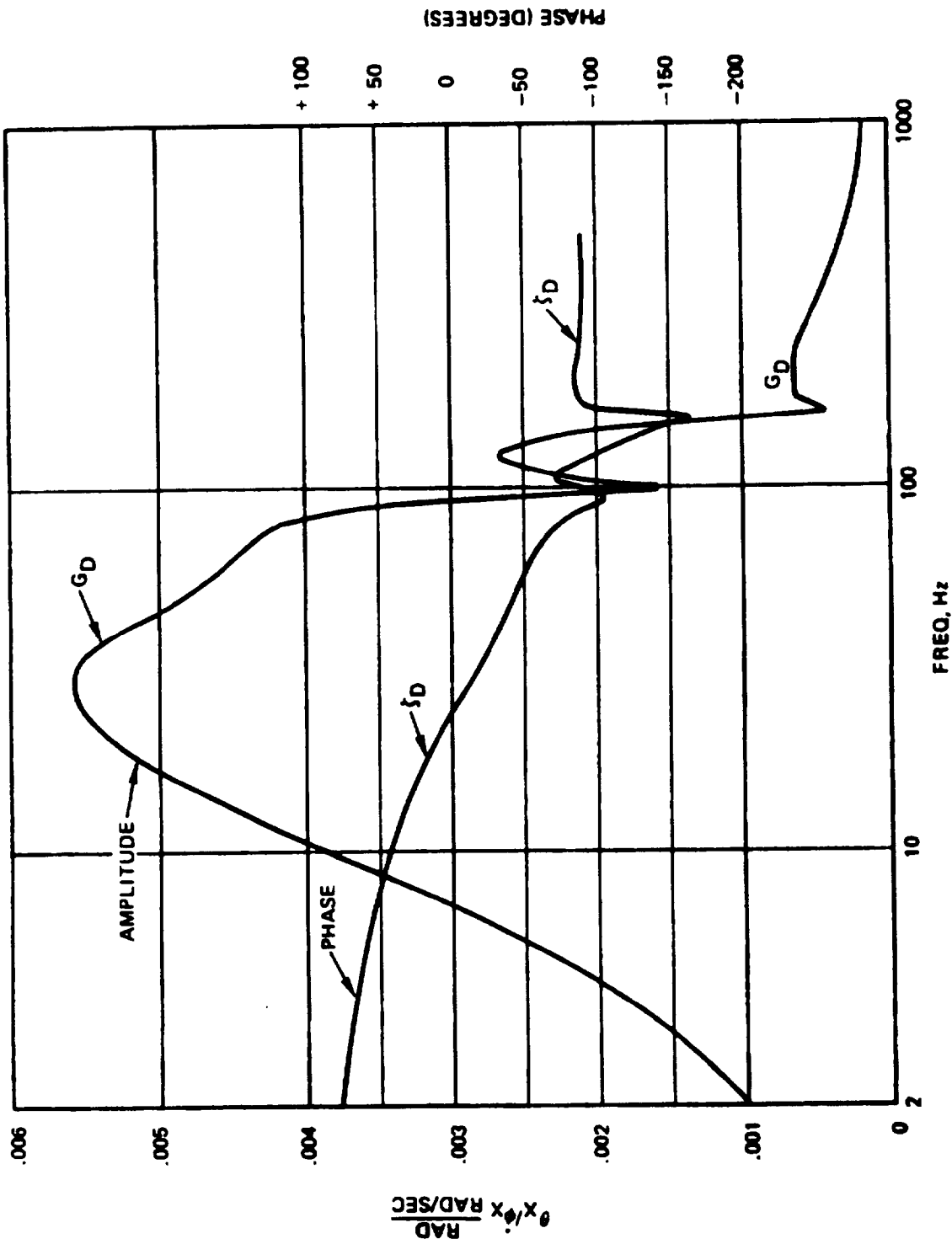


Figure 6-10. Strapdown Gyro Loop Pickoff Response (Direct)

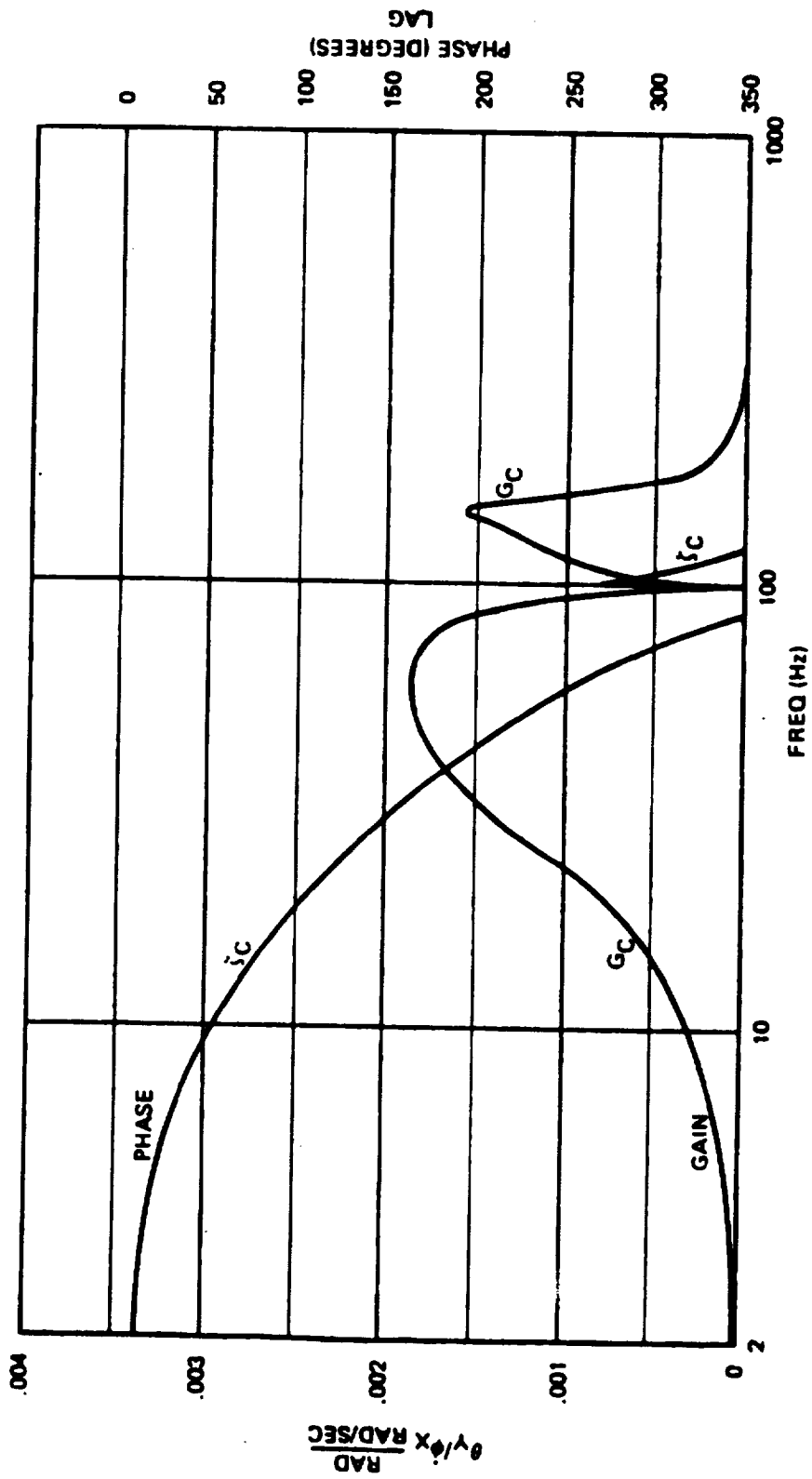


Figure 6-11. Strapdown Gyro Loop Pickoff Response (Cross Axis)

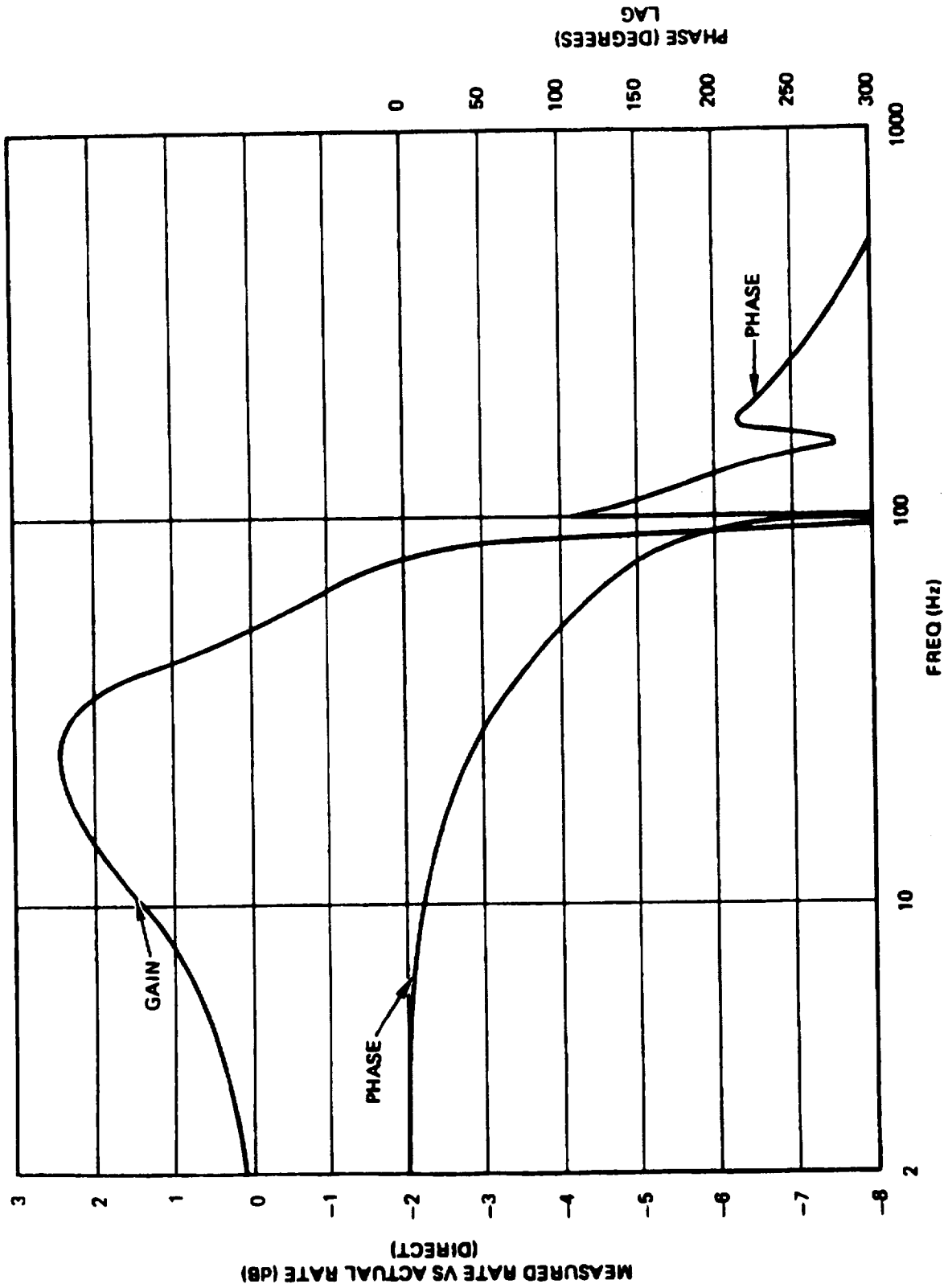


Figure 6-12. Strapdown Gyro Loop Frequency Response (Direct)

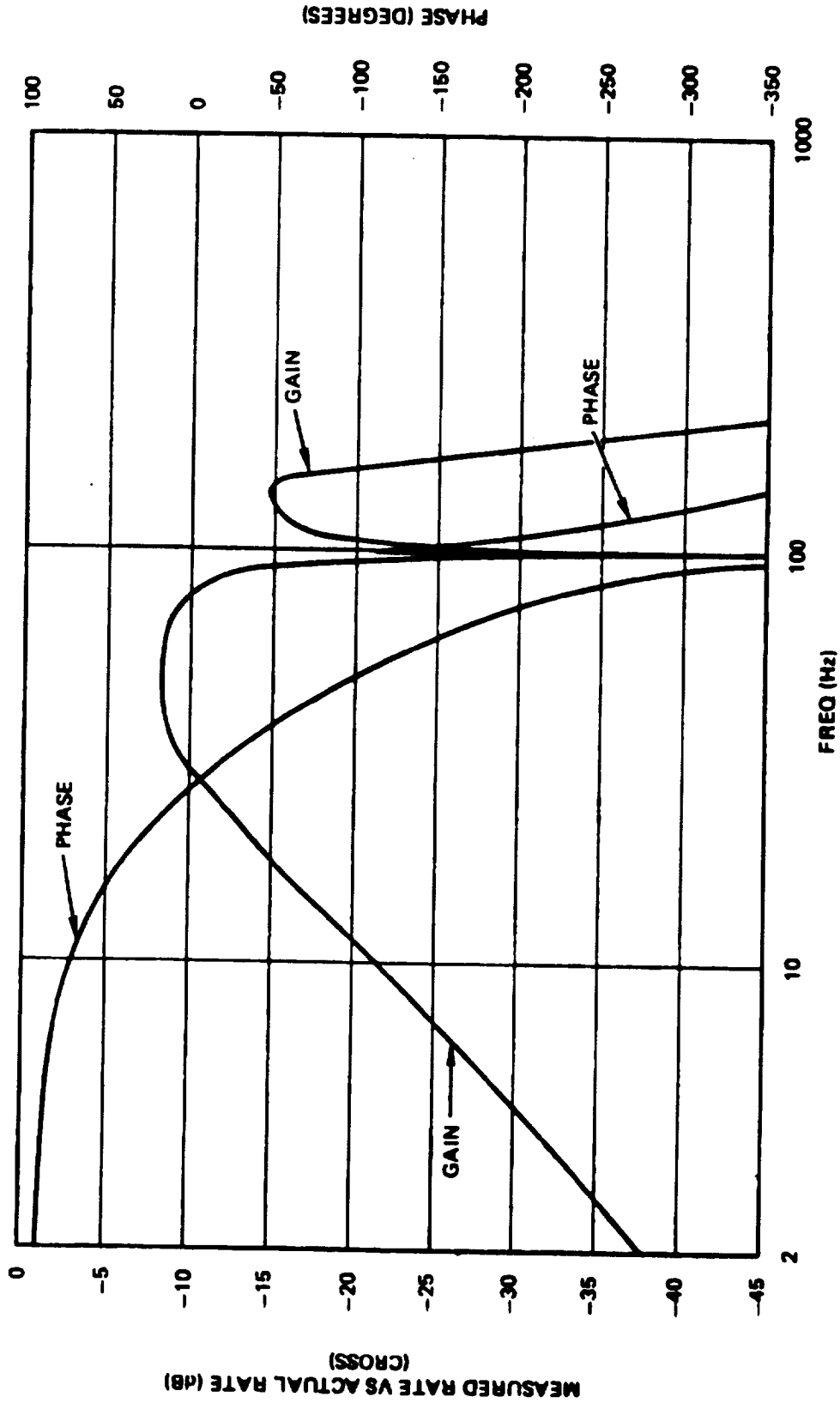


Figure 6-13. Strapdown Gyro Loop Frequency Response (Cross Measurement)

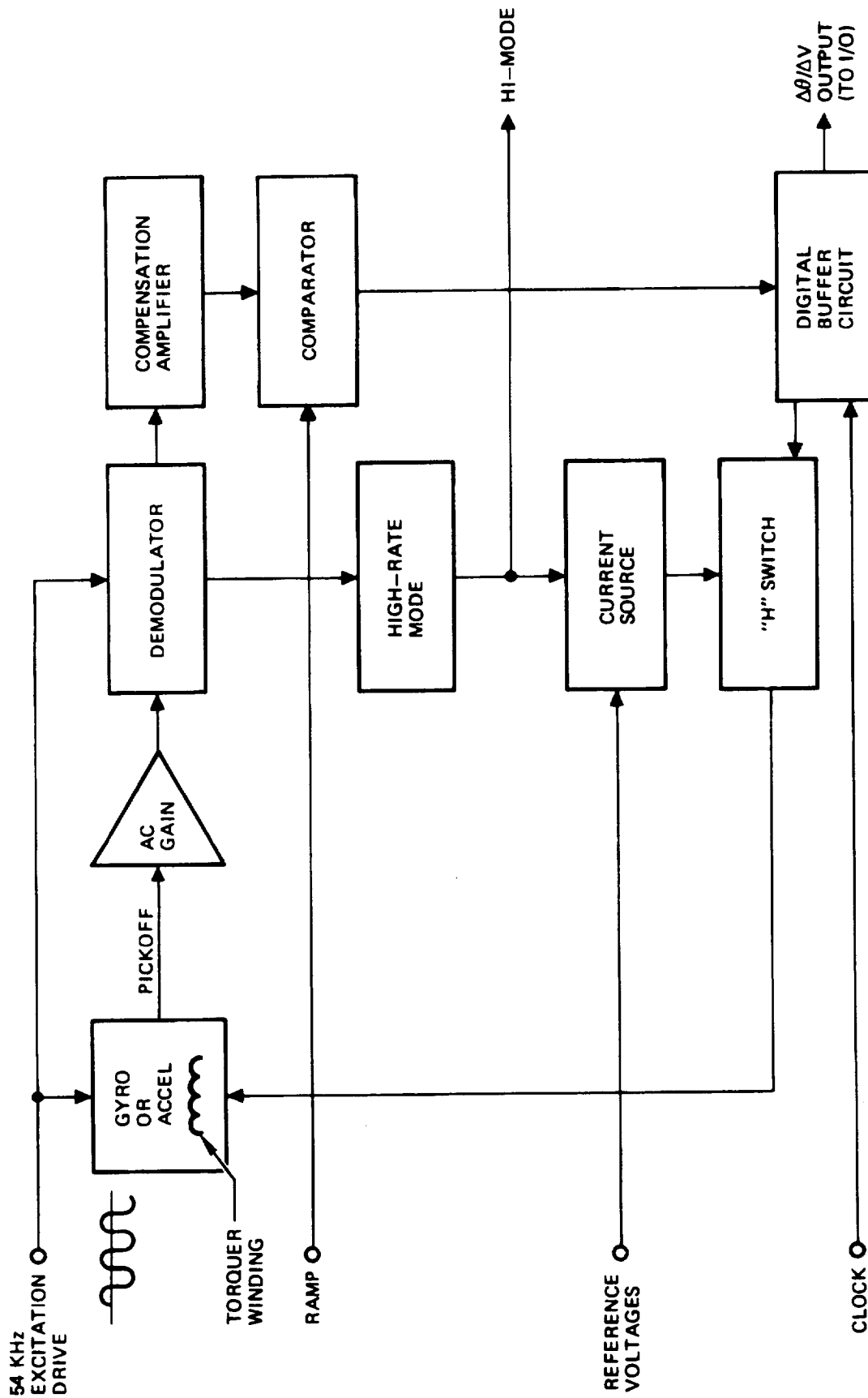


Figure 6-14. Typical Pulse-Rebalance Loop

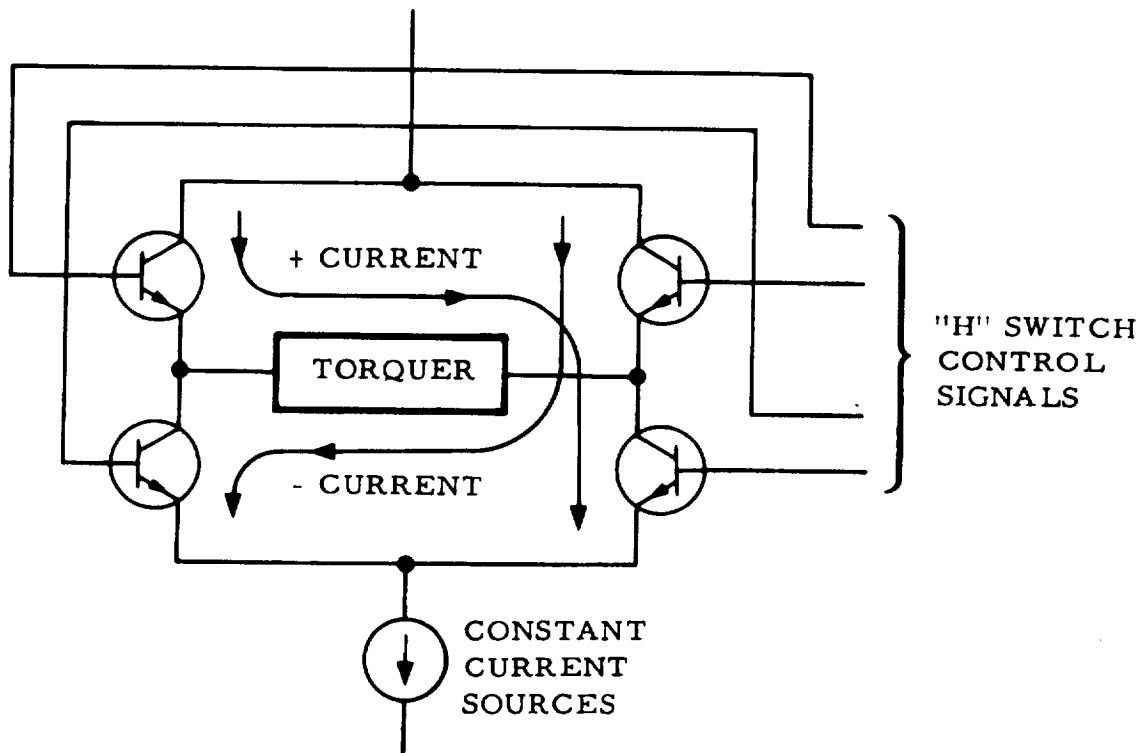


Figure 6-15. Rebalance Electronics Bridge Arrangement

The operation of the loop can be understood with the aid of figure 6-16. Input vehicle motions generate an error signal which is summed with a sawtooth waveform of a basic 2K Hz period called the limit cycle frequency. At the start of each limit cycle, the torquer current is positive until the error signal is equal to the sawtooth. The torquer current is then switched (by switching the torquer) to remain in the opposite direction until the end of the limit cycle. At time T, the bridge is again switched to a positive direction until another comparison is made during the second limit cycle. The net result is a current waveform whose average value is equivalent to that required to null the pickoff. Average current is therefore synchronous with the crossover time.

The master clock data pulses are synchronous with the limit cycle frequency. Since the bridge is permitted to be switched only at an integral number of clock pulses, the number of clock pulses between the start of the limit cycle and the time the bridge is switched is an extremely accurate measurement of average rebalance torque. The clock pulses (409.6 K Hz) and converter control signal are then fed to a counter in the serial data section to provide the equivalent incremental change in angle ($\Delta\theta_s$) in digital form to the computer. For a 2.048 K Hz limit cycle with a 409.6 K Hz data pulse rate, zero pulses per limit cycle represents full negative input rate, 200 pulses per limit cycle represents full positive input rate.

The electrical design success is predicated upon having an extremely accurate and stable rebalance current. Therefore all circuits associated with this function are considered critical. In general, all circuits employ state-of-the-art solid-state monolithic integrated circuits to the extent that available components are capable of performing the required task. Where performance requirements are beyond the capability of monolithic circuits, hybrids are employed. Discrete components are used where the ultimate in performance demands their use. All circuits are designed to meet the most stringent applicable specifications.

The input (front-end) section of each pulse-rebalance loop employs presently existing, well-proven, production hybrid circuits. The H-switch uses FET technology to minimize current imbalance between the two switched output current directions and to minimize leakage and base-drive-current contamination at the torquer coil. This coil is RC tuned to cause the winding to appear as a purely resistive load to the current switch, preventing switching transients from appearing at the current source.

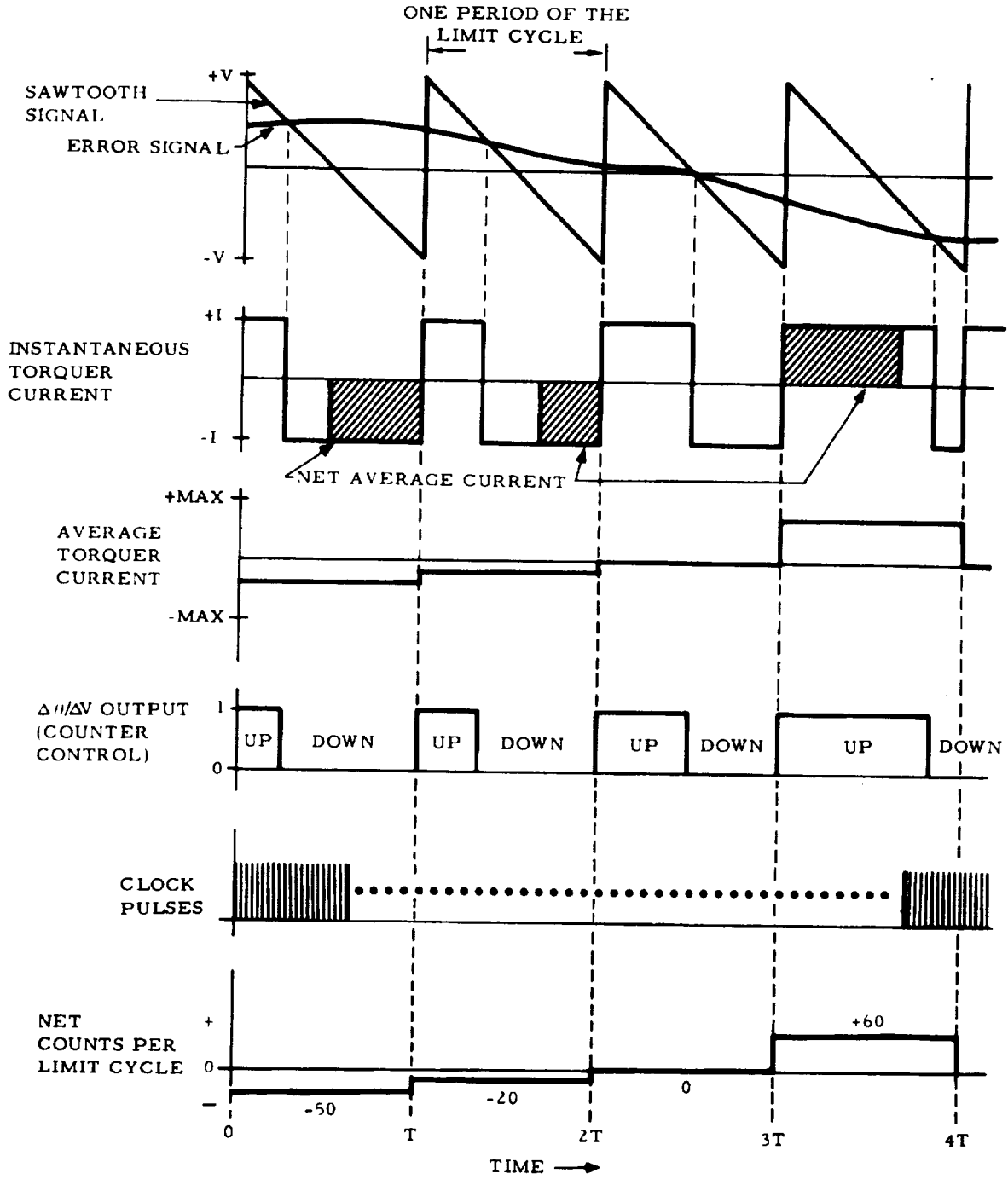


Figure 6-16. Rebalance Loop Waveforms

6.2.3 A-1000 Accelerometer and Loop Dynamics

Description

The A-1000 accelerometer, figure 6-17 is a flexure-supported, pendulous, torque-to-balance instrument characterized by simplicity, small size, and high precision. Its design has a demonstrated capability of withstanding a wide range of operational environments. Key design features are:

- a. Extremely simple, small, and lightweight.
- b. Low threshold, providing excellent gyrocompass performance.
- c. Single metalization pattern forming capacitive pickoff plates, circuitry, and flexure.
- d. Minimal thermal lag.

Excellent rapid reaction and extremely low temperature sensitivity is achieved by a combination of mechanical design and electrical compensation.

Principle of Operation

The sensitive element of the accelerometer is a disc supported by flexures which permit rotation about a diameter. The disc is made pendulous by the addition of a weight which displaces the center of gravity in the plane of the disc and normal to the hinge axis. Accelerations perpendicular to the plane of the disc result in rotation about the hinge axis. This rotation is sensed by the capacitive pickoff which produces a phase-sensitive signal proportional to the angular displacement. This output is amplified and is compared with a ramp which pulse-width-modulates the error signal in digital increments. This signal is used to control the timing of the current switches which produce precise amplitude current pulses whose timing is related to the loop error signal and drive the accelerometer torquer coil. The current in the torquer magnet produces a torque equal and opposite to the acceleration induced torque.

A-1000 Loop Dynamics

A block diagram representing the dynamics of the A-1000 is shown in figure 6-18. This model includes (a) the back EMF generated by the torquer, (b) the circuit placed in parallel with the torquer for optimizing the pulse-torqued wave-shape, and (c) the resonance and anti-resonance (node) of the suspension.

By using standard servo techniques the optimum gain and phase was determined. A computer was programmed to determine the frequency

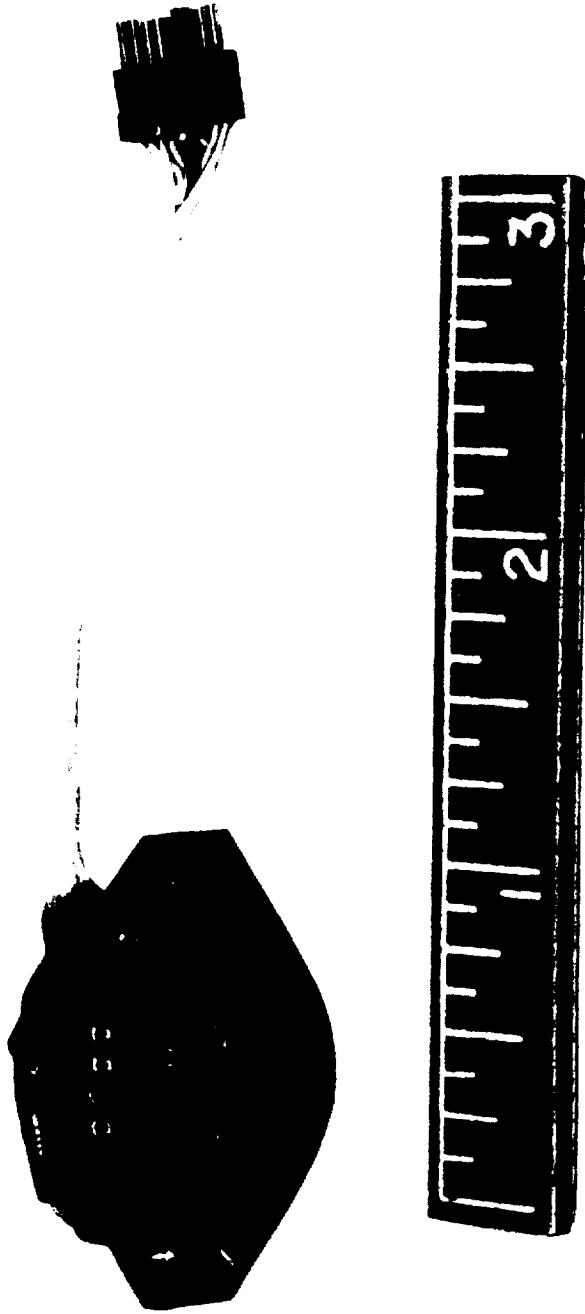


Figure 6-17. A-1000 Accelerometer

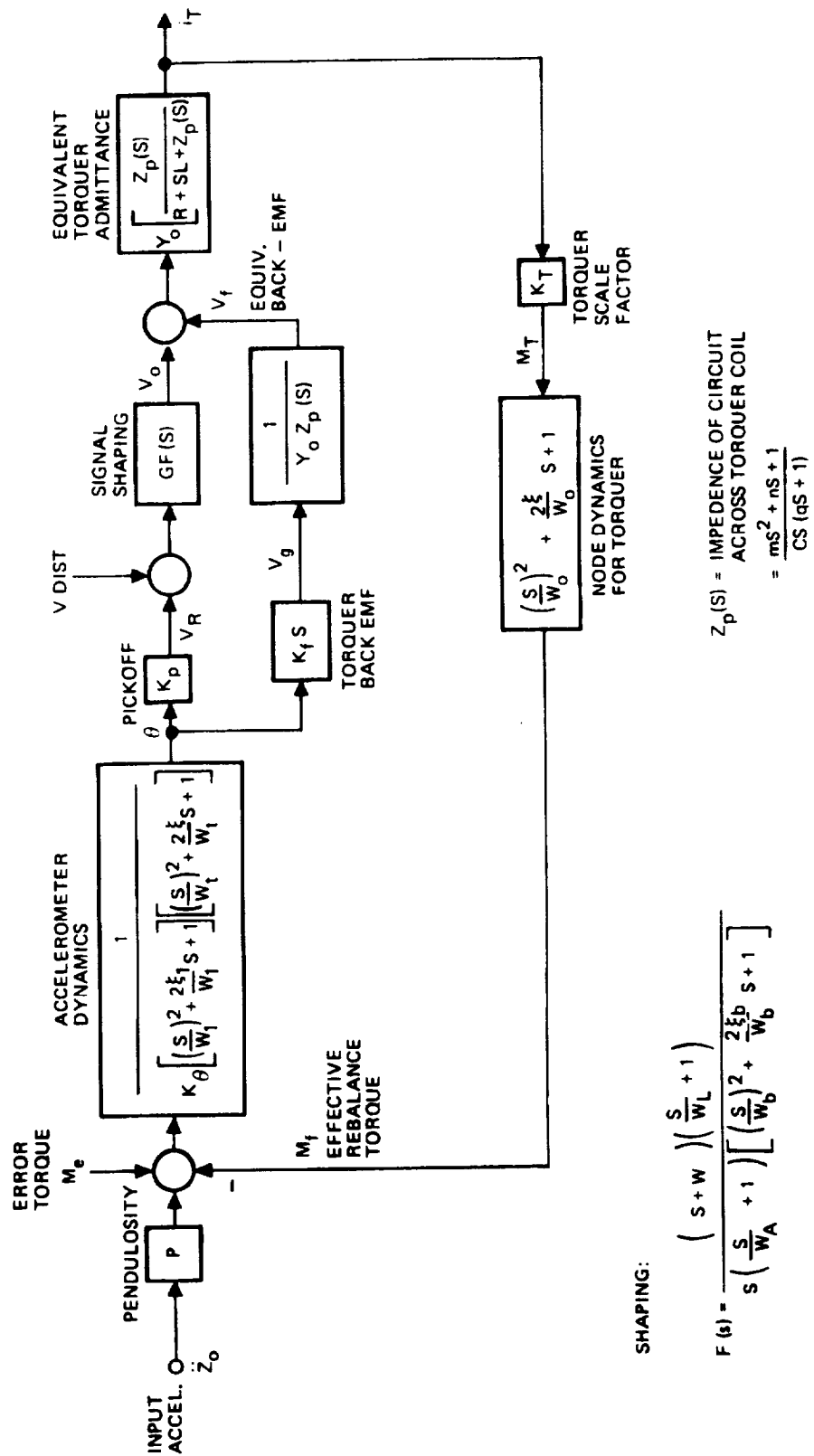


Figure 6-18. Strapdown Accelerometer Block Diagram

responses for this configuration. Figure 6-19, shows the pickoff excursion (proof mass rotation relative to the case) for applied accelerations.

Figure 6-20 relates the frequency response for acceleration inputs. For a pulse-torqued system this is determined by noting the output V_O (to the pulse-torquing network) for acceleration inputs \ddot{Z}_O . Definitions of the various terms are given in table 6.2.

6.2.4 Accelerometer Rebalance Electronics

The accelerometer rebalance electronics are virtually identical to that of the gyro. Loop gain and compensation and torquer current levels are different, however. The accelerometer circuit implementation is simpler since a less sophisticated transfer function is needed, and dual-mode current level is not required.

Table 6-3 gives pertinent information on the accelerometer digital rebalance loop.

6.2.5 IMM/Computer Interface

The IMM/Computer interface functions as a pulse accumulator for the two gyro and two accelerometer data channels. Parallel pulse data from the accelerometers and gyros is counted at a 409.6 KHz clock rate. Data is gathered for a period of 7.8125 msec. At the completion of each data gathering period an interrupt is generated to the computer which functions as a real-time clock (128 Hz) and cues the system software to retrieve the accumulated pulse data from this channel and all other channels.

Accumulation of pulse data is performed with a "micro-processor" up-down counter as illustrated in figure 6-21.

Pulse data are sampled each data clock time; a data level of "1" causes the counter to count up while a data level of "0" causes it to count down. For the gyro signals, a Hi-Mode discrete is sampled which applies a scale factor to the accumulated pulses. Pulses are accumulated for one data gathering period and the resultant count is stored for computer readout. The counters are zeroed at the start of each data gathering period and the process is repeated.

In addition to the four accumulated gyro and accelerometer data channels, a self-test channel will be implemented to help detect any faults. This channel will always count up at each clock time. This function, when accessed by the computer at the end of a data gathering period, will always yield the same value when the system is functioning properly.

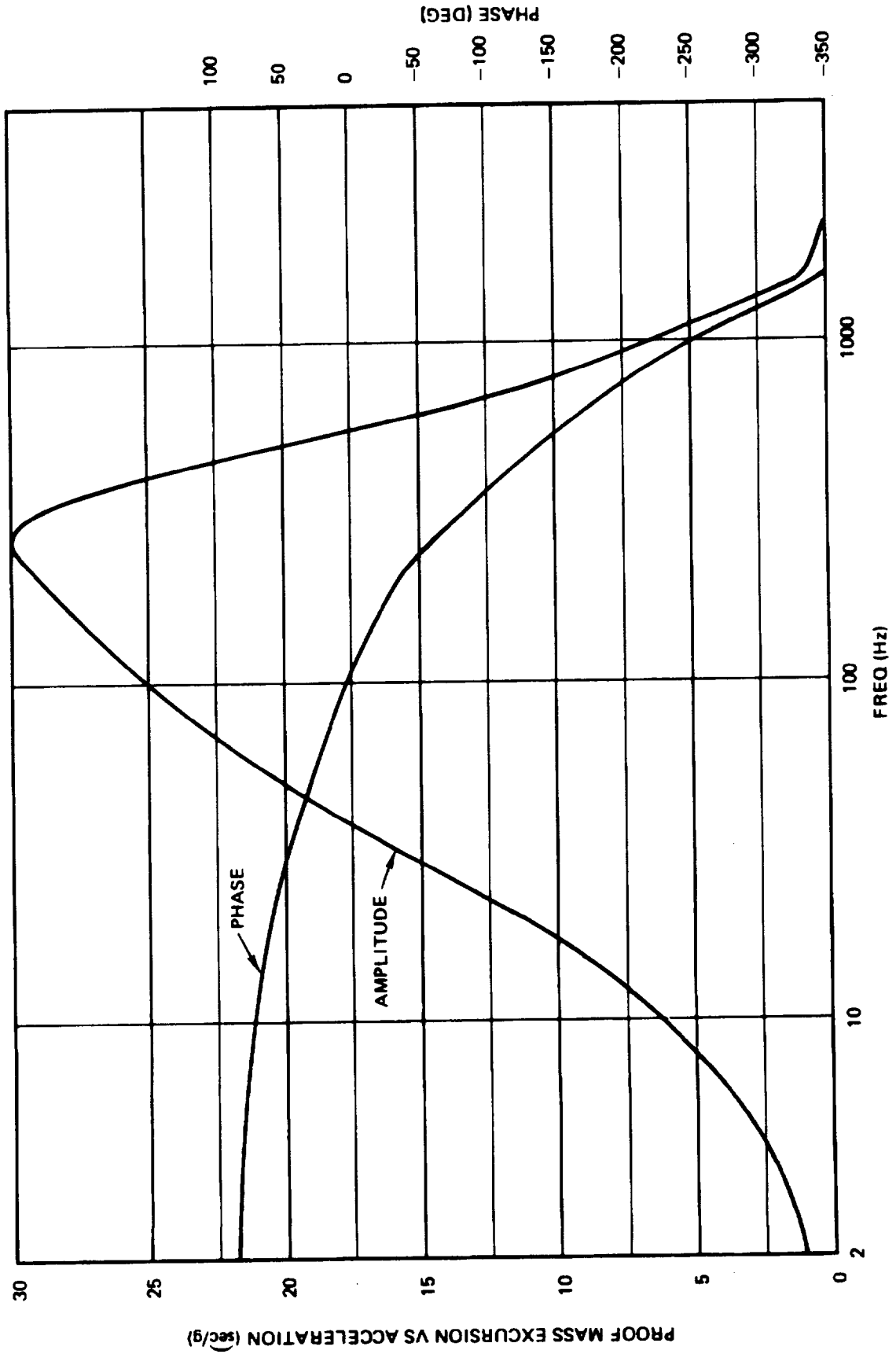


Figure 6-19. Accelerometer Loop Pickoff Response

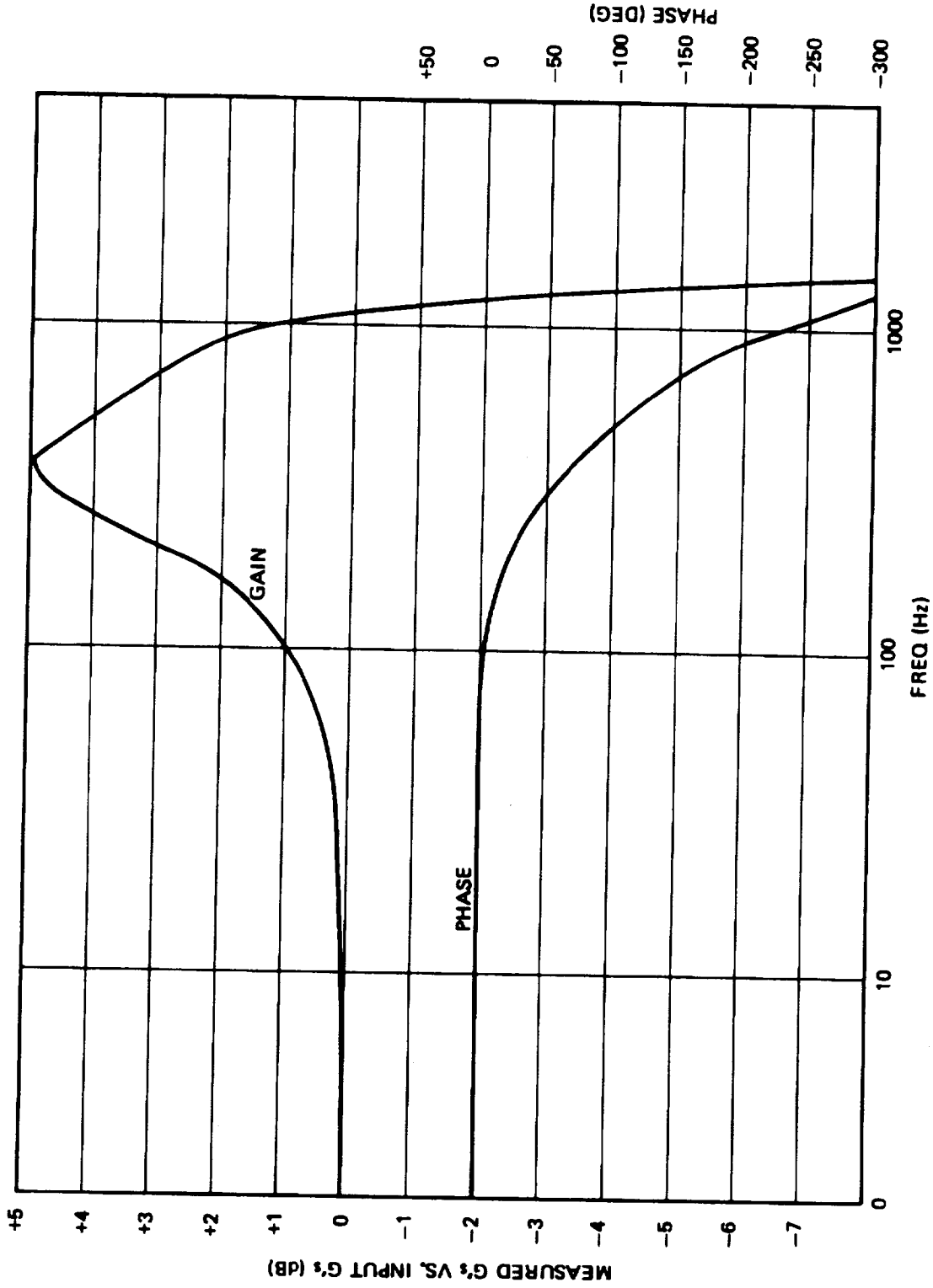


Figure 6-20. Accelerometer Loop Frequency Response

TABLE 6-2. ACCELEROMETER NOMENCLATURE

B	Damping about output axis
G	Gain of servo compensation
J_{OA}, J_{IA}, J_{PA}	Moments of inertia of sensitive element about OA, IA and PA respectively
K_f	Torquer back-emf coefficient
K_p	Pickoff scale factor
K_T	Torquer scale factor
K_θ	Torsional spring rate of suspension
L	Torquer inductance
m, n, q, C	Coefficients for impedance function Z_p for tuning circuit across torquer coil
OA, IA, PA	Output axis, input axis, and pendulous axis
P	Pendulosity
R	Torquer resistance
Y_o	Equivalent DC admittance for pulse-torquing
ξ	Damping factors of structural frequencies
ξ_b	Damping factor for ω_b
ξ_l	Damping factor for ω_l
ω	Lead recovery frequency for integral gain
ω_A	Demodulator roll-off frequency
ω_b	Complex-lag natural frequency
ω_L	Lead frequency
ω_o	Mechanical node frequency
ω_l	Open-loop pendulous oscillation frequency
ω_t	Structural resonant frequency

TABLE 6-3. SENSOR LOOP OPERATIONAL PARAMETERS

PARAMETER	ACCELEROMETER
Maximum range	12 g's
Usable range	11 g's
Pulse repetition rate	409.6 KHz
Pulse weight (scale factor)	5.88×10^{-4} m/sec (0.00193 ft/sec)/pulse
Pulse width	2.5 μ sec
Pulse modulation frequency	4.096 KHz
Sensor stops	± 3 mr
Torquer current	20 ma

A RAM within the microprocessor is used as a memory device. This memory is partitioned into two sectors, a "count-memory" and a storage memory. During a data-gathering period, one sector accumulates counts from the accelerometers and gyros while the other sector stores the data from the previous data gathering period. After completion of a data gathering period the two sectors change functions and the first sector becomes available for computer readout. The storage memory sector is zeroed as it transitions to a "count-memory" sector. Management of the RAM memory functions is done within the control logic function of the microprocessor.

In addition, the IMM/Computer interface will be capable of transferring factory derived instrument constants from local PROMs within the IMM to the software. Temperature sensor data (from A/D converters) will also utilize this interface. Data paths for all these variables may be routed through the same "microprocessor" up-down counter.

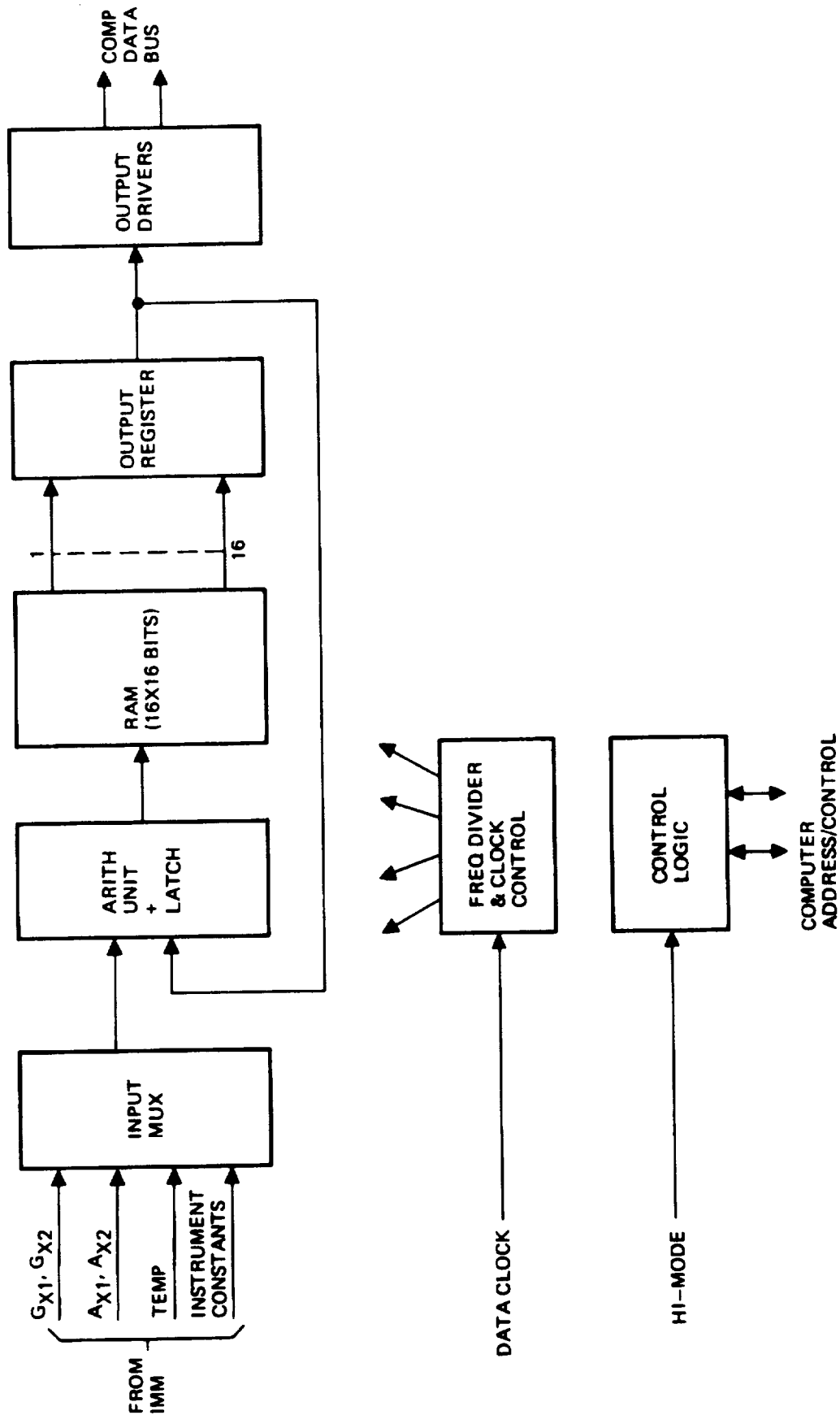


Figure 6-21. Functional Block Diagram IMM/Computer Interface

6.2.6 Computer Description

The computer for the redundant strapdown INS will be assumed to have an architecture similar to the Litton 4516 family of computers. In production since the early '70's, this family of microprogrammable Central Processing Units has been used extensively in various system configurations, notably B-1 RFS/ECMs, AGM-86A (SCAD), LN-33 (F-5E), MPU (CP-1149 for DD-963), TERC (RF-4), and ECU (DD-963).

Designed to economically satisfy a wide range of applications, the 4516 architecture employs a microprogrammable control structure that provides design flexibility and growth to an extended instruction set through the reprogramming of PROMs within its control structure. The 4516 is a 16-bit, fully parallel general purpose digital computer. Its basic instruction length is 16 bits but a full complement of 32 bit instructions is also included, permitting a powerful selection of addressing modes. Arithmetic processing includes provisions for both single (16-bit) and double (32-bit) precision arithmetic as well as a complete set of logical operations.

Maximum size of storage addressable by the 4516 family is 65,536 words. The dominant mode of addressing is relative through the use of base/index registers. However, all four modes of addressing are provided; direct, indirect, relative and immediate.

The computer proposed for the strapdown INS will be mechanized utilizing LSI circuits, solid state Random Access memories (RAMS) for temporary storage of dynamic system variables, non-volatile solid-state Read-Only-Memories (ROMs) for microprogram control and instruction memories. The RAM power will be battery-supported for storage of system variables that need to be retained after power has been turned off.

Various hardware implementation approaches utilizing microprocessor LSI circuits from the semiconductor industry are applicable. Companies active in this field include Fairchild, Intel, Advanced Micro Devices, Texas Instruments, American Microsystems, Inc., and National Semiconductor. All of the currently available microprocessor designs, with the exception of the AMD AM2901 which utilizes a low-power Schottky TTL process are somewhat marginal for the strapdown problem.

COMPUTER PROCESSING UNIT (CPU)

The following description is an example of the type of microprocessors that are currently available in the semiconductor marketplace. AMD's AM2900 microprocessor system consists of a family of bipolar LSI building blocks that can be configured in numerous system configurations. Figure 6-22 is a functional block diagram of a typical central processor unit (CPU) using microprogrammed high-speed bipolar microprocessor circuits.

The heart of the system is the AM2901 bipolar microprocessor (figure 6-23). This four-bit element consists of a 16-word by four-bit two-port random access memory, a high speed arithmetic and logic unit and associated shifting, decoding and multiplexing circuitry. Four such chips are used to form the data path portion of the CPU. All machine level data operations (i.e., add, subtract, multiply, divide, etc.) are performed utilizing these chips.

Control of the CPU is performed primarily with the microprogrammed PROM memory and the microcode sequencer which is used to control the microstep operations within each instruction cycle. The microprogrammed memory contains 256 28-bit words and is provided by seven 256 x 4 bit PROMS. (For production machines, it may be more cost effective to replace this part with a comparable ROM.)

The A/B address registers control the data sources of the Random Access Memory (RAM) within the microprocessor. This RAM contains the program counters (old and new values), the base register, the general registers (9), the accumulators, and the stack and Z registers as required by the 4516 architecture. Data in any of the 16 words of the RAM can be read from the A-port of the RAM as controlled by the 4-bit, A-address field. Likewise, data in any of the 16 words of the RAM as defined by the four-bit B-address field can be simultaneously read from the B-port of the RAM. (See figure 6-23.)

When enabled by the RAM write enable signal, new data is written into the 16-bit word defined by the B-address field. The RAM data input field is driven by a three-input multiplexer which allows shifting of the ALU output if desired.

The ALU can perform any of three binary arithmetic or five logical operations on the two inputs (R, S) of the ALU. The R-field is driven from a two-input multiplexer, while the S field is driven from a three-input multiplexer. Both multiplexers have an inhibit capability in which no data is passed. This multiplexer scheme gives the capability of selecting a large number of source operand pairs together with the eight possible operations to yield a very powerful microprocessor. The output of the ALU is controlled by microcode bits which route the ALU function to either

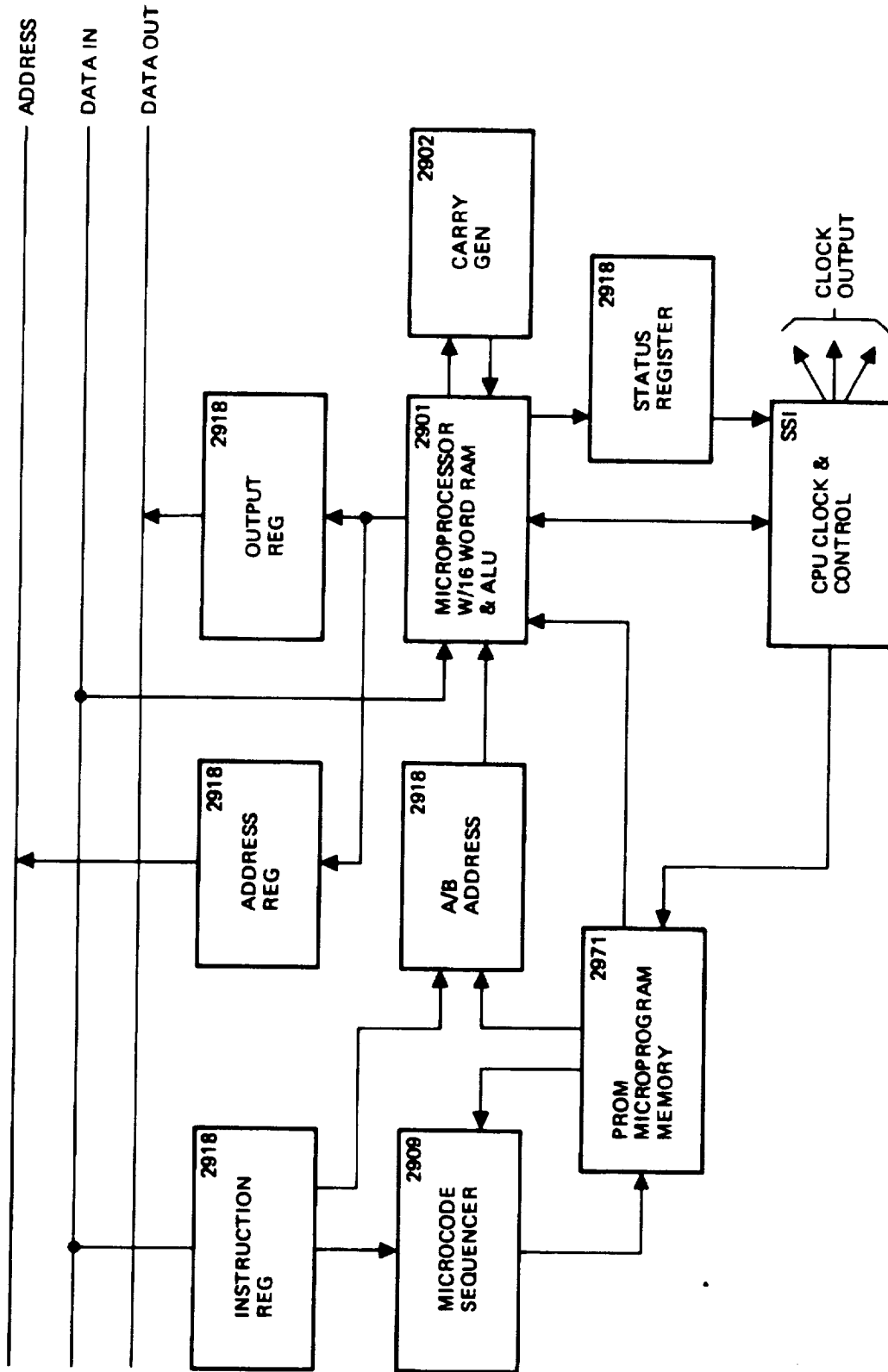


Figure 6-22. Functional Block Diagram of CPU Using AMD Chips

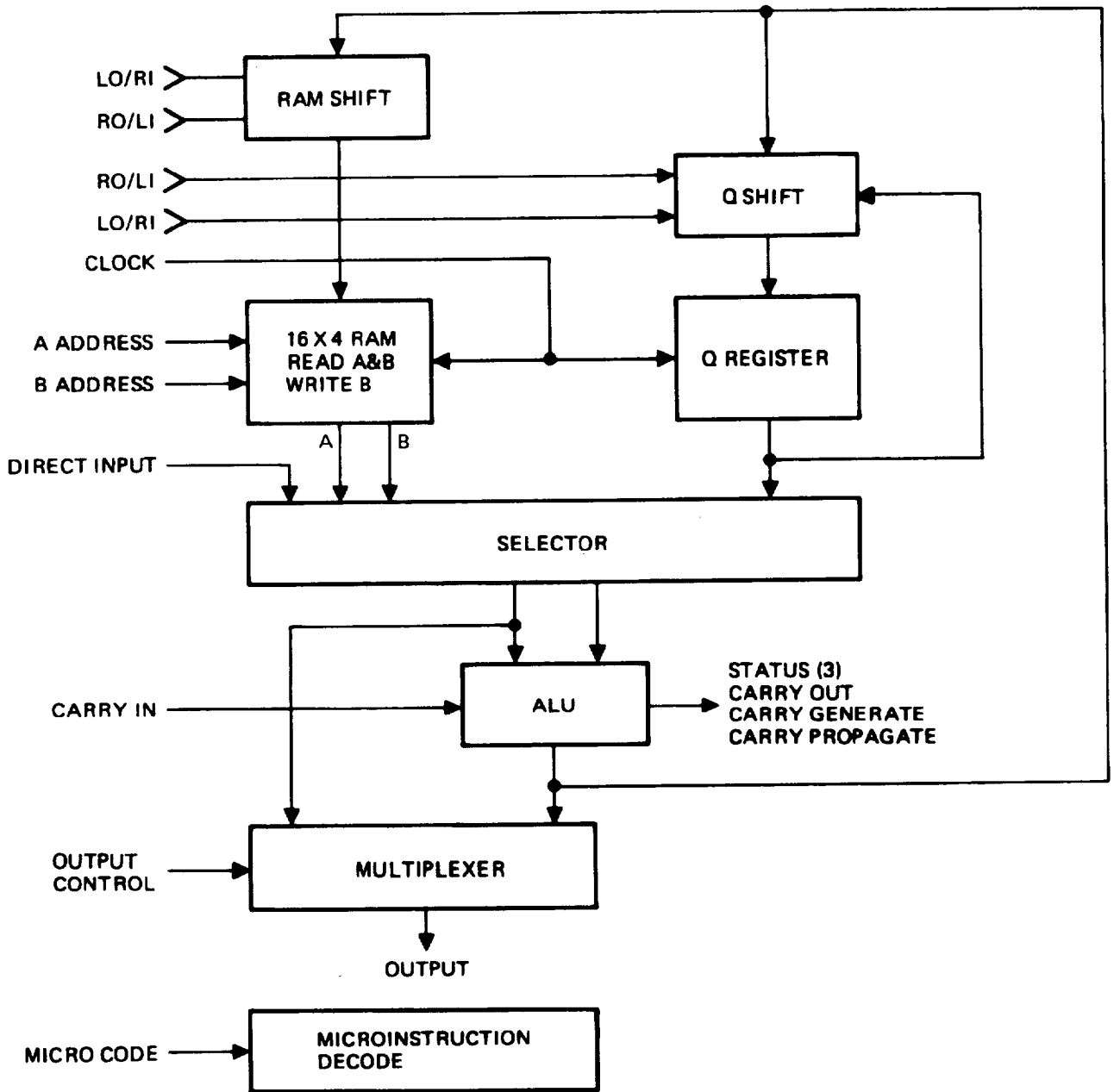


Figure 6-23. 4-Bit Bipolar Microprocessor Slice

the output register, the Q register, or the RAM. In combination with the input multiplexers of the RAM and Q register, this microcode enables the processor to perform the necessary micro-steps of more complicated functions such as multiply and divide.

AMD also provides a look-ahead carry generator (AM2902) chip which provides the capability of multi-level look-ahead operation for high speed arithmetic operation over large word lengths (i.e. larger than four-bits). This chip has a typical propagation delay of approximately six nsec.

The AM2918 Quad D-type flip-flop register provides additional flexibility in system configurations. It is used in typical designs as the address register, the instruction register, the status register, and the data output register. Both three-state and standard totem-pole outputs are provided for interfacing with data buses or for internal registers.

Thus the entire central processing unit for a complex 16-bit machine can be implemented using this family of LSI components in conjunction with some standard SSI circuitry for clock and control.

A summary of the 4516 General Characteristics is given in table 6-4.

The LC-4516 instruction set consists of 49 instructions. These are grouped into nine load and store, 9 logic and arithmetic, 8 transfer, and 23 register-to-register, I/O, and control. The main features of each of these four groups are as follows:

Load and Store (9 total)

- 16, 32-bit lengths

Logic and Arithmetic (9 total)

- 16 and 32-bit fixed-point add/subtract
- 16 and 32 bit fixed point multiply
- Overflow and fault detection
- High-speed multiply and divide
- Double-add-of-carry for 64-bit summing

Transfer (8 total)

- Minus, zero, register test conditionals
- Automatic PC save and return
- Increment-test-transfers

TABLE 6-4. 4516 GENERAL CHARACTERISTICS

Word Lengths	16 or 32 bits (data word) 16 bits (instruction word)
Instruction Type	Single-address, single instruction, indexable
Computation Process	Parallel
Data Format	Fixed-point, fractional binary 2's complement
Input-Output	Programmable I/O Direct Memory Access External Interrupt System
Addressing Range	65,536 words
Addressing Modes	Direct Address Relative Addressing Indirect Base Addressing Indexing Literal Register-Register
Number of Instructions	49

Register-to-Register, Shift, and I/O (23 total)

- Compare register-to-register
- Copy/exchange register-to-register
- Add/Sub register-to-register
- Single/double-length shifts
- Complements
- Input/output to/from accumulator
- Double-length normalization
- Interrupt mask control
- Hardware/software reset/restart

Utilizing microprocessing chips with the assumed speed characteristics, the instruction speeds of table 6-5 are achievable.

TABLE 6-5. TYPICAL INSTRUCTION TIMES

Microprocessor Cycle Time	100 nsec
Memory Cycle Time	600 nsec
Memory Access Time	200 nsec
Load/Store	1.4 usec
Add/Subtract/Logical (16 bits)	1.4 usec
Double Precision Add/Sub (32 bits)	2.2 usec
Multiply	3.2 usec
Double Precision Multiply	11.0 usec
Divide	3.4 usec
Transfers	1.0 usec

MEMORY SYSTEM

The memory requirements for the system are as follows:

<u>MEMORY TYPE</u>	<u>NO. WORDS (16-bit)</u>
Random Access Memory (RAM)	1024
Read Only Memory (ROM)	8192

In addition, there is a microprogram control store memory requirement which is considered a part of the Control Processing Unit.

Random Access Memory (RAM)

The RAM memory chosen for this application is a high-speed CMOS-SOS static storage device which is organized as 1024 words x 4-bit with an access time of 200 nsec and a cycle time of 300 nsec. The chip uses DC stable (static) circuitry and requires no clocks or refreshing to operate. Data are read out nondestructively and are compatible with TTL circuits in all respects. While devices of this storage capacity are not yet available, it is assumed that they will be so by the time the redundant strapdown INS begins its final design phase.

Each RAM memory interfaces with the other three computers in the system via memory ports as shown in figure 6-2. Also, the microprocessor is tentatively organized as a 3 bus system: an address bus, a data input bus and a data output bus. These internal busses communicate with all the functional elements (i.e. the ROMs, the IMM interface, and the external memory controller, etc.) of the individual channel. The port method of intercomputer interfacing provides read-only capability for the other channels in the redundant system. Priority control logic in the memory unit assures that multiple requests can be effectively serviced and that a failed channel cannot swamp out or nullify any other channel. A battery is also provided, normally in a charge mode, for data non-volatility.

Read-Only Memory (ROM)

The ROM for each channel is mechanized with LSI chips contained in 24 pin dual-in-line packages that have 16K memory elements/chip organized in a 2048 words x 8 bits/word configuration. The ROM memory requires only eight mask-programmable LSI chips. Instructions and constants are permanently stored in the devices by use of a special metallization pattern supplied to the vendor.

The ROM memory elements feature advanced Schottky processing, low power dissipation (0.5w) and fast access time (200 nsec). Cycle time is 600 nsec. The LSI chips are organized in a 4 x 2 matrix to form an 8192 word x 16-bit memory. The output is tri-state and similar outputs of each column are connected together. All devices except the pair selected are placed in the high impedance state thus giving the output the characteristics of a TTL totem pole output.

6.2.7 Input/Output System Description

Communication with the external aircraft system will be replicated in all four channels. It has been designated to be all-digital, serial and in the format defined in ARINC 575. It is assumed that the output transmission system of each channel will be directed at another avionics subsystem that can accept the four outputs and perform its own voting and fault-masking routines. In addition, each channel will accept inputs from three separate transmission systems. This is consistent with the concept that failure in any element of one channel will cause the failure of that channel but not the failure of another channel.

The ARINC 575 digital message format consists of a serial transmission scheme in which data, word synchronization and clock are transmitted over a single pair of wires at a frequency of $11 \pm \frac{2.0}{3.5}$ KHz. Each word consists of 32 bits with a minimum of

four bit lengths (91 +42/-14 usec) of blanks (zero voltage) between words. The data word can be either in a binary coded decimal (BCD) data format or a fractional two's complement binary (BNR) format. In either case the eight Least Significant Bits (LSB's) of the word contain address/label information while the rest of the word (24 bits) contains the data and a two-bit coded designation matrix indicating sign and validity information. In the case of binary data, the Most Significant Bit (MSB) is used for odd parity checking. Details of the transmission scheme are found in ARINC 575.

Three receivers will be provided in each channel. One receiver will provide altitude information, and the second receiver will provide initial position and mode information from an avionics display unit. This input will be used only at system start up or infrequently in flight for mode changes. The third receiver is provided for interfacing with another avionics subsystem in order to provide position and velocity up-date information.

6.2.8 Power Supply and Support Electronics

The remainder of electronics needed to complete a redundant strapdown INS is shown in block diagram form in figure 6-24. Primary aircraft power is converted to DC which is used to derive the various voltages needed by the electronic components. It is also used to charge the battery which provides the backup power in the event of aircraft power interruptions.

Mode sequencing circuits are used to initiate gyro spin power when power supply voltages are stabilized and close gyro and accelerometer digital rebalance loops when gyro motors are up to speed.

Self-test circuits monitor critical gyro, accelerometer, and power supply signals. When a failure is detected, the computer is sent an interrupt so it can perform its shutdown subroutine, and a failure indication is provided to other aircraft avionics.

A variety of frequency references are provided by the crystal oscillator and countdown circuitry for such things as instrument pickoff excitation, gyro spin power, digital rebalance loop control, I/O circuit counting and timing, computer clock, the software executive interrupt, and a computer-read time word used in the solution of the equations to compensate for computational time delays. A watch-dog timer is also incorporated, reset periodically by software. If a problem develops and software cannot reset the timer, self-test circuits are activated to indicate a computer failure. This timer is run off a separate oscillator to be able to detect main crystal oscillator failures.

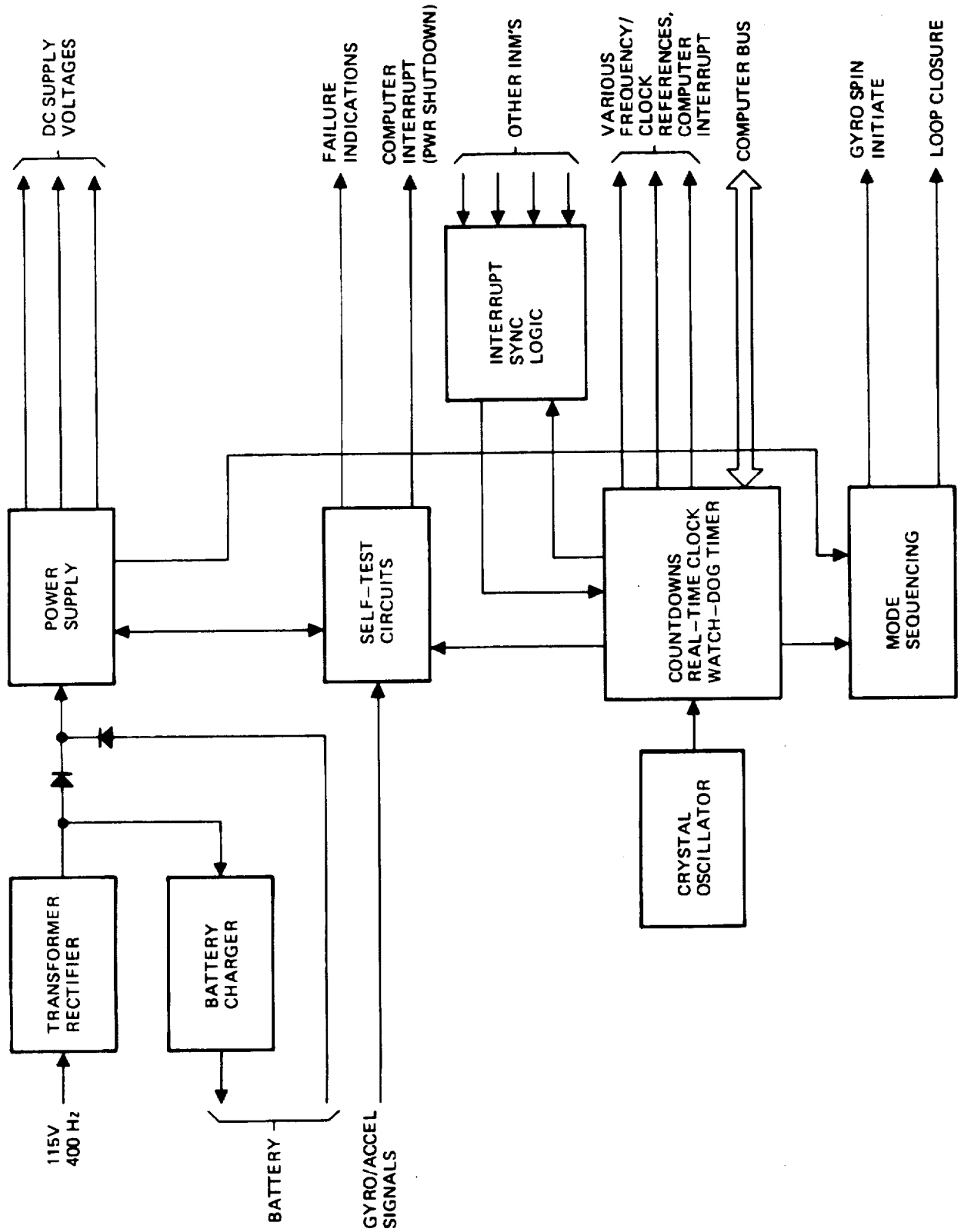


Figure 6-24. Power Supply and Support Electronics Block Diagram

The software executive interrupt pulses between the four computers are synchronized with the included logic circuitry. Since a minimum IMM/computer I/O implementation is achieved with computer interrupts derived by count-down from gyro/accelerometer marker pulses, synchronization at this level is also desirable. Circuit design of this element is also subject to the fail-op/fail-op requirement. Failure modes which cause loss of interrupt pulses or non-synchronization of more than one channel must be avoided.

6.2.9 Self-Test

The self-test requirements for the redundant strapdown INS are reduced from those of a single-string system. Voting methods provide very effective, high-coverage failure detection and isolation for both fail-op levels.

Self-test goals are:

- To prevent chain-type failure modes which could lead to extensive equipment or aircraft damage.
- To provide a high level of capability of detecting failures of each gyro to reduce the probability of a failure occurring within the 3-gyro isolation singularities.
- To contribute to making the third failure a fail-safe condition, that is, to indicate to the aircraft flight crew that a failure has occurred.
- To provide information to maintenance personnel for use in determining the failed module for repair.

Because of the high effectiveness of redundancy management, a minimum amount of circuitry should be used for self-test, except for that needed to protect the equipment against self-destruction. The main self-test features providing this protection are in the power supply. Over-voltage, under-voltage, and over-current detectors sense potentially destructive conditions and shut down channel power. An interrupt is sent to the computer which then executes a shut-down subroutine, as shown in the system block diagram of figure 6-2.

Gyro self-tests consist of loop closure monitors which detect uncontrolled pickoff excursions, a high rate mode timer which indicates a failure if a gyro axis is in the high rate mode for an unreasonable length of time, and a wheel pickoff monitor which detects differences between actual and synchronous spin speed. Accelerometer self-test consists of a pickoff monitor to detect loop closure problems. Temperature sensors amplifiers detect open and short circuit conditions.

The digital subsystem has a variety of simple test provisions. IMM/computer I/O has a separate self-test input channel, other digital I/O has simple wrap-around provisions and parity tests as applicable, the computer cycle is checked with the watch-dog timer, the instrument PROM would have test words and parity bits. The A/D converter has a separate, constant DC reference channel.

A computer software subroutine provides assistance to hardware provisions by means of wrap-around comparisons, comparison of reference or test inputs to expected values, and reasonableness tests on temperature and other measurement data. Software memory and op-code tests are also performed.

Mode/BITE logic assembles hardware self-test results into a word available for input into the computer during a power supply shutdown interrupt. Software self-test and redundancy management results are also available in non-volatile memory for subsequent review by maintenance personnel during repair. Failure of either type actuates a failure indicator, visible from the front of the unit.

6.2.10 Packaging Design

General Concept

Estimates were made of electronics needed to implement one complete channel of the redundant strapdown INS. From the numbers of printed circuit boards and power supply components, a preliminary packaging design was conceived, shown in figure 6-25.

One channel of the redundant strapdown INS, consisting of one gyro, two accelerometers, supporting electronics, a computer with I/O, and a power supply is expected to fit within the dimensions of 0.36 m x 0.11 m x 0.19 m, and weigh approximately 5.9 Kg. Cam-lock handles are used to engage the rear-mounting connector and lock the unit in place.

A mechanism is required to withdraw the instrument block to allow the unit to slide freely into or out of a holding chassis/mount during maintenance. For this purpose, the instrument block is attached to the chassis by means of a pivoted lever. The pivot, shown in figure 6-25, is fixed to the chassis.

During insertion or removal, the return spring causes the instrument block to be held so the alignment feet are kept within the unit. When the unit is locked in place, the engagement lever is depressed by external means, causing motion of the instrument block, in the direction shown in figure 6-25. The alignment feet then protrude from the side of the unit to engage a precision alignment block for precise registration between gyros and to the aircraft.

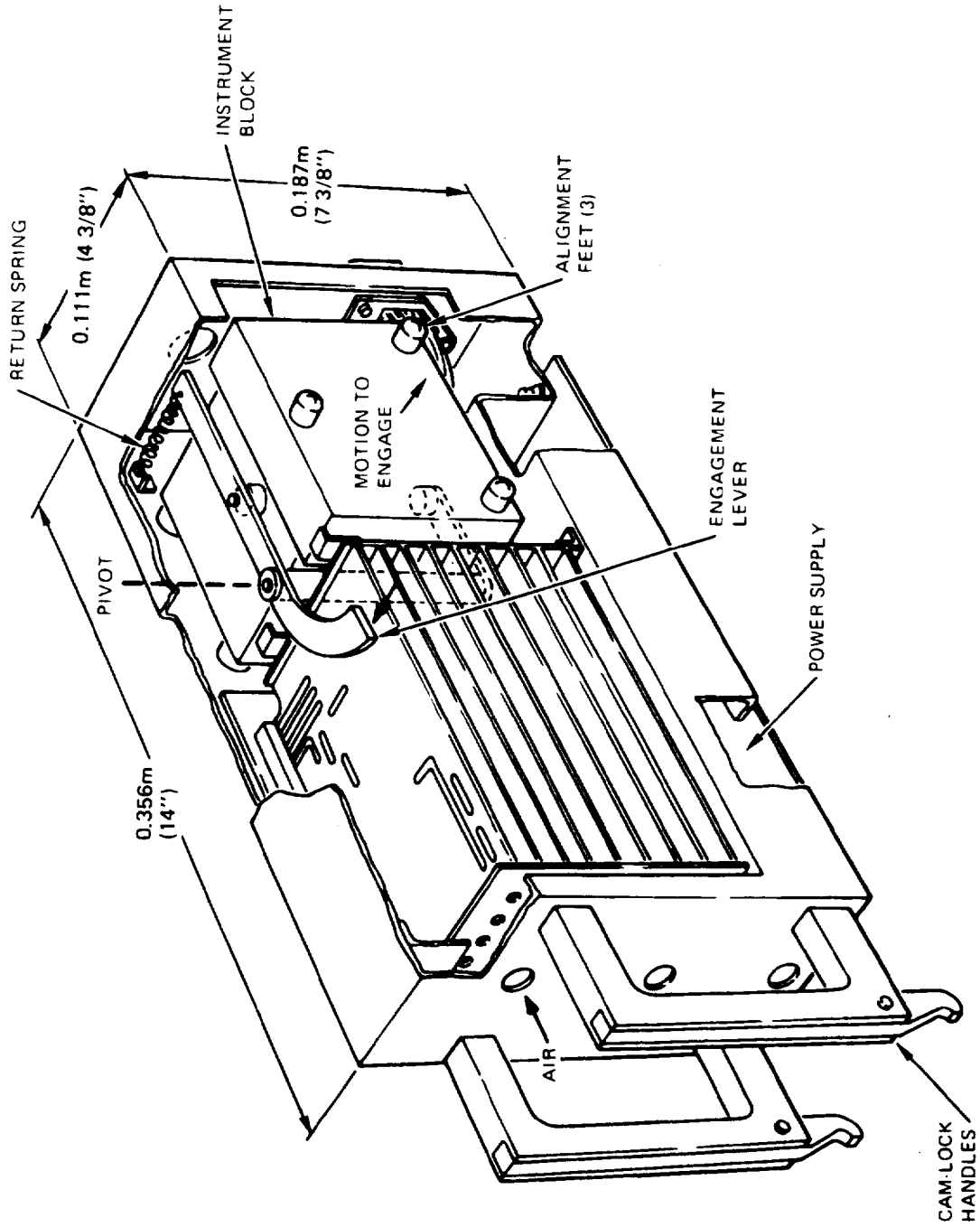


Figure 6-25. One Channel of the Redundant Strapdown INS

Figure 6-26 shows one of the Inertial Navigation Modules (INM) installed into a common chassis/mount. The orientations of the other three INM's are rotated 90° from each other to provide the required gyro axis skewing. An actuator assembly on the front of the chassis/mount is used to depress the engagement lever within each INM following installation. The INM instrument block is then pressed against a central alignment block in the center of the chassis/mount assembly.

The actuator assembly and alignment block are more clearly shown in figure 6-27. The 90° rotation of the INM rectangular shape leaves a hollow core in the chassis mount. This area is then available for installation of the actuator assembly and alignment block. Figure 6-27 also shows a view of instrument blocks in the withdrawn and depressed conditions.

Figure 6-28 shows the G-6 gyro and A-1000 accelerometers with the remainder of the instrument block. A printed circuit card would also be attached containing critical portions of the rebalance loops. Thus these components would thermally track the instruments, avoiding the need for separate calibration.

The size of the entire fail-op/fail-op redundant INS is expected to be 0.33 m x 0.33 m x 0.36 m. Weight would be under 28 Kg. Elaborate measures were not taken for size reduction since low-cost is a major system design requirement.

Instrument Alignment Mechanism

Alignment from gyro-to-gyro is required to be better than 20 arc seconds, including long term effects of handling by maintenance personnel. The baseline design was selected to provide proximity between instruments thus minimizing bending between modules due to temperature gradients or g-loading.

Alignment repeatability requirements will dictate the final design of the alignment mechanism. Forces on the block stemming from the actuator must be analyzed with regard to potential friction forces which might prevent proper seating of the instrument block alignment feet onto the chassis/mount block. Wear effects and thermal gradient susceptibility need consideration in the selection of material and finishes. In addition, pressures produced by the mechanism would need to be analyzed under vibration conditions to avoid angular block-to-block motions which could produce system errors.

Alignment of the instruments relative to the aircraft is much less critical. Six arc minute alignment accuracy can be achieved using normal bore-sight and installation techniques.

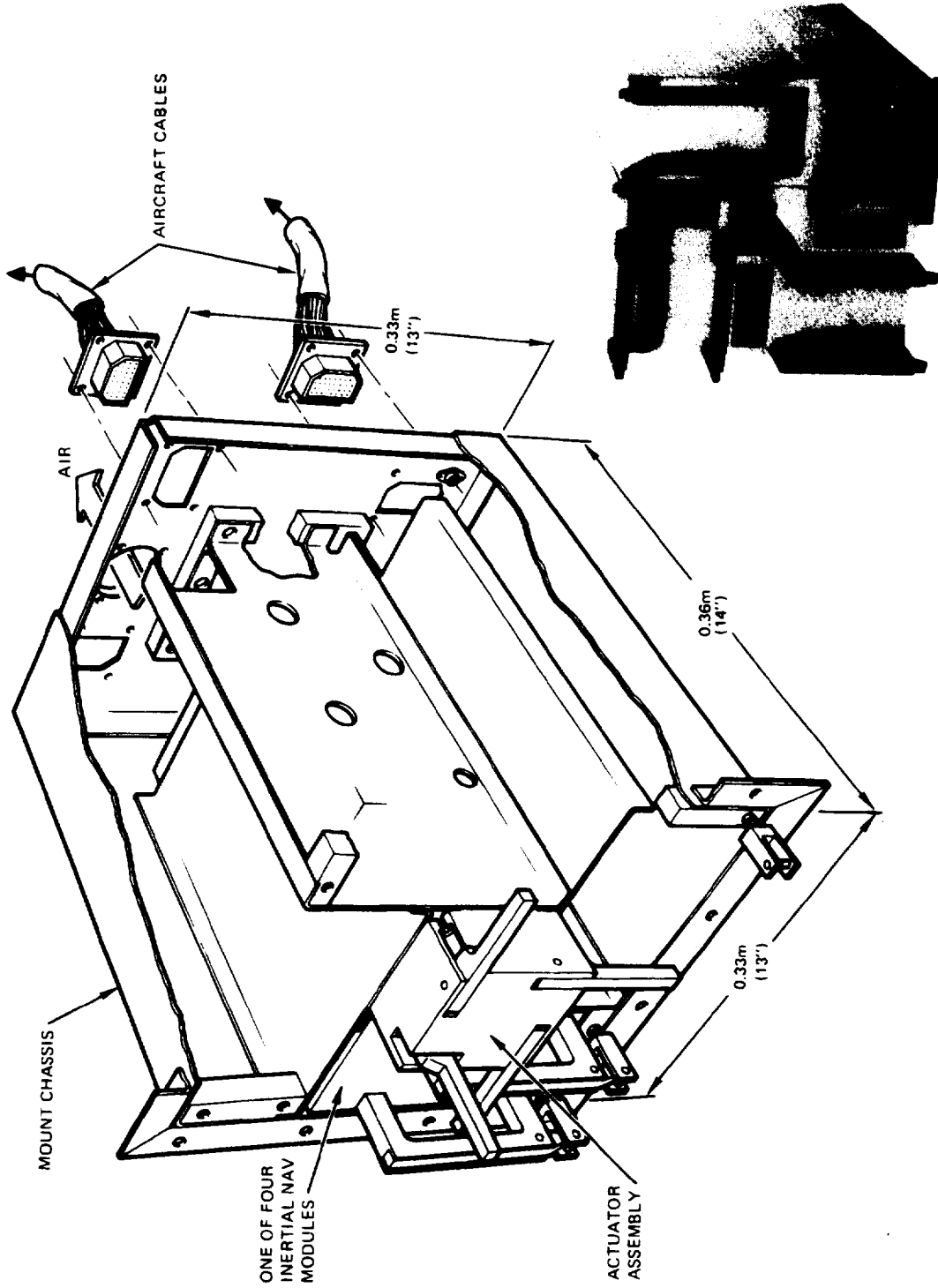


Figure 6-26. Redundant Strapdown INS Installation

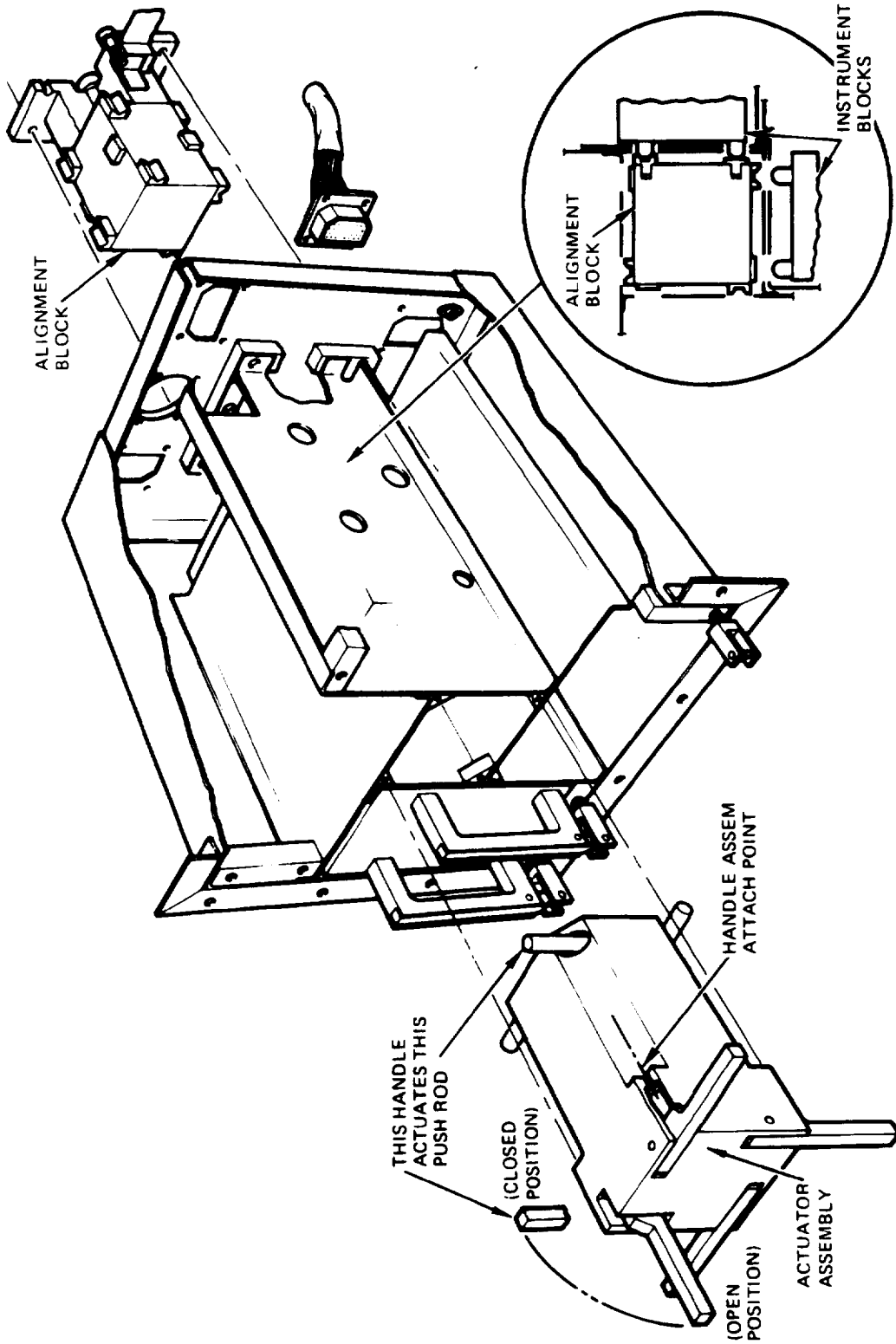


Figure 6-27. Redundant Strapdown INS Mount Details

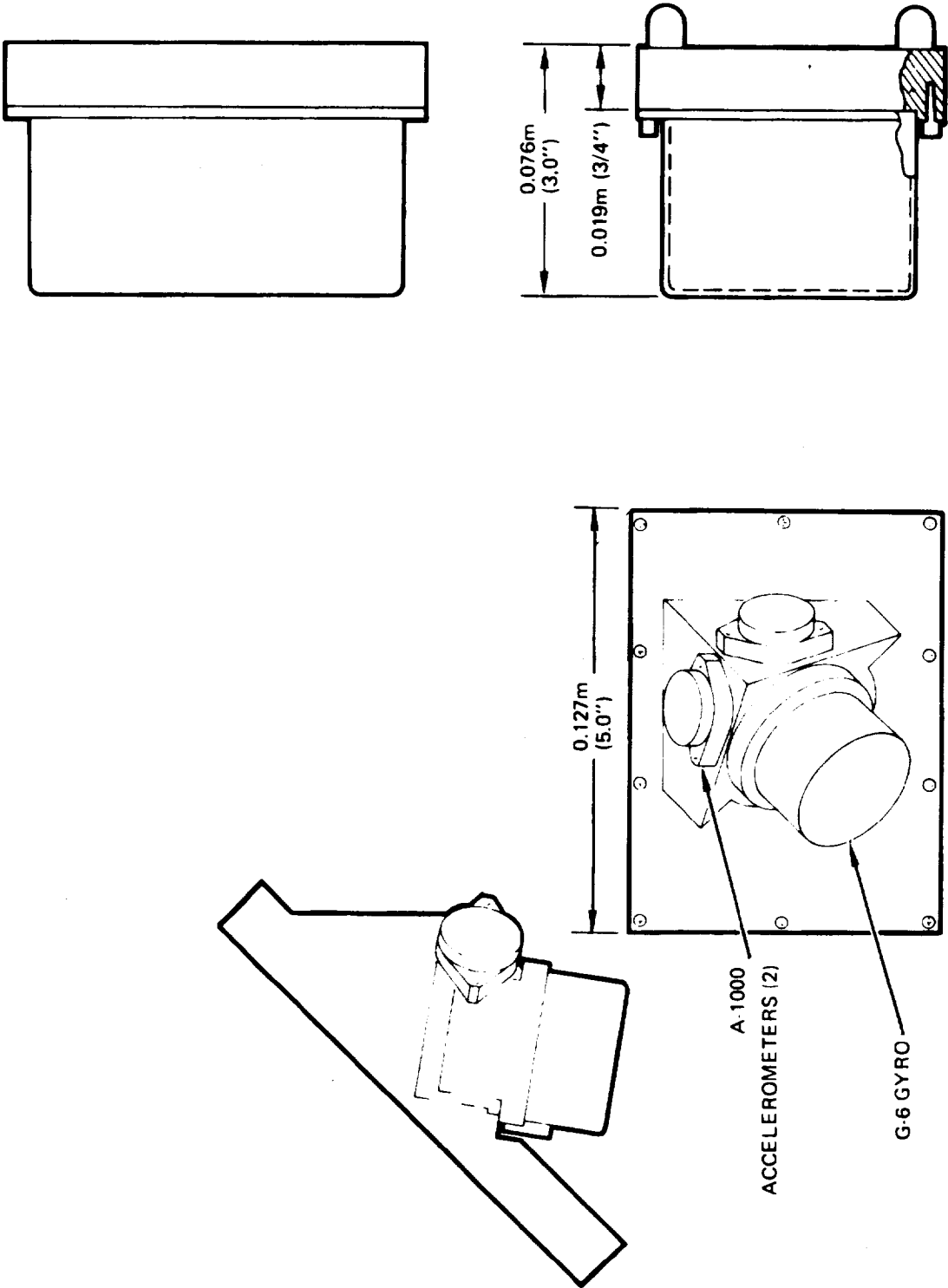


Figure 6-28. Instrument Block

Thermal Design

Power dissipation within each INM is expected to be under 135 watts. New ARINC 600 cooling provisions need review for the unique installation requirements of the redundant, skewed-sensor INS.

The preliminary packaging design included provision for the drawing of cabin air through openings in the front of each INM. Some sealing of the face of the INM against the chassis/mount is needed to avoid air pressure losses. Since ARINC cooling has such a low pressure drop, highly effective sealing is not needed.

The cooling air flow directly impinges electronic components and the cover of the instrument block. It then exits at the rear of the chassis mount, which forms a plenum between units for even pressure and flow distribution. While impingement cooling is undesirable due to potential contamination, it is very effective. Installation of filters on the front of each INM, as used on present commercial INS, would prevent some of the internal contamination. Other methods should be reviewed in the final design for optimum balance between maximum component temperature (and thus reliability), contamination and unit cost.

Structural Design

Sufficient structural rigidity must be provided to avoid self-destruction or damage during the normal and emergency shock and vibration incurred during flight and handling. The preliminary design has not included analysis for these factors. However, the general concepts and size are expected to apply for the required environment.

Special Test Equipment Constraints

The equipment used in the factory for calibration of an INM includes a high-cost, computer-controlled rate table. In order to defray cost of this item, it is essential that it be fully occupied, day and night. It is thus also essential that the capability of calibrating more than one INM at a time be provided.

The volume and form available on this table is limited. It appears on a preliminary basis that 3 INM's can be installed on the table side-by-side. There is no room, however, to include mounting hardware between units for the side-engagement of the instrument block. It would be preferable to provide instrument block engagement at the rear or connector end of the INM if possible. This will require further analysis during the final design phase.

6.3 Software Design

The major divisions of software are:

- a. Instrument Compensation
- b. FDI - Design Equation
- c. Coordinate Conversion
- d. Navigation

These major divisions have been further divided into smaller blocks of software to increase computational throughput. Figure 6-29 illustrates the minor software blocks and denotes the repetition rates.

The INM software has been organized to enable interchangeability of computers. Only the plug-in instrument calibration coefficient programmable read-only memory (PROM) would be a unique circuit. Since the software in each INM is interchangeable, some means of identifying the particular position in the semi-octahedron is necessary. This is accomplished by hard-wire programming of the system interconnection harness. The system harness is wired into a computer input discrete word. Upon power turn-on the computer program pre-alignment routine will initialize pointers to enable branching to the section of software pertinent to the individual INM.

6.3.1 Computational Considerations

Assuming that a 16-bit digital computer is utilized for this application, a standard set of double precision instructions is required. In addition, a hardware double precision (32 x 32) multiply is very useful.

A computer throughput of 198,000 instructions per second is required to perform the redundant strapdown INS problem with a double precision multiply instruction along with the instruction mix of table 6-6. If this DMPY instruction were not available, approximately 460,000 instructions per second are required with the instruction mix of table 6-6, using normal programming techniques. These throughput estimates are based on actual LN-50 coding.

Applying this same instruction mix to a state-of-the-art computer in table 6-7, results in a duty cycle estimate (the ratio of the strapdown throughput requirement to the computer throughput capability) of 60 percent. Note that if a double precision multiply instruction were not available, the computer would be quite marginal in this application. However, with this instruction, approximately 132,000 spare instructions/second are available for other computations, assuming the same instruction mix.

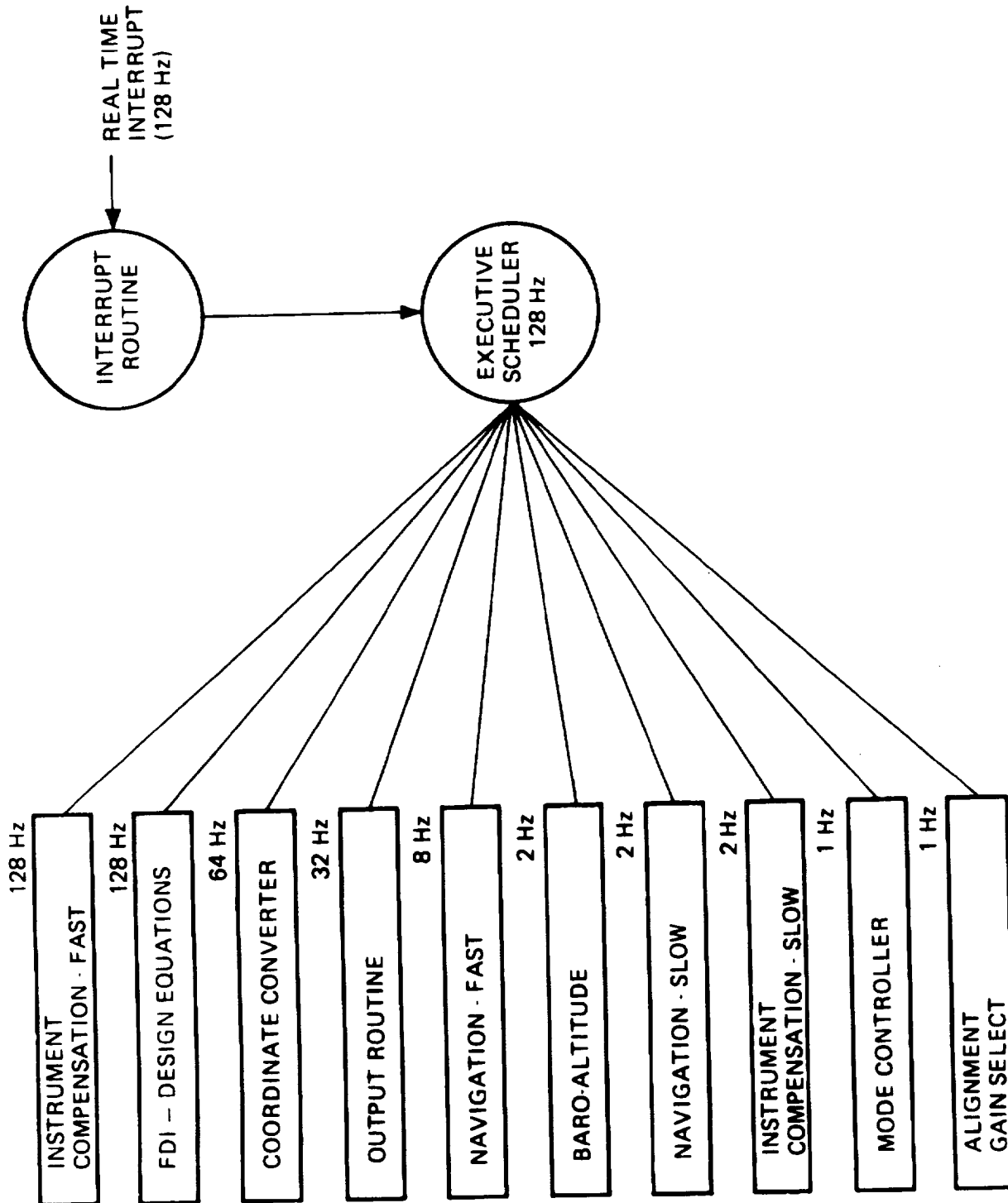


Figure 6-29. INM Software

TABLE 6-6. INSTRUCTION MIX FOR REDUNDANT STRAPDOWN INS

Type	Percentages With Double-Multiply Instruction	Percentages Without Double-Multiply Instruction
Load/Store	11.9	20.3
D-Load/Store	31.8	18.2
Copy	5.5	7.4
Exchange	4.2	1.6
D-Shift	9.1	14.0
Add/Sub	10.5	9.4
D-Add/Sub	13.1	10.4
Multiply	6.4	10.2
D-Multiply	5.5	-
Divide	0.6	0.2
Transfer	1.4	8.3

6.3.2 Equation Summary

The following paragraphs summarize the equations of the flight software. The coordinate frames and a glossary are included. Preliminary computer software flow charts are presented in Appendix H.

6.3.2.1 Instrument Compensation

Figure 6-30 illustrates the compensation computations per single channel. The gyros are compensated for the following terms:

- a. Scale factor linearity
- b. Scale factor temperature sensitivity
- c. Sensitive axes misalignment
- d. Inertia dynamic compensation
- e. Mass unbalance drift
- f. Mass unbalance temperature sensitivity
- g. Bias
- h. Bias temperature sensitivity

TABLE 6-7. DUTY CYCLE ESTIMATE FOR
A STATE OF THE ART 16-BIT COMPUTER

Type	Hardware D-Multiply			Software D-Multiply	
	Ex. Time (μ sec)	Mix	Ex. Time/ Ins.	Mix	Ex. Time/ Ins.
Load/Store	1.4 X	0.119 =	0.1904	0.203	0.3248
D-Load/Store	2.2	0.318	0.7632	0.182	0.4368
Copy	1.4	0.055	0.088	0.074	0.1184
Exchange	1.4	0.042	0.0672	0.016	0.0256
D-Shift	2.2	0.091	9.4368	0.140	0.672
Add/Sub	1.4	0.105	0.168	0.094	0.1504
D-Add/Sub	2.2	0.131	0.3144	0.104	0.2496
Multiply	3.2	0.064	0.2688	0.102	0.4284
D-Multiply	11.0	0.055	0.66	-	-
Divide	3.4	0.006	0.0216	0.002	0.0072
Transfer	1.0	0.014	0.0504	0.083	0.2988
μ sec/avg instr				3.0288	2.712
Throughput = 330,164 instr/sec				368,732 instr/sec	
Duty Cycle = $\frac{198,000}{330,164} = 60.0\%$				$\frac{460,000}{368,732} = 125\%$	

The accelerometers are compensated for the following terms:

- a. Scale factor
- b. Scale factor temperature sensitivity
- c. Sensitive axes misalignment
- d. Bias
- e. Bias temperature sensitivity

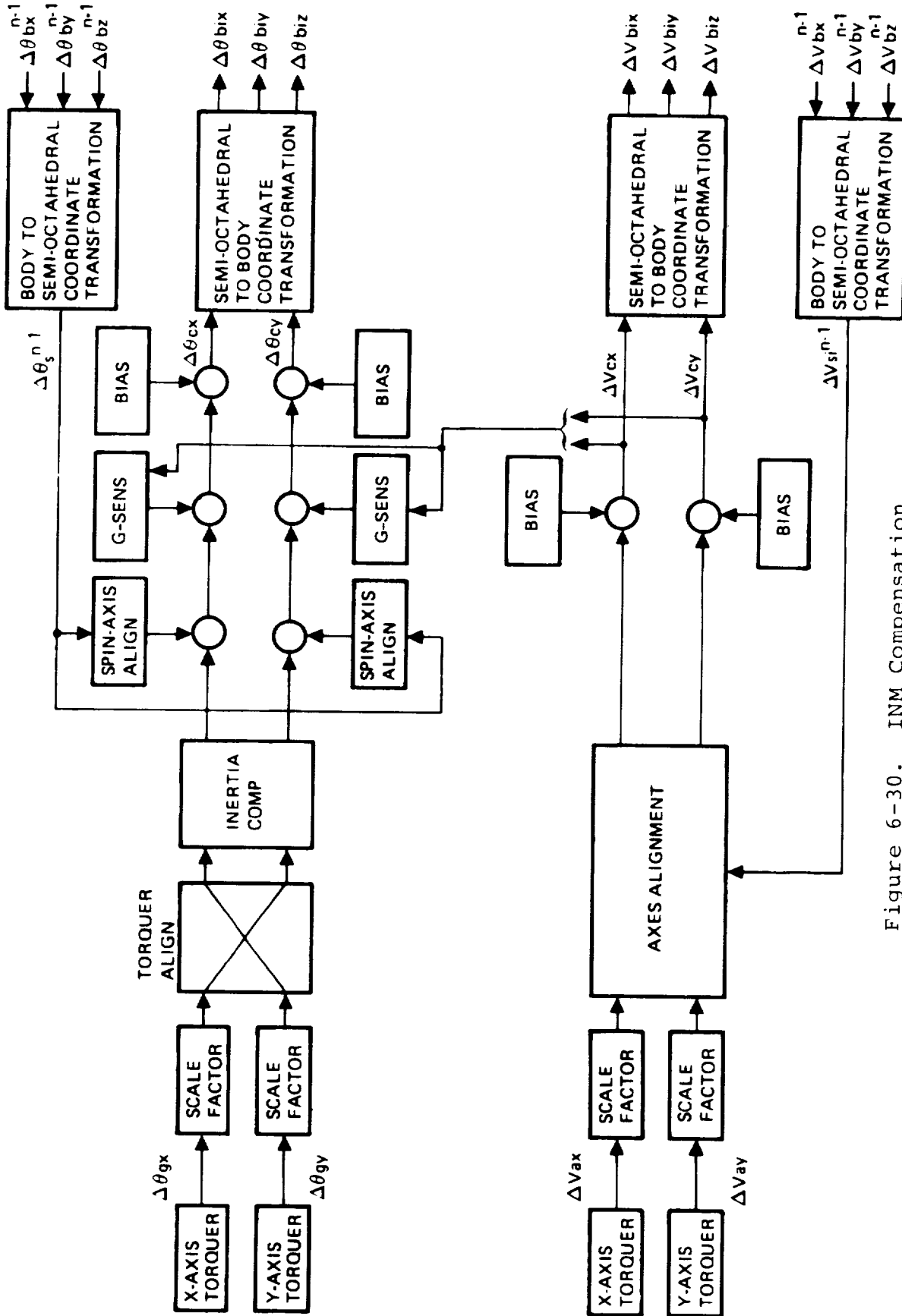


Figure 6-30. INM Compensation

Equations 1 to 18 describe the compensation equations. Equation 19 provides the components necessary for axis misalignment correction. Equation 20 transforms the 2-axis instrument outputs to the body frame. Reference table 6-12 for a definition of symbols.

GYRO SCALE FACTOR

$$\begin{aligned}
 S_{GX} = & \left. \begin{aligned} & \left[S_{GX1}^+ + \frac{S_{GX2}^+}{\Delta t} \cdot \Delta \theta_{GX} \right] \cdot S_{gn}(\Delta \theta_{GX}) \\ & + \left[S_{GX1}^- + \frac{S_{GX2}^-}{\Delta t} \cdot \Delta \theta_{GX} \right] \cdot S_{gn}(\Delta \theta_{GX}) \end{aligned} \right\} \text{NORMAL MODE} \\
 & \left. \begin{aligned} & \left[S_{GX1}^{++} + \frac{S_{GX2}^{++}}{\Delta t} \cdot \Delta \theta_{GX} \right] \cdot S_{gn}(\Delta \theta_{GX}) \\ & + \left[S_{GX1}^{--} + \frac{S_{GX2}^{--}}{\Delta t} \cdot \Delta \theta_{GX} \right] \cdot S_{gn}(\Delta \theta_{GX}) \end{aligned} \right\} \text{HIGH RATE MODE}
 \end{aligned} \tag{1}$$

$$\begin{aligned}
 S_{GY} = & \left. \begin{aligned} & \left[S_{GY1}^+ + \frac{S_{GY2}^+}{\Delta t} \cdot \Delta \theta_{GY} \right] \cdot S_{gn}(\Delta \theta_{GY}) \\ & + \left[S_{GY1}^- + \frac{S_{GY2}^-}{\Delta t} \cdot \Delta \theta_{GY} \right] \cdot S_{gn}(\Delta \theta_{GY}) \end{aligned} \right\} \text{NORMAL MODE} \\
 & \left. \begin{aligned} & \left[S_{GY1}^{++} + \frac{S_{GY2}^{++}}{\Delta t} \cdot \Delta \theta_{GY} \right] \cdot S_{gn}(\Delta \theta_{GY}) \\ & + \left[S_{GY1}^{--} + \frac{S_{GY2}^{--}}{\Delta t} \cdot \Delta \theta_{GY} \right] \cdot S_{gn}(\Delta \theta_{GY}) \end{aligned} \right\} \text{HIGH RATE MODE}
 \end{aligned} \tag{2}$$

NOTE: $\left. \begin{aligned} S_{gn}(\Delta \theta_{GX}) &= 1 \\ S_{gn}(\Delta \theta_{GX}) &= 0 \end{aligned} \right\} \text{if } \Delta \theta_{GX} \text{ is negative.}$

GYRO COMPENSATION

SCALED GYRO RATES

$$\begin{aligned}\Delta \theta_X &= S_{GX} \cdot \Delta \theta_{GX} \\ \Delta \theta_Y &= S_{GY} \cdot \Delta \theta_{GY}\end{aligned}\quad (3)$$

TORQUER AXIS TRANSFORMATION

$$\begin{aligned}\Delta \theta_{TX} &= \delta_{GXX} \cdot \Delta \theta_X + \delta_{GXY} \cdot \Delta \theta_Y \\ \Delta \theta_{TY} &= \delta_{GYX} \cdot \Delta \theta_X + \delta_{GYY} \cdot \Delta \theta_Y\end{aligned}\quad (4)$$

INERTIA COMPENSATION

$$\begin{aligned}\Delta \theta_{IX} &= -I_G \cdot (\Delta \theta_{TY}^n - \Delta \theta_{TY}^{n-1}) \\ \Delta \theta_{IY} &= I_G \cdot (\Delta \theta_{TX}^n - \Delta \theta_{TX}^{n-1})\end{aligned}\quad (5)$$

SPIN-AXIS ALIGNMENT

$$\begin{aligned}\Delta \theta_{PX} &= \Delta \theta_{IX} - \gamma_{GX} \cdot \Delta \theta_S^{n-1} \\ \Delta \theta_{PY} &= \Delta \theta_{IY} + \gamma_{GY} \cdot \Delta \theta_S^{n-1}\end{aligned}\quad (6)$$

G SENSITIVE DRIFTS

$$\begin{aligned}\Delta \theta_{MX} &= \Delta \theta_{PX} + M_{XX} \cdot \Delta v_{CX} + M_{XY} \cdot \Delta v_{CY} + M_{XZ} \cdot \Delta v_S^{n-1} \\ \Delta \theta_{MY} &= \Delta \theta_{PY} + M_{YX} \cdot \Delta v_{CX} + M_{YY} \cdot \Delta v_{CY} + M_{YZ} \cdot \Delta v_S^{n-1}\end{aligned}\quad (7)$$

GYRO COMPENSATION

NON-G SENSITIVE BIASES

$$\begin{aligned}\Delta \theta_{CX} &= \Delta \theta_{MX} + B_X \cdot \Delta t \\ \Delta \theta_{CY} &= \Delta \theta_{MY} + B_Y \cdot \Delta t\end{aligned}\quad (8)$$

ACCELEROMETER COMPENSATION
SCALED INCREMENTAL VELOCITIES

$$\begin{aligned}\Delta v_X &= S_{AX} \cdot \Delta v_{AX} \\ \Delta v_Y &= S_{AY} \cdot \Delta v_{AY}\end{aligned}\quad (9)$$

AXIS ALIGNMENT

$$\begin{aligned}\Delta v_{TX} &= \delta_{AXX} \cdot \Delta v_X + \delta_{AXY} \cdot \Delta v_Y + \delta_{AXZ} \cdot \Delta v_S^{n-1} \\ \Delta v_{TY} &= \delta_{AYX} \cdot \Delta v_X + \delta_{AYY} \cdot \Delta v_Y + \delta_{AYZ} \cdot \Delta v_S^{n-1}\end{aligned}\quad (10)$$

BIAS

$$\begin{aligned}\Delta v_{CX} &= \Delta v_{TX} + A_{BX} \cdot \Delta t \\ \Delta v_{CY} &= \Delta v_{TY} + A_{BY} \cdot \Delta t\end{aligned}\quad (11)$$

INSTRUMENT TEMPERATURE COMPENSATION

Gyro

$$DSGX = SGTX0 + SGTX1(TGX) + SGTX2(TGX)^2 \quad (12)$$

$$DSGY = SGTY0 + SGTY1(TGY) + SGTY2(TGY)^2$$

$$B_X = BGTX0 + BGTX1(TGX) + BGTX2(TGX)^2 \quad (13)$$

$$B_Y = BGTY0 + BGTY1(TGY) + BGTY2(TGY)^2$$

$$M_{XX} = MGTX0 + MGTX1(TGX) + MGTX2(TGX)^2 \quad (14)$$

$$M_{YY} = MGTY0 + MGTY1(TGY) + MGTY2(TGY)^2$$

$$S_{GX1}^+ = S_{GX0}^+ + DSGX, \quad S_{GX1}^- = S_{GX0}^- + DSGX \quad (15)$$

$$S_{GY1}^- = S_{GY0}^- + DSGY, \quad S_{GY1}^+ = S_{GX0}^+ + DSGY \quad (16)$$

Accel

$$S_{AX} = SATX0 + SATX1(TAX) + SATX2(TAX)^2 \quad (17)$$

$$S_{AY} = SATY0 + SATY1(TAY) + SATY2(TAY)^2$$

$$A_{BX} = BATX0 + BATX1(TAX) + BATX2(TAX)^2 \quad (18)$$

$$A_{BY} = BATY0 + BATY1(TAY) + BATY2(TAY)^2$$

TRANSFORMATIONS

Spin Axis Components

$$\Delta \theta_S^{n-1} = \bar{S} \cdot (\Delta \bar{\theta}_b)^{n-1} \quad (19)$$

$$\Delta V_S^{n-1} = \bar{S} \cdot (\Delta \bar{V}_b)^{n-1}$$

Body Components

$$\begin{aligned} \overline{\Delta\theta}_b &= \begin{bmatrix} \bar{X} & \bar{Y} \end{bmatrix} \begin{bmatrix} -\cos 45^\circ & -\sin 45^\circ \\ +\sin 45^\circ & -\cos 45^\circ \end{bmatrix} \begin{bmatrix} \overline{\Delta\theta CX} \\ \overline{\Delta\theta CY} \end{bmatrix} \\ \overline{\Delta V}_b &= \begin{bmatrix} \bar{X} & \bar{Y} \end{bmatrix} \begin{bmatrix} -\cos 45^\circ & -\sin 45^\circ \\ \sin 45^\circ & -\cos 45^\circ \end{bmatrix} \begin{bmatrix} \overline{\Delta VCX} \\ \overline{\Delta VCY} \end{bmatrix} \end{aligned} \quad (20)$$

NOTE: Refer to Table 6-8 for definition of (\bar{X} , \bar{Y} , \bar{S}) vectors.

TABLE 6-8. SEMI-OCTAHEDRON UNIT VECTORS

INM	\bar{S}_i	\bar{X}_i	\bar{Y}_i
#1	$\frac{1}{\sqrt{3}} (-1, -1, -1)$	$\frac{1}{\sqrt{6}} (-2, 1, 1)$	$\frac{1}{\sqrt{2}} (0, 1, -1)$
#2	$\frac{1}{\sqrt{3}} (-1, 1, -1)$	$\frac{1}{\sqrt{6}} (-2, -1, 1)$	$\frac{1}{\sqrt{2}} (0, 1, 1)$
#3	$\frac{1}{\sqrt{3}} (-1, +1, +1)$	$\frac{1}{\sqrt{6}} (-2, -1, -1)$	$\frac{1}{\sqrt{2}} (0, -1, 1)$
#4	$\frac{1}{\sqrt{3}} (-1, -1, 1)$	$\frac{1}{\sqrt{6}} (-2, 1, -1)$	$\frac{1}{\sqrt{2}} (0, -1, -1)$

EDGE VECTORS

$$\bar{e}_{12}: \frac{1}{\sqrt{2}} (-1, 0, 1)$$

$$\bar{e}_{23}: \frac{1}{\sqrt{2}} (-1, -1, 0)$$

$$\bar{e}_{34}: \frac{1}{\sqrt{2}} (-1, 0, -1)$$

$$\bar{e}_{41}: \frac{1}{\sqrt{2}} (-1, 1, 0)$$

$$\bar{e}_{13}: \frac{1}{\sqrt{2}} (0, 1, -1)$$

$$\bar{e}_{24}: \frac{1}{\sqrt{2}} (0, 1, 1)$$

6.3.2.2 Failure, Detection and Isolation

Figure 6-31 illustrates the mechanization of the gyro Failure, Detection and Isolation software. An equivalent set of software exists for the accelerometers, the differences are in the filter time constants, detection levels, and scaling.

GYRO PARITY EQUATIONS

$$\left. \begin{aligned} \Delta P_{g12}^n &= \sqrt{2} (\overline{\Delta\theta}_{b1} \cdot \bar{e}_{12} - \overline{\Delta\theta}_{b2} \cdot \bar{e}_{12}) \\ \Delta P_{g23}^n &= \sqrt{2} (\overline{\Delta\theta}_{b2} \cdot \bar{e}_{23} - \overline{\Delta\theta}_{b3} \cdot \bar{e}_{23}) \\ \Delta P_{g34}^n &= \sqrt{2} (\overline{\Delta\theta}_{b3} \cdot \bar{e}_{34} - \overline{\Delta\theta}_{b4} \cdot \bar{e}_{34}) \\ \Delta P_{g41}^n &= \sqrt{2} (\overline{\Delta\theta}_{b4} \cdot \bar{e}_{41} - \overline{\Delta\theta}_{b1} \cdot \bar{e}_{41}) \\ \Delta P_{g13}^n &= \sqrt{2} (\overline{\Delta\theta}_{b1} \cdot \bar{e}_{13} - \overline{\Delta\theta}_{b3} \cdot \bar{e}_{13}) \\ \Delta P_{g24}^n &= \sqrt{2} (\overline{\Delta\theta}_{b2} \cdot \bar{e}_{24} - \overline{\Delta\theta}_{b4} \cdot \bar{e}_{24}) \end{aligned} \right\} \text{PARITY EQUATIONS (21)}$$

$$\left\{ \begin{aligned} P_{gij}^n &= P_{gij}^{n-1} - \frac{\Delta t}{\tau} \cdot P_{gij}^{n-1} + \Delta P_{gij}^n \\ i, j &= 1, 2, 3, 4 \quad i \neq j \end{aligned} \right\} \text{FIRST ORDER FILTER (22)}$$

$$L_{gij} = 1 \quad \text{if } |P_{gij}| > \delta_g$$

$$L_{g1} = (L_{g12} \odot L_{g41}) \oplus (L_{g12} \odot L_{g13}) \oplus (L_{g41} \odot L_{g13}) \text{ GYRO \#1 FAIL (23)}$$

$$L_{g2} = (L_{g12} \odot L_{g23}) \oplus (L_{g12} \odot L_{g24}) \oplus (L_{g23} \odot L_{g24}) \text{ GYRO \#2 FAIL}$$

$$L_{g3} = (L_{g23} \odot L_{g34}) \oplus (L_{g23} \odot L_{g13}) \oplus (L_{g34} \odot L_{g13}) \text{ GYRO \#3 FAIL}$$

$$L_{g4} = (L_{g34} \odot L_{g41}) \oplus (L_{g34} \odot L_{g24}) \oplus (L_{g41} \odot L_{g24}) \text{ GYRO \#4 FAIL}$$

NOTE: 1. \odot = LOGICAL 'AND', \oplus = LOGICAL 'OR'

2. Refer to table 6-10 for definition of \bar{e}_{ij} vectors

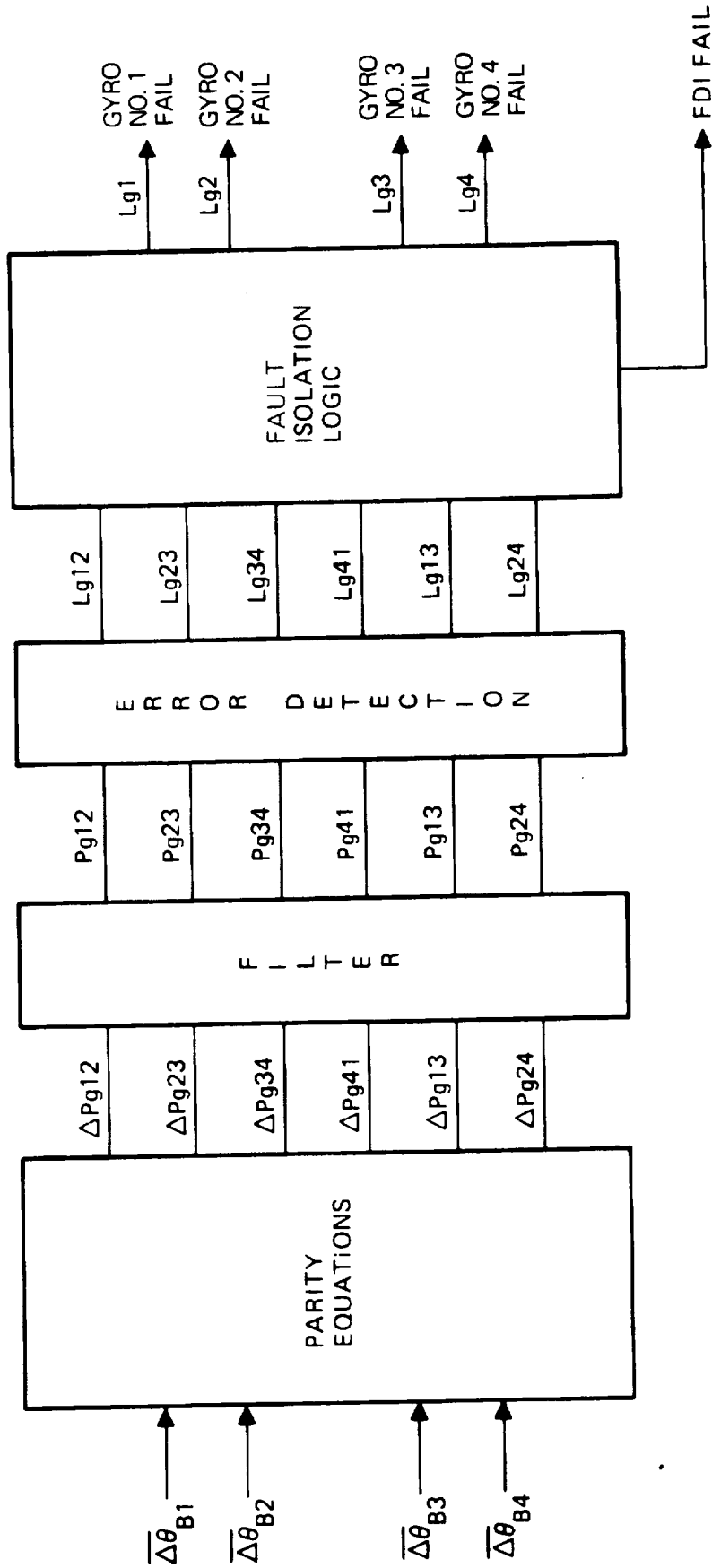


Figure 6-31. Gyro Failure Detection and Isolation Block Diagram

GYRO PARITY EQUATIONS

$$\begin{aligned}
 L_{gn9} = & L_{g12} \odot (\overline{L_{g1} \odot L_{g2}}) \oplus L_{g23} \odot (\overline{L_{g2} \odot L_{g3}}) \\
 & \oplus L_{g34} \odot (\overline{L_{g3} \odot L_{g4}}) \oplus L_{g41} \odot (\overline{L_{g4} \odot L_{g1}}) \\
 & \oplus L_{g13} \odot (\overline{L_{g1} \odot L_{g3}}) \oplus L_{g24} \odot (\overline{L_{g2} \odot L_{g4}})
 \end{aligned}$$

GYRO (24)
PARITY
EQUATION
ERROR
DISCRETE

ACCEL PARITY EQUATIONS

$$\left. \begin{aligned}
 \Delta P_{a12}^n &= \sqrt{2} (\overline{\Delta v}_{b1} \cdot \bar{e}_{12} - \overline{\Delta v}_{b2} \cdot \bar{e}_{12}) \\
 \Delta P_{a23}^n &= \sqrt{2} (\overline{\Delta v}_{b2} \cdot \bar{e}_{23} - \overline{\Delta v}_{b3} \cdot \bar{e}_{23}) \\
 \Delta P_{a34}^n &= \sqrt{2} (\overline{\Delta v}_{b3} \cdot \bar{e}_{34} - \overline{\Delta v}_{b4} \cdot \bar{e}_{34}) \\
 \Delta P_{a41}^n &= \sqrt{2} (\overline{\Delta v}_{b4} \cdot \bar{e}_{41} - \overline{\Delta v}_{b1} \cdot \bar{e}_{41}) \\
 \Delta P_{a13}^n &= \sqrt{2} (\overline{\Delta v}_{b1} \cdot \bar{e}_{13} - \overline{\Delta v}_{b3} \cdot \bar{e}_{13}) \\
 \Delta P_{a24}^n &= \sqrt{2} (\overline{\Delta v}_{b2} \cdot \bar{e}_{24} - \overline{\Delta v}_{b4} \cdot \bar{e}_{24})
 \end{aligned} \right\}$$

PARITY EQUATIONS (25)

$$\left. \begin{aligned}
 P_{aij}^n &= P_{aij}^{n-1} - \frac{\Delta t}{\tau} P_{aij}^{n-1} + \Delta P_{aij}^n \\
 i, j &= 1, 2, 3, 4 \quad i \neq j
 \end{aligned} \right\}$$

FIRST ORDER FILTER (26)

$$L_{aij} = 1 \quad \text{if} \quad |P_{aij}| > \delta_a$$

NOTE: \odot = LOGICAL 'AND' \oplus = LOGICAL 'OR'

ACCEL PARITY EQUATIONS

$$L_{a1} = (L_{a12} \odot L_{a41}) \oplus (L_{a12} \odot L_{a13}) \oplus (L_{a41} \odot L_{a13}) \quad \text{ACCEL \#1 FAIL (27)}$$

$$L_{a2} = (L_{a12} \odot L_{a23}) \oplus (L_{a12} \odot L_{a24}) \oplus (L_{a23} \odot L_{a24}) \quad \text{ACCEL \#2 FAIL}$$

$$L_{a3} = (L_{a23} \odot L_{a34}) \oplus (L_{a23} \odot L_{a13}) \oplus (L_{a34} \odot L_{a13}) \quad \text{ACCEL \#3 FAIL}$$

$$L_{a4} = (L_{a34} \odot L_{a41}) \oplus (L_{a34} \odot L_{a24}) \oplus (L_{a41} \odot L_{a24}) \quad \text{ACCEL \#4 FAIL}$$

$$L_{\text{ang}} = L_{a12} \odot (L_{a1} \odot L_{a2}) \oplus L_{a23} \odot (L_{a2} \odot L_{a3}) \oplus L_{a34} \odot (L_{a3} \odot L_{a4}) \oplus L_{a41} \odot (L_{a4} \odot L_{a1}) \oplus L_{a13} \odot (L_{a1} \odot L_{a3}) \oplus L_{a24} \odot (L_{a2} \odot L_{a4}) \quad \text{ACCEL PARITY EQUATION ERROR DISCRETE (28)}$$

NOTE: \odot = LOGICAL 'AND' \oplus = LOGICAL 'OR'

6.3.2.3 Design Equations

The design equations combine the outputs of two instruments in a least square solution to form the total body axes inertial rates.

Equations (29) and (30) summarize the equations in vector form. The weighting factors are defined in table 6-10. The logic variables SG12, SG13, etc are set to 1 or 0 according to the logic formulated in table 6-9.

$$\begin{aligned} \overline{\Delta\theta}_b &= W_{12}(\overline{\Delta\theta}_{b1} + \overline{\Delta\theta}_{b2})SG12 \\ &+ W_{13}(\overline{\Delta\theta}_{b1} + \overline{\Delta\theta}_{b3})SG13 \\ &+ W_{14}(\overline{\Delta\theta}_{b1} + \overline{\Delta\theta}_{b4})SG14 \end{aligned} \quad (29)$$

$$\begin{aligned} \overline{\Delta V}_b &= W_{12}(\overline{\Delta V}_{b1} + \overline{\Delta V}_{b2})SV12 \\ &+ W_{13}(\overline{\Delta V}_{b1} + \overline{\Delta V}_{b3})SV13 \\ &+ W_{14}(\overline{\Delta V}_{b1} + \overline{\Delta V}_{b4})SV14 \end{aligned} \quad (30)$$

Note: Design equations are written for INM-1, similar sets apply for INM2-4 as indicated in table 6-11.

TABLE 6-9. INSTRUMENT PAIR SELECTION VS FAILURE INDICATION

CHAN	FAILURE INDICATION										
	0	1	2	3	4	1&2	1&3	1&4	2&3	2&4	3&4
1	1,2	1,2	1,3	1,2	1,2	1,3	1,2	1,2	1,4	1,3	1,2
2	2,3	2,3	2,3	2,4	2,3	2,3	2,4	2,3	2,4	2,3	2,1
3	3,4	3,4	3,4	3,4	3,1	3,4	3,4	3,2	3,4	3,1	3,1
4	4,1	4,2	4,1	4,1	4,1	4,3	4,2	4,2	4,1	4,1	4,1

6.3.2.4 Coordinate Converter

Figure 6-32 illustrates the strapdown conversion computations. The integration algorithm listed under equation set (31), represents a partial 5th order Taylor series quaternion integration algorithm. The total quaternion integration procedure is accomplished at two rates, the body rate integration performed at 64/sec and the computational frame rate integration at 8/sec. The velocity transformations, equation (33) performed at 64/sec. Note that the quaternions are converted to a direction cosine matrix followed by a matrix multiply to accomplish the velocity transformation.

TABLE 6-10. LEAST SQUARES WEIGHTING FACTORS

$$W_{12} = [S_1 + S_2]^{-1} = 1/4 \begin{bmatrix} 4 & 0 & 2 \\ 0 & 3 & 0 \\ 2 & 0 & 4 \end{bmatrix}$$

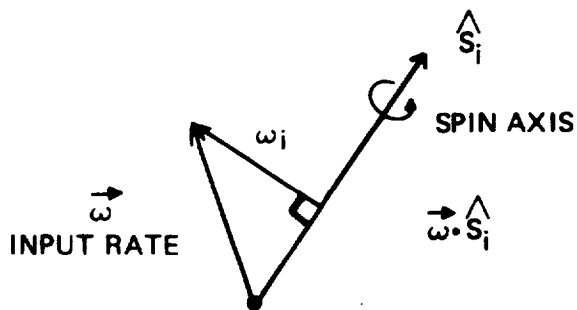
$$W_{13} = [S_1 + S_3]^{-1} = -1/4 \begin{bmatrix} 3 & 0 & 0 \\ 0 & 4 & 2 \\ 0 & 2 & 4 \end{bmatrix}$$

$$W_{23} = [S_2 + S_3]^{-1} = 1/4 \begin{bmatrix} 4 & -2 & 0 \\ -2 & 4 & 0 \\ 0 & 0 & 3 \end{bmatrix}$$

$$W_{24} = [S_2 + S_4]^{-1} = 1/4 \begin{bmatrix} 3 & 0 & 0 \\ 0 & 4 & -2 \\ 0 & -2 & 4 \end{bmatrix}$$

$$W_{34} = [S_3 + S_4]^{-1} = 1/4 \begin{bmatrix} 4 & 0 & -2 \\ 0 & 3 & 0 \\ -2 & 0 & 4 \end{bmatrix}$$

$$W_{14} = [S_1 + S_4]^{-1} = 1/4 \begin{bmatrix} 4 & -2 & 0 \\ -2 & 4 & 0 \\ 0 & 0 & 3 \end{bmatrix}$$

DEFINITION OF $[S_i]$ 

$$\vec{\omega}_i = \vec{\omega} - (\omega \cdot \hat{S}_i) \hat{S}_i = [S_i] \vec{\omega}$$

$$\begin{pmatrix} \text{GYRO OUTPUT RATE} \end{pmatrix} = \begin{pmatrix} \text{INPUT RATE} \end{pmatrix} - \begin{pmatrix} \text{PROJECTION OF INPUT RATE ALONG SPIN AXIS} \end{pmatrix} = \begin{pmatrix} \text{PROJECTION OF INPUT ON PLANE NORMAL TO SPIN AXIS} \end{pmatrix}$$

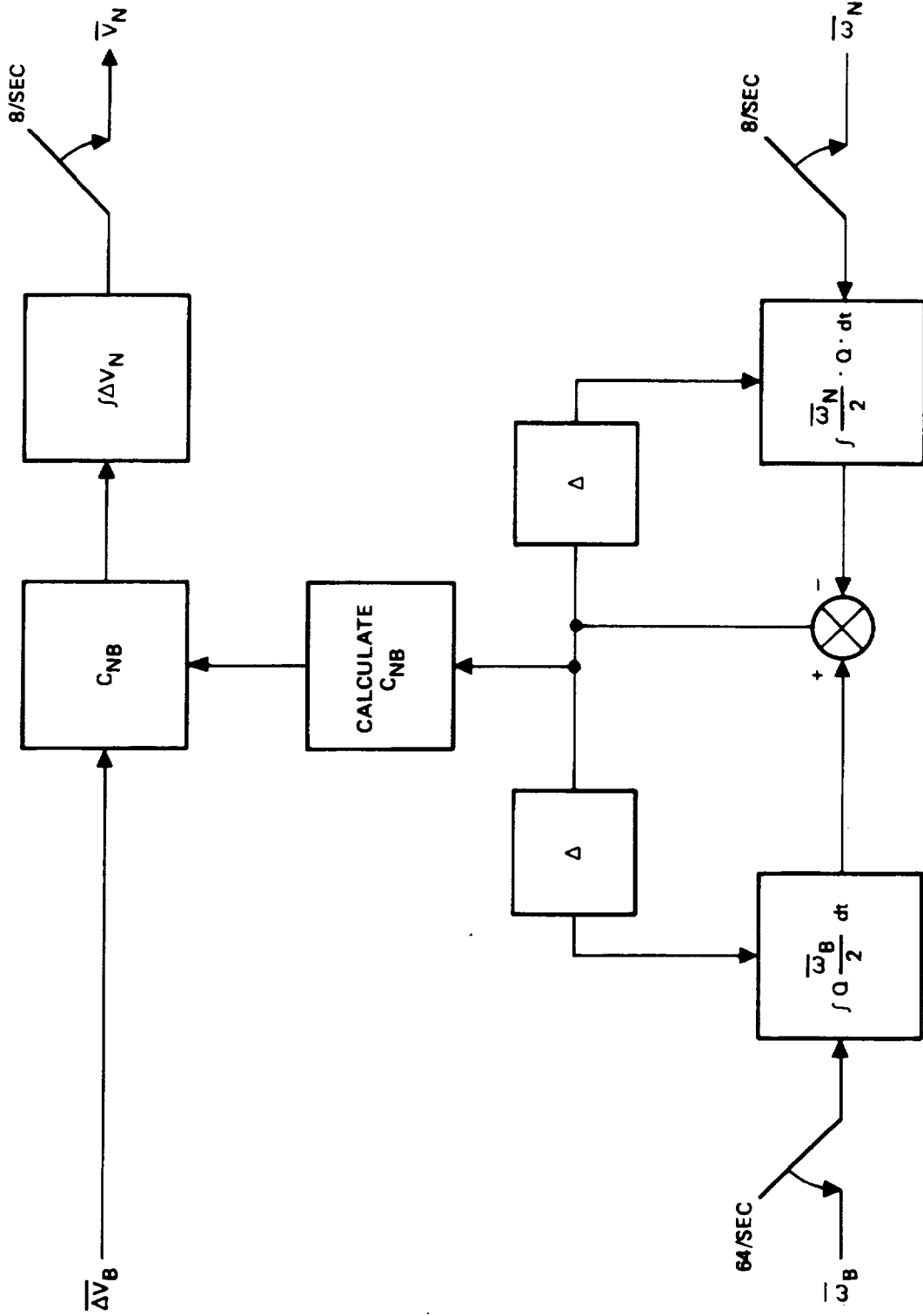


Figure 6-32. Coordinate Conversion

QUATERNION INTEGRATION

ALGORITHM

$$\dot{Q} = Q\bar{\omega}/2$$

GYRO SAMPLES

$$\overline{\Delta\theta}_A = \int_{n\Delta t}^{(n+1/2)\Delta t} \bar{\omega} dt \qquad \overline{\Delta\theta}_B = \int_{(n+1/2)\Delta t}^{(n+1)\Delta t} \bar{\omega} dt$$

DIFFERENCE
APPROXIMATIONS

$$\overline{\Delta\theta} = \overline{\Delta\theta}_A + \overline{\Delta\theta}_B$$

$$C = 1 - \frac{|\overline{\Delta\theta}|^2}{2!} + \frac{|\overline{\Delta\theta}|^4}{4!}$$

$$S = 1 - \frac{|\overline{\Delta\theta}|^2}{3!} + \frac{|\overline{\Delta\theta}|^4}{5!}$$

$$Q^{n+1} = Q^n \left(C, S \left(\frac{\overline{\Delta\theta}}{2} + \frac{\overline{\Delta\theta}_A \times \overline{\Delta\theta}_B}{3} \right) \right) \quad (31)$$

Note: $\overline{\Delta\theta}_A$ and $\overline{\Delta\theta}_B$ are two samples of $\overline{\Delta\theta}_b$

DIRECTION COSINES

$$\begin{aligned}
C_{XX}^n &= (Q_1^n)^2 - (Q_2^n)^2 - (Q_3^n)^2 + (Q_4^n)^2 \\
C_{XY}^n &= 2 \cdot (Q_1^n \cdot Q_2^n - Q_3^n \cdot Q_4^n) \\
C_{XZ}^n &= 2 \cdot (Q_1^n \cdot Q_3^n + Q_2^n \cdot Q_4^n) \\
C_{YX}^n &= 2 \cdot (Q_1^n \cdot Q_2^n + Q_3^n \cdot Q_4^n) \\
C_{YY}^n &= (Q_2^n)^2 - (Q_1^n)^2 - (Q_3^n)^2 + (Q_4^n)^2 \\
C_{YZ}^n &= 2 \cdot (Q_2^n \cdot Q_3^n - Q_1^n \cdot Q_4^n) \\
C_{ZX}^n &= 2 \cdot (Q_1^n \cdot Q_3^n - Q_2^n \cdot Q_4^n) \\
C_{ZY}^n &= 2 \cdot (Q_2^n \cdot Q_3^n + Q_1^n \cdot Q_4^n) \\
C_{ZZ}^n &= (Q_3^n)^2 - (Q_1^n)^2 - (Q_2^n)^2 + (Q_4^n)^2
\end{aligned} \tag{32}$$

COORDINATE CONVERSION

$$\begin{aligned}
\Delta V_{XN}^{n+1/2} &= C_{XX}^n \cdot \Delta V_{Xb}^{n+1/2} + C_{XY}^n \cdot \Delta V_{Yb}^{n+1/2} + C_{XZ}^n \cdot \Delta V_{Zb}^{n+1/2} \\
\Delta V_{Yn}^{n+1/2} &= C_{YX}^n \cdot \Delta V_{Xb}^{n+1/2} + C_{YY}^n \cdot \Delta V_{Yb}^{n+1/2} + C_{YZ}^n \cdot \Delta V_{Zb}^{n+1/2} \\
\Delta V_{Zn}^{n+1/2} &= C_{ZX}^n \cdot \Delta V_{Xb}^{n+1/2} + C_{ZY}^n \cdot \Delta V_{Yb}^{n+1/2} + C_{ZZ}^n \cdot \Delta V_{Zb}^{n+1/2}
\end{aligned} \tag{33}$$

NAVIGATION VELOCITY SUMMATION

$$\begin{aligned}
V_{XN}^{n+1/2} &= V_{XN}^{n-1/2} + \Delta V_{XN}^{n+1/2} \\
V_{YN}^{n+1/2} &= V_{YN}^{n-1/2} + \Delta V_{YN}^{n+1/2} \\
V_{ZN}^{n+1/2} &= V_{ZN}^{n-1/2} + \Delta V_{ZN}^{n+1/2}
\end{aligned} \tag{34}$$

6.3.2.5 Navigation

Equation (35) represents the integration of the navigation frame rates, comparable to gyro torquing for a gimballed platform inertial navigation system.

The inertial navigation equations are the standard set common to all Litton inertial navigation systems. The alignment equations again use a proven technique common to Litton inertial navigation systems. It consists of two independent 3rd order leveling loops with Kalman gains. The technique accomplishes simultaneous leveling and gyrocompassing with a minimum of computations.

Figure 6-33 illustrates the 3rd order Baro-Inertial Vertical Channel. It is modified to compensate for barometric altimeter errors.

QUATERNION UPDATE (NAV RATES)

$$\begin{aligned}
 1) \quad |\Delta\phi|^2 &= (WXN \cdot WXN + WYN \cdot WYN + WZN \cdot WZN)(\Delta t_N)^2 \\
 2) \quad S|\phi| &= -\frac{|\Delta\phi|^2}{48} \\
 3) \quad C|\phi| &= -\frac{|\Delta\phi|^2}{8} + \frac{E^n}{2} \quad (E^0 = 0) \\
 4) \quad T1 &= (-Q_2 \cdot WZN + Q_3 \cdot WYN + Q_4 \cdot WXN) \cdot \Delta t_N \\
 \quad T2 &= (-Q_3 \cdot WXN + Q_4 \cdot WYN + Q_1 \cdot WZN) \cdot \Delta t_N \\
 \quad T3 &= (Q_4 \cdot WZN - Q_1 \cdot WYN + Q_2 \cdot WXN) \cdot \Delta t_N \\
 \quad T4 &= (-Q_1 \cdot WXN - Q_2 \cdot WYN - Q_3 \cdot WZN) \cdot \Delta t_N \\
 5) \quad Q_1 &= Q_1 + Q_1 \cdot C|\phi| + 1/2 \cdot T_1 + 1/2 \cdot S|\phi| \cdot T_1 \\
 \quad Q_2 &= Q_2 + Q_2 \cdot C|\phi| + 1/2 \cdot T_2 + 1/2 \cdot S|\phi| \cdot T_2 \\
 \quad Q_3 &= Q_3 + Q_3 \cdot C|\phi| + 1/2 \cdot T_3 + 1/2 \cdot S|\phi| \cdot T_3 \\
 \quad Q_4 &= Q_4 + Q_4 \cdot C|\phi| + 1/2 \cdot T_4 + 1/2 \cdot S|\phi| \cdot T_4 \\
 6) \quad E^{n+1} &= (1 - (Q_1^2 + Q_2^2 + Q_3^2 + Q_4^2)) \quad (35)
 \end{aligned}$$

NAVIGATION VELOCITY

$$\begin{aligned}
 V_X^N &= V_X^{N-1} + V_{XN} + (VXCR + VXCL) \cdot \Delta t_N \\
 V_Y^N &= V_Y^{N-1} + V_{YN} + (VYCR + VYCL) \cdot \Delta t_N \\
 V_Z^N &= V_Z^{N-1} + V_{ZN} + (VZCR + VZCL) \cdot \Delta t_N
 \end{aligned}
 \tag{36}$$

ALIGNMENT EQUATIONS

$$\begin{aligned}
 TPX &= TPX - VYA \cdot KT \cdot \Delta t_N \\
 TPY &= TPY + VXA \cdot KT \cdot \Delta t_N \\
 WXC &= TPX \cdot 8 \\
 WYC &= TPY \cdot 8 \\
 TPX &= TPX - WXC \cdot \Delta t_N \\
 TPY &= TPY - WYC \cdot \Delta t_N \\
 VXCL &= - VXA \cdot KV - GEE \cdot TPY \\
 VYCL &= - VYA \cdot KV + GEE \cdot TPX \\
 BXC &= BXC - VYA \cdot KZ \cdot \Delta t_N \\
 BYC &= BYC + VXA \cdot KZ \cdot \Delta t_N
 \end{aligned}
 \tag{37}$$

NAVIGATION DIRECTION COSINES

$$\begin{aligned}
 RHOX &= - VY \cdot RE2 - VX \cdot RE3 \\
 RHOY &= VX \cdot RE1 + VY \cdot RE3 \\
 WX &= WXS + RHOX \\
 WY &= WYS + RHOY \\
 WZ &= WZS \\
 B11 &= B11 - RHOY \cdot B31 \cdot \Delta t_N \\
 B21 &= B21 + RHOX \cdot B31 \cdot \Delta t_N \\
 B31 &= B31 + (RHOY \cdot B11 - RHOX \cdot B21) \cdot \Delta t_N \\
 B12 &= B12 - RHOY \cdot B32 \cdot \Delta t_N \\
 B22 &= B22 + RHOX \cdot B32 \cdot \Delta t_N \\
 B32 &= B32 + (RHOX \cdot B12 - RHOY \cdot B22) \Delta t_N
 \end{aligned}
 \tag{38}$$

NAVIGATION RATES

$\begin{aligned} \text{WXN} &= - (\text{WX} + \text{WXC} + \text{BXC}) \\ \text{WYN} &= - (\text{WY} + \text{WYC} + \text{BYC}) \\ \text{WZN} &= - (\text{WZ}) \end{aligned}$

$$\begin{aligned} \text{WXC}, \text{WYC} &= 0 : \text{NAV} \\ \text{BXC}, \text{BYC} &= 0 \quad \text{MODE} \end{aligned} \quad (39)$$

MISCELLANEOUS CALCULATIONS

ATTITUDE

$$\text{PITCH} = \text{SIN}^{-1} (\text{CZY})$$

$$\text{ROLL} = \text{TAN}^{-1} \left(\frac{-\text{CZX}}{\text{CZZ}} \right)$$

$$\text{AZIMUTH} = \text{TAN} \left(\frac{-\text{CXY}}{\text{CYY}} \right)$$

$$\text{HEADING} = - \text{AZIMUTH} - \text{ALPHA} \quad (40)$$

RADII OF CURVATURE

$$\begin{aligned} \text{RE1} &= \frac{1}{a} \cdot \left(1 - \frac{1}{a} \cdot h_b - f \cdot \left(1 - 3 \cdot (\text{B12})^2 - (\text{B22})^2 \right) \right) \\ \text{RE2} &= \frac{1}{a} \cdot \left(1 - \frac{1}{a} \cdot h_b - f \cdot \left(1 - 3 \cdot (\text{B22})^2 - (\text{B12})^2 \right) \right) \\ \text{RE3} &= \frac{1}{a} \cdot (2 \cdot f \cdot \text{B12} \cdot \text{B22}) \end{aligned} \quad (41)$$

CORIOLIS ACCELERATION

$$\begin{aligned} \text{VXCR} &= (2 \cdot \text{WZN} \cdot \text{VY}) - (2 \cdot \text{WYN} - \text{RHOY}) \cdot \text{VZ} \\ \text{VYCR} &= (2 \cdot \text{WZN} \cdot \text{VX}) + (2 \cdot \text{WXN} - \text{RHOX}) \cdot \text{VZ} \\ \text{AZCR} &= V_X (\text{RHOY} + 2\Omega\text{B22}) - V_Y (\text{RHOX} + \Omega\text{B12}) \end{aligned} \quad (42)$$

POSITION CALCULATIONS

$$\text{LONGITUDE} = \text{Tan}^{-1} \frac{\text{B31}}{\text{B11} \cdot \text{B22} - \text{B12} \cdot \text{B21}}$$

$$\text{LATITUDE} = \text{Sin}^{-1} -(\text{B32})$$

$$\text{ALPHA} = \text{Tan}^{-1} \frac{\text{B12}}{\text{B22}} \quad (43)$$

EARTH RATES

$$\omega_{XS} = \Omega(\text{B12}) \quad (44)$$

$$\omega_{YS} = \Omega(\text{B22})$$

$$\omega_{ZS} = \Omega(\text{B32})$$

NAVIGATION DIRECTION COSINE INITIALIZATION

$$\text{B11} = \cos(\alpha) \cos(\lambda) - \sin(\lambda) \sin(\phi) \sin(\alpha) \quad (45)$$

$$\text{B21} = -\cos(\lambda) \sin(\alpha) - \sin(\lambda) \cdot \sin(\phi) \cdot \cos(\alpha)$$

$$\text{B31} = \sin(\lambda) \cdot \cos(\phi)$$

$$\text{B21} = \sin(\alpha) \cdot \cos(\phi)$$

$$\text{B22} = \cos(\alpha) \cdot \cos(\phi)$$

$$\text{B32} = \sin \phi$$

where λ = Longitude

ϕ = Latitude

α = Alpha

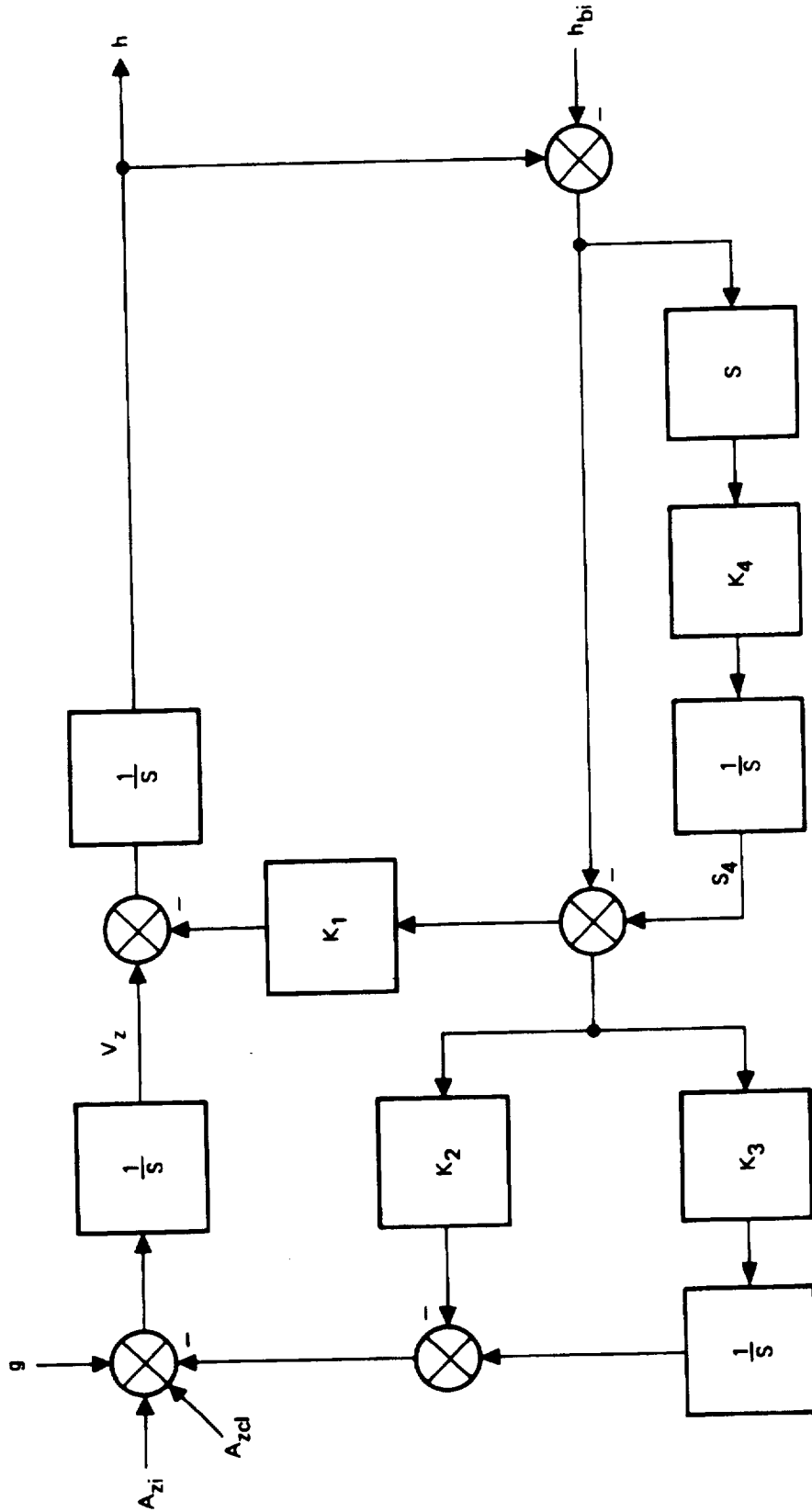


Figure 6-33. Baro-Inertial Loop

BARO-INITIAL COMPUTATIONS

$$\begin{aligned}
 \text{HBDOT} &= (\text{HB} - \text{HBO})/\text{DT} & (46) \\
 \text{KTA} &= (1/\text{TH})/(1 + (\frac{\text{HBDOT}}{\text{EHBDOT}})^2) \\
 \text{K1} &= 3 \cdot (\text{KTA}) \\
 \text{K2} &= 4 \cdot (\text{KTA})^2 \cdot + \frac{2 \cdot \text{g}_0}{\text{a}} \\
 \text{K3} &= 2 \cdot (\text{KTA})^3 \\
 \text{K4} &= (\text{HBDOT})^2/(\text{EHBDOT}^2 + \text{HBDOT}^2) \\
 \text{S4} &= \text{S4} + \text{K4} \cdot \text{HBDOT} \cdot \text{DT} \\
 \text{DH} &= (\text{HB} - \text{HBO}) - \text{S4} \\
 \text{HBO} &= \text{HB} \\
 \text{S3} &= \text{S3} + \text{K3} \cdot \text{DH} \cdot \text{DT} \\
 \text{Vz} &= \text{Vz} + (\text{S}_3 + \text{K2} \cdot \text{DH}) \cdot \text{DT} \\
 \text{h} &= \text{h} + (\text{Vz} + \text{K1} \cdot \text{DH}) \cdot \text{DT} \\
 \text{g} &= \text{g}_0 (1 + \text{Beta} \cdot \text{B32} - \frac{2\text{h}}{\text{a}})
 \end{aligned}$$

6.3.2.6 Coordinate Frames and Glossary

Figures 6-34 and 6-35 illustrate the pertinent coordinate frames for the preceding equations. Table 6-11 summarizes these coordinate frames.

Table 6-12 is a glossary of major terms in these equations.

6.3.3 Computer Resource Estimates

With the INM software tasks broken down as illustrated in figure 6-29, an estimate of memory and computer duty cycle requirements using the computer characteristics of table 6-7 has been made. The results are listed in table 6-13. The estimates of duty cycle requirements are conservative. Various means of reducing computation time will be reviewed during the final design phase of the redundant strapdown INS.

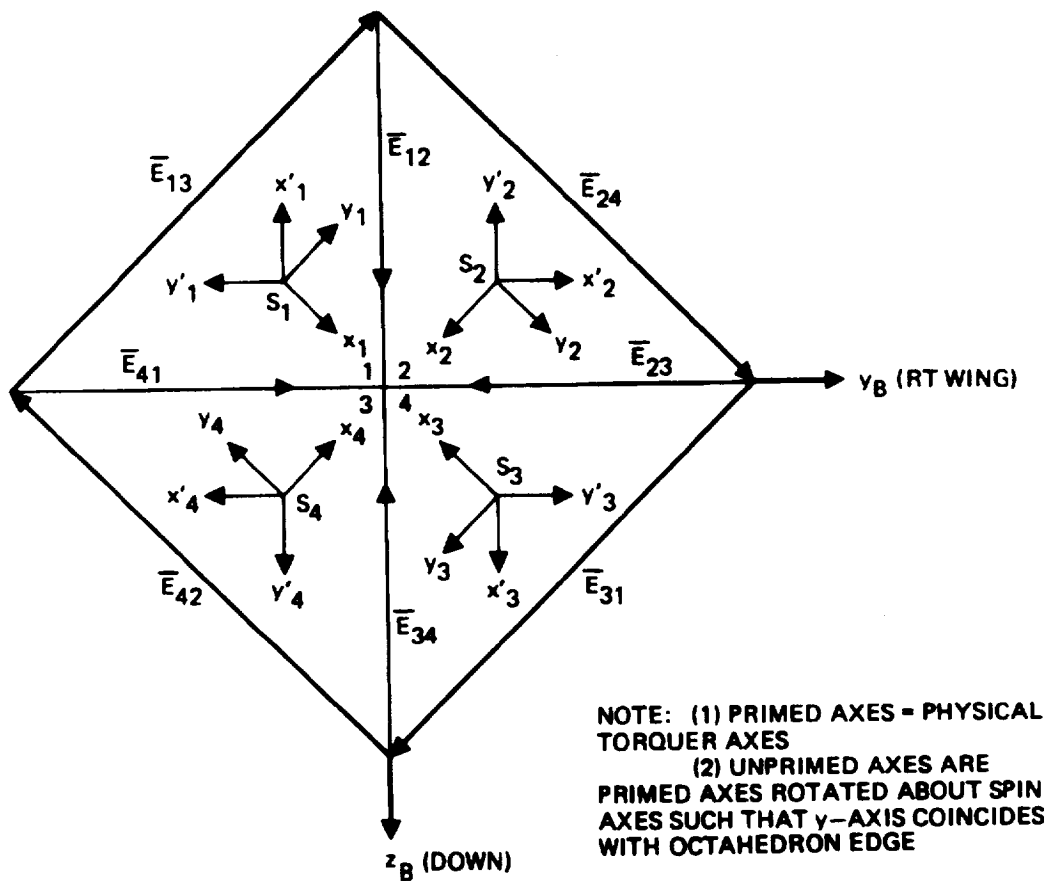


Figure 6-34. Semi-Octahedral Coordinate Frames

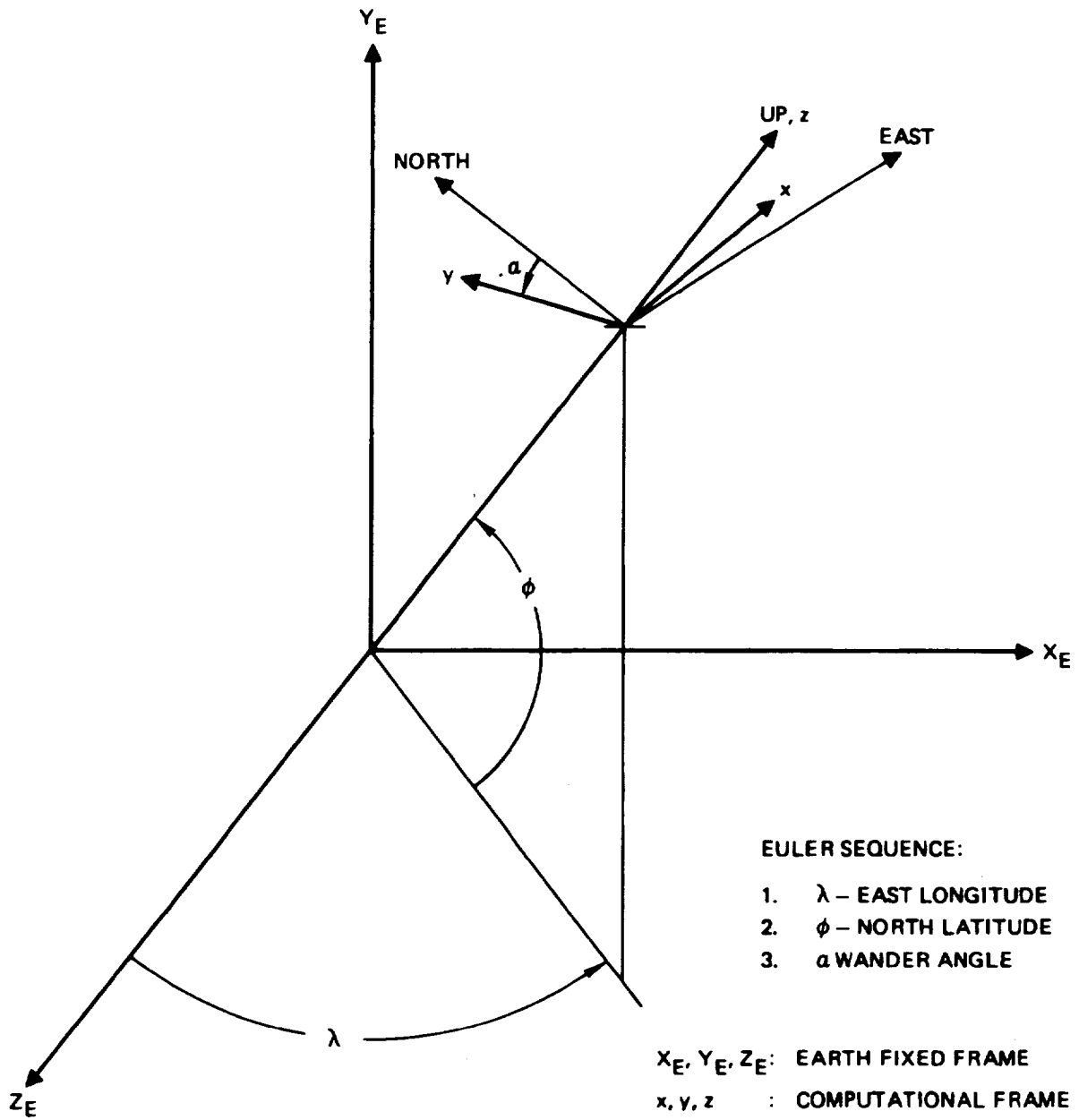


Figure 6-35. Navigation Frame Relationship

TABLE 6-11. COORDINATE FRAMES

X_B, Y_B, Z_B	Body Frame: X-forward along airframe longitudinal axis. Y along right wing and Z-axis down
x_i', y_i', s_i'	Instrument physical axis of the ith inertial navigation module: the s_i' axis is normal to the ith surface of a semi-octahedron, the x_i' and y_i' axis lie in the ith surface such that the bisector of the x_i' and y_i' axis is perpendicular to the base of the semi-octahedron.
x_i, y_i, s_i	Instrument axis of ith inertial navigation module: this axis is obtained by rotating the physical axes (x_i', y_i', s_i') about the $-s_i'$ axis through -135° to make the Y_i axes parallel to an outside semi-octahedral edge
x, y, z	Computational frame: locally leveled, with y-axis displaced from geographic north through azimuth angle ' α '. z-axis is up.
X_E, Y_E, Z_E	Earth fixed frame: X_E - Z_E plane coincident with earth's equatorial plane, Z_E axis passing through Greenwich meridian. x, y, z frame obtained by rotations through angles λ and ϕ about Y_E and X_E and finally through ' α ' about z axis.

TABLE 6-12. GLOSSARY

Symbol	Definition
a	Earth's equatorial radius, 6378.163 Km
A_{BX} , A_{BY}	Accelerometer biases
BATX0, BATX1, BATX2	Accelerometer bias temperature sensitivity coefficients
Beta	Gravity constant 0.0517993209 Km/Sec ²
BGTX0, BGTX1, BGTX2	Gyro bias temperature sensitivity coefficients
B_x , B_y	Gyro biases
B11, B21, B31, B12, B22, B32	Earth - Navigation frame direction cosines
γ_{GX} , γ_{GY}	Gyro spin axis misalignment coefficients
C_{ij} , $i, j = x, y, z$	Body to navigation frame direction cosines
δ_{ZXX} , δ_{AXY} , δ_{AXZ}	Accelerometer misalignment coefficients
δ_{ZYX} , δ_{AYY} , δ_{AYZ}	
δ_{GXX} , δ_{GYG} , δ_{GYX} , δ_{GXY}	
$\Delta\theta_{bx}^{n-1}$, $\Delta\theta_{by}^{n-1}$, $\Delta\theta_{bz}^{n-1}$	Body rates from previous iteration
$\Delta\theta_{cx}$, $\Delta\theta_{cy}$	Compensated gyro rates about instrument axes
$\Delta\theta_{gx}$, $\Delta\theta_{gy}$	Raw outputs of gyros
$\Delta\theta_s^{n-1}$	Inertial rate about spin axis from last iteration

TABLE 6-12. GLOSSARY (cont)

Symbol	Definition
$\Delta V_{ax}, \Delta V_{ay}$	Raw outputs of accelerometers
$\Delta V_{bx}, \Delta V_{by}, \Delta V_{bz}$	Incremental body velocities along body axes
ΔV_s^{n-1}	Incremental inertial velocity along s - axis of accelerometer
$\Delta V_{xn}, \Delta V_{yn}$	Incremental inertial velocities in navigation frame
E HBDOT	Empirically derived constant for baro-inertial loop
f	Earth's flattening, $3.3541005459 \times 10^{-3}$
g, GEE	Vertical component of Earth's gravitational field
g_0	Equatorial gravity. At equator, sea level, $9.780270477 \text{ Km/sec}^2$
h	Inertial altitude
I_g	gyro inertial compensation coefficient
k1, k2, k3, k4	Baro-inertial loop gains
MGTX0, MGTX1, MGXTX ²	Gyro mass imbalance temperature sensitivity coefficients
$M_{XX}, M_{XY}, M_{XZ}, M_{YX}, M_{YY}, M_{YZ}$	Gyro direct and quadrature mass imbalance coefficients
Ω	Earth's rate, $15.041067^\circ/\text{hr}$
S_{ax}, S_{ay}	Accelerometer scale factors
S_{GX1}^+, S_{GX2}^+	Gyro scale factor, normal mode, for positive inputs

TABLE 6-12. GLOSSARY (cont)

Symbol	Definition
S_{GX1}^{-}, S_{GX2}^{-}	Gyro scale factor, normal mode, for negative inputs
$S_{GX1}^{++}, S_{GX2}^{++}$	Gyro scale factor, high rate for positive inputs
$S_{GX1}^{--}, S_{GX2}^{--}$	Gyro scale factor, high rate mode, for negative inputs
S_{GX}, S_{GY}	Total gyro scale factor
SATX0, SATX1, SATX2	Accelerometer scale factor temperature sensitivity coefficients
SGTX0, SGTX1, SGTX2	Gyro scale factor, temperature sensitivity coefficients.
T_{GX}, T_{AX}	Normalized relative gyro and accelerometer temperature input
V_x, V_y, V_z	Ground velocities in navigation frame.
$V_{XCR}, V_{YCR}, V_{ZCR}$	Coriolis acceleration correction

TABLE 6-13. COMPUTER RESOURCE ESTIMATES

TASK	DUTY CYCLE (%)	MEMORY	RATE (Hz)
COMPENSATION - FAST	15.2	500	128
COMPENSATION - SLOW	0.3	200	2
FDI - DESIGN EQN	16.6	700	128
COORDINATE CONVERTER	15.9	750	64
NAVIGATION - FAST	2.1	650	8
NAVIGATION - SLOW	2.1	300	2
ALIGNMENT GAIN SELECT	0.1	100	1
MODE CONTROLLER	0.7	600	1
BARO-ALTITUDE	0.1	150	2
EXECUTIVE-SCHEDULER	4.8	250	128
OUTPUT FORMATTER	2.1	200	32
DATA BASE-SUBROUTINES		2000	
TOTALS	60.0	6400	

6.3.4 Future Software Refinements

The flow charts presented in Appendix H include all major processing requirements. There are additional functions which would be considered for the software of a final design. They do not represent a major impact on duty cycle and word-count.

The details of processing of variables for output to other avionics and self-test implementations have not been included in the flow charts, for example. Special formatting and/or filtering requirements need to be determined in consultations with potential users and would vary with the detailed hardware design of the redundant strapdown INS. Rough computer estimates have been included, however.

Gyro/accelerometer selection in design equations is based on only one alternate rather than the two described in paragraph 4.5.1 of this report. The decision to use the second alternate for improved fail-safe operation during the third system failure was reached too late for incorporation into flow charts.

There are various refinements to the redundancy management discussed in Section IV, not incorporated into flow charts, but worthy of future consideration. These refinements include:

- a. Processing of filtered parity equation outputs, including compensation of nominal gyro scale factor errors, for improved FDI sensitivity to performance degradations.
- b. Derivation of error probabilities from parity equation outputs to determine weighting factors for use by external equipment in combining the three or four channel output, for reduction of total system error just prior to actuation of FDI thresholds.
- c. Transfer of the FDI filter lag to a pure integration following detection (but not isolation) of a drift, for potential noise reduction and better isolation sensitivity.
- d. Reincorporation of a previously failed but only marginal gyro to resolve three-gyro isolation ambiguity or cover a 3rd failure, for improved system reliability.
- e. Cross-feed of computer output tables to detect computer transient errors and reinitialize quaternions and navigation solution, for improved system reliability and as an aid in fault isolation between the computer and external I/O.

- f. Reinitialization of those computers using an instrument which was switched out by redundancy management with information from a known good computer, to eliminate errors which needed to accumulate to trip the FDI mechanism.
- g. Monitor of accumulated position and velocity updates from the external computer and perform redundancy switching, for elimination of degraded gyros and flagging maintenance personnel. (This could be done by the external computer, but a self-contained capability may be preferred.)
- h. Storing various data at the time of a redundancy management or self-test action, such as self-test results, vehicle rates, acceleration, velocity, attitude and some prior time history of parity equations (e.g., 10 seconds), for use by maintenance personnel in determination of repair requirements.

The basic navigation function may also be augmented with refinements for improved performance or in-service usability. These refinements include:

- a. An estimate of each of the skewed-gyro biases can be made, following each ground alignment based on:
 - (1) a North level bias calculation which assumes knowledge of latitude to some accuracy, e.g., 1.85 Km, (since aircraft parking heading is generally different from alignment to alignment, all level components of drift gradually get compensated),
 - (2) differences between each channel's computation of aircraft heading during gyrocompassing (aggregate heading using data from all four channels should be more accurate than from one channel alone),
 - (3) the difference in indicated heading from the end of the previous flight to that resulting from the following gyrocompass (azimuth drift), assuming the aircraft had not been moved. (Protection against movement by means of a reasonableness test would be needed. Also, normal scale-factor errors contaminate this measurement, but it may be sufficiently accurate over a number of flights.)

- b. The various indications of aircraft pitch and roll may be averaged to improve accelerometer bias errors. (Accelerometer bias is a significant contributor to the velocity error of a strapdown INS, much more so than in a gimballed INS.)
- c. An automatic transfer from align to navigate when accelerometer outputs cross a threshold is often included as a protection against operator error.
- d. Factory test equipment (FTE) can be simplified by having a special counting subroutine in the airborne equipment for use during unit calibration prior to delivery. A trade-off is needed to compare cost of FTE counters versus a small amount of additional airborne computer memory.
- e. A back-up, pendulous attitude mode could be added for use with previously switched degraded accelerometers or gyros, following a third failure detected and isolated by self test, for improved pitch/roll reliability.

VII. FACTORY TEST EQUIPMENT

7.1 Module Testing

Integration and acceptance testing is performed at the module level, consistent with the standardization and interchangeability concept of the four module Redundant Strapdown System. To support high production rates economically and insure consistency and thorough testing, all final test is performed on automatic stations supported by software test programs.

7.1.1 Manufacturing Flow

Figure 7-1 represents the module manufacturing and test flow. Integration or "Build-Up" is the assembly of assets which have been tested at lower levels into the module chassis. Electronic cards have been tested on card testers, harnesses on FACT machines and instruments on their respective gyro and accelerometer test stations. The Manufacturing Test Procedure (MTP) is performed in two parts to accommodate the special requirements of instrument rate testing and axis alignment calibration. MTP 1A provides a functional test of the module and specifies a six position "static" calibration. Testing for MTP 1B is performed on a Rate Calibration Station which has angular rate testing capability. To screen for component and assembly problems, all modules are run through a multi-cycle hi-lo temperature burn-in. The temperature chambers include vibration equipment and vibration testing is also performed. To support the modules during this period a third station, the Burn-In Monitor, is utilized. After burn-in, the Final Acceptance Test is run.

7.1.2 Test Programs

Build Up Software Program

The Build Up Program executes on the Load Station. Build Up begins with inserting subassemblies or groups of subassemblies into the chassis. First the power supply is inserted and checked for voltage levels and operation of automatic shutdown safety features. Next the computer is added. It is initialized and allowed to execute self-test programs first and when these are successfully completed to drive the I/O cards. The next to last assemblies added are the instrument rebalance electronics which are supplied with dummy loads to insure safe operation prior to installation of the final subassembly, the instrument block. This step by step procedure assures incrementally good assets and inspection of intermediate test points not normally accessible at the module test connectors.

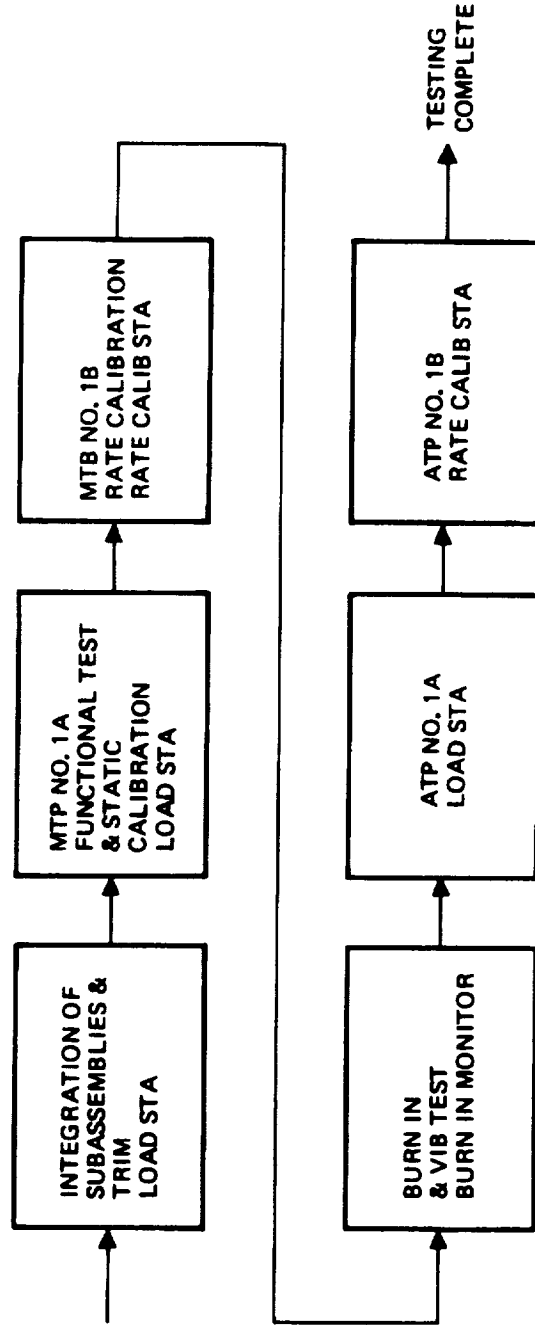


Figure 7-1. Module Manufacturing Flow

The final operation of Build Up is Trim. For the INM this is primarily setting the frequency characteristics of the instrument loops. A frequency response is made of each loop automatically and the computer then calculates the required trim resistance to adjust each to the nominal. With this information, the module is returned to Operations for resistor installation.

Manufacturing Test Procedure (MTP) 1A

MTP 1A begins when the trimmed module is returned. The test consists of:

- a. Turn-On Test
 - Turn on sequence timing.
 - Supply voltage and test point monitor.
 - Performance versus time from start-up.
- b. Computer Diagnostics
- c. Mode Test
 - Test of the module operating modes Test, OFF, BITE, Forced Hi-Rate Mode
- d. I/O Tests
 - Tests of the Lo Speed and Hi Speed data buses.
 - Test of input and output discretes.
- e. Instrument loop frequency response
 - Verification of the Build Up Trim.
- f. Static Calibration
 - Six position tests to determine accelerometer alignment coefficients, and gyro biases. A skewed holding fixture is used to align the instrument axes parallel and at right angles to vertical. Constants determined here are stored for later insertion into the module PROM.

Rate Calibration Program, MTP-1B

Rate Calibration is performed on the Rate Calibration Station which incorporates a precision, automatic rate table. Four units are tested concurrently and the software is so arranged that a module may be loaded independent of the test status of the other modules. Testing consists of introducing CW and CCW rates over precise angles and measuring the instrument outputs and the elapsed time. These tests are performed about the gyro input

axes and include multiple rates in both the hi and lo rate range. Rotations are also performed about other axis to determine axis misalignments. These data and previous data are then written into the module PROM.

Burn-In Program

The Burn-In stage of the manufacturing flow is unique in that modules are operated as a system rather than as independent modules. Several factors lead to this as the most desirable implementation. Operation as a System during burn-in maximizes operation of the modules at minimum support equipment expense. Moreover, the System level redundancy management and self-test provides a real time monitor of functional and inertial performance. Most significantly however, is that when operated as a module in the navigation mode, they can easily be tested across a vibration environment.

During Burn-In the Burn-In Monitor (BIM) tracks hardware, initiates background tests in the operational units, executes I/O and monitors test points while undergoing temperature cycling and vibration.

Acceptance Test Procedure (ATP) 1A, 1B

ATP 1A and 1B parallels tests performed in MTP 1A and 1B; however, it is an "end to end" test and must be entered at the start and completed without failure.

7.1.3 Test Equipment

The proposed test equipment is an extension of Litton's LSS-370 family of automatic test equipment. It is derived from almost a decade of automatic and semi-automatic test equipment. Current applications include:

CAINS IMU Test Station

LN-31 INU Test Station with multiplex capability

CGATS Platform Test Station.

Figure 7-2 shows the LN-31 INU multiplex station. Fundamental to the LSS-370 concept is a powerful real time operating system which controls all user tasks, disc management memory allotment and task queing. The system provides effective CPU management and allows concurrent multiple users, or partitions.

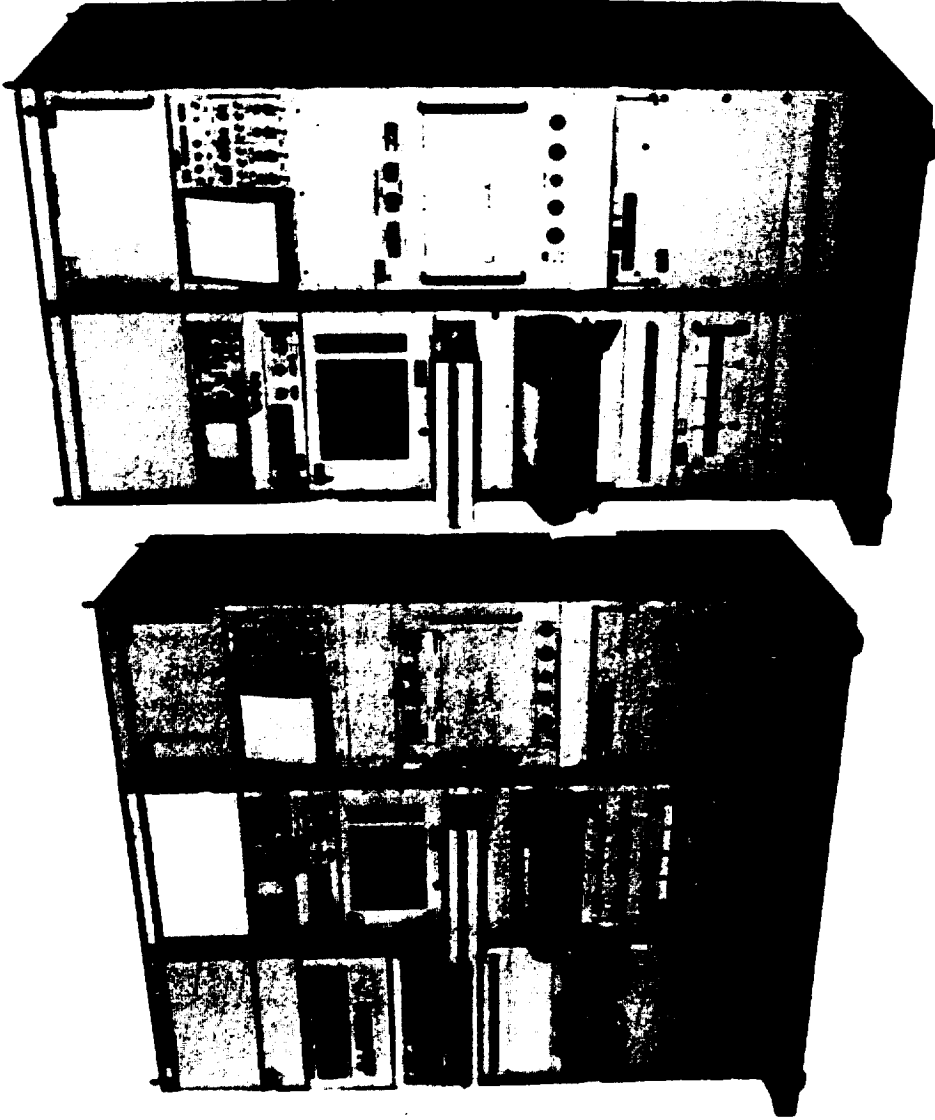


Figure 7-2. LN-31 INU Multiplex Station

Load Station

The Load Station is configured as shown in figure 7-3 with three partitions. Rack 0 controls all three partitions. It houses the computer complex:

PDP-11-35
 Disc
 Extended Core Memory
 Tape Loader

The operating system controls and communicates with each partition via a bus system. Also housed in Rack 0 are the common commercial equipment with low utilization, namely the frequency measurement equipment. This is used to measure the instrument loop frequency characteristics.

Each partition of Racks 1 and 2 behaves identically and independently of the other partitions though they share a common master computer. This multiplex mode is currently in operation in the LN31 INU Test Station. Both the programmable digital multimeter (DMM) and scope have access to 300 signal channels via the scanner; signal routing and measurement are all under software control.

The operator interface is through the CRT, Keyboard and Printer. The CRT displays time, test mode, test number, unit under test (UUT) status and current test results. In the lower 1/3 of the CRT, operator messages are displayed. Messages are only displayed when operator action is required and a keyboard response is needed. The keyboard allows the operator to select, initiate or terminate a test as well as input data and respond to messages. A printer provides hard copy of all test results and requested operator transactions.

In addition to the Scan Control and the Scanner, Rack 2 contains the Rack Control Unit (RCU) and System Interface Unit (SIU). The RCU furnishes the digital interface with the computer bus system, formatting all inputs and deciphering outputs. The RCU interfaces the commercial equipment including the CRT, DMM, Keyboard, Printer, etc. as well as the unique UUT interface electronics. The latter are housed in the SIU. Typical of these devices are the hi and lo speed data bus receiver and drivers, discrete monitors, loads, time interval monitors and input test stimulus. The SIU uniquely identifies a configuration of the LSS-370 for a given application.

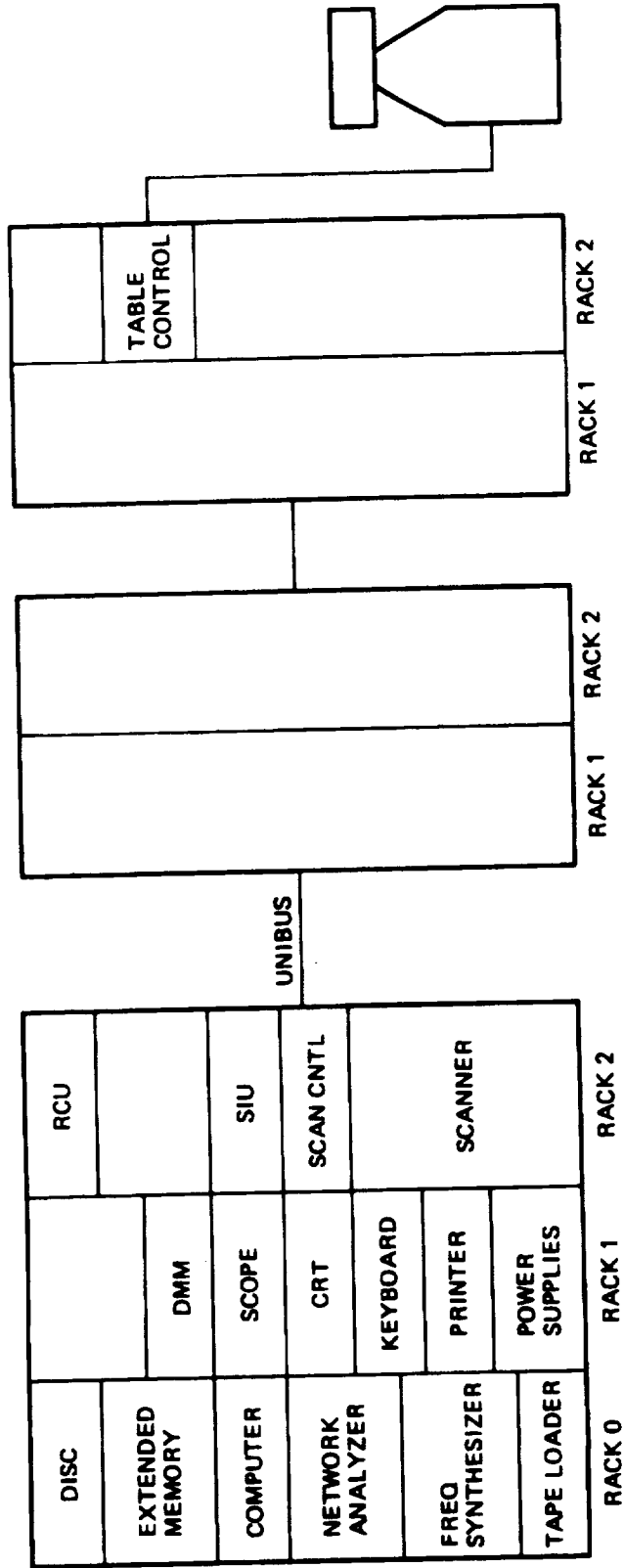


Figure 7-3. Load Station

Not shown in figure 7-3 are the granite block, work surface and module indexing fixture provided for each partition. The work surface provides an inertially stable and level reference for orienting the module in its fixture into all six test positions.

The Rate Calibration Station (RCS) has been configured for production testing and therefore to support factory troubleshooting, a single axis rate table has been provided in the third partition of the Load Station.

Rate Calibration Station

The RCS is shown in figure 7-4. Rack 0 and 1 are essentially identical to those of the Load Station with the exception of the frequency measuring equipment. It is not required here and is deleted. Rack 2 has a unique SIU designed to interface with the 8 units under test. This interface is restricted to communication via the low frequency serial bus for transmittal of data and commands. The RCU of Rack 2 now houses a new complement of interfaces to service the multi-module SIU, Data, Display and Recording devices, and two rate tables. Rack 3 contains auxiliary printers and displays to support test monitoring without interfacing with test control displays of Rack 1.

High angular rate testing of large packages requires specialized rate tables. The proposed Rate Table, shown in figure 7-5 has high angular acceleration, and provides the accuracy and precision control required for rate testing. Currently Litton is using a version of the multi-gimbal table shown here. The table is capable of rates to $1000^\circ/\text{sec}$ and test packages to 34 kg (75 pounds).

Inertial Navigation Modules will be calibrated individually rather than in a 4-module system. Because of the high cost of the Rate Table, however, up to 4 modules will be calibrated in parallel. The orientation of the 4 INM's must be identical rather than rotated 90° from each other as in an aircraft installation. In order to fit 4 modules on the Rate Table, they should be mounted side-by-side. Therefore, the instrument block engagement should be at the rear, connector end of the unit rather than at the side as indicated in paragraph 6.2.10.

Burn-In Monitor (BIM)

The BIM supports the burn-in of two systems, 8 modules. The BIM station is configured similar to Racks 0, 1, 2, 3 and 4 of the Calibration Rate Station since both stations handle 8 units on a limited access basis. The BIM interfaces with an environmental chamber housing the systems under test. Fixtures within the chamber orient the systems and provide wrap-around of signals to allow self monitoring of input and output circuitry.

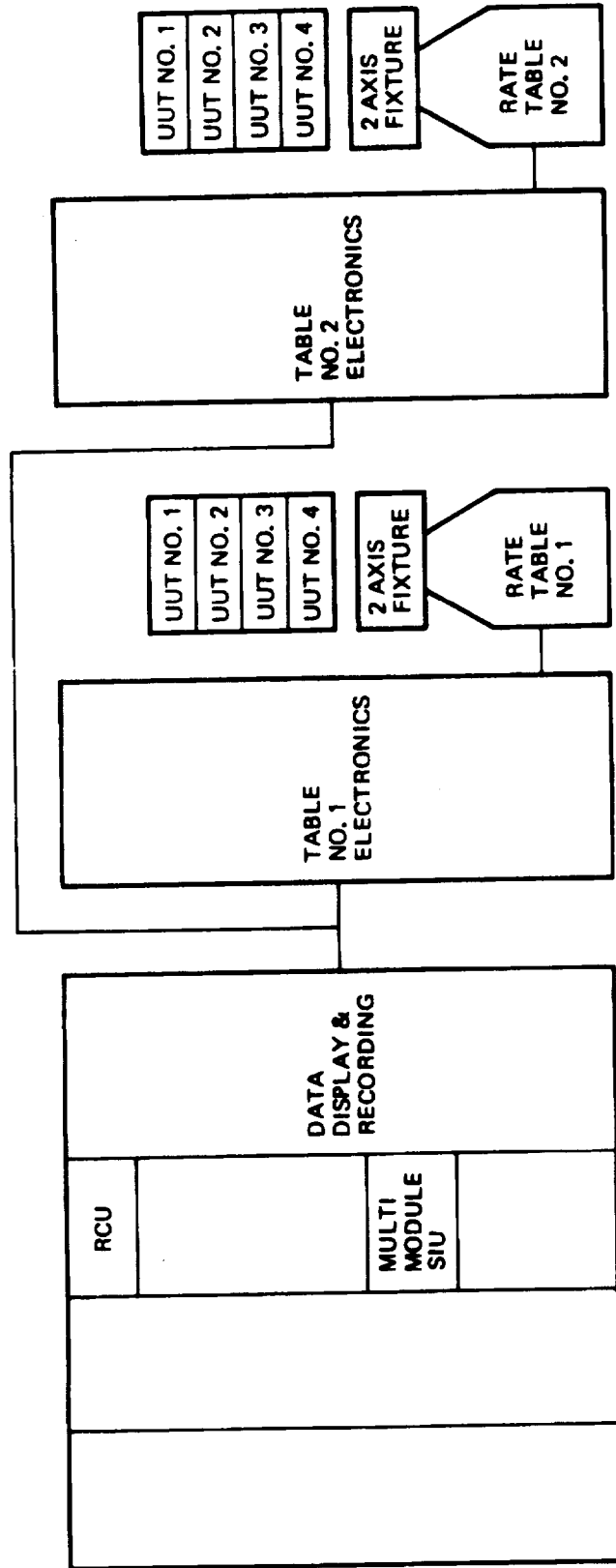
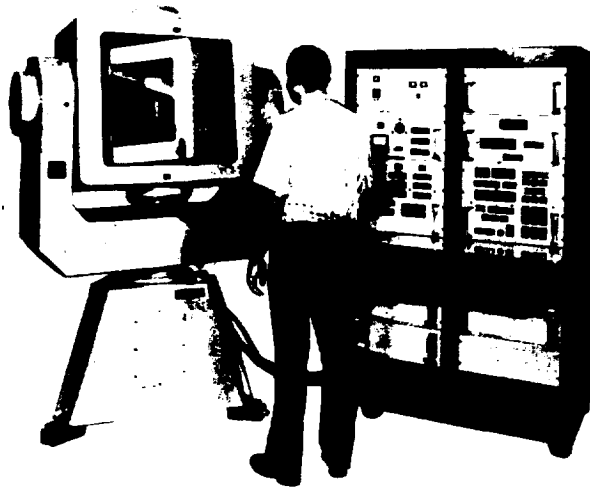


Figure 7-4. Rate Calibration Station



301 ALPHA DRIVE, PITTSBURGH, PA. 15238 • TEL. 412-782-3516 • TWX 710-864-2082



MODEL 555 THREE-AXIS AUTOMATIC TEST STAND

GENERAL

The Model 555 Three-Axis Automatic Test Stand is a multi-axis fixture designed to test inertial guidance and control systems. It is fitted with digital position transducers that allow the test stand to be operated by a variety of automatic control devices such as a digital computer or tape reader.

Motion about all axes is produced by direct drive DC torque motors. Rate control to 1,000 degrees per second about these axes is achieved by means of 0.1% ripple direct mounted DC tachometers. Three modes of automatic digital positioning and readout are available at ± 3 arc second accuracy and 0.0005 degree resolution up to 1,000 degrees per second, at 0.0001 degree resolution to 200 degrees per second, or a dual 0.001 and 0.0001 degree resolution system providing both 1,000 and 200 degrees per second maximum speed selection. A Scorsby motion generator is also provided.

The mechanical structure of the test stand is in the azimuth, roll, pitch axis configuration. Since slippings are provided for both stand components and the unit under test (UT) signal and power connections, continuous rotation capability is provided.

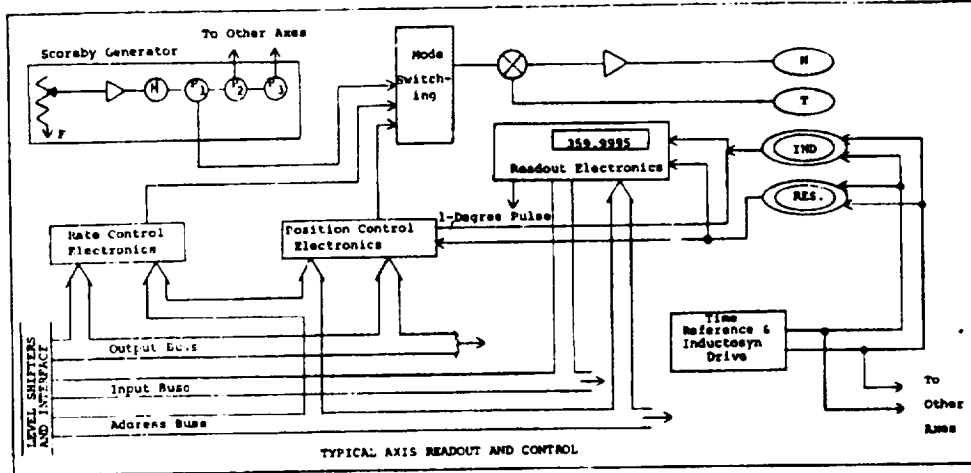
SPECIFICATIONS

Servo Components			
Azimuth	-----	22 ft-lb torque motor	
Roll	-----	Two 11 ft-lb torque motors	
Pitch	-----	7 ft-lb torque motor	
All Axes	-----	0.1% tachometer, 720-pole Inductosyn and 2-pole resolver	
Axis Inertia, Torque and Acceleration			
Inertia	----- (slug-foot squared)	Azimuth	100
Stall Torque	----- (ft-lbs)	Roll	34
Stall Acceleration	----- (rad/s ²)	Pitch	5
			6
			0.8
Orthogonality of Axes	-----		
Bearing Wobble	-----		
Intersection of Axes	-----		
Three Point Mounting	-----		
Range	-----		
Resolution	-----		
Trunnion Shaft Deflection	-----		
Test Package	-----		
Size	-----		
Weight	-----		
ELECTRICAL SPECIFICATIONS			
Slippings	-----		
Resistance Variation	-----		

D-150



Figure 7-5. Three Axis Automatic Test Stand



MODES OF OPERATION/SPECIFICATIONS

Position Mode
Range

Maximum Readout Speed	High Resolution	High Speed	Dual	
	200 degrees per second	1,000 degrees per second	200 degrees per second	1,000 degrees per second
Readout Range	A000.0000 to B359.9999 degrees	A000.0000 to B359.9995 degrees	A000.0000 to B359.9999 degrees	A000.0000 to B359.999 degrees

- Accuracy ----- ±3 arc second
 Stability ----- ±0.5 arc second
- Control
 Local ----- Front panel 7-decade thumbwheel switch plus Enter Command pushbutton for each axis
 Remote ----- Remote digital input per Report TR-2036
- Rate Mode
 Ranges ----- X1, X10, X100, X1000 degrees per second
 Resolution ----- 0.1% of full scale on each range
 Accuracy ----- 0.1% or 0.0001 degree per second whichever is greater averaged over 10-degree intervals or larger
- Control
 Local ----- Front panel 4-decade thumbwheel switch plus Enter Command pushbutton for each axis
 Remote ----- Remote digital input per Report TR-2036
- Scoreby Mode
 Sine Wave Motion ----- Applied to all three axes at a selected frequency
 Phase Shift ----- Adjustable between axes
 Amplitude Control ----- Provided independently for each axis
 Frequency Range Adjustment ----- 10/1
 Amplitude Range Control with a 10-Turn Potentiometer ----- 0.1 degree to 30 degrees
 Accuracy of Motion ----- ±0.1 degree from a perfect sine wave
 Frequency Range ----- 10 cycles per minute to 1 cycle per minute
- Angle Encoding System
 Transducer
 Fine ----- 720-pole, ±2 arc second Inductosyn
 Coarse ----- 1-speed Resolver
- Absolute Angle Encoding System
 Rate Range ----- (0 to 1,000 degrees per second)
 a) Accuracy and Stability ----- 1.8 arc second
 b) Quantisation ----- High Resolution System - 0.36 arc second
 ----- High Speed System - 1.8 arc second
 ----- Dual System - 0.36 and 3.6 arc second
 c) Velocity Error ----- 0.2 arc second per radian per second
 (When sampled at submultiples of reference frequency)
 d) Output Display ----- High Resolution System - 0.0001 degree to 359.9999 degrees absolute angle
 ----- High Speed System - 0.0005 degree to 359.9995 degrees absolute angle
 ----- Dual System - 0.0001 or 0.001 degree to 359.9999 or 359.999 degrees absolute angle
- e) Position Pulse Outputs ----- (Available up to 1,000 degrees per second)
 Pulse Width ----- 1 usec
 Intervals ----- 1-degree intervals
 Accuracy ----- ±0.5 arc second, +0, -0.4 millisecond
- f) Digital Output ----- Available for transfer to a digital computer. Outputs are transferred to a data bus on receipt of an address and freeze command per Report TR-2036.

7.2 G-6 Gyro Test

7.2.1 G-6 Process Flow

A projected G-6 gyro process flow is shown in figure 7-6. This process flow is then used to determine projected factory test equipment requirements. The G-6 gyro design is very similar to the Litton G-1200. Present production test equipment was used as the basis for this description, with redesigns and modifications as required to meet the needs of the G-6.

7.2.2 G-6 Test Stations

a. G-6 Final Test Station

List of Tests

- Measure pickoff parameters (ln, P O SF, P O Offset, etc.)
- Measure torquer parameters (SF, axis align)
- Measure rotor and flexure parameters (G and Non-G sensitive, drift and repeatability, random drift, resonant frequency etc.)
- Measure motor parameters (watts start/run, milli-watts with torquer-bearing quality, run-up time, etc.)
- Rapid reaction (if any).
- Time constant, etc.
- Possibly a limited rate table test capability.

Description

Uses a computer data acquisition system (standard module), and automatic table to collect and reduce data. All excitations are under computer control. KSR 33 keyboard and printer provide the final data printout, and operator control. Temporary data, operator instructions, UUT status and test station condition are displayed on a CRT.

b. Flexure Frequency Station

List of Tests

- Test for the value of the natural resonant frequency of the G-6 rotor flexure.

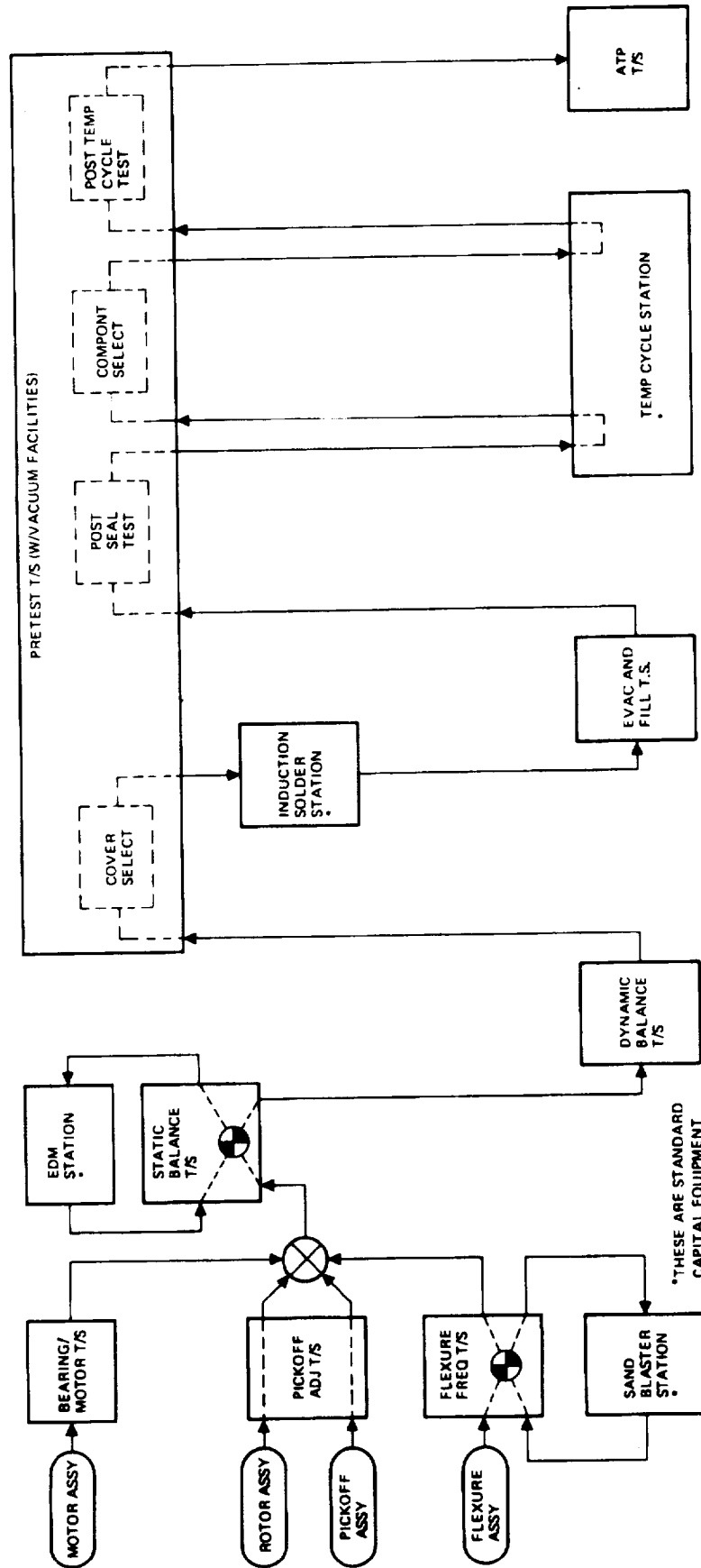


Figure 7-6. G6 Factory T/E Process Flow

Description

Contains vibration exciter and photonic displacement sensor to create a closed loop system with the flexure. Frequency counter readout and functional electronics are included.

c. Pickoff Adjustment StationList of Tests

- Takes data required to determine dimensional and magnetic properties of rotor pickoff surfaces.
- Measures pickoff assembly parameters.
- Provides test verification capability after lapping.

Description

Uses master rotor and master pickoff elements (permanently mounted to fixtures). Provides a plotter output to chart the rotor characteristics. Includes PAVM and PO excitation electronics. Lapping facilities must be provided to augment this station.

d. Pretest StationList of Tests

- Cover select.
- Component select.
- All ATP tests.

Description

Contains a full set of electronics to spin, capture and temp control (if required) the gyro. Measurement capabilities include: P O parameters, torquer parameters, spin and motor parameters, temperature sensitivity parameters and are provided through use of a data acquisition system (standard module) and computer. No shake capability is included. Vacuum backfill capabilities are included. The station will operate semi-automatically. The CRT will display manufacturing test procedures for manual operations. Analog strip chart recording (or plotter) can be provided as augmenting data.

e. Evacuation and Fill StationList of Tests

- Provide "bakeout".
- Purge.
- Final backfill.
- Seal.
- Leak check.

Description

This station is similar to the G-1200 evacuation and fill station in system capabilities but different in design.

f. Static Rotor Balance StationList of Tests

- Collect data to determine static values of radial, mass, etc., rotor unbalance.
- Determine equivalent dynamic values.
- Reduce data and determine position and amounts of material that must be removed to meet rotor balance specifications.

Description

This station contains a computer or calculator to collect and reduce data. It controls the test for consistency, provides printout of how much material to remove, where, and the final static parameter values. Equivalent dynamic values are also printed. Modules include the data acquisition system (standard panel), temperature control (fixture), test cube or auto table, loop closure electronics and augmenting functional electronics.

g. Dynamic Balance StationList of Tests

- Adjust radial unbalance of motor.

Description

A Schenk dynamic balance machine is used for measurement and verification after adjustment. The station also contains a spin supply, a mounting fixture, and a control panel.

h. Motor Test and Run-In StationList of Tests

- 100 hour run-in of 18 gyro's simultaneously.
- Data collection of milliwatt meter data for bearing evaluation throughout run-in.
- Temperature monitor throughout run-in.
- Self logging of elapsed time on each gyro.

Description

This station uses a minicomputer or microprocessor as a test controller and data organizer. A high speed data acquisition system (proposed throughout this gear and is a standard module) is used to scan all 18 gyro positions for millivolts, temperature, and elapsed time. This spin supply is a square wave with individually controllable output stages (18). An historical window of data (e.g., 30 minutes) is stored in case of power failure, or in the event a gyro is "seen" as bad. All data available can be dumped on a KSR 33 (thermal printer with keyboard). An xy plotter may be included to yield the effect of a stripchart recorder output for the last hour of each gyro run-in.

i. Resistance and ContinuityList of Tests

- Resistance test of all circuits.
- Hi-pot insulation resistance tests.
- Intercircuit short test.

Description

This station is similar to the G-1200 Resistance and Continuity station.

7.3 A-1000 Accelerometer Test

The A-1000 accelerometer is a production design. The redundant strapdown INS accelerometers will use the test procedures and equipment currently in use with minor modifications. Descriptions are not supplied as part of this study since the technology is not new.

VIII. COST ANALYSIS

8.1 Baseline Cost Estimate

Table 8-1 is an itemized breakdown of the projected cost of the redundant strapdown INS as described in Sections V and VI, and tested with Factory Test Equipment similar to that shown in Section VII.

TABLE 8-1. REDUNDANT STRAPDOWN INS PREDICTED
AVERAGE COST, 200 SYSTEMS

<u>ELEMENT</u>	<u>COST (1976 \$)</u>
GYRO	4,331
ACCELEROMETERS (2)	3,751
COMPUTER/MEMORY	3,697
BLOCK/REBALANCE ELECT.	2,862
MODE/IMM I/O	1,252
INTERNAL/EXTERNAL I/O	2,246
POWER SUPPLY/INTERRUPT	3,864
CHASSIS	<u>2,481</u>
	<u>TOTAL, PER CHANNEL</u>
	24,484
TOTAL SYSTEM	97,936
SYSTEM LESS MOUNT	95,560

"Cost" is defined as cost to an airline based on 1976 dollars. Therefore, the estimate of table 8-1 includes not only the average cost to build 200 INS (800 channels), but also an estimate of amortized development, production tooling, and test equipment costs. The amortization schedule also includes delivery of redundant strapdown INS equipment to other users beyond the requirements of short-haul VTOL. The total build of systems is assumed to be similar to the quantity of first-generation, commercial inertial systems, LTN-51, built by Litton to date. Approximately 14% of the net cost is due to this amortization.

Cost items generally incurred by airlines but not included in this total cost estimate are warranty, training and maintenance. These are somewhat variable, depending upon customer requirements.

8.2 Basis of Estimate

The cost estimate was prepared from an estimated bill of material of electronic components and the preliminary chassis design shown in paragraph 6.1.10. Component costs were then estimated from the current catalog prices of these or similar items. Some limited extrapolation of prices was needed based on cost trends (not including inflation) especially in the area of digital circuits. Material costs are then factored to include line-flow, attrition and common stores items.

Allocation of components to printed circuit cards was made, from which assembly and test hours were derived. Cost of assembly and test labor also included factory allocables such as manufacturing engineering, production control, quality assurance, test equipment maintenance and sustaining design engineering.

The chassis mount costs were spread among the various system elements, based on the ratio of that element's cost to total channel cost. System cost excluding the chassis mount is also shown in table 8-1. Some form of installation provisions would probably be supplied by the airframe designer in many applications.

An estimate was then made of the total developmental cost of the redundant strapdown INS including productionizing the design, environmental and EMI testing, handbooks, software, etc. Cost of design or modification of test equipment and production tooling was estimated as well as the procurement or build of a sufficient quantity of items needed to support the production rate.

The total sum of development, tooling and test equipment was then amortized over an assumed number of systems, with the amortized amount then added to unit production cost. The amortized amount added to each system element was based on the ratio of that element's build cost to total channel build cost. Final element costs include a factor for profit.

8.3 Cost Reduction Prospects

One area of potential system cost reduction is in the use of less accurate gyros. Use of the Litton G-7 gyro instead of the G-6 could reduce system cost by nearly \$3,000. A more sophisticated filter combining radio and inertial data would be needed, however, as described in Section 5.2 and paragraph 4.5.2.

Further cost reduction may be obtainable from the advancements of digital technology. No attempt will be made to quantify such a reduction, however.

403314

APPENDIX A
REDUNDANT STRAPDOWN INERTIAL
NAVIGATION SYSTEM SPECIFICATION

DEVELOPMENT SPECIFICATION
REDUNDANT STRAPDOWN INERTIAL NAVIGATION UNIT

1. SCOPE

1.1 Identification

This specification establishes the design requirements for a low-cost, twice fail-operational redundant strapdown inertial navigation unit, using two-degree-of-freedom, tuned-gimbal gyroscopes.

1.2 Introduction

Improved integration of the various aircraft avionics functions can lead to significant aircraft cost reductions. Sharing of sensors between navigation and flight control functions, and sharing of computers by navigation, flight control and air data functions, tends to produce a low system cost with improved capability. Modern fly-by-wire aircraft using such a system require extremely high reliability to achieve sufficient flight safety. The specified redundant strapdown INS achieves the required reliability. It is initially directed toward short haul VTOL aircraft but shall be designed to be applicable to the full range of civil and general aviation. Low cost is a firm design objective.

2. APPLICABLE DOCUMENTS

2.1 The following documents, of the issue in effect on the date of invitation for bids or request for proposal, form a part of this exhibit to the extent specified herein.

SPECIFICATIONS

TITLE

ARINC 404

Specification, Air Transport Equipment
Cases and Racking

<u>SPECIFICATIONS</u>	<u>TITLE</u>
ARINC 413	Report, Guidance for Aircraft Electrical Power Utilization and Transient Protection
ARINC 414	Project Paper, General Guidance for Equipment and Installation Designers
ARINC 571	Characteristic, Inertial Sensor System (ISS)
ARINC 575	Characteristic, Mark 3 Sub-Sonic Air Data System (Digital) DADS
RTCA Paper 120-61/DO-108	Environmental Test Procedures, Airborne Electronic Equipment

3. REQUIREMENTS

3.1 Item Definition

The redundant strapdown inertial navigation unit, hereinafter referred to as INU_{RS}, shall provide multiply redundant sensing of inertial quantities and redundant output of aircraft states (angular rates, linear accelerations, attitude, heading, velocities, position coordinates) to other avionics. Essentially, inertial sensing devices, gyros and accelerometers, shall be rigidly mounted to the airframe (strapped down), without intervening gimbals. The INU_{RS} shall be capable of withstanding any combination of two failures without degradation of system performance. It shall also be capable of accepting position and velocity updates from external avionics.

3.1.1 System Diagrams

The complete INU_{RS} shall consist of four identical and interchangeable channels, as shown in the system block diagram, figure A-1. Each channel, designated an inertial navigation module (INM), consists of the following elements.

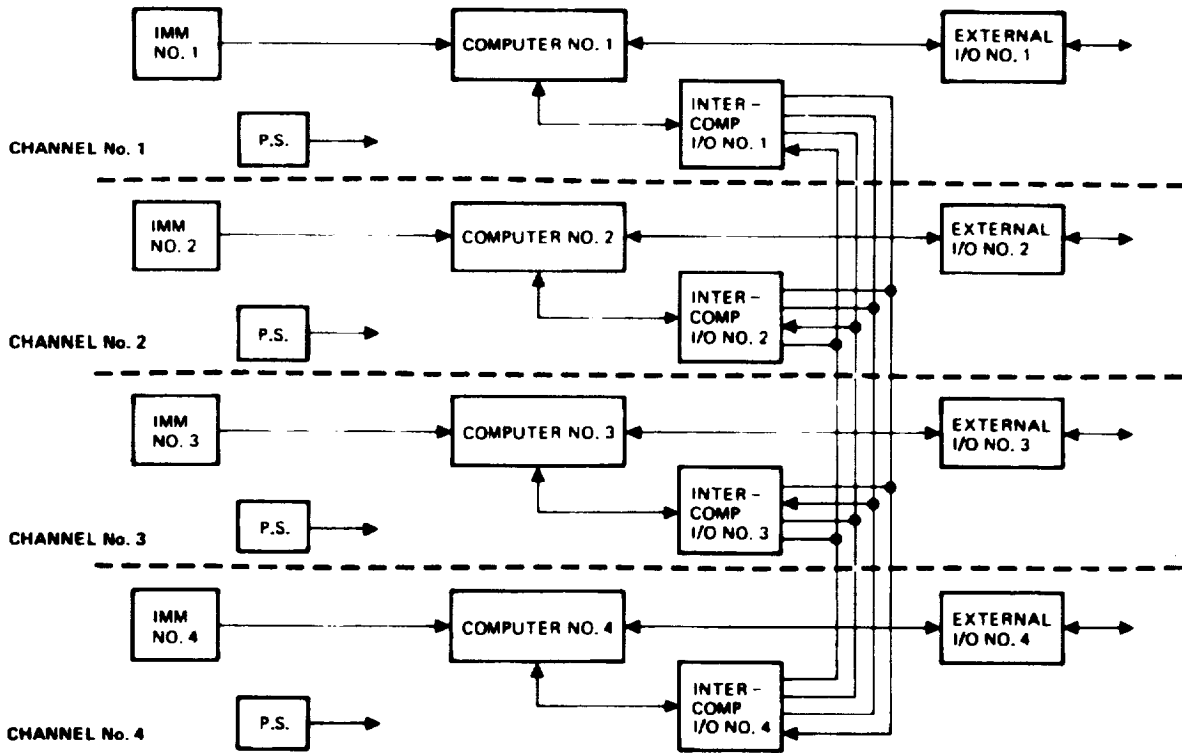


Figure A-1. Redundant Strapdown INS

- a. An Inertial Measurement Module (IMM) with one two-degree-of-freedom tuned gimbal gyroscope and two axes of acceleration measurement with associated electronics to provide digital outputs.
- b. A general purpose digital computer including low cost, semiconductor memory.
- c. Digital I/O for two-way communication with external avionics.
- d. Digital I/O for read-capability of other INM's.
- e. Power supplies, clock generators, and other support electronics needed for proper INM operation.

The gyro and accelerometers of each INM shall be skewed relative to INM axes. When the 4 INM's are installed into a common mount, rotated 90° relative to one another, the 4 gyro spin axes shall be normal to four non-parallel faces of an octahedron.

Fail-operational/fail-operational capability is obtained since if two complete channels fail, two channels remain and these are sufficient to derive the required three axes of output data. Redundancy management shall be contained in the software in each computer and in external equipment using the INU_{RS} data.

Software implementation in the four computers shall be mechanized as shown in figure A-2. Software functions shall be as follows:

- a. Read-in gyro data, accelerometer data, and calibration constants.
- b. Compensate measured angular rate and acceleration using the input calibration constants and known gyro characteristics, and then transform measurements from skewed axes to aircraft body axes.
- c. Solve parity equations which allow extraction of measurement errors from vehicle angular rates and linear accelerations, process outputs to detect and isolate failed instruments. Failure detection and isolation (FDI) results shall be combined with self-test results to determine instrument status.

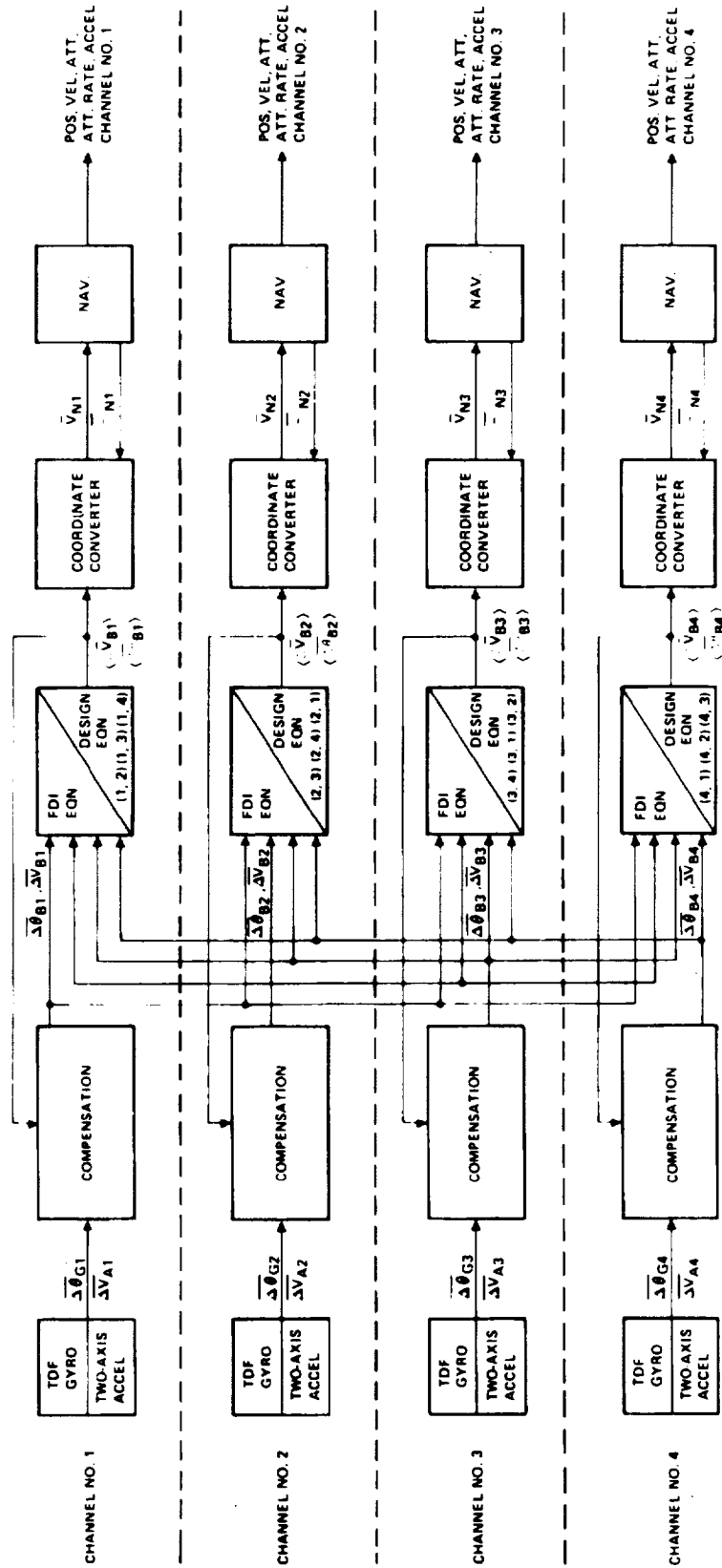


Figure A-2. Four-Channel Software Mechanization

- d. Combine outputs of two gyros and two pairs of accelerometer outputs in a least-squares solution in the design equations to derive three axes of acceleration and angular velocity, in aircraft coordinates. The selection logic of instruments shall be based on use of the local channel's instruments plus another channel's inputs, the next cyclic* channel number satisfying FDI/self-test.
- e. Perform integration of angular rate inputs to determine the transformation from aircraft coordinates to navigation coordinates, and resolve accelerometer outputs through this transformation.
- f. Solve inertial navigation equations to derive required outputs and derive inertial rate of the navigation coordinate system to rotate the aircraft-to-navigation coordinate transformation.
- g. Perform additional functions such as software executive control, ground gyrocompassing alignment, initialization and update from a display or external computer, self-test and cross-fed output table comparisons, redundancy management reinitialization, and gyro bias trimming based on entered latitude and longitude and terminal errors.

In order to avoid time-skew errors, the executives of each of the four computers shall be driven by an interrupt, and the four computer interrupts shall be synchronized by fail-op/fail-op circuitry contained within each INM.

The INU_{RS} shall be capable of operation as a fail-op navigator with installation of only three INMs.

* Cyclic is defined as the ordered sequence of channel numbers, e.g. 1,2,3,4,1,2

3.1.2 Interface Definitions

Output requirements are as follows:

CATEGORY	QUANTITY	RESOLUTION	RANGE	BITS	CYCLE TIME
Attitude	Pitch (Elevation)	$2\pi/2^{15}$	$\pm\pi/2^*$	14	0.03125
	Roll	$2\pi/2^{15}$	$\pm\pi$	15	0.03125
	Heading, true	$2\pi/2^{15}$	$\pm\pi$	15	0.03125
Attitude Rate	Pitch Rate	0.05°/sec	± 4 rad/sec	14	0.03125
	Roll Rate	0.05°/sec	± 4 rad/sec	14	0.03125
	Yaw Rate	0.05°/sec	± 4 rad/sec	14	0.03125
Body** Acceleration	Longitudinal Accel.	0.003 m/sec ²	± 10 g	11	0.03125
	Lateral Accel.	0.003 m/sec ²	± 10 g	11	0.03125
	Vertical Accel. (body)	0.003 m/sec ²	± 10 g	11	0.03125
Navigation Outputs	North Velocity	0.03 m/sec	± 1686 m/sec	16	0.125
	East Velocity	0.03 m/sec	± 1686 m/sec	16	0.125
	Vertical Vel. (earth)	0.03 m/sec	± 1686 m/sec	16	0.125
	Latitude	$2\pi/2^{19}$	$\pm\pi/2^*$	18	0.5
	Longitude	$2\pi/2^{19}$	$\pm\pi$	19	0.5
	Altitude	0.3 m	-305 m to 18.3 km	16	0.5
Other	Mode/Status	N/A	N/A	16	0.03125

*These outputs are generally scaled at $\pm\pi$.

**Installation is assumed to be at the aircraft center of gravity so lever-arm accelerations are not included.

These outputs shall be provided separately from each INM on an ARINC 575 format serial data channel. An additional discrete

relay closure shall be provided from each INM to indicate normal INM operation, opening during a failed or off condition.

Three ARINC 575 receivers shall be provided in each INM. One receiver shall be used to input aircraft barometric altitude with resolution, range, and cycle time TBD. The second receiver shall be used to input a system mode word, and position and velocity updates with resolution, range, and cycle time TBD. The third receiver shall be for growth purposes.

A discrete input shall be provided to each INM by means of external jumper wires to identify the channel number to software for use in skewed-axis to aircraft-axis transformations and parity equations. Two additional jumper wires shall be monitored to determine $\pm 90^\circ$ installation from the nominal orientation described in paragraph 3.2.2.1.

3.1.3 Inter-Channel Interface

The following variables shall be received by each channel from the other three channels:

- Compensated velocity increments (3)
- Compensated angular increments (3)
- Attitude matrix, e.g., quaternions (4)
- Vehicle velocity components (3)
- Navigation direction cosines (6)
- Inertial altitude
- Accumulated velocity updates (2)
- Accumulated position updates (2)
- Output table (15)
- Status

Some variables require transmission of more than one computer word to obtain sufficient precision. Transmission of all 37 variables shall be completed in 1/128 second. Transmission of the

first six variables shall be completed within 50 microseconds after initiation of transmission. Scaling and resolution are TBD.

3.1.4 Major Components

The INU_{RS} shall consist of four interchangeable line replaceable INM and one chassis/mount. The chassis/mount shall contain provisions as follows:

- a. A shell to house the four INMs.
- b. A central alignment block to register the INM gyros and accelerometers to each other.
- c. Attachment for four aircraft cable connectors, one for each INM.
- d. A latching mechanism to hold each INM into the chassis mount, provide connector engagement between the INM connector and the aircraft connector, and lock the INM instrument block to the central alignment block.
- e. Attachment for aircraft cooling methods.
- f. A plenum for even distribution of cooling air through the 4 INM's.
- g. Provisions for bolting the INU_{RS} to the aircraft and providing for boresight alignment of the central alignment block to the aircraft axes.

3.2 Characteristics

3.2.1 Performance

3.2.1.1 Modes of Operation

The basic operating modes of the INU_{RS} are as follows:

- | | |
|-------|--|
| OFF | All power is removed from the system. |
| ALIGN | Automatic sequencing through the various steps needed for alignment shall be provided. The align mode is initiated only on the ground. Automatic transfer to |

- ALIGN (cont) the navigate mode shall occur if aircraft motion is detected via the INS accelerometers.
- NAV All outputs shall be provided to full accuracy in this mode.
- ATTITUDE Consideration shall be given to use of a pendulous attitude mode in flight during certain failure conditions if the end reliability of attitude and attitude rate outputs can be improved.

These modes are mutually exclusive and, with the exception of ATTITUDE, are selected from an operator's panel external to the INU_{RS}. The ATTITUDE mode, if provided, shall be selected by redundancy management software in the event of a third channel failure.

Other software-controlled operating modes shall be provided.

These are:

- UPDATE Accept position and velocity coordinate errors (4) and correct INU_{RS} outputs. Provide growth capability for tilt, heading, and gyro bias updates. Updates will be made asynchronously, with a minimum time duration of 1 second between updates.
- RECON-FIGURE Based on results of FDI and self-test, change selection of instrument channel number being used in design equation solution. Reuse of a previously failed channel shall be provided if it again satisfies FDI thresholds.
- REIN-INITIALIZE A computer shall reinitialize its attitude transformation, velocity, and position calculations to another channel's values following reuse of a previously failed channel, including one that was removed and replaced during maintenance. In addition, consideration shall be given to reinitialization under the following conditions:
- a. Following any channel reconfiguration activated by FDI provisions.
 - b. Following detection of a large error in software output tables, which may have been caused by a computer transient.

3.2.1.2 Accuracy

The INU_{RS} shall have the following output accuracy:

Attitude rate	0.05°/sec, rms, per axis
Body acceleration	0.003 m/sec ² , rms, per axis
Attitude	0.1°, rms, per axis
Heading	0.2°, rms, VTOL flight profile
	TBD°, rms, CTOL* flight profile
Velocity (no updates)	3 m/sec/axis, 1σ, VTOL flight profile
	TBD ft/sec/axis, 1σ, CTOL flight profile
Position (no updates)	7.4 km/HR, CEP, VTOL flight profile
	TBD NM/HR, CEP, CTOL flight profile

This accuracy shall apply with either 0, 1 or 2 hardware failures, through the operational environment described. It is assumed that aircraft installation errors are not included, aircraft parking coordinates have been entered perfectly, and a full gyrocompassing alignment has been completed at a latitude of 45° prior to first aircraft motion.

3.2.1.3 Ground Alignment Time

The redundant strapdown INU shall complete its self-contained alignment in less than 10 minutes from system turn-on. No external inputs shall be required, with the exception of aircraft latitude and longitude entered within two minutes after system turn-on. Aircraft motion during alignment shall consist of the model described in Paragraph 3.2.5.2.3. The alignment time required applies for a starting ambient temperature greater than 0°C and less than 50°C and for a latitude less than 70°.

* Conventional take-off and landing aircraft.

3.2.1.4 Redundancy Management

3.2.1.4.1 Redundancy Management Logic

Redundancy management logic shall consist of the following:

- a. A computer shall always use the instruments within its own INM chassis.
- b. A computer's output calculations shall be based on only two channels of instrument data.
- c. The second channel used in a given calculation shall be the next working cyclic channel number.
- d. Accelerometer and gyro redundancy management shall be independent of each other except for major failures detected by self-test.
- e. Detection and isolation of a failure of one axis of a channel shall cause rejection of both axes of data, except (a.) supersedes.
- f. An instrument's outputs shall continue to be monitored following its rejection, but not included in output calculation, except (a.) supersedes.
- g. If a failed instrument returns to working condition as determined by FDI, it shall be reinstated into output calculations, based on normal instrument selection logic. The computer of the same channel number of the reinstated instrument shall reinitialize to the state of a non-failed channel.
- h. Logic shall be incorporated to detect and isolate two simultaneous failures within information limits of a 4-gyro skewed array.
- i. During the condition of isolation ambiguity, monitoring shall continue. A status word output shall indicate presence of a failure and approximate magnitude.
- j. Indicated instrument failures shall be placed into 3 categories:
 - a. HARD - inoperative (self-test)
 - b. GF₃ - nav and flight control failure
 - c. GF₂ - nav failure

- k. Instruments with category HARD failures shall never be reused even if failure condition disappears.
- l. Instruments with category GF₃ failures should be used following a third channel failure or to resolve a category GF₃ 3-gyro isolation ambiguity

3.2.1.4.2 Error Detection/Switching Levels* and Time

The levels which shall be used in the FDI mechanism to indicate failure of an instrument are given in table A-I. An instrument error and its integral are shown. The threshold error is the minimum detectable instrument error. The error integral, e.g., angle delta or velocity delta, may be used to determine the time to detect large errors. FDI solution time shall be sufficiently fast that errors greater than these amounts do not reach system outputs regardless of instrument error amplitude.

TABLE A-I. PRELIMINARY ERROR DETECTION/SWITCHING LEVELS PER INSTRUMENT

FAILURE TYPE	GROUND	FLIGHT NO TURNS	FLIGHT TURNS
NAV FAILURE			
Acceleration Threshold	0.003 m/ sec ²	0.001 m/ sec ²	TBD
Velocity Delta	1.5 m/sec	4 m/sec	TBD
Angular Rate Threshold	0.1°/hr	1°/hr	TBD
Angle Delta	30 $\overline{\text{sec}}$	60 $\overline{\text{sec}}$	TBD
NAV/FLT CONTROL FAILURE			
Acceleration Threshold	N/A	0.03 m/ sec ²	0.03 m/sec ²
Velocity Delta	N/A	12 m/sec	12 m/sec
Angular Rate Threshold	N/A	1°/sec	1°/sec
Angle Delta	N/A	1°	1°

* Detection/switching levels indicated in the table are approximate. Further testing and/or analysis are needed to establish reasonable levels. Corrective maintenance action will occur if one or more nav failures is indicated before takeoff.

3.2.1.4.3 Performance Transients

System error buildups following occurrence of a failure, but before FDI action, shall be minimized. Performance shall return to normal following redundancy management actions.

3.2.1.5 Performance/Environment

A typical flight profile for the VTOL application consists of:

- a. System turn-on at 20°C, start alignment, passenger loading/refueling in progress, aircraft subject to wind gusts, ground power applied to the aircraft.
- b. Engine turn-on after five minutes.
- c. System advanced to Navigate Mode after 10 minutes, remove ground power
- d. Engage rotors, perform vertical take-off.
- e. Climb to 305 m altitude, turn left 90° at a turn rate of 3°/sec.
- f. Accelerate to 103 m/sec and cruise for 6 minutes.
- g. Turn left 90° then spiral down at turn rates of 3°/sec. (typical peak turn rate of 30°/sec).
- h. Decelerate and perform vertical descent to touchdown.
- i. Disengage rotors, unload/reload passengers for 3.5 minutes.
- j. Repeat d thru h two additional times, then turn off system power.

The non-VTOL applications are assumed to have the flight profile as follows:

- a.)
- | } Same as above
- c.)

- d. Take-off, climb to 9,000 m altitude, accelerate to 257 m/sec.

- e. Turn left 90° at a turn rate of 3°/sec.
- f. Cruise for 2 hours with two 10° course changes at turn rates of 1°/sec.

The required and desired aircraft operational performance limits are:

	<u>VTOL</u>	<u>CIVIL OR GENERAL AVIATION</u>
Angular Rates	4 rad/sec	4 rad/sec
Angular Acceleration	50 rad/sec ²	50 rad/sec ²
Linear Accel. (maneuver)	±3 g	±3 g
Velocity (max.)	154 m/sec	1029 m/sec
Altitude	3048 m	18,300 m
Aircraft tilt (parked)	±5°	±5°
Range of operation (latitude)	±70°	Worldwide

3.2.1.6 Power

The aircraft power supply characteristics, utilization and general guidance, are given in ARINC 413. The redundant strap-down INU shall be designed to use 115V AC single phase power, per MIL-STD-704, Category B. A separate input shall be utilized for each redundant power supply.

Capability of operation from an external battery, equivalent to Sonotone P/N CA-51N, shall be provided with each redundant power supply. In addition, each supply shall contain a battery charger, as required by ARINC 561. The redundant strapdown INS shall also have the capability of operating from redundant standby computer DC buses for backup power, as defined in ARINC 571, paragraph 2.4.5.1, in lieu of the battery.

Maximum average power drawn by each INM during flight conditions shall be under 150 watts. The chassis/mount shall require no power.

3.2.1.7 Cooling

Cooling air having the characteristics of ARINC 404 may be utilized if required. Maximum cooling air flow shall be 14 kg/hour/100 watts. Cooling air attachment method, if other than that specified in ARINC 404, shall be TBD.

3.2.1.8 Operational Service Life

The redundant strapdown INS shall be capable of operation for at least 3,000 hours, preferably 5,000 hours, without additional lubrication, adjustment or replacement of components (per ARINC 414). Scheduled calibrations required to be performed during Level 2 maintenance, shall be minimized.

3.2.1.9 Built-In Self-Test

Minimum self-contained self-test features shall be incorporated within each INM:

- To prevent chain-type failure modes which could lead to extensive equipment or aircraft damage.
- To provide a high level of capability of detecting failures of each gyro to reduce the probability of a failure occurring within the 3-gyro isolation singularities.
- To contribute to making the third failure a fail-safe condition, that is, to indicate to the aircraft flight crew that a failure has occurred.
- To provide information to maintenance personnel for use in determining the failed module for repair.

3.2.2 Physical Characteristics

3.2.2.1 Inertial Measurement Skewed Axis Geometry

Figure A-3 shows the nominal orientation of the accelerometer and gyro input axes, and gyro spin axes relative to aircraft axes. The angles between axes shall be as determined by the faces of

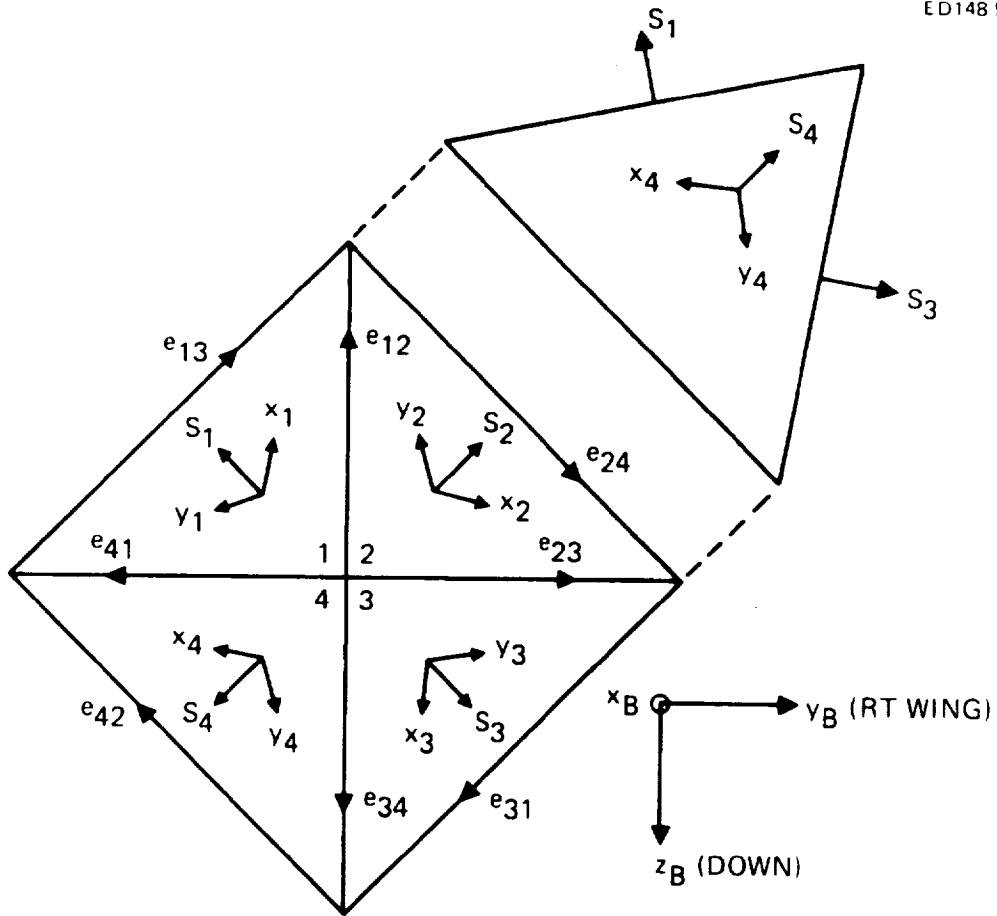


Figure A-3. Inertial Measurement Axis Geometry (Nominal)

half of a regular octahedron. The two orthogonal gyro/accelerometer input axes shall be oriented symmetrically relative to the outside edge of the octahedron.

Normal orientation of the octahedron relative to aircraft axes is shown in figure A-3. Some applications may require installation into the aircraft with the INU_{RS} rotated $\pm 90^\circ$ about z_B from the nominal. Means of computing the outputs in either rotated installation shall be provided by means of jumper wires on the INM connectors.

3.2.2.2 Dimensions

The maximum INU_{RS} dimensions are shown in figure A-4. These dimensions do not include protrusions such as handles, latching mechanisms, connectors, or boresight adjustment provisions. They do include the holding chassis/mount.

3.2.2.3 Weight

The weight of the INU_{RS} shall not exceed 32 kg. The weight of each INM shall not exceed 7 kg.

3.2.2.4 Alignment Repeatability

The angular alignment between the instrument blocks of adjacent INM's shall be $90^\circ \pm 30$ arc seconds (3 sigma). This alignment shall be maintained following repeated insertions of each INM, and through the environments specified in paragraph 3.2.5. Removal and replacement of one INM shall not disturb the alignment of the remaining three.

The angular alignment between the alignment block and aircraft axes shall be capable of being boresighted to, and maintaining through the environments of paragraph 3.2.5, an accuracy of ± 12 arc minutes in pitch, roll, and yaw.

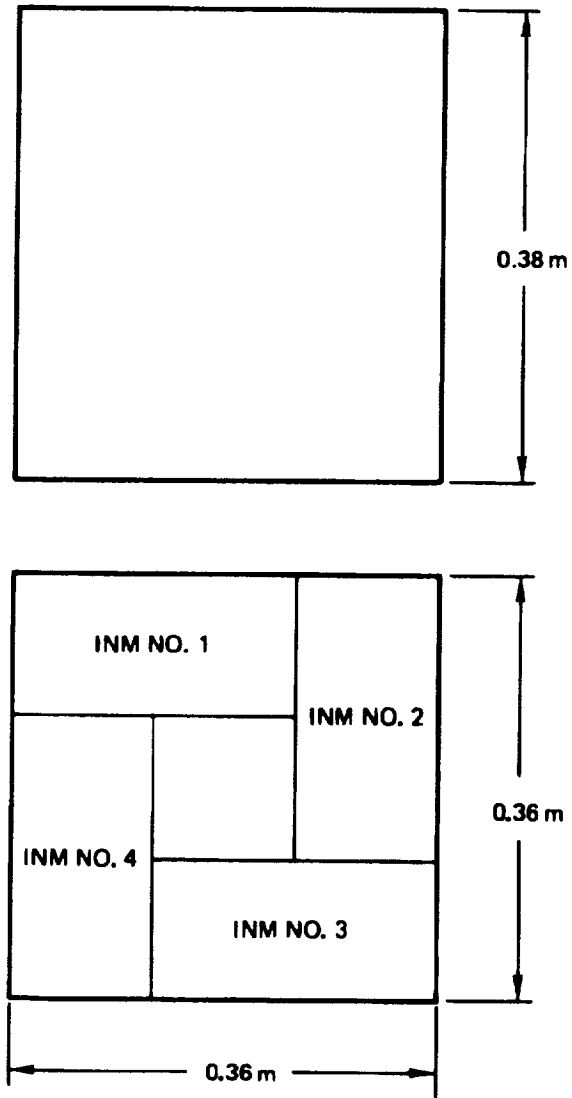


Figure A-4. INU_{RS} Installation Dimensions

3.2.2.5 Packaging of Redundant Elements

The four INM's shall each be packaged into a separate housing. The chassis mount shall provide EMI, thermal, and as much mechanical shielding between INM's as practical within weight and size limitations, to reduce the probability of multiple INM failures due to a single cause. There shall be no electrical interconnection between INMs within the confines of the INU_{RS} envelope.

It is assumed that the aircraft designer will locate the INU_{RS} away from the path of rotating machinery such as engines or APUs which might shed debris during certain failure modes.

3.2.3 Reliability

The probability of failure of the INU_{RS} during a 0.5 hour flight, assuming no failures are present at takeoff, shall be less than 10^{-9} , including effects of self-contained FDI coverage.* A failure is said to occur when undetected or unisolated gyro or accelerometer errors exceed the navigation performance detection levels given in table I of paragraph 3.2.1.4.2. Coverage of FDI capability external to the INU_{RS} shall be assumed to be unity for both fail-op levels.

The probability of failure of the attitude rate and acceleration outputs of the INU_{RS} during a 1.0 hour flight, assuming no failures are present at takeoff, shall be less than 5×10^{-10} , including effects of self-contained FDI coverage. A failure is said to occur when undetected or unisolated gyro or accelerometer errors exceed the flight control system performance detection levels given in table I of paragraph 3.2.1.4.2. Coverage of FDI capability external to the INU_{RS} shall be assumed to be unity for both fail-op levels.

* Coverage is defined as the probability of recovery from a given failure.

Provisions for reliability improvement by use of external radio aid update information to resolve the rare 3-gyro isolation ambiguity shall be included. Increased coverage from this means shall not be included in the previous INU_{RS} reliability calculations.

The mature in-service MTBF of each INM shall be greater than 3000 hours.

3.2.4 Maintainability

3.2.4.1 Maintainability Design

Plug-in assembly construction shall be used to the greatest extent practical. All modules bearing the same part number shall be interchangeable. As a goal, electronic modules shall not require adjustment or recalibration after replacement. Care should be exercised in locating and mounting of modules and components for ease of accessibility.

Each aircraft-replaceable unit shall have a failure indicator, visible from the front panel which indicates that one or more of the internal modules has failed. This indication shall be present with or without power applied to the system and shall only be reset after repair.

Highly reliable self-test shall be included, consistent with redundancy management requirements. All self-test provisions shall be continuous and automatic, with no pilot-initiated tests.

Sufficient unit test points shall be included to allow fault isolation to the module level using factory or field test equipment. Module test points shall be provided to allow fault isolation to the failed component without probing.

3.2.4.2 Maintainability Specification

The time to remove and replace an INM in the aircraft, assuming adequate accessibility, shall be less than one minute,

including mechanical alignment registration as defined in paragraph 3.2.2.4. Normal functioning of the other three INMs shall not be disturbed during this process.

3.2.4.3 Adjustments

Manually-activated on-aircraft adjustments, alignments or calibrations shall not be required by the INU_{RS}. Adjustment, alignment, or calibration devices shall not be accessible during normal, on-aircraft handling. The INU_{RS} shall require no periodic maintenance.

Automatic self-biasing methods using entered ramp position coordinates (accurate to ± 2 km), gyrocompassing alignment procedures, and terminal position and velocity indications shall be used to the extent practical to maintain system performance within required bounds over long periods of time.

3.2.5 Environmental Conditions

The redundant strapdown INS shall be designed in accordance with ARINC 414 except as modified herein, and be capable of being tested in accordance with RTCA Paper 120-61/DO-108, with conditions modified to be consistent with this specification.

3.2.5.1 Ambient Temperature

Normal ambient temperature:	30°C
Maximum continuous operation:	50°C
Short term (30 min) overtemp:	71°C
Low operating temp:	-15°C

3.2.5.2 Vibration3.2.5.2.1 General

The INU_{RS} shall be capable of operation during vibration as specified by RTCA Paper 120-61/DO-108, Category A. This vibration level consists of a constant total excursion of 0.76 mm from 10 to 55 cps with a maximum of 5 g, and of 5 g from 55 to 500 cps.

3.2.5.2.2 Performance Vibration

The angular and linear vibrations present during flight to be used for performance estimates are shown in table A-II. These shall be considered 3 sigma environments, present during 50 percent of the flight, with a phase correlation between axes of 0.3.

TABLE A-II. MAXIMUM PERFORMANCE ENVIRONMENT

	SINUSOIDAL	RANDOM
Linear	0.3 g _{rms} @28 Hz	0.00045 (g _{rms}) ² /Hz 0-200 Hz (0.3 g _{rms})
Angular	1.0 deg/sec _{rms} @15 Hz	0.033 (deg/sec _{rms}) ² /Hz 0-30 Hz (1.0 deg/sec _{rms})
Linear/angular	0.1 g _{rms} -deg/sec _{rms} @15 Hz	0.0033 (g _{rms} -deg/sec _{rms})/Hz 0-30 Hz (0.1 g _{rms} -deg/sec _{rms})

3.2.5.2.3 Motion During Ground Alignment

Coning motion of the vehicle shall be assumed to occur during ground alignment with a cone whole-angle of four arc minutes, at a frequency between 1 and 4.5 Hz. Sudden pitch or roll rotations of 0.5° shall also be assumed. Motion of the aircraft due to wind gusts shall be assumed to be a first-order Markov process with a standard deviation of 4 mm with a correlation time of 20 seconds.

3.2.5.3 Shock

Operational: 6 g with a time duration of at least 10 milli-sec., in accordance with the procedure of RTCA Paper 120-61/DO-108.

Crash Safety: 15 g with a time duration of at least 10 milli-sec., in each direction.

3.3 Design and Construction

3.3.1 Electromagnetic Interference

The redundant strapdown INS shall meet the conducted and radiated susceptibility and emission requirements of ARINC 413, and the test requirements of RTCA Paper 120-61/DO-108, for Category A equipment. Grounding and shielding practices shall be used in accordance with ARINC 413.

3.3.2 Humidity

The redundant strapdown INS shall be capable of normal operation during conditions of a relative humidity varying from 10 percent to 100 percent, combined with temperature and altitude cycling encountered in normal aircraft operation, as defined by ARINC 414, for Category A (Std) environment.

3.3.3 Explosive Atmosphere

Explosive atmosphere is not normally encountered by electronics equipment in airline type aircraft. Specific installations where explosive vapor presents an operating hazard are normally defined by the airframe manufacturer.

3.3.4 Atmospheric Pressure

Normal atmospheric pressure range is from -305 m to 13,700 m. Decompression from a pressure altitude of 2100 m to 13,700 m in 15 seconds or less shall not degrade system performance, per ARINC 414.

3.4 Logistics

The INU_{RS} design shall be compatible with the following maintenance structure:

Level 1	Unit replacement, in aircraft
Level 2	Module replacement, in the shop
Level 3	Module repair (excluding gyros and accelerometers)
Level 4	Gyro/Accelerometer repair

Level 1 maintenance shall not require the use of any standard or special test equipment.

3.5 Major Component Characteristics

3.5.1 Inertial Measurement Module (IMM)

The IMM shall consist of one two-degree-of-freedom, tuned-gimbal gyro, two single-degree-of-freedom accelerometers, with supporting loop-closure electronics. Compensation coefficients for use in software for correction of systematic instrument errors shall be contained in a memory which, when installed, may not be

altered by any means. Self-test capability shall be included to detect loop-closure failures.

3.5.2 Digital Computer

The digital computer shall be of the general purpose type with the instruction sequence and constants stored in a memory which, when installed, may not be altered by any means.

Space in the INM chassis shall be included for expansion of instruction memory by 100 percent from that needed for the INU_{RS} problem as defined in this specification. Spare computer execution time shall also be provided, for greater than 100,000 instructions per second with an average instruction mix as shown in table A-III.

TABLE A-III. SPARE CAPACITY INSTRUCTION MIX

<u>TYPE</u>	<u>PERCENTAGE UTILIZATION</u>
Load/Store	11.9
D-Load/Store	31.8
Copy	5.5
Exchange	4.2
D-Shift	9.1
Add/Sub	10.5
D-Add/Sub	13.1
Multiply	6.4
D-Multiply	5.5
Divide	0.6
Transfer	1.4

A portion of the computer memory shall be non-volatile with removal of aircraft power. Last-computed values of the following variables shall be retained following normal or failure-mode power shut down, for a time duration of over 30 days without external power:

- a. Calibration constants which are modified during the course of normal operation.
- b. Latitude, longitude, velocities, and quaternions.
- c. Maintenance data, e.g., self-test results, FDI information, etc.

Computer self-test provisions shall be included such as:

- a. A watchdog timer not driven from the main computer clock, periodically reset under software control, indicating a failure if not reset
- b. Instruction tests
- c. Memory tests
- d. I/O tests

3.5.3 Computer I/O

Input/output provisions for interfacing the computer with the various peripheral elements shall be included:

- a. Interface with one IMM including the calibration constant memory and temperature sensors.
- b. Interface with external avionics via ARINC 575 transmitter/receivers.
- c. Interface with up to three other INMs. Particular care must be taken in the design of this circuitry to avoid single-point INU_{RS} failure modes.

3.5.4 Power Supply and Support Electronics

The power supply design shall include monitoring circuits for over-voltage, under-voltage, and short circuit protection. Automatic shutdown shall occur during failure modes to avoid potentially hazardous or chain-failure conditions.

Computer and IMM clock and timing circuitry shall be included. Provision for synchronization of all software executive interrupts shall be included to avoid errors due to time-skew of sensor data readouts. Particular care must be taken in the design of this circuitry to avoid single-point INU_{RS} failure modes.

403314

APPENDIX B
PARITY EQUATIONS

Parity Equations

Parity equations will now be derived for the semioctahedral spin axis orientation. Equations are based on TDF gyro measurements.

Test relations for a semioctahedral array are obtained as follows. Four unit spin vectors are defined (S_i , $i = 1, 2, 3, 4$) normal to and directed outward from the four triangular faces of a semioctahedron, (figure B-1). From symmetry considerations the following useful relations can be obtained.

$$\left\{ \begin{array}{l} \sum_{i=1}^4 (-1)^i S_i = 0 = \hat{S}_1 - \hat{S}_2 + \hat{S}_3 - \hat{S}_4 \\ \hat{S}_i \cdot \hat{S}_j = -\frac{(-1)^{i+j}}{3} \quad i \neq j \end{array} \right\} \quad (1)$$

The output planes (sensitive axes) of the TDF gyros lie in the triangular faces of the pyramid, hence, a set of parity equations can be constructed by resolving the gyro output rates along the pyramid edges and comparing them. This leads to six independent comparisons and can be formalized as follows. First, find the unit edge vectors of the pyramid. These edge vectors must be perpendicular to the adjacent spin vectors. Thus edge vector \hat{e}_{ij} can be defined from the spin vectors \hat{S}_i and \hat{S}_j as:

$$\hat{e}_{ij} = \frac{\hat{S}_i \times \hat{S}_j}{|\hat{S}_i \times \hat{S}_j|} \quad i \neq j$$

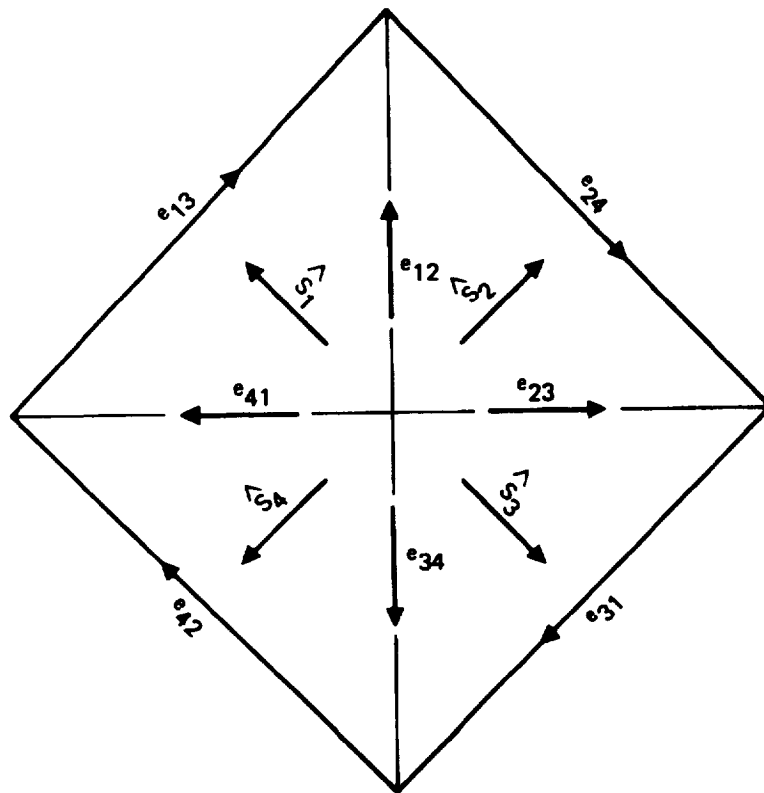


Figure B-1. Semioctahedral Spin and Edge Vectors

Since

$$|\hat{s}_i \cdot \hat{s}_j| = \frac{1}{3}$$

we have

$$|\hat{s}_i \times \hat{s}_j| = \sqrt{1 - \left(\frac{1}{3}\right)^2} = \sqrt{\frac{8}{9}}$$

thus

$$\hat{e}_{ij} = \sqrt{\frac{9}{8}} (\hat{s}_i \times \hat{s}_j) \quad i \neq j \quad (2)$$

Now suppose the output rate of the i th gyro is \vec{w}_i and the j th gyro \vec{w}_j . Then we can define the parity test as:

$$T_{ij}^* = \vec{w}_i \cdot \hat{e}_{ij} - \vec{w}_j \cdot \hat{e}_{ij} \quad i \neq j$$

or

$$T_{ij}^* = (\vec{w}_i - \vec{w}_j) \cdot \hat{e}_{ij} \quad i \neq j \quad (3)$$

Now, before proceeding, note that $T_{ij}^* = T_{ji}^*$, since both the sign of the rate difference and the edge vector sign change on interchange of index. Thus the test equations can be written as

$$T_{ij}^* = (\vec{w}_i - \vec{w}_j) \cdot \hat{e}_{ij} \quad i < j$$

or expanding

$$\begin{aligned}
 T_{12}^* &= (\vec{w}_1 - \vec{w}_2) \cdot \hat{e}_{12} \\
 T_{13}^* &= (\vec{w}_1 - \vec{w}_3) \cdot \hat{e}_{13} \\
 T_{14}^* &= (\vec{w}_1 - \vec{w}_4) \cdot \hat{e}_{14} \\
 T_{23}^* &= (\vec{w}_2 - \vec{w}_3) \cdot \hat{e}_{23} \\
 T_{24}^* &= (\vec{w}_2 - \vec{w}_4) \cdot \hat{e}_{24} \\
 T_{34}^* &= (\vec{w}_3 - \vec{w}_4) \cdot \hat{e}_{34}
 \end{aligned} \tag{4}$$

In reality the gyros do not output rates but incremental angles

$$\Delta \vec{\theta}_i = \int_{n\Delta t}^{(n+1)\Delta t} \vec{w}_i dt$$

Furthermore, these incremental angles have "noise" components. Hence, it is desirable (necessary) to filter them. For the

purposes of this treatment we define $T_{ij} = \text{filtered}^1 (T_{ij}^*)$ thus the test equations become

$$T_{ij} = \text{filtered} \left\{ \vec{w}_i - \vec{w}_j \right\} \cdot e_{ij}$$

$$i = 1 \dots 4, \quad i < j \leq 4$$

¹For example a first order filter of the form

$$T_{ij}((n+1)\Delta t) = K T_{ij}(n\Delta t) + T_{ij}^*((n+1)\Delta t)$$

$$\cong \int_0^{(n+1)\Delta t} e^{-k(t-\tau)} T_{ij}^* dt$$

might be employed.

403314

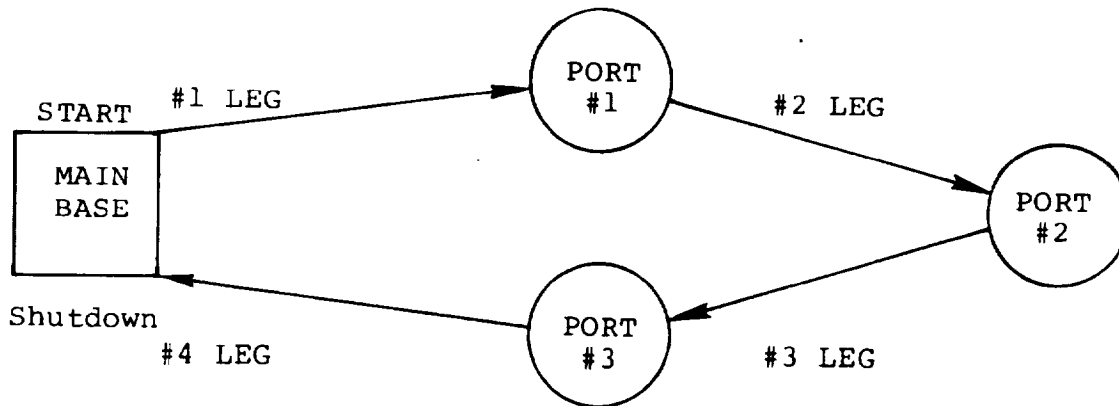
APPENDIX C
LOGISTICS ANALYSIS

LOGISTICS ANALYSIS
VTOL Operations

1. OPERATIONAL CRITERIA

1.0 SYSTEM UTILIZATION

TYPICAL ROUTE PLAN



ACTIVITY	#1 LEG	#2 LEG	#3 LEG	#4 LEG
Ground Operations (Power on)	6.5			
Unloading/Loading:	3.5	3.5	3.5	3.5
Ascent	2.5	2.5	2.5	2.5
Cruise	6.0	6.0	6.0	6.0
Descent	3.0	3.0	3.0	3.0
Servicing (Power off)				8.5
Total Time (Minutes)	21.5	15.0	15.0	23.5
Total Flight Time per Route			46.0 Minutes	
Total Ground Operating Time (Power On)			20.5 Minutes	
Total Time for One Complete Cycle			75.0 Minutes	

1.1 OPERATIONAL MODES:

Peak Demand Period 6:00 AM to 6:00 PM
 Reduced Operational Period - 6:00 PM to 6:00 AM

OPTIONS:

	Time Between Port Stops	
	<u>Peak</u>	<u>Reduced</u>
A. 1 Aircraft per Route	90 Minutes	120 Minutes
B. 2 Aircraft per Route	45 Minutes	60 Minutes
C. 3 Aircraft per Route	30 Minutes	45 Minutes
D. 5 Aircraft per Route	15 Minutes	30 Minutes

	<u>A</u>	<u>B</u>	<u>C</u>	<u>D</u>
Total Routes Flown per day:	14	28	40	72
Peak Period	8	16	24	48
Reduced Operations Period	6	12	16	24
Slack Time Between Flights (Minutes)				
Peak Period	15	15	15	0
Reduced Operations Period	45	34	60	75
Total Operating Hours per day	15.52	31.10	44.33	79.80
Avg. Operating Hours Per A/C/ day	15.52	15.50	14.78	15.96
Total Flight Hours per day	10.73	21.47	30.67	55.20
Avg. Flight Hours per A/C/ day	10.73	10.73	10.22	11.04

1.2 OPERATIONAL SITES:

Given 200 Aircraft In Inventory
 Assuming 90% Operational
 Readiness = 180 Aircraft Operational
 = 20 Aircraft In Maintenance

Assuming one (1) Main Base has five (5) separate routes, then:

OPTION	OP:A/C REQD	BACKUP A/C	TOTAL A/C	TOTAL		
				MAIN BASES	SATELLITE PORTS	
				TOTAL	OPER. SITES	
A	5	1	6	30	450	480
B	10	1	11	16	240	256
C	15	1	16	11	165	176
D	25	1	26	7	105	112

1.3 OPERATING TIME:

OPTION	AVG. FLIGHT HRS. PER DAY	NO. OF A/C IN USE	TOTAL FLIGHT HRS. PER MON.	OP/FT HR RATIO
A	10.73	150	48,285	1.444:1
B	10.73	160	51,504	1.444:1
C	10.22	165	50,589	1.446:1
D	11.04	175	57,960	1.445:1

1.4 ESTIMATED RELIABILITY:

Channel: 3,000 Hours MTBF (4 per aircraft)

Consisting of:

IMM: 6,000 Hours MTBF

COMPUTER: 7,500 Hours MTBF

POWER SUPPLY: 30,000 Hours MTBF

Unit: 750 Hours MTBF (1 per aircraft)

1.5 FAILURES

1.5.1 "Hard" Failures, or "Soft" Failures exceeding system degradation limits, encountered in flight will require removal and replacement of failed unit at next ground operational site. Take-off for next leg of route will not be attempted until all INS Units operational.

1.5.2 "Soft" failures in flight, not exceeding system degradation limits, will require system monitoring until return to the main base where the faulty unit will be removed and replaced.

1.6 MAINTENANCE:

1.6.1 Maintenance at satellite ports restricted to removal and replacement of INS units within 3 minutes (1 minute installation time) using minimal, common hand tools.

1.6.2 Maintenance at the main operating base shall consist of:

- a. Fault verification and removal and replacement of failed INS Units.
- b. Fault detection and isolation to replaceable assembly within the INS unit; removal and replacement of failed replaceable assembly; and repair verification.

2.0 INITIAL AND REPLACEMENT SPARES COSTS. (INS Unit only - modules not included)

$$C_1 = (STK)(M)(UC) + \frac{(PFH)(UF)(QPA)(1-RIP)}{MTBF} (DRCT)(UC)$$

Where:

		<u>1 Box</u>	<u>4 Box</u>
STK	= Stock Level at a site (units)	-	1
M	= Number of Operating Sites	-	Ref. Para. 1.2
UC	= Unit Cost	90K	23.75K
PFH	= Peak Flying Hours per Month	-	Ref. Para. 1.3 -
UF	= Ratio of Operating Hours to Flying Hours	-	Ref. Para. 1.3 -
QPA	= Quantity of Like Items per Aircraft	1	-
RIP	= Fraction of Failures which can be repaired in place	-	.00
MTBF	= Mean Time Before Failure in Operating Hours/Box	750	3000
DRCT	= Average Repair Cycle Time (In months)	.0667	-
			.0500

2.1 Spare Units Stocked at Sites:

2.1.1 One Box Inertial Navigation System

$$\begin{aligned} \text{Option A.} &= (1)(480)(90K) + \frac{(48,285)(1.444)(1)(1-0)}{750} (.0667)(90K) \\ &= \$43,758,067. \end{aligned}$$

$$\begin{aligned} \text{B.} &= (1)(256)(90K) + \frac{(51,504)(1.444)(1)}{750} (\$6,003.) \\ &= \$23,635,272. \end{aligned}$$

$$\begin{aligned} \text{C.} &= (1)(176)(90K) + \frac{(50,589)(1.446)(1)}{750} (\$6,003.) \\ &= \$16,425,506. \end{aligned}$$

$$\begin{aligned} \text{D.} &= (1)(112)(90K) + \frac{(57,960)(1.445)(1)}{750} (\$6,003.) \\ &= \$10,750,353. \end{aligned}$$

2.1.2 Four Box Inertial Navigation System

$$\begin{aligned} \text{Option A.} &= (1)(480)(23.75K) + \frac{(48,285)(1.444)(4)(1-0)}{3000} (.05)(23.75K) \\ &= \$11,510,396 \end{aligned}$$

$$\begin{aligned} \text{B.} &= (1)(256)(23.75K) + \frac{(51,504)(1.444)(4)}{3000} (\$1,187.50) \\ &= \$6,197,755. \end{aligned}$$

$$\begin{aligned} \text{C.} &= (1)(176)(23.75K) + \frac{(50,589)(1.446)(4)}{3000} (\$1,187.50) \\ &= \$4,295,824 \end{aligned}$$

$$\begin{aligned} \text{D.} &= (1)(112)(23.75K) + \frac{(57,960)(1.445)(4)}{3000} (\$1,187.50) \\ &= \$2,792,608 \end{aligned}$$

2.2 On-Board Spares (1 Replacement Unit per Aircraft)

$$C_2 = (\text{Operational Aircraft}) + (\text{Standby Aircraft}) + (\text{Repair Pipeline Units})$$

2.2.1 One Box Inertial Navigation System:

$$\begin{aligned} \text{Option A.} &= (1)(150)(90K) + (1)(30)(90K) + 558,067 \\ &= \$16,758,067. \end{aligned}$$

$$\begin{aligned} \text{B.} &= (1)(160)(90) + (1)(16)(90) + 595,272 \\ &= \$16,435,272 \end{aligned}$$

$$\begin{aligned} \text{C.} &= (1)(165)(90) + (1)(11)(90) + 585,506 \\ &= \$16,425,506 \end{aligned}$$

$$\begin{aligned} \text{D.} &= (1)(175)(90) + (1)(7)(90) + 670,353 \\ &= \$17,050,353 \end{aligned}$$

2.2.2 Four Box Inertial Navigation System:

$$\begin{aligned} \text{Option A.} &= (1)(150)(23.75K) + (1)(30)(23.75K) + 110,396 \\ &= \$4,385,396 \end{aligned}$$

$$\begin{aligned} \text{B.} &= (1)(150)(23.75K) + (1)(16)(23.75K) + 117,755 \\ &= \$4,060,255 \end{aligned}$$

$$\begin{aligned} \text{C.} &= (1)(165)(23.75K) + (1)(11)(23.75K) + 115,824 \\ &= \$4,295,824 \end{aligned}$$

$$\begin{aligned} \text{D.} &= (1)(175)(23.75K) + (1)(7)(23.75K) + 132,608 \\ &= \$4,455,108 \end{aligned}$$

3.0 ON-AIRCRAFT MAINTENANCE COSTS (MONTHLY)

$$C_3 = \frac{(\text{PFH})(\text{UF})(\text{QPA})}{\text{MTBF}} [\text{PAMH} + (\text{RMH} + \text{RVH})] (\text{BLR} + \text{DDR})$$

Where :

	<u>1 BOX</u>	<u>4 BOXES</u>
PFH = Peak Flying Hours per Month	- Ref. Para. 1.3	-
UF = Ratio of Operating Hours to Flying Hours	- Ref. Para. 1.3	-
QPA = Quantity of Like Items per Aircraft	1	4
MTBF = Mean Time Before Failure in Operating Hours	750	3000
PAMH = Average Manhours for Preparation and Access to Unit	- 1 Min/4 Min	-
RMH = Average Manhours to Remove and Replace Unit	- 2 Min	-
RVH = Average Time to Verify Restoration of System to Operational Status	10 Min	.5 Min
BLR = Basic Labor Rate for Maintenance Personnel	- \$24. Hr	-
DDR = Dispatch Delay Rate	- \$3,000. Hr	-

3.1 Not Requiring System Shutdown

3.1.1 Four Box Inertial Navigation System

3.1.1.1 On-Board Spare Available

$$\text{Option A.} = \frac{(48,285)(1.444)(1)}{750} [0.0166 + (.0333 + .0083)] (\$24. + \$3,000.)$$

$$= \$18,681$$

$$\text{B.} = \frac{(51,504)(1.444)(1)}{750} (.0582) (\$3,024.)$$

$$= \$17,207.$$

$$\text{C.} = \frac{(50,589)(1.446)(1)}{750} (.0582) (\$3,024.)$$

$$= \$17,165.$$

$$\text{D.} = \frac{(57,960)(1.445)(1)}{750} (.0582) (\$3,024.)$$

$$= \$19,653.$$

3.1.1.2 Replacement Spare Stocked at Site

$$\text{Option A.} = \frac{(48,285)(1.444)(1)}{750} [.0667 + (.0333 + .0083)] (\$24. + \$3,000)$$

$$= \$35,512$$

$$\text{B.} = \frac{(51,504)(1.444)(1)}{750} (.1083) (\$3,024.)$$

$$= \$32,036.$$

$$\text{C.} = \frac{(50,589)(1.446)(1)}{750} (.1083) (\$3,024.)$$

$$= \$31,941.$$

$$\text{D.} = \frac{(57,960)(1.445)(1)}{750} (.1083) (\$3,024.)$$

$$= \$36,572.$$

3.2 Requiring System Shut Down During Maintenance

3.2.1 One Box Inertial Navigation System

3.2.1.1 On-Board Spare Available

$$\text{Option A.} = \frac{(48,285)(1.444)(4)}{3000} [.0166 + (.0333 + .1667)]$$

$$(\$24. + \$3,000.) = \$69,561$$

$$\text{B.} = \frac{(51,504)(1.444)(4)}{3000} (.2167) (\$3,024.)$$

$$= \$64,102$$

$$\text{C.} = \frac{(50,589)(1.446)(4)}{3000} (.2167) (\$3,024.)$$

$$= \$63,912.$$

$$\text{Option D.} = \frac{(57,960)(1.445)(4)}{3000} (.2167) (\$3,024.)$$

$$= \$73,177.$$

3.2.1.2 Replacement Spare Stocked at Site

$$\text{Option A.} = \frac{(48,285)(1.444)(4)}{3000} [.0667 + (.0333 + .1667)]$$

$$= \$87,452$$

$$\text{B.} = \frac{(51,504)(1.444)(4)}{3000} (.2667) (\$3,024.)$$

$$= \$78,892.$$

$$\text{C.} = \frac{(50,589)(1.446)(4)}{3000} (.2667) (\$3,024.)$$

$$= \$78,658.$$

$$\text{D.} = (57,960)(1.445)(4)(.2667)(\$3,024.)$$

$$= \$90,062.$$

4.0 OFF-AIRCRAFT MAINTENANCE COSTS: (MONTHLY)

$$C_4 = \frac{(PFH)(UF)(QPA)}{MTBF} [(RTS)(BMH)(SLR + SMR)]$$

Where:

		<u>1 BOX</u>	<u>4 BOXES</u>
PFH	= Peak Flying Hours per Month	-	- Ref. Para. 1.3 -
UF	= Ratio of Operating Hours to Flying Hours	-	- Ref. Para. 1.3 -
QPA	= Quantity of Like Items per Aircraft	1	4
MTBF	= Mean Time Between Failure in Operating Hours	750	3000
RTS	= Fraction of Units Expected to be Repaired at Main Base	1.00	-

		<u>1 BOX</u>	<u>4 BOXES</u>
BMH	= Average Manhours to Perform Shop Maintenance on failed units including fault isolation, repair, and verification (INS Unit only - module repair not included)	3	2
SLR	= Shop Labor Rate per Hour	-	\$34.
SMR	= Shop Material Consumption Rate per Hour	-	\$16.

4.1 One Box Inertial Navigation System

$$\text{Option A.} = \frac{(48,285)(1.444)(1)}{750} [(1)(3)(\$34 + \$16)] = \$16,265$$

$$\text{B.} = \frac{(51,504)(1.444)(1)}{750} (\$150.) = \$14,673.$$

$$\text{C.} = \frac{(50,589)(1.446)(1)}{750} (\$150.) = \$14,628.$$

$$\text{D.} = \frac{(57,960)(1.445)(1)}{750} (\$150.) = \$16,750.$$

4.2 Four Box Inertial Navigation System

$$\text{Option A.} = \frac{(48,285)(1.444)(4)}{3000} [(1)(2)(\$34. + \$16.)] = \$10,843.$$

$$\text{B.} = \frac{(51,504)(1.444)(4)}{3000} (\$100.) = \$9,783.$$

$$\text{C.} = \frac{(50,589)(1.446)(4)}{3000} (\$100.) = \$9,753.$$

$$\text{D.} = \frac{(57,960)(1.445)(4)}{3000} (\$100.) = \$11,167.$$

5.0 LIFE CYCLE MAINTENANCE COSTS

Assuming:

Service Life of Inertial Navigation System = 10 years

Increase in Reliability = 5000 Hours MTBF for mature system

5.1 On Aircraft Maintenance Costs

$$C_5 = [C_3 - (K)(C_3)](LUP)$$

Where:

C_3	= Monthly On-Aircraft Maintenance Costs	Ref. Para. 3.0
K	= Adjustment Factor to establish Average Monthly Costs over Program Period	20%
LUP	= Inventory Usage Period (Operational Service Life of System in Months)	120

5.1.1 Spares at Site

<u>OPTION</u>	<u>BOXES</u>	
A	1	[87,452 - (.2)(87,452)] (120) = \$8,395,390.
	4	[35,512 - (.2)(35,512)] (120) = \$3,409,130.
B	1	[78,892 - (.2)(78,892)] (120) = \$7,573,632
	4	[32,036 - (.2)(32,036)] (120) = \$3,075,456.
C	1	[78,658 - (.2)(78,658)] (120) = \$7,546,848.
	4	[31,941 - (.2)(31,941)] (120) = \$3,066,336.
D	1	[90,062 - (.2)(90,062)] (120) = \$8,645,952.
	4	[36,572 - (.2)(36,572)] (120) = \$3,510,912.

5.1.1.2 Spares On-Board

<u>OPTION</u>	<u>BOXES</u>	
A	1	[69,561 - (.2)(69,561)] (120) = \$6,598,907.
	4	[18,681 - (.2)(18,681)] (120) = \$1,793,413.
B	1	[64,102 - (.2)(64,102)] (120) = \$6,153,792.
	4	[17,207 - (.2)(17,207)] (120) = \$1,651,872.

<u>OPTION</u>	<u>BOXES</u>	
C	1	[63,912 - (.2)(63,912)] (120) = \$6,135,552.
	4	[17,165 - (.2)(17,165)] (120) = \$1,647,840.
D	1	[73,177 - (.2)(73,177)] (120) = \$7,024,992.
	4	[19,653 - (.2)(19,653)] (120) = \$1,886,688.

5.2 Off Aircraft Maintenance Costs

$$C_6 = [(C_4) - (K)(C_4)](1UP)$$

Where:

C_4 = Monthly Off Aircraft Maintenance Costs

<u>OPTION</u>	<u>BOXES</u>	
A	1	[16,265 - (.2)(16,265)] (120) = \$1,561,454.
	4	[10,843 - (.2)(10,843)] (120) = \$1,040,969.
B	1	[14,673 - (.2)(14,673)] (120) = \$1,408,608.
	4	[9,783 - (.2)(9,783)] (120) = \$ 939,168.
C	1	[14,628 - (.2)(14,628)] (120) = \$1,404,288.
	4	[9,753 - (.2)(9,753)] (120) = \$ 936,288.
D	1	[16,750 - (.2)(16,750)] (120) = \$1,608,000.
	4	[11,167 - (.2)(11,167)] (120) = \$1,072,032.

6.1 One Unit vs Four Unit Inertial Navigation System

6.1.1 Spares Stocked at Sites:

<u>OPTION</u>	<u>UNITS PER A/C</u>	<u>INITIAL & RPL'MT SPARES COST</u>	<u>LIFE CYCLE M COST ON A/C</u>	<u>OFF A/C</u>	<u>TOTAL (\$000,000)</u>
A	1	43.8	8.4	1.6	53.8
	4	11.5	3.4	1.0	15.9
DELTA COST:		32.3	5.0	.6	37.9

OPTION	UNITS PER A/C	INITIAL & RPL'MT SPARES COST	LIFE CYCLE M COST		TOTAL (\$000,000)
			ON A/C	OFF A/C	
B	1	23.6	7.6	1.4	32.6
	4	<u>6.2</u>	<u>3.1</u>	<u>.9</u>	<u>10.2</u>
DELTA COST:		17.4	4.5	.5	22.4
C	1	16.4	7.6	1.4	25.4
	4	<u>4.3</u>	<u>3.1</u>	<u>.9</u>	<u>8.3</u>
DELTA COST:		12.1	4.5	.5	17.1
D	1	10.8	8.7	1.6	21.1
	4	<u>2.8</u>	<u>3.5</u>	<u>1.1</u>	<u>7.4</u>
DELTA COST:		8.0	5.2	.5	13.7

6.1.2 On Board Spares:

A	1	16.8	6.6	1.6	25.0
	4	<u>4.4</u>	<u>1.8</u>	<u>1.0</u>	<u>7.2</u>
DELTA COST:		12.2	4.8	.6	17.8
B	1	16.4	6.2	1.4	24.0
	4	<u>4.1</u>	<u>1.7</u>	<u>.9</u>	<u>6.7</u>
DELTA COST:		12.5	4.5	.5	17.3
C	1	16.4	6.2	1.4	24.0
	4	<u>4.3</u>	<u>1.7</u>	<u>.9</u>	<u>6.9</u>
DELTA COST:		12.1	4.5	.5	17.1
D	1	17.1	7.0	1.6	25.7
	4	<u>4.5</u>	<u>1.9</u>	<u>1.1</u>	<u>7.5</u>
DELTA COST:		12.6	5.1	.5	18.2

7.0 CONCLUSIONS:

- a. Initial and Replacement Spares Costs for a four unit Inertial Navigation System are from 71 percent to 76 percent less than a one unit Inertial Navigation System, regardless of whether the spare units are stocked at the site or onboard the aircraft.
- b. On-aircraft maintenance costs for a four unit Inertial Navigation System are 72 percent less than a one unit INS when onboard spares are available and 59 percent less when the spare unit is stored on site. The difference is due, in part, to bringing the replacement unit aboard and removal of the faulty unit from the aircraft.
- c. Although initial and replacement spares costs are lower when stored at the site (when the number of aircraft exceeds the number of sites), the difference in cost is offset by the increased on-aircraft maintenance costs.
- d. Off-aircraft maintenance costs for a four unit INS are from 31 percent to 35 percent less than a one unit INS due to the added equipment complexity and time required to fault isolate and verify repair of the single unit INS.
- e. Total life cycle maintenance costs including cost of spares is over \$13M greater for a one unit INS than for a four unit INS. Initial INS procurement penalty is only 5K x 200, or \$1M, for a net savings of \$12M.

403314

APPENDIX D
STRAPDOWN GYRO TRANSFER FUNCTION

Strapdown Gyro Transfer Function

The dynamic model of the strapdown gyro is shown in figure D-1. The basic equations of motion of the strapdown gyro are determined by balancing all the torques acting on the rotor.

Torques about X:

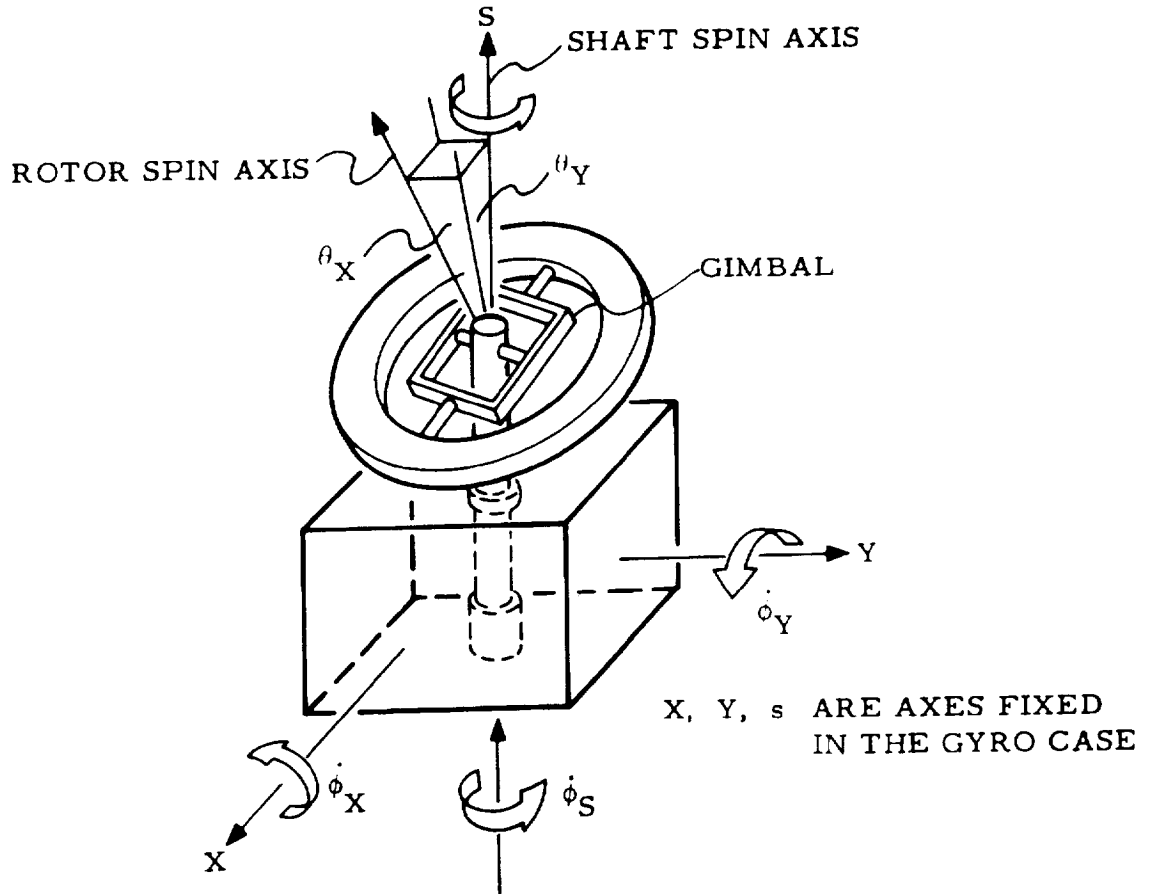
$$A\ddot{\theta}_X + D\dot{\theta}_X + K_D \theta_X + H_C \dot{\theta}_Y + K_Q \theta_Y = -H\dot{\phi}_Y - A\ddot{\phi}_X + M_{eX} + M_{aX} \quad (1)$$

and torques about Y:

$$A\ddot{\theta}_Y + D\dot{\theta}_Y + K_D \theta_Y - H_C \dot{\theta}_X - K_Q \theta_X = H\dot{\phi}_X - A\ddot{\phi}_Y + M_{eY} + M_{aY} \quad (2)$$

where:

- A = Rotor moment of inertia about output axes
- D = Damping on rotor about output axes relative to case,
D = 2A/τ
- τ = Gyro dynamic time constant
- K_D = In-phase spring rate between rotor and case (function of mistuning parameter ΔN) K_D = H_C ΔN/F_m
- K_Q = Quadrature spring rate between rotor and case:
K_Q = H_C/τ
- H_C = Angular momentum of rotor for rotor displacements relative to case for no case rates, i.e., $\dot{\phi}_X = \dot{\phi}_Y = 0$,
H_C = (C + A_g)N
- H = Effective angular momentum of rotor for case rates about input axes for rotor moving with case, i.e., $\dot{\theta}_X = \dot{\theta}_Y = 0$,
H = {H_C - N (A_g + B_g - C_g)/2} = H_C [1 - 1/2F_m]
- F_m = Figure of merit = H_C N /K_T, where K_T = sum of all torsional spring rates of suspension.



$\dot{\phi}_X, \dot{\phi}_Y, \dot{\phi}_S$: ANGULAR RATES OF CASE
RELATIVE TO INERTIAL SPACE

θ_X, θ_Y : ROTOR ANGULAR DISPLACEMENTS
RELATIVE TO THE CASE (PICKOFFS)

N : SPIN SPEED

N_o : TUNED SPEED = $\sqrt{K_T / (A_g + B_g - C_g)}$

K_T : SUM OF TORSIONAL SPRING RATES ATTACHED TO GIMBAL

A_g : GIMBAL MOMENT OF INERTIA ABOUT SHAFT-ATTACHED AXIS

B_g : GIMBAL MOMENT OF INERTIA ABOUT ROTOR-ATTACHED AXIS

C_g : GIMBAL POLAR MOMENT OF INERTIA

C : ROTOR POLAR MOMENT OF INERTIA

$\Delta N = N_o - N$

Figure D-1. Dynamic Model of Strapdown Gyro

M_{ax} and M_{ay} are torques applied to rotor about X and Y respectively. M_{ex} and M_{ey} are error torques generated primarily by the non-linear terms in the equations of motion. The primary terms are:

$$M_{cx} = -(C - A) \dot{\phi}_S \dot{\phi}_Y - H\dot{\phi}_S \theta_X - (C - 2A) \dot{\phi}_S \dot{\theta}_Y + A\ddot{\phi}_S \theta_Y$$

$$M_{cy} = (C - A) \dot{\phi}_S \dot{\phi}_X - H\dot{\phi}_S \theta_Y + (C - 2A) \dot{\phi}_S \dot{\theta}_X - A\ddot{\phi}_S \theta_X$$

The first term is the expression for the anisoinertia term and is present even for an ideal perfectly captured gyro, where $\theta_X = \theta_Y = 0$. The second term is the cross coupling error generated if the capture loop is not ideal (θ_X and θ_Y not equal to zero). The third and fourth terms are other error terms which are also generated for imperfect rebalancing. Additional terms due to motor hunting are discussed in another section.

Gyro Transfer Function (Open Loop)

The output angle θ (pickoff) versus input angle ϕ can be determined from Equations (1) and (2). Assume $\dot{\phi}_S = 0$ and inoperative capture loops.

Taking the Laplace transform and expressing in matrix form:

$$\begin{bmatrix} AS^2 + DS + H_C \Delta N/F_m & H_C(S + 1/T) \\ -H_C(S + 1/T) & AS^2 + DS + H_C \Delta N/F_m \end{bmatrix} \begin{bmatrix} \theta_X(S) \\ \theta_Y(S) \end{bmatrix} = \begin{bmatrix} -HS\phi_Y(S) - AS^2\phi_X(S) \\ HS\phi_X(S) - AS^2\phi_Y(S) \end{bmatrix}$$

(3)

Solving (3) yields (for $D \ll H_C$):

$$\frac{\theta_X(S)}{\phi_X(S)} = \frac{-S(S + 1/T) (S^2 - DS/2A + HH_C/A^2)}{\left[(S + 1/T)^2 + (\Delta N/F_m)^2 \right] \left[S^2 + DS/A + (H_C/A)^2 \right]} \quad \text{Direct Axis}$$

$$\frac{\theta_Y(S)}{\phi_X(S)} = \frac{-H_C S \left[S - F_m/T + \sqrt{(F_m/T)^2 + 2\Delta NH/A} \right] \left[S - F_m/T - \sqrt{(F_m/T)^2 + 2\Delta NH/A} \right]}{2AF_m \left[(S + 1/T)^2 + (\Delta N/F_m)^2 \right] \left[S^2 + DS/A + (H_C/A)^2 \right]} \quad \text{Cross Axis}$$

$$\frac{H_C}{A} = \text{Nutation frequency } \omega_n$$

$$\sqrt{\frac{HH_C}{A^2}} = \omega_o \approx \omega_n \left[1 - \frac{1}{4} F_m \right]$$

for

$$F_m \gg 1$$

A typical frequency response for such an open-loop gyro is shown in figure D-2.

RATIO OF PICKOFF OUTPUT θ TO ANGULAR DISPLACEMENT INPUT ϕ VS. FREQUENCY (OPEN-LOOP)

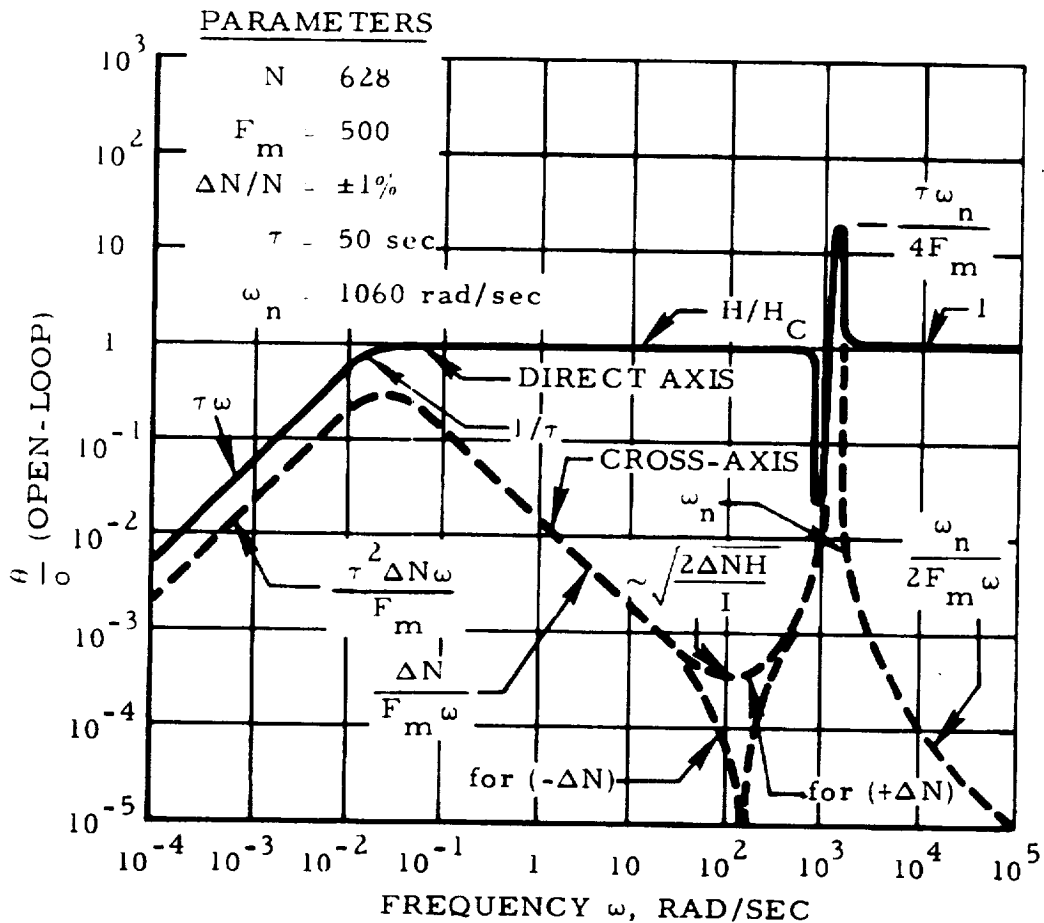


Figure D-2. Open-Loop Frequency Response of Strapdown Gyro

403314

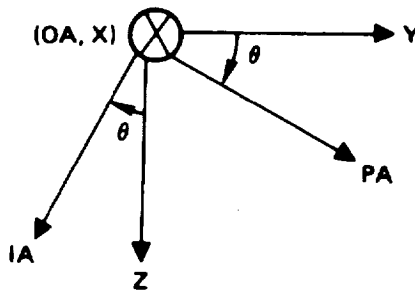
APPENDIX E
PENDULOUS ACCELEROMETER ANALYSIS

Pendulous Accelerometer Analysis

Below is a brief analysis of a Pendulous Accelerometer. Instrument level errors and dynamics are derived and error magnitudes evaluated.

Instrument axes defined by:

(X, Y, Z)	Case fixed axes
(OA, PA, IA)	Principal axes of accelerometer
OA	Output axis
PA	Pendulous axis
IA	Input axis
θ	Pickoff angle



Resolving input case rates along principal axes to first order in θ .

$$\omega_{IA} = \omega_Z - \theta \omega_Y$$

$$\omega_{PA} = \omega_Y + \theta \omega_Z$$

$$\omega_{OA} = \omega_X + \dot{\theta}$$

Input acceleration as measured by instrument is:

$$A_{IA} = A_Z - \theta A_Y$$

Since (OA, PA, IA) are principal axes, angular momentum, H, is related to angular velocity by principal moments of inertia J_{OA} , J_{IA} , J_{PA}

$$H_{IA} = J_{IA} (\omega_Z - \theta \omega_Y)$$

$$H_{PA} = J_{PA} (\omega_Y + \theta \omega_Z)$$

$$H_{OA} = J_{OA} (\omega_X + \dot{\theta})$$

Equations of motion are obtained from:

$$\dot{\vec{H}}_{\text{SPACE}} = \vec{M}$$

$$\dot{\vec{H}}_{\text{SPACE}} = \dot{\vec{H}}_{\text{BODY}} + \vec{\omega} \times \vec{H}$$

The equation for torques along the OA axis is then:

$$\dot{H}_{OA} + \omega_{PA} H_{IA} - \omega_{IA} H_{PA} = M_{OA}$$

Substituting for ω and H and collecting terms:

$$J_{OA} (\dot{\omega}_X + \ddot{\theta}) + \omega_Y \omega_Z (J_{IA} - J_{PA}) + \theta (\omega_Z^2 - \omega_Y^2) (J_{IA} - J_{PA}) = M_{OA}$$

External torques to the system along OA axis are:

$$M_{OA} = P A_{IA} - K_{\theta} \theta - B \dot{\theta} + M_e$$

Where

- P = Pendulosity (Ml)
 K_0 = Torsional restraint of suspension
 B = Rotational damping
 M_e = Applied rebalance torque

Applying equilibrium of moments, we have:

$$J_{OA} \ddot{\theta} + B \dot{\theta} + K_0 \theta = PA_Z + PA_e + M_e$$

Where A_e are the error terms measured by the instrument:

$$PA_e = \omega_Y \omega_Z (J_{PA} - J_{IA}) + 0(\omega_Z^2 - \omega_Y^2) (J_{PA} - J_{IA}) - J_{OA} \dot{\omega}_X - P\theta A_Y$$

The magnitudes of these error terms will now be evaluated using the A-1000 design parameters.

Anisoinertia

$$\alpha_e = \omega_Y \omega_Z (J_{PA} - J_{IA}) / P$$

$$\frac{\alpha_e}{\omega_Y \omega_Z} = 0.5 \mu G / (\text{°/sec})^2$$

Output Axis Sensitivity (Not Rectification)

$$\alpha_e = \frac{J_{OA}}{P} \dot{\omega}_X$$

With

$$J_{OA} = 0.9 \text{ gm} - \text{cm}^2 \quad ,$$

$$\omega_X = \omega_O \text{ SIN } (2\pi ft)$$

$$\frac{\alpha_e}{\dot{\omega}_X} = 210 \text{ } \mu\text{G}/(\text{ }^\circ/\text{sec})\text{Hz}$$

Governor Effect

$$\alpha_e = \theta(\omega_Z^2 - \omega_Y^2) (J_{PA} - J_{IA})/P$$

$$\frac{\alpha_e}{\theta(\omega_Z^2 - \omega_Y^2)} = 0.5 \text{ } \mu\text{G}/(\text{ }^\circ/\text{sec})^2/\text{rad}$$

Vibropendulous

$$\alpha_e = \theta A_Y$$

403314

APPENDIX F
DERIVATION OF DESIGN EQUATIONS
FOR TETRAHEDRAL ARRAY
OF 4 TDF GYROS

APPENDIX F

DERIVATION OF LEAST SQUARES DESIGN MATRIX FOR n
TWO-DEGREE-OF-FREEDOM GYROS WHOSE SPIN AXES
ARE NOT COLLINEAR

When the instrument cluster consists of n TDF gyros, then there are $2n$ channels that contain information of angular rate of the cluster. The computed angular rate of the cluster, $\langle \omega \rangle$, is related to the measured angular rates of the cluster, $\bar{\omega}$, through the matrix $[D]$ as shown in Equation (1).

$$\langle \omega \rangle = [D] \bar{\omega} \quad (1)$$

The purpose of this section is to derive and define the design matrix in such a way that the sum of squares of the errors contributed by all $2n$ channels is minimized.

Let $\bar{\omega}$ represent the total angular rate of the instrument cluster.

Let the unit vector \hat{S}_i coincide with the spin vector of the i^{th} gyro and $\bar{\omega}_i$ represent the component of ω that is perpendicular to the spin axis of the i^{th} gyro. The relationship between the spin axis of the i^{th} gyro and the various vectors is shown in figure F-1.

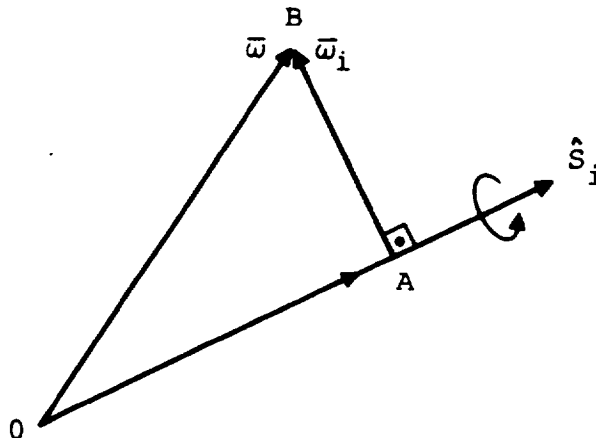


Figure F-1. Spin Axis of the i^{th} Gyro and the Angular Velocity Vectors

It is noted that $\bar{\omega}_i$ is the angular velocity vector measured by a perfect i th gyro and this vector is given by Equation (2)

$$\bar{\omega}_i = \bar{\omega} - \hat{S}_i (\hat{S}_i \cdot \bar{\omega}) \quad (2)$$

The dot product written in matrix form becomes

$$\hat{S}_i \cdot \bar{\omega} = \begin{bmatrix} \hat{S}_i^T \end{bmatrix} [\bar{\omega}] , \quad (3)$$

where

$$\begin{bmatrix} \hat{S}_i^T \end{bmatrix} [\bar{\omega}] = \begin{bmatrix} S_{xi} & S_{yi} & S_{zi} \end{bmatrix} \begin{bmatrix} \omega_x \\ \omega_y \\ \omega_z \end{bmatrix}$$

$$= \begin{bmatrix} S_{xi} \omega_x + S_{yi} \omega_y + S_{zi} \omega_z & 0 & 0 \\ 0 & 0 & 0 \\ 0 & 0 & 0 \end{bmatrix} . \quad (4)$$

Where S_{xi} , S_{yi} and S_{zi} are components of the unit vector, \hat{S}_i , resolved along the reference coordinate set xyz , and ω_x , ω_y and ω_z are components of total angular velocity of the cluster also resolved along the same set.

Substitute (3) into (2) and express in matrix form.

$$\begin{aligned} [\bar{\omega}_i] &= [\bar{\omega}] - [\hat{S}_i] [\hat{S}_i^T] [\bar{\omega}] \\ &= ([I] - [\hat{S}_i] [\hat{S}_i^T]) [\bar{\omega}] \end{aligned} \quad (5)$$

Let

$$[S_i] = [I] - [\hat{S}_i] [\hat{S}_i^T] \quad (6)$$

Substitute (6) into (5)

$$[\bar{\omega}_i] = [S_i] [\bar{\omega}] \quad (7)$$

Expanding (6) we obtain

$$[S_i] = \begin{bmatrix} 1 - S_{xi}^2 & -S_{xi} S_{yi} & -S_{xi} S_{zi} \\ -S_{xi} S_{yi} & 1 - S_{yi}^2 & -S_{yi} S_{zi} \\ -S_{xi} S_{zi} & -S_{yi} S_{zi} & 1 - S_{zi}^2 \end{bmatrix} \quad (8)$$

Examination of Equation (7) reveals that when the total angular rate vector, $\bar{\omega}$, is premultiplied by the $[S_i]$ matrix the resulting product yields a component of the total angular input rate that is perpendicular to the spin vector of the i th gyro. Thus $\bar{\omega}_i$ represents the rate vector as would be measured by a perfect i th gyro. Similar relationships may be written for the n TDF gyros contained within the instrument cluster. Thus,

$$\begin{aligned}
 [\bar{\omega}_1] &= [s_1] [\bar{\omega}] \\
 [\bar{\omega}_2] &= [s_2] [\bar{\omega}] \\
 &\vdots \\
 [\bar{\omega}_i] &= [s_i] [\bar{\omega}] \\
 &\vdots \\
 [\bar{\omega}_n] &= [s_n] [\bar{\omega}] .
 \end{aligned} \tag{9}$$

Equation (9) may be written as

$$\begin{bmatrix} [\bar{\omega}_1] \\ [\bar{\omega}_2] \\ \vdots \\ [\bar{\omega}_i] \\ \vdots \\ [\bar{\omega}_n] \end{bmatrix} = \begin{bmatrix} [s_1] \\ [s_2] \\ \vdots \\ [s_i] \\ \vdots \\ [s_n] \end{bmatrix} [\bar{\omega}] , \tag{10}$$

or

$$[\tilde{\omega}] = [A] [\bar{\omega}] , \tag{11}$$

Where $[\tilde{\omega}]$ is 1 by 3n matrix representing 2n measured rates and $[A]$ is the 3 by 3n matrix (sometimes referred to as the mapping matrix). $[\tilde{\omega}]$ and $[A]$ are defined by Equations (12) and (13).

$$[\tilde{\omega}] = \begin{bmatrix} [\omega_1] \\ [\omega_2] \\ \vdots \\ [\omega_i] \\ \vdots \\ [\omega_n] \end{bmatrix} \quad (12)$$

$$[A] = \begin{bmatrix} [s_1] \\ [s_2] \\ \vdots \\ [s_i] \\ \vdots \\ [s_n] \end{bmatrix} \quad (13)$$

Assuming that the spin axes of the n gyros used are not collinear then we have 2n available measurements that represent the total rate of the cluster. There is a variety of ways of extracting the desired information out of the 2n measurements available. In our approach we will consider the least squares regression method which is given by Equation (14)

$$\langle \omega \rangle = \left[A^T A \right]^{-1} \left[A^T \right] \bar{\omega} \quad (14)$$

Comparing Equation (14) with Equation (1) it is noted that

$$[D] = \left[A^T A \right]^{-1} \left[A^T \right] \quad (15)$$

Next we will evaluate the least squares solution for matrix [D] when n TDF gyros are present and operating within the instrument cluster.

Using (13) we obtain

$$\left[A^T \right] = \left[\left[S_1^T \right], \left[S_2^T \right], \dots, \left[S_i^T \right], \dots, \left[S_n^T \right] \right] \quad (16)$$

Examination of Equation (8) indicates that

$$\left[S_i^T \right] = \left[S_i \right] \cdot \quad (17)$$

Applying (17) to (16)

$$\left[A^T \right] = \left[\left[S_1 \right], \left[S_2 \right], \dots, \left[S_i \right], \dots, \left[S_n \right] \right] \quad (18)$$

And thus

$$\begin{aligned}
 [A^T] [A] &= \left[[s_1], [s_2], \dots, [s_i], \dots, [s_n] \right] \begin{bmatrix} [s_1] \\ [s_2] \\ \vdots \\ [s_i] \\ \vdots \\ [s_n] \end{bmatrix} \\
 &= [s_1]^2 + [s_2]^2 + \dots + [s_i]^2 + \dots + [s_n]^2 . \quad (19)
 \end{aligned}$$

From Equation (6)

$$\begin{aligned}
 [s_i]^2 &= \left[I - \hat{S}_i \hat{S}_i^T \right] \left[I - \hat{S}_i \hat{S}_i^T \right] \\
 &= I - 2 \hat{S}_i \hat{S}_i^T + \hat{S}_i \hat{S}_i^T \hat{S}_i \hat{S}_i^T \quad (20)
 \end{aligned}$$

But since

$$\hat{S}_i^T \hat{S}_i = 1 \quad (21)$$

Then Equation (20) becomes

$$[s_i]^2 = 1 - \hat{s}_i \hat{s}_i^T = [s_i] \quad (22)$$

Using Relationship (22) in Equation (19) we have

$$[A^T] [A] = \left[[s_1] + [s_2] + \dots + [s_i] + \dots + [s_n] \right] \quad (23)$$

Substitute (18) and (23) into (14) we obtain

$$\begin{aligned} \langle \omega \rangle &= \left[[s_1] + [s_2] + \dots + [s_i] + \dots + [s_n] \right]^{-1} \left[[s_1], [s_2], \dots, [s_i], \dots, [s_n] \right] \tilde{\omega} \\ &= \left[\sum_{i=1}^{i=n} [s_i] \right]^{-1} \left[[s_1], [s_2], [s_3], \dots, [s_n] \right] \tilde{\omega} \\ \langle \omega \rangle &= \left[\sum_{i=1}^{i=n} [s_i] \right]^{-1} \tilde{\omega} \end{aligned} \quad (24)$$

since $[s_i] \bar{\omega}_i = \bar{\omega}_i$.

Equation (24) states the computed angular velocity, $\langle \omega \rangle$, of the instrument cluster based on outputs of the individual instruments. In this equation the outputs of the individual instruments are so weighted that the sum of the squares of the errors associated with all the instrument axes is minimized.

Equation (24) is a general one and prior to its solution, instrument orientations have to be specified. This is done in the following paragraphs for tetrahedral orientation.

DESIGN MATRIX FOR FOUR GYROS

Thus let us assume that $n = 4$. Using Equation (6)

$$\begin{aligned} \sum_{i=1}^{i=4} [S_i] &= \sum_{i=1}^{i=4} \left[[I] - [\hat{S}_i] [S_i^T] \right] \\ &= 4 [I] - \sum_{i=1}^{i=4} [\hat{S}_i] [S_i^T]. \end{aligned} \quad (25)$$

Next we evaluate the value of the sum of the products in Equation (25).

$$\begin{aligned} \sum_{i=1}^{i=4} [\hat{S}_i] [S_i^T] &= \sum_{i=1}^{i=4} \begin{bmatrix} S_{xi} \\ S_{yi} \\ S_{zi} \end{bmatrix} [S_{xi} \ S_{yi} \ S_{zi}] \\ &= \begin{bmatrix} S_{xi}^2 & S_{xi} S_{yi} & S_{xi} S_{zi} \\ S_{yi} S_{xi} & S_{yi}^2 & S_{yi} S_{zi} \\ S_{zi} S_{xi} & S_{zi} S_{yi} & S_{zi}^2 \end{bmatrix} \end{aligned} \quad (26)$$

Assuming orientation of the spin axes on the faces of a tetrahedron as shown in figure F-2, it may be proven that the direction cosines for the \hat{S}_i unit vectors are:

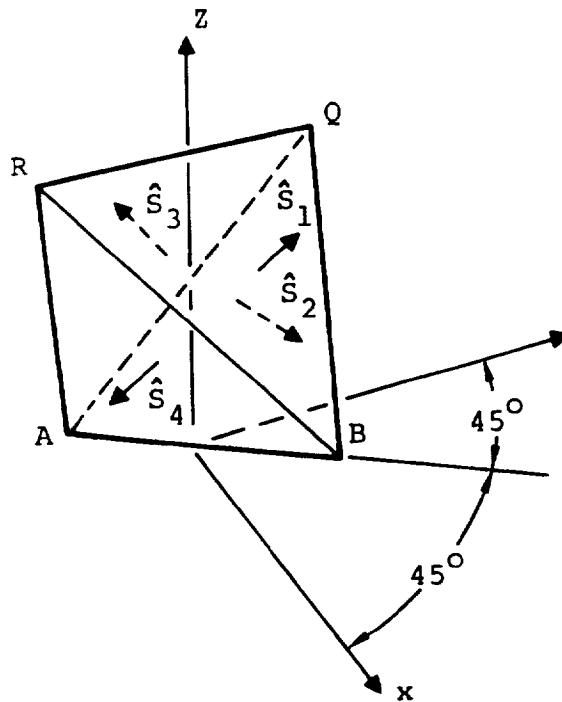


Figure F-2. Regular Tetrahedron

for

$$\begin{aligned}
 i = 1 \quad s_{x1} &= \frac{1}{\sqrt{3}}, & s_{y1} &= \frac{1}{\sqrt{3}}, & s_{z1} &= \frac{1}{\sqrt{3}} \\
 2 \quad s_{x2} &= -\frac{1}{\sqrt{3}}, & s_{y2} &= \frac{1}{\sqrt{3}}, & s_{z2} &= -\frac{1}{\sqrt{3}} \\
 3 \quad s_{x3} &= -\frac{1}{\sqrt{3}}, & s_{y3} &= -\frac{1}{\sqrt{3}}, & s_{z3} &= -\frac{1}{\sqrt{3}} \\
 4 \quad s_{x4} &= \frac{1}{\sqrt{3}}, & s_{y4} &= -\frac{1}{\sqrt{3}}, & s_{z4} &= -\frac{1}{\sqrt{3}}
 \end{aligned} \tag{27}$$

$$\sum_{i=1}^{i=4} s_{xi}^2 = \frac{4}{3}, \quad \sum_{i=1}^{i=4} s_{yi}^2 = \frac{4}{3}, \quad \sum_{i=1}^{i=4} s_{zi}^2 = \frac{4}{3} \tag{28}$$

$$\sum_{i=1}^{i=4} s_{xi} s_{yi} = \sum_{i=1}^{i=4} s_{xi} s_{zi} = \sum_{i=1}^{i=4} s_{y1} s_{z1} = 0 \tag{29}$$

Substitute (28) and (29) into (26) we obtain

$$\sum_{i=1}^{i=4} \begin{bmatrix} \hat{S}_i \\ \hat{S}_i \end{bmatrix} \begin{bmatrix} \hat{S}_i^T \\ \hat{S}_i^T \end{bmatrix} = \begin{bmatrix} \frac{4}{3} & 0 & 0 \\ 0 & \frac{4}{3} & 0 \\ 0 & 0 & \frac{4}{3} \end{bmatrix} = \frac{4}{3} \begin{bmatrix} \mathbf{I} \\ \mathbf{I} \\ \mathbf{I} \end{bmatrix} \quad (30)$$

Substitute (30) into (25)

$$\sum_{i=1}^{i=4} \begin{bmatrix} S_i \\ S_i \end{bmatrix} = 4 \begin{bmatrix} \mathbf{I} \\ \mathbf{I} \\ \mathbf{I} \end{bmatrix} - \frac{4}{3} \begin{bmatrix} \mathbf{I} \\ \mathbf{I} \\ \mathbf{I} \end{bmatrix} = \frac{8}{3} \begin{bmatrix} \mathbf{I} \\ \mathbf{I} \\ \mathbf{I} \end{bmatrix} \quad (30a)$$

and

$$\left[\sum_{i=1}^{i=4} \begin{bmatrix} S_i \\ S_i \end{bmatrix} \right]^{-1} = \frac{1}{\frac{8}{3} \begin{bmatrix} \mathbf{I} \\ \mathbf{I} \\ \mathbf{I} \end{bmatrix}} = \frac{3}{8} \begin{bmatrix} \mathbf{I} \\ \mathbf{I} \\ \mathbf{I} \end{bmatrix} \quad (31)$$

Substitute (31) into (24)

$$\hat{\omega} = \frac{3}{8} \left[\begin{bmatrix} S_1 \\ S_1 \end{bmatrix}, \begin{bmatrix} S_2 \\ S_2 \end{bmatrix}, \begin{bmatrix} S_3 \\ S_3 \end{bmatrix}, \begin{bmatrix} S_4 \\ S_4 \end{bmatrix} \right] \tilde{\omega} \quad (32)$$

Substitute (12) into (32)

$$\begin{aligned} \langle \hat{\omega} \rangle &= \frac{3}{8} \begin{bmatrix} [s_1] \\ [s_2] \\ [s_3] \\ [s_4] \end{bmatrix} \begin{bmatrix} [\omega_1] \\ [\omega_2] \\ [\omega_3] \\ [\omega_4] \end{bmatrix} \\ &= \frac{3}{8} \left[[s_1][\omega_1] + [s_2][\omega_2] + [s_3][\omega_3] + [s_4][\omega_4] \right] \end{aligned} \quad (33)$$

But since in general

$$[s_i][\omega_i] = [\omega_i] \quad (34)$$

Then, the least squares solution for four gyros arranged in tetrahedron configuration is given by Equation (35)

$$\langle \omega \rangle_{1234} = \frac{3}{8} [\bar{\omega}_1 + \bar{\omega}_2 + \bar{\omega}_3 + \bar{\omega}_4] \quad (35)$$

Where $\bar{\omega}_1, \bar{\omega}_2, \bar{\omega}_3$ and $\bar{\omega}_4$ are vectors representing outputs of the four gyros.

The subscript 1234 to $\langle \omega \rangle$ indicates that solution is based on the output data of all four gyros.

The relationship stated by Equation (34) may be derived from physical reasoning as follows: Premultiplication of a vector by the matrix $[s_i]$ yields the component of that vector that is perpendicular to the \hat{s}_i vector. Now, since $\bar{\omega}_i$ is defined as being perpendicular to \hat{s}_i , then premultiplication of $\bar{\omega}_i$ by the matrix $[s_i]$ must yield $\bar{\omega}_i$.

DESIGN MATRIX FOR THREE GYROS

Next let us assume that $n=3$. When one of the gyros in a tetrahedral set fails, then we wish to process only the outputs from the remaining three properly operating gyros. Let us make an arbitrary assumption that gyro number 4 has failed.

The sum of matrices in Equation (24) becomes

$$\sum_{i=1}^{i=3} [S_i] = [S_1] + [S_2] + [S_3] + [S_4] - [S_4] \quad (36)$$

Note that the matrix involving the failed gyro, $[S_4]$, was added and subtracted in Equation (36). Substitute (30a) into (36)

$$\begin{aligned} \sum_{i=1}^{i=3} [S_i] &= \frac{8}{3} [I] - [S_4] \\ &= \left(\frac{8}{3} [I] - \frac{3}{8} [S_4] \right) \end{aligned} \quad (37)$$

Assume that the inverse of Equation (37) is given by Equation (38). Thus

$$\left[\sum_{i=1}^{i=3} [S_i] \right]^{-1} = \frac{3}{8} \left([I] + \frac{3}{5} [S_4] \right) \quad (38)$$

The relationship stated by the Equation (38) may be verified by performing multiplication indicated by Equation (39)

$$\left[\sum_{i=1}^{i=3} [S_i] \right] \left[\sum_{i=1}^{i=3} [S_i] \right]^{-1} = [I] \quad (39)$$

Substitute Equation (37) and Equation (38) into Equation (39)

$$\begin{aligned} & \left[\frac{8}{3} [I] - \frac{3}{8} [S_4] \right] \left[\frac{3}{8} [I] + \frac{3}{5} [S_4] \right] \\ &= [I] + \frac{3}{5} [S_4] - \frac{3}{8} [S_4] - \frac{9}{40} [S_4]^2 \\ &= [I] + \frac{24-15}{40} [S_4] - \frac{9}{40} [S_4]^2 \\ &= [I] \quad \text{Q.E.D.} \end{aligned}$$

Where it was noted that relationship stated by Equation (22) was used.

Substituting (38) into (24) and noting (34) we obtain

$$\langle \omega \rangle_{123} = \frac{3}{8} \left[[I] + \frac{3}{5} [S_4] \right] \left[\bar{\omega}_1 + \bar{\omega}_2 + \bar{\omega}_3 \right] \quad (40)$$

Equation (40) states the least squares solution for the tetrahedral set when it is desired to process the data from gyros 1, 2 and 3 and disregard the data provided by gyro number 4. In a similar manner when the data from gyro number 3 are disregarded we obtain

$$\langle \omega \rangle_{124} = \frac{3}{8} \left[\left[I \right] + \frac{3}{5} \left[S_3 \right] \right] \left[\bar{\omega}_1 + \bar{\omega}_2 + \bar{\omega}_4 \right] \quad (41)$$

When the data from gyro number 2 are disregarded we obtain

$$\langle \omega \rangle_{134} = \frac{3}{8} \left[\left[I \right] + \frac{3}{5} \left[S_2 \right] \right] \left[\bar{\omega}_1 + \bar{\omega}_3 + \bar{\omega}_4 \right] \quad (42)$$

When the data from gyro number 1 are disregarded we obtain

$$\langle \omega \rangle_{234} = \frac{3}{8} \left[\left[I \right] + \frac{3}{5} \left[S_1 \right] \right] \left[\bar{\omega}_2 + \bar{\omega}_3 + \bar{\omega}_4 \right] \quad (43)$$

DESIGN MATRIX FOR TWO GYROS

Finally let us assume that $n=2$, i.e., when two of the gyros in a tetrahedral set fail, then, of course, we wish to process only the outputs from the remaining two properly operating gyros. As before, let us make an arbitrary assumption that gyro numbers 3 and 4 have failed.

The sum of matrices in Equation (24) becomes

$$\sum_{i=1}^{i=2} \left[S_i \right] = \left[S_1 \right] + \left[S_2 \right] \quad (44)$$

Assume that the inverse of Equation (44) is given by Equation (45)

$$\left[\sum_{i=1}^{i=2} [S_i] \right]^{-1} = \frac{11}{4} [I] - \frac{9}{4} \left[[S_1] + [S_2] \right] + \frac{9}{16} \left[[S_1] + [S_2] \right]^2 \quad (45)$$

As before, the relationship stated by Equation (45) will be verified by performing the following evaluation.

Define

$$[B] = \left[[S_1] + [S_2] \right]^{-1} \quad (46)$$

Substitute from Equation (45)

$$[B] = \frac{11}{4} [I] - \frac{9}{4} \left[[S_1] + [S_2] \right] + \frac{9}{16} \left[[S_1] + [S_2] \right]^2 \quad (47)$$

Noting relationship expressed by Equation (6) we obtain

$$[S_1] = [I] - [S_{11}] \quad (48)$$

$$[S_2] = [I] - [S_{22}] \quad (49)$$

Where

$$[S_{11}] = \hat{S}_1 \hat{S}_1^T \quad (50)$$

$$[S_{22}] = \hat{S}_2 \hat{S}_2^T \quad (51)$$

Thus

$$[[S_1] + [S_2]] = [2[I] - [S_{11}] - [S_{22}]] \quad (52)$$

Also

$$\begin{aligned} [[S_1] + [S_2]]^2 &= [2[I] - [[S_{11}] + [S_{22}]]]^2 \\ &= [2[I] - [[S_{11}] + [S_{22}]]] [2[I] \\ &\quad - [[S_{11}] + [S_{22}]]] \\ &= 4[I] - 2[I] [[S_{11}] + [S_{22}]] \\ &\quad - [[S_{11}] + [S_{22}]] 2[I] + [[S_{11}] \\ &\quad + [S_{22}]] [[S_{11}] + [S_{22}]] \\ &= 4[I] - 4 [[S_{11}] + [S_{22}]] + [S_{11}][S_{11}] \\ &\quad + [S_{11}][S_{22}] + [S_{22}][S_{11}] + [S_{22}][S_{22}] \end{aligned} \quad (53)$$

Evaluate

$$[s_{11}] [s_{11}] = [s_{11}]^2 \quad (54)$$

Substitute Equation (50) into (54)

$$\begin{aligned} [s_{11}] [s_{11}] &= \hat{s}_1 \hat{s}_1^T \hat{s}_1 \hat{s}_1^T \\ &= \hat{s}_1 \hat{s}_1^T \\ &= [s_{11}] \end{aligned} \quad (54)$$

Because $\hat{s}_1^T \hat{s}_1$ is the dot product of the same vector and this is equal to unity.

Similarly

$$[s_{22}] [s_{22}] = [s_{22}] \quad (55)$$

Next evaluate $[s_{11}] [s_{22}]$

Substituting from Equation (50) and (51)

$$\begin{aligned} [s_{11}] [s_{22}] &= \hat{s}_1 \hat{s}_1^T \hat{s}_2 \hat{s}_2^T \\ &= -\frac{1}{3} \hat{s}_1 \hat{s}_2^T \\ &\triangleq -\frac{1}{3} [s_{12}] \end{aligned} \quad (56)$$

Because $\hat{S}_1^T \hat{S}_2$ is the dot product of two unit vectors and for the case of tetrahedron orientation this dot product is equal to $-1/3$.

Similarly

$$\begin{aligned} [s_{22}] [s_{11}] &= -\frac{1}{3} \hat{S}_2 \hat{S}_1^T \\ &\triangleq -\frac{1}{3} [s_{21}] \end{aligned} \quad (57)$$

Substitute Equations (54), (55), (56) and (57) into (53) obtaining

$$\begin{aligned} \left[[s_1] + [s_2] \right]^2 &= 4 [I] - 4 \left[[s_{11}] + [s_{22}] \right] \\ &\quad + [s_{11}] - \frac{1}{3} [s_{12}] - \frac{1}{3} [s_{21}] + [s_{22}] \\ &= 4 [I] - 3 \left[[s_{11}] + [s_{22}] \right] - \frac{1}{3} \left[[s_{12}] \right. \\ &\quad \left. + [s_{21}] \right] \end{aligned} \quad (58)$$

Substitute Equation (52) and (58) into (47)

$$\begin{aligned}
 [B] &= \frac{11}{4} [I] - \frac{9}{4} \left[2 [I] - [S_{11}] - [S_{22}] \right] \\
 &\quad + \frac{9}{16} \left[4 [I] - 3 \left[[S_{11}] + [S_{22}] \right] - \frac{1}{3} \left[[S_{12}] + [S_{21}] \right] \right] \\
 &= \left[\frac{11}{4} - \frac{18}{4} + \frac{9}{4} \right] [I] + \left[\frac{9}{4} - \frac{27}{16} \right] \left[[S_{11}] + [S_{22}] \right] \\
 &\quad - \frac{3}{16} \left[[S_{12}] + [S_{21}] \right] \tag{59}
 \end{aligned}$$

Noting definition of [B] from Equation (46) multiply both sides of Equation (59) by the inverse of [B].

$$\begin{aligned}
 [I] &= \left\{ \frac{1}{2} [I] \right. \\
 &\quad \left. + \frac{9}{16} \left[[S_{11}] + [S_{22}] \right] \right. \\
 &\quad \left. - \frac{3}{16} \left[[S_{12}] + [S_{21}] \right] \right\} \left\{ 2 [I] - \left[[S_{11}] + [S_{22}] \right] \right\} \\
 &= [I] - \frac{1}{2} \left[[S_{11}] + [S_{22}] \right] \\
 &\quad + \frac{9}{8} \left[[S_{11}] + [S_{22}] \right] - \frac{9}{16} \left[[S_{11}] + [S_{22}] \right]^2 \\
 &\quad - \frac{3}{8} \left[[S_{12}] + [S_{21}] \right] + \frac{3}{16} \left[[S_{12}] + [S_{21}] \right] \left[[S_{11}] + [S_{22}] \right]
 \end{aligned}$$

$$\begin{aligned}
&= [I] + \left[-\frac{1}{2} + \frac{9}{8}\right] \left[[s_{11}] + [s_{22}]\right] \\
&\quad - \frac{9}{16} \left[[s_{11}] + [s_{22}]\right]^2 \\
&\quad - \frac{3}{8} \left[[s_{12}] + [s_{21}]\right] \\
&\quad + \frac{3}{16} \left[[s_{12}] [s_{11}] + [s_{12}] [s_{22}] + [s_{21}] [s_{11}] + [s_{21}] [s_{22}]\right] \quad (60)
\end{aligned}$$

Evaluate components of the last term of equation (60) using definitions stated by Eqs. (50), (51), (56) and (57)

$$[s_{12}] [s_{11}] = \hat{S}_1 \hat{S}_2^T \hat{S}_1 \hat{S}_1^T = -\frac{1}{3} [s_{11}] \quad (61)$$

$$[s_{12}] [s_{22}] = \hat{S}_1 \hat{S}_2^T \hat{S}_2 \hat{S}_2^T = [s_{12}] \quad (62)$$

$$[s_{21}] [s_{11}] = \hat{S}_2 \hat{S}_1^T \hat{S}_1 \hat{S}_1^T = [s_{21}] \quad (63)$$

$$[s_{21}] [s_{22}] = \hat{S}_2 \hat{S}_1^T \hat{S}_2 \hat{S}_1^T = -\frac{1}{3} [s_{22}] \quad (64)$$

Evaluate the term

$$\begin{aligned}
\left[[s_{11}] + [s_{22}]\right]^2 &= \left[[s_{11}] + [s_{22}]\right] \left[[s_{11}] + [s_{22}]\right] \\
&= [s_{11}]^2 + [s_{11}] [s_{22}] + [s_{22}] [s_{11}] + [s_{22}]^2 \\
&= [s_{11}] + [s_{22}] - \frac{1}{3} \left[[s_{12}] + [s_{21}]\right] \quad (65)
\end{aligned}$$

Substitute Eqs. (61), (62), (63), (64) and (65) into (60).

$$\begin{aligned}
 [I] &= [I] + \frac{5}{8} \left[[S_{11}] + [S_{22}] \right] \\
 &\quad - \frac{9}{16} \left[[S_{11}] + [S_{22}] - \frac{1}{3} \left[[S_{12}] + [S_{21}] \right] \right] \\
 &\quad - \frac{3}{8} \left[[S_{12}] + [S_{21}] \right] \\
 &\quad + \frac{3}{16} \left[[S_{12}] + [S_{21}] - \frac{1}{3} \left[[S_{11}] + [S_{22}] \right] \right] \\
 &= [I] + \left[\frac{5}{8} - \frac{9}{16} - \frac{1}{16} \right] \left[[S_{11}] [S_{22}] \right] \\
 &\quad + \left[\frac{3}{16} - \frac{3}{8} + \frac{3}{16} \right] \left[[S_{12}] + [S_{21}] \right] \\
 &= [I] \quad \text{Q.E.D.}
 \end{aligned}$$

Table F-1 shows the design equations to be used for the special gyro failures. Note that the matrices $[S_1]$, $[S_2]$, $[S_3]$ and $[S_4]$ are only dependent upon the specific orientation of the tetrahedron relative to the reference coordinate axes selected and are entirely independent of the orientation of the gyro sensing axes. The i^{th} matrix is given by

$$[S_i] = \begin{bmatrix} 1 - S_{xi}^2 & -S_{xi}S_{yi} & -S_{xi}S_{zi} \\ -S_{xi}S_{yi} & 1 - S_{yi}^2 & -S_{yi}S_{zi} \\ -S_{xi}S_{zi} & -S_{xi}S_{zi} & 1 - S_{zi}^2 \end{bmatrix}$$

where $i = 1, 2, 3, 4$.

Table F-I. Design Equations

GYRO FAILED	DESIGN EQUATION TO BE USED
NONE	$\langle \omega \rangle_{1234} = \frac{3}{8} (\bar{\omega}_1 + \bar{\omega}_2 + \bar{\omega}_3 + \bar{\omega}_4)$
1	$\langle \omega \rangle_{234} = \frac{3}{8} \left([I] + \frac{3}{5} [S_1] \right) (\bar{\omega}_2 + \bar{\omega}_3 + \bar{\omega}_4)$
2	$\langle \omega \rangle_{134} = \frac{3}{8} \left([I] + \frac{3}{5} [S_2] \right) (\bar{\omega}_1 + \bar{\omega}_3 + \bar{\omega}_4)$
3	$\langle \omega \rangle_{124} = \frac{3}{8} \left([I] + \frac{3}{5} [S_3] \right) (\bar{\omega}_1 + \bar{\omega}_2 + \bar{\omega}_4)$
4	$\langle \omega \rangle_{123} = \frac{3}{8} \left([I] + \frac{3}{5} [S_4] \right) (\bar{\omega}_1 + \bar{\omega}_2 + \bar{\omega}_3)$
1 & 2	$\langle \omega \rangle_{34} = \left(\frac{11}{4} [I] - \frac{9}{4} [[S_3] + [S_4]] + \frac{9}{16} [[S_3] + [S_4]]^2 \right) (\bar{\omega}_3 + \bar{\omega}_4)$
1 & 3	$\langle \omega \rangle_{24} = \left(\frac{11}{4} [I] - \frac{9}{4} [[S_2] + [S_4]] + \frac{9}{16} [[S_2] + [S_4]]^2 \right) (\bar{\omega}_2 + \bar{\omega}_4)$
1 & 4	$\langle \omega \rangle_{23} = \left(\frac{11}{4} [I] - \frac{9}{4} [[S_2] + [S_3]] + \frac{9}{16} [[S_2] + [S_3]]^2 \right) (\bar{\omega}_2 + \bar{\omega}_3)$

Table F-I. Design Equations (Continued)

GYRO FAILED	DESIGN EQUATION TO BE USED
2 & 3	$\langle \omega \rangle_{14} = \left(\frac{11}{4} [I] - \frac{9}{4} [[S_1] + [S_4]] + \frac{9}{16} [[S_1] + [S_4]] \right)^2$ $(\bar{\omega}_1 + \bar{\omega}_4)$
2 & 4	$\langle \omega \rangle_{13} = \left(\frac{11}{4} [I] - \frac{9}{4} [[S_1] + [S_3]] + \frac{9}{16} [[S_1] + [S_3]] \right)^2$ $(\bar{\omega}_1 + \bar{\omega}_3)$
3 & 4	$\langle \omega \rangle_{12} = \left(\frac{11}{4} [I] - \frac{9}{4} [[S_1] + [S_2]] + \frac{9}{16} [[S_1] + [S_2]] \right)^2$ $(\bar{\omega}_1 + \bar{\omega}_2)$

403314

APPENDIX G
RELIABILITY DATA

RELIABILITY DATA

Attached are two separate reliability predictions, of 18 pages each, for the redundant strapdown INS. Both predictions are based upon MIL-HDBK-217B failure rates. The first assumes an Airborne Inhabited application with the part ambient temperatures stabilized at a maximum of 70°C. The second prediction assumes an Airborne Uninhabited application with a part case temperature of 90°C.

The Airborne Uninhabited prediction is applicable to military aircraft applications and is, therefore, conservative for the VTOL application. The Airborne Inhabited condition is applicable to Commercial Airline installations for inertial systems.

RELIABILITY PREDICTION DATA SHEET

AIRBORNE INHABITED

DATE: _____ ASSY AMBIENT TEMP: 70 °C SHEET 1 OF 1
 PROGRAM: Langley Strapdown Inertial Nav. ASSY: Gyro Spin/Interrupt Card
 NHA: _____ SCHEMATIC NO: _____

QUANT (n)	PART TYPE/ASSEMBLY	STRESS RATIO	INDIVIDUAL FAILURE RATE (λ)	TOTAL FAILURE RATE (nλ)
1	I.C., SSI/MSI Digital (M38510/05001) (C24011)	—	0.060	0.060
3	I.C., SSI/MSI Digital (M38510/05102) (C24027)	—	0.191	0.573
1	I.C., SSI/MSI Digital () (C24029)	—	0.201	0.201
3	I.C., SSI/MSI Digital (M38510/01306) (SM54161)	—	0.151	0.453
3	I.C., SSI/MSI Digital () (SM7095)	—	0.075	0.225
2	I.C., SSI/MSI Digital () (SN54LS112)	—	0.079	0.158
2	I.C., SSI/MSI Digital (M38510/00104) (SM5400)	—	0.065	0.130
2	I.C., SSI/MSI Digital (M38510/00105) (SM5404)	—	0.070	0.140
1	I.C., SSI/MSI Digital (M38510/00102) (SM5420)	—	0.053	0.053
1	I.C., SSI/MSI Digital (M38510/00901) (SM5495)	—	0.138	0.138
1	I.C., SSI/MSI Digital (M38510/01403) (SN54153)	—	0.094	0.094
5	I.C., SSI/MSI Digital (M38510/01304) (SM54163)	—	0.140	0.700
1	I.C., SSI/MSI, Linear (LM105)	—	0.171	0.171
1	I.C., SSI/MSI, Linear (LM112)	—	0.227	0.227
1	I.C., SSI/MSI, Linear (LM139)	—	0.208	0.208
1	Transistor, NPN, Logic Switch (JANTX)	0.2	0.019	0.019
6	Transistor, NPN, Linear (JANTX)	0.2	0.040	0.240
1	Transistor, PNP, Linear (JANTX)	0.2	0.059	0.059
3	Diode, General Purpose (JANTX)	0.2	0.053	0.159
12	Diode, SCR (JANTX)	0.2	0.098	1.176
8	Capacitor, Ceramic (CMR)	0.4	0.009	0.072
5	Capacitor, Tant. Solid (CSR)	0.4	0.004	0.020
30	Resistor, Film (RLR)	0.2	0.004	0.120
1	Resistor, W.W., Power (RWR)	0.2	0.011	0.011
1	Connector, 90 Pin	—	2.034	2.034

ASSEMBLY FAILURE RATE 7.322 FAILURES/10⁶ HOURS

G-8 ASSEMBLY MTBF 136,575 HOURS

PAGE 6 OF 18

RELIABILITY PREDICTION DATA SHEET

AIRBORNE INHABITED

DATE: _____ ASSY AMBIENT TEMP: 70 °C SHEET 1 OF 1
 PROGRAM: Langley Strapdown Inertial Nav. ASSY: Mode Card
 NHA: _____ SCHEMATIC NO: _____

QUANT (M)	PART TYPE/ASSEMBLY	STRESS RATIO	INDIVIDUAL FAILURE RATE (A)	TOTAL FAILURE RATE (MA)
1	I.C., SSI/MSI Digital (CD 4053)	—	0.162	0.162
1	I.C., SSI/MSI Digital (AM 1500)	—	0.045	0.045
1	I.C., SSI/MSI Digital (SN 54LS30)	—	0.045	0.045
1	I.C., SSI/MSI Digital (SN 54LS00)	—	0.075	0.075
1	I.C., SSI/MSI Digital (SN 54164)	—	0.148	0.148
2	I.C., SSI/MSI Digital (M38510/01303) (SN 54160)	—	0.151	0.302
4	I.C., SSI/MSI Digital (M38510/00202) (SN 5473)	—	0.087	0.348
4	I.C., SSI/MSI Digital (M38510/00105) (SN 5404)	—	0.070	0.280
1	I.C., SSI/MSI Digital (M38510/00102) (SN 5420)	—	0.053	0.053
6	I.C., SSI/MSI Digital (M38510/01306) (SN 54161)	—	0.151	0.906
2	I.C., SSI/MSI Linear (M38510/10101) (LM 741)	—	0.181	0.362
3	I.C., SSI/MSI Linear (LM 112)	—	0.227	0.681
3	I.C., SSI/MSI Linear (LM 118)	—	0.254	0.762
1	I.C., SSI/MSI Linear (LM 139)	—	0.208	0.208
4	Transistor, NPN, Linear (JANTX)	0.2	0.040	0.160
1	Transistor, PNP, Linear (JANTX)	0.2	0.059	0.059
1	Transistor, Field Effect, Linear (JANTX)	0.2	0.360	0.360
9	Diode, General Purpose (JANTX)	0.2	0.053	0.477
17	Capacitor, Ceramic (CKR)	0.4	0.009	0.153
4	Capacitor, Tant Solid (CSR)	0.4	0.004	0.016
2	Capacitor, Metalized (CHR)	0.4	0.001	0.002
25	Resistor, Film (RLR)	0.2	0.004	0.100
5	Resistor, Film (RMC)	0.2	0.004	0.020
2	Resistor, W.W., Power (RWR)	0.2	0.011	0.022
15	Resistor, w.w., Accurate (RBR)	0.2	0.020	0.300
1	Resistor, Variable (RTR)	0.2	0.032	0.032
1	Inductor, Power	—	0.054	0.054
1	Crystal Oscillator	—	0.054	0.054
1	Heater	—	1.000	1.000
1	Connector, 90 Pin	—	2.034	2.034

ASSEMBLY FAILURE RATE 9.220 FAILURES/10⁶ HOURS

G-16 ASSEMBLY MTBF 108,460 HOURS

PAGE 14 OF 18

RELIABILITY PREDICTION DATA SHEET

AIRBORNE UNINHABITED

DATE: _____ ASSY AMBIENT TEMP: 90 °C SHEET 1 OF 1
 PROGRAM: Langley Strapdown Inertial Nav. ASSY: Gyro Spin/Interrupt Card
 NHA: _____ SCHEMATIC NO: _____

QUANT (n)	PART TYPE/ASSEMBLY	STRESS RATIO	INDIVIDUAL FAILURE RATE (λ)	TOTAL FAILURE RATE (nλ)
1	I.C., SSI/MSI Digital (M38510/05001) (CD4011)	—	0.094	0.094
3	I.C., SSI/MSI Digital (M38510/05102) (CD4027)	—	0.313	0.939
1	I.C., SSI/MSI Digital () (CD4029)	—	0.330	0.330
3	I.C., SSI/MSI Digital (M38510/01306) (SN54161)	—	0.246	0.738
3	I.C., SSI/MSI Digital (DM7095)	—	0.119	0.357
2	I.C., SSI/MSI Digital (SN54LS112)	—	0.126	0.252
2	I.C., SSI/MSI Digital (M38510/00104) (SN5400)	—	0.103	0.206
2	I.C., SSI/MSI Digital (M38510/00105) (SN5404)	—	0.111	0.222
1	I.C., SSI/MSI Digital (M38510/00102) (SN5420)	—	0.082	0.082
1	I.C., SSI/MSI Digital (M38510/00901) (SN5493)	—	0.224	0.224
1	I.C., SSI/MSI Digital (M38510/01403) (SN54153)	—	0.150	0.150
5	I.C., SSI/MSI Digital (M38510/01304) (SN54163)	—	0.246	1.230
1	I.C., SSI/MSI, Linear (LM105)	—	0.395	0.395
1	I.C., SSI/MSI, Linear (LM112)	—	0.533	0.533
1	I.C., SSI/MSI, Linear (LM139)	—	0.482	0.482
1	Transistor, NPN, Logic Switch (JANTX)	0.2	0.037	0.037
6	Transistor, NPN, Linear (JANTX)	0.2	0.079	0.474
1	Transistor, PNP, Linear (JANTX)	0.2	0.130	0.130
3	Diode, General Purpose (JANTX)	0.2	0.120	0.360
12	Diode, SCR (JANTX)	0.2	0.244	2.928
8	Capacitor, Ceramic (CCR)	0.4	0.022	0.176
5	Capacitor, Tant. Solid (CSR)	0.4	0.026	0.130
30	Resistor, Film (RLR)	0.2	0.010	0.300
1	Resistor, W.W., Power (RWR)	0.2	0.026	0.026
1	Connector, 90 Pin	—	7.840	7.840

ASSEMBLY FAILURE RATE 10.635 FAILURES/10⁶ HOURS

G-26 ASSEMBLY MTBF 53,662 HOURS

PAGE 6 OF 18

RELIABILITY PREDICTION DATA SHEET

Airborne Uninhabited

DATE: _____ ASSY AMBIENT TEMP: 90 °C SHEET 1 OF 1
 PROGRAM: Langley Strapdown Inertial Nav. ASSY: Mode Card
 NHA: _____ SCHEMATIC NO: _____

QUANT (M)	PART TYPE/ASSEMBLY	STRESS RATIO	INDIVIDUAL FAILURE RATE (λ)	TOTAL FAILURE RATE (Mλ)
1	I.C., SSI/MSI Digital (CD 4053)	—	0.263	0.263
1	I.C., SSI/MSI Digital (AM1500)	—	0.071	0.071
1	I.C., SSI/MSI Digital (SN54LS30)	—	0.071	0.071
1	I.C., SSI/MSI Digital (SN54LS00)	—	0.119	0.119
1	I.C., SSI/MSI Digital (SN54164)	—	0.241	0.241
2	I.C., SSI/MSI Digital (M38510/01303) (SN54160)	—	0.246	0.492
4	I.C., SSI/MSI Digital (M38510/00202) (SN 5473)	—	0.139	0.556
4	I.C., SSI/MSI Digital (M38510/00105) (SN5404)	—	0.111	0.444
1	I.C., SSI/MSI Digital (M38510/00102) (SN 5420)	—	0.082	0.082
6	I.C., SSI/MSI Digital (M38510/01306) (SN 54161)	—	0.246	1.476
2	I.C., SSI/MSI Linear (M38510/10101) (LM741)	—	0.420	0.840
3	I.C., SSI/MSI Linear (LM112)	—	0.533	1.599
3	I.C., SSI/MSI Linear (LM110)	—	0.641	1.923
1	I.C., SSI/MSI Linear (LM139)	—	0.482	0.482
4	Transistor, NPN, Linear (JANTX)	0.2	0.079	0.316
1	Transistor, PNP, Linear (JANTX)	0.2	0.130	0.130
1	Transistor, Field Effect, Linear (JANTX)	0.2	0.744	0.744
9	Diode, General Purpose (JANTX)	0.2	0.120	1.080
17	Capacitor, Ceramic (CKR)	0.4	0.022	0.374
4	Capacitor, Tant Solid (CSR)	0.4	0.026	0.104
2	Capacitor, Metalized (CHR)	0.4	0.001	0.002
25	Resistor, Film (RLR)	0.2	0.010	0.250
5	Resistor, Film (RNC)	0.2	0.011	0.055
2	Resistor, W.W., Power (RWR)	0.2	0.026	0.052
15	Resistor, W.W., Accurate (RBR)	0.2	0.047	0.705
1	Resistor, Variable (RTR)	0.2	0.083	0.083
1	Inductor, Power	—	0.101	0.101
1	Crystal Oscillator	—	2.100	2.100
1	Heater	—	1.000	1.000
1	Connector, 90 Pin	—	7.840	7.840

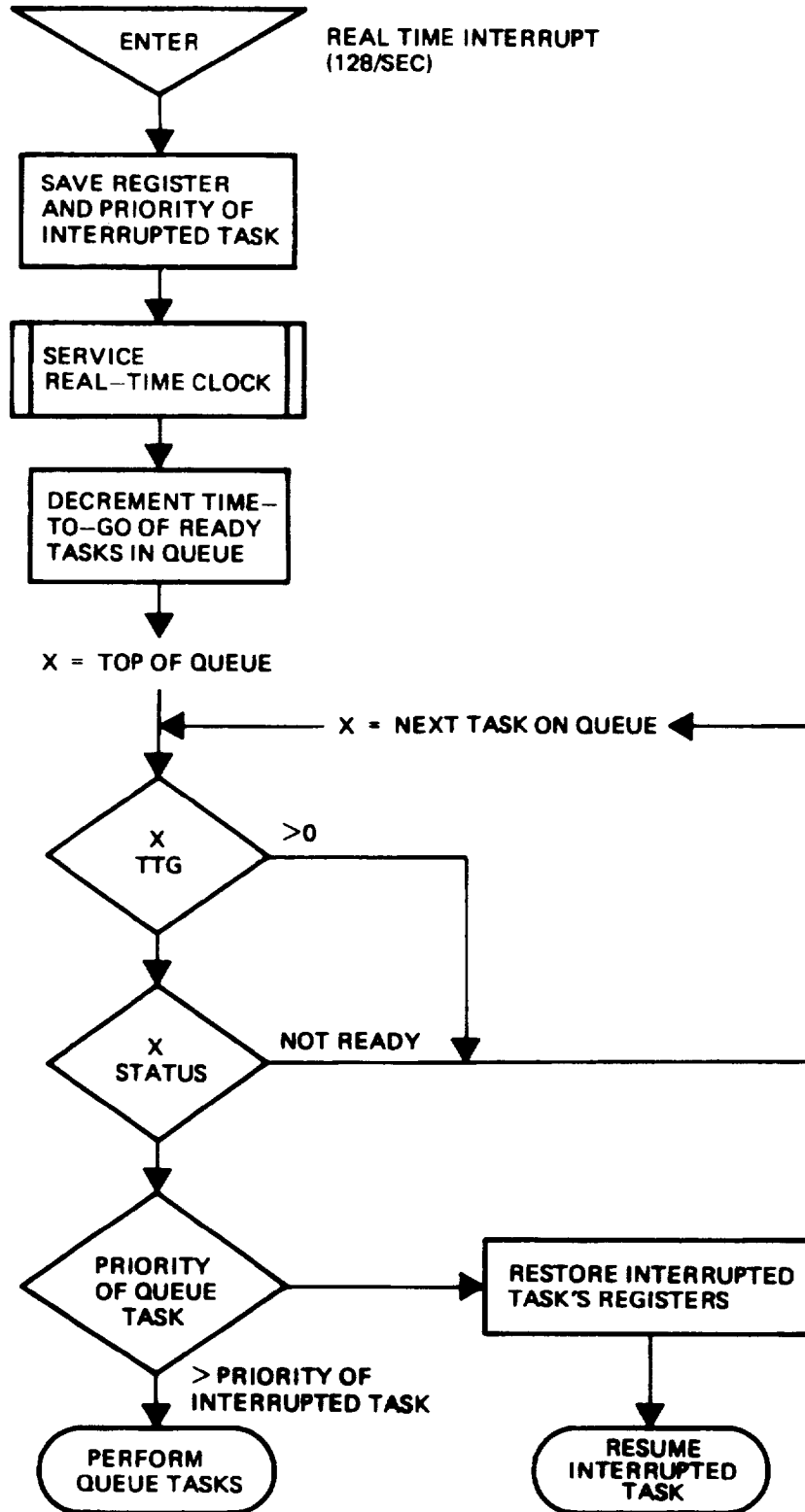
ASSEMBLY FAILURE RATE 23.595 FAILURES/10⁶ HOURS

42,382

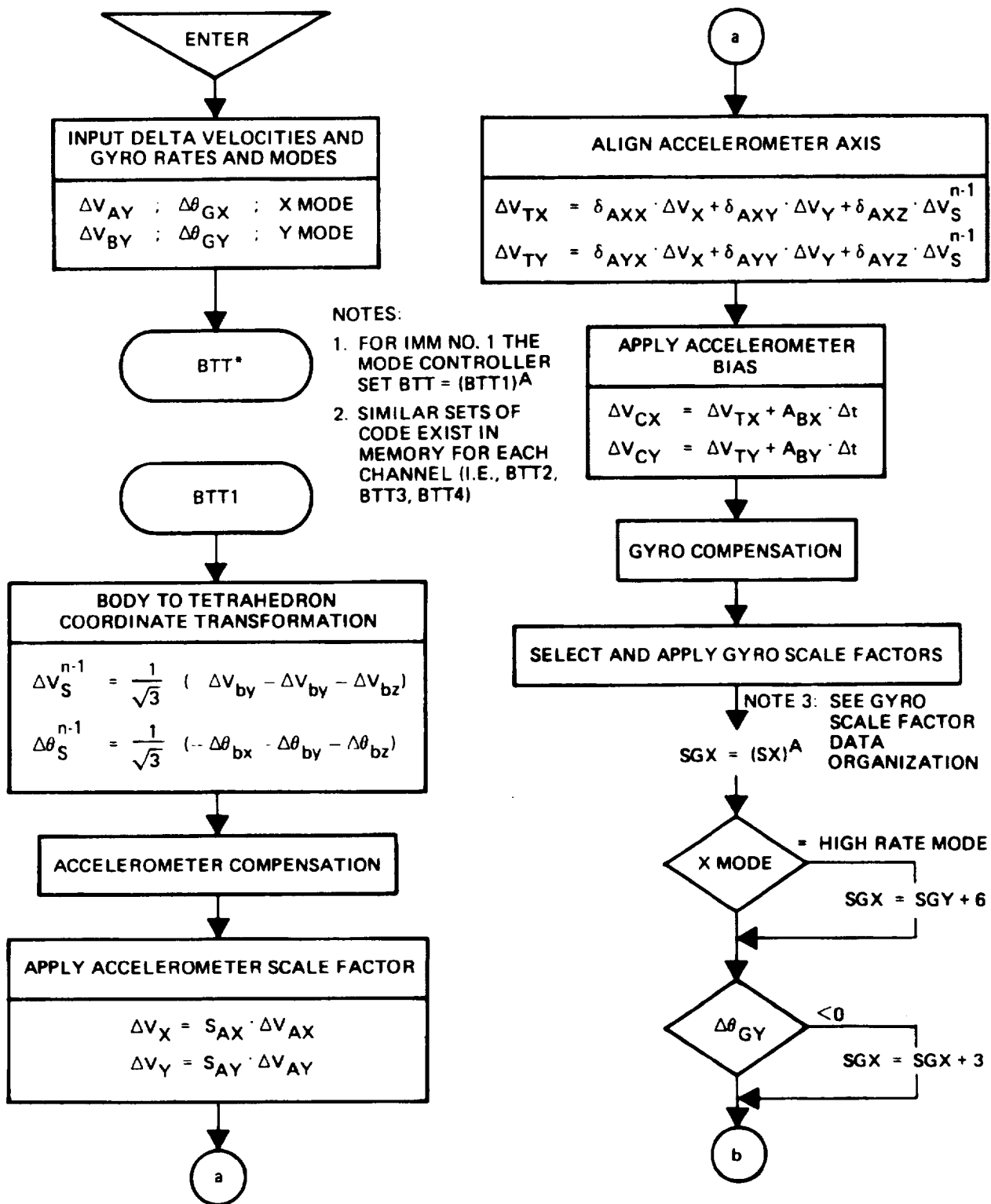
HOURS

PAGE 14 OF 18

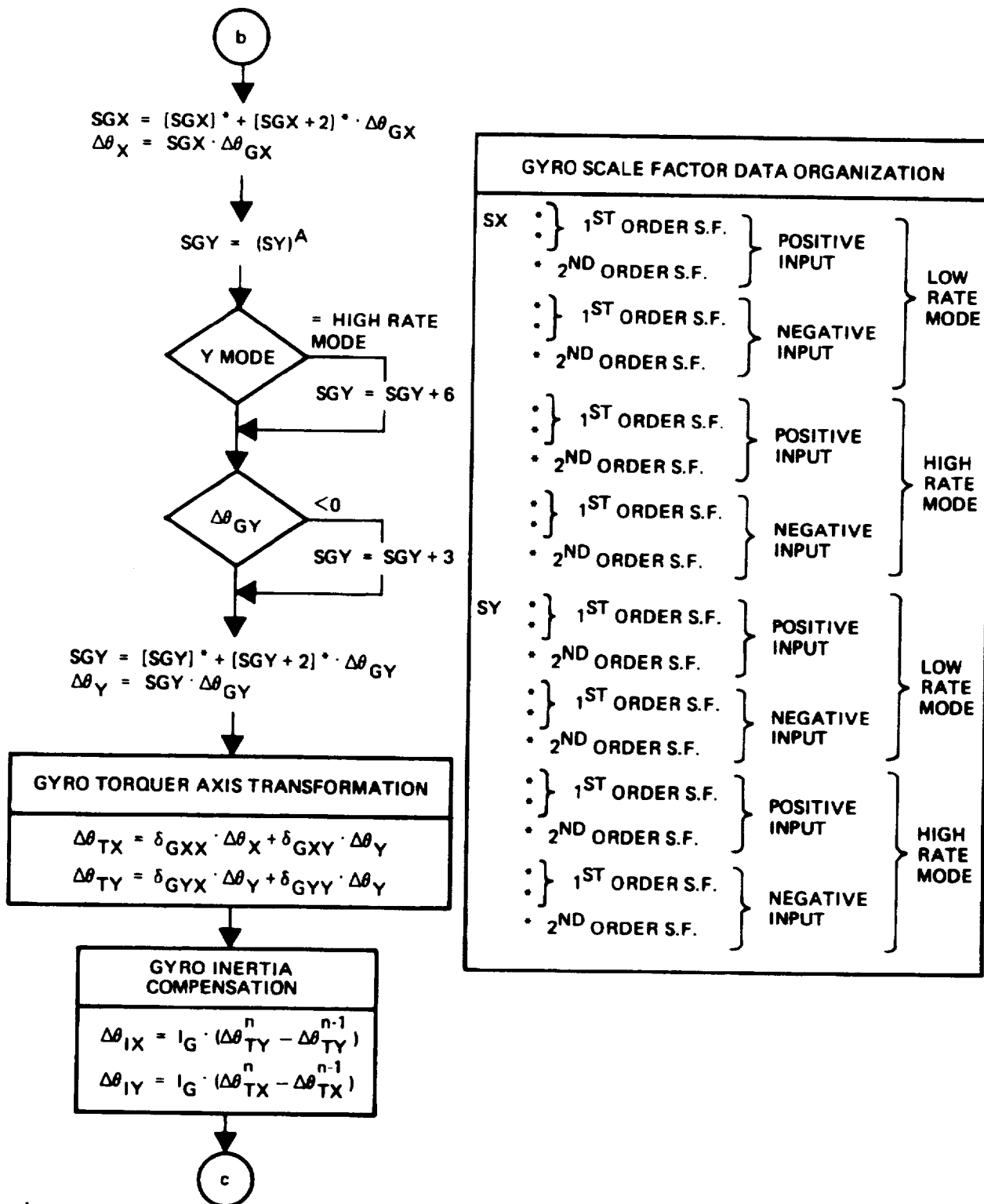
APPENDIX II
COMPUTER FLOW CHARTS



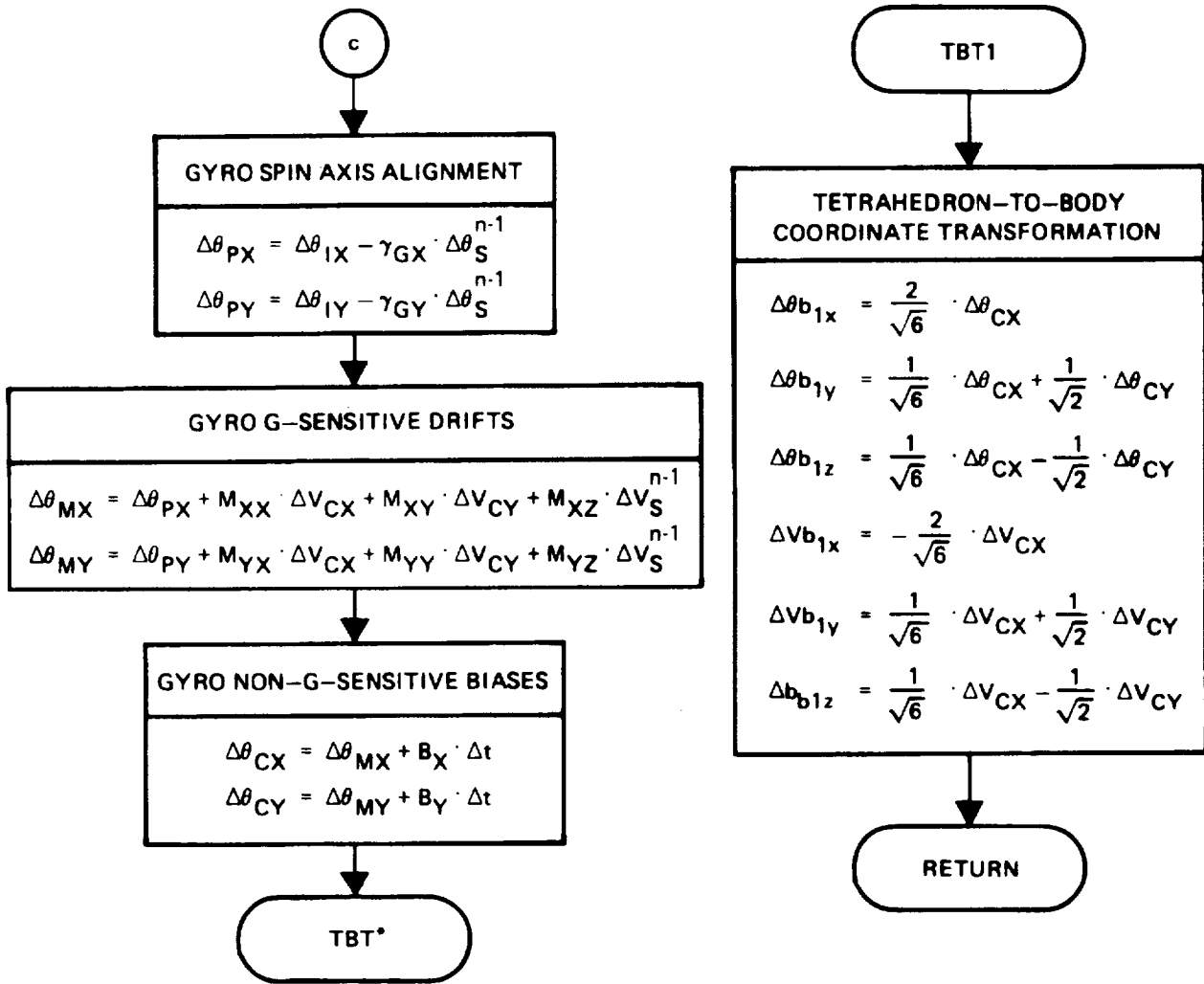
Flowchart H-1. Executive Scheduler (128/sec)



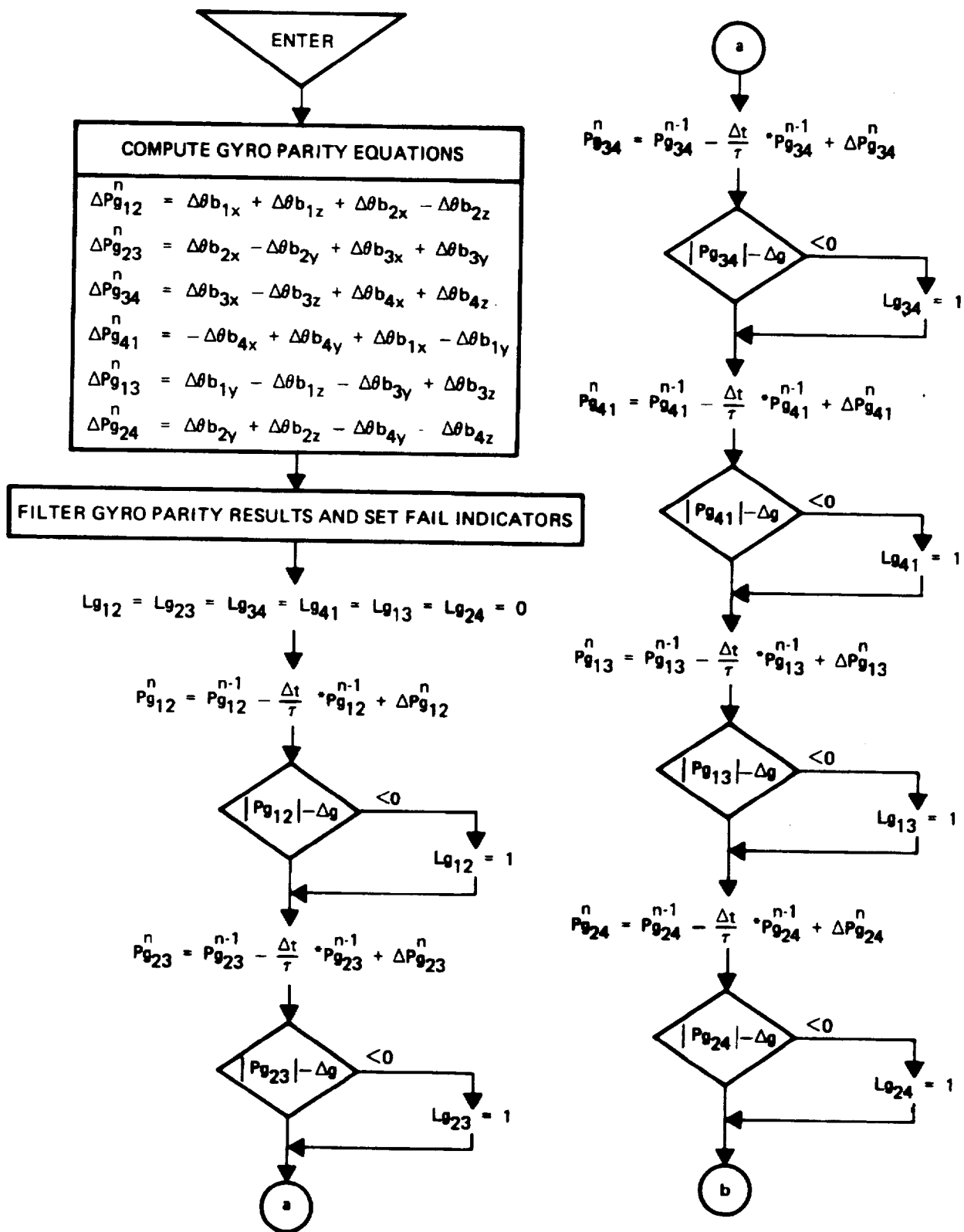
Flowchart H-2. Instrument Compensation Fast (128/sec)
(Sheet 1 of 3)



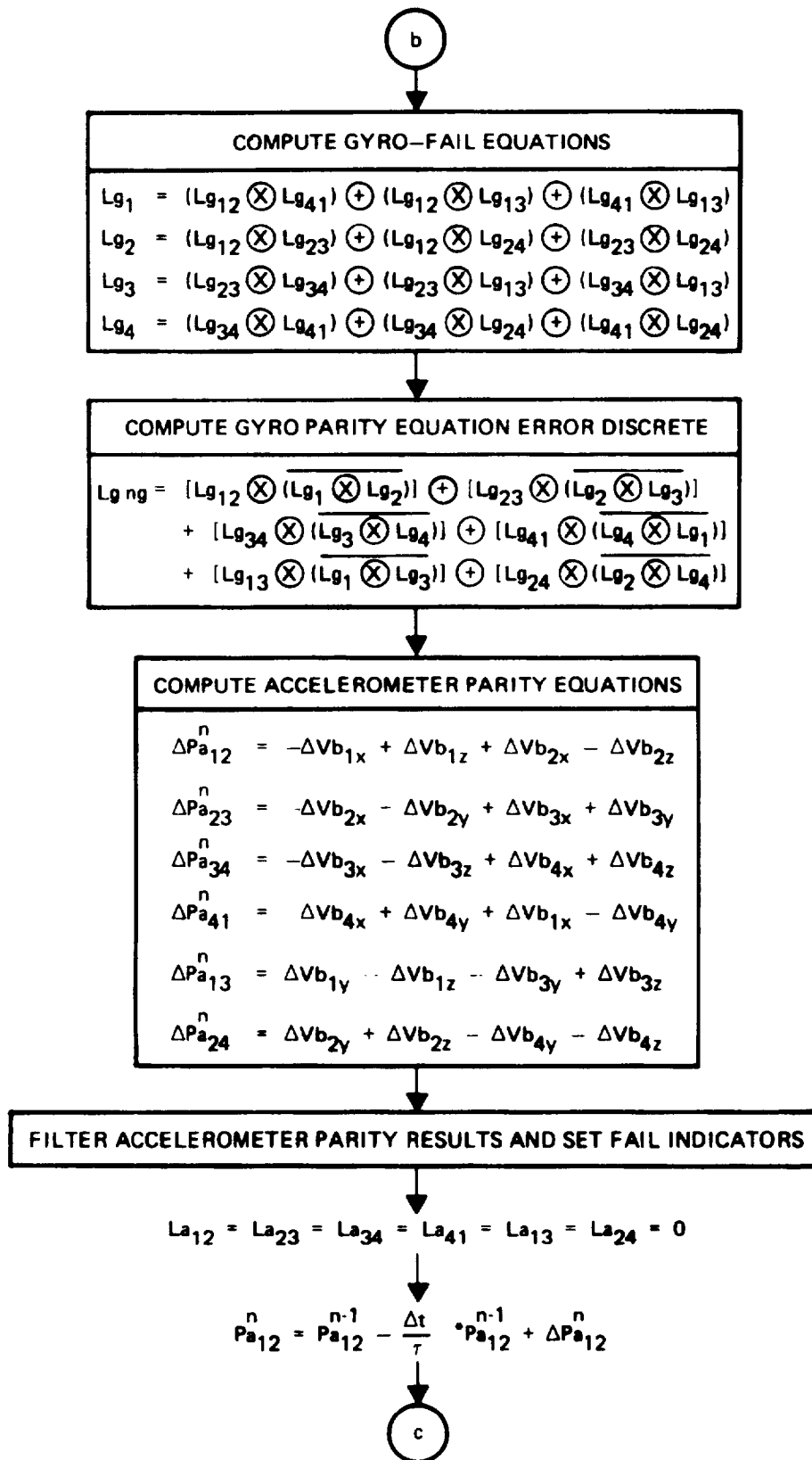
Flowchart H-2. Instrument Compensation Fast (128/sec)
(Sheet 2 of 3)



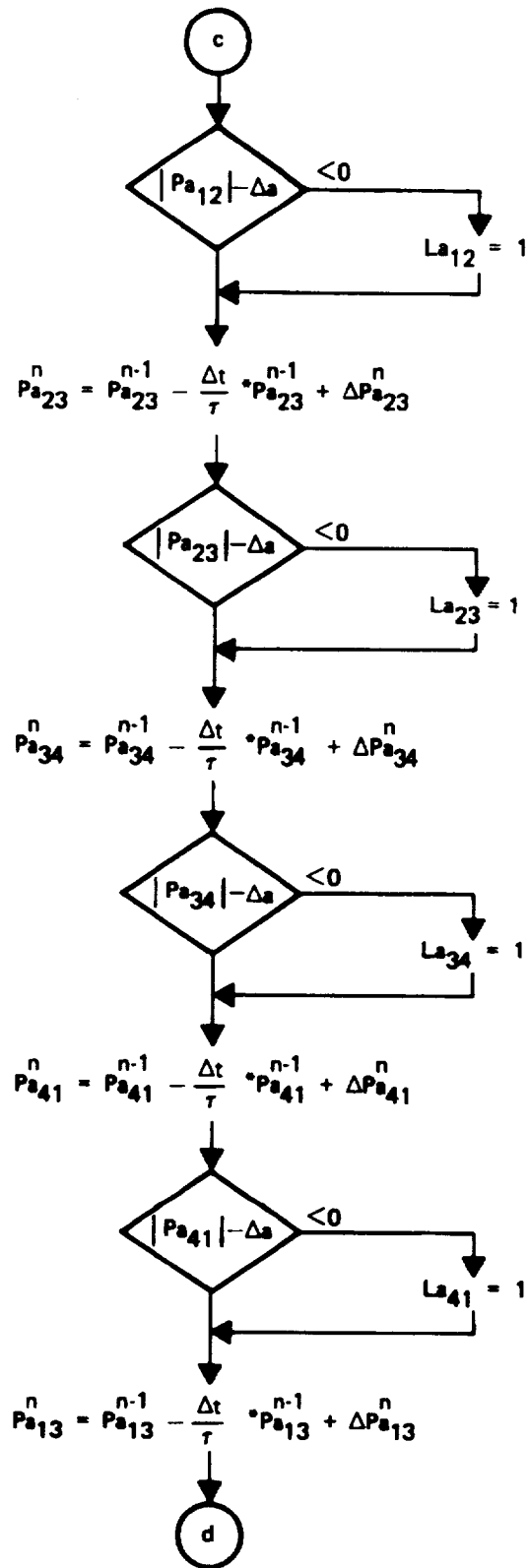
- NOTES: 4. FOR IMM NO. 1 THE MODE
CONTROLLER SET
TBT = (TBT1)^A
5. SIMILAR SETS OF CODE
EXIST IN MEMORY FOR EACH
CHANNEL (I.E., TBT2, TBT3,
TBT4)



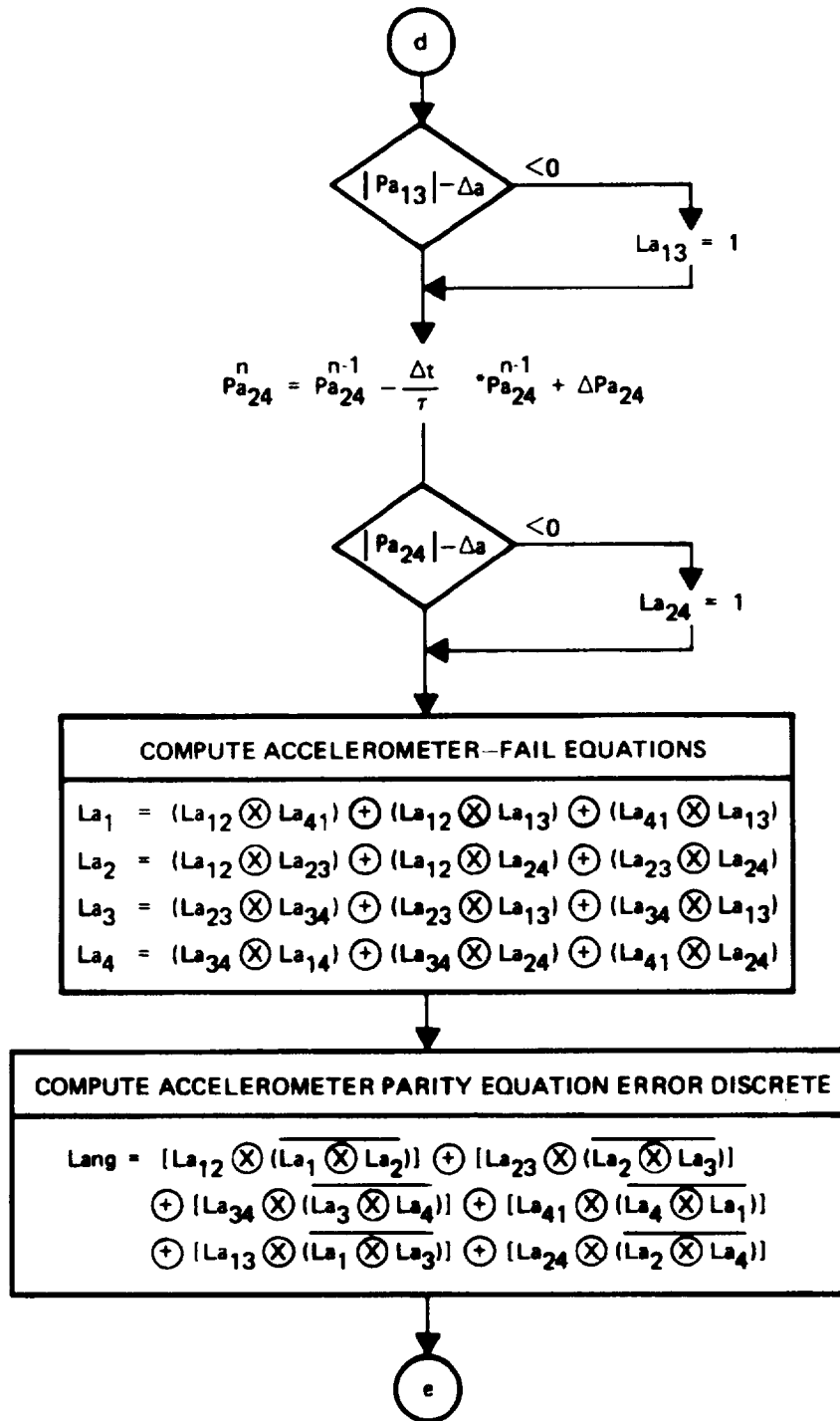
Flowchart H-3. Parity Equations/Design Equations (128/sec)
(Sheet 1 of 5)



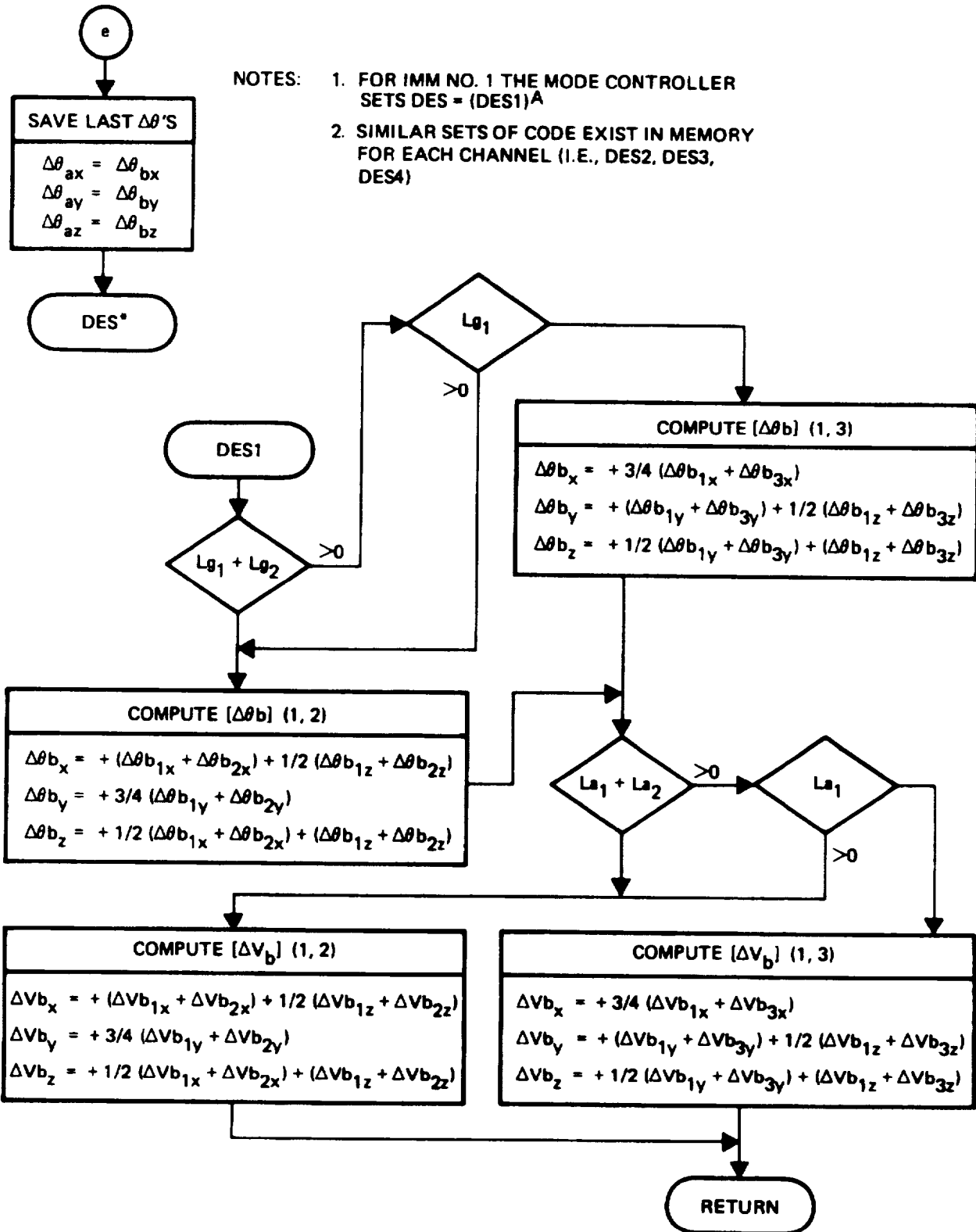
Flowchart H-3. Parity Equations/Design Equations (128/sec)
(Sheet 2 of 5)



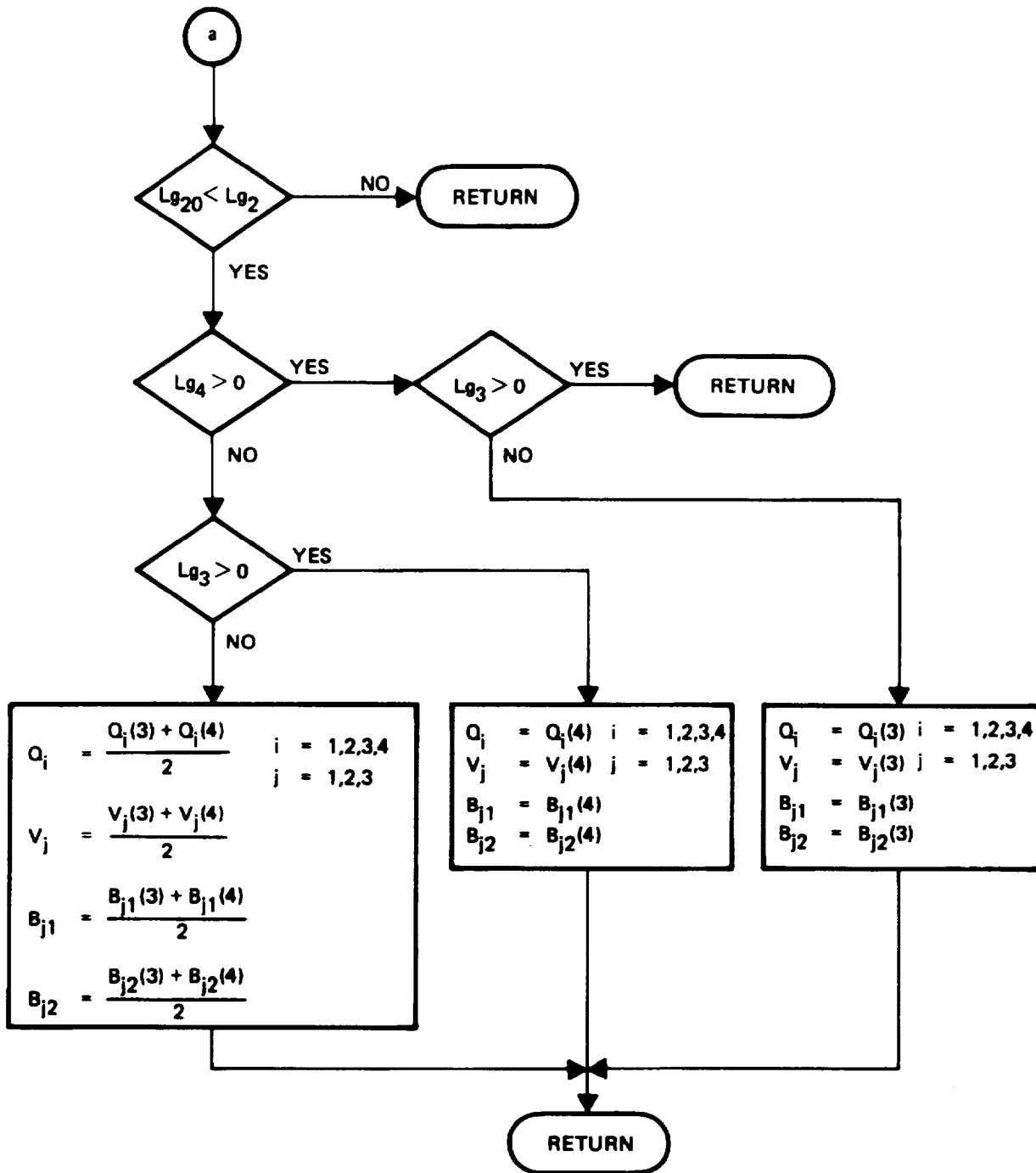
Flowchart H-3. Parity Equations/Design Equations (128/sec)
(Sheet 3 of 5)



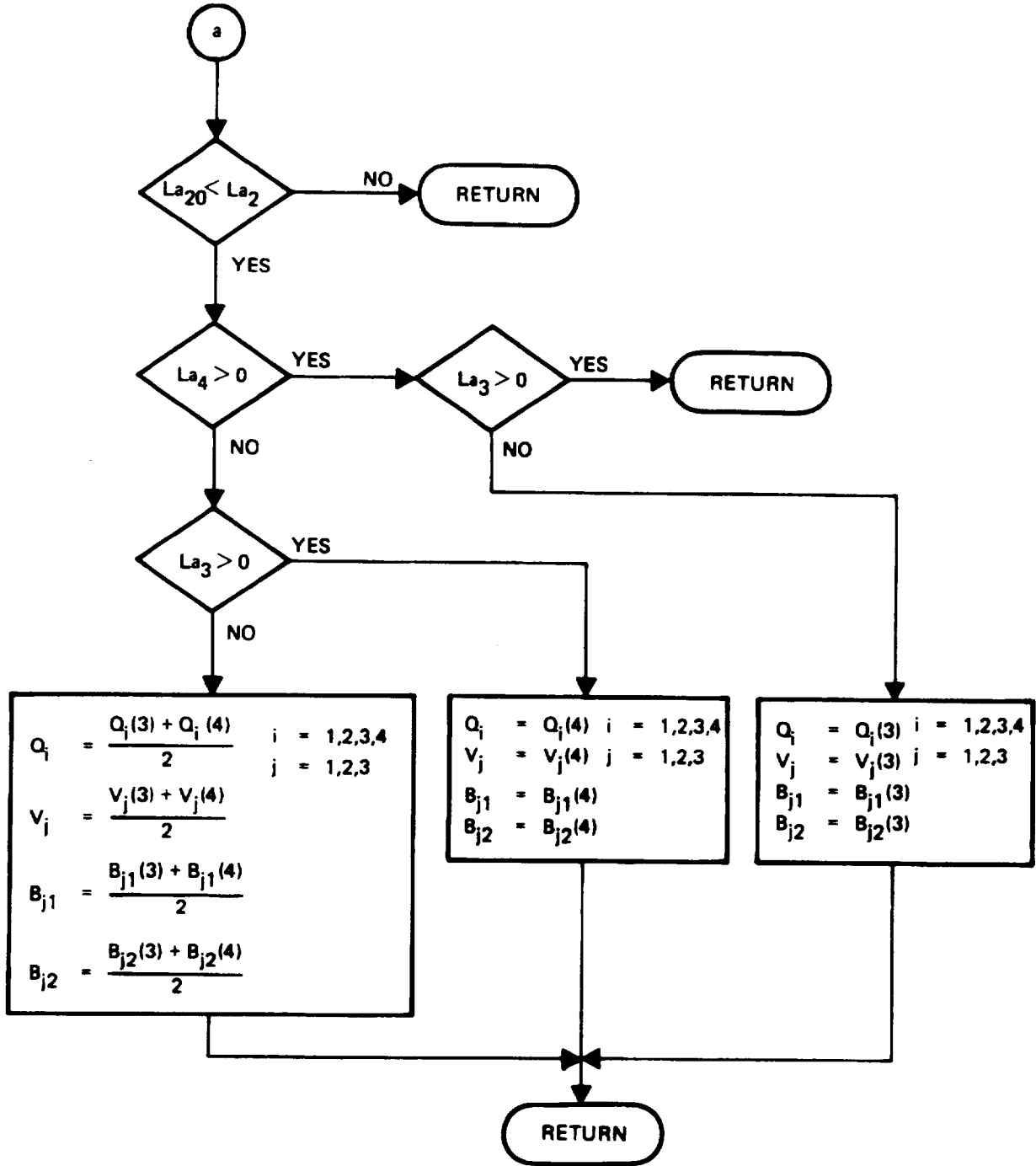
Flowchart H-3. Parity Equations/Design Equations (128/sec)
(Sheet 4 of 5)



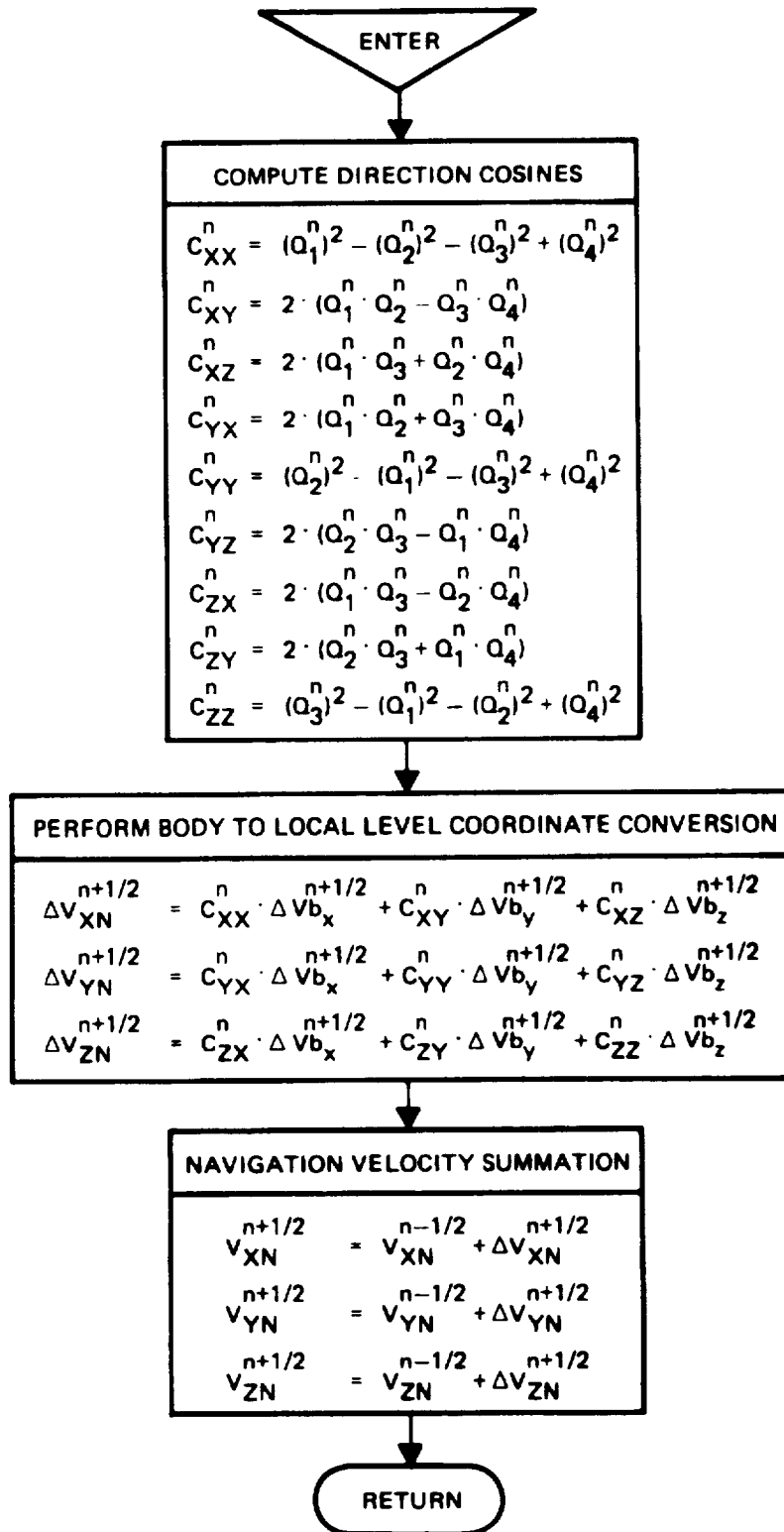
Flowchart H-3. Parity Equations/Design Equations (128/sec)
 (Sheet 5 of 5)



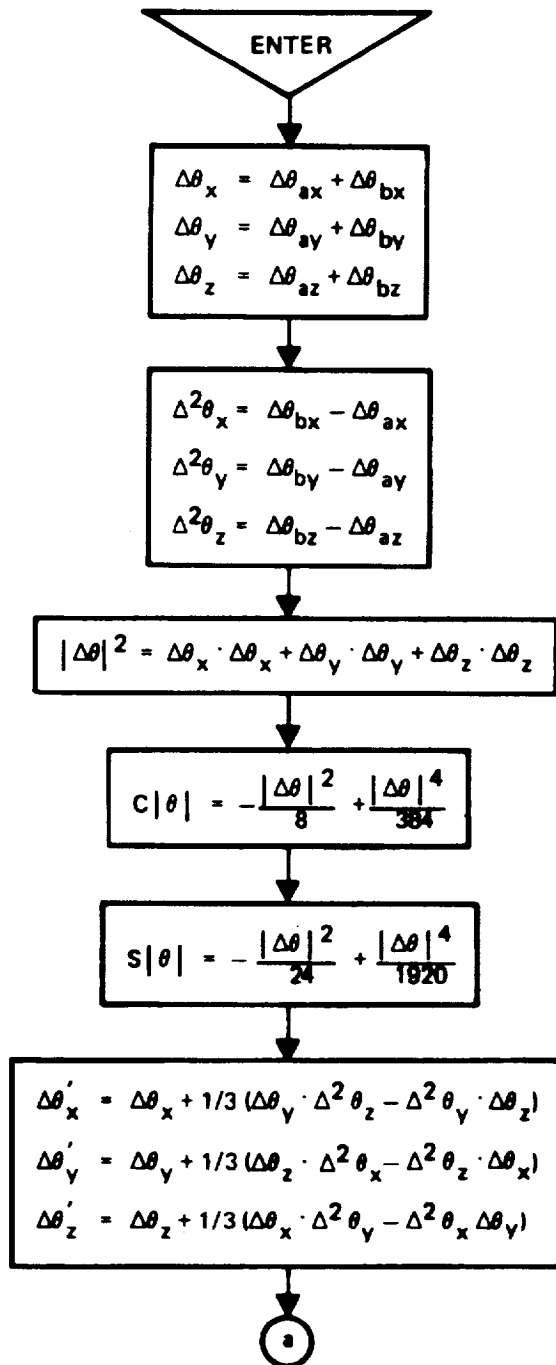
Flowchart H-4. IMM Initialization (128/sec) (Sheet 2 of 2)



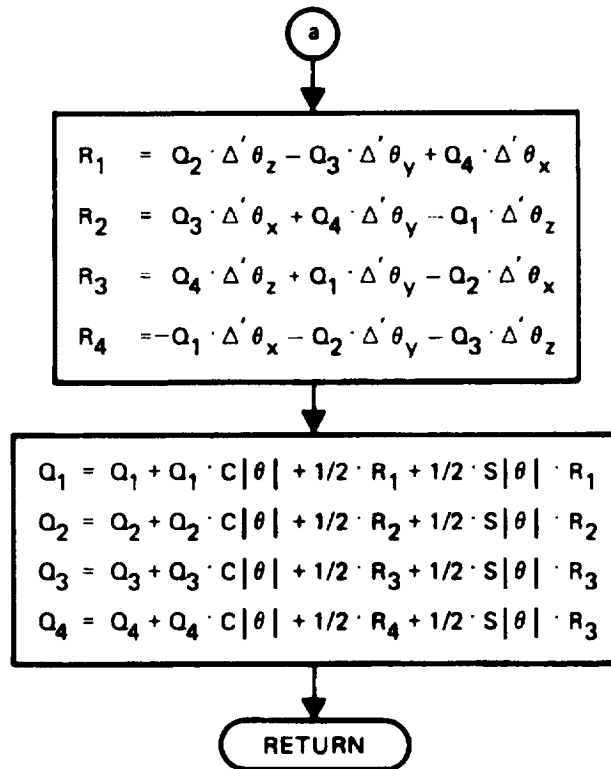
Flowchart H-5. IMM Initialization (128/sec) (Sheet 2 of 2)



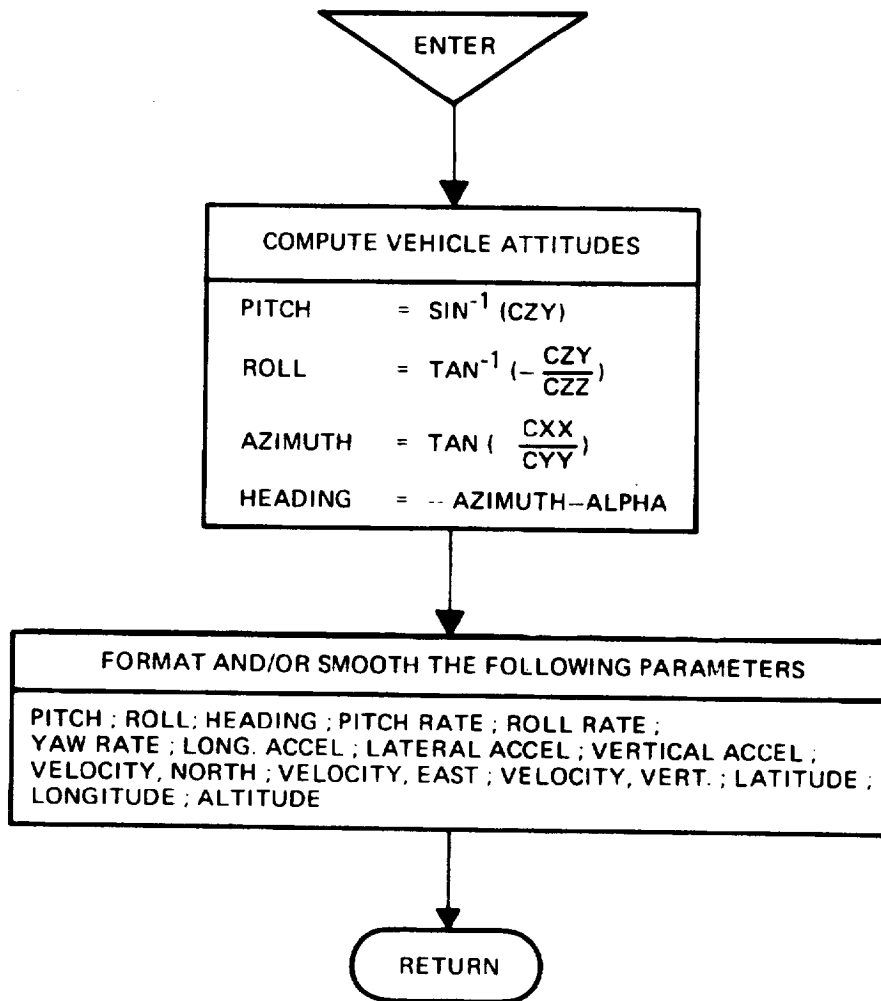
Flowchart H-6. Coordinate Transformation



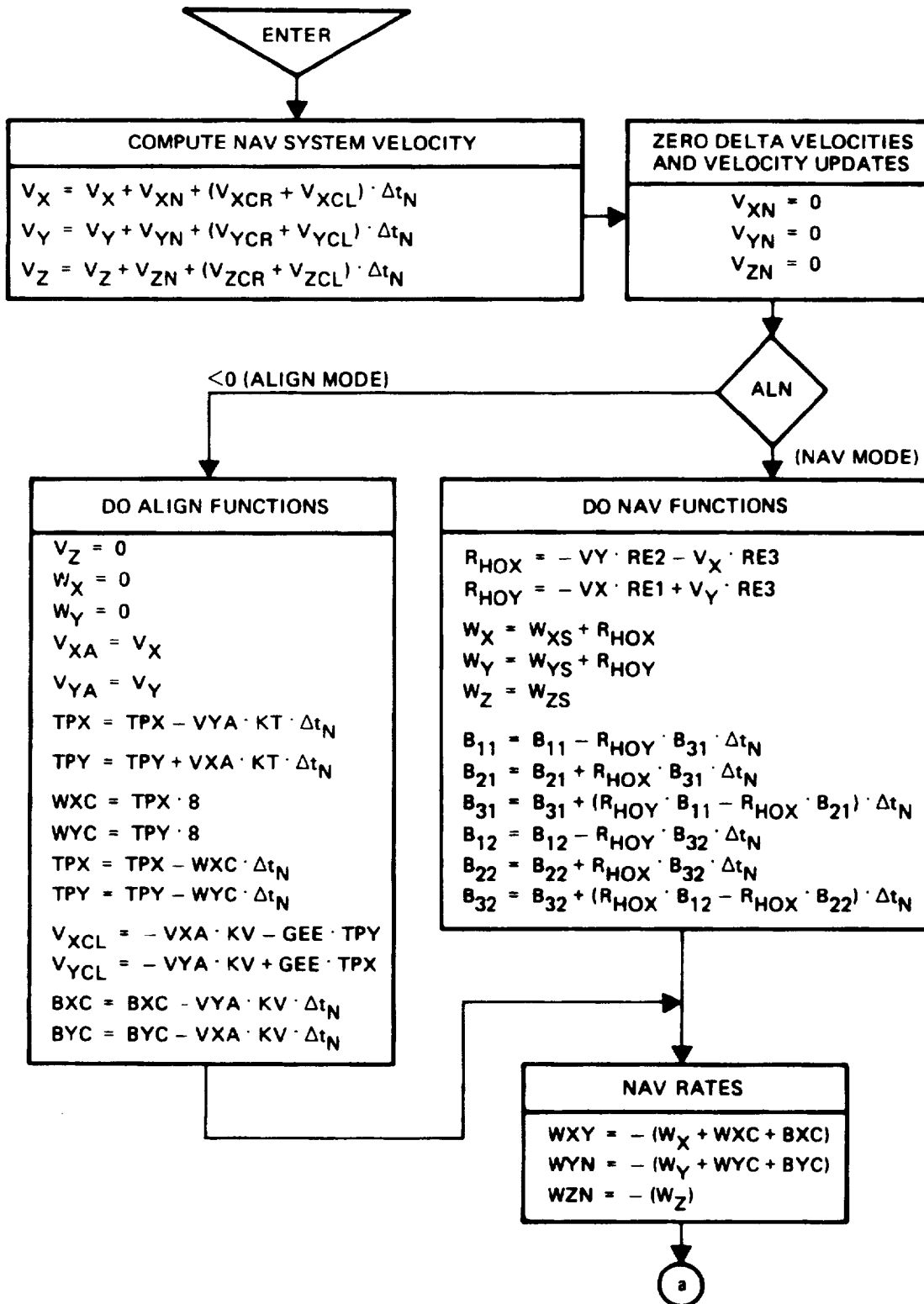
Flowchart H-7. Quaternion Body Rate (64/sec) Sheet 1 of 2)



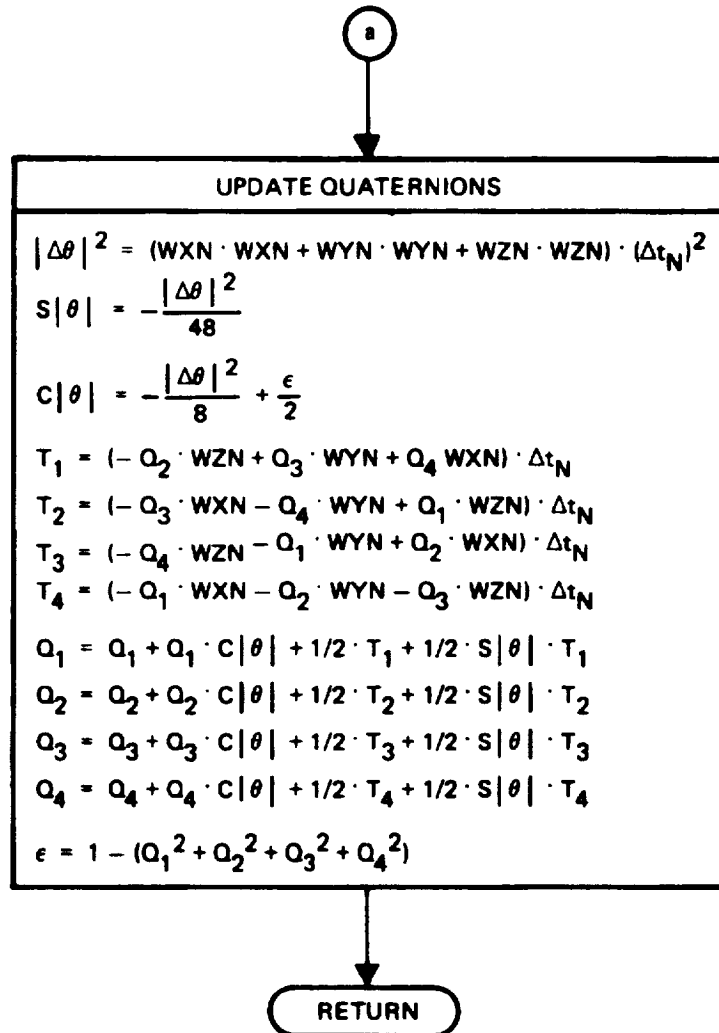
Flowchart H-7. Quaternion Body Rate (64/sec) (Sheet 2 of 2)



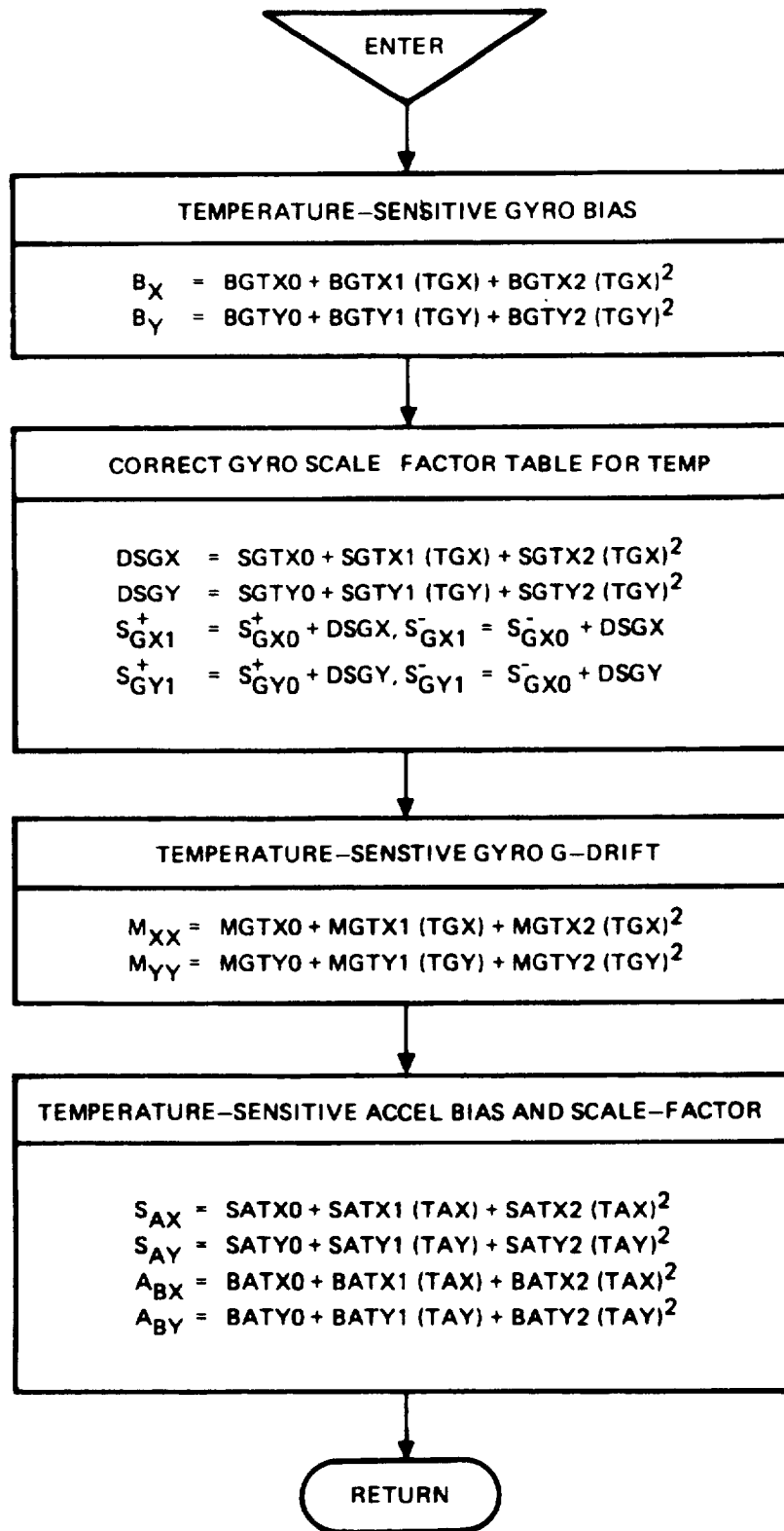
Flowchart H-8. Output Formatter (32/sec)



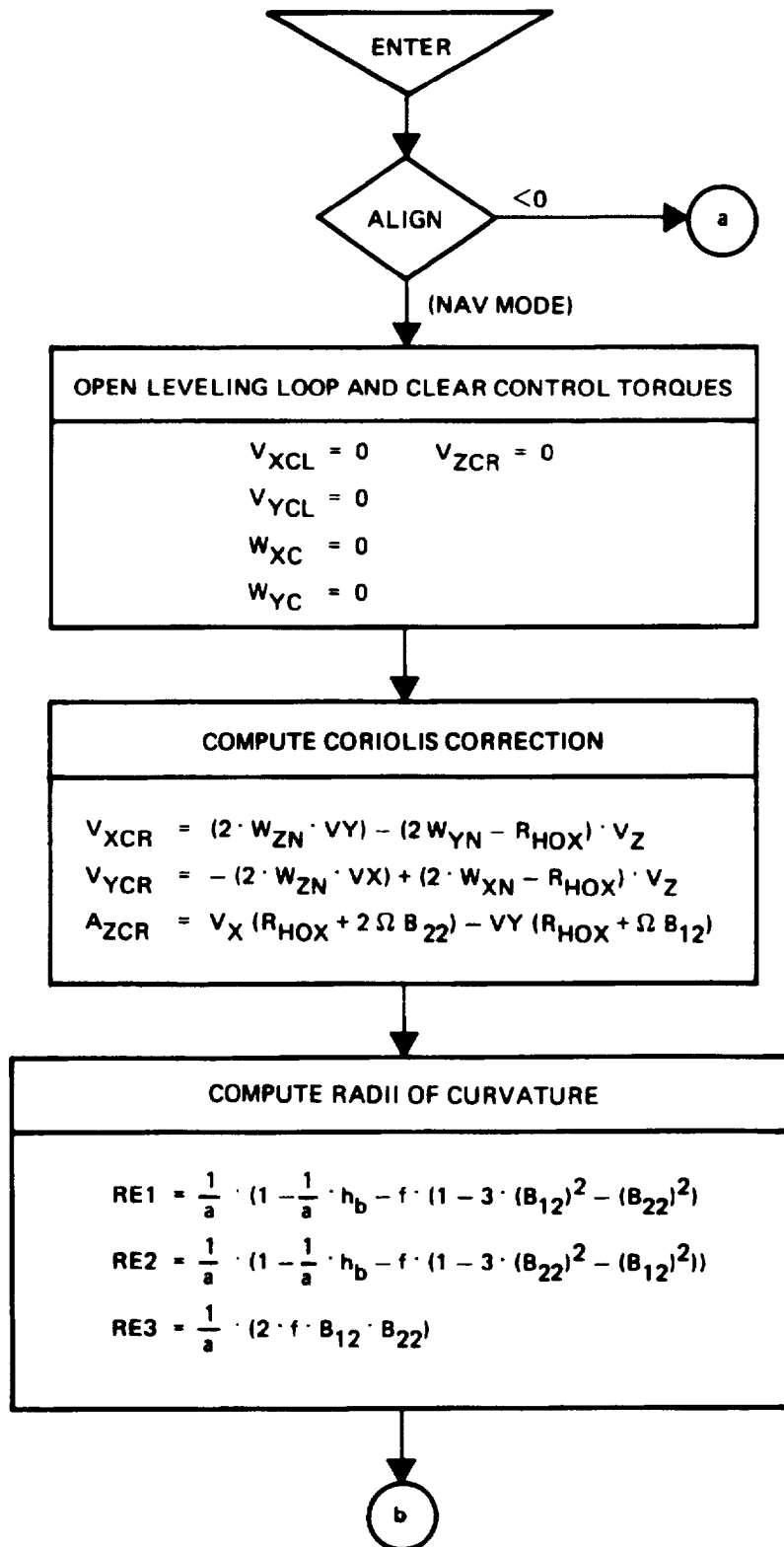
Flowchart H-9. Nav Fast/Align (8/sec) (Sheet 1 of 2)



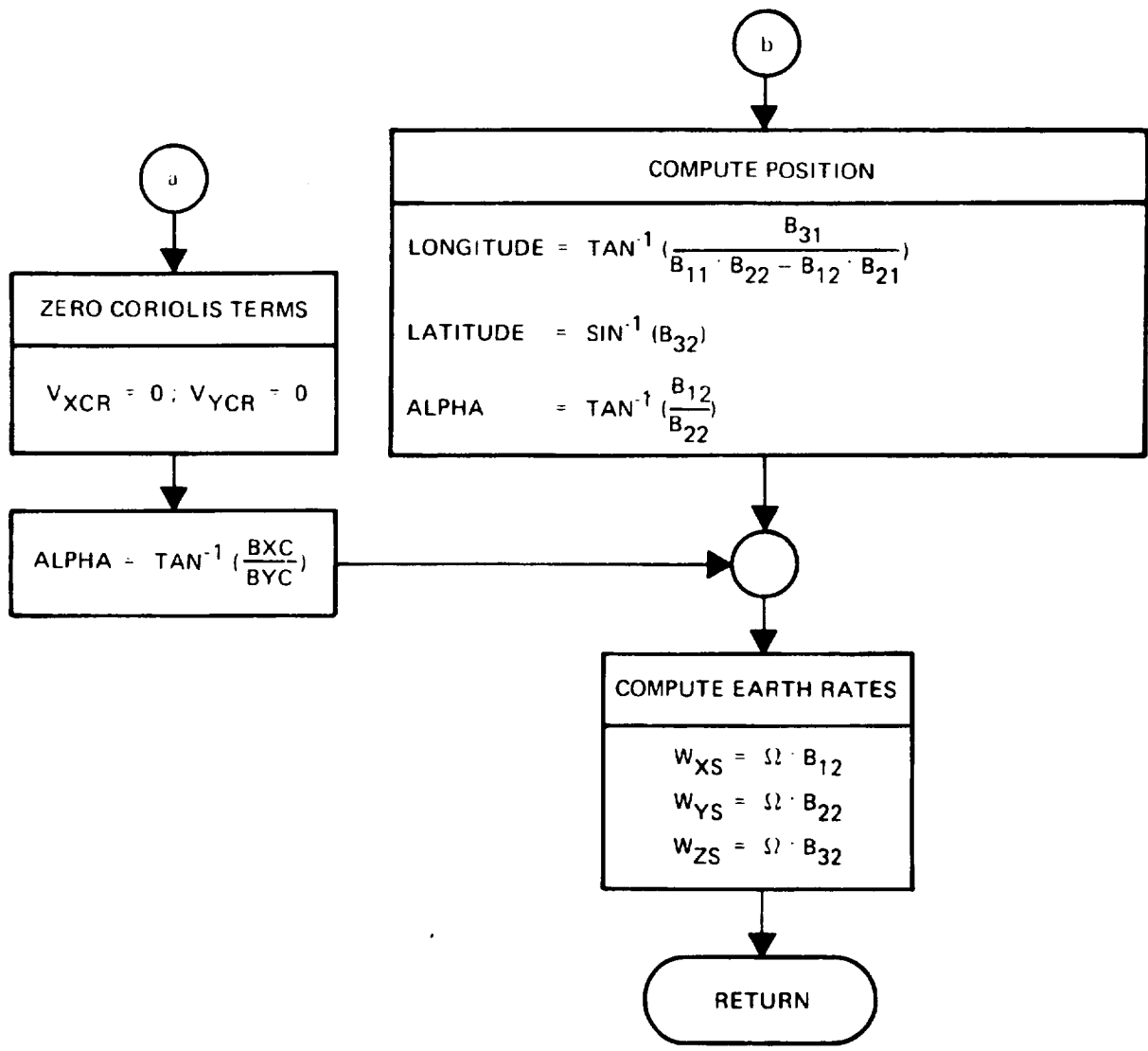
Flowchart H-9. Nav Fast/Align (8/sec) (Sheet 1 of 2)



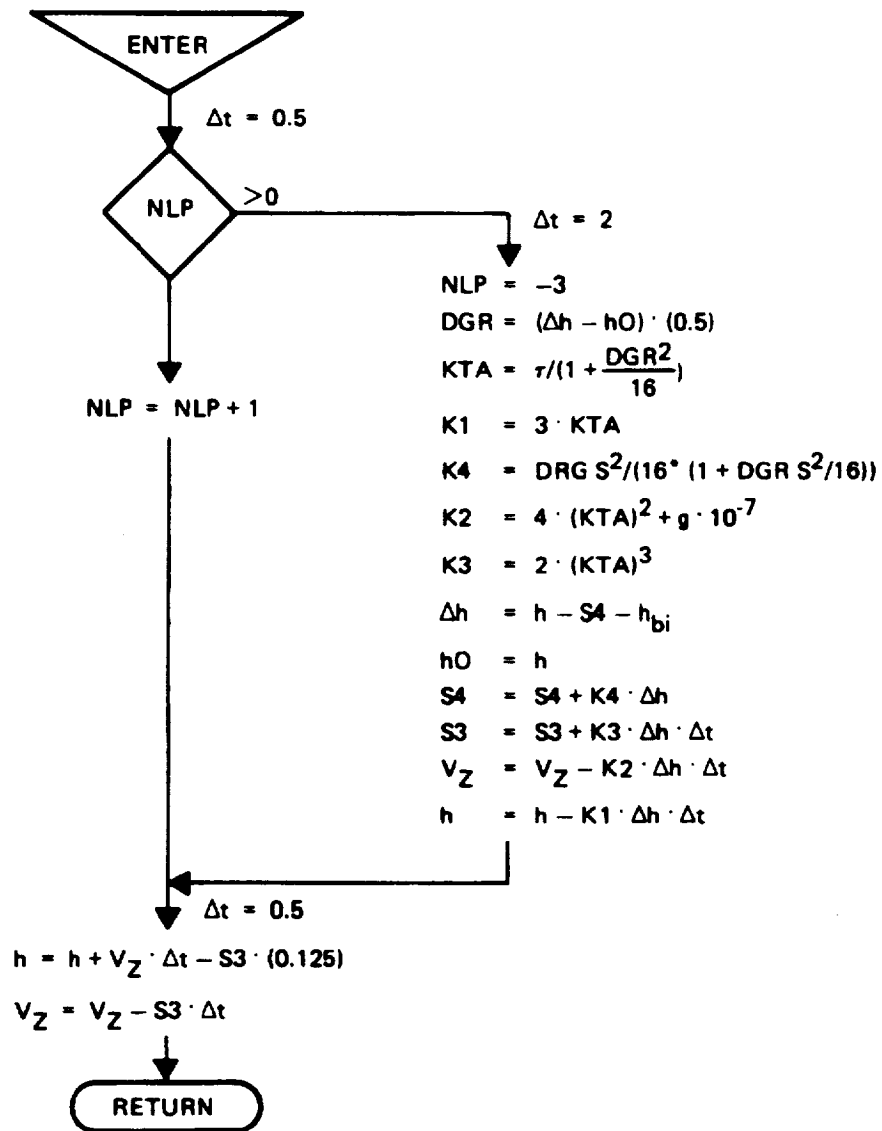
Flowchart H-10. Instrument Compensation, Slow (2/sec)



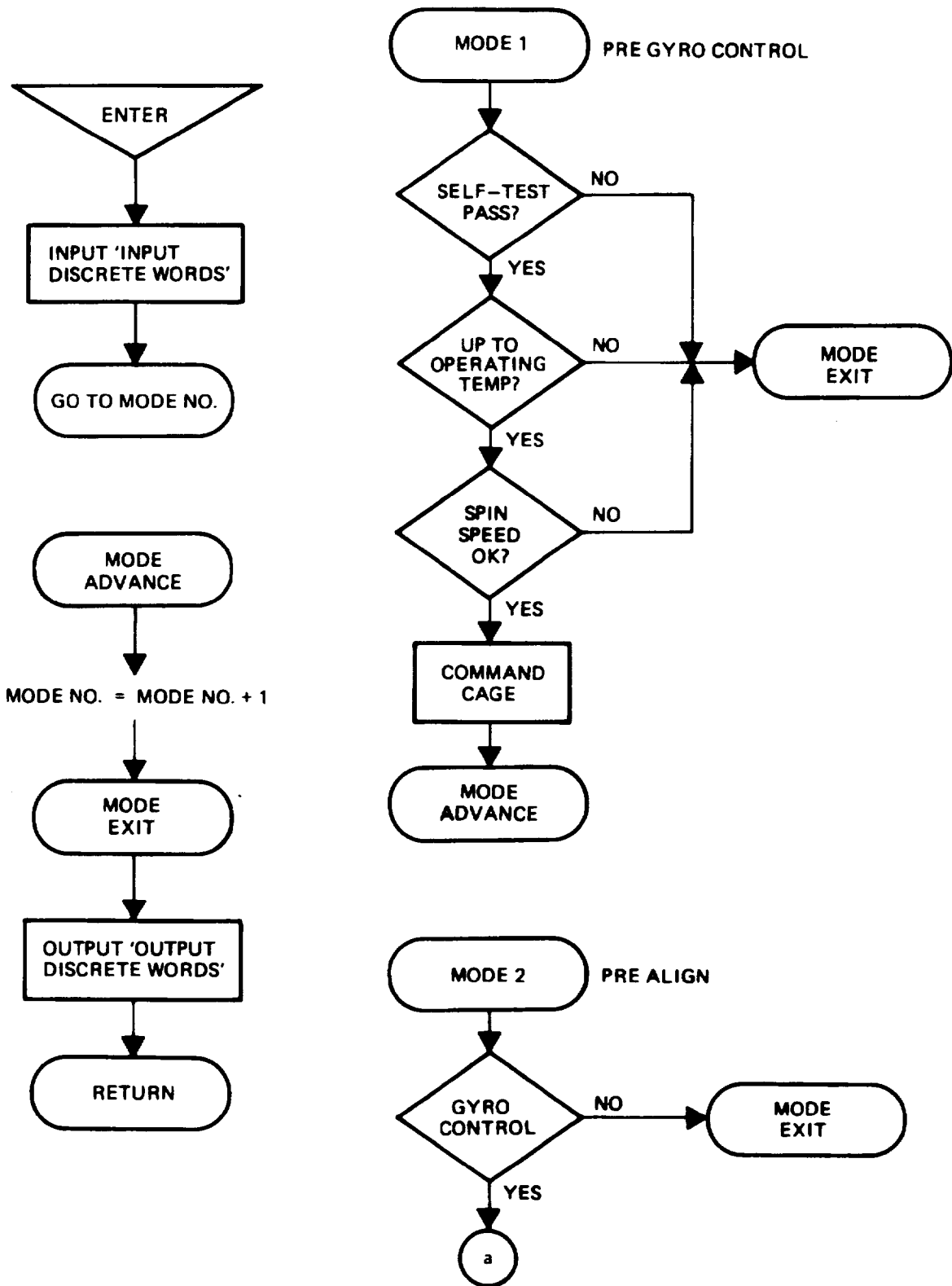
Flowchart H-11. Nav Slow (2/sec) (Sheet 1 of 2)



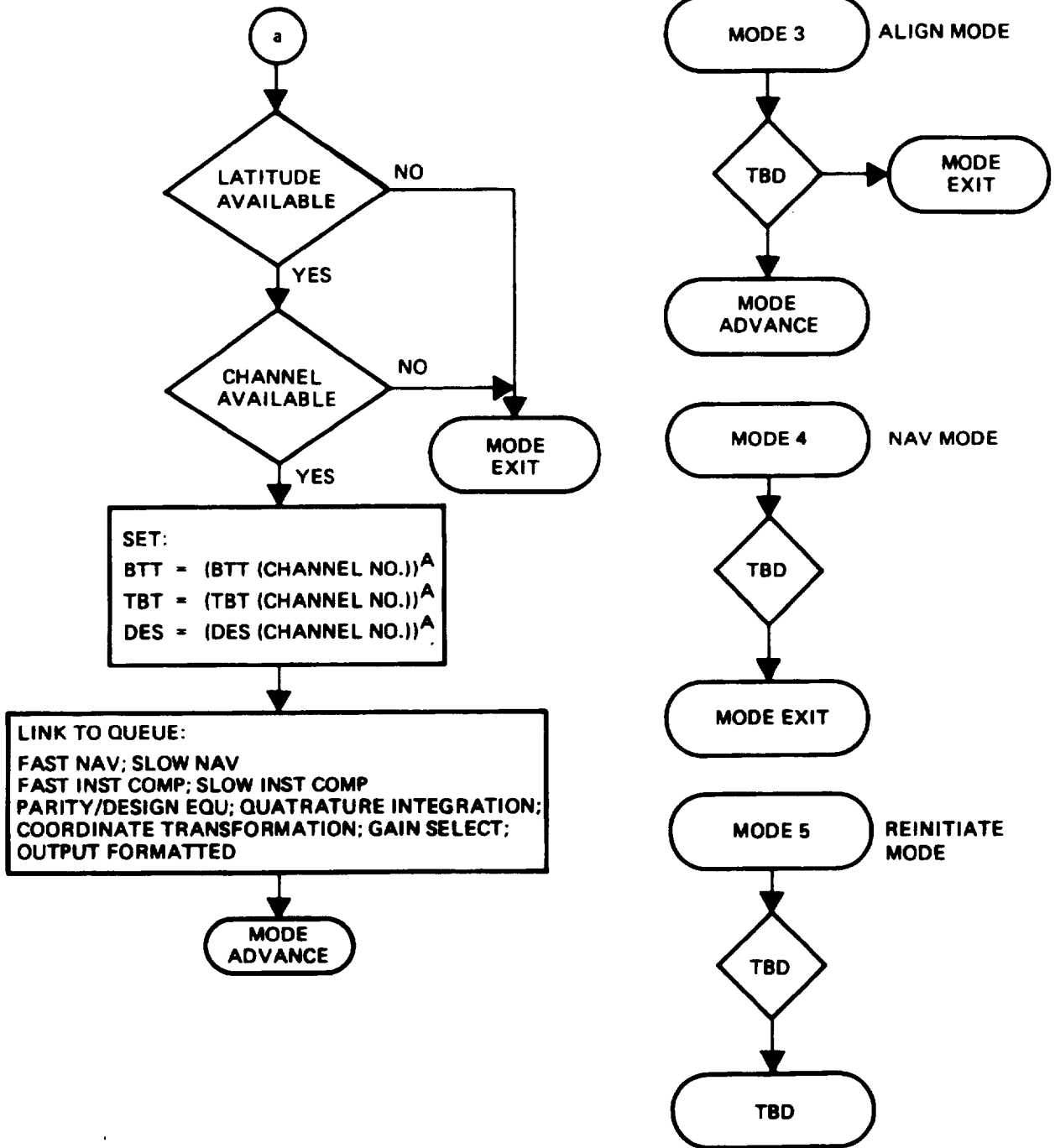
Flowchart H-11. Nav Slow (2/sec) (Sheet 2 of 2)



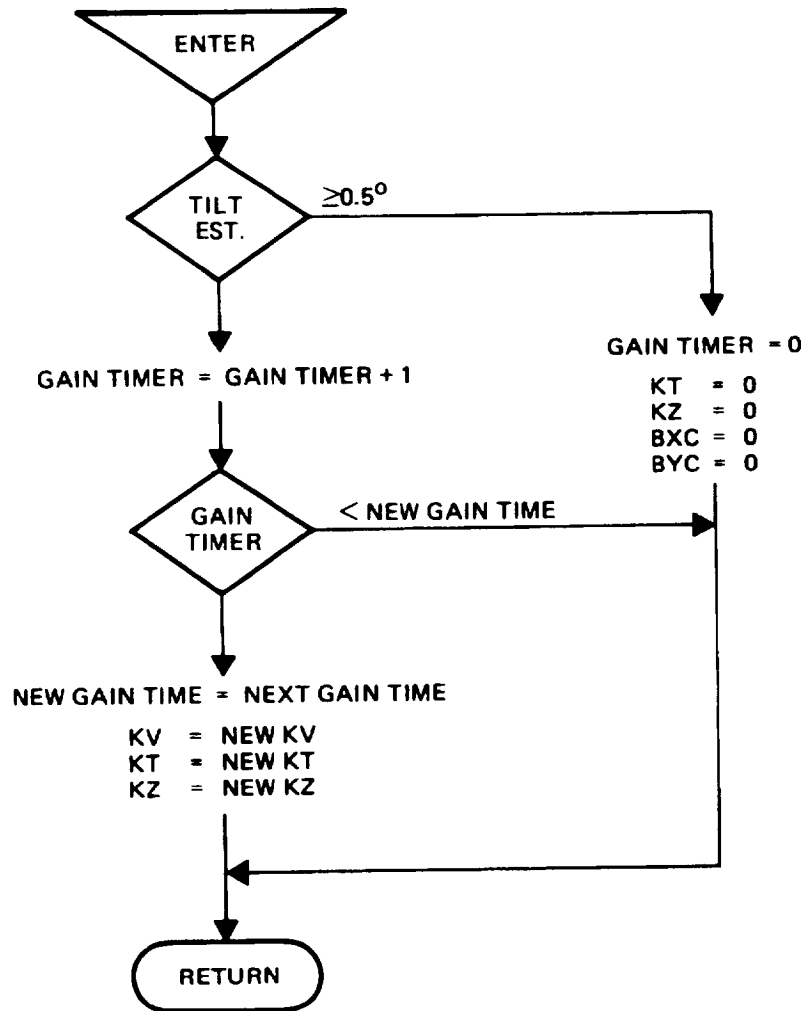
Flowchart H-12. Altitude (2/sec)



Flowchart H-13. Mode Controller (1/sec) (Sheet 1 of 2)



Flowchart H-13. Mode Controller (1/sec) (Sheet 2 of 2)



Flowchart H-14. Gain Select (1/sec)

APPENDIX I
ADVANCED FAILURE DETECTION AND
ISOLATION ALGORITHM

1. Failure Detection and Isolation Algorithm for Tetrahedral Array of Four Valid Gyros

Test relations for a tetrahedral array are obtained from the centroid relation

$$\vec{e}_{13} - \vec{e}_{23} + \vec{e}_{33} - \vec{e}_{43} = 0 \quad (1)$$

where spin axes \vec{e}_{r3} are taken outward from sides of a pyramid. For test directions

$$\vec{e}_{T_{rs}} = \frac{\vec{e}_{r3} \times \vec{e}_{s3}}{S_0} \quad \text{where } S_0 = \frac{\sqrt{3}}{2}$$

Note, by multiplying (1) by \vec{e}_{r3} ,

$$\vec{e}_{T_{r1}} - \vec{e}_{T_{r2}} + \vec{e}_{T_{r3}} - \vec{e}_{T_{r4}} = 0$$

Since

$$\vec{e}_{T_{rs}} = -\vec{e}_{T_{sr}} \quad \text{and} \quad \vec{e}_{T_{rr}} = 0$$

Then

$$\begin{aligned} \vec{e}_{T_{14}} &= \vec{e}_{T_{13}} - \vec{e}_{T_{12}} \\ \vec{e}_{T_{13}} &= \vec{e}_{T_{23}} - \vec{e}_{T_{34}} \\ \vec{e}_{T_{12}} &= \vec{e}_{T_{23}} - \vec{e}_{T_{24}} \\ \vec{e}_{T_{14}} &= \vec{e}_{T_{24}} - \vec{e}_{T_{34}} \end{aligned} \quad (2)$$

Using the first relation, the absolute value yields $C_{T_{13}T_{14}} = 1/2$ and multiplying by $\vec{\theta}$, a relation for test duration rotations is

$$\theta_{14} = \theta_{13} - \theta_{12} \quad (3)$$

where subscripts indicate the test direction.

Note, the unit vector

$$\begin{aligned} \vec{e}_{N_{14}} &= (\vec{e}_{T_{13}} + \vec{e}_{T_{12}}) / \sqrt{2(1 + C_{T_{13}T_{12}})} \\ &= (\vec{e}_{T_{13}} + \vec{e}_{T_{12}}) / \sqrt{3} \end{aligned}$$

is normal to $\vec{e}_{T_{14}}$, hence, in the No. 1 gyro sensitive plane

$$\vec{\theta} = \theta_{14} \vec{e}_{T_{14}} + \frac{(\theta_{13} + \theta_{12})}{\sqrt{3}} \vec{e}_{N_{14}} \quad (4)$$

The magnitude of the rotation is

$$\begin{aligned} \theta^2 &= \vec{\theta} \cdot \vec{\theta} = \theta_{14}^2 + (\theta_{13} + \theta_{12})^2 / 3 \\ &= \frac{2}{3} (\theta_{12}^2 + \theta_{13}^2 + \theta_{14}^2) + \frac{1}{3} [\theta_{14}^2 - (\theta_{12} - \theta_{13})^2] \\ &= \frac{2}{3} (\theta_{12}^2 + \theta_{13}^2 + \theta_{14}^2) \end{aligned} \quad (5)$$

using (3)

Defining T_{rs} as the test difference of r gyro and s gyro outputs in the direction $\vec{e}_{T_{rs}}$, then it follows the square of rotation amplitude θ_1 of gyro No. 1, if other gyros are perfect is given by the calculation,

$$F_1^* = \frac{2}{3} (T_{12}^2 + T_{13}^2 + T_{14}^2)$$

, that is $F_1^* = \theta_1^2$ for only gyro No. 1 drifting.

Multiplying (2) by $\vec{\theta}$ obtain relations

$$\theta_{13} = \theta_{23} - \theta_{34}$$

$$\theta_{12} = \theta_{23} - \theta_{24} \tag{6}$$

$$\theta_{14} = \theta_{24} = \theta_{34}$$

hence if only gyro No. 3 drifts,

$$T_{13} = -\theta_{13} = -\theta_{23} + \theta_{34} = T_{23} + T_{34}$$

and if only gyro No. 2 drifts,

$$T_{12} = -\theta_{12} = -\theta_{23} + \theta_{24} = -T_{23} + T_{24}$$

and if only gyro No. 4 drifts,

$$T_{14} = -\theta_{14} = -\theta_{24} + \theta_{34} = T_{24} - T_{34}$$

It follows that the calculation

$$F_1 = \frac{2}{3} \left[(T_{12}^2 + T_{13}^2 + T_{14}^2) - (T_{23} + T_{34} - T_{24})^2 \right] \quad (6a)$$

has the output

$$F_1 = \begin{cases} \theta_1^2 & \text{if only gyro No. 1 drifts} \\ 0 & \text{if only gyro No. 2 drifts} \\ 0 & \text{if only gyro No. 3 drifts} \\ 0 & \text{if only gyro No. 4 drifts} \end{cases}$$

Thus F_1 serves to detect failure of gyro No. 1 if only one gyro fails at a time.

It may be similarly shown that test functions for the other gyros are:

$$\begin{aligned} F_2 &= \frac{2}{3} \left[T_{12}^2 + T_{23}^2 + T_{24}^2 - (T_{14} + T_{34} - T_{13})^2 \right] \\ F_3 &= \frac{2}{3} \left[T_{13}^2 + T_{23}^2 + T_{34}^2 - (T_{12} + T_{14} - T_{24})^2 \right] \\ F_4 &= \frac{2}{3} \left[T_{14}^2 + T_{24}^2 + T_{34}^2 - (T_{12} + T_{23} - T_{13})^2 \right] \end{aligned} \quad (6b)$$

In order to evaluate the response of the test functions for general drifts of all gyros we shall express the drifts in terms used in a later section.

Extending (17) for four gyros in tetrahedral configuration it may be shown

$$T_{12} = D_{F_1} C_{\theta_1 - 30^\circ} - D_{F_2} C_{\theta_2 - 30^\circ}$$

$$T_{13} = D_{F_1} S_{\theta_1} + D_{F_3} C_{\theta_3 - 30^\circ}$$

$$T_{23} = D_{F_2} S_{\theta_2} + D_{F_3} S_{\theta_3}$$

$$T_{14} = D_{F_1} S_{\theta_1 - 60^\circ} - D_{F_4} C_{\theta_4 - 30^\circ}$$

$$T_{24} = D_{F_2} S_{\theta_2 - 60^\circ} - D_{F_4} S_{\theta_4}$$

$$T_{34} = -D_{F_3} S_{\theta_3 - 60^\circ} - D_{F_4} S_{\theta_4 - 60^\circ}$$

where θ_k are drift directions relative worst case directions.

Where

$$X_r = D_{F_r} C_{\theta_r + 30^\circ} \quad , \quad Y_r = D_{F_r} S_{\theta_r + 30^\circ}$$

it may then be obtained,

$$T_{12} = (X_1 - X_2) \cdot \frac{1}{2} + (Y_1 - Y_2) \frac{\sqrt{3}}{2}$$

$$T_{13} = (X_3 - X_1) \cdot \frac{1}{2} + (Y_3 + Y_1) \frac{\sqrt{3}}{2}$$

$$T_{23} = -(X_2 + X_3) \cdot \frac{1}{2} + (Y_2 + Y_3) \frac{\sqrt{3}}{2}$$

$$T_{14} = -X_1 - X_4 \cdot \frac{1}{2} - Y_4 \frac{\sqrt{3}}{2}$$

$$T_{24} = -X_2 + X_4 \cdot \frac{1}{2} - Y_4 \frac{\sqrt{3}}{2}$$

$$T_{34} = X_3 + X_4$$

(6c)

Note,

$$(T_{12} + T_{23} - T_{13}) = X_1 - X_2 - X_3$$

$$(T_{12} + T_{14} - T_{24}) = \frac{-X_1}{2} + \frac{X_2}{2} - X_4 + (Y_1 - Y_2) \frac{\sqrt{3}}{2}$$

$$(T_{14} + T_{34} - T_{13}) = \frac{-X_1}{2} + \frac{X_3}{2} + \frac{X_4}{2} - (Y_1 + Y_3 + Y_4) \frac{\sqrt{3}}{2}$$

$$(T_{23} - T_{24} + T_{34}) = \frac{X_2}{2} + \frac{X_3}{2} + \frac{X_4}{2} + (Y_2 + Y_3 + Y_4) \frac{\sqrt{3}}{2}$$

The selection of variables X_r , Y_r leads to analysis of F_4 of (6b) which is simpler than other F_r .

Obtain

$$\begin{aligned}
 F_4 &= D_{F_4}^2 + \frac{2}{3} X_4 (X_1 - X_2 + 2X_3) + \frac{2}{\sqrt{3}} Y_4 (X_1 + X_2) \\
 &\quad + \frac{4}{3} (X_1 X_2 + X_1 X_3 - X_2 X_3) \\
 F_3 &= D_{F_3}^2 + \frac{2}{3} X_3 \cdot \left(2X_4 - \frac{X_1}{2} + \frac{X_2}{2} + \frac{\sqrt{3}}{2} (Y_1 - Y_2) \right) \quad (7) \\
 &\quad + \frac{2}{3} Y_3 \cdot \left(\frac{3}{2} Y_1 + \frac{3}{2} Y_2 - \frac{\sqrt{3}}{2} (X_1 + X_2) \right) \\
 &\quad + \frac{2}{3} X_1 \left(\frac{X_2}{2} - X_4 - Y_2 \frac{\sqrt{3}}{2} \right) + \frac{2}{3} X_2 \left(X_4 - Y_1 \frac{\sqrt{3}}{2} \right) \\
 &\quad + \frac{2}{\sqrt{3}} (X_4 Y_1 - X_4 Y_2) + Y_1 Y_2
 \end{aligned}$$

where $D_{F_r}^2 = X_r^2 + Y_r^2$. Consider the mean and standard deviation of F_r if gyro No. r fails with given D_{F_r} over the set of random phases. Note, $\overline{F_r} = D_{F_r}^2$

assuming independent gyro drifts. Also,

$$\begin{aligned}
 \overline{(F_4 - F_4)^2} &= \overline{X_4^2} \cdot \frac{4}{9} \overline{(X_1 - X_2 + 2X_3)^2} + \overline{Y_4^2} \cdot \frac{4}{3} \overline{(X_1 + X_2)^2} \\
 &\quad + \frac{16}{9} \overline{(X_1 X_2 + X_1 X_3 - X_2 X_3)^2} \\
 &= \frac{4}{3} D_{F_4}^2 \cdot \sigma_N^2 + \frac{4}{3} \sigma_N^4
 \end{aligned}$$

using $\overline{X_r^2} = \overline{Y_r^2} = \sigma_N^2/2$ for $r = 1, 2, 3$ and $\overline{X_4^2} = \overline{Y_4^2} = D_{F_4}^2/2$.

Then

$$\sigma_{F_4/\bar{F}_4} = \frac{2}{\sqrt{3}} r \sqrt{1+r^2} \quad \text{where } r = \sigma_N/D_{F_4} \quad (8)$$

If the noise is .1°/hr and the failure rate 1.°/hr then the 1σ variation of F_4 is 11.6 percent about the average due to noise of the other gyros. By symmetry the same relation holds for all F_r , however to demonstrate the consistency of the above relations for F_3 , obtain as expected,

$$\begin{aligned} \overline{(F_3 - \bar{F}_3)^2} &= \overline{x_3^2} \cdot \frac{4}{9} \left(2x_4 - \frac{x_1}{2} + \frac{x_2}{2} + \frac{\sqrt{3}}{2} (y_1 - y_2) \right)^2 \\ &+ \overline{y_3^2} \cdot \frac{4}{9} \left(\frac{3}{2} y_1 + \frac{3}{2} y_2 - \frac{\sqrt{3}}{2} (x_1 + x_2) \right)^2 \\ &+ \overline{x_1^2} \cdot \frac{4}{9} \left(\frac{x_2}{2} - x_4 - y_2 \frac{\sqrt{3}}{2} \right)^2 + \overline{x_2^2} \cdot \frac{4}{9} \left(x_4 - y_1 \frac{\sqrt{3}}{2} \right)^2 \\ &+ \frac{4}{3} \overline{(x_4 y_1 - x_4 y_2)^2} + \overline{y_1^2} \cdot \overline{y_2^2} \\ &= \frac{4}{3} D_{F_3}^2 \cdot \sigma_N^2 + \frac{4}{3} \sigma_N^4 \end{aligned}$$

If none of the gyros failed, then $\bar{F}_4 = \overline{D_{F_r}^2} = \sigma_N^2$ and

$$\sigma_{F_r}^2 = \overline{(F_r - \bar{F}_r)^2} = \frac{8}{3} \sigma_N^4$$

Expressed as a fraction of the output with a test failure rate D_F , then the 1 σ spread of outputs is given by

$$\frac{F_r}{D_F} = r^2 \left(1 \pm 2 \sqrt{\frac{2}{3}} \right)$$

where $r = \sigma_N/D_F$. If $\sigma_N = .1^\circ/\text{hr}$ and $D_F = 1.^\circ/\text{hr}$ then the output ranges 1 σ from $-.63\%$ to $+1.63\%$ of the output for an actual failure with test level magnitude D_F .

In order to evaluate the probability of no detection of a failure and false alarm a more detailed analysis of the probability distribution of errors is necessary. This can be done by examining F_4 of (7) assuming the gyro noises are Gaussian.

The analysis of probability distribution of F_r is facilitated by putting F_4 of (7) in the form,

$$F_4 = R^2 - r^2$$

where

$$R^2 = X_4^{*2} + Y_4^{*2}$$

$$r = \frac{2}{3} (X_3 + X_2 - X_1)$$

$$X_4^* = X_4 + \frac{1}{3} (2X_3 + X_1 - X_2)$$

$$Y_4^* = Y_4 + \frac{1}{\sqrt{3}} (X_1 + X_2)$$

It is readily shown using $\overline{X_r^2} = \overline{Y_r^2} = \sigma_N^2/2$ for $r = 1, 2, 3$

$$\sigma_{X_4^*}^2 = \sigma_N^2/3$$

$$\sigma_{Y_4^*}^2 = \sigma_N^2/3$$

$$\sigma_r^2 = 2 \sigma_N^2/3 \quad \text{Regarding } X_4, Y_4 \text{ given}$$

$$\overline{X_4^*} = X_4$$

$$\overline{Y_4^*} = Y_4$$

$$\overline{r} = 0$$

$$\overline{(X_4^* - \overline{X_4^*})(r - \overline{r})} = 0$$

$$\overline{(Y_4^* - \overline{Y_4^*})(r - \overline{r})} = 0$$

$$\overline{(X_4^* - \overline{X_4^*})(Y_4^* - \overline{Y_4^*})} = 0$$

regarding X_4, Y_4 as given rather than random variables. Regarding X_4, Y_4 as random variables with $\overline{X_4^2} = \overline{Y_4^2} = \sigma_{D_F}^2/2, \overline{X_4} = \overline{Y_4} = 0$ then,

$$\sigma_{X_4^*}^2 = \sigma_{D_F}^2/2 + \sigma_N^2/3$$

$$\sigma_{Y_4^*}^2 = \sigma_{D_F}^2/2 + \sigma_N^2/3 \quad \text{Regarding } X_4, Y_4 \text{ as random variables}$$

$$\sigma_r^2 = 2 \sigma_N^2/3$$

$$\overline{X_4^*} = 0$$

$$\overline{Y_4^*} = 0$$

$$\overline{r} = 0$$

$$\overline{(X_4^* - \bar{X}_4^*)(r - \bar{r})} = 0$$

$$\overline{(Y_4^* - \bar{Y}_4^*)(r - \bar{r})} = 0$$

$$\overline{(X_4^* - \bar{X}_4^*)(Y_4^* - \bar{Y}_4^*)} = 0$$

Since X_1, X_2, X_3 are assumed normally distributed then so is r . It follows r^2 has a Rayleigh distribution

$$\phi(r^2) = \frac{1}{\sigma_r^2} \cdot e^{-r^2/\sigma_r^2}$$

Since r is independent of X_4^*, Y_4^* the joint probability density of X_4^*, Y_4^*, r^2 is

$$\phi(X_4^*, Y_4^*, r^2) dx_4^* dy_4^* dr^2 = \phi(X_4^*, Y_4^*) e^{-r^2/\sigma_r^2} d(r^2/\sigma_r^2) dx_4^* dy_4^*$$

The probability distribution of F_4 is obtained substituting $r^2 = X_4^{*2} + Y_4^{*2} - F_4$ and integrating over X_4^*, Y_4^* such that $X_4^{*2} + Y_4^{*2} \geq G(F_4, 0)$,

$$\phi(F_4) dF_4 = \iint dx_4^* dy_4^* \phi(X_4^*, Y_4^*) e^{-\frac{(X_4^{*2} + Y_4^{*2})}{\sigma_r^2} + \frac{F_4}{\sigma_r^2}} \frac{dF_4}{\sigma_r^2} \quad (9)$$

$$(X_4^{*2} + Y_4^{*2}) \geq G(F_4, 0)$$

where $G(F_4, 0)$ is the greater of F_4 and 0, and F_4 has the range $-\infty$ to $(X_4^{*2} + Y_4^{*2})$. Consider the case where gyro No. 4 has not failed and simply has noise. Then

$$\begin{aligned} dX_4^* dY_4^* \cdot \phi(X_4^*, Y_4^*) &= \frac{dX_4^* dY_4^*}{2\pi \sigma_{X_4^*} \sigma_{Y_4^*}} e^{-\frac{1}{2} \left(\frac{X_4^{*2}}{\sigma_{X_4^*}^2} + \frac{Y_4^{*2}}{\sigma_{Y_4^*}^2} \right)} \\ &= 2R \frac{d\theta}{2\pi} \frac{dR}{\sigma_R^2} e^{-R^2/\sigma_R^2} \end{aligned}$$

where $\sigma_R^2 = 2 \sigma_{X_4^*}^2 = 2 \sigma_{Y_4^*}^2 = \frac{5}{3} \sigma_N^2$ and $R^2 = X_4^{*2} + Y_4^{*2}$. Then

$$\begin{aligned} \phi(F_4) dF_4 &= \iint_{R^2 \geq G(F_4, 0)} \frac{2R d\theta}{2\pi} \frac{dR}{\sigma_R^2} e^{-\frac{R^2}{\sigma_R^2}} \frac{dF_4}{\sigma_r^2} \\ &= dF_4 \cdot e^{-\frac{F_4}{\sigma_r^2}} \cdot \int_{R \geq G(F_4, 0)} \frac{dR^2}{\sigma_R^2 \sigma_r^2} \cdot e^{-R^2 \left(\frac{1}{\sigma_R^2} + \frac{1}{\sigma_r^2} \right)} \\ &= dF_4 \cdot e^{-\frac{F_4}{\sigma_r^2}} \cdot \frac{e^{-G(F_4, 0) \cdot \left(\frac{1}{\sigma_R^2} + \frac{1}{\sigma_r^2} \right)}}{\left(\sigma_R^2 + \sigma_r^2 \right)} \\ &= \begin{cases} \frac{dF_4}{7/3 \sigma_N^2} e^{-F_4/5/3 \sigma_N^2} & \text{if } F_4 > 0 \\ \frac{dF_4}{7/3 \sigma_N^2} e^{+F_4/2/3 \sigma_N^2} & \text{if } F_4 < 0 \end{cases} \end{aligned} \tag{10}$$

The probability of false alarm, PFA, using test level ϵ^2 against F_4 is

$$\begin{aligned} \text{PFA} &= \int_{\epsilon^2}^{\infty} \frac{dF_4}{7/3\sigma_N^2} \cdot e^{-F_4/5/3\sigma_N^2} \\ &= \frac{5}{7} e^{-\frac{3}{5} \left(\frac{\epsilon}{\sigma_N}\right)^2} \end{aligned} \quad (11)$$

If $\sigma_N = .1^\circ/\text{hr}$ and $\epsilon = .5^\circ/\text{hr}$ then $\text{PFA} = 2. \times 10^{-7}$. Raising ϵ to $.6^\circ/\text{hr}$ reduces PFA to $\text{PFA} = 2.6 \times 10^{-10}$. The fraction of false alarms to actual failures is

$$f_{\text{FA}} = \frac{\text{PFA}}{\lambda_s} \cdot (\text{MTBF})$$

MTBF = Mean time before failure
 λ_s = Test smoothing time

For MTBF = 3000 hr, $\lambda_s = 1/60$ hr we see in the last example with $\epsilon = .5^\circ/\text{hr}$ we have $f_{\text{FA}} = .036$ and with $\epsilon = .6^\circ/\text{hr}$ we have $f_{\text{FA}} = .00005$.

Consider the case of failure of gyro No. 4 having occurred where the distribution of failure magnitude is $\phi(D_F)$ and the distribution drift direction is flat with respect to angle θ_F . The probability distribution of X_4^* , Y_4^* is

$$\begin{aligned} \phi(X_4^*, Y_4^*) dX_4^* dY_4^* &= \int_{D_F=0}^{\infty} \int_{\theta_F=0}^{2\pi} \frac{e^{-\frac{1}{2} \left[\frac{(X_4^* - D_F C_{\theta_F})^2}{\sigma_{X_4^*}^2} + \frac{(Y_4^* - D_F S_{\theta_F})^2}{\sigma_{Y_4^*}^2} \right]}}{2\pi \sigma_{X_4^*} \sigma_{Y_4^*}} dX_4^* dY_4^* \cdot \phi(D_F) \\ &\quad dD_F \frac{d\theta_F}{2\pi} \end{aligned}$$

assuming $(X_4^* - X_4)$, $(Y_4^* - Y_4)$ are normally distributed where
 $X_4 = D_F C_{\theta_F}$, $Y_4 = D_F S_{\theta_F}$. Using $\sigma X_4^{*2} = \sigma Y_4^{*2} = \sigma R^2/2$,
 $R^2 = X_4^{*2} + Y_4^{*2}$

$$\phi(X_4^*, Y_4^*) dx_4^* dy_4^* = \frac{dx_4^* dy_4^*}{\pi \sigma^2} \cdot e^{-\frac{R^2}{\sigma^2}} \cdot \int_{D_F=0}^{\infty} e^{-\frac{D_F^2}{\sigma^2}} \phi(D_F) dD_F \int_{\theta_F=0}^{2\pi} e^u \frac{d\theta_F}{2\pi} \quad (12)$$

where

$$u = \frac{2D_F}{\sigma^2} (X_4^* C_{\theta_F} + Y_4^* S_{\theta_F}) = \frac{2D_F \cdot R}{\sigma^2} (C_{\theta} C_{\theta_F} + S_{\theta} S_{\theta_F}) = \frac{2D_F \cdot R}{\sigma^2} C_{\theta_F - \theta}$$

using $X_4^* = R C_{\theta}$, $Y_4^* = R S_{\theta}$. Except* in rare cases $K = 2 \frac{D_F R}{\sigma^2} \gg 1$.

Then,

$$\begin{aligned} \int_{D_F=0}^{2\pi} e^u \frac{d\theta_F}{2\pi} &= \int_{\phi=0}^{2\pi} e^{KC_{\phi}} \frac{d\phi}{2\pi} = e^K \cdot \int_{\phi=0}^{2\pi} e^{-K(1-C_{\phi})} \frac{d\phi}{2\pi} = e^K \cdot \int_{-\infty}^{\infty} e^{-\frac{K\phi^2}{2}} \frac{d\phi}{2\pi} \\ &\approx \frac{e^K}{\sqrt{2\pi K}} \int_{t=0}^{\infty} e^{-t^2/2} \frac{dt}{\sqrt{2\pi}} \approx \frac{e^K}{\sqrt{2\pi K}} = e^{2 \frac{D_F R}{\sigma^2}} \frac{\sigma_R}{2\sqrt{\pi D_F R}} \quad (12a) \end{aligned}$$

*Cases unimportant to non-detection of failure.

Substituting this result in (12), obtain

$$\phi(X_4^*, Y_4^*) dX_4^* dY_4^* = \frac{dX_4^* dY_4^*}{2\pi^{3/2} \sigma_R \sqrt{R}} \int_{D_F=0}^{\infty} e^{-\frac{(R-D_F)^2}{\sigma^2 R}} \phi(D_F) \frac{dD_F}{\sqrt{D_F}} \quad (13)$$

where $R^2 = X_4^{*2} + Y_4^{*2}$. Substituting (13) into (9) obtain

$$\phi(F_4) dF_4 = \iint_{R \geq G(F_4, 0)} \frac{dX_4^* dY_4^*}{2\pi^{3/2} \sigma_R \sqrt{R}} \cdot e^{-R^2/\sigma^2 R} \int_{D_F=0}^{\infty} e^{-\frac{(D_F-R)^2}{\sigma^2 R}} \phi(D_F) \frac{dD_F}{\sqrt{D_F}} \cdot e^{\frac{F_4/\sigma^2 R}{\sigma^2 R}}$$

Changing variables of integration X_4^*, Y_4^* to R, θ using

$$\frac{dX_4^* dY_4^*}{2\pi^{3/2} \sigma_R \sqrt{R}} = \frac{R d\theta dR}{2\pi^{3/2} \sigma_R \sqrt{R}} = \sqrt{\frac{R}{\pi}} \frac{dR d\theta}{\sigma_R 2\pi}$$

and noting that the integrand does not involve θ ,

$$\phi(F_4) dF_4 = J(\sqrt{G(F_4, 0)}) \cdot e^{\frac{F_4}{\sigma^2 R}} \cdot \frac{dF_4}{\sigma^2 R} \quad (14)$$

where

$$J(Y) = \int_{R=Y}^{\infty} \sqrt{\frac{R}{\pi}} \frac{dR}{\sigma_R} \cdot e^{-\frac{R^2}{\sigma_R^2}} \cdot \int_{D_F=0}^{\infty} e^{-\frac{(D_F-R)^2}{\sigma_R^2}} \phi(D_F) \frac{dD_F}{\sqrt{D_F}}$$

Consider the probability of non-detection of a failure, PND, using the test $F_4 > \epsilon^2$ in which case

$$\begin{aligned} \text{PND} &= \int_{-\infty}^{\epsilon^2} \phi(F_4) dF_4 \\ &= \int_0^{\epsilon^2} \phi(F_4) dF_4 \end{aligned}$$

Using (14), and integrating by parts

$$\begin{aligned} \text{PND} &= \int_0^{\epsilon^2} J(\sqrt{F_4}) d\left(\frac{F_4}{\sigma_R^2}\right) \\ &= \int_{Y=0}^{\epsilon} J(Y) d\left(\frac{Y^2}{\sigma_R^2}\right) \\ &= J(\epsilon) \cdot \frac{\epsilon^2}{\sigma_R^2} - J(0) \\ &\quad + \int_{Y=0}^{\epsilon} \sqrt{\frac{Y}{\pi}} \frac{dY}{\sigma_R} \int_{D_F=0}^{\infty} e^{-\frac{(D_F-Y)^2}{\sigma_R^2}} \phi(D_F) \frac{dD_F}{\sqrt{D_F}} \\ &= \int_0^{\epsilon} \sqrt{\frac{Y}{\pi}} \frac{dY}{\sigma_R} \left\{ e^{-\frac{(Y^2 - \sigma_R^2)}{\sigma_R^2}} - e^{-\frac{Y^2}{\sigma_R^2}} \right\} \cdot \int_{D_F=0}^{\infty} e^{-\frac{(D_F-Y)^2}{\sigma_R^2}} \phi(D_F) \frac{dD_F}{\sqrt{D_F}} \quad (15) \end{aligned}$$

on collecting integral forms $J(\epsilon)$, $J(0)$.

Consider the case of a distribution of failure rates

$$\phi(D_F) = \begin{cases} \lambda \sqrt{D_F} & \text{for } D_{F_L} \leq D_F \leq D_{F_U} \\ 0 & \text{otherwise} \end{cases}$$

where $\lambda = \frac{3}{2} \left(D_{F_U}^{3/2} - D_{F_L}^{3/2} \right)^{-1}$. The distribution is rather flat with bias toward higher values. Since non-detection occurs mostly in a band of D_F values less than σ_N wide at the lower end of the distribution, consider the probability

$$\begin{aligned} P \left(D_{F_L} \leq D_F \leq (D_{F_L} + \sigma_N) \right) &= \int_{D_{F_L}}^{D_{F_L} + \sigma_N} \phi(D_F) dD_F \\ &= \frac{\left(1 + \frac{1}{u} \right)^{3/2} - 1}{\left(r_D^{3/2} - 1 \right)} \approx \frac{3}{2u r_D^{3/2}} \end{aligned}$$

where $u = D_{F_L}/\sigma_N$, $r_D = D_{F_U}/D_{F_L}$. For $u = 11$, $r_D = 10$, the probability is 4.5×10^{-3} for occurrence of D_F value where non-detection is modeled as practically possible.

For $R < D_{F_L} - \sigma_R$,

$$\begin{aligned}
 \int_{D_F=0}^D e^{-\frac{(D_F - R)^2}{\sigma_R^2}} \phi(D_F) \frac{dD_F}{\sqrt{D_F}} &= \lambda \cdot \sigma_R \int_{\frac{D_{F_L} - R}{\sigma_R}}^{\frac{D_{F_U} - R}{\sigma_R}} e^{-y^2} dy \\
 &\approx \lambda \cdot \sigma_R \left[\frac{e^{-\frac{(D_{F_L} - R)^2}{\sigma_R^2}}}{2 \left(\frac{D_{F_L} - R}{\sigma_R} \right)} - \frac{e^{-\frac{(D_{F_U} - R)^2}{\sigma_R^2}}}{2 \left(\frac{D_{F_U} - R}{\sigma_R} \right)} \right] \\
 &\approx \lambda \cdot \frac{\sigma_R^2}{2 \left(\frac{D_{F_L} - R}{\sigma_R} \right)} e^{-\frac{(D_{F_L} - R)^2}{\sigma_R^2}} \quad (16)
 \end{aligned}$$

since $(D_{F_U} - D_{F_L}) \gg \sigma_R$ and using the asymptotic property of the normal function. Substituting (16) into (15), obtain

$$\text{PND} \approx \int_0^{D_{F_L} - \sigma_R} \frac{1}{\sqrt{\frac{y}{\pi}}} \frac{dy}{\sigma_R} \left\{ e^{-G\left(\frac{(y^2 - \epsilon^2)}{\sigma_r^2}, 0\right)} e^{-\frac{y^2}{\sigma_r^2}} \right\} \frac{\lambda \sigma_R^2}{2(D_{F_L} - y)} e^{-\frac{(D_{F_L} - y)^2}{\sigma_R^2}} \quad (17)$$

assuming $D_{F_L} - \epsilon \gg \sigma_R$, that is, ϵ , the test level is many noise sigma less than the failure rate.

The exponential terms dominate variation of the magnitude of the integrand where appreciable contributions to PND occur. For the tetrahedral case $\sigma_R^2 = \sigma_r^2 = \frac{2}{3} \sigma_N^2$ hence for $y, \epsilon \gg \sigma_N$

$$\left(e^{-G\left(\frac{y^2 - \epsilon^2}{\sigma_r^2}, 0\right) - \frac{y^2}{\sigma_r^2}} \right) \cdot e^{-\frac{(D_{FL} - y)^2}{\sigma_R^2}} \cdot \frac{1}{\sigma_r^2} \left[\epsilon^2 - 2 \left(y - \frac{D_{FL}}{2} \right)^2 - D_{FL}^2/2 \right]$$

$$\approx e^{-\frac{1}{\sigma_r^2} \cdot (y - D_F)^2}$$

for $y \geq \epsilon$

for $y < \epsilon$

(18)

The maximum of this function occurs at $y = D_{FL}/2$ when $\epsilon \leq D_{FL}/2$ and at $y = \epsilon$ when $D_{FL}/2 < \epsilon < D_{FL}$ hence

$$y_{\max} = G(D_{FL}/2, \epsilon)$$

It is desirable to use the least ϵ , so as to minimize PND, consistent with acceptable PFA which by (11) is $\epsilon \geq 5.5 \sigma_N$. For $D_{FL}/\sigma_N \geq 11$ then $\epsilon \leq D_{FL}/2$ using $\epsilon = 5.5 \sigma_N$ and the integrand of (17) is approximately maximized at $y = D_{FL}/2$. When $D_{FL}/\sigma_N \geq 11$, we model GF_2 failure. In general, (17) is approximately evaluated setting y in non-exponential terms to $y = D_{FL}/2$ where $y > \epsilon$ and $y = \epsilon$ where $y < \epsilon$, and integrating. Then, for $\epsilon \leq D_{FL}/2$, obtain

$$PND = \frac{1}{3} \frac{\sigma_N^2 \cdot \lambda}{\sqrt{D_{FL}}} \left[e^{\frac{\epsilon^2 - D_{FL}^2}{\frac{2}{3} \sigma_N^2}} \cdot G\left(\frac{\epsilon - D_{FL}/2}{\sigma_N/\sqrt{6}}\right) + \sqrt{\frac{\epsilon D_{FL}}{D_{FL} - \epsilon}} \cdot G\left(\frac{D_{FL} - \epsilon}{\sigma_N/\sqrt{3}}\right) \right]$$

where $G(x) = \int_X^{\infty} e^{-\frac{1}{2}y^2} \frac{dy}{\sqrt{2\pi}}$ and $\sigma_R = \sigma_r = \sqrt{\frac{2}{3}} \sigma_N$. Note, since $(D_{FL} - \epsilon)/\sigma_N/\sqrt{3}$ is large for the GF_2 failure model,

$$\frac{\sqrt{\epsilon \cdot D_{FL}}}{(D_{FL} - \epsilon)} G\left(\frac{D_{FL} - \epsilon}{\sigma_N/\sqrt{3}}\right) = \sqrt{\frac{3}{2\pi}} \frac{\sqrt{\epsilon \cdot D_{FL}} \sigma_N}{(D_{FL} - \epsilon)^2} e^{-\frac{1}{2}\left(\frac{D_{FL} - \epsilon}{\sigma_N/\sqrt{3}}\right)^2}$$

using the asymptotic expansion. Modeling $r_D = D_{FU}/D_{FL} \gg 1$

then $\lambda = \frac{3/2}{(r_D \cdot D_{FL})^{3/2}}$. For cases where $\epsilon < D_{FL}/2$,

$$PND = \frac{1}{2U^2 \cdot r_D^{3/2}} \cdot \left[e^{-\frac{3}{2}(u/2-v)^2} \cdot G(\sqrt{6}(v-u/2)) + \sqrt{\frac{3}{2\pi}} \frac{\sqrt{u \cdot v}}{(u-v)^2} \cdot e^{-\frac{3}{2}(u-v)^2} \right] \quad (20)$$

where $u = D_{FL}/\sigma_N$, $v = \epsilon/\sigma_N$. Adopt a nominal value of $r_D = 10$, noting adjustment of PND is readily made with any change of assumption regarding r_D . Consider the marginal case for GF_2 failure with $u = 11$ where $v = 5.5$ to hold PFA to an acceptable level, $PFA = 10^{-8}$ obtaining

$$PND = 1.3 \times 10^{-4} \cdot \left[.50 \cdot e^{-45.3} + .18 \cdot e^{-45.3} \right] \approx 10^{-24}$$

$$\begin{aligned} GF_2 \text{ Failure Model } \epsilon &= D_{FL}/2 \\ D_{FL} &= 11 \cdot \sigma_N \end{aligned}$$

When $u = D_{FL}/\sigma_N < 11$ and $v = \epsilon/\sigma_N = 5.5$, since $\epsilon > D_{FL}/2$ the maximum value of (18) is at $y = \epsilon$. Substituting $y = \epsilon$ for non-exponential terms of (17) and otherwise making the same approximations as in (20), obtain for $\epsilon > D_{FL}/2$,

$$\text{PND} \approx \frac{1}{2u^2 \cdot r_D^{3/2}} \cdot \frac{\sqrt{uv}}{(u-v)^2} \cdot \left[e^{-\frac{3}{2}(u^2/2-v^2)} \cdot \frac{(u-v)}{\sqrt{2}} \cdot G\left(\sqrt{6}(v-u/2)\right) + \sqrt{\frac{3}{2\pi}} \cdot e^{-\frac{3}{2}(u-v)^2} \right] \quad (21)$$

A table of PND for several u values is:

D_{FL}/σ_N	PND
11	10^{-24}
9	1.3×10^{-12}
8	$1. \times 10^{-6}$
7	2.7×10^{-5}

$r_D = 10$
 $\epsilon/\sigma_N = 5.5$

Consider the statistical properties of

$$F_0 = T_{12}^2 + T_{13}^2 + T_{23}^2 + T_{14}^2 + T_{24}^2 + T_{34}^2$$

Using (6c),

$$\begin{aligned} T_{14}^2 + T_{24}^2 + T_{34}^2 &= \left(-x_1 - \frac{x_4}{2} - y_4 \frac{\sqrt{3}}{2}\right)^2 + \left(-x_2 + \frac{x_4}{2} - y_4 \frac{\sqrt{3}}{2}\right)^2 \\ &\quad + (x_3 + x_4)^2 \\ &= \left(\frac{-x_1}{\sqrt{2}} - \frac{x_2}{\sqrt{2}} - \sqrt{\frac{3}{2}} y_4\right)^2 + \left(-\frac{x_1}{\sqrt{2}} + \frac{x_2}{\sqrt{2}} - \frac{x_4}{\sqrt{2}}\right)^2 \\ &\quad + (x_3 + x_4)^2 \\ &= \left(\frac{-x_1}{\sqrt{2}} - \frac{x_2}{\sqrt{2}} - \sqrt{\frac{3}{2}} y_4\right)^2 + \left(\frac{-x_1}{\sqrt{6}} + \frac{x_2}{\sqrt{6}} - \sqrt{\frac{3}{2}} x_4 - \sqrt{\frac{2}{3}} x_3\right)^2 \\ &\quad + \left(-\frac{x_1}{\sqrt{2}} + \frac{x_2}{\sqrt{3}} + \frac{x_3}{\sqrt{3}}\right)^2 \end{aligned}$$

where the identity $U_1^2 + U_2^2 = (\alpha U_1 - \sqrt{1-\alpha^2} U_2)^2 + (\sqrt{1-\alpha^2} U_1 + \alpha U_2)^2$ is used with $\alpha = 1/\sqrt{2}, 1/\sqrt{3}$ to isolate y_4, x_4 to single terms to remove correlation of variables. Introducing the variables

$$x_D = \frac{x_1}{\sqrt{2}} - \frac{x_2}{\sqrt{2}}, \quad x_S = \frac{x_1}{\sqrt{2}} + \frac{x_2}{\sqrt{2}} \text{ with variance } \sigma_N^2,$$

$$\begin{aligned} T_{14}^2 + T_{24}^2 + T_{34}^2 &= \left(x_S + \sqrt{\frac{3}{2}} y_4\right)^2 + \left(\frac{x_D}{\sqrt{3}} + \sqrt{\frac{3}{2}} x_4 + \sqrt{\frac{2}{3}} x_3\right)^2 \\ &\quad + \left(-\sqrt{\frac{2}{3}} x_D + \frac{x_3}{\sqrt{3}}\right)^2 \end{aligned}$$

where correlation of variables due to x_4, y_4 was removed.

Where we also introduce variables $y_D = \frac{y_1}{\sqrt{2}} - \frac{y_2}{\sqrt{2}}$, $y_S = \frac{y_1}{\sqrt{2}} + \frac{y_2}{\sqrt{2}}$ then by (6c),

$$\begin{aligned} T_{12}^2 + T_{13}^2 + T_{23}^2 &= \left(\frac{x_D}{\sqrt{2}} + \sqrt{\frac{3}{2}} y_D \right)^2 + \left[\frac{(x_3 - x_1)}{2} + (y_3 + y_1) \frac{\sqrt{3}}{2} \right]^2 \\ &\quad + \left[-\frac{(x_2 + x_3)}{2} + (y_2 + y_3) \frac{\sqrt{3}}{2} \right]^2 \\ &= \left(\frac{x_D}{\sqrt{2}} + \sqrt{\frac{3}{2}} y_D \right)^2 + \left(-\frac{x_S}{2} + \sqrt{\frac{3}{2}} y_3 + \frac{\sqrt{3}}{2} y_S \right)^2 \\ &\quad + \left(\frac{x_3}{\sqrt{2}} - \frac{x_D}{2} + y_D \frac{\sqrt{3}}{2} \right)^2 \end{aligned}$$

using the above identity with $\alpha = 1/\sqrt{2}$. Adding the two results, and introducing the variables

$$\begin{aligned} x_4 &= \frac{x_D}{\sqrt{3}} + \sqrt{\frac{3}{2}} x_4 + \sqrt{\frac{2}{3}} x_3 \\ y_4 &= x_S + \sqrt{\frac{3}{2}} y_4 \\ y_3 &= -\frac{x_S}{2} + \sqrt{\frac{3}{2}} y_3 + \frac{\sqrt{3}}{2} y_S \\ x_3 &= \sqrt{\frac{5}{6}} x_3 + \frac{3}{2\sqrt{5}} y_D - \frac{7}{6} \sqrt{\frac{3}{5}} x_D \\ U &= \sqrt{\frac{3}{5}} x_D + \frac{3}{\sqrt{5}} y_D \end{aligned}$$

obtain

$$F_0 = X_4^2 + Y_4^2 + Y_3^2 + \mu$$

where

$$\begin{aligned} \mu &= \left(-\sqrt{\frac{2}{3}} x_D + \frac{x_3}{\sqrt{3}} \right)^2 + \left(\frac{x_3}{\sqrt{2}} - \frac{x_D}{2} + y_D \frac{\sqrt{3}}{2} \right)^2 + \left(\frac{x_D}{\sqrt{2}} + \sqrt{\frac{3}{2}} y_D \right)^2 \\ &= \left(\frac{x_D}{\sqrt{10}} + \sqrt{\frac{3}{10}} y_D \right)^2 + \left(\sqrt{\frac{5}{6}} x_3 + \frac{3}{2\sqrt{5}} y_D - \frac{7}{6} \sqrt{\frac{3}{5}} x_D \right)^2 + \left(\frac{x_D}{\sqrt{2}} + \sqrt{\frac{3}{2}} y_D \right)^2 \\ &= U^2 + X_3^2 \end{aligned}$$

using $\alpha = \sqrt{\frac{3}{5}}$ in the identity, then collecting terms. Note that variables generated by the identity have a covariance

$$\begin{aligned} \overline{U_1 U_2} &= \overline{(\alpha U_1 - \sqrt{1-\alpha^2} U_2)(\sqrt{1-\alpha^2} U_1 + \alpha U_2)} \\ &= \alpha \sqrt{1-\alpha^2} (\overline{U_1^2} - \overline{U_2^2}) - (1-2\alpha^2) \cdot \overline{U_1 U_2} \end{aligned}$$

In the case, $\overline{U_1^2} = \overline{U_2^2}$ then the new variables are uncorrelated using $\alpha = 1/\sqrt{2}$. Since

$$\overline{Y_4^2} = \overline{Y_3^2} = \frac{5}{2} \sigma_N^2$$

we may apply the identity with $\alpha = 1/\sqrt{2}$ to obtain

$$Y_4^2 + Y_3^2 = U_4^2 + U_3^2$$

where

$$U_4 = \frac{\sqrt{3}}{2} (y_4 + y_3 + y_s/\sqrt{2}) + \frac{x_s}{2\sqrt{2}}$$

$$U_3 = \frac{\sqrt{3}}{2} (y_4 - y_3 - y_s/\sqrt{2}) + \frac{3 x_s}{2\sqrt{2}}$$

and $\overline{U_4 \cdot U_3} = 0$. Also note U_4, U_3 are uncorrelated with X_4, X_3, U .

Note, $\overline{X_4^2} = \frac{5}{2} \sigma_N^2$, $\overline{U^2} = \frac{12}{5} \sigma_N^2$. To use the identity to form uncorrelated variables when the variances are unequal, use the following general result

$$\alpha = \sqrt{\frac{1 - \lambda\sqrt{1 + \lambda^2}}{2}} \quad \lambda = \frac{\overline{U_1^2} - \overline{U_2^2}}{2 \overline{U_1 U_2}}$$

Where $U_1 = X_4$, $U_2 = U$ then $\overline{U_1 U_2} = \overline{X_4 U} = \sigma_N^2/\sqrt{5}$ so obtain $\lambda = \frac{1}{4\sqrt{5}}$ then $\alpha = \frac{2}{3}, \sqrt{1 - \alpha^2} = \frac{\sqrt{5}}{3}$.

The new independent variables are

$$V_1 = -\frac{1}{3\sqrt{3}} x_D - y_D + \sqrt{\frac{2}{3}} x_4 + \frac{2}{3} \sqrt{\frac{2}{3}} x_3$$

$$V_2 = \frac{11}{3\sqrt{15}} x_D + \frac{2}{\sqrt{5}} y_D + \sqrt{\frac{5}{6}} x_4 + \frac{1}{3} \sqrt{\frac{10}{3}} x_3$$

where $\overline{V_1 \cdot V_2} = 0$ and $x_4^2 + U^2 = V_1^2 + V_2^2$. We know V_1, V_2 are uncorrelated also with U_3, U_4 , but must determine correlation with X_3 to obtain

$$\overline{V_1 X_3} = 0$$

$$\overline{V_2 X_3} = \frac{3}{10} \sigma_N^2$$

The only non-zero covariance is $\overline{V_2 X_3}$ which is removed using the identity with $U_1 = V_2, U_2 = X_3$ using $\sigma_{X_3}^2 = 21/10 \sigma_N^2$, $\sigma_{V_2}^2 = 29/10 \sigma_N^2$, for which $\lambda = 4/3$ to obtain $a = 1/\sqrt{10}$, $\sqrt{1 - a^2} = 3/\sqrt{10}$ hence

$$U_1 = -\frac{7}{6\sqrt{3}} x_3 - \frac{y_D}{2\sqrt{2}} + \frac{1}{2\sqrt{3}} x_4 + \frac{17}{6\sqrt{6}} x_D$$

$$U_2 = \frac{3}{2\sqrt{3}} x_3 + \frac{3}{2\sqrt{2}} y_D + \frac{3}{2\sqrt{3}} x_4 + \frac{3}{2\sqrt{6}} x_D$$

where

$$\overline{U_1 U_2} = 0, \quad x_3^2 + v_2^2 = U_1^2 + U_2^2$$

Collecting results,

$$\begin{aligned} F_0 &= T_{12}^2 + T_{13}^2 + T_{23}^2 + T_{14}^2 + T_{24}^2 + T_{34}^2 \\ &= U_1^2 + U_2^2 + U_3^2 + U_4^2 + V_1^2 \end{aligned}$$

where the variables

$$\begin{aligned} U_1 &= -\frac{7}{6\sqrt{3}} x_3 - \frac{y_D}{2\sqrt{2}} + \frac{1}{2\sqrt{3}} x_4 + \frac{17}{6\sqrt{6}} x_D \\ U_2 &= \frac{3}{2\sqrt{3}} x_3 + \frac{3}{2\sqrt{2}} y_D + \frac{3}{2\sqrt{3}} x_4 + \frac{3}{2\sqrt{6}} x_D \\ U_3 &= \frac{\sqrt{3}}{2} (y_4 - y_3 - y_s/\sqrt{2}) + \frac{3}{2\sqrt{2}} x_s \\ U_4 &= \frac{\sqrt{3}}{2} (y_4 + y_3 + y_s/\sqrt{2}) + \frac{1}{2\sqrt{2}} x_s \\ V_1 &= \frac{2}{3}\sqrt{\frac{2}{3}} x_3 - y_D + \sqrt{\frac{2}{3}} x_4 - \frac{1}{3\sqrt{3}} x_D \end{aligned}$$

are uncorrelated where

$$X_D = (X_1 - X_2) / \sqrt{2}$$

$$X_S = (Y_1 - Y_2) / \sqrt{2}$$

$$Y_D = (Y_1 - Y_2) / \sqrt{2}$$

$$Y_S = (Y_1 + Y_2) / \sqrt{2}$$

It is assumed X_r, Y_r $r = 1, 4$ are independent with variance σ_N^2 so

$$\sigma_{U_1}^2 = 2\sigma_N^2$$

$$\sigma_{U_2}^2 = 3\sigma_N^2$$

$$\sigma_{U_3}^2 = 3\sigma_N^2$$

$$\sigma_{U_4}^2 = 2\sigma_N^2$$

$$\sigma_{U_1}^2 = 2\sigma_N^2$$

Since $\sigma_{T_{rs}}^2 = 2\sigma_N^2$, $\overline{F_0} = 12\sigma_N^2$ in agreement with the result for the new independent variables.

Consider evaluation of the probability distribution of F_0 , which involves the sum of independent Rayleigh distributed variables with differing means. First consider the case where

means are equal. It may be shown that the probability distribution for the case of sum of two and three Rayleigh variables with equal mean is

Distribution of:

$$\phi(S_2) dS_2 = \frac{e^{-S_2/M_2}}{M_2^2} S_2 dS_2 \quad \text{Sum of Two Rayleigh Variables, Means } M_2$$

$$\phi(S_3) dS_3 = \frac{e^{-S_3/M_3}}{M_3^3} \cdot \frac{S_3^2}{2} dS_3 \quad \text{Sum of Three Rayleigh Variables, Means } M_3$$

Let $S_2 = U_2^2 + U_3^2$ where $M_2 = 3\sigma_N^2$ and $S_3 = U_1^2 + U_4^2 + V_1^2$ where $M_3 = 2\sigma_N^2$. Then $F_0 = S_2 + S_3$ has a probability distribution given by integrating the product of the two distributions with substitutions $dF_0 = dS_2$, $S_2 = F_0 - S_3$

$$\begin{aligned} \phi(F_0) dF_0 &= \int_{S_3=0}^{\infty} e^{-\frac{(F_0 - S_3)/M_2 - S_3/M_3}{2M_2^2 M_3^3}} (F_0 - S_3) \cdot S_3^2 dS_3 dF_0 \\ &= \frac{dF_0 \cdot e^{-F_0/M_2}}{2M_2^2 \cdot M_3^3} \cdot I \end{aligned}$$

where

$$I = \int_{x=0}^{F_0} e^{-\alpha x} (F_0 - x) x^2 dx, \quad \alpha = \left(\frac{1}{M_3} - \frac{1}{M_2} \right)$$

It may be shown by integration and taking $M_2 = 3\sigma_N^2$, $M_3 = 2\sigma_N^2$ that

$$\phi(F_0) dF_0 = 54 [2 (u-3) e^{-2u} + (u^2 + 4u + 6) \cdot e^{-3u}] du$$

where $u = F_0/6 \sigma_N$. The probability that noise causes F_0 to exceed ϵ^2 is

$$\begin{aligned} P(F_0 > \epsilon^2) &= \int_{\epsilon^2}^{\infty} \phi(F_0) dF_0 \\ &= [-27 (5-2u) + 2 (68 + 42u + 9u^2) e^{-u}] e^{-2u} \end{aligned}$$

where $u = 1/6 (\epsilon/\sigma_N)^2$.

2. Failure Detection and Isolation Algorithm for Tetrahedral Array with Three Valid Gyros

When one of four gyros in tetrahedral array is invalid, say gyro No. 4 then θ_{14} in (5) must be estimated using data of other gyros using (3), hence

$$\begin{aligned}\theta^2 &= \frac{2}{3} \left[\theta_{12}^2 + \theta_{13}^2 + \theta_{14}^2 \right] \\ &= \frac{2}{3} \left[\theta_{12}^2 + \theta_{13}^2 + (\theta_{13} - \theta_{12})^2 \right] \\ &= \frac{4}{3} \left[\theta_{12}^2 + \theta_{13}^2 - \theta_{12}\theta_{13} \right]\end{aligned}$$

The test function

$$\bar{F}_1 = \frac{4}{3} \left[T_{12}^2 + T_{13}^2 - T_{12} \cdot T_{13} \right],$$

correctly estimates $D_{F_1}^2$ if only gyro No. 1 drifts and at drift rate D_{F_1} . When a gyro other than gyro No. 1 fails it is important that the test function for gyro No. 1 be minimized, in order to isolate the failure. This may be done by elaborating the test to the bilinear function

$$F_1 = \frac{4}{3} \left\{ T_{12}^2 + T_{13}^2 - T_{12} \cdot T_{13} - T_{23} \cdot \left[K_1 \cdot T_{12} + \bar{K}_1 \cdot T_{13} + K_2 \cdot T_{23} \right] \right\} \quad (22)$$

which correctly estimates $D_{F_1}^2$ when only gyro No. 1 drifts since $T_{23} = 0$. Constants K_1, \bar{K}_1, K_2 are chosen to minimize F_1 if either gyro No. 2 fails or gyro No. 3 fails.

Consider the case only gyro No. 2 drifts. Then (22) reduces to

$$F_1 = \frac{4}{3} \left\{ T_{12}^2 - K_1 T_{23} T_{12} - K_2 T_{23}^2 \right\} \quad (23)$$

Using (2) it may be shown $(\vec{e}_{T_{12}} \cdot \vec{e}_{T_{23}}) = 1/2$, hence when gyro No. 2 drifts in a direction with angle ϕ_2 from $\vec{e}_{T_{12}}$, we have $T_{12} = -D_{F_2} C \phi_2$ and $T_{23} = D_{F_2} C_{60^\circ - \phi_2}$

When only gyro No. 2 drifts, it may be shown

$$\begin{aligned} F_1 &= \frac{4}{3} D_{F_2}^2 \left\{ C_{\phi_2}^2 + K_1 C_{\phi_2} \cdot C_{60^\circ - \phi_2} - K_2 C_{60^\circ - \phi_2}^2 \right. \\ &= \frac{2}{3} D_{F_2}^2 \left\{ \left(1 + \frac{K_1}{2} - K_2 \right) + D \cdot C_{z \phi_2 - \Delta} \right\} \end{aligned} \quad (24)$$

where

$$D = \sqrt{\left(1 + \frac{K_1}{2} + \frac{K_2}{2} \right)^2 + \frac{3}{4} (K_1 - K_2)^2}$$

$$C_{\Delta} = \left(1 + \frac{K_1}{2} + \frac{K_2}{2} \right) / D$$

$$S_{\Delta} = \frac{\sqrt{3}}{2} (K_1 - K_2) / D$$

The worse case direction of drift ϕ_2 is $\phi_{2\omega} = \Delta/2$ for which F_1 is maximized to

$$F_1 = \frac{2}{3} D_{F_2}^2 \left\{ K_2^* + D \right\}$$

where $K_2^* = 1 + \frac{K_1}{2} - K_2$

Eliminating K_2 show

$$D = \sqrt{\frac{3}{4} (1 + K_1)^2 + (K_2^* - \frac{3}{2})^2}$$

so F_1 is a function of K_1, K_2^* . Note F_1 is minimized taking $K_1 = -1$ in which case (11) reduces to

$$F_1 = \frac{2}{3} D_{F_2}^2 \cdot \left\{ K_2^* + \left| \frac{3}{2} - K_2^* \right| \cdot C_{2\phi_2 - \Delta} \right\} \quad (25)$$

For the worse case direction of drift $\phi_2 = -\Delta/2$ it is readily shown

$$F_1 \geq D_{F_2}^2$$

the equal sign holding for $K_2^* \leq 3/2$, which is desirable to hold done worse case F_1 . Measuring drift rate direction relative the worst case direction with $\theta_2 = \phi_2 - \Delta/2$ note $C_{2\phi_2 - \Delta} = C_{2\theta_2} = 1 - 2 S_{\theta_2}^2$, hence (25) takes the form

$$\begin{aligned} F_1 &= \frac{2}{3} D_{F_2}^2 \cdot \left\{ K_2^* + \left| \frac{3}{2} - K_2^* \right| (1 - 2S_{\theta_2}^2) \right\} \\ &= D_{F_2}^2 \cdot \left\{ 1 - \frac{4}{3} \left(\frac{3}{2} - K_2^* \right) S_{\theta_2}^2 \right\} \end{aligned}$$

for $K_2^* \leq 3/2$.

Then F_1 is seen to be minimized by making K_2^* as large negative as possible (noise being the counter consideration). Since $K_2 = \frac{1}{2} - K_2^*$, it follows K_2 should be as large as possible. Note, with $K_1 = -1$, generally $\Delta = -60^\circ$ so the worst case drift direction is $\phi_2 = -30^\circ$, that is 90° to $\vec{e}_{T_{23}}$.

For only gyro No. 3 drifting, the same relations hold except for sense of T_{23} , T_{13} so $\bar{K}_1 = 1$.

The derived algorithm is

$$F_1 = \frac{4}{3} \left\{ T_{12}^2 + T_{13}^2 - T_{12} \cdot T_{13} - T_{23} \cdot \left[T_{13} - T_{12} + K_2 \cdot T_{23} \right] \right\} \quad (26)$$

which has properties

$$\left\{ \begin{array}{ll} D_{F_1}^2 & \text{if only gyro No. 1 drifts} \\ D_{F_2}^2 \cdot \left\{ 1 - \frac{4}{3} (1 + K_2) S_{\theta_2}^2 \right\} & \text{if only gyro No. 2 drifts} \\ D_{F_3}^2 \cdot \left\{ 1 - \frac{4}{3} (1 + K_2) S_{\theta_3}^2 \right\} & \text{if only gyro No. 3 drifts} \end{array} \right.$$

where K_2 is as large as consistent with noise levels. To investigate the behavior of F_1 in the general case where all gyros drift, use

$$\begin{aligned} T_{12} &= D_{F_1} C_{\phi_1} - D_{F_2} \cdot C_{\phi_2} \\ T_{13} &= D_{F_1} C_{60^\circ - \phi_1} + D_{F_3} C_{\phi_3} \\ T_{23} &= D_{F_2} C_{60^\circ - \phi_2} + D_{F_3} C_{60^\circ - \phi_3} \end{aligned} \quad (27)$$

where

ϕ_1 is the angle from $\vec{e}_{T_{12}}$ to \vec{D}_{F_1} about \vec{e}_{S_1}

ϕ_2 is the angle from $\vec{e}_{T_{12}}$ to \vec{D}_{F_2} about \vec{e}_{S_2}

ϕ_3 is the angle from $\vec{e}_{T_{13}}$ to \vec{D}_{F_3} about \vec{e}_{S_3}

as seen in figure I-1.

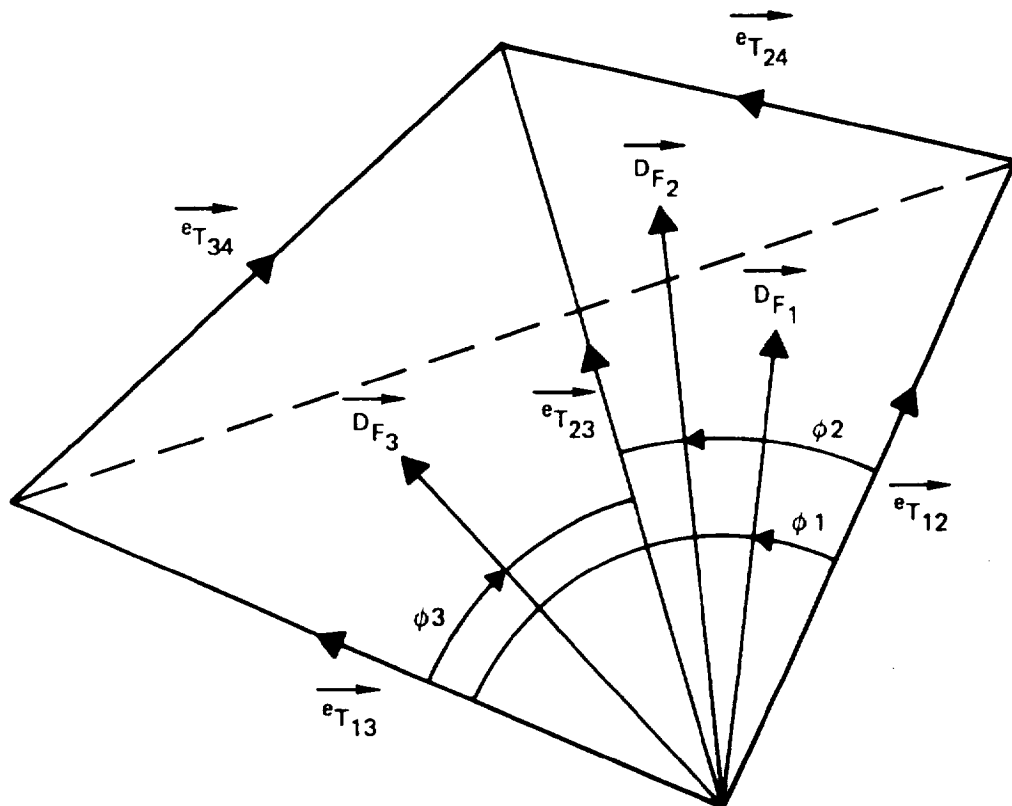


Figure I-1

Note, Eq (26) may be put in the form

$$F_1 = \frac{2}{3} \left\{ (T_{12}^2 + T_{13}^2 + T_{23}^2) + (T_{12} - T_{13} + T_{23})^2 \right\} - \frac{4}{3} K \cdot T_{23}^2 \quad (28)$$

where $K = K_2 + 1$, where, using (27)

$$\begin{aligned} (T_{12} - T_{13} + T_{23}) &= D_{F_1} (C_{\phi_1} - C_{60^\circ - \phi_1}) - D_{F_2} (C_{\phi_2} - C_{60^\circ - \phi_2}) - D_{F_3} (C_{\phi_3} - C_{60^\circ - \phi_3}) \\ &= -D_{F_1} \cdot S_{\phi_1 - 30^\circ} + D_{F_2} \cdot S_{\phi_2 - 30^\circ} + D_{F_3} \cdot S_{\phi_3 - 30^\circ} \\ (T_{12}^2 + T_{13}^2 + T_{23}^2) &= D_{F_1}^2 \cdot \left(\frac{3}{2} - S_{\phi_1 - 30^\circ}^2 \right) + D_{F_2}^2 \left(\frac{3}{2} - S_{\phi_2 - 30^\circ}^2 \right) \\ &\quad + D_{F_3}^2 \cdot \left(\frac{3}{2} - S_{\phi_3 - 30^\circ}^2 \right) - 2 D_{F_1} D_{F_2} C_{\phi_1} C_{\phi_2} \\ &\quad + 2 D_{F_1} D_{F_3} C_{60^\circ - \phi_1} C_{\phi_3} + 2 D_{F_2} D_{F_3} C_{60^\circ - \phi_2} C_{60^\circ - \phi_3} \end{aligned}$$

$$\text{using } (C\phi - C_{60^\circ - \phi}) = -S_{\phi - 30^\circ} \text{ and } (C_\phi^2 + C_{60^\circ - \phi}^2) = \frac{3}{2} - S_{\phi - 30^\circ}^2$$

Then

$$\begin{aligned} \frac{2}{3} \left\{ (T_{12}^2 + T_{13}^2 + T_{23}^2) + (T_{12} - T_{13} + T_{23})^2 \right\} &= D_{F_1}^2 + D_{F_2}^2 + D_{F_3}^2 \\ &\quad - \frac{4}{3} D_{F_1} D_{F_2} \cdot \lambda_{12} \\ &\quad - \frac{4}{3} D_{F_1} D_{F_3} \cdot \lambda_{13} \\ &\quad + \frac{4}{3} D_{F_2} D_{F_3} \cdot \lambda_{23} \end{aligned}$$

where

$$\lambda_{12} = C_{\phi_1} \cdot C_{\phi_2} + S_{\phi_{1-30^\circ}} \cdot S_{\phi_{2-30^\circ}} = C_{\theta_{1-30^\circ}} C_{\theta_{2-30^\circ}} + C_{\theta_{1+30^\circ}} C_{\theta_{2+30^\circ}}$$

$$\lambda_{13} = -C_{60^\circ-\phi_1} C_{\phi_3} + S_{\phi_{1-30^\circ}} S_{\phi_{3-30^\circ}} = -S_{\theta_1} C_{\theta_{3-30^\circ}} + C_{\theta_{1+30^\circ}} C_{\theta_{3+30^\circ}}$$

$$\lambda_{23} = C_{60^\circ-\phi_2} C_{60^\circ-\phi_3} + S_{\phi_{2-30^\circ}} S_{\phi_{3-30^\circ}} = S_{\theta_2} S_{\theta_3} + C_{\theta_{2+30^\circ}} C_{\theta_{3+30^\circ}} \quad (29)$$

using $\phi_r = \theta_{r-30^\circ}$ noting θ_2, θ_3 are angles measured from worst case directions in terms of which, using (27),

$$T_{12} = D_{F_1} \cdot C_{\theta_{1-30^\circ}} - D_{F_2} \cdot C_{\theta_{2-30^\circ}}$$

$$T_{13} = D_{F_1} \cdot S_{\theta_1} + D_{F_3} \cdot C_{\theta_{3-30^\circ}} \quad (30)$$

$$T_{23} = D_{F_2} \cdot S_{\theta_2} + D_{F_3} \cdot S_{\theta_3}$$

Then, in general

$$F_1 = D_{F_1}^2 + D_{F_2}^2 + D_{F_3}^2 - \frac{4}{3} \left\{ D_{F_1} \cdot D_{F_2} \cdot \lambda_{12} + D_{F_1} \cdot D_{F_3} \cdot \lambda_{13} - D_{F_2} \cdot D_{F_3} \cdot \lambda_{23} + K \left(D_{F_2} S_{\theta_2} + D_{F_3} S_{\theta_3} \right)^2 \right\} \quad (31)$$

where by expanding cosines

$$\lambda_{12} = \left(\frac{3}{2} C_{\theta_1} C_{\theta_2} + \frac{1}{2} S_{\theta_1} S_{\theta_2} \right) = C_{\theta_2 - \delta_2} \cdot \sqrt{2C_{\theta_1}^2 + \frac{1}{4}} \quad (32)$$

$$\lambda_{13} = - \left(\frac{3}{2} S_{\theta_1 - 30^\circ} C_{\theta_3} + \frac{1}{2} C_{\theta_1 - 30^\circ} S_{\theta_3} \right) = -C_{\theta_3 - \delta_3} \cdot \sqrt{2C_{\theta_1 + 60^\circ} + \frac{1}{4}}$$

$$\lambda_{23} = C_{\theta_2 - \theta_3} - \frac{1}{2} S_{\theta_2 + \theta_3 + 30^\circ} = \left(\frac{3}{2} C_{\theta_2 + 60^\circ} C_{\theta_3 + 60^\circ} + \frac{1}{2} S_{\theta_2 + 60^\circ} S_{\theta_3 + 60^\circ} \right)$$

It may be shown $|\lambda_{12}| \leq 3/2, |\lambda_{13}| \leq 3/2, |\lambda_{23}| \leq 3/2.$

Note the phase of \vec{D}_{F1} cannot maximize λ_{12} with $\theta_1 = 0, 180^\circ$ for $\theta_2 = \delta_2$ and maximize λ_{13} with $\theta_1 = -60^\circ, 120^\circ$ for $\theta_3 = \delta_3$ simultaneously, rather $|\lambda_{12}| + |\lambda_{13}| \leq \sqrt{7}.$

The selection of K should at last be held so if gyro No. 1 fails, the noise level in terms of $D_{F2} D_{F3}$ does not reduce the apparent failure magnitude by more than a fraction ϵ on average. This occurs when

$$(1-\epsilon)^2 D_F^2 = F_1 = D_F^2 - \frac{4}{3} K \cdot \sigma_N^2$$

for which

$$K \approx \frac{3}{2} \epsilon D_F^2 / \sigma_N^2$$

In the worst case when noises of gyro No. 2 and No. 3 are equal and $\theta_2 = \theta_3 = \pi/2,$

$$K \approx \frac{3}{8} \epsilon D_F^2 / \sigma_N^2 \quad (33)$$

would be necessary to hold the apparent failure rate reduction to $\epsilon \cdot D_F.$

The apparent failure magnitude can also be reduced by the terms λ_{12} , λ_{13} , λ_{23} by worst case phase relationships subject to (32) so it may be shown the worst case reduction factor in apparent failure magnitude is,

$$\epsilon^* \leq \frac{2\sqrt{7} \sigma_N}{3 D_F}$$

The total reduction in apparent failure magnitude from the K term and λ terms of (31) is $(\epsilon + \epsilon^*) D_F$ which may be compensated for in testing by lowering the test level accordingly.

The derived algorithm* tests $F_r < \delta$ $r = 1, 2, 3$ where

$$F_1 = \bar{F}_4 - \alpha \cdot T_{23}^2$$

$$F_2 = \bar{F}_4 - \alpha \cdot T_{13}^2$$

$$F_3 = \bar{F}_4 - \alpha \cdot T_{12}^2$$

where

$$\bar{F}_4 = \frac{2}{3} \left\{ T_{12}^2 + T_{13}^2 + T_{23}^2 + (T_{12} - T_{13} + T_{23})^2 \right\}$$

$$\alpha = \frac{4}{3} (1 + K_2) = \frac{4}{3} K$$

If a single test fails, say $F_r^* \geq \delta$ then the gyro No. r^* is concluded to have failed. The functions F_r have the properties:

$$F_1 = \begin{cases} D_{F_1}^2 & \text{if only gyro No. 1 drifts} \\ D_{F_2}^2 \cdot \{ 1 - \alpha \cdot S_{\theta_2}^2 \} & \text{if only gyro No. 2 drifts} \\ D_{F_3}^2 \cdot \{ 1 - \alpha \cdot S_{\theta_3}^2 \} & \text{if only gyro No. 3 drifts} \end{cases} \quad (35a)$$

$$F_2 = \begin{cases} D_{F_1}^2 \cdot \{ 1 - \alpha \cdot S_{\theta_1}^2 \} & \text{if only gyro No. 1 drifts} \\ D_{F_2}^2 & \text{if only gyro No. 2 drifts} \\ D_{F_3}^2 \cdot \{ 1 - \alpha S_{\theta_3^*}^2 \} & \text{if only gyro No. 3 drifts} \end{cases} \quad (35b)$$

where $\theta_3^* = \theta_3 + 60^\circ$, θ_3^* being zero for drift normal to $\vec{e}_{T_{13}}$

$$F_3 = \begin{cases} D_{F_1}^2 \cdot \{ 1 - \alpha S_{\theta_1^*}^2 \} & \text{if only gyro No. 1 drifts} \\ D_{F_2}^2 \cdot \{ 1 - \alpha S_{\theta_2^*}^2 \} & \text{if only gyro No. 2 drifts} \\ D_{F_3}^2 & \text{if only gyro No. 3 drifts} \end{cases} \quad (35c)$$

where $\theta_1^* = \theta_1 + 60^\circ$ and $\theta_2^* = \theta_2 + 60^\circ$
 θ_1^* , θ_2^* being zero for drift normal to $\vec{e}_{T_{12}}$

*Which amounts to testing T_{23}^2 , T_{13}^2 , T_{12}^2 relative $(\bar{F}_4 - \delta)/\alpha$

The variation of \bar{F}_4 due to noise of other gyros when gyro No. r failed is limited to

$$|\delta\bar{F}_4| \leq \frac{4}{3}\sqrt{7} D_{F_r} \cdot \sigma_N \text{ if } \delta_N \ll D_{F_r} \quad (36)$$

where σ_N is the noise amplitude and worse phases of the other gyro drifts occurred (by (31) with $K = 0$). Writing the algorithm (21) in the form,

Test No. 1:	$T_{23}^2 > \delta^*$	If <u>only</u> Test No. 1 fails the gyro No. 1 failed
Test No. 2:	$T_{13}^2 > \delta^*$	If <u>only</u> Test No. 2 fails the gyro No. 2 failed
Test No. 3:	$T_{12}^2 > \delta^*$	If <u>only</u> Test No. 3 fails the gyro No. 3 failed

(37)

where

$$\delta^* = (\bar{F}_4 - \delta)/\alpha$$

Consider the case when two of the tests fail, say Test No. 1 and Test No. 2. This can occur when only one gyro actually failed, say gyro No. 1, as seen by (35a), (35b) if $S_{\theta_1}^2$ is sufficiently small. Deciding which gyro failed may use (34) to compare F_1 and F_2 . If $F_1 > F_2$ then it is more probable that gyro No. 1 failed than gyro No. 2. The exact probability depends on noise level of $F_1 - F_2$ whereby (34)

$$F_1 - F_2 = \alpha (T_{13}^2 - T_{23}^2)$$

Using (17) and the general relation $(C_{\theta_3}^2 - 30^\circ - S_{\theta_3}^2) = \frac{\sqrt{3}}{2} C_{2\theta_3-30^\circ}$, consider the statistic Δ ,

$$\begin{aligned} \Delta &\equiv T_{13}^2 - T_{23}^2 \\ &= \left(D_{F1} S_{\theta_1} + D_{F3} C_{\theta_3-30^\circ} \right)^2 - \left(D_{F2} S_{\theta_2} + D_{F3} S_{\theta_3} \right)^2 \\ &= D_{F1}^2 S_{\theta_1}^2 + 2 D_{F1} D_{F3} S_{\theta_1} C_{\theta_3-30^\circ} + D_{F3}^2 \cdot \frac{\sqrt{3}}{2} C_{2\theta_3-30^\circ} \\ &\quad - D_{F2}^2 S_{\theta_2}^2 - 2 D_{F2} D_{F3} S_{\theta_2} S_{\theta_3} \end{aligned} \quad (38)$$

If gyro No. 1 failed at angle θ_1 and other gyros have only noise, the mean value of Δ is

$$\bar{\Delta}_1 = D_{F1}^2 S_{\theta_1}^2 - \sigma_N^2 / 2 \quad (39)$$

using $\overline{C^2} = \overline{S^2} = 1/2$, $\bar{C} = \bar{S} = 0$, $\overline{D_{F2}^2} = \overline{D_{F3}^2} = \sigma_N^2$. If gyro No. 2 failed at angle θ_2 and other gyros have only noise, the mean value of Δ is

$$\bar{\Delta}_2 = -D_{F2}^2 S_{\theta_2}^2 + \sigma_N^2 / 2 \quad (40)$$

using also $\overline{D_{F1}^2} = \overline{D_{F3}^2} = \sigma_N^2$.

If gyro No. 1 failed at angle θ_1 , using (26)

$$\begin{aligned}\sigma_{\Delta_1}^2 &= \overline{(\Delta - \bar{\Delta}_1)^2} = \overline{\left[\left(\Delta - D_{F_1}^2 S_{\theta_1} \right)^2 + \sigma_N^2 / 2 \right]^2} \\ &= \overline{\left(\Delta - D_{F_1}^2 S_{\theta_1} \right)^2} + \left(\bar{\Delta}_1 - D_{F_1}^2 S_{\theta_1} \right) \sigma_N^2 \\ &\quad + \sigma_N^4 / 4 \\ &= \overline{\left(\Delta - D_{F_1}^2 S_{\theta_1} \right)^2} - \sigma_N^4 / 4\end{aligned}$$

Denoting drifts of other gyros as noises N_2, N_3 ,

$$\begin{aligned}\overline{\left(\Delta - D_{F_1}^2 S_{\theta_1} \right)^2} &= \overline{\left[-N_2^2 S_{\theta_2}^2 + N_3^2 \cdot \frac{\sqrt{3}}{2} C_{2\theta_3-30^\circ} + 2N_3 D_{F_1} S_{\theta_1} C_{\theta_3-30^\circ} - 2N_2 N_3 S_{\theta_2} S_{\theta_3} \right]^2} \\ &= \overline{N_2^4} \cdot \overline{S^4} + \overline{N_3^4} \cdot \frac{3}{4} \overline{C^2} + 4 D_{F_1}^2 S_{\theta_1}^2 \cdot \overline{N_3^2} \cdot \overline{C^2} + 4 N_3^2 \overline{N_2^2} \cdot \overline{S^2} \cdot \overline{S^2}\end{aligned}$$

since none of the cross product terms contribute. Using *

$$\overline{N_2^4} = \overline{N_3^4} = 2 \sigma_N^4, \quad \overline{S^4} = 3/8 \text{ then}$$

$$\overline{\left(\Delta - D_{F_1}^2 S_{\theta_1} \right)^2} = 2 \sigma_N^2 \cdot \left[D_{F_1}^2 S_{\theta_1}^2 + \frac{5}{4} \sigma_N^2 \right]$$

*An amplitude distribution of two components which are normally distributed is modeled.

Hence

$$\sigma_{\Delta_1}^2 = 2 \sigma_N^2 \cdot \left[D_{F_1}^2 \cdot S_{\theta_1}^2 + \frac{9}{8} \sigma_N^2 \right]$$

If gyro No. 2 failed at angle θ_2 ,

$$\begin{aligned} \sigma_{\Delta_2}^2 &= (\Delta - \bar{\Delta}_2)^2 = \overline{\left[\left(\Delta + D_{F_2}^2 \cdot S_{\theta_2}^2 \right) - \sigma_N^2/2 \right]^2} \\ &= \overline{\left(\Delta + D_{F_2}^2 \cdot S_{\theta_2}^2 \right)^2} - \left(\bar{\Delta}_2 + D_{F_2}^2 \cdot S_{\theta_2}^2 \right) \cdot \sigma_N^2 + \sigma_N^4/4 \\ &= \overline{\left(\Delta + D_{F_2}^2 \cdot S_{\theta_2}^2 \right)^2} - \sigma_N^4/4 \end{aligned}$$

Denoting drifts of other gyros as noises

$$\begin{aligned} \overline{\left(\Delta + D_{F_2}^2 \cdot S_{\theta_2}^2 \right)^2} &= \overline{\left[N_1^2 \cdot S_{\theta_1}^2 + N_3^2 \cdot \frac{\sqrt{3}}{2} \cdot C_{2\theta_3-30^\circ} + 2N_1 N_3 \cdot S_{\theta_1} \cdot C_{\theta_3-30^\circ} - 2 D_{F_2} N_3 S_{\theta_2} S_{\theta_3} \right]^2} \\ &= \overline{N_1^4} \cdot \overline{S^4} + \overline{N_3^4} \cdot \frac{3}{4} \overline{C^2} + 4 \overline{N_1^2} \overline{N_3^2} \overline{S^2} \cdot \overline{C^2} + 4 D_{F_2}^2 \overline{S_{\theta_2}^2} \overline{N_3^2} \overline{S^2} \\ &= 2 \sigma_N^2 \cdot \left[D_{F_2}^2 \cdot S_{\theta_2}^2 + \frac{5}{4} \sigma_N^2 \right] \end{aligned}$$

Hence,

$$\sigma_{\Delta_2}^2 = 2 \sigma_N^2 \cdot \left[D_{F_2}^2 \cdot S_{\theta_2}^2 + \frac{9}{8} \sigma_N^2 \right] \quad (42)$$

The observable $\Delta \equiv T_{13}^2 - T_{23}^2$ is approximately normally distributed when the failure term exceeds the noise level according to probability density

$$\phi(\Delta) = \frac{e^{-\frac{1}{2} \left(\frac{\Delta - \bar{\Delta}_1}{\sigma_{\Delta_1}} \right)^2}}{\sqrt{2\pi} \sigma_{\Delta_1}} \quad \text{if gyro No. 1 failed} \quad (43)$$

$$\phi(\Delta) = \frac{e^{-\frac{1}{2} \left(\frac{\Delta - \bar{\Delta}_2}{\sigma_{\Delta_2}} \right)^2}}{\sqrt{2\pi} \sigma_{\Delta_2}} \quad \text{if gyro No. 2 failed}$$

To investigate the maximum probability density for $X = D_{F_1}^2 S_{\theta_1}^2$ put (43) for gyro No. 1 fail in the form

$$\phi(\Delta) = \frac{1}{\sqrt{2\pi}} e^{-\frac{1}{2} Q}$$

where

$$Q = \frac{(\Delta - \bar{\Delta}_1)^2}{\sigma_{\Delta_1}^2} + \ln(\sigma_{\Delta_1}^2). \quad \text{Using (39), (41)}$$

$$\bar{\Delta}_1 = x - \sigma_N^2/2$$

$$\sigma_{\Delta_1}^2 = 2 \sigma_N^2 \cdot \left(x + \frac{9}{8} \sigma_N^2 \right)$$

$$\text{Note } Q = \frac{(y - \delta)^2}{2\sigma_N^2 y} + \ln 2 \sigma_N^2 y \quad \text{where } y = x + \frac{9}{8} \sigma_N^2 \quad (44)$$

$$\delta = \Delta + \frac{13}{8} \sigma_N^2$$

Since $\phi(\Delta)$ is maximized when Q is minimized, take $\partial Q/\partial y = 0$ to obtain

$$0 = \frac{y^2}{2\sigma_N^2} + y - \frac{\delta^2}{2\sigma_N^2}$$

so

$$y = \sigma_N^2 \left[-1 + \sqrt{1 + (\delta/\sigma_N^2)^2} \right] \quad (45)$$

Since $\sigma_{\Delta 1}^2 > 0$, consider only the positive root. For $\delta \gg \sigma_N$ note $y \approx \delta$. For $\Delta > 3/8 \sigma_N^2$,

$$y \approx \delta + \frac{1}{2} \sigma_N^4 / \delta - \sigma_N^2$$

that is

$$\hat{x} = \Delta + \frac{1}{2} \sigma_N^2 / (13/8 + \Delta/\sigma_N^2) \quad (46)$$

minimizes Q and maximizes $\phi(\Delta)$ when $\Delta > 0$. The probability density for $\hat{x} = \Delta$ approximates

$$\text{Max}_{\left| D_{F1} S_{\theta 1} \right|} \phi(\Delta \mid \#1 \text{ fail}) \approx \frac{1}{\sqrt{2\pi} \cdot 2\sigma_N^2} \frac{e^{-\frac{1}{4} \frac{\sigma_N^2}{\left(\Delta + \frac{13}{8} \sigma_N^2\right)}}}{\left(\Delta + \frac{5}{8} \sigma_N^2 + \frac{1}{2} \sigma_N^4 / \delta\right)} \cdot \Delta > \frac{3}{8} \sigma_N^2 \quad (47)$$

For the same Δ observation, $\Delta > 0$, if we assume gyro No. 2 failed we have using (43), (40), (42) and redefining $x = D_{F2}^2 S_{\theta 2}^2$

$$\phi(\Delta) = \frac{1}{\sqrt{2\pi}} e^{-\frac{1}{2} Q}$$

where

$$Q = \frac{(\Delta - \bar{\Delta}_2)^2}{\sigma_{\Delta_2}^2} + \ln(\sigma_{\Delta_2}^2) = \frac{(y - \delta^*)^2}{2\sigma_N^2 y} + \ln 2\sigma_N^2 y \quad (48)$$

where

$$y = x + \frac{9}{8} \sigma_N^2$$

$$\delta = -\Delta + \frac{13}{8} \sigma_N^2$$

Since (48) and (44) have the same form except δ^* replaces δ the solution (45) for the maximum density holds with $\delta \rightarrow \delta^*$ provided $y > \frac{9}{8} \sigma_N^2$ (since $x > 0$) hence

$$y = \sigma_N^2 \left[-1 + \sqrt{1 + (\delta^*/\sigma_N^2)^2} \right] = |\delta^*| + \sigma_N^2 \cdot \left(\frac{\sigma_N^2}{2|\delta^*|} - 1 \right) \quad (49)$$

if $|\delta^*| > \frac{15}{8} \sigma_N^2$, which by (48) requires $\Delta > \frac{7}{2} \sigma_N^2$. For cases $\frac{7}{2} \sigma_N^2 > \Delta > 0$, where $|\delta^*| < \frac{15}{8} \sigma_N^2$ let us examine Q and its derivative using (44) with $\delta \rightarrow \delta^*$,

$$Q = \frac{1}{2\sigma_N^2} \left[y - 2\delta^* + \frac{\delta^{*2}}{y} \right] + \ln y + \ln 2\sigma_N^2$$

$$\frac{dQ}{dy} = \frac{1}{2\sigma_N^2} \left[1 - \frac{\delta^{*2}}{y^2} \right] + \frac{1}{y}$$

Try $y = \frac{9}{8} \sigma_N^2$, the minimum value of y for which $x > 0$, obtaining

$$Q = \left(\frac{3}{4} - \frac{2}{3} u \right)^2 + \ln \left(\frac{9}{4} \sigma_N^4 \right) \text{ where } u = \frac{\delta^*}{\sigma_N^2} \quad (50)$$

$$\frac{dQ}{dy} = \frac{25}{18\sigma_N^2} \left[1 - \left(\frac{8}{15} u \right)^2 \right] \quad \frac{7}{2} \sigma_N^2 > \Delta > 0$$

Since we consider the case $\frac{8}{15} u = \frac{8 \delta^*}{15 \sigma_N^2} < 1$, it follows $\frac{dQ}{dy} > 0$ and that Q is larger for values of $y = \frac{9}{8} \sigma_N^2$. The probability density for the most likely value of $D_{F2}^2 S_{\theta 2}^2$ if gyro No. 2 failed is by (50), (48)

$$\begin{aligned} \text{Max}_{\left| D_{F2}^2 S_{\theta 2}^2 \right|} \phi(\Delta \mid \text{No. 2 fail}) &= \frac{1}{\sqrt{2\pi} \frac{3}{2} \sigma_N^2} \cdot e^{-\frac{2}{9} \left(\frac{\Delta}{\sigma_N^2} - \frac{1}{2} \right)^2} \quad \frac{7}{2} \sigma_N^2 > \Delta > 0 \\ & \quad - \left| \frac{\Delta}{\sigma_N^2} - \frac{13}{8} \right| \quad (51) \\ \text{Max}_{\left| D_{F2}^2 S_{\theta 2}^2 \right|} \phi(\Delta \mid \text{No. 2 fail}) &= \frac{1}{\sqrt{2\pi} 2 \sigma_N^2} e^{-\left| \frac{\Delta - \frac{13}{8} \sigma_N^2}{\sigma_N^2} \right|^2} \quad \Delta > \frac{7}{2} \sigma_N^2 \end{aligned}$$

3. Calculation of the Probability of Isolating a Gyro-Failure in the Three Gyro Case

When only one edge test clearly fails in the three gyro case it is clear that one or the other gyros associated with the edge test that failed was a failed gyro. The best that can be done is estimate the probability that one gyro failed rather than the other, on the basis of the three test values. The principle by which this is calculated here is the relative probability densities of the test results for alternate hypothesis of failure, the probability densities being those for maximum likelihood values with respect to amplitude and direction of the hypothesized failure rate. This procedure then is

$$\frac{PF_1}{PF_2} = \frac{\left(\begin{matrix} \text{Max} & \phi(\Delta | \#1 \text{ Fail}) \\ D_{F1} & S_{\theta 1} \end{matrix} \right)}{\left(\begin{matrix} \text{Max} & \phi(\Delta | \#2 \text{ Fail}) \\ D_{F2} & S_{\theta 2} \end{matrix} \right)} \equiv \frac{1}{r}$$

where $PF_1 + PF_2 = 1$ so $PF_1 = \frac{1}{1+r}$, $PF_2 = 1 - PF_1$ where (34), (38) are used for the peak probability densities for given $\Delta \equiv (T_{13}^2 - T_{23}^2)$ when T_{12} failed. Using (34), (38) obtain

$$P_{F1} = \left[1 + \sqrt{\frac{\Delta + \frac{5}{8} \sigma_N^2}{\Delta - \frac{13}{8} \sigma_N^2}} \cdot e^{-\left(\frac{\Delta}{\sigma_N^2} - \frac{13}{8}\right)} \right]^{-1} \quad \text{for } \Delta > \frac{7}{2} \sigma_N^2$$

$$P_{F1} = \left[1 + \frac{2\sqrt{2}}{3} \sqrt{\frac{\Delta}{\sigma_N^2} + \frac{5}{8}} \cdot e^{-\frac{2}{9} \left(\frac{\Delta}{\sigma_N^2} - \frac{1}{2}\right)^2} \right]^{-1} \quad \text{for } \frac{7}{2} \sigma_N^2 \geq \Delta \geq \frac{3}{8} \sigma_N^2$$

A table of a number of values is

Δ/σ_N^2	P_{F1}	
2.	.52	
3.5	.80	$\Delta = T_{13}^2 - T_{23}^2$
5.	.956	
10.	.999746	

For values of $\Delta/\sigma_N^2 \leq 1.5$ the formulae are in accurate because of approximations made in the deviation.

4. Navigating with Improved Accuracy with Four Valid Gyros

The proposed configuration generates four navigation program outputs in parallel. To minimize navigation error the parallel outputs x_i of any navigation parameter x can be estimated by use of weighting coefficients, ω_i ,

$$\hat{x} = \frac{\sum_{i=1}^4 \omega_i x_i}{\sum_{i=1}^4 \omega_i}$$

where ω_i should be selected according to quality of the i th channel estimates. When no failure has occurred and all gyros behave according to specification, selection $\omega_i = 1/4$ is a practical selection. Consider the case of soft failure of one gyro, GF₁ type, where already available test functions F_r , $r = 1, 4$ do not indicate failure. In this case, the use of

$$\omega_i = \left[F_j + F_k + C \right]^{-1}$$

where the i th channel uses gyro j and k , and $C = \text{constant}$, will reduce the weights on two channels using the degraded gyro. This selection of weights is further justified as follows:

- a. For errors in x_i independent from channel to channel, the theoretical weight is $\omega_i = 1/\sigma_{x_i}^2$
- b. Actually errors in x_i are correlated because certain pairs of channels have one gyro in common. However, the correlation of drift rates in the constructed reference using two gyros is $|\rho| < 1/3$. Neglect this correlation since the effect on magnitude is fairly small, by $\sqrt{1 - \rho^2} \approx .943$.
- c. The reference error of the constructed reference; using two gyros has variance proportional to $(\sigma_{D_j}^2 + \sigma_{D_k}^2)$.

where $\sigma_{D_{j \text{ or } k}}^2$ is the variance of gyro j or k. Gyro cluster orientation is such that most navigation variables relate to total reference error, so

$$\sigma_{x_i}^2 = C_1 \left(\sigma_{D_j}^2 + \sigma_{D_k}^2 \right) + C_0$$

where C_0 includes errors not related to reference error.

- d. For four gyros, the test function F_j for test of gyro j approximates $F_j \approx D_j^2$, when one gyro j has distinctly larger drift than the other gyros, for which F_k is noisy but small.
- e. Then

$$\omega_i = 1/\sigma_{x_i}^2 \approx [F_j + F_k + C]^{-1}$$

$$\text{where } C = \frac{C_0}{C_1}$$

Note: This weighting technique is contemporaneous to the smoothing time of the test so that if a gyro shows some recovery, the channels using it are given more weight.

5. Preliminary Gyro Failure Detection and Isolation Program FORTTRAN Listing

$$S(4) = T_{23} * T_{23}$$

$$S(5) = T_{24} * T_{24}$$

$$S(6) = T_{34} * T_{34}$$

$$\bar{F}(1) = S(6) + S(5) + S(4)$$

$$S(2) = T_{13} * T_{13}$$

$$S(3) = T_{14} * T_{14}$$

$$\bar{F}(2) = S(3) + S(6) + S(2)$$

$$S(1) = T_{12} * T_{12}$$

$$\bar{F}(3) = S(1) + S(3) + S(5)$$

```

 $\bar{F}(4) = S(1) + S(2) + S(4)$ 
 $F\emptyset = (\bar{F}(4) + \bar{F}(3) + \bar{F}(2) + \bar{F}(1)) * .5 - \delta 4$ 
 $\bar{F}(1) = (T_{23} - T_{24} + T_{34}) ** 2 + \bar{F}(1)$ 
 $\bar{F}(2) = (T_{14} + T_{34} - T_{13}) ** 2 + \bar{F}(2)$ 
 $\bar{F}(3) = (T_{12} + T_{14} - T_{24}) ** 2 + \bar{F}(3)$ 
 $\bar{F}(4) = (T_{12} - T_{13} + T_{23}) ** 2 + \bar{F}(4)$ 
4  v(5) = v5
   TL   = ( $\bar{F}(JB) - \delta 3$ ) *  $\bar{a}$ 
   DO 10 J = 1,4

   IF (v(5).EQ.0.) Go to 1
   IF (F(J)-F $\emptyset$ ) > 0 Go to 10
   v5   = 0.
   IF (F( $\delta$ ).LT. $\delta 2$ ) Go to 7
   2BAD = 1.
   SM   = S(1)
   Go to 4
7  v(J) = 0
   JB   = J

```

} For 2BAD } Four Gyro Case

```

1  IF (v(J).EQ.0.) Go to 10
   DO 2 K = 1,4
   IF (K,LE.J) Go to 2
   IF (v(K).EQ.0.) Go to 2
   L = J + K -1
   IF (J.EQ.1) L = L-1
   IF (2BAD.EQ.1.) TL = SM
   IF (S(L).GT.TL) Go to 2
   IF (2BAD.EQ.0.) Go to 7
   SM = S(L)
   JM = J
   KM = K
   Go to 2
7  KBØ = KB
   KB = TEN-J-K-JB
   v(KB) = 0.
   ARG - S(L)-ARG
2  CONTINUE
10 CONTINUE
   IF (v5*FØ.LT.0.) Go to 5
   2BAD = 1.
   v5 = 0.
   Go to 4
5  IF (2BAD.EQ.0.) Go to 6
   JB = 3
   IF (JM.GT.1) JB = 1
   IF (KM.LT.4) JB = 4
   v(JB) = 0.
   2BAD = 0.
   Go to 4

```

For 2BAD

For 2BAD

Three Gyro Case

} Optional (Long Shot Case)

For 2BAD

```
6  IF (KBØ.EQ.0.) Go to 3
    READ P(ARG) Table
    v(KBØ) = P(ARG)
    v(KB) = 1.-v(KB)
3  CONTINUE
```

Initialize:

v(1) = 1.	2 BAD = 0.
v(2) = 1.	KB = 0.
v(3) = 1.	KBØ = 0.
v(4) = 1.	ARG = 0.
v 5 = 1	
JB = 1	
TEN = 10.	

APPENDIX J
PROBABILITY OF EFFECTIVELY SIMULTANEOUS FAILURE OF
TWO GYROS AND IMPACT ON FAILURE ISOLATION AND
SYSTEM FAILURE

Probability of Effectively Simultaneous Failure of Two Gyros and Impact on Failure Isolation and System Failure

On missions where two gyros failed during a half hour period, the probability the failures occurred within 60 seconds of each other is $P_{SF} = 60/1800 = 0.033$. Since testing involves a smoothing time, two failures within 60 seconds can involve testing in the presence of effectively simultaneous failures. To see the impact of simultaneous failures on testing substitute (6c) of Appendix I for say gyro No. 1 and No. 2 failed into (6a), (6b) to obtain an algebraic reduction the test functions F_r of the sophisticated procedure:

$$F_1 = D_{F_1}^2 - \frac{4}{3} D_{F_1} D_{F_2} C_{\theta_1-30^\circ} C_{\theta_2-30^\circ}$$

$$F_2 = D_{F_2}^2 - \frac{4}{3} D_{F_1} D_{F_2} C_{\theta_1-30^\circ} C_{\theta_2-30^\circ} \quad D_{Fr} = \text{failure drifts}$$

$$F_3 = \frac{4}{3} D_{F_1} D_{F_2} S_{\theta_1} S_{\theta_2} \quad \theta_r = \text{angle of drift}$$

$$F_4 = \frac{4}{3} D_{F_1} D_{F_2} C_{\theta_1+30^\circ} C_{\theta_2+30^\circ}$$

Say $D_{F_1} > D_{F_2} > D_{F_{MIN}}$ where $D_{F_{MIN}}$ is the minimum rate for failure. Note that testing $F_1 > \epsilon^2$ where $\epsilon = D_{F_{MIN}}/2$ for detection of gyro No. 1 failure is unsuccessful if D_{F_2} satisfies

$$\frac{D_{F_2}}{D_{F_1}} > \left[\frac{3}{4} - \frac{3}{16} \left(\frac{D_{F_{MIN}}}{D_{F_1}} \right)^2 \right] / A$$

$> \frac{3}{4A}$ usually when $D_{F_{MIN}} < D_{F_1 \text{ or } 2} < D_{F_{MAX}}$

where

$$A = C_{\theta_1^*} \cdot C_{\theta_2^*}, \quad \theta_1^* = \theta_1 - 30^\circ, \quad \theta_2^* = \theta_2 - 30^\circ.$$

The probability given θ_1^*, θ_2^* that the drift rate satisfies $\frac{3}{4A} D_{F_1} < D_{F_2} < D_{F_1}$ is:

$$P_D = \frac{\left(1 - \frac{3}{4A}\right) D_{F_1}}{\left(D_{F_{MAX}} - D_{F_{MIN}}\right)} \approx \frac{3}{8} \frac{\left(\frac{2}{3} - \theta_1^{*2} - \theta_2^{*2}\right) D_{F_1}}{\left(D_{F_{MAX}} - D_{F_{MIN}}\right)}$$

where $\theta_1^{*2} + \theta_2^{*2} < 2/3$, assuming a flat distribution of failure drift rates. It is believed that the actual distribution of failure rates is a combination of two flat distributions of 0.5 area each in the ranges 1.°/hr to 20.°/hr and 20.°/hr - 100.°/sec (360,000°/hr), in which case failures of near equal magnitude practically always occur in the range 1.°/hr to 20.°/hr with half the probability for a single flat distribution.

The probability that gyro No. 1 will not be isolated by F_1 test is

$$P_{F_1 \text{ PASS}} = \int_{-\sqrt{\frac{2}{3}}}^{\sqrt{\frac{2}{3}}} \frac{d\theta_2^*}{2\pi} \int_{-\theta}^{\bar{\theta}} \frac{d\theta_1^*}{\pi} P_D$$

$$\bar{\theta} = \sqrt{\frac{2}{3} - \theta_2^{*2}}$$

where

$$P_D = a \left(\bar{\theta}^2 - \theta_1^{*2} \right), \quad a = 3D_{F1} / 8 (D_{FMAX} - D_{FMIN})$$

Integrating,

$$\begin{aligned} P_{F1 \text{ PASS}} &= \int_{-\sqrt{\frac{2}{3}}}^{\sqrt{\frac{2}{3}}} \frac{d\theta^*}{2\pi} \cdot \frac{a}{\pi} \cdot \frac{4}{3} \bar{\theta}^3 \\ &= \frac{4a}{3\pi^2} \int_0^{\sqrt{\frac{2}{3}}} \left(\frac{2}{3} - \theta^{*2} \right)^{3/2} d\theta^* \\ &\approx \frac{8a}{27\pi^2} \\ &\approx \frac{D_{F1}}{90 (D_{FMAX} - D_{FMIN})} \end{aligned}$$

averaging with respect to D_{F1}

$$P_{F1 \text{ PASS}} \approx \frac{1}{180}$$

for $D_{FMAX} \gg D_{FMIN}$. The fraction of flights where two failures occurred in which non-isolation of the larger failure rate resulted from simultaneous failures is

$$P_G = P_{SF} \cdot P_{F_1 \text{ PASS}} = 1.8 \times 10^{-4} \quad \text{Non-detection probability of greater failure}$$

The probability that the gyro which failed with a lesser drift rate is not detected may be shown to be

$$P_L \approx \frac{D_{F \text{ MAX}} - \frac{3}{2} D_{F 2}}{2(D_{F \text{ MAX}} - D_{F \text{ MIN}})} \quad \text{Non-detection probability of lesser failure}$$

On average, for $\frac{2}{3} D_{F \text{ MAX}} > D_{F 2} > D_{F \text{ MIN}}$

$$P_L \approx \frac{(D_{F \text{ MAX}} - \frac{3}{2} D_{F \text{ MIN}})}{4(D_{F \text{ MAX}} - D_{F \text{ MIN}})} \approx \frac{1}{4}$$

for $D_{F \text{ MAX}} \gg D_{F \text{ MIN}}$. Thus about 25% of the cases of dual failures the lesser failure is not detected by its Fr test.

Tests Fr with dual failure not involving r can fail. The average value of F_3 , F_4 for positive cases, which occur 50% of the time is

$$\begin{aligned} \bar{F}_3 &= \frac{1}{2} \left[\bar{D}_F \cdot \bar{S}_\theta \right]^2 \\ &= \frac{1}{2} \left[\frac{(D_{F \text{ MAX}} + D_{F \text{ MIN}})}{2} \cdot \frac{2}{\pi} \right]^2 \\ &= \left[\frac{(D_{F \text{ MAX}} + D_{F \text{ MIN}})}{4.45} \right]^2 \end{aligned}$$

Comparing with a test level

$$\epsilon^2 = \left(\frac{D_{F\text{MIN}}}{2} \right)^2$$

it is clear that almost half the time (when sign of F_3 positive) it will fail the test.

Consider the probability that no test fails, $F_r < \epsilon^2$ ($r = 1, 2, 3, 4$), in the dual failure case. The probability $r = 1$ passes is $1/180$, that $r = 2$ passes is near 1, in this case, while the probabilities of $r = 3$ pass or $r = 4$ pass are near equal as

$$P_{r\text{PASS}} = 2 \left(\frac{\theta_1}{1 \text{ rad}} \right) \quad \text{where } \theta_1 = 2 \left(\frac{D_{F\text{MIN}}}{D_{F\text{AVERAGE}}} \right)^2 \quad r = 3, 4$$

$$\approx 2 \left(\frac{D_{F\text{MIN}}}{D_{F\text{MAX}}} \right)^2$$

$$\approx 1.3 \times 10^{-3} \quad \text{for } D_{F\text{MAX}} = 40 D_{F\text{MIN}}$$

Then the probability of system failure because no test fails is

$$P_{\text{SYS FAILURE}}^{\text{ALL PASS}} = \left(\frac{1}{180} \right) (1.0) (1.3 \times 10^{-3})^2 = 10^{-8}$$

In the extremely likely case one or more F_r tests fail, it is proposed that dual failures be handled as follows. For four gyros, if a test F_{r^*} failed, make the three gyro test not using gyro r^* and if any test fails conclude that dual failure has occurred.

In the event of deciding that dual failure has occurred, revert to the simple test procedure

$$|T_{rs}| < \epsilon$$

If only one test passes, $T_{r^*s^*} < \epsilon$, it is concluded gyro r^* and gyro s^* are good and that the remaining gyros are bad, a certain conclusion. If two tests pass, $T_{r^*s^*}$ and $T_{q^*r^*}$, having a gyro in common then conclude certainly that r^* is good and the fourth gyro p^* is bad (since either s^* gyro or q^* gyro is good and it is known two gyros are bad), thus reducing the situation to the ambiguous case of three gyros, r^* , s^* , q^* where p^* is known bad, r^* is known good but s^* gyro or q^* gyro is bad with calculable probability based on the magnitude of $|T_{r^*s^*}|$ and $|T_{r^*q^*}|$. The probability of a test passing given that two GF_2 failures occurred is^{**}:

$$P_{\text{PASS, 1 BAD}} \approx \frac{D_{F \text{ MIN}}}{\pi} \int_{D_{F \text{ MIN}}}^{D_{F \text{ MAX}}} \frac{1}{D_F} \cdot \frac{dD_F}{(D_{F \text{ MAX}} - D_{F \text{ MIN}})} \quad \text{Pass Probability: if either gyro r or gyro s failed}$$

* $D_{\text{max}} = 20$. D_{min} for a range 1.°/hr - 20.°/hr, but half the time GF_3 failure occurs so we may usually take $D_{\text{max}} = 40 D_{\text{min}}$ and get

** correct results.

Using notation defined in 5.3.3 on attitude rate failure.

$$\begin{aligned}
 & \approx \frac{D_{F\text{MIN}}}{\pi} \cdot \frac{\ln\left(\frac{D_{F\text{MAX}}}{D_{F\text{MIN}}}\right)}{D_{F\text{MAX}}} \\
 P_{\text{PASS, 2 BAD}} & \approx \frac{D_{F\text{MIN}}}{2\pi} \int_{D_{F\text{MIN}}}^{D_{F\text{MAX}}} \frac{1}{D_F} \cdot \frac{dD_F}{(D_{F\text{MAX}} - D_{F\text{MIN}})} \quad \text{if both gyro r or gyro s failed} \\
 & \approx \frac{D_{F\text{MIN}}}{2\pi} \cdot \frac{\ln\left(\frac{D_{F\text{MAX}}}{D_{F\text{MIN}}}\right)}{D_{F\text{MAX}}}
 \end{aligned}$$

Only the case where a test with both gyros bad has $|T_{rs}| < \epsilon$ leads to system failure directly associated with simultaneity of failures of two gyros, having probability within the subclass of missions in which two gyro failures occurred:

$$\begin{aligned}
 P_{\text{SYSTEM FAILURE}} &= P_{\text{SF}} \cdot P_{\text{PASS, 2 BAD}} \quad \text{Probability of system failure due to simultaneous failure of 2 gyros. Given: 2 gyros failed during mission}
 \end{aligned}$$

$$= 0.33 \cdot \frac{D_{F\text{MIN}}}{2\pi} \cdot \frac{\ln\left(\frac{D_{F\text{MAX}}}{D_{F\text{MIN}}}\right)}{D_{F\text{MAX}}}$$

$$\approx 0.8 \times 10^{-3}$$

$$\text{using } D_{F\text{MAX}} = 20 D_{F\text{MIN}}$$

403314

REFERENCE SECTION

REFERENCES

- [1] Statement of Work for a "Preliminary Design of a Redundant Strapped Down Inertial Navigation Unit Using Two-Degree-of-Freedom Tuned Gimbal Gyroscopes," 1-16-5138 Exhibit A, August 2, 1974, Langley Research Center, Hampton, Va.
- [2] Proposal for a Preliminary Design of a Redundant Strapdown Navigator, Pub. No. 130001, December 1974, Litton Systems, Inc., Woodland Hills, Ca.
- [3] "Investigation of Application of Two-Degree-of-Freedom Dry Tuned-Gimbal Gyroscopes to Strapdown Navigation Systems," Final Report, NASA CR-132419, April 1974, Teledyne Systems Company, Northridge, Ca.
- [4] ARINC Characteristic No. 561-11, "Air Transport Inertial Navigation System - INS," April 30, 1974, Aeronautical Radio, Inc., Annapolis, Md.
- [5] ARINC Characteristic No. 571, "Inertial Sensor System (ISS)," August 10, 1970, Aeronautical Radio, Inc., Annapolis, Md.
- [6] ARINC Project Paper No. 414, "General Guidance for Equipment and Installation Designers," August 18, 1964, Aeronautical Radio, Inc., Annapolis, Md.
- [7] RTCA Paper 120-61/DO-108, "Environmental Test Procedures Airborne Electronic Equipment," July 13, 1961, Radio Technical Commission for Aeronautics, Washington, D.C.
- [8] ARINC Specification No. 404-8, "Air Transport Equipment Cases and Racking," December 31, 1970, Aeronautical Radio, Inc., Washington, D.C.
- [9] Measurement of the Motion of Parked Aircraft by a Photographic Method," by A. P. Worgan, Royal Aircraft Establishment Technical Report 67132, June 1967.
- [10] "Linear and Angular Vibration Measurement of V/STOL Aircraft," by D. Isakson, Final Report, April 1970, Contract NAS12-2028, Hamilton Standard Division, United Aircraft Corp., Windsor Locks, Conn.

- [11] "Strapdown Navigator Errors in a Vibration Environment," by L. Sher of Air Force Weapons Laboratory, Kirtland Air Force Base, New Mexico, and J. H. Fagan, The Analytic Sciences Corp., Reading, Mass., Presented at the Fifth Inertial Guidance Test Symposium.
- [12] ARINC Project Paper No. 413, "Guidance for Aircraft Electrical Power Utilization and Transient Protection," July 1, 1965, Aeronautical Radio, Inc., Washington, D.C.
- [13] "Evaluation of Selected Strapdown Inertial Instruments and Pulse Torque Loops," by J. S. Sinkiewicz, et al, Charles Stark Draper Laboratory, Inc., July 1974, NASA Marshall Space Flight Center Contract NAS12-2033, N74-32099.
- [14] "Reliability Improvement Through Redundancy at Various System Levels," by B. J. Flehinger, Convention Record of the 1958 IRE National Convention, Part 6, pp 137-151.
- [15] "Reliability Modeling Techniques for Self-Repairing Computer Systems," by W. G. Bouricius, W. R. Carter and P. R. Schneider, Proceedings of the ACM, 1969 Annual Conference.
- [16] "Digital Computer Design Guidelines for a Full Authority Fly-by-Wire Flight Control System," by J. G. Allen, AIAA Digital Avionics System Conference, April 2-4, 1975.
- [17] "Design of a Fault Tolerant Airborne Digital Computer," Stanford Research Institute, October 1973, NASA CR-132252.
- [18] "Definition and Tradeoff Study of Reconfigurable Airborne Digital Computer System Organizations," Ultrasystems, Inc., November 1974, NASA CR-132552.
- [19] "Redundancy Management of Inertial Systems," by R. A. McKern and H. Musoff, Charles Stark Draper Laboratory, AIAA Guidance and Control Conference, Key Biscayne, Fla., August 20-22, 1973, AIAA Paper No. 73-852.
- [20] "A Redundant Strapdown Inertial Reference Unit (SIRU)," by J. P. Gilmore and R. A. McKern, Charles Stark Draper Laboratory, Journal of Spacecraft and Rockets, Vol. 9, No. 1, January 1972.

- [21] "An Adaptive Technique for a Redundant Sensor Navigation System," by Tze-Thong Chien, Massachusetts Institute of Technology, AIAA Guidance and Control Conference, Stanford, Calif., August 14-16, 1972, AIAA Paper No. 72-863.
- [22] "Minimax Failure Detection and Identification in Redundant Gyro and Accelerometer Systems," by J. E. Potter and J. C. Deckert, Charles Stark Draper Laboratory, Journal of Spacecraft and Rockets, Vol. 10, No. 4, April 1973.
- [23] "SIRU Utilization, Vol. I, Theory, Development, and Test Evaluation," by H. Musoff, Charles Stark Draper Laboratory, NASA Johnson Space Center Contract NAS9-8242, N74-28098.
- [24] "Experimental Strapdown Redundant Sensor Inertial Navigation System," by F. A. Evans and J. C. Wilcox, TRW Systems Group, Journal of Spacecraft and Rockets, Vol. 7, No. 9, September 1970.
- [25] "Maximum Likelihood Failure Detection for Redundant Inertial Instruments," by J. C. Wilcox, TRW Systems Group, AIAA Guidance and Control Conference, Stanford, Calif., August 14-16, 1972, AIAA Paper No. 72-864.
- [26] "Competitive Evaluation of Failure Detection Algorithms for Strapdown Redundant Inertial Instruments," by J. C. Wilcox, TRW Systems Group, Journal of Spacecraft and Rockets, Vol. 11, No. 7, July, 1974.
- [27] "Optimum Skewed Redundant Inertial Navigators," by A. J. Pejisa, Honeywell, Inc., AIAA Journal, Vol. 12, No. 7, July 1974.
- [28] "Strapdown Cost Trend Study and Forecast," by A. J. Eberlein, et al, Honeywell, Inc., NASA Ames Research Center Contract No. NAS2-8065, N75-17328.
- [29] "Optimal Gyro Mounting Configurations for a Strapdown System," by C. R. Giardina, Singer-Kearfott Division, NAECON '74 Record.
- [30] "New Voters For Redundant Systems," by R. B. Broen, McDonnell Aircraft Co., Journal of Dynamic Systems, Measurement, and Control, March 1975.
- [31] "Theory of Operation of an Elastically Supported, Tuned Gyro," by R. J. G. Craig, IEEE Trans. Aerospace and Electronic Systems, Vol. AES-8, pp. 280-288, May 1972.

- [32] "Theory of Errors of a Multigimbal, Elastically Supported, Tuned Gyro," by R. J. G. Craig, IEEE Trans. Aerospace and Electronic Systems, Vol. AES-8, pp. 289-297, May 1972.
- [33] "Dynamically Tuned Gyros in Strapdown Systems," by Robert J. G. Craig, 1972 AGARD Conference Proceedings No. 116 on Inertial Navigation Components and Systems.
- [34] "Application of the Complex Method to Transform Analysis of Spinning Systems with Rotating Non-Symmetries," by Dr. J. S. Lipman, Proc 1968 Joint Automatic Control Conf., Ann Arbor, Mich.

